THE UNIVERSITY *of* EDINBURGH

Behavioural, Genetic and Epigenetic Determinants of White Matter Pathology in a New Mouse Model of Chronic Cerebral Hypoperfusion

Yanina Tsenkina M.Sc.

Doctor of Philosophy

The University of Edinburgh

2012

DECLARATION

In accordance with the regulations of the University of Edinburgh I declare that this dissertation in its entirety is not substantially the same as any that the author has previously submitted for a degree or diploma or any other qualification at any other university. The work is solely that of the author, except where and if indicated.

Yanina Tsenkina

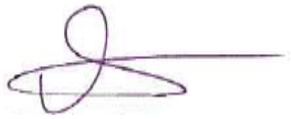

ACKNOWLEDGEMENTS

First of all, I would like to thank my supervisors Drs Karen Horsburgh and Paul De Sousa for their professional advice and guidance during the experimental work and the write- up of my thesis. I would also like to acknowledge Dr Emma Wood for help and professional guidance. My special thanks to Prof Richard Ribchester for being an excellent chairman of my thesis committee, for his help, support and guidance during my postgraduate studies. I would like to thank Profs Siddharthan Chandran and Stephen Dunnett for reviewing my thesis and for their useful recommendations.

During my PhD years in Edinburgh, I had the opportunity to work and make friends with extraordinary people who helped me both professionally and morally to go through all stages (ups and downs) of my PhD studies. Here, I would like to express my gratitude to Drs Catherine Gliddon and Alexey Ruzov for being great colleagues and friends, for their professional advice, support and friendship.

I would also like to thank all the PhD students, postdocs and technical staff at the Centers for Cognitive and Neural Systems and Regenerative Medicine at the University of Edinburgh who contributed to all aspects of my PhD in particular, Jessica Smith, Karim Khallout, Aisling Spain, Robin Coltman, Rachel James, Michell Reimer, Gillian Scullion, Philip Holland, Fiona Scott, Severine Launay, Veronika Ganeva, Steve Pells, Eirini Koutsouraki, Heidi Mjoseng, Alexander Ermakov, Cairnan Duffy, Jieuqian Zhou. My special thanks to Drs Anna Williams, Veronique Miron and Maurits Jansen for their help with some of the experimental work presented in my thesis.

Lastly, I would like to thank my family and friends for their love and support.

Thank you.

CONTENTS

Declaration I

Acknowledgments II

Table of contents III

List of figures XXVI

List of tables XXXI

List of abbreviations XXXV

Abstract XXIX

TABLE OF CONTENTS

CHAPTER 1

Introduction

1.1. Cerebral white matter 1

1.2. Age- related white matter pathology and cognitive decline 6

1.3. Mechanisms of damage to white matter 9

1.3.1. Excitotoxicity and oxidative stress 9

1.3.2. Inflammation 10

1.3.3. Gene mutations 11

1.4. Methods for detection of white matter integrity 12

1.4.1. Magnetic resonance imaging (MRI) 12

1.4.1.1. Diffusion tensor imaging (DTI) 13

1.4.1.2. Magnetization transfer ration (MTR) 14

1.4.2. Ex vivo (postmortem) histopathological evaluation of white matter integrity 14

1.5. Chronic cerebral hypoperfusion 15

1.5.1. Chronic cerberal hypoperfusion, age- related white matter pathology and cognitive decline 16

1.5.2. Animal models of chronic cerebral hypoperfusion 19

1.5.2.1. Rat model of chronic cerebral hypoperfusion 19

1.5.2.2. Gerbil model of chronic cerebral hypoperfusion 21

1.5.2.3. Mouse model of chronic cerebral hypoperfusion 22

1.6. Apolipoprotein E (APOE) 23

1.6.1. Differences between human and mouse APOE 26

1.6.2. APOE deficient mice 27

1.6.3. APOE, age- related white matter pathology and cognitive decline 27

1.6.4. APOE- related mechanisms impacting on white matter integrity 29

1.6.4.1. Role of APOE in the transport and metabolism 29
of brain lipids and cholesterol

1.6.4.2. Anti- excitotoxic function of APOE 31

1.6.4.3.Anti- oxidative function of APOE 31

1.6.4.4. Immunomodulatory function of APOE 32

1.7. Epigenetics **33**

1.7.1. DNA methylation 33

1.7.1.1. DNA methylation, age- related neuropathology 36
and cerebrovascular disease

1.7.2. DNA hydroxymethylation 38

1.7.2.1. DNA hydroxymethylation and age- related neuropathology 39

1.7.3. Ten- Eleven- Translocation proteins (TETs) 40

1.8. Thesis aims **41**

CHAPTER 2

Materials and methods

2.1. Animals **42**

2.1.1. C57Bl6J mice 42

2.1.2. APOEKO mice 42

2.2. Chronic cerebral hypoperfusion **43**

2.3. Behavioural tests **43**

2.3.1. Vision test 44

2.3.1.1. Principle and apparatus 44

2.3.1.2. Procedure 44

2.3.2. Spatial working memory task on a radial arm maze paradigm 46

2.3.2.1. Principle and apparatus 46

2.3.2.2. Procedures 46

2.3.2.2.1. Pretraining 46

2.3.2.2.2. Training 47

2.3.3. Serial spatial learning and memory task on a water maze paradigm 47

2.3.3.1. Principle and apparatus 47

2.3.3.2. Procedures 48

2.3.3.2.1. Cue task 48

2.3.3.2.2. Serial spatial learning and memory task 49

2.3.3.2.2.1. Training 49

2.3.3.2.2.2. Probe trails 49

2.4. Transcardiac perfusion- fixation 50

2.5. Histology 50

2.5.1. Paraffin embedding 50

2.5.1.1. Processing of brain slices 51

2.5.1.2. Processing of whole brains 51

2.5.2. Microtome cutting 51

2.5.3. Haemotoxylin and eosin (H&E) 53

2.6. Immunohistochemistry 53

2.6.1. Avidin- biotin immunohistochemistry 53

2.6.1.1. Peroxidase ABC based immunohistochemistry 55

2.6.1.2. Fluorescent immunohistochemistry 56

2.6.1.3. DNA fluorescent immunohistochemistry 56

2.7. Pathology assessment **58**

2.7.1. Light microscopy 58

2.7.2. Neuroanatomical regions of interest 58

2.7.3. Grey matter integrity and neuronal perikarya ischemic damage 58

2.7.4. White matter integrity and inflammation 61

2.7.4.1. Evaluation of axonal integrity by means 61
of amyloid precursor protein (APP) immunoreactivity

2.7.4.2. Evaluation of myelin structural integrity by means 62
of myelin associated glycoprotein (MAG) immunoreactivity

2.7.4.3. Evaluation of degraded myelin by means 64
of degraded myelin basic protein (dMBP) immunoreactivity

2.7.4.4. Evaluation of inflammation activity by means 64
of ionized calcium binding antigen 1 (Iba1) immunoreactivity

2.7.5. Other immunomarkers 65

2.7.5.1. 5- Methylcytosine (5mC) 65

2.7.5.2. 5- Hydroxymethylcytosine (5hmC) 65

2.7.5.3. Single stranded DNA (ssDNA) 67

2.7.5.4. Ten- eleven translocation protein 2 (TET2) 67

2.7.5.5. CC1 or also called adenomatous polyposis coli (APC) 67

2.7.5.6. Chondroitin sulfate proteoglycan (NG2) 67

2.8. Quantification of 5mC, 5hmC, TET2, CC1, NG2 and Iba1 positive cells 69

2.8.1. Fluorescent microscopy and imaging 69

2.8.2. Cell counting 69

2.9. Ex vivo MRI- DTI 70

2.9.1. Small rodent MRI scanner 70

2.9.2. Brain preparation prior to ex vivo MRI scanning 70

2.9.3. Ex vivo MRI- DTI procedure 73

2.9.4. MRI image analysis 73

2.10. In vitro culture and maturation of oligodendroglial cells 74

2.11. In vitro culture of activated and nonactivated microglial cells 75

2.12. Fixation of oligodendroglial and microglial cells 75

2.13. Statistics 75

CHAPTER 3

Effects of chronic cerebral hypoperfusion on white matter integrity and cognitive abilities in mice

3.1. Introduction and aims **76**

3.2. Materials and methods **81**

3.2.1. Animals and surgery 81

3.2.2. Behavioural tests 81

3.2.3. Pathological assessment 82

3.2.4. Statistics 83

3.2.3.1. Statistical analysis of the behavioural data 83

3.2.3.1.1. Statistical analysis of the radial arm maze behavioural data 83

3.2.3.1.2. Statistical analysis of the water maze behavioural data 83

3.2.3.2. Statistical analysis of the pathological data 84

3.2.3.3. Correlation analysis 84

3.3. Results **86**

3.3.1. Post- surgery recovery and physiological status 86

3.3.2. Effects of chronic cerebral hypoperfusion 86

on spatial working memory, memory flexibility,

learning capacity, short- and long- term memory recall in mice

3.3.2.1. Chronic cerebral hypoperfusion leads to spatial working memory impairment 86

3.3.2.2. Chronic cerebral hypoperfusion does not affect spatial memory flexibility 89

3.3.2.3. Chronic cerebral hypoperfusion does not affect spatial learning capacity 89

3.3.2.4. Chronic cerebral hypoperfusion does not impact on spatial short and long term memory recall 89

3.3.3. Effects of chronic cerebral hypoperfusion on white and grey matter integrity, inflammation 91

3.3.3.1. Chronic cerebral hypoperfusion leads to a significant axonal injury in white and grey matter 91

3.3.3.2. Chronic cerebral hypoperfusion leads to a significant myelin pathology 96

3.3.3.3. Chronic cerebral hypoperfusion leads to a significantly increased inflammation 97

3.3.3.4. Chronic cerebral hypoperfusion leads to neuronal ischemic damage 99

3.3.4. Inflammation in white matter correlates significantly with working memory, but not executive function in hypoperfused mice. 100

3.4. Discussion **102**

3.4.1. Cognition and memory in chronically hypoperfused mice 102

3.4.1.1. Spatial working memory impairment in chronically hypoperfused mice 102

3.4.2. Spectrum of white and grey matter pathology in chronically hypoperfused mice 105

3.4.2.1. Axonal injury in white and grey matter of chronically hypoperfused mice 105

3.4.2.2. Myelin pathology in chronically hypoperfused mice 108

3.4.2.3. Neuronal ischemic injury in chronically hypoperfused mice 111

3.4.2.4. Increased inflammation in white and grey matter of chronically hypoperfused mice 113

3.4.3. Is hypoperfusion- induced white matter pathology associated with cognitive impairment in mice? An unresolved question. 117

3.4.4. Methodological strengths, limitations and future behavioural and pathological experiments on chronically hypoperfused mice 121

3.4.4.1. Strengths of the applied behavioural and pathological approach 121

3.4.4.2. Limitations of the applied behavioural and pathological approach 122

3.4.4.3. Future behavioural and pathological studies 124

on chronically hypoperfused mice

3.4.5. Implications of the new mouse model of chronic cerebral hypoperfusion and future directions 128

3.5. Summary **129**

CHAPTER 4

Effects of APOE on white matter integrity under normal physiological and chronically hypoperfused conditions in mice

4.1. Introduction and aims **130**

4.2. Materials and methods **134**

4.2.1. Animals and surgery 134

4.2.2. Ex vivo MRI- DTI procedure 134

4.2.3. Pathological assessment 136

4.2.4. Statistics 136

4.2.4.1. Statistical analysis of the ex vivo MRI (FA and MTR) data 136

4.2.4.2. Statistical analysis of the pathological data 137

4.3. Results **138**

4.3.1. Post- surgery recovery and physiological status 138

4.3.1. Ex vivo MRI results 138

4.3.1.1. APOE deficiency and chronic cerebral hypoperfusion impact on MRI parameters of white matter integrity 138

4.3.1.1.1. APOE deficiency is associated with significant FA reductions in white, but not grey matter after chronic cerebral hypoperfusion 139

4.3.1.1.2. APOE deficiency is associated with significant MTR reductions in white, but not grey matter after chronic cerebral hypoperfusion 139

4.3.1.1.3. APOE deficiency does not affect grey matter structural integrity under normal physiological and chronically hypoperfused conditions: T2-weighted scans 141

4.3.2. Pathological data 141

4.3.2.1. APOE deficiency does not impact on axonal integrity under normal physiological and chronically hypoperfused conditions 141

4.3.2.2. APOE deficiency does not impact on myelin integrity under normal physiological and chronically hypoperfused conditions 144

4.3.2.3. APOE deficiency does not impact on myelin degradation 145

under normal physiological and chronically hypoperfused

4.3.2.4. APOE deficiency does not impact on inflammatory levels under normal physiological and chronically hypoperfused conditions 146

4.3.2.5. APOE deficiency does not affect grey matter integrity under normal physiological and chronically hypoperfused conditions 148

4.4. Discussion **149**

4.4.1. APOE effects on white matter integrity under normal physiological and chronically hypoperfused conditions in mice 149

4.4.1.1. APOE does not affect white matter integrity under normal physiological conditions in mice 149

4.4.1.2. APOE affects hypoperfusion- induced white matter pathology in mice 151

4.4.2. APOE effects on grey matter integrity under normal physiological and chronically hypoperfused conditions in mice 154

4.4.3. APOE effects on inflammation under normal physiological and chronically hypoperfused conditions in mice 156

4.4.4. Sensitivity of ex vivo MRI to white matter integrity 157

4.4.5. Differential sensitivity of ex vivo MRI and immunohistochemistry to APOE genotype differences in white matter integrity in mice 160
4.4.6. Strengths and limitations of the applied methodology and future experimental work 161
4.4.6.1. Strengths and limitations of ex vivo MRI and future experiments to further develop and characterize this newly developed neuroimaging procedure 161
4.4.6.1.1. Strengths of the ex vivo MRI procedure 161
4.4.6.1.2. Limitations of the ex vivo MRI procedure 162
4.4.6.1.3. Future experiments to further develop and characterize ex vivo MRI 163
4.4.6.2. Strengths and limitations of the immunochemical pathological approach and future experiments 165
4.4.6.2.1. Strengths of the immunochemical approach 165
4.4.6.2.2. Limitations of the immunohistochemical approach 165
4.4.6.2.3. Future pathological studies 165
4.4.6.3. Other methodological limitations and future experiments to examine APOE effects on white matter integrity under normal physiological and hypoperfused conditions in mice 166

4.4.7. Implications of the study and future directions 169

4.5. Summary 170

CHAPTER 5

Characterization of methylation and hydroxymethylation in white matter under normal physiological and chronically hypoperfused conditions in mice

5.1. Introduction and aims 171

5.2. Materials and methods 175

5.2.1. Animals and surgery 175

5.2.2. In vivo evaluation of the proportion 175
of 5mC, 5hmC and TET2 immunopositive cells in
the mouse brain under normal physiological and
chronically hypoperfused conditions

5.2.3. In vivo evaluation of the proportion of 175
CC1, NG2, Iba1 immunopositive cells in
the mouse brain under normal physiological and
chronically hypoperfused conditions

5.2.4. In vitro evaluation of 5hmC 176
immunochemical distribution in oligodendroglial

cells at different stages of maturation (0, 2, 6 DIV),
in IFNγ/ LPS activated and nonactivated microglia in vitro
5.2.5.Statistics 176
5.2.5.1. Statistical analysis of the regional group proportions of biomarker positive cells 176
5.2.5.2. Correlation analyses 176
5.2.5.2.1. Correlation analysis among epigenetic marks (5mC, 5hmC and TET2) 177
5.2.5.2.2. Correlation analysis between hydroxymethylation and cells composing the cerebral white matter 177

5.3.Results **178**
5.3.1. Chronic cerebral hypoperfusion leads to the development of white matter pathology 178
5.3.2. Chronic cerebral hypoperfusion does not affect brain 5mC distribution 178
5.3.3. Chronic cerebral hypoperfusion leads to significant white matter tract- specific changes in brain 5hmC distribution 178
5.3.4. Chronic cerebral hypoperfusion leads to significant grey matter- specific changes in TET2 distribution 181
5.3.5. Hydroxymethylation does not correlate significantly 183

with methylation and TET2 in white matter (the CC)

5.3.6. Chronic cerebral hypoperfusion does not affect the proportion of mature oligodendrocytes 183

5.3.7. Chronic cerebral hypoperfusion is associated with a significant increase in the proportion of OPC 183

5.3.8. Chronic cerebral hypoperfusion leads to a significant increase in the proportion of microglia 186

5.3.9. Hydroxymethylation significantly correlates with microglia in the CC 186

5.3.10.In vitro 5hmC immunochemical distribution decreases with oligodendroglial maturation and it is abundant in both activated and non activated microglia 188

5.4. Discussion **190**

5.4.1. Methylation dynamics in white and grey matter under normal physiological conditions and one month after chronic cerebral hypoperfusion in mice 190

5.4.2. Hydroxymethylation in white and grey matter under normal physiological 193

conditions and one month after chronic
cerebral hypoperfusion in mice
5.4.3. In search of the cellular basis of 5hmC in white matter. An unresolved question. 195
5.4.4. TET2 in white and grey matter under normal physiological conditions and one month after chronic cerebral hypoperfusion in mice 199
5.4.5. Is hydroxymethylation associated with methylation and TET2 in white matter? 200
5.4.6. Methodological strengths, limitations and future epigenetic experiments in chronically hypoperfused mice 203
5.4.6.1. Strengths of the applied methodology to examine epigenetic marks in the mouse brain under normal physiological and chronically hypoperfused conditions 203
5.4.6.2. Limitations of the applied methodology to examine epigenetic marks in the mouse brain under normal physiological and chronically hypoperfused conditions 203
5.4.6.3. Future experiments to examine epigenetic mechanism in the mouse brain under normal physiological and chronically hypoperfused conditions 205
5.4.7. Implications of the study and future directions 207

5.5. Summary **208**

CHAPTER 6

General discussion

6.1. Future research directions using the new mouse model of chronic cerebral hypoperfusion 209

6.1.1. Effects of chronic cerebral hypoperfusion on alternative (non- examined) brain processes in mice 209

6.1.1.1. Effects of chronic cerebral hypoperfusion on the cerebral metabolism in mice 209

6.1.1.2. Effects of chronic cerebral hypoperfusion on the cerebrovasculature in mice 211

6.1.1.3. Effects of chronic cerebral hypoperfusion on neurotransmission in mice 213

6.1.2. Effects of chronic cerebral hypoperfusion on neuropathology and cognitive impairment in the context of aging 215

6.1.3. Pathophysiological mechanisms in chronically hypoperfused mice 217

6.1.3.1. A role of excitotoxicity in hypoperfusion- induced neuropathology and cognitive deficits in mice? 218

6.1.3.2. A role of oxidative stress in hypoperfusion- induced 220

neuropathology and cognitive deficits in mice?

6.1.3.3. A role of inflammation in hypoperfusion- induced neuropathology and cognitive deficits in mice? 221

6.1.4. Preclinical development of therapeutic strategies for the treatment of age- related cognitive decline using chronically hypoperfused mice 223

6.1.4.1. Cerebral reperfusion 223

6.1.4.2. APOE modulation 224

6.1.4.3. Epigenetic modulation 226

6.1.4.4. Alternative therapeutic interventions 229

6.1.4.5. Cellular therapies 229

6.1.5. Future application of the microcoils surgery on genetically modified mice 231

6.2. Summary 233

REFERENCES **234**

LIST OF PUBLICATIONS

1) Coltman, R.*, Spain, A.*, **Tsenkina, Y**.*, Fowler, J.H., Smith, J., Scullion, G., Allerhand, M., Scott, F., Kalaria, R.N., Ihara, M., Daumas, S., Deary, I.J., Wood, E., McCulloch, J., Horsburgh, K. (2011) Selective white matter pathology induces specific impairment in spatial working memory. *Neurobiology of Aging.* 32 (12). 2324.e7-12.

2) Titomanlio, L., Bouslama, M., Le Verche, V., Dalous, J., Kaindl, A., **Tsenkina, Y**., Lacaud, A., Peineau, S., Elghouzzi, V., Lelievre, V., Gressens, P. (2011) Implanted neurosphere- derived precursors promote recovery after neonatal excitotoxic brain injury. *Stem cells and Development*. 20(5), 865-879.

3) Ruzov, A., **Tsenkina, Y.**, Serio, A., Dudnakova, T., Fletcher, J., Chebotareva, T., Pells, Hannoun, Z., Sullivan, G., Chandran, S., Hay, D., Bradley, M., Wilmut, I., De Sousa, P. (2011) Lineage specific distribution of high levels of genomic 5-hydroxymethylcytosine in mammalian development. *Cell research*. 21(9).1332-42.

4) Moreau, P.H.*, **Tsenkina, Y.***, Lecourtier, L., Lopez, J., Cosquer, B., Wolff, M., Dalrymple-Alford, J., Cassel, J.C. (2012). Lesions of the anterior thalamic nuclei and intralaminar thalamic nuclei: place and visual discrimination learning in the water maze. *Brain Structure and Function.* Epub 2012 Apr 29 DOI: 10.1007/s00429-012-0419-0 (in press)

5) Zhang, R., Mjoseng, H.K., Hoeve, M.A., Bauer, N.G., Pells, S., Besseling, R., Velugotla, S., Tournier, G., Kischen, R.E.B., **Tsenkina, Y.,** Armit, C., Duffy, C.R.E., Helfen, M., Edenhofer, F., De Sousa, P.A., Bradley, M. (2013). A thermoresponsive chemically-defined hydrogel for long term culture of human embryonic stem cells. *Nature Communications.* Jan 8: 4:1335. doi: 10.1038/ncomms2341

*these authors contributed equally to this work

APPENDICES I

S.3.1. Additional behavioural analysis from the radial arm maze study presented in the main thesis 300

S.3.1.1. Chronic cerebral hypoperfusion does not 300

affect the visual abilities in mice

S.3.1.2. Chronic cerebral hypoperfusion leads to significant spatial working memory impairment on a radial arm maze paradigm 303

S.3.1.2.1. Results: total number of arm entries and trial duration 303

S.3.2. Replica of the radial arm maze study (not presented in the main thesis body) 305

S.3.2.1 Materials and methods 305

S.3.2.1.1. Animals and surgery 305

S.3.2.1.2.Behavioural testing 305

S.3.2.1.3. Pathological assessment 305

S.3.2.1.4. Statistical analysis of the behavioral performance 305

S.3.2.2. Results 306

S.3.2.2.1. Post- surgery recovery and physiological status of the animals 306

S.3.2.2.2. Chronic cerebral hypoperfusion leads to spatial working memory impairment in mice 308

S.3.3. Additional behavioural data from the water maze experiment presented in the main thesis body 310

S.3.3.1. Chronic cerebral hypoperfusion does not impact on a cue task performance 310

APPENDICES II

S.4.1. Correlation analysis between regional MRI metrics and pathological grades 344

S.4.1.1. Statistics 344

S.4.1.2. Results 344

APPENDICES III

S.5.1. Pathological assessment 346

S.5.1.1. Materials and methods 346

S.5.1.2. Statistical analysis 346

S.5.1.3. Results 347

5.3.1.1. Chronic cerebral hypoperfusion affects significantly axonal integrity 347

5.3.1.2. Chronic cerebral hypoperfusion leads to significant myelin structural abnormalities in EC and IC, but not in CC 347

5.3.1.3. Chronic cerebral hypoperfusion is associated with a significant myelin degradation 347

5.3.1.4. Chronic cerebral hypoperfusion does not affect grey matter structural integrity 348

LIST OF FIGURES

CHAPTER 1

1.1. Cerebral white matter 2

1.2. Cellular composition of the cerebral white matter 4

1.3. Hypoperfusion- induced white matter pathology 18

1.4. APOE structure and potential APOE effects on white matter integrity 25

1.5. Methylation and hydroxymethylation 34

CHAPTER 2

2.1. Behavioural paradigms 45

2.2. Neuroanatomical levels at which the brains were microtome cut 52

2.3. Principles of immunohistochemistry 54

2.4. Neuroanatomical regions of interest (ROI) 59

2.5.1. H&E staining 60

2.5.2. APP, MAG, dMBP, Iba1 immunoreactivity 63

2.6. 5mC, 5hmC, ssDNA, TET2, CC1, NG2 immunoreactivity 66

2.7. Composing elements of a MRI scanner 71

2.8. Brains set up for ex vivo MRI- DTI procedure 72

CHAPTER 3

3.1. Group performance on a spatial working memory radial arm maze task 88

3.2. Group performance on a serial spatial learning and memory water 90

3.3. White matter integrity and inflammation in sham and hypoperfused mice 92

3.4. Grey matter integrity in sham and hypoperfused mice 98

3.5. Correlation analysis between white matter cellular 101
components and behavioural parameters of
working memory and executive function in hypoperfused mice

CHAPTER 4

4.1. Representative ex vivo MRI generated 135
T2- weighted, FA, and MTR scans

4.2. White matter integrity in WT and APOEKO 142
sham and hypoperfused mice

4.3. Grey matter integrity in WT and APOEKO 147
sham and hypoperfused mice

CHAPTER 5

5.1. Methylation, hydroxymethylation and TET2 179

immunochemically evidenced distribution in the
CC of sham and chronically hypoperfused mice
5.2. Hydroxymethylation does not correlate significantly with methylation and TET2 in the CC 182
5.3. Mature oligodendrocytes (CC1), OPC (NG2) and microglia (Iba1) immunoreactivity in the CC of sham and chronically hypoperfused mice 184
5.4. Hydroxymethylation correlates significantly with inflammatory microglia, but not with mature and progenitor oligodendroglia in the adult mouse CC 187
5.5. In vitro 5hmC immunochemical distribution in oligodendroglia at different stages of maturation (0-6DIV), in IFNγ/ LPS activated and nonactivated microglia 189

APPENDICES I

S.3.1.1. Visual abilities of sham and hypoperfused mice 301
S.3.1.2. Physiological status of sham and hypoperfused mice 302
S.3.1.3. Group performance on a spatial working memory radial arm maze task 304
S.3.2.1.Physiological status of sham and hypoperfused 307

tested on a radial arm maze (replica)

S.3.2.2. Group performance on a spatial working memory radial arm maze task (replica) 309

S.3.3. Cue task performance on a water maze paradigm 311

S.3.4.1. A-E. White matter regional group median pathological grades of axonal integrity (the radial arm maze experiment) 319

S.3.4.1. F-G. Grey matter regional group median pathological grades of axonal integrity (the radial arm maze experiment) 320

S.3.4.2. A-E. White matter regional group median pathological grades of axonal integrity (the water maze experiment) 321

S.3.4.2. F-G. Grey matter regional group median pathological grades of axonal integrity (the water maze experiment) 322

S.3.4.3. Regional group median pathological grades of myelin integrity (the radial arm maze experiment) 323

S.3.4.4. A-E. Regional group median pathological grades of myelin integrity (the water maze experiment) 324

S.3.4.5. A-E. White matter regional group median pathological grades of inflammation (the radial arm maze experiment) 325

S.3.4.5. F-G. Grey matter regional group median pathological grades of inflammation (the radial arm maze experiment) 326

S.3.4.6. A-E. White matter regional group median pathological 327

grades of inflammation (the water maze experiment)

S.3.4.6. F-G. Grey matter regional group median pathological grades of inflammation (the water maze experiment) 328

APPENDICES II

S.4.1. Physiological status of WT and APOE sham and hypoperfused mice 336

S.4.2.1. Regional FA in WT and APOEKO sham and hypoperfused mice 337

S.4.2.2. Regional MTR in WT and APOEKO sham and hypoperfused mice 338

S.4.3.1. Regional group median pathological grades of axonal integrity 339

S.4.3.2. Regional group median pathological grades of myelin integrity (MAG) 340

S.4.3.3. Regional group median pathological grades of degraded myelin (dMBP) 341

S.4.3.4. Regional group median pathological grades of inflammation 342

S.4.4. Grey matter structural integrity on T2- weighted scans of WT and APOEKO sham and hypoperfused mice 343

APPENDICES III

S.5.1. White matter integrity in sham and hypoperfused mice 349

S.5.2.1.: Brain 5mC immunochemical distribution in sham and hypoperfused mice 351

S.5.2.2.: Brain 5hmC immunochemical distribution in sham and hypoperfused mice 352

S.5.2.3.: Brain TET2 immunochemical distribution in sham and hypoperfused mice 354

LIST OF TABLES

CHAPTER 2

2.1. Primary and secondary antibodies, their manufacturer, cellular target, optimal dilution and specifics of the immunohistochemical procedure 57

2.2. Fluorochromes with their detection wavelengths (nm) used for the visualization of immunofluorescence- stained biomarkers 68

CHAPTER 3

3.1.1. Regional group median pathological grades: Radial arm maze experiment 94

3.1.2. Regional group median pathological grades: Water maze experiment 95

CHAPTER 4

4.1. Regional MRI biomarker values 140

4.2. Regional group median pathological grades 143

CHAPTER 5

5.1. Regional mean proportions of 5mC, 5hmC, TET2 immunopositive cells 180

5.2. Regional mean proportions of mature oligodendrocytes (CC1), OPC (NG2), and microglia (Iba1) 185

APPENDICES I

S.3.1. Short and long term memory recall in sham and hypoperfused mice: additional group statistical analysis 312

S.3.2.1. Individual regional pathological grades of axonal (APP) integrity of sham and hypoperfused mice (the radial arm maze experiment) 313

S.3.2.2. Individual regional pathological grades of axonal (APP) integrity of sham and hypoperfused mice (the water maze experiment) 314

S.3.2.3. Individual regional pathological grades of myelin (MAG) integrity of sham and hypoperfused mice (the radial arm maze experiment) 315

S.3.2.4. Individual regional pathological grades of myelin (MAG) integrity of sham and hypoperfused mice (the water maze experiment) 316

S.3.2.5. Individual regional pathological grades of Inflammation (Iba1) of sham and hypoperfused mice (the radial arm maze experiment) 317

S.3.2.6. Individual regional pathological grades of 318

Inflammation (Iba1) of sham and hypoperfused mice
(the water maze experiment)

S.3.3.1. Total individual pathological scores across white matter ROIs of sham and hypoperfused mice tested on a radial arm maze paradigm 329

S.3.3.2. Total individual pathological scores across white matter ROIs of sham and hypoperfused mice tested on a water maze paradigm 330

S.3.3.3. Total group median pathological scores across white matter ROIs of sham and hypoperfused mice tested on a radial arm maze and water maze paradigm and group statistics 331

APPENDICES II

S.4.1.1. Individual regional grades of axonal (APP) integrity in WT and APOEKO sham and hypoperfused mice 332

S.4.1.2. Individual regional grades of myelin (MAG) integrity in WT and APOEKO sham and hypoperfused mice 333

S.4.1.3. Individual regional grades of myelin (dMBP) integrity in WT and APOEKO sham and hypoperfused mice 334

S.4.1.4. Individual regional grades of inflammation (Iba1) in WT and APOEKO sham and hypoperfused mice 335

S.4.2. Correlation analysis of MRI parameters and pathological grades of axonal (APP), myelin (MAG) integrity, degraded myelin (dMBP), and inflammation (Iba1) 345

APPENDICES III

S.5.1. Regional group median pathological grades 350

S.5.2. Regional number of 5mC, 5hmC, TET2 positive cells and total number of cells 356

S.5.3.Regional number of CC1, NG2, Iba1 positive cells and total number of cells 357

LIST OF ABBREVIATIONS

ABC	Avidin- biotin complex
Aβ	Beta- amyloid
AMPA	α-amino-3-hydroxy-5-methyl-4-isoxazoleproprionic acid
APOE	Apolipoprotein E
APOEKO	Apolipoprotein E knockdown mouse

APP	Amyloid precursor protein
ATP	Adenosine-5'-triphosphate
BDNF	Brain- derived neurotrophic factor
C	Cytosine
ChAT	Choline acetyltransferase
CC	Corpus callosum
CC1	Adenomatous polyposis coli
CNP	2`-3`- cyclic nucleotide 3`- phosphate
CpG	5`- cytosine phosphate guanine- 3`
CSF	Cerebrospinal fluid
Cx	Cerebral cortex
DAB	Diaminobenzidine tetrachloride solution
DIV	Days in vitro
dMBP	Degraded myelin basic protein
DNMT	DNA methyltransferase
DTI	Diffusion tensor imaging
EC	External capsule
EGF	Epidermal growth factor
ERα	Estrogen receptor α
FA	Fractional anisotropy
FGF2	Fibroblast growth factor 2

fMRI	Functional magnetic resonance imaging
Fx	Fimbria fornix
GDNF	Glial cell line- derived neurotrophic factor
GFAP	Glial fibrillary acidic protein
HCL	Hydrochloric acid
HDAC	Histone deacetylase
HDL	High density lipoprotein
HDLR	High density lipoprotein receptor
H&E	Haemotoxylin and eosin
5hmC	5- Hydroxymethylcytosine
HIF	Hypoxia- inducible factor
HPLC	High performance liquid chromatography
Iba1	Ionized- calcium binding antigen 1
IC	Internal capsule
IFNγ	Interferon γ
IL	Interleukin
LDL	Low density lipoprotein
LDL-R	Low density lipoprotein receptor family
LDLR	Low density lipoprotein receptor
LPS	Lipopolysaccaride
LRP1	Low density lipoprotein receptor- related protein 1

MAG	Myelin associated glycoprotein
MAP2	Microtubule associated protein 2
MBD	Methyl- CpG- binding domain protein
MBP	Myelin basic protein
5mC	5- Methylcytosine
5MCDG	5- mC DNA glycosylase
MeCP2	Methyl- CpG- binding protein 2
MOG	Myelin oligodendrocyte glycoprotein
MRI	Magnetic resonance imaging
MTR	Magnetization transfer ratio
NBQX	2,3-dihydroxy-6-nitro-7-sulfamoyl-benzo[f]quinoxaline-2,3-dione
NG2	Chondroitin sulfate proteoglycan
NMDA	N-methyl-D-aspartate
NO	Nitric oxide
OPC	Oligodendroglial precursor cell
OT	Optic tract
PBS	Phosphate buffered saline
PDGF	Platelet- derived growth factor
PET	Positron emission tomography
PFA	Paraformaldehyde
PLP	Proteolipid protein

PT	Probe trial
RF	Radio frequency
ROI	Region of interest
rpm	Rounds per minute
RT	Room temperature
SAM	S-adenosylmethionine
ssDNA	Single stranded DNA
TET	Ten- eleven- translocation protein
TNFα	Tumor necrosis factor α
TTX	Tetrodoxin
VEGF	Vascular endothelial growth factor
VLDL	Very low density lipoprotein
VLDLR	Very low density lipoprotein receptor
WT	Wild- type

ABSTRACT

Recent clinical studies suggest that white matter pathology rather than grey matter abnormality is the major neurobiological substrate of age- related cognitive decline during "healthy" aging. According to this hypothesis, cerebrovascular (e.g. chronic cerebral hypoperfusion) and molecular (e.g. APOE, epigenetics) factors might contribute to age-related white matter pathology and cognitive decline. To test this, I used a new mouse model of chronic cerebral hypoperfusion and examined the following predictions:

1) hypoperfusion- induced white matter pathology might be associated with cognitive deficits, 2) APOE deficiency might be associated with white matter anomalies under normal physiological conditions and more severe hypoperfusion- induced white matter pathology, 3) chronic cerebral hypoperfusion might impact on hydroxymethylation (a newly discovered epigenetic marker) in white matter, via perturbations in associated epigenetic pathways, namely methylation and/ or TETs.

I. Effects of chronic cerebral hypoperfusion on white matter integrity and cognitive abilities in mice

To test the hypothesis suggesting that hypoperfusion- induced white matter pathology is associated with working memory and executive function impairment in mice, behavioural performance and neuropathology were systematically examined in two separate cohorts of sham and hypoperfused C57Bl6J mice. Spatial working memory, memory flexibility, learning capacity, short and long term memory recall were taxed using radial arm maze and water maze paradigms one month after surgery. At the completion of the behavioural testing white and grey matter integrity, inflammation were evaluated using standard immunohistochemistry with antibodies recognizing neuronal axons (APP), myelin sheath (MAG) and microglia (Iba1) as well as H&E histological staining to examine neuronal morphology and ischemic injury. In agreement with previous reports, the behavioral data indicated spatial working memory impairment in the absence of spatial memory flexibility, learning, short- and long- term memory recall deficits in hypoperfused mice However, in contrast to previous reports, a spectrum of white and grey matter abnormalities accompanied by an increased inflammation were observed in hypoperfused mice Although there was a significant association between hypoperfusion- induced inflammation in white matter and performance on a working memory radial arm maze task ($p<0.05$), the present pathological findings suggest that white matter abnormalities, neuronal ischemia and increased inflammation might be at the basis of hypoperfusion-induced cognitive impairment in mice. Further, chronic cerebral hypoperfusion might have affected alternative, non- examined brain processes (e.g. cerebral metabolism, neurotransmission) which might have contributed to the observed cognitive deficits in hypoperfused mice.

II. Effects of APOE on white matter integrity under normal physiological and chronically hypoperfused conditions in mice

To test the hypothesis suggesting that mouse APOE deficiency might be associated with white matter anomalies under normal physiological conditions and the development of more severe white matter pathology following chronic cerebral hypoperfusion, white and grey matter integrity, inflammation were examined in APOE deficient mice on a C57Bl6J background (APOEKO) and C57Bl6J wild- type (WT) counterparts one month after chronic cerebral hypoperfusion or sham surgery. A combined neuroimaging (MRI- DTI)/ immunochemical approach was attempted in these mice as an additional step towards translation of this research to human subjects. The ex vivo MRI- DTI findings demonstrated APOE genotype effects on the development of white matter abnormalities following chronic cerebral hypoperfusion in mice. Significant reductions in MRI metrics (FA and MTR) of white matter integrity were observed in examined white matter areas of APOEKO hypoperfused mice compared with WT hypoperfused counterparts ($p<0.05$). However, the neuroimaigng findings were not supported by the pathological analysis where no significant APOE differences were observed in hypoperfusion- induced axonal (APP), myelin (MAG, dMBP) pathology and inflammation (Iba1) ($p>0.05$). No significant differences in MRI parameters and pathological grades of white matter integrity were evidenced between APOEKO and WT sham mice ($p>0.05$). An absence of grey matter abnormalities was evidenced on T2- weighted scans and corresponding H&E stained brain sections in all experimental animals. However, significant reductions in MTR values and dMBP immunoreactivity (myelin pathology) ($p<0.05$) were observed in grey matter (the hippocampus) following chronic cerebral hypoperfusion in the absence of significant APOE genotype effect ($p>0.05$) suggesting the existence of both white and grey matter abnormalities in this animal model. Overall, the present neuroimaging data, but not pathological analysis, partially validated the main study hypothesis suggesting that APOE deficiency might be associated with the development of more severe white matter abnormalities in hypoperfused mice.

III. Characterization of methylation and hydroxymethylation in white matter under normal physiological and chronically hypoperfused conditions in mice

Lastly, I sought to test the hypothesis that chronic cerebral hypoperfusion might alter oxygen dependent DNA hydroxymethylation (5hmC) in white matter regions via perturbations in methylation (5mC) and/ or Ten- eleven translocation proteins (e.g. TET2) in mice. DNA methylation (5mC), hydroxymethylation (5hmC) and TET2 were immunochemically studied in white and grey matter of sham and chronically hypoperfused C57Bl6J mice a month after surgery. The immunochemical results demonstrated significant increases ($p<0.05$) in 5hmC in the hypoperfused corpus callosum (CC) in the absence of significant hypoperfusion- induced alterations in the distribution of 5mC and TET2 ($p>0.05$) in white matter. Significant hypoperfusion- induced increases were evident for TET2 in the cerebral cortex (Cx) ($p<0.05$). These data partially validated the main study hypothesis suggesting hypoperfusion- induced alterations in 5hmC in white matter. However, in contrast to the study hypothesis, the observed hypoperfusion- induced alterations in 5hmC occurred in the absence of changes in 5mC and TET2 in white matter. A subsequent correlation analysis between hydroxymethylation and 5mC, TET2 in the CC failed to show significant associations ($p>0.05$). In search of the cellular determinants of 5hmC in the CC, hydroxymethylation was examined in relation to some of the cell types in white matter- mature oligodendrocytes, oligodendrolial progenitors (OPC) and microglia both in vivo and in vitro. Specifically, a separate parametric correlation analysis between the proportion of 5hmC positive cells and the respective proportions of mature oligodendrocytes, OPC and microglia in the CC demonstrated that hydroxymethylation correlated significantly only with microglia in vivo ($p<0.05$). Following this, 5hmC immunochemical distribution was studied in vitro in oligodendroglia cells at different stages of maturation, and interferon γ/ lypopolisaccharide activated and nonactivated microglia. The in vitro analysis demonstrated that 5hmC is high in OPC, activated and nonactivated microglia, but it is low in mature oligodendrocytes. Taken together the in vivo and in vitro cellular analyses suggest that the processes of hydroxymethylation in white matter might be immunoregulated. However, it is possible that in vivo in addition to microglia, other cell types (e.g. astrocytes, OPC) contributed to the presently observed 5hmC upregulation in the hypoperfused CC.

Conclusion

The experimental work presented in this thesis further developed and characterized a new mouse model of chronic cerebral hypoperfusion by confirming previous behavioural findings (e.g. working memory deficits) and revealing previously undetected spectrum of white and grey matter pathology in this animal model. The thesis demonstrated for the first time by using a newly developed ex vivo MRI procedure that APOE might modulate hypoperfusion- induced white matter pathology in mice. Additional immunochemical analysis revealed important hypoperfusion- induced epigenetic alterations in white (5hmC) and grey (TET2) matter in this animal model. Future experiments on chronically hypoperfused mice would allow to get a better insight into the neurobiological determinants (e.g. white vs. grey matter) underlying the observed cognitive deficits in this animal model, the involved cellular and molecular pathways as well as the functional significance of genetic (APOE) and epigenetic (5hmC, TETs) alterations in the hypoperfused brain. Future experimental work on this animal model would potentially reveal new biological targets for the pre- clinical development of therapies for age- related cognitive decline. Further development and optimization of the newly developed ex vivo MRI procedure would allow its broader application in preclinical settings and would facilitate the translation of experimental findings to clinics.

Chapter 1

Introduction

1.1. Cerebral white matter

The cerebral white matter is composed of bundles of myelinated and non- myelinated neuronal axons (tracts) connecting cortico- cortical and cortico- subcortical grey matter regions. The Renaissance anatomist Andreas Vesalius was the first to clearly distinguish brain white matter regions from grey matter structures in 1543 in his work *De Humani Corporis Fabrica* (Vesalius, 1543) (figure 1.1. A). Since this pioneering work, the neuroanatomy, function, cellular and molecular composition of the cerebral white matter have been described and studied under both normal and pathological conditions.

The cerebral white matter constitutes 40- 50% of the total volume of the adult human brain (~16% of the total volume of the adult mouse brain) (Zhang and Sejnowski, 2000) (figure 1.1. B- C). The corpus callosum (CC), the external capsule (EC), the internal capsule (IC), the fimbria fornix (Fx), and the optic tract (OT) are the major white matter regions. The CC represents the main association fiber system connecting prefrontal, premotor and somatosensory areas between the two hemispheres and therefore supporting various cognitive, memory, and sensory- motor functions (Bloom and Hynd, 2005). The EC is a smaller white matter bundle primarily comprising cholinergic fibers from the basal forebrain to cortical areas (Selden et al., 1998). The IC is the major subcortical white matter tract separating the caudate nucleus and the thalamus from the lenticular nucleus (Sullivan et al., 2010). This white matter tract ensures cortico- subcortical connectivity and the associated cognitive, somatosensory and motor functions (Sullivan et al., 2010). The Fx is mainly involved in the support of hippocampal afferent and efferent connectivity and the structural integrity of this white matter region plays a critical role in cognition and memory (Adelmann et al., 1996). The OT mediates the transmission of visual impulses from the retinas to the occipital (visual) lobe (Andrews et al., 1997).

Therefore, pathological damage to the cerebral white matter could lead to a multitude of functional deficits depending on the extent and the localization of the lesion. White matter abnormalities are evidenced in different neurological, neurodegenerative and psychiatric disorders (Fields, 2008).

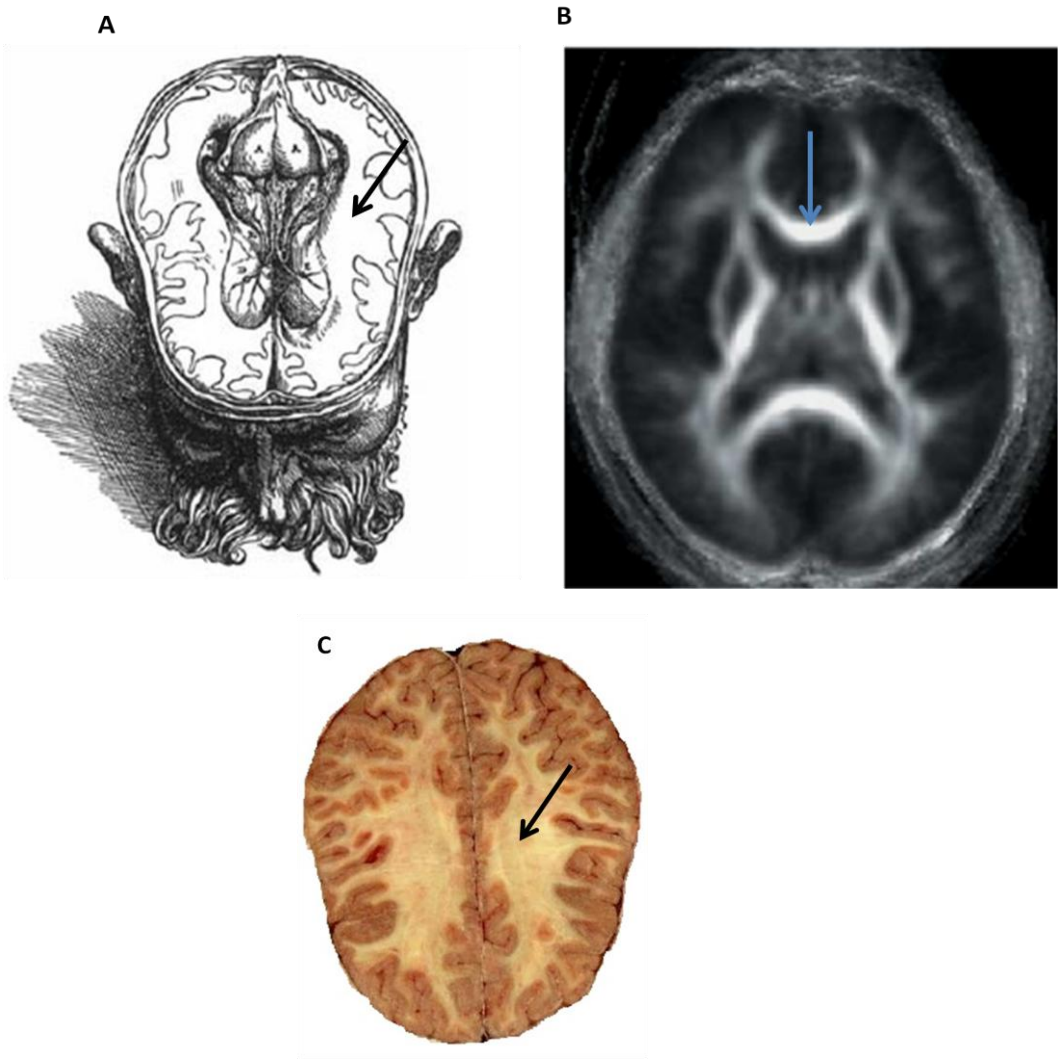

Figure 1.1.: Cerebral white matter

Different representations of the cerebral white matter (arrows in **A**, **B**, **C**) on horizontal brain sections. In (**A**) is shown the first neuranatomical schematic drawing of the cerebral white matter (black arrow) made by Vesalius in 1543 (image adapted from Vesalius, 1543). In (**B**) is presented the cerebral white matter of a healthy young adult appearing as bright hyperintesities (blue arrow) on a modern noninvasive diffusion tensor imaging (DTI) scan (image adapted from Hedden and Gabrielli, 2004). In (**C**) is shown a post-mortem sample of a healthy human adult brain where the white matter appears as white regions (black arrow) surrounded by cortical and subcortical grey matter structures (image adapted from Wikipedia: http://en.wikipedia.org/wiki/Human_brain)

At the microscopic level the cerebral white matter is composed of the neuronal axons covered by the myelin sheath and the myelin- producing oligodendroglial cells (figure 1.2.). The myelin sheath insulating the neuronal axons was first discovered by Rudolf Virchow in 1854 and since its structure has been characterized in details (Virchow, 1854). The myelin sheath is composed of myelin internodes interrupted by non- myelinated areas with a high sodium channels content called the nodes of Ranvier. The nodes of Ranvier support the evolutionary evolved phenomenon of saltatory conduction in vertebrates (Peters, 1966; Hartline and Colman, 2007). The saltatory axonal conduction accelerates the propagation of action potentials in myelinated fibers contributing to greater conduction velocity and speed of information processing in comparison with non- myelinated axons (Hartline and Colman, 2007). The myelin sheath is composed of ~ 40 % water with a dry mass constituted of ~70 - 85 % lipids and ~15 - 30 % proteins (de Vries and Hoekstra, 2000). The primary myelin lipid components are cholesterol, galactocerebrosides, phospholipids sphingomyelin (composed of ceramides and their bioproduct sulfatides) which serve to strengthen the myelin sheath (O`Brien and Sampson, 1965; Han et al., 2003; Dietschy et al., 2004; Marcus et al., 2006). For instance, mutation of the enzyme responsible for the production of galactocerebrosides- ceramide galactosyltransferase results in a thinner myelin sheath and the occurrence of hind limb ataxia and tremors in mice (Coetzee et al., 1996). Specific oligodendroglial- mutation of the squalene synthase, an enzyme catalyzing the first step in the production of sterols leads to abnormal myelin structure and motor deficits in mice (Saher et al., 2005). The myelin protein components are myelin basic protein (MBP), myelin oligodendrocyte glycoprotein (MOG), proteolipid protein (PLP), 2`,3`- cyclic nucleotide 3`- phosphodiesterase (CNP), and myelin-associated glycoprotein (MAG). Each of these proteins fulfills a distinct role in the maintenance of the myelin sheath (Jahn et al., 2009) and some examples are provided in Chapter 1, section 1.3.1.

The myelin- producing oligodendrocyte is the major cell type of the cerebral white matter. The term oligodendrocyte was first introduced by Rio Hortega in 1928 who used metallic impregnation techniques to study the cellular phenotypes in the mammalian brain (Hortega, 1928). Morphologically, the mature oligodendrocyte is characterized by a small soma surrounded by multiple processes branching and ensheathing hundreds of

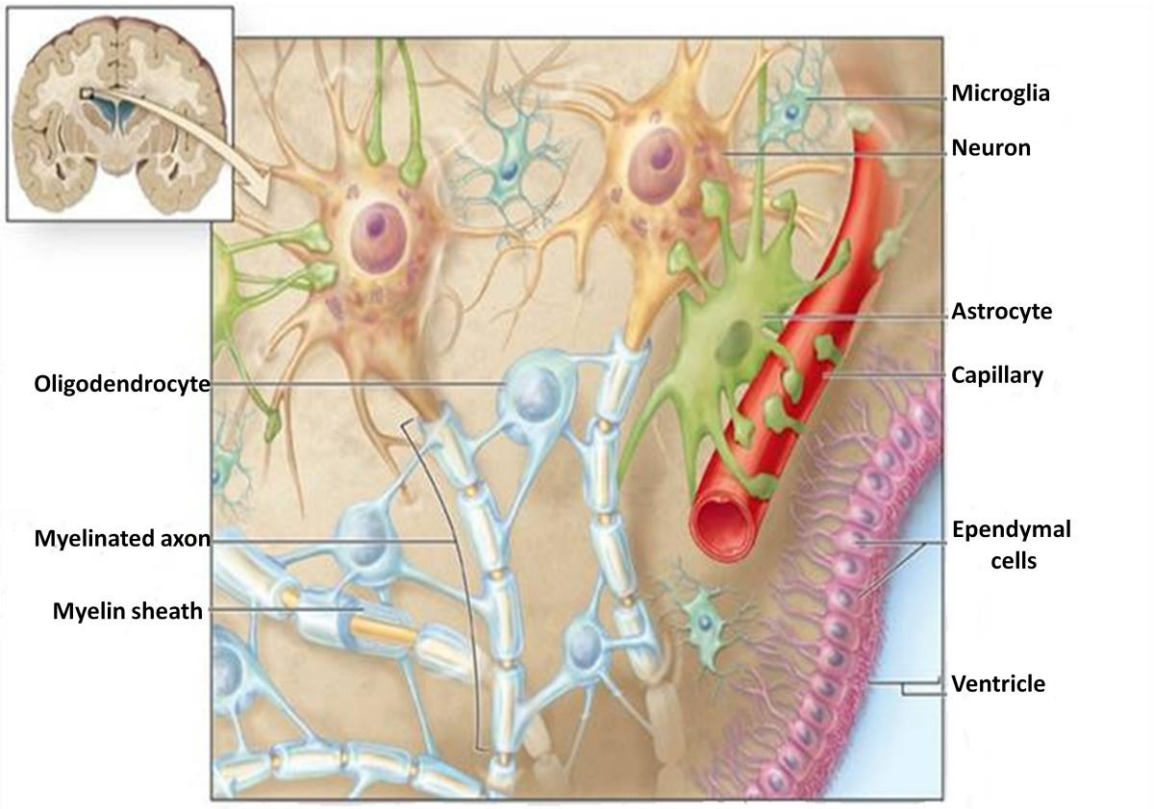

Figure 1.2.: Cellular composition of the cerebral white matter

A schematic representation of the cellular composition of the cerebral white matter as observed near the walls of the ventricles bordered by the ependymal cells. The major cellular component of the cerebral white matter is the olgiodendrocyte producing the myelin sheath enwrapping hundreds of neuronal axons. Astrocytes are another cell type present in white matter regions composing the blood brain barrier, providing trophic and metabolic support to neurons and oligodendrocytes and participating in the endogenous processes of brain repair in concert with inflammatory microglia. The cerebral white matter is irrigated by small arterioles and capillaries.

(adapted from http://multiple-sclerosis-research.blogspot.com/2011/07/death-receptor-in-myelination.html)

neuronal axons (Baumann and Pham- Dinh, 2001) (figure 1.2.). Only large diameter axons are myelinated by mature oligodendrocytes (Friede, 1972). The exact reasons for this selective myelination process during early neurodevelopment are unknown, but it is most likely the result of a complex cellular and molecular signaling orchestrating the interaction between immature oligodendroglial cells and neuronal axons (Sherman and Brophy, 2005). In mammals, myelination is a gradual process. Depending on the species it starts either prior to (human) or after birth (mouse). In humans axonal myelination continues for more than two decades, whereas in mice this process is completed for a couple of weeks postpartum (Marret et al., 1995; Lebel et al., 2008).

From a molecular perspective, the oligodendroglial cells are characterized by high metabolic- adenosine triphoshate (ATP) demands necessary for the production and maintenance of the myelin sheath (Ravera et al., 2009). Myelination requires iron and oligodendroglial cells at all stages of maturation are characterized by the highest intracellular iron content among neural cells which could under unfavourable extracellular conditions trigger free radicals production and lipid peroxidation (Braughler et al., 1986; Todorich et al., 2009). N-methyl-D-aspartate (NMDA), α-amino-3-hydroxy-5-methyl-4-isoxazoleproprionic acid (AMPA) and kainite glutamatergic receptors are expressed by oligodendrocytes and they are the principal mediators of excitotoxic injury to these cells occurring during various pathological conditions such as hypoxic- ischemic events (Karadottir and Attwell, 2007; Bakiri et al., 2009). The oligodendrocytes are also characterized by low levels of natural antioxidative defenses such as gluthatione limiting their chances to fight damaging oxidative, excitotoxic and inflammatory agents (Thornburne and Juurlink, 1996). Taken together, the intrinsic biological characteristics of the oligodendroglia put them at a greater risk of damage under pathological conditions.

Recent experimental data suggest that in addition to their basic myelination functions mature oligodendrocytes provide metabolic and trophic support to axons (Nave and Trapp, 2008). For instance, genetic manipulation of the normal metabolic machinery in oligodendroglial cells by mutation of the Pex 5 gene leading to an absence of functional peroxisomes in these cells has been associated with a progressive axonal degeneration in adult mice (Kassmann et al., 2007). Oligodendrocytes also synthesize growth factors such as glial cell line- derived neurotrophic factor (GDNF) and brain- derived

neurotrophic factor (BDNF) providing trophic support to axons (Dougherty et al., 2000; Wilkins et al., 2003).

In addition to mature oligodendrocytes, a small population of resident chondroitin sulfate proteoglycan (NG2) positive oligodendroglial progenitor cells (OPC) is also present in white matter tracts of the adult mammalian brain (Karadottir et al., 2008). The exact functional role of these progenitor cells remains not well understood, but they are likely to play a role in the endogenous processes of brain repair, namely by replacing injured and/ or apoptotic oligodendroglial cells and by remyelinating demyelinated axons (Chang et al., 2000; Reynolds et al., 2002). Interestingly, in contrast to mature oligodendrocytes, immature oligodendroglia are able to fire action potentials similar to neurons (Karadottir et al., 2008). Astrocytes are another glial cell type present in white matter regions. Morphologically, these cells are characterized by a stellar shape soma with multiple processes branching around neuronal axons, oligodendroglial cells and blood vessels composing the blood brain barrier (figure 1.2.). Functionally, astrocytes are involved in the formation of the blood brain barrier, maintenance of the extracellular homeostasis by glutamate buffering, provision of trophic and metabolic support (e.g. glycogen production) to the rest of the neural cells (Hertz and Zielke, 2004; Hawkins and Davis, 2005; Magistretti, 2006). Astrocytes also play a role in the endogenous brain repair mechanisms by secreting inflammatory agents and by actively participating in the formation of glial scars in the presence of neuropathology or brain injury (Volterra and Meldolesi, 2005). Microglia are inflammatory glial cells scattered throughout the brain which are usually quiescent (inactive) under normal physiological conditions, but become activated in the presence of neuropathology (figure 1.2.). Microglia secrete inflammatory agents and in concert with astrocytes and OPC, these inflammatory cells are active participants in the endogenous brain repair mechanisms (Parkhurst and Gan, 2010).

1.2. Age- related white matter pathology and cognitive decline

White matter abnormalities are a common neuropathological finding on magnetic resonance imaging (MRI) scans of both healthy* and demented elderly. These recent neuroimaging findings have revolutionized the long- lasting neurobiological concept of age- related cognitive decline as the functional outcome of grey matter volume loss.

*In the present thesis the term "healthy elderly" refers to aged individuals who do not present dementia- like neuropathological changes (e.g. amyloid plaques) and cognitive deficits.

Although there are subtle neuronal morphological changes such as reductions in synapses and dendrites, the number of neuronal cells remains unchanged in the aged mammalian brain (Anderson et al., 1983; Duan et al., 2003).

In 2001, O`Sullivan et al., suggested that cortical disconnections due to white matter pathology are the major neuropathological substrate of age- related cognitive deficits (O`Sullivan et al., 2001). These initial results have been subsequently repeated and extended by other groups and it is now largely accepted that widespread white matter abnormalities occur in the aging human brain and they are associated with cognitive decline (Salat et al., 2005; Bastin et al., 2009; Gunning- Dixon et al., 2009; Madden et al., 2009; Penke et al., 2010). Significant reductions in MRI metrics of white matter integrity, namely fractional anisotropy (FA) and magnetization transfer ratio (MTR) values are observed with increasing age and these neuroimaging parameters negatively correlated with performance on cognitive tasks taxing executive function, working memory, and processing speed (O`Sullivan et al., 2001; Charlton et al., 2006; Cook et al., 2007; Grieve et al., 2007; Wright, et al., 2008; Kennedy and Raz, 2009). These cognitive functions rely on the rapid transmission of information between cortical and subcortical regions (Rolls, 2000; Funahashi, 2001; Tekin and Cummings, 2002; Grieve et al., 2007). Specifically, a disruption of the prefrontal- hippocampal connectivity might be at the basis of the selective executive and working memory impairment observed in elderly people with white matter pathology (Grieve et al., 2007). Interestingly, general intelligence, semantic knowledge and episodic memory are relatively preserved in healthy elderly (Charlton et al., 2006; Kennedy and Raz, 2009). Further, white matter abnormalities are observed in individuals with mild cognitive impairment, vascular dementia and Alzheimer`s disease (Gootjes et al., 2004; Head et al., 2004). Neuroimaging data have demonstrated that there is a difference in the extent of the observed white matter alterations between healthy and demented elderly. In the healthy aging human brain white matter lesions affect primarily frontal association fibers, whereas in mild cognitive impairment, vascular dementia and Alzheimer` s disease patients white matter pathology is evidenced in both anterior and posterior brain regions suggesting that a more widespread white matter damage might contribute to the development and severity of senile dementia (Gootjes et al., 2004; Head et al., 2004).

At the microscopic level pathological postmortem analysis reveals that age- related white matter lesions are characterized by myelin loss, axonal injury and increased inflammation (Fernando et al., 2006; Gold et al., 2007; Ihara et al., 2010). Alterations in myelin lipid content are observed with increasing age. For instance, biochemical studies using post-mortem brain samples show a decrease in cholesterol, phospholipids, gangliosides, and sphingomyelin bioproducts- ceramides and sulfatides in the frontal and temporal cerebral white matter with advanced age (Svennerholm et al., 1994). Further, stereological comparisons of white matter integrity between healthy young and old adults show a significant decrease in the total length of the myelinated fibers accompanied by a significant increase in the mean axonal diameter in old adults in comparison with young controls indicating a substantial myelin loss with increasing age (Tang et al., 1997). Myelin pathology is also evidenced in aging rats and nonhuman primates (Knox et al., 1989; Peters et al., 2000; Peters and Sethares, 2002). For instance, in the prefrontal cortex, CC, and primary visual cortex of the aged rhesus monkey pathological abnormalities in myelin integrity such as a loosening of its compaction, a formation of liquid- filled ballons, an increase in the paranodes length, an accumulation of oligodendroglia- derived cytoplasm within the myelin lamella are observed by means of electron microscopy (Peters et al., 2000; Peters and Sethares, 2002). Interestingly, aged monkeys present similar cognitive impairments to healthy elderly people such as executive function (memory flexibility), working memory and processing speed deficits (Herndon et al., 1997; Luebke et al., 2004). Consequently, pathological disruption of the myelin integrity might lead to changes in the axonal conduction rates resulting in a loss of synchrony in cortico- subcortical neuronal circuits and a subsequent cognitive impairment. Indeed, in a study by Xi et al., 1999 comparing the conduction velocity of axons in the pyramidal tracts of aged cats with those in young cats it has been found that 51% of pyramidal tract neurons in young cats are fast conducting when compared with 26% in old cats. Aged cats exhibit an overall 43% decrease in median axonal conduction velocity compared with young animals (Xi et al., 1999).

1.3. Mechanisms of damage to white matter

1.3.1. Excitotoxicity and oxidative stress

Excitotoxic and oxidative insults are common molecular mechanisms leading to white matter pathology in many neurological and neurodegenerative conditions (Volpe, 2001; Park et al., 2004; Yi and Hazell, 2006; Baltan et al., 2008). From a mechanistic point of view, the excitotoxic damage to white matter is mediated via the glutamatergic NMDA, AMPA/ kainite receptors present on oligodendroglial cells at all stages of maturation (Karadottir and Attwell, 2007; Bakiri et al., 2009). Specifically, exposure of oligodendrocytes to glutamate induces cystine depletion through the action of a glutamate-cystine exchange system, thereby depleting gluthatione and causing free radical mediated cell death (Yonezawa et al., 1996). Under excitotoxic conditions gluthatione scavenges hydrogen peroxide by an electron donor. However, if hydrogen peroxide is not scavenged it drives the conversion of lipid hydroperoxides to alkoxyl radicals and in the presence of increased iron leading to the formation of peroxyl radicals attacking cellular mitochondrias and provoking apoptotic cell death. Oligodendrocytes have been shown to have 23 fold more iron than astrocytes while having less than half of their gluthatione amount (Thornburne and Juurlink, 1996). Hypoxic- ischemic conditions are characterized by increased excitotoxicity and the development of white matter pathology (Matute et al., 2001). For instance, using in situ model of adult brain slices transient oxygen and glucose deprivation has been found to result in white matter damage accompanied by widespread oligodendroglial cell death (Tekkok and Goldberg, 2001). However, application of 2,3-dihydroxy-6-nitro-7-sulfamoyl-benzo[f]quinoxaline-2,3-dione (NBQX)- an AMPA/ kainate antagonist during oxygen and glucose deprivation in the same in situ model prevents oligodendroglial cell death as well as the development of white matter pathology. Further, in vivo in a mouse model of periventricular leukamalacia characterized by hypoxic- ischemic white matter injury, the application of AMPA antagonists has neuroprotective effects (Follet et al., 2004). Periventricular leukomalacia is a common neurological disorder in preterm babies. It is characterized by excitotoxic white matter injury due to hypoxic- ischemic events during premature birth associated with long- term motor and cognitive morbidities (Volpe, 2001). Excitotoxic and oxidative damage to

cerebral white matter is also evidenced in adults specifically in individuals with traumatic brain and spinal cord injury as well as in elderly people as a result of an age- related increase in brain excitotoxicity (Park et al., 2004; Yi and Hazell, 2006; Baltan et al., 2008).

1.3.2. Inflammation

Increased inflammatory agents released by astrocytes and microglia under pathological conditions are known to cause demyelination, axonal injury and oligodendroglial cell death (Hu and Lucchinetti, 2009). The precise mechanisms via which inflammation affects white matter integrity are still not well understood. Oligodendrocytes express receptors for interleukins (IL) and cytokines such as IL- 2, IL- 1α/β, IL- 6 interferon γ (IFNγ), tumor necrosis factor α (TNFα) (Otero and Merrill, 1994; Dopp et al., 1997). These inflammatory agents are known to be important signaling cues governing oligodendroglial maturation, migration and myelination during neurodevelopment as well as in certain neuropathological conditions associated mainly with the processes of active remyeliantion (Diemel et al., 1998; Vela et al., 2002). However, in vitro experiments have demonstrated that elevated inflammatory levels such as an increase in IL- 2, IFNγ, TNFα are lethal to oligodendroglial cells (Otero and Merrill, 1994; McLaurin et al., 1995; Vartanian et al., 1995). In vivo experiments using transgenic mice overexpressing TNFα have confirmed the in vitro studies demonstrating that the toxic effects of this cytokine are directly related to the function of activated microglia and macrophages (Corbin et al., 1996). Further, intraneuronal injection of TNFα into the sciatic nerve of the adult rat produces demyelination, axonal degeneration and vascular pathology several days after injection (Redford et al., 1995). In addition, TNFα affects myelin integrity by stimulating the activity of sphingomyelinase an enzyme converting sphigophospolipids to toxic ceramides and sulfatides under pathological conditions. In vitro treatment of bovine or rat oligodendrocytes with ceramide analogue (C2) induces oligodendroglial apoptosis showing that inflammatory agents such as TNFα could indirectly impact on myelin integrity and oligodendrocytes by stimulating alternative molecular pathways (Larocca et al., 1997). Impaired immune response followed by increased inflammation, active demyelination, oligodendroglial apoptosis, axonal damage are all observed in patients

with multiple sclerosis, encephalomyelitis and acquired immunodeficiency syndrome (Minagar et al., 2002; Hu and Lucchinetti, 2009). These patients present functional impairments such as motor, visual and cognitive deficits, depression with a different degree of severity depending on the disease stage (Calabrese, 2006).

1.3.3. Gene mutations

Mutation in genes coding for major myelin proteins is associated with impaired white matter integrity and functional deficits in both laboratory mice and human patients with congenital dysmyelinating disorders (leukodystrophies).

PLP is one of the major myelin protein components playing an important role in myelin integrity and structural maintenance (Klugmann et al., 1997). A X- linked mutation in PLP gene occurs naturally in human patients with Pelizaeus- Merzbacher disease and spastic paraplegia as well as in mice presenting *jimpy* phenotype (Nave et al., 1986; Saugier-Veber et al., 1994). At the pathological level, naturally occurring PLP mutation in mice results in congenital dysmyelination with preserved axonal integrity and a very short life-span (~4 weeks) (Nave et al., 1986; Klugmann et al., 1997). However, experimental genetic deletion of the PLP gene leads to an increased life span (>12 months) allowing a better characterization of the functional importance of PLP (Griffiths et al., 1998). PLP null mice exhibit a late- onset neurodegeneration characterized by progressive axonal loss and swellings throughout the central nervous system affecting primarily the long spinal tracts. This neuropathological profile is associated with late onset ataxia in the absence of seizures and tremors and premature death similar to disease progression in human patients with Pelizaeus- Merzbacher disease and spastic paraplegia (Garbern et al., 2002).

MBP in addition to PLP constitutes one of the most abundant protein members of the compact myelin and it has similar to PLP function (Dupouey et al., 1979; Klugmann et al., 1997). In mice, mutation in MBP gene results in a *shiverer* phenotype characterized by hypomyelination with abnormal myelin structure (an impaired myelin compaction), subtle changes in axonal cytoarchitecture in the absence of swellings or salient axonopathy, motor (gait) disturbances, convulsions, and very short lifespan (between 50- 100 days) (Dupouey et al., 1979; Readhead and Hood; 1990; Kirkpatrick et al., 2001). In humans,

MBP protein is pathologically damaged in patients with multiple sclerosis and most likely contributes to the observed neuropathological features and functional deficits (Allegretta et al., 1990).

MAG is a transmembrane glycoprotein localized at the periaxonal space. It is functionally involved in the maintenance of the structural integrity and survival of both the neuronal axons and oligodendroglia (Quarles, 2007). MAG is also a molecular factor known to inhibit axonal regeneration and neurite outgrowth acting through the NOGO receptor pathway (Liu et al., 2002). This myelin protein is particularly vulnerable to hypoxic-ischemic insults (Aboul- Enein et al., 2003). Interestingly, MAG null mutation in mice does not impact significantly on the overall myelin structure (at the exception of some multiple ensheathed axons) (Schachner, 1994). The phenotype of MAG mutants is normal and no severe functional (motor and/ or cognitive) deficits are observed (Montag et al., 1994).

Additionally, mutation in the glial fibrillary acid protein (GFAP) present in astrocytes and radial glia indirectly impacts on myelin integrity (Song et al., 2002). Absence of endogenous astrocytes in both humans with Alexander disease and in genetically modified GFAP null mice results in a substantial dysmyelination associated with an impaired oligodendroglial function and short survival. In humans, GFAP mutation is associated with sever functional deficits such as seizures, muscle spasticity, cognitive deficits and a very short lifespan (~10 years after disease onset) (Johnson, 2002).

1.4. Methods for detection of white matter integrity

1.4.1. Magnetic resonance imaging (MRI)

Magnetic resonance imaging (MRI) is a neuroimaging technique used in both clinical and preclinical settings. It was initially developed about 40 years ago (Lauterber, 1973) and its principle relies on the physical properties of water molecules composing the body organs. The MRI scanner applies strong magnetic fields to the person/ animal/ biological sample resulting in an excitation of the water hydrogen atoms (protons) which align their own magnetic fields (spins) in the direction to the scanner magnetic field. Subsequently, the application of a brief radio frequency (RF) produces an electromagnetic field. The

generated RF is absorbed by the aligned protons and flips their own spin. The frequency at which the protons resonate depends on the strength of the applied magnetic field. Once the RF is turned off, the spin of the protons will return progressively to baseline. The time taken for the protons (the relaxation time) to return to their initial spin is measured by the MRI scanner. The protons from the different body tissues have different relaxation properties allowing the generation of MRI image contrast. The generation of high quality MRI images with a good spatial resolution depends on the strength of the applied magnet, the total imaging time and physiological artifacts (movement, respiration, blood circulation etc). MRI provides a good regional contrast between the different soft tissues of the body and unlike computer tomography (CT) scans or traditional X-rays, MRI does not apply ionizing radiation making this neuroimaging technique safer for clinical use.

1.4.1.1. Diffusion tensor imaging (DTI)

Diffusion tensor imaging (DTI) is a newly developed MRI approach first described by Moseley et al., in 1990 measuring the temperature driven directional diffusivity of water molecules in organized biological systems such as white matter tracts (Moseley et al., 1990). Specifically, DTI provides a quantitative evaluation of white matter structural integrity relying on the physical phenomenon of fractional anisotropy (FA). FA is defined by the axial diffusivity ($\lambda\parallel$) determined by the diffusion of water molecules along the neuronal axons and the radial diffusivity ($\lambda\perp$) characterized by the water diffusivity perpendicular to the neuronal axons (through the myelin sheath and the axonal cytoarchitecture). Under normal physiological conditions, the diffusion of water molecules in white matter tracts is mainly along the neuronal axons and it is highly anisotropic (~1.0). FA decreases in the presence of pathology due to a disruption of the myelin membranes, axonal injury and the occurrence of an isotropic (in all direction) water diffusivity (Basser, 1995; Beaulieu, 2002). FA is shown to be a sensitive noninvasive biomarker for white matter integrity and it is currently used in both clinical and preclinical settings. Recent neuroimaging studies have established that DTI is sensitive to changes in white matter integrity when applied on ex vivo samples (Filippi et al., 2001; Bozzali et al., 2002; Deary et al., 2003; Song et al., 2003; Song et al., 2005; Dhenain et al., 2006; Harms et al., 2006; Harsan et al., 2006; Sun et al., 2006a; Gouw et al., 2008; Bastin et al., 2009;

Penke et al., 2010; Holland et al., 2011). Although, postmortem brain tissue is characterized by a lower temperature and reduced overall water diffusivity due to the application of fixatives and the absence of active blood circulation, FA is relatively preserved (Guilfoyle et al., 2003; Sun et al., 2003; Sun et al., 2005). The advantage of ex vivo DTI application to biological samples is that it allows longer imaging time in the absence of physiological artifacts and therefore the generation of MRI images with a better spatial resolution. Ex vivo DTI provides a more detailed histological white matter analysis when combined with basic immunohistochemical/ biochemical techniques allowing the simultaneous examination of microstructural (axons and myelin integrity, inflammatory cells) and molecular (myelin gene expression, protein and lipid levels) basis of white matter pathology observed on MRI scans.

1.4.1.2. Magnetization transfer ratio (MTR)

Magnetization transfer ratio (MTR) is a new MRI technique first developed by Wolff and Balaban in 1989 providing information on white matter integrity by calculating a ratio between the free water protons and the macromolecular (myelin) bound water pool in the brain (Wolff and Balaban, 1989; Grossman et al., 1994). A decrease in MTR is usually associated with an increase in the free brain water pool due to white matter (primarily myelin) damage (McGowan et al., 1999; Schmierer et al., 2004; Blezer et al., 2007; Bastin et al., 2009; Ou et al., 2009; Holland et al., 2011). Similar to DTI, MTR is also successfully applied for the detection of white matter integrity both in vivo and ex vivo (McGowan et al., 1999; Schmierer et al., 2004; Blezer et al., 2007; Bastin et al., 2009; Ou et al., 2009; Holland et al., 2011).

1.4.2. Ex vivo (postmortem) histopathological evaluation of white matter integrity

Microstructural white matter axonal and myelin integrity are studied on postmortem brain samples by means of standard histological and immunohistochemical techniques. The most common histological stainings applied for the study of white matter integrity are Kluver Barrera allowing the visualization of gross white matter fiber disorganizations and Luxol fast blue allowing the differentiation of white matter abnormalities (pale areas) from normal appearing white matter (intensely stained in blue) (Kluver and Barrera, 1953;

Goto, 1987). These techniques are good indicators of the overall white matter integrity, however they lack a sufficient sensitivity as to the different cellular components of the cerebral white matter such as the neuronal axons and the myelin sheath, therefore they are not good biomarkers for subtle pathological changes in white matter integrity. Standard immunohistochemical techniques employing antibodies to the neuronal axons and the myelin proteins are much more sensitive to mild changes in the microstructural integrity of the cerebral white matter.

1.5. Chronic cerebral hypoperfusion

Chronic cerebral hypoperfusion is associated with age- related changes in the cerebrovasculature leading to subtle reductions in the cerebral blood supply and metabolism. Arteriosclerosis (affecting the arteries) and atherosclerosis (affecting the small blood vessels) are characterized by the accumulation of lipids, cholesterol, inflammatory macrophages in the walls of the cerebral blood vessel leading to their partial occlusion and the occurrence of a forebrain hypoperfusion (Kalback et al., 2004; Moore and Tabas, 2011) (figure 1.3. A). One of the major risk factors for the development of atherosclerotic lesions in elderly is an existing polymorphism in the human apolipoprotein E (APOE) gene (Chapter 1, section 1.6.) (Elosua et al., 2004). A detectable carotid stenosis is present in 75% of men and 62% of women aged $\geq$ 65 years and the prevalence of a $\geq$ 50% stenosis in this population being 7% in men and 5% in women (O`Leary et al., 1992). Peripheral carotid stenosis has been shown to impact on the cerebral microvasculature leading to thickening of the basement membrane, reductions in vascular smooth muscle content, and loss of vessels elasticity (de Leeuw et al., 2000; Farkas et al., 2006). All these morphological changes in the macro and micro cerebrovasculature impact on the overall vascular tone and could lead to impaired neural metabolism. Carotid occlusive disease is responsible for 15- 20% of all ischemic stroke (Chaturvedi et al., 2005). Whereas, stroke is a well- known cause for dementia, carotid stenosis itself is less well- established independent risk factor for a cognitive impairment. The mechanisms of cognitive impairment occurring in patients with carotid stenosis are poorly understood.

1.5.1. Chronic cerebral hypoperfusion, age- related white matter pathology and cognitive decline

Human studies have suggested that chronic cerebral hypoperfusion is the major pathophysioloigcal mechanism leading to the occurrence of age- related white matter pathology and cognitive decline (Fernando et al., 2006). Specifically, MRI evidenced white matter lesions coincided with pathologically observed increases in hypoxia-inducible factors (HIF) HIF1α and HIF2α suggesting that white matter lesions in elderly are most likely due to hypoxic environment. Furthermore, the increase in HIFs is also associated with an increase in inflammatory levels showing that complex cellular and molecular events following hypoperfusion contribute to the development of white matter pathology in elderly. In patients with small vessel disease a decreased cerebral blood flow in subcortical regions (putamen and thalamus) is negatively associated with the burden of white matter pathology in these brain areas (Kawamura et al., 1991). These data suggest that chronic cerebral hypoperfusion in cerebral regions supplied by the deep penetrating arteries most likely contributes to the occurrence of white matter lesions in periventricular and deep subcortical areas. Ischemic white matter lesions in Alzheimer`s patients exhibit oligodendroglial loss and microvessels pathology such as abnormal collagen deposition in the vessels wall indicating that cerebrovascular disease leading to hypoxic- ischemic events contributes to the development of neuropathology and dementia in elderly (Brown et al., 2000).

Although it is methodologically extremely challenging to study in isolation the effects of chronic cerebral hypoperfusion on cognitive function in elderly humans presenting very often additional neuropathological conditions (e.g. Alzheimer`s disease), several published reports have tried to address the impact of reduced cerebral blood flow on cognitive performance in the healthy aging population. A recent study (the Tromso study) applying MRI for the detection of white matter integrity, ultrasonography for the measurement of carotid stenosis and a battery of neuropsychological tests has demonstrated that subjects with carotid stenosis have significantly impaired attention, psychomotor speed, memory, and motor functioning, independent of MRI lesions (Mathiesen et al., 2004). Furthermore, a decreased cerebral blood flow due to hypoperfusion measured by transcranial Doppler

has been associated with a poorer performance on a battery of cognitive tests (Mini Mental State Examination) in both healthy and demented elderly (Ruitenberg et al., 2005). The results from a postmortem neuropathological study suggest that chronic reduction of the cerebral blood supply observed in Alzheimer`s patients contributes to the development of white matter lesions and the progression of dementia, especially in APOE4 carriers (Alafuzoff et al., 2000). Similar findings have been reported in vivo. Reductions in cerebral brain metabolism are usually observed with increasing age in both grey and white matter regions and they are associated with cognitive decline and dementia (Ogawa et al., 1996; Pardo et al., 2007). Alzheimer`s disease and vascular dementia patients present a significantly decreased cerebral blood flow in comparison with normal elderly (Schuff et al., 2009a). However, little is known about the exact contribution of chronic cerebral hypoperfusion to the occurrence of age- related changes in the cerebral metabolism. Derdeyn et al., 1999 have demonstrated that chronic cerebral hypoperfusion in patients with carotid stenosis leads to a reduced rate of cerebral metabolism (Derdeyn et al., 1999). However, the ratio between the oxygen extraction fraction and the rate of cerebral metabolism is normal in hypoperfused patients suggesting that collateral blood flow could compensate for normal cerebral metabolism.

From a mechanistic point of view, the cerebral white matter is particularly vulnerable to such changes in the cerebral blood supply due to its limited vascular irrigation. At the difference from the highly vascularized cerebral grey matter, the cerebral white matter is defined as an arterial end and border zone with a very low blood supply even under normal physiological conditions rendering this neuroanatomical structure particularly vulnerable to hypoxic- ischemic events (Nonaka et al., 2003). Chronic cerebral hypoperfusion is characterized by subtle blood flow reductions (<50% of baseline) which are usually compensated by the cerebral anastomosis provided by the cerebral arteries composing the Circle of Willis. This compensation could explain the relative absence of neuropathological changes after chronic cerebral hypoperfusion in the highly vascularized cortical and subcortical grey matter regions (Shibata et al., 2004; Shibata et

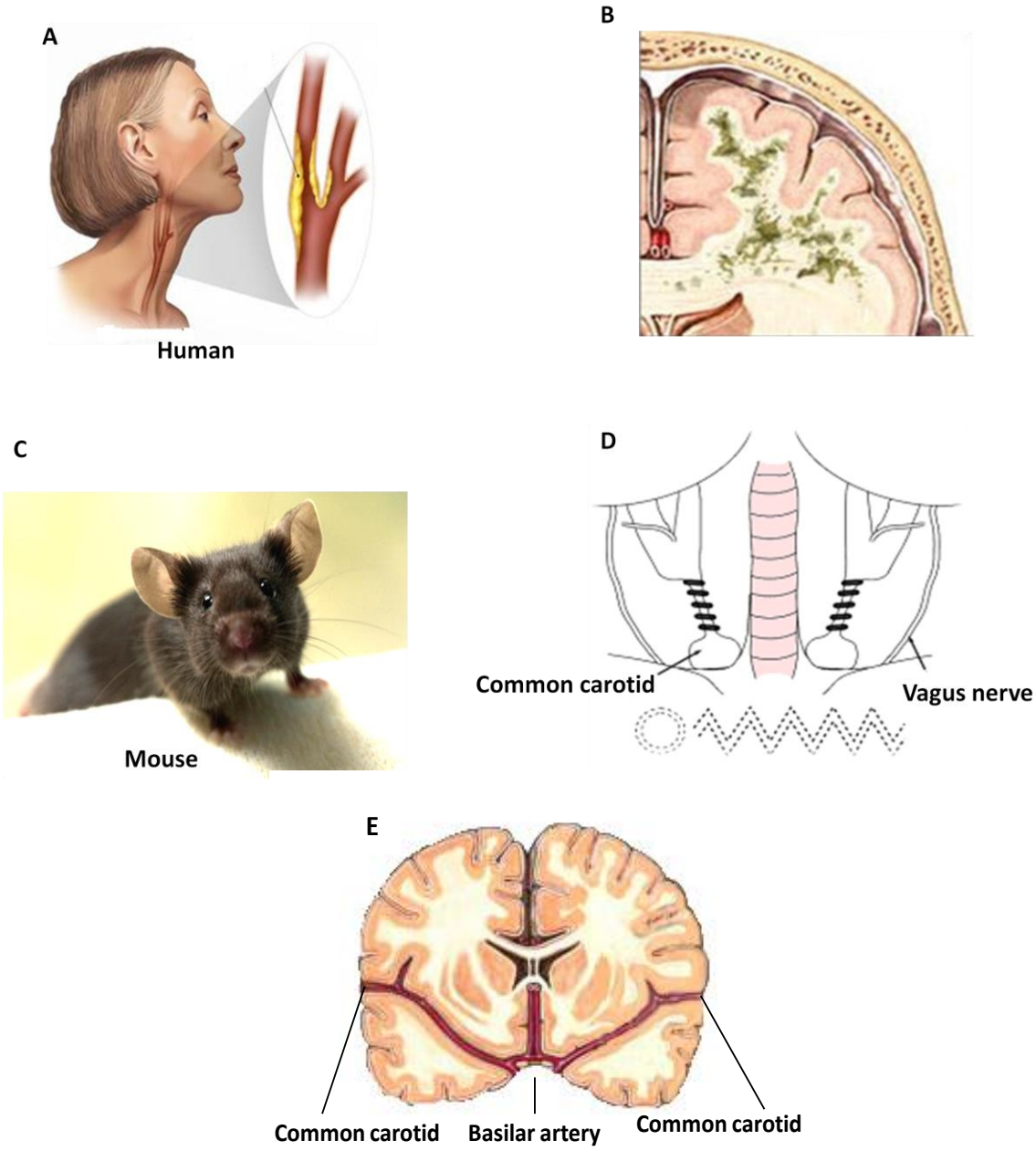

Figure 1.3.: Hypoperfusion- induced white matter pathology

In humans, age-related cerebrovascular changes (e.g. atherosclerosis) (**A**) lead to chronic cerebral hypoperfusion and the occurrence of white matter pathology (**B**). To model age-related neuropathology in preclinical settings, 0.18mm diameter piano microcoils (**D**) are bilaterally applied to the common carotid of mice (**C**) leading to chronic cererbral hypoperfusion and the development of white matter pathology. The cerebral white matter is defined as an arterial border end zone with a poor vascular irrigation rendering these neuroanatomical regions particularly vulnerable to subtle metabolic changes (**E**). (images adapted from ADAM Medical images http://adameducation.com/adam_images.aspx)

al., 2007; Coltman et al., 2011; Holland et al., 2011). However, this cerebrovascular compensation might be inefficient in sustaining a normal flow to the cerebral white matter which is mainly irrigated by small arterioles and veins emanating from the anterior cerebral artery (for the frontal white matter- CC, EC), the posterior and basilar cerebral arteries (for the subcortical white matter- IC, Fx, OT) (figure 1.3.B, E). Further, it is also possible that the reduced levels of glucose affect oligodendroglial metabolism. Oligodendrocytes are known to be the biggest consumers of lactate and glucose in the brain (Sanchez- Abarca et al., 2001; Rinholm et al., 2011). Pathological disruption of the oligodendroglial metabolism could affect their molecular and cellular machinery leading to impaired myelin production and maintenance promoting the subsequent development of white matter pathology. Furthermore, increased levels of excitotoxic and oxidative agents due to hypoperfusion might be harmful to the oligodendroglial cells (van Reempts et al., 1986; Siesjo et al., 1995; Matute et al., 2001).

1.5.2. Animal models of chronic cerebral hypoperfusion

In elderly people it is extremely difficult to study in isolation the effects of single etiological factors on neuropathology and cognition due to the presence of comorbidities such as diabetes, cardiac disease, hypertension, neurodegeneration (e.g. Alzheimer`s disease) (Van Swieten et al.; 1991; Lindgren et al., 1994; Ruitenberg et a., 2005; Verdelho et al., 2010). Therefore, animal models have been developed in order to study the cellular and molecular events following chronic cerebral hypoperfusion leading to the development of white matter pathology and cognitive deficits.

1.5.2.1. Rat model of chronic cerebral hypoperfusion

Chronic cerebral hypoperfusion was first experimentally modeled in rats due to the low experimental cost, the complete Circle of Willis in this rodent species, the relatively low mortality rate and the high reproducibility of both the neuropathological and behavioural outcome. To induce chronic cerebral hypoperfusion in the rat, the common carotid artery is bilaterally permanently ligated. This leads to ~30- 60% (of baseline level) initial reductions of the cerebral blood supply with a gradual flow recovery by 4 weeks post-surgery (Otori et al., 2003). The observed recovery of the cerebral blood flow is explained

by compensatory mechanisms such as enlargement of the arteries at the base of the brain. The posterior vessels constituting the Circle of Willis (the posterior cerebral artery, the posterior communicating artery, and the basilar artery) are considerably enlarged between 3- 6 months after the induction of chronic cerebral hypoperfusion (Olendorf, 1989; Choy et al., 2006). The blood- brain barrier integrity is also impaired in hypoperfused rats as measured by the presence of venously administered horseradish peroxidase in the CC. The blood- brain barrier permeability increases progressively from 3 hours after bilateral carotid ligation reaching maximum permeability by day 3 post- surgery. The blood brain barrier integrity shows progressive recovery from day 7 post- surgery (Ueno et al., 2001). These cerebrovascular alterations are accompanied by an impaired cerebral metabolism mainly observed as ATP depletion immediately after the artery ligations followed by hypoxia and hypoglycemia (Plaschke et al., 2005). Reduced intracellular concentrations of ATP as well as the increased levels of excitotoxicity and oxidation are the most likely molecular mechanisms leading to neuropathological changes in chronically hypoperfused rats. Neuronal ischemic damage in grey matter regions (mainly in the CA1 region of the hippocampus evidenced by 1 week post- surgery) accompanies the development of white matter abnormalities such as white matter rarefication, vacuoles formation, myelin disintegration, oligodendroglial apoptosis, amyloid precursor protein (APP) accumulation in bulbous axons, early microglial activation (20 min post- surgery) and long- term astrocytic response (6 months post- surgery) (Pappas et al., 1996; Abraham and Lazar, 2000; Farkas et al., 2004; Farkas et al., 2007; Otori et al., 2003; Tomimoto et al., 2003). White matter pathology in hypoperfused rats develops progressively over time and the very first abnormalities such as fibers disorganization are evidenced 3 days post- surgery (Wakita et al., 2002; Otori et al., 2003). Further, white matter pathology is accompanied by subtle changes in neuronal morphology demonstrated by alterations in mRNA and protein expression of synaptic (synaptophysin) and dendritic (microtubule- associated protein 2 (MAP2)) proteins (Liu et al., 2005). Chronically hypoperfused rats exhibit an early spatial reference memory impairment on a water maze task (7 days post- surgery) followed by a long- term spatial working and reference memory deficit on a radial arm maze task (63 days post- surgery) (Pappas et al., 1996; Sopala and Danysz, 2001). These results suggest that the observed learning and memory deficits in hypoperfused rats are

cumulative corresponding to the chronic nature of the cerebrovascular challenge and the progressive development of white matter pathology in this model. Further, in the rat, chronic cerebral hypoperfusion does not affect the locomotor and exploratory activity as well as the overall anxiety on an open- field test (de Bortoli et al., 2005). However, hypoperfused rats show increased anxiety levels on an open- arms T- maze task (de Bortoli et al., 2005). Overall, the rat model of chronic cerebral hypoperfusion reproduces most of the pathological and cognitive features associated with chronic cerebral hypoperfusion in humans, but the concomitant grey matter pathology renders difficult the evaluation of the effects of selective white matter pathology on cognition in hypoperfused rats.

1.5.2.2. Gerbil model of chronic cerebral hypoperfusion

The gerbil is another rodent species that has been used to model human age- related chronic cerebral hypoperfusion. In the gerbil, coiled stainless steel wire clips are applied to both common carotids leading to 24- 27% (of control baseline) chronic reduction of the cerebral blood flow observed up- to 8 weeks post- surgery (Kudo et al., 1990). At the neuropathological level hypoperfused gerbils exhibit varying degree of cortical atrophy, ventricular dilation, astroglial activation and white matter fibers rarefication occurring not earlier than 4 weeks post- surgery with increasing frequency and severity by 12 weeks post- surgery (Hattori et al., 1992; Kudo et al., 1993; Kurumatani et al., 1998). White matter pathology in hypoperfused gerbils is accompanied by neuronal ischemic loss in cortical and subcrotical (hippocampus) regions (Kudo et al., 1993). Further, in hypoperfused gerbils, Western blot analysis demonstrated significant decreases in MBP protein levels prior to changes in neuronal cytoarchitecture associated with reductions in neurofilament H and MAP2 two months after surgery. These results suggest that myelin pathology occurs prior to axonal damage in this model (Kurumatani et al., 1998). Additional immunohistochemical analysis demonstrated that MAP2 is significantly reduced in grey matter regions accompanied by an increased neurofilament phosphorylation 12 weeks post- surgery (Kudo et al., 1993). Learning and memory abilities in gerbils are studied by passive avoidance paradigms and hypoperfused gerbils show learning and memory deficits on this task 12 weeks post- surgery (Kudo et al.,

1990). The gerbil model of chronic cerebral hypoperfusion is a low experimental cost in vivo tool reproducing correctly some of the neuropathological features and functional impairments observed in human patients with carotid stenosis. However, the gerbil model shows some limitations that could be overcome by using rats or mice. First, it is more difficult to train gerbils on behavioural paradigms which is not the case for rats and mice. Although, similar to gerbils mice have underdeveloped Circle of Willis (at the difference from rats where this cerebrovascular structure is complete and similar to humans) the development of genetically modified mice makes this rodent species a preferred in vivo tool for the evaluation of cerebrovascular pathology in preclinical settings.

1.5.2.3. Mouse model of chronic cerebral hypoperfusion

The large preclinical use of genetically modified mice has prompted the recent development and characterization of a new mouse model of chronic cerebral hypoperfusion by our and other groups (Shibata et al., 2004; Shibata et al., 2007; Nishio et al., 2010; Coltman et al., 2011; Holland et al., 2011). This model consists of the bilateral application of piano wire coils around the common carotid artery (figure 1.3. C, D). The use of coils with different internal diameter allows experimental regulation of the cerebral blood flow reductions. In an initial work it has been demonstrated that using microcoils with an internal diameter of 0.18 mm leads to a 20- 30% (of baseline levels) reductions of the cerebral blood supply and the development of a predominant white matter pathology 1- 2 month(s) post- surgery (Shibata et al., 2004). The first white matter changes in this model are observed as soon as 2 weeks post- surgery (unpublished observations from Dr Horsburgh`s laboratory). Application of microcoils with a smaller internal diameter (0.16 mm) induces mixed grey and white matter pathology one month post- surgery (Shibata et al., 2004). Therefore, the 0.18 mm diameter is preferentially used by the groups working on this model because of the development of white matter pathology in the absence of neuronal ischemia. In chronically hypoperfused mice, white matter abnormalities are characterized by fibers rarefication, vacuolation, MAG debris, degraded MBP (dMBP) accumulations, and increased inflammatory levels in white matter tracts (Shibata et al., 2004; Shibata et al., 2007; Coltman et al., 2011; Holland et al., 2011). Myelin pathology in chronically hypoperfused mice is accompanied by mild to moderate axonal injury

(Coltman et al., 2011). These pathological observations have been confirmed by a recent in vivo MRI- DTI study reporting significant reductions in FA and MTR values in white matter tracts one month after chronic cerebral hypoperfusion (Holland et al., 2011). Long-term studies on this model have demonstrated accumulative pathological changes in the brains of hypoperfused mice. Specifically, hippocampal neuronal loss occurs at 8 months after surgery (Nishio et al., 2010). Furthermore, cerebral blood flow reductions in chronically hypoperfused mice are associated with late- occurring reductions in cerebral metabolism in grey matter regions (striatum, hippocampus and cortex) 6 months after microcoils application (Nishio et al., 2010). At the functional level, one month after surgery chronically hypoperfused mice perform as well as sham on a comprehensive battery of tests such as a startle prepulse inhibition test, hot plate test, rotarod and grip strength motor tests, open field test, light/ dark transition test, porsolt forced swim test, cue and fear conditioning (Shibata et al., 2007). At the same post- surgery time point, chronically hypoperfused mice exhibit deficits on a radial arm maze spatial working memory task in the absence of learning and memory deficits on radial arm maze and water maze reference memory tasks (Shibata et al., 2007; Coltman et al., 2011). Interestingly, 8 months after surgery hypoperfused mice show an impaired reference memory on a radial arm maze paradigm most likely due to grey matter structural abnormalities (Nishio et al., 2010).

Due to its recent development in 2004, this new mouse model of chronic cerebral hypoperfusion has not been fully characterized and more work needs to be done in order to get a better insight into the molecular and cellular events underlying the occurrence of white matter pathology and functional deficits in chronically hypoperfused mice. Since most of the currently available genetically modified mice used in research settings are on a C57Bl6J background the microcoil surgery has been specifically optimized for experimental application in C57Bl6J mice.

1.6. Apolipoprotein E (APOE)

Apolipoproteins are formed by the binding of an apoprotein to a lipoprotein. Lipoproteins are biochemical assemblies composed of a core of triglycerides and cholesterol esters surrounded by a layer of phospholipids allowing the transport of insoluble lipids

throughout the body. Apoproteins support the stability of the lipopoprotein allowing its targeted transport and receptor binding. Apopoprotein E binds specifically to high density lipoproteins (HDL) involved in the peripheral metabolism of cholesterol, mainly by collecting cholesterol from the different body organs and delivering it back to the liver; to very low density lipoproteins (VLDL) distributing newly synthesized cholesterol from the liver to the rest of the body organs; and to chylomicrons transporting triglycerides from the intestine to the liver, skeletal muscle, and the adipose tissue) (figure 1.4. A).

Apolipoprotein E (APOE) is a glycoprotein of 299 amino acids with a molecular weight of ~34- kDa first discovered by Shore and Shore in 1973. APOE is found in both the periphery (spleen, liver, macrophages) as well as in the central nervous system.

In the periphery APOE is synthesized predominantly by the liver which is the integral organ of lipid metabolism (Elshourbagy et al., 1985).

In the brain, APOE is found in the parenchyma as well as in the cerebrospinal fluid (CSF). APOE mRNA is detected in the cerebral cortex, the cerebellum, the brain stem, the choroid plexus, the thalamus, the hypothalamus and the hippocampus (Elshourbagy et al., 1985; Lorent et al., 1995). Astrocytes are the neural cells expressing APOE under normal physiological conditions (Boyles et al., 1985). Low APOE levels are also detected in microglia, oligodendrocytes, ependymal cells. In primates and humans, APOE is present at lower levels in neurons under normal physiological conditions (Han et al., 1994; Metzger et al., 1996). In rodents, neuronal APOE expression is evidenced only in the presence of ongoing neuropathology (Horsburgh et al., 1996; Horsburgh et al., 1997).

APOE mediates its effects via the low density lipoprotein receptor (LDL- R) family- a class of single transmembrane glycoproteins containing large extracellular and relatively short intracellular domains, generally recognized as cell surface endocytic receptors, which bind and internalize extracellular ligands for lysosomal degradation. The LDL- R consists of more than 10 members of receptors, but the most important ones for APOE function are the low density lipoprotein receptor (LDLR), the very low density lipoprotein receptor (VLDLR), the low density lipoprotein receptor- related protein

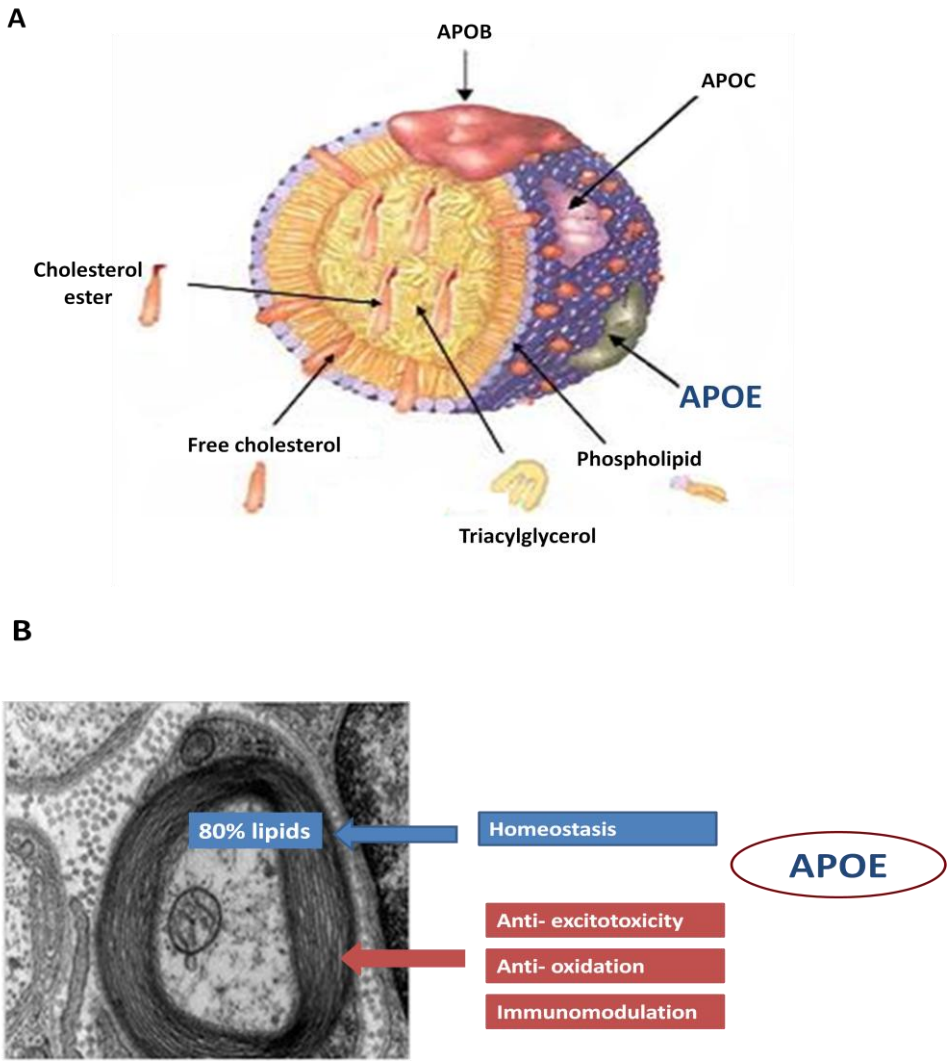

Figure 1.4.: APOE structure and potential APOE effects on white matter integrity

A schematic representation of a lipoprotein particle composed of triacyglycerol and cholesterol esters surrounded by a layer of phospholipids allowing the transport of insoluble lipids through the body. Apoproteins are attached to lipoproteins resulting in apolipoprotein complexes (**A**). APOE might impact on the integrity of the cerebral white matter under both normal and pathological conditions either directly via the regulation of the homeostasis of the lipid component of the myelin sheath or via APOE- modulated mechanisms such as excitotoxicity, oxidation and immune response (**B**). The electron microscopy image of myelin sheath in (**B)** is adapted from Wikipedia http://en.wikipedia.org/wiki/Myelin.

(LRP1). The LDL- R family members are involved in multiple signaling pathways playing an important role during early neurodevelopment as well as in the adult mammalian brain (Cooper and Howell, 1999).

1.6.1. Differences between human and mouse APOE

In humans, the APOE gene is located on chromosome 19q13.2. It is composed of 5 exons and 4 introns. Human APOE exists in three different isoforms- APOE2, APOE3, and APOE4 coded by three different alleles- ε2, ε3, and ε4 respectively (Utermann et al., 1977; Zannis et al., 1981). The resulting three human APOE proteins differ in their amino acid composition at residues 112 and 158 leading to differences in their functionality. APOE3 has a cysteine at residue 112 and an arginine at residue 158, APOE2 has cysteine at both positions, and APOE4 contains arginine at both positions. In APOE4, arginine-112 (Arg-112) impairs domains interaction between Arg- 61 (N terminal domain) and glutamate-255 (Glu- 255) (C terminal domain) and reduces the stability of the protein leading to a so- called molten globule state (Weisgraber, 1994). The APOE4 structural conformation has been shown to mediate its negative effects on neurobiology such as increase in beta amyloid (Aβ) production, potentiation of Aβ induced leakage and apoptosis, and its enhanced proteolytic cleavage in neurons (Mahley et al., 2006).

In other mammalian species, including the great apes, APOE gene does not present multiple isoforms and the resulting protein is molecularly similar to APOE4, but functionally behaves like human APOE3 (Hanlon and Rubinsztein, 1995).

In the mouse, the APOE gene is situated on chromosome 7 and its amino acid sequence homology to the human APOE gene is >90% (Maloney et al., 2007). However, the homology between the human and the mouse APOE gene promoter is <40% which might account partially for the observed species differences in the APOE cell distribution. From a structural point of view, similar to human APOE4, mouse APOE contains arginine at residue 112, but arginine at residue 61 is replaced by thryonine (Thr- 61) thus abolishing the human APOE4- specific domain interaction between Arg- 112 and Glu- 255. Replacing Thr- 61 with arginine introduces domain interaction and allows mouse APOE

to behave like human APOE4 (Raffai et al., 2001). Functionally, similar to other mammalian species, mouse APOE preferentially binds to HDL, but not VLDL.

1.6.2. APOE deficient mice

To experimentally address APOE function in the central nervous system under normal physiological and pathological conditions, APOE deficient (APOEKO) mice have been created as described in Chapter 2, section 2.1.2. These animals are characterized by increased plasma cholesterol levels (Van Ree et al., 1994), early development of atherosclerosis (Piedrihta et al., 1992; Van Ree et al., 1994), impaired immune response (Laskowitz et al., 2000), blood brain barrier anomalies (Fullerton et al., 2001; Methia et al., 2001; Hafezi- Moghadam et al., 2006), increased lipid peroxidation in the plasma (Witting et al., 2000) and in the central nervous system (Lomnitski et al., 1999; Ramassamy et al., 2001; Pratico et al., 2002; Choi et al., 2004), and early onset of neurodegeneration (Masliah et al, 1995; Masliah et al., 1997). At the functional level, APOEKO mice exhibit learning and memory deficits when compared with wild- type (WT) counterparts (Gordon et al., 1995; Masliah et al., 1997). After experimentally induced brain injury APOEKO animals present a poor neuropathological and functional recovery as shown in models of traumatic brain injury (Chen et al., 1997; Lomnitski et al., 1997; Lomnitski et al., 1999; Lynch et al., 2002), global ischemia (Hosrburgh et al., 1999; Sheng et al., 1999; Kitagawa et al., 2002), focal ischemia (Laskowitz et al., 1997a), entorhinal cortex lesion (Champagne et al., 2005). Intraventricular infusion of human recombinant apolipoprotein E rescues the pathological and the functional deficits associated with APOE deficiency after global ischemia (Horsburgh et al., 2000a), during normal aging (Masliah et al., 1995), after kainic acid induced lesion (Buttini et al., 1999). These results suggest that APOE is an important molecular factor in the endogenous neuroregenerative processes.

1.6.3. APOE, age- related white matter pathology and cognitive decline

APOE and its human isoforms have been primarily studied in the context of Alzheimer`s disease and senile dementia, due to the increased risk of Alzheimer`s disease in APOE4

carriers. Therefore, so far, the major research focus on APOE has been primarily on its effects on grey matter structural integrity (Saunders et al., 1993; Mahley et al., 2006).

Little attention has been paid to APOE and its effects on white matter integrity during healthy aging. Recent combined functional MRI (fMRI) and neuropsychological studies have demonstrated that non demented APOE4 adults activate a significantly higher number of cerebral regions during the performance of a working memory task suggesting the existence of compensatory mechanisms (e.g. a recruitment of larger neuronal networks) allowing these individuals to perform the cognitive task at the same level as APOE3 carriers (Bookheimer et al., 2000; Wishart et al., 2006). In regards to APOE involvement in the turnover of myelin lipids and cholesterol one could suspect that this apolipoprotein and its different human isoforms impact differentially on white matter integrity. Indeed, recent neuroimaging studies discovered that cognitively intact middle aged APOE4 individuals exhibit white matter abnormalities compared with age and cognitive status- matched APOE3 carriers (Filippini et al., 2009; Heise et al., 2010; Ryan et al., 2011). Specifically, in cognitively intact APOE4 adults, white matter abnormalities have been detected in prefrontal transcollosal tracts, the genu and the splenium of the CC years prior to the onset of dementia. By calculating MRI transversal relaxation rates (an indirect measure of myelin integrity) it has been established that the APOE4 genotype is directly related to myelin integrity in white matter regions (Bartzokis et al., 2007). On the basis of these results it has been proposed that APOE initially mediates its effects on cognition via its decreased functionality leading to impaired myelin metabolism and white matter pathology. Further, the observed human APOE isoform differences in white matter integrity among healthy APOE3 and APOE4 carries is most likely due to isoform- related functional and/ or quantity (brain APOE4 levels are estimated to be 12- 20% lower than APOE3 levels) differences (Bartzokis et al., 2006). Therefore, the inability of APOE4 to sustain normal myelin lipid and cholesterol metabolism or the reduced brain levels of this apolipoprotein might be at the basis of the observed white matter abnormalities in cognitively intact APOE4 carriers. Interestingly, positron emission tomography (PET) neuroimaging studies have revealed that young and middle aged cognitively intact APOE4 adults present reduced cerebral metabolism in the same brain regions which are subsequently affected in Alzheimer`s patients, namely parietal, temporal, prefrontal and

posterior cingulated regions (Reiman et al., 1996; Reiman et al., 2004). These results suggest the existence of asymptomatic cerebrovascular abnormalities in cognitively normal APOE4 carriers. Further it has been established using fMRI that MRI signal intensity is significantly increased in the anterior cingulated and dorsal prefrontal cortex of cognitively intact APOE4 adults during the recall phase of a working memory task (Bookheimer et al., 2000). Overall, these results suggest that subjects at genetic risk for Alzheimer`s disease show white matter abnormalities accompanied by a reduced cerebral metabolism and a widespread brain activation during cognitive effort years prior to the occurrence of dementia. However, future clinical and preclinical studies should elucidate the exact cellular and molecular events via which APOE and its isoforms impact on white matter integrity, cerebral metabolism and cognitive function.

1.6.4. APOE- related mechanisms impacting on white matter integrity

APOE could impact on white matter integrity under both normal physiological and pathological (e.g. chronic cerebral hypoperfusion) conditions due to its role in the maintenance of the myelin lipid and cholesterol homeostasis as well as its involvement in the endogenous brain repair mechanism via its anti- excitotoxic, anti- oxidative and immunomdulatory functions (figure 1.4. B).

1.6.4.1. Role of APOE in the transport and metabolism of brain lipids and cholesterol

APOE plays an important role in the turnover of lipid and cholesterol content in the central nervous system. The brain cholesterol is synthesized locally primarily by glia and it is delivered to neurons by APOE (Boyles et al., 1985; Elshourbagy et al., 1985). The brain is the body organ with the highest cholesterol content mainly present in white matter regions (Dietschy et al., 2001). Cholesterol is found in myelin, glial and neuronal cell membranes and it is essential for neuronal plasticity (Goritz et al., 2002), synaptogenesis (Mauch et al., 2001), neuroregeneration and remyelination (Poirier et al., 1993). Cholesterol is cleared from the brain by its neuronal conversion to 24S-hydroxycholesterol which passes through the blood- brain barrier (Bjorkhem et al., 2006). With age, brain cholesterol levels decrease (Thelen et al., 2006) and 24S-hydroxycholesterol levels increase (Lutjohann et al., 1996) and this is more pronounced in

the presence of neuropathology such as Alzheimer` s disease (Lutjohann et al., 2000; Yanagisawa et al., 2002). Further, during neuroregeneration of experimentally injured sciatic nerve APOE levels increase significantly with a peak at the time of active remyelination (Boyles et al., 1989). It has been shown that APOE plays an important role in the delivery of newly synthesized cholesterol to damaged cells and to actively participate in the clearance of cellular debris promoting neuroregeneration and remyelination.

APOE is also involved in the transport and metabolism of other brain lipids such as phospholipids. Phospholipids are integral constituents of cell membranes and myelin. APOE deficient mice show a significant reduction in cortical phospholipids and their constituent fatty acids in comparison to WT littermates (Montine et al., 1999). Furthermore, oxidized phospholipids have been shown to participate in concert with cholesterol in the formation of atherosclerotic plaques occurring with increasing age in the majority of APOE4 human carriers and in APOE deficient mice due to an inefficient lipid and cholesterol turnover and the pathological accumulation of the latter in the walls of the blood vessels followed by the occurrence of brain hypoperfusion (Piedrihta et al., 1992; Van Ree et al., 1994; Elosua et al., 2004).

APOE is involved in the metabolism of sulfatides which are exclusively synthesized by oligodendrocytes (Poduslo and Miller, 1985). Sulfatides are part of the myelin lipid component, but they also participate in the regulation of cell growth, protein trafficking, cell adhesion, and neural plasticity (Marcus et al., 2006). The hippocampal and cortical sulfatide mass is higher in the brains of APOE deficient mice than in WT counterparts (Han et al., 2003). Similarly human APOE4 carriers have increased sulfatide content compared to APOE3 carriers. Although sulfatides are important for myelin maintenance (Marcus et al., 2006), when the level of these lipids increases excessively as in the case of metachromatic leukodystrophies, they exert a toxic effect on the myelin- producing oligodendroglia and by consequence contribute to the appearance of substantial demyelination and functional deficits such as motor and gait disturbances as well as cognitive and memory dysfunction (Ramakrishnan et al., 2007).

1.6.4.2. Anti- excitotoxic function of APOE

In vitro and in vivo studies have shown that APOE is involved in the modulation of excitotoxicity and this in an isoform- dependent manner. For instance, an excitotoxic kainic acid intra- amygdalar administration in rats induces APOE mRNA and protein up-regulation in neurons as evidenced 7 days post- injury (Montpied et al., 1999; Boschert et al., 1999). These results have been confirmed in vitro using organotypic cultures, where kainite acid treatment is found to increase APOE mRNA expressions by 72% (Montpied et al., 1999). In vitro exposure of primary neural culture and a neuronal cell line to a human recombinant APOE prior to NMDA- induced excitotoxic challenge partially reduces cell death (Aono et al., 2002). Subsequent in vitro experiments have determined that APOE modulates excitotoxicity by its direct binding to LDL- R receptors modulating Ca^{2+} influx through the NMDA receptors (Bacskai et al., 2000, Qiu et al., 2002). These preclinical findings have been confirmed by preclinical and clinical studies. After intracerebral kainite injection, human APOE3 transgenic animals show significantly reduced lesion size in comparison with human APOE4 transgenic mice (Buttini *et al*., 1999). In humans, APOE4 carriers show poorer functional and pathological outcome after traumatic brain injury- a neurological disorder characterized by increased levels of excitotoxicity (Chiang et al., 2003; Yi and Hazell, 2006). APOE4 traumatic brain injury patients also develop more severe white matter pathology and cognitive deficits in comparison with APOE2 and APOE3 carriers (Ariza et al., 2006).

1.6.4.3. Anti- oxidative function of APOE

APOE has been associated with oxidative stress mainly because of its effects on neuropathology and functional outcome in different neurological and neurodegenerative conditions. Young APOEKO mice (6 months old) have been found to have 2 fold greater total protein oxidation in the hippocampus in comparison with age- matched WT controls and this level of protein oxidation is similar to the one observed in aged WT and APOEKO deficient mice (18 months). Absence of significant differences in protein oxidation has been observed between the old APOE deficient and age- matched WT mice (Choi et al., 2004). These results demonstrate an impaired oxidative modulation in young APOE deficient mice which might impact on their neuropathological and functional

outcome after injury to the central nervous system. Indeed, APOE deficient mice show an inadequate oxidative response after experimental head trauma associated with a poor neurological outcome (Lomnitski et al., 1999). Further in the same study, using an in vitro system it has been found that human recombinant APOE3 is able to modulate the oxidative effects of Cu^{2+} - induced lipid peroxidation. Additionally, pretreatment of APOE deficient mice with the anti- oxidant vitamin E significantly reduces ischemic damage after experimental infarction (Kitagawa et al., 2002). Infusion of recombinant APOE in APOE deficient mice significantly reduces free radical levels following global ischemia (Horsburgh et al., 2000a). These in vivo results have been confirmed in vitro. Specifically, recombinant APOE and APOE conditioned media prevent peroxide free radical induced cytotoxicity in vitro in an isoform- dependent manner APOE2> APOE3> APOE4 (Miyata and Smith, 1996). Interestingly, similar results have been reported in a postmortem study on brain tissue samples from Alzheimer`s patients showing the same gradient of APOE-isoform susceptibility to oxidation (APOE2> APOE3> APOE4) (Jolivalt et al., 2000). The in vivo and in vitro data on APOE demonstrates that this apolipoprotein has anti-oxidative properties and APOE deficiency can impact on neuropathology via impaired anti- oxidative defenses.

1.6.4.4. Immunomodulatory function of APOE

APOE has also been studied in relation to its immunomodulatory properties due to its implication in various neurological and neuropathological disorders (Laskowitz et al., 1998). In vivo studies have demonstrated that APOEKO mice exhibit increased TNFα and IL6 mRNA levels after lipopolysaccaride (LPS) venous injection compared to WT controls. These results have been confirmed in vitro where mixed glial cultures prepared from APOE deficient mouse pups express higher TNFα, IL1-β, and IL6 mRNA levels after LPS treatment (Lynch et al., 2001). Pretreatment of APOE deficient mixed neuronal-glial cultures with human recombinant APOE blocks glial secretion of TNFα after LPS stimulation (Lynch et al., 2001). APOE has also been shown to modulate microglial nitric oxide (NO) synthesis and this in an isoform- specific manner. In vitro studies using peritoneal and brain macrophage (microglia) from human APOE3 and human APOE4 transgenic mice show that significantly higher NO levels are produced by APOE4

microglia in comparison with APOE3 cultures (Colton et al., 2002). Similar results have been observed in monocyte- derived macrophages from human APOE3 and human APOE4 carriers. Human APOE4 macrophages produce significantly more NO than human APOE3 macrophages (Colton et al., 2002). Increased inflammatory levels are observed in many brain disorders such as multiple sclerosis and Alzheimer` s disease and for these conditions a significantly increased inflammatory levels are evidenced for APOE4 carriers corresponding with the accelerated disease progression in these individuals (Fazekas et al., 2005).

1.7. Epigenetics

Epigenetics (from Greek *επί*- above genetics) is defined as changes in gene expression in the absence of alterations in the underlying DNA sequence. The term epigenetics was first introduced by Waddington in 1942 in an attempt to describe the evolutionary perspective of gene- environment interactions, but he had no scientific idea of the molecular aspects of the phenomenon (Waddington, 1942). Over the last decades a substantial insight has been gained in epigenetic mechanisms, namely methylation, hydroxymethylation, histone acetylation, histone deacetylation, microRNAs. These epigenetic marks have been shown to regulate gene expression during early mammalian development as well as in adults (Bird, 2002; Hernandez et al., 2011). Epigenetic changes have been associated with many neurodevelopmental, neurodegenerative, cerebrovascular, and psychiatric conditions (Mehler, 2008).

1.7.1. DNA methylation

DNA methylation is one of the major epigenetic mechanisms in eukaryotic cells associated with transcriptional repression (gene silencing) (Bird, 2002). Inversely, hypomethylation of regulatory elements correlates with transcriptional activity (gene expression). Methylation was first discovered in calf thymus in 1948 by Hotchkiss (Hotchkiss, 1948) and confirmed two years later by Wyatt (Wyatt, 1951). However, 5-methylcytosine (5mC) role in gene regulation was first proposed in 1975 (Holliday and Pugh, 1975; Riggs, 1975) and accumulative supporting evidence has been gathered over the years. This epigenetic mark occurs mostly at the 5 position of cytosine by the transfer

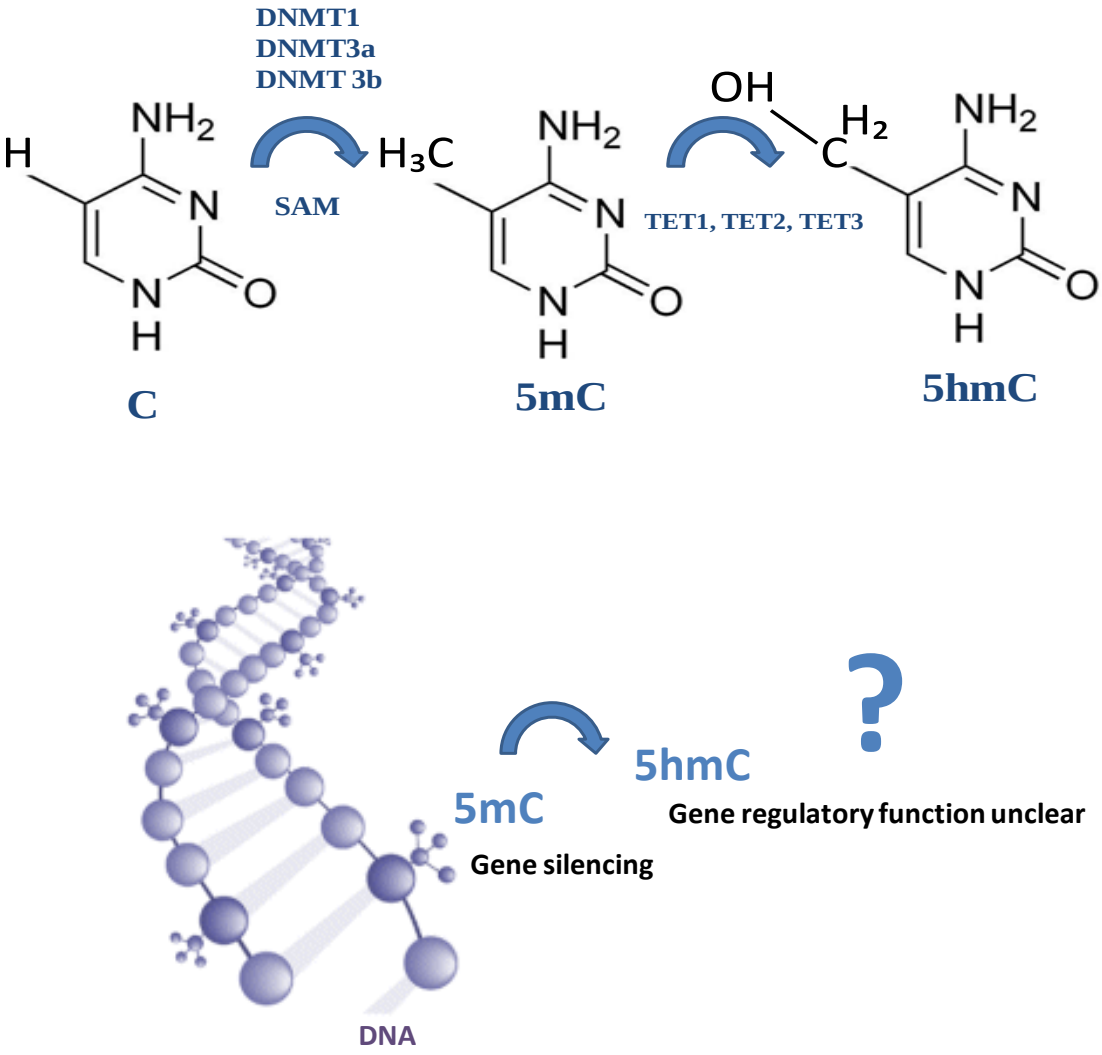

Figure 1.5.: Methylation and hydrohyxmethylation

5mC is an epigenetic mark resulting from the transfer of a methyl group (CH_3) from S-adenosylmethionine (SAM) to C- a reaction dependent on the activity of DNMT1, DNMT3a, DNMT3b. 5mC is primarily associated with transcriptional repression. 5hmC is a newly discovered epigenetic mark resulting from the oxidation of 5mC- a reaction catalyzed by the TETs. The exact gene regulatory role of 5hmC is still unclear. Although both methylation and hydroxymethylation have been associated with age- related neurodegeneration, nothing is known about the effects of these two epigenetic marks on white matter integrity under both normal physiological and chronically hypoperfused conditions.

of a methyl group (CH_3) from S- adenosylmethionine (SAM) to cytosine (C) producing 5mC (figure 1.5.). In the mammalian genome approximately 4% of C is methylated and it is predominantly found in the context of 5`- cytosine phosphate guanine- 3` (CpG) dinuclotides. Between 60- 90% of all CpG in the mammalian genome are methylated and they are transcriptionally inactive. However, the rest of the CpG (called CpG islands) remain non- methylated and they are closely associated with active transcriptional activity. In mammals methylation patterns are maintained by the enzymatic activity of DNA methyltransferase (DNMT). Absence of DNMT will result into two non- methylated daughter strands during replication and this would be associated with passive demethylation. Three DNMTs with a different functional activity have been identified in mammals: DNMT1, DNMT2, DNMT3a and 3b. DNMT1 is involved in the maintenance of methyltransferase activity during the S phase of cellular replication because of its preference for hemimethylated DNA as compared with non- methylated DNA (Yoder et al., 1997). DNMT2 has no detectable methyltransferase activity (Okano et al., 1998). DNMT3a and 3b are methyltransferases regulating the set up of *de novo* DNA methylation patterns during early mammalian development (Okano et al., 1999). Methylation can impact on gene transcription by 1) impeding transcription factors from binding to their promoters or 2) binding of specific transcriptional inhibitory proteins to methylated DNA such as methyl-CpG-binding domain proteins (MBDs) and methyl-CpG-binding protein 2 (MeCP2). Additionally, chromatin modifiers such as histone deacetylases (HDACs) are recruited by MBDs leading to complex methylation- deacetylation process, compact chromatin structure and transcriptional repression at heterochromatic genomic regions (Nan et al., 1998). Mutation in MeCP2 gene is the major cause of Rett syndrome- the most common form of mental retardation in females showing a role of methylation during neurodevelopment (Amir et al., 1999). Further, methylation of neural specific genes governs neuronal vs. glial fate specification during early neurodevelopment. Specifically, hypermethylation of the GFAP promoter is associated with predominantly neuronal cell fate, whereas hypomethyaltion of the GFAP promoter triggers glial differentiation (Okada et al., 2008).

DNA demethylation also occurs and it involves at least two established mechanisms (Wu and Zhang, 2010). Demethylation is associated with a functional deficiency of one or

more DNMTs leading to an absence of newly methylated DNA during replication or inefficient maintenance of established methylation patterns (Yoder et al., 1997; Okano et al., 1999). The second mechanism involves DNA demethylases such as 5mC DNA glycosylase (5-MCDG) and requires RNA for its demethylation function (Zhu, 2009). Further, one of the MBDs- MBD4 has also been shown to act as a demethylase similar to 5- MCDG (Zhu et al., 2000). Recent reports suggest that the newly discovered epigenetic mark 5 hydroxymethylcytosine (5hmC) (Chapter 1, section 1.7.2.) might also participate in DNA demethylation machinery by its DNA glycosylase function leading to replacement of 5mC with C (Cannon et al., 1988).

1.7.1.1. DNA methylation, age- related neuropathology and cerebrovascular disease

DNA methylation patterns are not fixed and they change with aging in a complex fashion due to the specific cellular and molecular environment of the aging mammalian organism. A recent study has demonstrated that 5mC distribution on CpG islands in frontal and temporal cortex, cerebellum, and pons from neurologically intact humans (from 1 to 102 years of age) increases significantly with chronological age and it is most likely associated with a transcriptional repression (Hernandez et al., 2011). However, results from other published work suggest that age- related changes in brain methylation are disease- and gene- specific (Tohgi et al., 1999; Wang et al., 2008; Mastroeni et al., 2009; Mastroeni et al., 2010). Data from studies on homozygote twins with discordant Alzheimer`s disease have shown that the twin suffering from Alzheimer`s disease exhibited significantly decreased 5mC immunoreactivity in the temporal cortex than his cognitively intact twin brother (Mastroeni et al., 2009). Further global DNA hypomethylation was observed in the enthorhinal cortex of Alzheimer`s patients (the cerebral region where the first signs of neurodegeneration are observed) in comparisons with controls (Mastroeni et al., 2010). There is increasing evidence that the promoter region of the APP gene is significantly demethylated after the age of 70 which might be associated with the deposition of Aβ in the aging brain (Tohgi et al., 1999). Interestingly, the APOE regulatory sequence in the prefrontal brain tissue and in the peripheral lymphocytes was significantly hypermethylated in Alzeheimer`s patients (Wang et al., 2008). Several mechanisms have been proposed to impact on DNA methylation in the aging brain such as altered DNMTs

expression or function, increased oxidative stress and free radical species as well as environmental factors such as diet and drugs. For instance, comparison of DNMTs and MeCP2 protein mRNA expression with aging in the brains of control and DNMT1 heterozygous KO mice an age- dependent decrease in MeCP2 in the control but not the KO brain was observed suggesting that a decrease in MeCP2 associated with histone deacetylation might be parallel to changes in 5mC genomic content in the aging brain (Bird and Wolffe, 1999). Further, an increase in 8- hydroxyguanine free radical levels induces not only DNA damage, but it is also associated with impaired methylation as 8-hydroxyguanine profoundly alters the methylation of adjacent C (Cerda and Weitzan, 1997). A diet deficient in vitamin B is associated with increased methylation and accelerated neurodegeneration in Alzheimer` s and Parkinson` s disease (Duan et al., 2002; Kruman et al., 2002). Altered methylation has been reported to occur in age- related cerebrovascular conditions such as atherosclerosis and stroke (Post et al., 1999; Endres et al., 2000; Endres et a., 2001; Westberry et al., 2008). For instance, a hypermethylation of the estrogen receptor α (ERα) has been evidenced in vascular tissue (arteries and veins) of human patients with clinically diagnosed atherosclerosis (Post et al., 1999). These results suggest that methylation plays a role in the development of age- related cerebrovacular changes. Further, stroke is a common neurological condition occurring in middle- aged and aged patients. Severe oxygen and glucose reductions to the brain are associated with global genomic hypermethylation and an increase in DNA methylation results in a more severe ischemic injury (Enders et al., 2000). This data is confirmed by preclinical studies where DNMT heterozygous mutants have reduced ischemic damage in the cortex and the striatum after transient middle carotid occlusion (a model of focal ischemia) (Enders et al., 2000; Enders et al., 2001). Interestingly, in a rat model of stroke, a sex- specific alteration in ERα methylation patterns are observed, specifically ERα gene promoter was hypomethylated in female, but not in male rats (Westberry et al., 2008). However, in this particular study the authors did not provide information on the association between ERα methylation patterns and the pathological/ functional outcome after stroke. So far, nothing is known about the role of methylation in the development of age- related white matter pathology and how changes in methylation could impact on cognition in elderly.

1.7.2. DNA hydroxymethylation

5- Hydroxymethylcytosine (5hmC) was first discovered in 1952 in bacteriophages (Wyatt and Cohen, 1952). In the mammalian genome 5hmC was described for the first time in 1972 when Penn et al. reported that 5hmC constitutes about 15% of total C in DNA in brains of adult rats, mice and frogs (Penn et al., 1972). However, as this finding could not be reproduced by others (Kothari et al., 1976), 5hmC received only limited attention over the next 30 years until 2009 when Kriaucious and Heintz rediscovered 5hmC in Purkinje neurons and granule cells of the adult mouse cerebellum (Kriaucious and Heintz, 2009) (figure 1.5.). 5hmC is produced by oxygenation of 5mC- an oxygen- dependent reaction catalyzed by the Ten- Eleven Translocation protein family (TET1, TET2, TET3) (Tahiliani et al., 2009; Ito et al., 2010) (Chapter 1, section 1.7.3.). At the difference from 5mC which is equally distributed in differentiated and undifferentiated cells, 5hmC shows lineage specific genomic distribution (Kinney et al., 2011; Ruzov et al., 2011). Specifically, 5hmC is high in embryonic stem cells, but it decreases with cell maturation (Globish et al., 2010; Ito et al., 2010; Ficz et al., 2011; Kinney et al., 2011; Ruzov et al., 2011). In adult mammalian organisms 5hmC is low or absent in most somatic tissues (kidney, heart, spleen, muscle, liver, intestine), but it is highly enriched in brain where it constitutes about 0.6% and 0.4% of the total DNA nucleotides in Purkinje neurons and granule cells respectively (Kriaucious and Heintz, 2009; Globish et al., 2010; Li and Liu, 2011; Kinney et al., 2011; Ruzov et al., 2011). So far, nothing is known about 5hmC content in other neural cell types (e.g. glia). Using a selective genome- wide labeling of 5hmC in mouse cerebellum at different stages of neurodevelopment it has been found that brain hydroxymethylation gradually increases from postnatal day 7 (~0.1% of total nucleotides in the genome) to adult stage (~ 0.4% of total nucleotides) (Song et al., 2010). These results suggest that this new epigenetic mark might play an important role during neurodevelopment. A further comparison of 5hmC content in adult cerebellum of 10 months old male and female mice has revealed an absence of sex differences in its genomic distribution (Song et al., 2010). Little is known about the functional role of 5hmC in the central nervous system. Recent studies on human frontal lobe tissue using deep genome sequencing as well as studies on mouse embryonic stem cells have demonstrated that 5hmC is particularly enriched at euchromatin rich genomic regions and it is most

likely to be involved in facilitation of gene expression (Ficz et al., 2010; Jin et al., 2011). Other reports suggest a role of 5hmC in active DNA demethylation and base excision mechanisms, but none of these has been fully proven yet (Surani and Hajkova, 2010). These hypotheses are based on findings showing that 5hmC prevents DNMT1- mediated methylation of the target C which will interfere with the methylation maintenance during cell replication and may lead to passive demethylation (Tahiliani et al., 2009). Further, on the basis of a previous identification of 5hmC- specific glycosylase activity it has been suggested that 5hmC might be a key intermediate of active demethylation involving DNA repair mechanisms (Cannon et al., 1988). Interestingly, methyl- CpG- binding proteins including MBD1, MBD2, MBD4 and MeCP2 have reduced affinity for 5hmC which might have a direct impact on the transcription of genes with enriched 5hmC content at their regulatory sequences (Valinluck et al., 2004; Jin et al., 2010). Our group and others have recently discovered that the process of active demethylation of the paternal pronuclei in the zygote coincides with high hydroxymethylation (Iqbal et al., 2011; Ruzov et al., 2011; Wossidlo et al., 2011).

1.7.2.1. DNA hydroxymethylation and age- related neuropathology

The initial study reporting the presence of 5hmC in adult brain failed to show changes in 5hmC cerebellar content with age (Kriaucious and Heintz, 2009). However, applying a new 5hmC genome- wide labeling approach it has been found that intragenic 5hmC genomic content increases in adult mouse cerebellum with age and it is associated with an increased expression of genes related to neuropathology (Song et al., 2010). Specifically, 5hmC intragenic increase is associated with genes involved in Alzheimer`s, Huntington`s, Parkinson`s disease as well as with angiogenesis and hypoxia. However, nothing is known about the functional importance of 5hmC increase with neurdegeneration and future studies should try to elucidate 5hmC role in both the healthy and diseased mammalian brain.

1.7.3. Ten- Eleven- Translocation proteins (TETs)

The Ten- Eleven Translocation protein family includes three members (TET1, TET2, TET3) all having the capacity to catalyze the conversion of 5mC to 5hmC in a 2-oxoglutarate- and Fe(II)- dependent manner (Tahiliani et al., 2009; Ito et al., 2010) (figure 1.5.). So far, all three TETs have been extensively studied in mouse and human embryonic stem cells as well as in different types of myeloid cancers, but little is known about the distribution and functional significance of these proteins in the central nervous system (Tahiliani et al., 2009; Ito et al., 2010; Ko et al., 2010; Ficz et al., 2011; Ruzov et al., 2011). In consistency with 5hmC high genomic content, all three TETs have been shown to be expressed in mouse embryonic stem cells as well as in human embryonic stem cells- derived neural stem cells (Ruzov et al., 2011). However, at the difference from mouse embryonic stem cells, human embryonic stem cells express only TET1 and TET3 at least at the mRNA level (Ruzov et al., 2011). These data suggest important species differences in the expression of these proteins implicating potential functional differences. TET family members are differentially expressed in mouse tissues with TET2 being the most widely expressed (including brain). At the functional level, both TET1 and TET2 are important regulators of mouse embryonic stem cells self- renewal and pluripotency (Ficz et al., 2011; Ito et al., 2010). Double knockdown of TET1 and TET2 is associated with a down- regulation of pluripotency genes and an increase in methylaiton of their promoters in mouse embryonic stem cells (Ficz et al., 2011). Most of the mutant embryonic stem cells differentiate predominantly into extraembryonic tissue (trophectoderm) (Ficz et al., 2011). Under normal conditions, a decrease of hydroxymethylation is evidenced at the level of pluripotency genes during mouse embryonic stem cells differentiation. Natural TET2 mutation is observed in some human patients with myeloid cancers (Ko et al., 2010). In these individuals, low 5hmC content accompanied by hypomethylation is evidenced in bone marrow suggesting that TET2 is involved in DNA demethylation potentially via hydroxymethylation- dependent mechanism. Nothing is known about TETs functional role in the central nervous system in health and disease (e.g. chronic cerebral hypoperfussion).

1.8. Thesis aims

The major aim of the present thesis was to experimentally study the effects of single etiological factors as well as their interactive effects on white matter integrity and cognitive abilities in mice. An attempt was made to translate the findings to humans and a specific focus was given to cerebrovascular (chronic cerebral hypoperfusion), genetic (APOE) and epigenetic (methylation and hydroxymethylation) mechanisms with known or suspected impact on white matter integrity and cognition in elderly people.

The specific aims of the present thesis were to:

- Determine the effects of hypoperfusion- induced white matter pathology on cognitive and memory abilities in mice.

- Investigate the effects of APOE on white matter integrity under normal physiological and chronically hypoperfused conditions in mice.

- Characterize methylation and hydroxymethylation in white matter under normal physiological and chronically hypoperfused conditions in mice.

Chapter 2

Materials and methods

2.1. Animals

All animal procedures were carried out in accordance with the United Kingdom Animals (Scientific Procedures) Act 1986.

All mice were group- housed in transparent Plexiglas cages (20 x 30 x 20 x 30 cm) and kept at the laboratory animal facilities under standard laboratory conditions. The humidity, the ambient temperature (22ºC) as well as the light/ dark cycle (14h light/ 10h dark) in the animal facility were maintained constant during the entire experimental period. Food and water were provided *ad libitum*. After chronic cerebral hypoperfusion, all animals were fed with a mashed chow during the first post- surgery week composed of normal mouse chow dissolved in water to facilitate food intake and prevent weight loss. Food restriction was applied for the purposes of the radial arm maze experiment (Chapter 3). The food restriction procedure started one week prior to the behavioural testing and was maintained until the end of the experiment in order to reduce the weight of the animals to 85- 90% from their original one. During the first week of food deprivation the animals were introduced to the flavour of the reward pellets (Bio- Serve, UK) used for the radial arm maze task.

2.1.1. C57Bl6J mice

Male adult C57Bl6J mice (Charles River, UK) were used for the purposes of this thesis. The C57Bl6J is the most commonly used inbred mouse strain in research. It is also a background strain for the majority of the existing genetically modified mouse lines.

2.1.2. APOEKO mice

The APOEKO mice used for the purposes of this thesis were purchased from Charles River, UK. The APOE deficient mice were generated as described in Piedrahita et al., 1992. The targeted deletion of the APOE gene was achieved by a targeting plasmid via homologous recombination in 129J embryonic stem cells. The selected APOE deficient embryonic stem cells were subsequently microinjected into blastocysts reintroduced into the uteri of pseudopregnant C57Bl6J mice. Heterozygous and homozygous F1 chimeric mice were born at the expected Mendelian frequency. Using immunodiffusion test, it was confirmed that the generated homozygous animals were unable to synthesize APOE. The

F1 APOEKO homozygous mice were backcrossed for six generation to C57Bl6J mice in order to derive the APOEKO line used for this study (Piedrahita et al., 1992).

2.2. Chronic cerebral hypoperfusion

Mice were anaesthetized with 5% isofluorane in 95% O_2 and anesthesia was maintained during the entire surgical procedure. Chronic cerebral hypoperfusion was induced by the bilateral application of piano microcoils (0.18mm internal diameter; Sawane Spring Co.) to the common carotid artery (Coltman et al., 2011; Holland et al., 2011). During surgery, body temperature was maintained between 36.5°C - 37°C. To prevent an acute reduction of the cerebral blood flow due to the simultaneous application of microcoils to both common carotids, a 30min period was left between the application of each microcoil during which the animal was placed in an incubator at 32°C in order to prevent hypothermia. Sham-operated mice underwent exactly the same surgical procedure except that microcoils were not applied to the common carotid arteries. The post- surgery recovery of the mice was closely monitored. Their eating and drinking activities as well as signs of overt neurological dysfunction (eg. circling, rolling, hunching, seizures) were recorded. Any mouse which exhibited a poor recovery including $\geq$ 20% loss of the pre-surgery body weight was culled. The animals which did not survive the entire prescribed experimental period were excluded from the subsequent data analysis. The surgeries for the experiments described in my thesis were kindly performed by Dr. Karen Horsburgh (the first radial arm maze and the water maze experiments, Chapter 3), Dr. Catherine Gliddon (experiments, Chapter 4, Chapter 5), and Dr. Phillip Holland (the second radial arm maze experiment, Chapter 3).

2.3. Behavioural tests

Prior to all behavioural procedures, the animals were handled by an experimenter for 5 days. During the training period the mice were transported every day to the experimental room 30min before the actual start of the behavioural test. Due to the large experimental numbers, the behavioural experiments described in my thesis were performed with the help of Jessica Smith (all tests), Aisling Spain (the first radial arm maze experiment; the water maze experiment), Robin Coltman (the first radial arm maze experiment), Dr Gillian

Scullion (the second radial arm maze experiment). All behavioural tests were performed blindly to the treatment (sham vs. hypoperfusion) of the animals.

2.3.1. Vision test

Preliminary studies in our laboratory showed that chronic cerebral hypoperfusion induces pathological damage to the myelin sheath and neuronal axons in the optic tract. Therefore, the visual abilities of the animals from the first radial arm maze experiment were tested at three different time points: 1) 3 days prior to surgery (control baseline level), 2) 6 days before the behavioural testing (24 days after surgery), and 3) at the end of the behavioural testing (50 days after surgery).

2.3.1.1. Principle and apparatus

The vision test is based on the principle that a mouse with an intact vision will move its entire head into the direction of a moving visual stimulus (figure 2.1. A).

The apparatus was the same as the one described in Thaung et al., 2002 and it was placed in an experimental room with ambient lighting. The apparatus consisted of a motorized drum, 30.5 cm in diameter and 54.5 cm in height, which could rotate at 2 revolutions per minute (rpm) clockwise and counterclockwise. A stationary circular metal platform (8.0 cm in diameter, situated at 20 cm above the bottom of the drum) was located at the interior of the drum. A black and white stripe card (2 degrees, 5.3 mm wide) was used as a pattern to test the visual acuity of the mice. The behavioral procedure was recorded by a camera fixed above the drum and connected to a video recorder.

2.3.1.2. Procedure

At the beginning of the test the mouse was left on the central platform for 5min to habituate to the apparatus. Afterwards, the drum was rotated for 60 sec clockwise, stopped for 30 sec (pause) and again rotated counterclockwise for another 60 sec. The head movement in the direction of the rotating stripes was considered a visual response. If an animal did not show a directional (head) response to the moving stripe pattern, it was retested in the following couple of days.

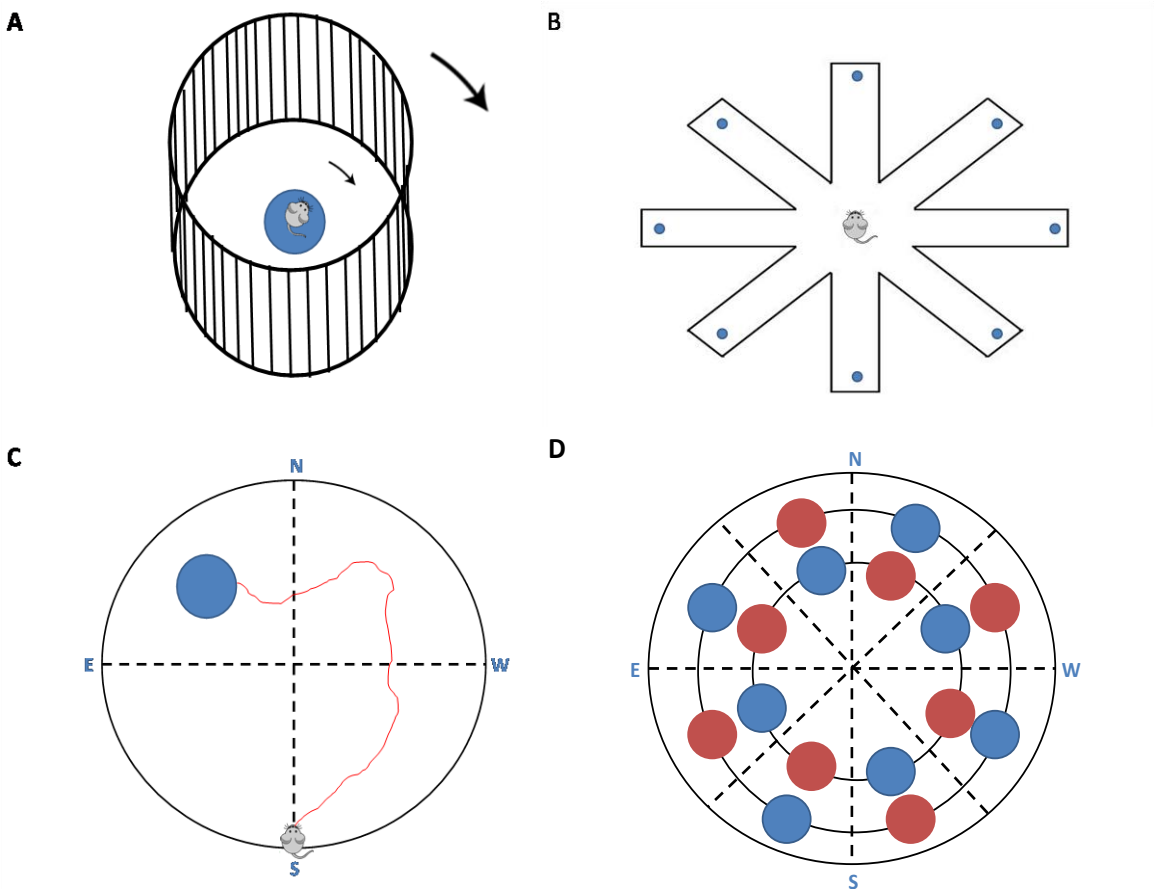

Figure 2.1.: Behavioral paradigms

A schematic representation of the applied behavioural paradigms.

The visual abilities of sham and hypoperfused mice were tested using a circular visual drum with automatically rotated visual pattern and a central circular platform on which the animal was placed during testing. The head movement into the direction of the moving visual pattern was considered a visual response (**A**). Spatial working memory was tested using an 8- arm radial arm maze paradigm where the animal had to learn to retrieve a food reward situated at the end of each of the 8-arms without revisiting previously visited arms (**B**). Spatial memory flexibility was challenged using a water maze apparatus (**C**) where the animal had to learn and remember 5 different spatial locations of a hidden escape platform for a set criterion (<20sec swimming latency to platform over 3 consecutive trials) when released from a different start point (S, N, E, W) on each trail. The spatial location of the hidden platform varied on virtual inner and outer ring in the water maze (**D**).

2.3.2. Spatial working memory task on a radial arm maze paradigm

2.3.2.1. Principle and apparatus

In the radial arm maze, a food deprived rodent (a mouse or a rat) has to learn and remember the spatial location (usually the end of one or all of the 8 maze arms) of a food pellet using intra and/ or extramaze environmental cues. Depending on the experimental protocol and the type of the cognitive function that is challenged, the number of pellets, the presence/ the absence of environmental spatial cues could vary. An indication of a successful learning and memory process on this behavioural paradigm is the rapid retrieval of all reward pellets in the absence of revisiting errors, the higher number of the new entries in the first 8 arm choices, the lower total number of arm entries and the shorter latency to complete the task.

The apparatus used for this study was a mouse version of the 8- arm radial maze which was first described by Olton and Samuelson, 1976 (figure 2.1. B). It was made of white plastic with Plexiglas arm walls. The diameter of the maze central platform was 20 cm. The dimensions of each of the 8 arms were 47 cm length/ 7 cm width/ 20 cm height. At the end of each arm was placed a white plastic well 3.5 cm in diameter and 2 cm deep. The maze was elevated 1m from the floor of the experimental room. A recording camera connected to a computer was fixed on the ceiling just above the central platform of the maze. The ongoing behavior of the animal during testing was distantly monitored by an experimenter using ANY- maze tracking software (Stoelting Co.). All experimental procedures were conducted in a dim- lit room provided with salient extra maze cues.

2.3.2.2. Procedures

2.3.2.2.1. Pretraining

Two pretraining days were scheduled before the real training procedure in order to familiarize the animals with the experimental environment, the apparatus and the task itself. On pretraining day 1, food pellets were scattered all around the maze and each animal was left to explore freely the maze for 5 min. On pretraining day 2, a food pellet

was placed at the end of each of the 8 arms. The mouse was placed at the distal end of each of the 8 arms of the maze and left to retrieve and consume the food pellet.

2.3.2.2.2. Training

During the training procedure, a food pellet was located at the end of all 8 arms. At the beginning of every trial (one trial/ training day) the animal was placed on the central platform. Once it had entered one of the 8 arms, the other 7 arms were closed automatically. When the animal exited the visited arm it was confined on the central platform for 5 sec. After the 5 sec delay the mouse was allowed to make a new arm choice. A trial was ended when the animal had retrieved all 8 pellets or 25 min had elapsed. For each trial, the number of novel arm entries within the first 8 arm visits, the total number of arm entries, the number of arm re- entries (the revisiting errors), and the trial latency were recorded.

2.3.3. Serial spatial learning and memory task an a water maze paradigm

2.3.3.1. Principle and apparatus

In the water maze, a rodent (a mouse or a rat) has to learn and remember the spatial location of a hidden escape platform using intra and/ or extramaze environmental cues (figure 2.1. C). The training procedure as well as the nature of the surrounding spatial environment could vary depending on the type of the cognitive function that is challenged. An indication of intact learning and memory processes on this behavioural paradigm is the rapid acquisition of the task (the platform location) and it is usually translated by a reduction of the swimming latency and the trajectory to the platform as well as a longer time spent swimming in the platform quadrant during probe trials (performed in the absence of the escape platform).

For this experiment, an open field water maze was used (Morris, 1984). The apparatus was a white metal tank (2.0 m diameter) filled with water (0.5 m depth, temperature 25 ± 1ºC) rendered opaque by the addition of 400mL liquid latex. A hidden escape platform (20 cm in diameter for the cue task; 13 cm in diameter for the serial spatial memory task) was positioned 1.5 cm below the water surface in one of the four virtual quadrants of the water

maze ((northeast (NE), northwest (NW), southeast (SE), southwest (SW)). All behavioural testing was conducted in the same experimental room provided with prominent extra maze cues and an appropriate level of diffuse lighting. For the cue task, white curtains were drawn around the pool to prevent the animals to use any distal cues during spatial navigation. A red plastic ball (10 cm in diameter) situated 20 cm above the platform was the only available landmark. The swimming behaviour of the animals was monitored by an automated tracking system (Watermaze) connected to a recording camera fixed in a position that allowed the viewing of the entire water surface. The animals were carried manually to the apparatus and placed in the water facing the tank wall. On each trial, the mouse was released from a randomly allocated start point ((north (N), south (S), east (E), west (W)) and allowed 90 sec to find the hidden platform. When on the platform, the mouse was left there for additional 30 sec. If the mouse had not found the escape platform within the allocated 90 sec it was guided to it by a paint roller moved on the water surface. The mouse was taken out of the water by allowing it to mount on the paint roller and then it was transferred to a standard cage placed under a heating lamp to avoid hypothermia.

2.3.3.2. Procedures

2.3.3.2.1. Cue task

As mice are not natural swimmers, their ability and motivation to swim were tested a day prior to surgery by using a cue task protocol in the water maze. Mice showing difficulties to swim or a floating behaviour were not included in the study. A month post- surgery, all experimental mice were trained again on the same task for 4 days prior to the beginning of the serial spatial learning and memory task in order to exclude any potential surgery effects on the swimming behaviour of the animals. For the correct performance of the cue task, the mice had to find a hidden escape platform in the absence of extra maze cues by navigating to a local landmark (a red ball) that was consistently associated with the hidden escape platform. The platform location was moved systematically from one trial to another. There were 4 trials per training day. The animal was released from a different start point (N, S, E, W) on each trial. The duration of an individual trial was 90 sec, but it was terminated as soon as the mouse had climbed on the platform. When on the platform, the animal was left there for 30 sec. If the mouse could not find the platform within the

allocated 90 sec it was guided to it by a paint roller and again left on the platform for 30 sec. On each training day, all four quadrants and all four start points were used.

2.3.3.2.2. Serial spatial learning and memory task

2.3.3.2.2.1. Training

The animals were trained on a serial spatial learning and memory task as described by Chen et al., 2000. This behavioural procedure consisted of 5 spatial reference memory tasks, each of them constituting a separate spatial problem. All tasks were performed in the same experimental environment (figure 2.1.D).

The mice had to learn the 5 separate spatial tasks for a period of 10 training days with a maximum of 32 trials per task (except task 1 for which the number of trials was 40). The platform location varied from one task to another on virtual inner (1m diameter) and outer (1.5m diameter) rings. For each task, there were 8 trials per day with 10 min intertrial interval. Each trial lasted 90 sec. An animal had learned one of the 5 spatial problems, when it reached a preliminary established criterion of an average escape latency of less than 20 sec over 3 consecutive trials. After this criterion had been reached, on the following experimental day, the animal was trained on the next spatial task. All animals were trained until they learned a minimum of 5 spatial tasks. The animals that learned easily the first 5 spatial tasks were trained up to 10 tasks.

2.3.3.2.2.2. Probe trials

Two probe trials (PT) were conducted in order to test the strength of the established memory for task 1 to task 5. The first PT was conducted 10 min (short- term recall) after the criterion had been reached, the second PT was 3h later (long- term recall). For the PTs, an automatically raised (Atlantis) platform was used (Spooner et al., 1994). The start points for the probe trials were counterbalanced among the mice. The platform was placed in the training quadrant and was unavailable for the animal during the first 60 sec of the trial. After 60 sec had elapsed, the platform was automatically raised and the animal was given additionally 30 sec to find it. If the mouse had not found the platform within 90 sec, it was guided to it and after 30 sec removed from the pool. For each PT, the percentage of

time the animal spent searching for the hidden platform in the training quadrant (during the first 60 sec of each PT), the swimming speed, the number of platform crossings, the percentage of time spent swimming near the pool walls (thigmotaxis) and the latency to the platform when it reappeared (during the last 30 sec of each PT) were recorded.

2.4. Transcardiac perfusion- fixation

At the end of each of the experiments included in this thesis, the animals were perfusion fixed. Prior to the perfusion- fixation procedure, the mice were deeply anesthetized with 5% isoflurane. An absence of a reflex response to a pinch on the hind limb was considered as a deeply anesthetized state. The anesthesia was maintained using a face mask during the procedure. The thoracic cage was widely open with surgical scissors in order to provide an access to the heart. Twenty ml 0.9% heparanized saline (NaCl) solution was infused at a speed of 2.1 ml/ min through the left cardiac ventricle and flushed with the vascular blood through the right cardiac atrium. Liver and spleen pallor was considered an indication of a successful removal of the blood from the body. Following this, a 20 ml 4% paraformaldehyde buffer (PFA) solution was infused through the vasculature at the same speed. The fixation was considered successful when the body was rigid at the end of the procedure. The brains were taken immediately out of the skull and immersed in 4% PFA for additional 24h fixation at 4°C prior to transfer in 0.1% phosphate buffer saline (PBS) where they were kept until paraffin embedding. For the ex vivo MRI experiments (Chapter 4), the whole mouse head was immersed in 4% PFA for two hours at room temperature (RT) before the brain was taken out of skull and left in 4% PFA overnight at 4°C prior to imaging.

2.5. Histology

2.5.1. Paraffin embedding

Brains were paraffin embedded manually as 3 mm thick coronal brain slices (Chapter 3) or automatically with a processor as whole brains (Chapter 4, Chapter 5). The 3 mm brain slices were cut using a mouse metal brain mould and sharp histological knives.

2.5.1.1. Processing of brain slices

The manually cut coronal brain slices were placed in individual plastic embedding cassettes labeled with the experimental number of the animal, washed under running water for 15min, dehydrated in increasing grades of ethanol (70% ethanol (2 x 30min), 90% ethanol (2 x 30min), 100% ethanol (2 x 30min)) and xylene (2 x 30min). Subsequently, the brain slices were processed in paraffin (3 x 30 min) at 60°C and left there overnight. On the following day, the brain slices were placed in metal moulds, embedded in fresh paraffin, left for 2h at RT and transferred to 4°C for 24h. Following this, the paraffin embedded tissue was stored at RT until requested for microtome cutting.

2.5.1.2. Processing of whole brains

The whole brains were placed in individual plastic embedding cassettes labeled with the experimental number of the animal and paraffin embedded using an automatic processor with 16h cycle programme: the tissue was dehydrated in increasing grades of ethanol baths (70% ethanol (1h); 85% ethanol (1h); 90% ethanol (1h); 100% ethanol (4 x 1h)) and xylene (3 x 1h). Brains were left in paraffin (3 x 3h) and finally automatically embedded in fresh paraffin. The paraffin tissue blocks were stored at RT prior to microtome cutting.

2.5.2. Microtome cutting

Six µm coronal brain sections were cut on a microtome from paraffin- embedded blocks. The neuroanatomical levels of interest were: 0.38 mm bregma, -2.12mm bregma (Chapter 3); 0.74 mm bregma, 0.38 mm bregma, -0.94 mm bregma, -2.12 mm bregma (Chapter 4) (Franklin and Paxinos, 1997) (figure 2.2. A-D). Special care was taken to preserve the intrahemispheric symmetry using a mouse brain atlas (Franklin and Paxinos, 1997) and major neuroanatomical landmarks. The brain sections were stretched in water (~ 40°C), mounted on poly- L- lysine coated glass slides and left to dry on a hot plate. The slides were stored in plastic boxes at RT until required for histological and immunohistochemical staining.

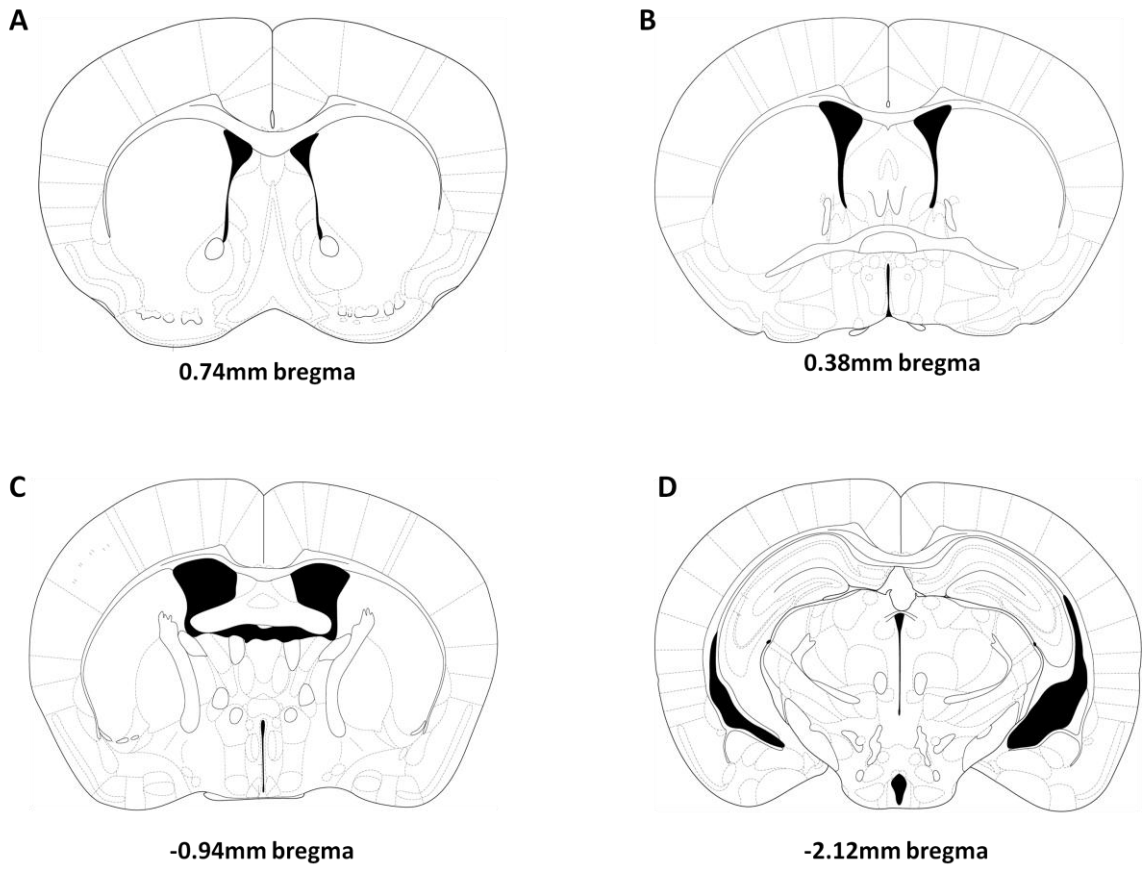

Figure 2.2.: Neuroanatomical levels at which the brains were microtome cut

A schematic representation of coronal brain sections from the neuroanatomical levels (Franklin and Paxinos, 1997) at which the brains were serially microtome cut.

For Chapter 3 the brains were microtome cut at levels 0.38mm bregma and -2.12mm bregma (**B, D**). For Chapter 4 the brains were microtome cut at levels 0.74mm bregma, 0.38mm bregma, -0.94mm bregma, -2.12mm bregma (**A- D**).

2.5.3. Haemotxylin and eosin (H&E)

Haemotxylin and eosin **(**H&E) histological staining was used for the examination of the overall brain morphology and the presence of neuronal ischemic damage. Haemotoxylin is a nuclear staining that stains in blue nucleic acids such as RNA. Eosin is a cytoplasmic staining that stains in light purple acidophilic elements such as the cytosol.

Brain sections were deparaffinized at 60°C for 30 min, cleaned in 2 x xylene (10 min; 5 min), rehydrated in decreasing grades of ethanol baths (100% ethanol (2 x 5 min); 90% ethanol (2 min); 70% ethanol (2 min)), washed under running water (2 min) and stained with haemotoxylin for 2 min (for 30 sec when haemotoxylin was applied for an immunohistochemical counterstain, Chapter 2, section 2.6.1.1.). Subsequently, the sections were washed under running water (2min), immersed in acidic alchohol (10 sec), washed under running water (2 min), immersed in Scots tap water solution (2 min), washed under running water (2 min), and stained with eosin (2 min). Brain sections were washed under running water (2 min), dehydrated in increasing grades of ethanol baths (70% ethanol (10 sec); 90% ethanol (2 min), 100% ethanol (2 x 5min) and xylene (15 min), and mounted on coverslips with DPX.

2.6. Immunohistochemistry

2.6.1. Avidin- biotin immunohistochemistry

The avidin- biotin based immunohistochemical approach developed by Hsu et al, in 1981 was used for the purposes of this thesis. The avidin- biotin method relies on the strong affinity (four binding sites) of avidin (a tetrameric protein derived from the white of avian, amphibian and reptile eggs) to the vitamin biotin (vitamin B7). The biotin molecule is easily conjugated to antibodies and enzymes. In the avidin- biotin immunohistochemical method, secondary antibody is conjugated to biotin and binds to the primary tissue antigen- bound antibody. The species in which the secondary antibody is raised determines the species of the serum used for blocking of the nonspecific binding sites performed prior to primary antibody application. During the primary- secondary antibody reaction, a biotinylated enzyme (horseradish peroxidase or alkaline phosphatase) binds to avidin and forms the avidin- biotin complex (ABC). The ABC

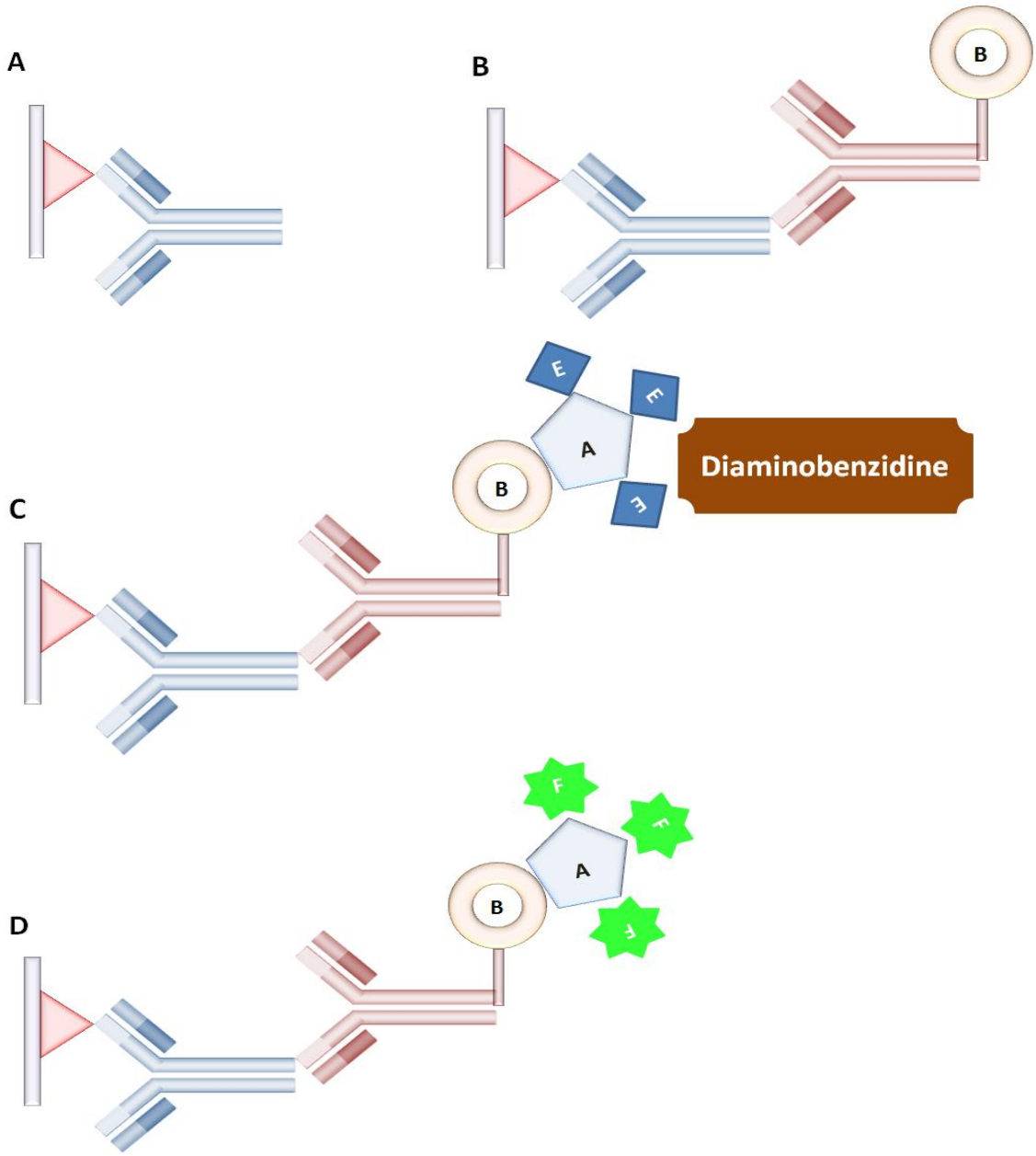

Figure 2.3.: Principles of immunohistochemistry

A schematic representation of the basic principle of a standard immunohistochemical procedure.

The primary antibody binds to its specific antigen (**A**). The biotinylated secondary antibody binds to the primary antibody (**B**). In the case of the peroxidase- based immunohistochemical procedure, the ABC diaminobenzidine complex binds to the secondary antibody allowing the visualization of the primary- secondary antibody reaction (**C**). In the case of the fluorescent immunohisto(cyto)chemistry, the secondary antibody is conjugated to a fluorochrome resulting in a fluorescent visualization of the primarimary- secondary antibody reaction (**D**).

reaction and by consequence the antigen of interest is revealed by the application of 3′3′-diaminobenzidine, tyramide or fluorochromes (figure 2.3.A-D).

For the experimental purposes of the present thesis, a negative control for all immunohistochemical staining was an omission of the primary antibody on a subset of samples.

The details of all primary and their respective secondary antibodies are given in table 2.1.

2.6.1.1. Peroxidase ABC based immunohistochenistry

Day1: Brain sections were deparaffinized at 60°C for 30 min, cleaned in 2 x xylene (10 min; 5 min) and dehydrated in 2 x 100% ethanol (10 min; 5 min). Endogenous peroxidase activity was blocked by incubation with 0.5% H_2O_2 in methanol at RT for 30 min. Sections were washed under running water for 15min. An antigen retrieval step consisting of microwaving the sections at high temperature with citric acid (pH6.0) for 10 min was applied for some of the antibodies. The sections were washed in PBS for 5min to normalize the pH. After the antigen retrieval a blocking step consisting of sample incubation with 10% normal serum was performed for an hour at RT in humidified chambers. All primary antibodies were diluted in 10% normal serum at their specific optimal dilution (table 2.1.). The brain sections were incubated with primary antibody in humidified chambers overnight at 4°C.

Day 2: Primary antibody was washed 3 x PBS (5 min/ each). Secondary antibody diluted (1:100) in PBS was applied on the sections for an hour at RT in humidified chambers. After 3 x PBS washes (5 min/ each) the sections were incubated in an avidin- biotin complex enzyme solution (ABC kit, Vector laboratories, UK) for an hour at RT in humidified chambers. After 3 x PBS washes (5 min/ each) an incubation with 3, 3-diaminobenzide tetrachloride solution (DAB) (Vector laboratories, UK) was performed for 2 min in order to visualize the antigen of interest (in brown colour). Subsequently, the sections were washed under running water for 10 min. A haemotxylin counterstain was performed for some stainings (Iba1; MAG) as described in Chapter 2, section 2.5.3. At the end of the procedure the sections were dehydrated into increasing grades of ethanol baths

(70% (2 min), 90% (5 min), 100% (2 x 5 min)), washed in xylene for 15 min and mounted on glass coverslips with DPX.

2.6.1.2. Fluorescent immunohistochemstry

Day 1: The procedure was exactly the same as for the peroxidase ABC based immunohistochemistry day 1 described in Chapter 2, section 2.6.1.1.

Day 2: Primary antibody was washed 3 x PBS (5 min/ each). The sections were incubated with secondary antibody (1:200) diluted in 10% normal serum for an hour at RT in humidified chamber. After 3 x PBS washes (5 min/ each), the sections were incubated with DAPI (1:1000) in 0.1% PBS for 10 min at RT in humidified. The DAPI was washed 3 x PBS (5 min/ each) and the sections were covesliped with Fluoromount solution (Sigma, UK). Immunofluorescent samples were covered with aluminum folio to prevent bleaching and stored at 4°C until imaging.

2.6.1.3. DNA fluorescent immunohistochemistry

Day 1: Brain sections were deparaffinized at 60°C for 30 min, cleaned in 2 x xylene (10 min; 5 min) and dehydrated in 2 x 100% ethanol (10 min; 5 min). Endogenous peroxidase activity was blocked by incubation with 0.5% H_2O_2 in methanol at RT for 30 min. Sections were washed under running water for 15 min. Cell membranes were permeabilized by incubation in 1% Tryton- X in 0.1% PBS solution for 30 min at RT (for immunocytochemistry this was the first step of this protocol). Subsequently, the DNA was denaturated by 4M hydrochloric acid (HCL) treatment at 37°C for an hour. After 5 x 0.1% Tween washes (5 min/ each), a blocking step was performed by sample incubation with 10% fetal calf serum (FCS) for an hour at RT in humidified chambers. Following this, the primary antibodies ssDNA, 5mC or 5hmC were diluted in 10% FCS at their optimal dilution (table 2.1.) and the tissue/ cell samples were incubated at 4°C overnight in humidified chambers.

Day 2: Primary antibodies were washed in 5 x 0.1% Tween solution (5 min/ each) and the corresponding secondary antibodies (1:200) (table 2.1.) diluted in 10% FCS were

Primary antibody *manufacturer*	**Target**	**Dilution**	**Secondary antibody** *manufacturer*	**Dilution**	**Hydrochloric acid**	**Citric acid**	**Chromogen** *manufacturer*
Mouse monoclonal APP *Millipore*	axons	1:1000	**Horse anti- mouse** *Invitrogen*	1:100	no	yes	Peroxidase ABC kit *Vector laboratories*
Goat polyclonal MAG *Santa Cruz*	myelin	1:500	**Horse anti- goat** *Invitrogen*	1:100	no	no	Peroxidase ABC kit *Vector laboratories*
Rabbit polyclonal dMBP *Millipore*	degraded myelin	1:300	**Goat anti-rabbit** *Invitrogen*	1:100	no	yes	Peroxidase ABC kit *Vector laboratories*
Rabbit polyclonal Iba1 *Biocare medical*	microglia	1:750	**Horse anti- rabbit** *Invitrogen*	1:100	no	yes	Peroxidase ABC kit *Vector laboratories*
Rat monoclonal 5hmC *Diagenode*	5hmC	1:1000	**Chicken anti- mouse** *DAKO*	1:200	yes	no	Tyramide *Perkin Elmer*
Mouse monoclonal 5mC *Eurogentec*	5mC	1:200	**Chicken anti- mouse** *DAKO*	1:200	yes	no	Tyramide *Perkin Elmer*
Rabbit polyclonal ssDNA *Zymo research*	ssDNA	1:200	**Donkey anti- rabbit** Alexa 555 *Invitrogen*	1:200	yes	no	
Rabbit polyclonal TET2 *Santa Cruz*	TET2	1:50	**Donkey anti- rabbit** Alexa 555 *Invitrogen*	1:200	no	no	
Mouse monoclonal CC1 *Calbiochem*	mature oligodendrocytes	1:50	**Chicken anti- mouse** *DAKO*	1:200	no	yes	Tyramide *Perkin Elmer*
Rabbit polyclonal NG2 *Millipore*	OPC	1:50	**Donkey anti- rabbit** Alexa 555 *Invitrogen*	1:200	no	yes	

Table 2.1.: Primary and secondary antibodies, their manufacturer, cellular target, optimal dilution and specifics of the immuno(cyto)histochemical procedure

applied for an hour at RT in humidified chambers. After 5 x 0.1% Tween washes (5 min/ each) the samples were incubated with tyramide solution (Perkin Elmer, USA) for 15 min at RT in humidified chambers. The tyramide was washed 5 x 0.1% Tween solution (5 min/ each) and the samples were mounted on glass coverslips with Fluoromount solution (Sigma, UK). Immunofluorescent samples were covered with aluminum folio to prevent bleaching and stored at 4°C until imaging.

For DNA immunocytochemical staining of oligodendroglia (Chapter 2, section 2.10.) and microglia (Chapter 2, section 2.11.) cells exactly the same staining procedure was applied at the exception of the tissue specific deparaffinization, dehydration and blocking of endogenous peroxidase activity. For immunocytochemistry, the 5hmC immunostaining protocol begins with an immediate cell membrane permeabilization with 0.1% Triton X solution of 4%PFA fixed cells.

2.7. Pathology assessment

2.7.1. Light microscopy

Neuronal perikarya ischemic damage, white matter pathology (myelin and axonal integrity) as well as inflammatory activity were examined using an inverted light microscope (Leica). Images of the corresponding pathology were taken using Quick capture software and a camera connected to a computer.

2.7.2. Neuroanatomical regions of interest

The neuroanatomical regions of interest (ROIs) examined in this thesis were major white matter tracts (the CC, EC, and IC). The Fx and OT were also examined in the studies presented in Chapter 3 and Chapter 4 (figure 2.4.B) Grey matter ROIs were the hippocampus, the striatum and the cortex (Cx) (figure 2.4.A, B).

2.7.3. Grey matter integrity and neuronal perikarya ischemic damage

The overall tissue morphology and neuronal perikarya ischemic damage were assessed on H&E stained brain sections in cortical and subcortical grey matter regions. Ischemic and non ischemic neurons were identified on the basis of their cellular morphology (figure

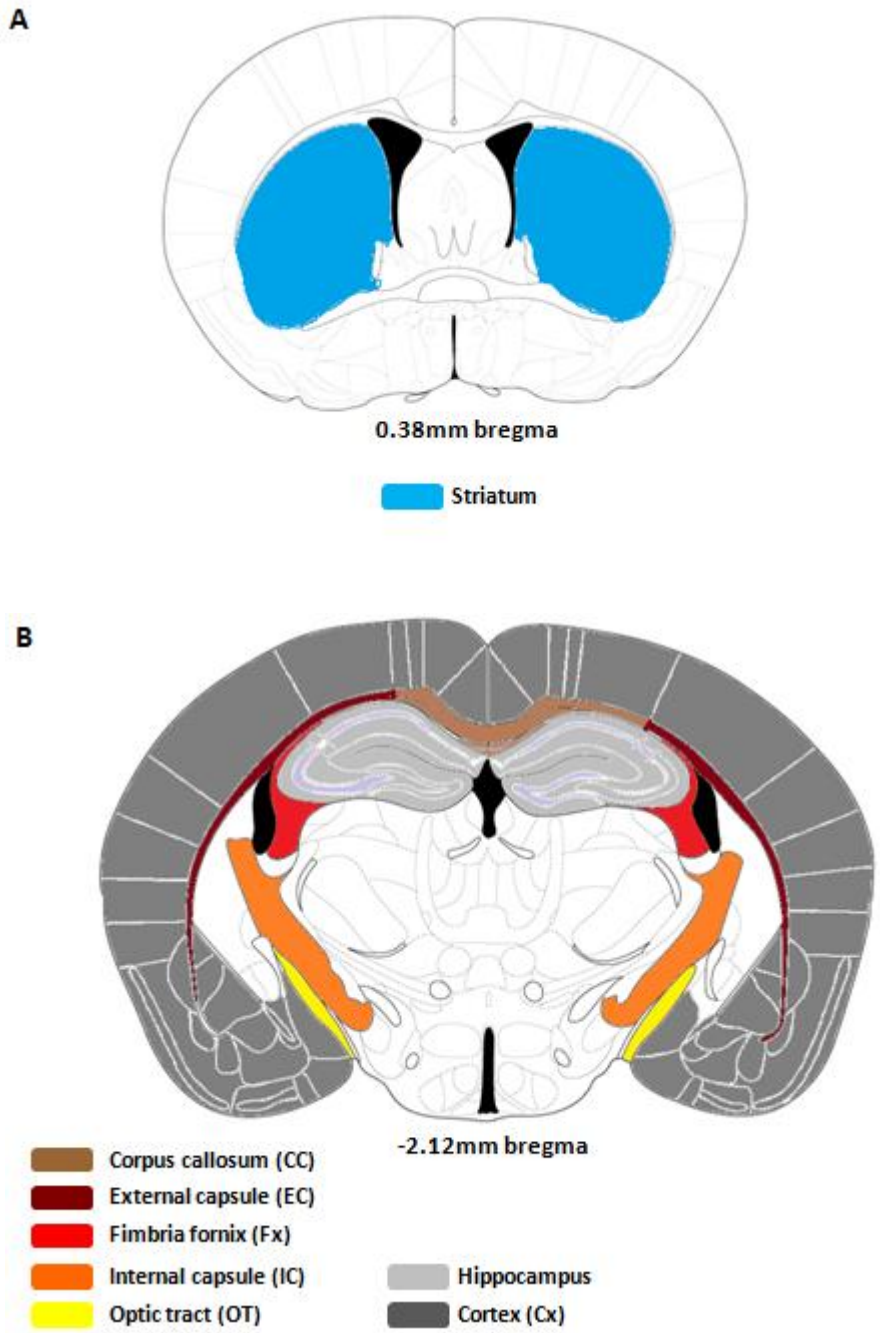

Figure 2.4.: Neuroanatomical regions of interest (ROI)

A schematic representation of the neuroanatomical regions of interest.

The neuroanatomical levels of interest were 0.38mm bregma (**A**) and -2.12mm bregma (**B**). The regions of interest (ROIs) used for the pathological evaluation of grey and white matter microstructural integrity as well as the characterization of epigenetic and glial biomerkers were cortical (Cx) (**B**) and subcortical (striatum hippocampus) (**A-B**) grey matter regions as well s major white matter tracts (CC, EC, Fx, IC, OT) (**B**).

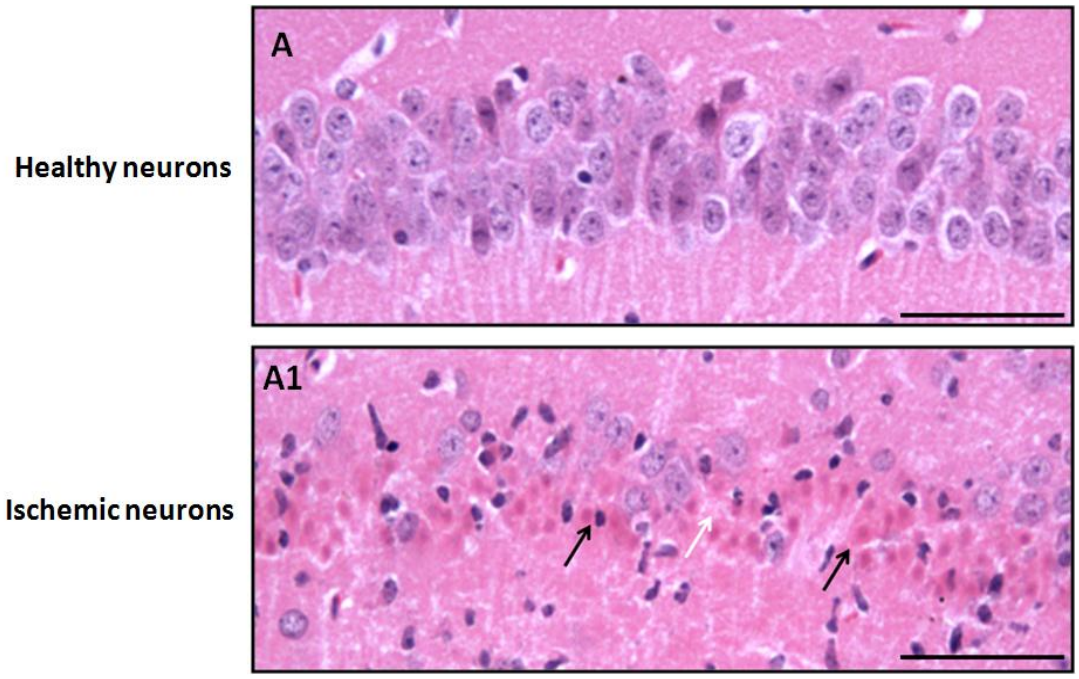

Figure 2.5.1.: H&E staining

Representative images of H&E stained healthy (**A**) and ischemic (**B**) neurons in the CA1 region of the hippocampus. Healthy neurons are characterized with light blue stained nuclei are shown in (**A**). Ischemic neurons are identified by their shrunken, dark nuclei and eosinphilic cytoplasm are indicated with black arrows in (**A1**). A typical "ghost" neuron is indicated with a white arrow in (**A1**).

Scale bar represents 15µm (magnification x60).

2.5.1.A, A1). Ischemic neurons present small pyknotic dark blue shrunken nuclei compared with the morphologically normal big light blue nuclei of healthy neurons. The cytoplasm of ischemic neurons is intensely eosinophilic. With long survival times after injury, damaged neurons are difficult to detect often become "ghost neurons" and engulfed by macrophages (figure 2.5.1. A1). Thus, due to the relatively long survival times after the initial induction of chronic cerebral hypoperfusion (2 month for the experiments in Chapter 3; 1 month for the experiments in Chapter 4, Chapter 5) and the formation of glial scars in ischemic brain regions it was difficult to quantify the exact number of ischemic cells in the different ROIs. Therefore, the neuronal perikarya ischemic damage was reported as present or absent, but was not quantified.

2.7.4. White matter integrity and inflammation

White matter structural integrity and inflammatory activity were examined by means of standard immunohistochemistry (Chapter 2, section 2.6.1.1.). The pathology was evaluated by means of a semi- quantitative pathological grading scale shown to be sensitive to white matter pathology in chronically hypoperfused mice (Coltman et al., 2011; Holland et al., 2011). Using this system the severity and the extent (relative percentage of affected area) of the observed pathology were numerically categorized: grade 0 (normal), grade 1 (mild pathology), grade 2 (moderate pathology), grade 3 (severe pathology). A pathological grade was attributed to all ROIs for all biomarkers. For the experimental purposes of chapter 3, a global score of axonal (APP), myelin (MAG) integrity, inflammation (Iba1) in each experimental animal was calculated by a separate summation of the pathological grades in the examined white matter areas (Coltman et al., 2011; Holland et al., 2011). The total biomarker score is considered to be a representative nonquantitative measure of the overall extent and severity of the observed pathology.

2.7.4.1. Evaluation of axonal integrity by means of amyloid precursor protein (APP) immunoreactivity

Axonal integrity was examined using an antibody targeted to amyloid precursor protein (APP), an integral membrane protein transported from the cell body along the neuronal axons. Under normal physiological conditions APP is immunodetected in neuronal

synapses and soma as well as in glial cell bodies (Forloni et al., 1992; Palacios et al., 1992). Axonal pathology disturbs normal axonal transport resulting in abnormal APP accumulation in swollen and/ or bulbous axons. Axonal integrity was examined in both white and grey matter ROIs.

The axonal integrity was estimated by analyzing the presence or absence of immunodetectable axonal APP aggregations in one or more of the examined ROIs (figure 2.5.2.A, A1). Normal axonal integrity (grade 0) was associated with the absence of immunodetectable axonal APP aggregations with localization of the protein solely in neuronal and glial cell bodies. A mild axonal injury (grade 1) corresponded to a minimal immunodetection of amyloid clumps within the neuronal axons covering less than 30% of the total surface of the examined ROI. A moderate axonal injury (grade 2) was associated with axonal APP aggregations covering between 30- 60% of the total surface of the ROI. A severe axonal injury (grade 3) corresponded to a substantial distribution of axonal APP aggregations affecting more than 60% of the total surface of the ROI.

2.7.4.2. Evaluation of myelin structural integrity by means of myelin associated glycoprotein (MAG) immunoreactivity

Myelin structural integrity was examined on MAG immunostained brain sections. MAG is a minor myelin protein (~2% of myelin protein content) and details on this protein function are given in Chapter 1, section 1.3.3. Myelin pathology with a different degree of severity was reported when disorganization of myelin fibers, vacuole formation and myelin debris with a different extent were observed in one or more of the white matter ROIs (figure 2.5.2.B, B1).

Normal appearing myelin (grade 0) was characterized by tightly organized myelin fibers, a lack of vacuole formation and an absence of myelin debris. A slight disorganization of the myelin fibers translated by the formation of small vacuoles and the accumulation of myelin debris covering relatively less than 30% of the total surface of the examined white matter ROI was considered as mild myelin pathology (grade 1). A moderate myelin comprising more than 40% vacuole formations surrounded by accumulated myelin debris

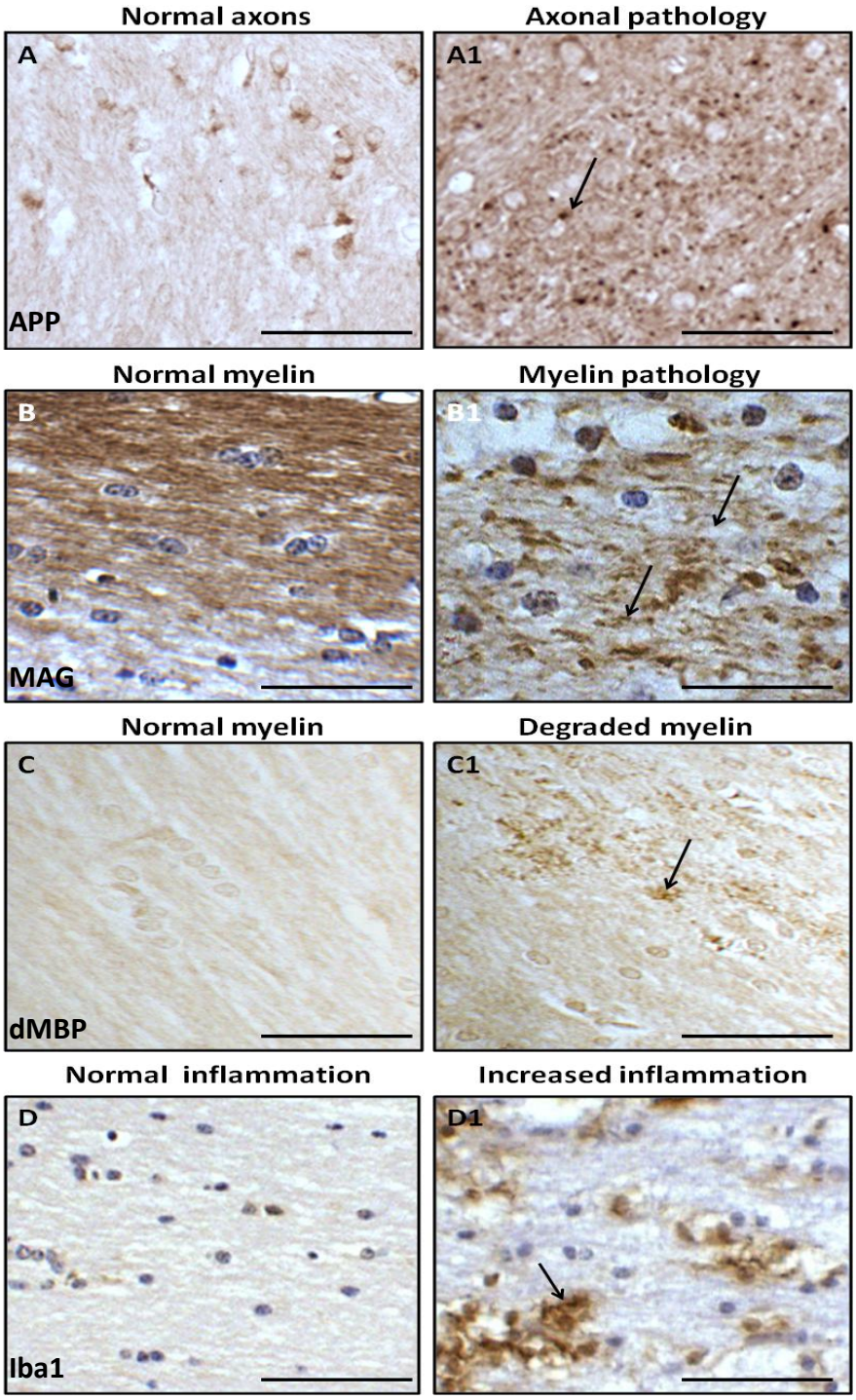

Figure 2.5.2.: APP, MAG, dMBP, Iba1 immunohistochemistry

Axonal (**A-A1**), myelin (**B-B1, C-C1**) integrity and inflammation (**D-D1**) in health (**A-D**) and disease (**A1-D1**). Axonal injury is revealed by APP immunoreactivity in bulbous/ swollen axons (arrow in **A1**). Myelin structural abnormalities are detected by MAG immunoreactivity as disorganized fibers, myelin debris, vacuoles (arrow in **B1**). Additional indication of myelin pathology is the presence of dMBP immunoreactivity (arrow in **C1**). Inflammatory levels are evaluated by Iba1 immunoreactive microglial cells (arrow in **D1**). All images are from the OT. Scale bar represents 15µm (magnification x60).

pathology (grade 2) was associated with a higher degree of myelin fiber disorganization with an extent reaching between 30- 40% of the total surface of the examined white matter area. The myelin pathology was considered severe (grade 3) when the structure and the organization of the myelin sheath were compromised by extensive vacuole formations and substantial aggregations of myelin debris scattered over relatively more than 60% of the total surface of the examined white matter area.

2.7.4.3. Evaluation of degraded myelin by means of degraded myelin basic protein (dMBP) immunoreactivity

Degraded myelin was detected by degraded myelin basic protein (dMBP) immunoreactivity- dMBP is a MBP isoform expressed only in pathological conditions (Matsuo et al., 1997). Myelin pathology with a different degree of severity was reported when immunodetectable dMBP was observed in one or more of the examined ROIs (figure 2.5.2.C, C1).

The myelin sheath was considered normal (grade 0) in the absence of immunodetetable dMBP levels in the examined white matter ROI. A minimal myelin pathology (grade 1) was attributed to small circular dMBP aggregations covering relatively less than 30% of the total surface of the ROI. A moderate myelin pathology (grade 2) was associated with dMBP aggregations covering between 30 and 60% of the total surface of the ROI. A severe myelin pathology (grade 3) corresponded to an extensive distribution of dMBP aggregations in more than 60% of the total area of the examined ROI.

2.7.4.4. Evaluation of inflammatory activity by means of ionized calcium binding antigen 1 (Iba1) immunoreactivity

Inflammatory levels were assessed on immunostained sections with an antibody targeted to ionized calcium binding antigen- 1 (Iba1) expressed by microglia and macrophages (Ito et al., 1998). Under normal physiological conditions the brain inflammatory levels are low, but they increase in the presence of neuropathological events (figure 2.5.2.D, D1). Inflammation was examined in both white and grey matter ROIs.

Inflammatory activity was evaluated on the basis of the relative microglia/ macrophages activation (relative distribution of Iba1 positive cells in a given area). Normal microglial activation (grade 0) was associated with a minimal number (0- 3) of Iba1 positive cells evidenced within the ROI. A minimal inflammatory activity (grade 1) was characterized by a slight increase in the distribution of Iba1 positive cells affecting less than 30% of the total surface of the examined ROI. A moderate inflammatory activity (grade 2) was attributed to a higher degree of inflammatory activity related to an increase in the number and reactivity of Iba1 positive cells evidenced in between 30- 60% of the total surface of the ROI. A severe inflammatory activity (grade 3) corresponded to the presence of reactive Iba1 positive cells in more than 60% of the total surface of the examined ROI.

For the purposes of the last experimental chapter (Chapter 5) presented in this thesis, the inflammatory levels were quantified by counting Iba1 positive cells on five random imaged fields taken from each ROI (Chapter 2, sections 2.8.).

2.7.5. Other immunomarkers

For the experimental purposes of Chapter 5, additional biomarkers were used for the immunodetection of cellular DNA components (5mC, 5hmC, single- stranded DNA), TET2 protein**,** mature (CC1) and precursor (NG2) oligodendroglial cells.

2.7.5.1. 5- Methylcytosine (5mC)

5mC is an epigenetic mark constituting ~1% of the total nucleotides of the mammalian DNA (Chapter 1, section 1.7.1.). It is immunodetected in cellular nuclei (figure 2.6. A- A2). 5mC immunoreactivity was quantified as explained in Chapter 2, section 2.8.

2.7.5.2. 5- Hydroxymethylcytosine (5hmC)

5hmC is a newly discovered epigentic mark resulting from the oxidation of 5mC (Chapter 1, section 1.7.2.). Similar to 5mC, 5hmC is immunodetected in cellular nuclei (figure 2.6. B- B2). 5hmC immunoreactivity was quantified as explained in Chapter 2, section 2.8.

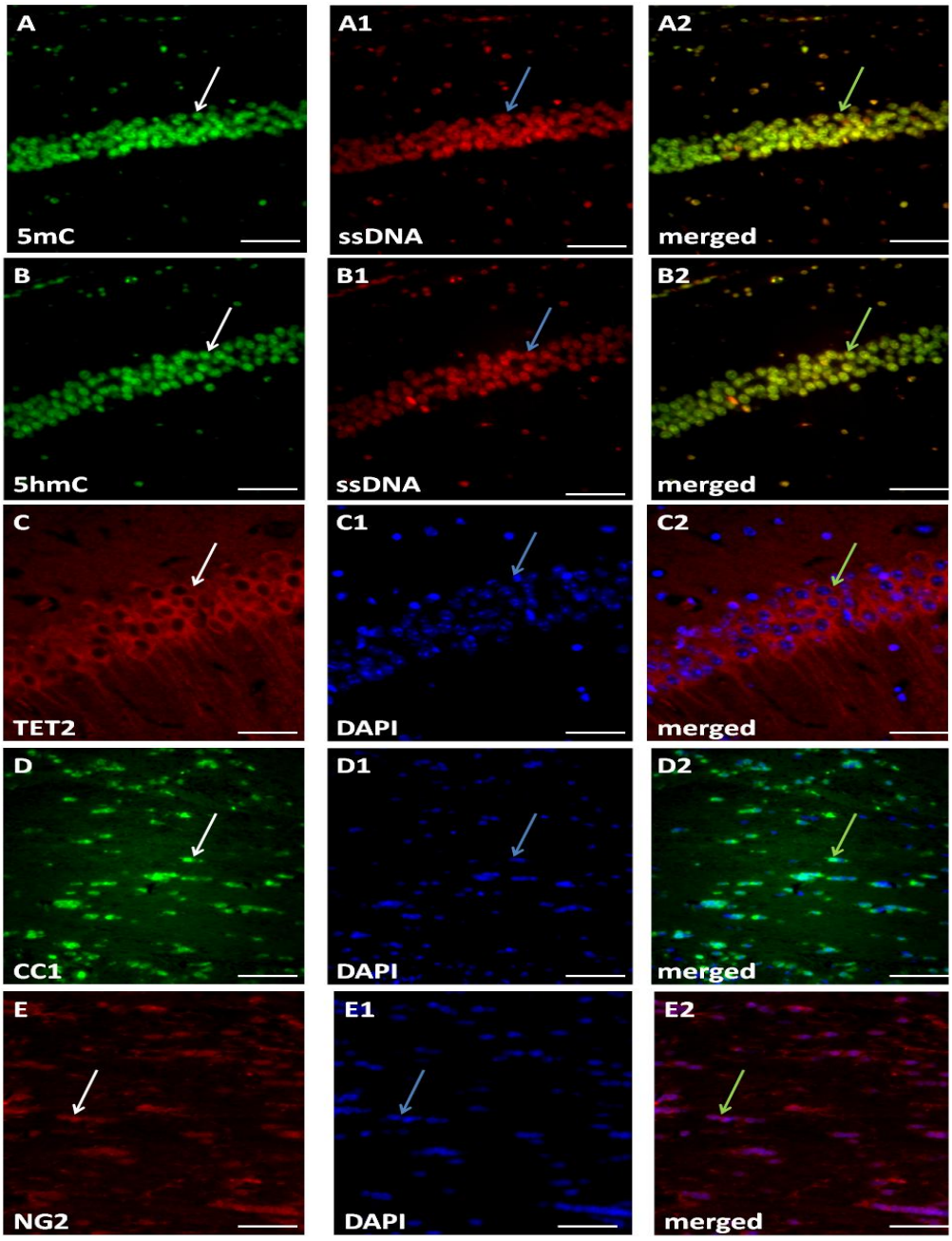

Figure 2.6.: 5mC, 5hmC, ssDNA, TET2, CC1, NG2 immunoreactivity

Representative images from the healthy mouse brain of 5mC (**A-A2**) 5hmC (**B-B2**), TET2 (**C-C2**), CC1 (**D-D2**), NG2 (**E-E2**) immunoreactivity with the corresponding counterstaining ssDNA (for 5mC and 5hmC) (**A1, B1**) or DAPI (for TET2, CC1, NG2) (**C1-E1**). Merged images of the biomarker of interest and the counterstain are presented in **A2-E2**. 5mC, 5hmC, and TET2 images are taken from the CA1 region of the hippocampus. CC1 and NG2 images are from the CC. Scale bar represents 20µm (magnification x40).

2.7.5.3. Single stranded DNA (ssDNA)

ssDNA is a biomarker for cellular DNA and is immunodetected in cellular nuclei (figure 2.6. A1- B1). ssDNA was quantified as explained in Chapter 2, section 2.8.

2.7.5.4. Ten- eleven translocation protein 2 (TET2)

Ten- eleven translocation protein 2 (TET2) catalyzes the oxidative reaction leading to the production of 5hmC (Chapter 1, section 1.7.3.). TET2 brain distribution was studied using an immunohistochemical approach for the first time in the present thesis and a representative image of TET2 immunostaining is given in figure 2.6. C- C2. TET2 was quantified as explained in Chapter 2, section 2.8.

2.7.5.5. CC1 or also called adenomatous polyposis coli (APC)

Adenomatous polyposis coli (APC) (CC1) is a protein detected in mature oligodendrocytes (figure 2.6. D- D2) (Armstrong et al., 2002). CC1 was quantified as explained in Chapter 2, section 2.8.

2.7.5.6. Chondroitin sulfate proteoglycan (NG2)

NG2 is a membrane proteoglycan found in OPC in the central nervous system (figure 2.6. E- E2) (Chang et al., 2000; Reynolds et al., 2002). NG2 immunoreactivity was quantified as explained in Chapter 2, section 2.8.

Biomarker	Fluorochrome	Wavelenght (nm)
5hmC	*GFP*	488
5mC	*GFP*	488
ssDNA	*Rhodamine*	594
CC1	*GFP*	488
NG2	*Rhodamine*	555
TET2	*Rhodamine*	555
DAPI	*DAPI*	358

Table 2.2.: Fluorochromes with their detection wavelengths (nm) used for the visualization of immunofluorescence- stained biomarkers.

2.8. Quantification of 5mC, 5hmC, TET2, CC1, NG2, and Iba1 positive cells

2.8.1. Fluorescent microscopy and imaging

Immunofluorescent brain samples were examined on an Axiovert (Carl Zeiss) fluorescence- detecting microscope. Each fluorochrome was detected at its corresponding excitation wave length (table 2.2.). Fluorescent images were generated using a lens magnification x40 and Axiovison software (Carl Zeiss) installed on a computer connected to the microscope camera. Five random fields were taken from each ROI and for each biormarker. Three separate images were generated from each of the five regional fields: one corresponding to the biomarker of interest, one corresponding to the ssDNA or DAPI staining, and a merged image of the biomarker of interest and ssDNA or DAPI (figure 2.6.). For the Iba1 immunostained samples a light microscopy (Chapter 2, section 2.7.1.) was applied using the same microscope and imaging system.

2.8.2. Cell counting

Cell counts were performed manually on images generated as described in Chapter 2, section 2.8.1. Cells positive for the biomarker of interest (5hmC, 5mC, CC1, NG2, TET2, Iba1) were counted on each of the five random images taken from a given ROI and their number was averaged across the five imaging fields in order to obtain a regional average number of biomarker positive cells. Subsequently, the number of ssDNA, DAPI or haemotoxylin positive cells was counted on the same five imaging ROI fields where the cells positive for the corresponding biomarker of interest were previously counted and their number was averaged across the five imaging fields in order to obtain a regional average number of total cells. A proportion of cells positive for each of the biomarkers was calculated for each of the ROIs using the following formula:

$$\textbf{Biomarker positive cells} = \frac{\textbf{Average number of biomarker positive cells in ROI}}{\textbf{Average number of total number of cells in ROI}}$$

During cell counting a special care was taken to avoid counting cells in neighbouring neuroanatomical regions which sometimes were also partially observed on the images and distinguished by their specific morphological and cellular landmarks.

2.9. Ex vivo MRI- DTI

MRI- DTI was applied on perfusion- fixed whole brain sample for the experimental purposes of Chapter 4. The aim was to achieve a better image resolution by using a longer imaging time in the absence of physiological artifacts allowing the detection of potentially subtle genotype differences in white matter integrity. Further, the experimental costs were reduced as more than 1 (3 to 4) brain samples were scanned by imaging session.

2.9.1. Small rodent MRI scanner

A small rodent 7T (T for tesla) Direct Drive MRI scanner (Varian Inc., Oxford, UK) was used for the ex vivo MRI experiment presented in this thesis. The apparatus consisted of a covering shield and a sliding table where the samples were positioned for imaging. The scanner was equipped with a 60 mm inner diameter gradient coil (1000 mT/ m) and a radiofrequency (RF) bird cage coil with an inner diameter of 26 mm (Rapid Biomedical, Wurzburg, Germany). The MRI system was controlled by a computer and the generated data was acquired using in- house software. The composing elements of a MRI scanner are schematically represented in figure 2.7.

2.9.2. Brain preparation prior to ex vivo MRI scanning

Within the 24h following transcardiac perfusion, 1- 2 brain(s) from the different experimental groups were placed and immobilized with a small piece of foam in a 2 ml plastic tube filled with 4% PFA to prevent tissue dehydration during imaging. Special care was taken to remove air bubbles from the tubes as they might impact on the image quality. The tubes were labeled tube 1 and 2 and each brain was given a number 1, 2, (tube 1) 3, 4 (tube 2) which allowed the subsequent identification of the samples. Three- four brains were imaged per scanning session (figure 2.8.).

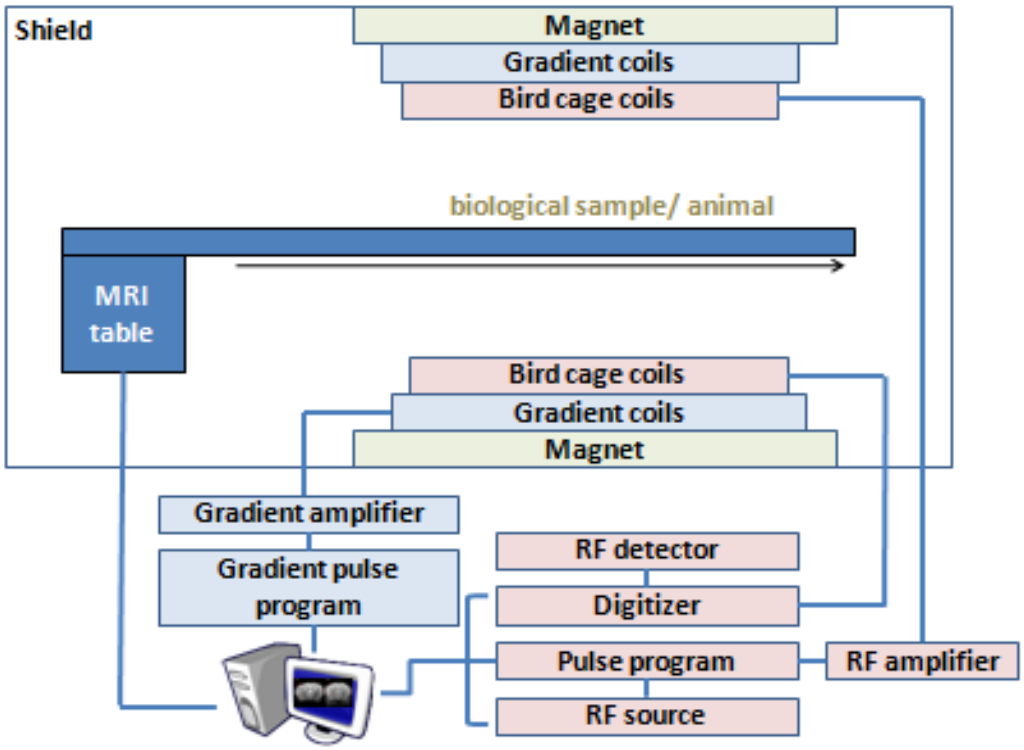

Figure 2.7.: Composing elements of a MRI scanner

A schematic representation of the composing elements of a MRI scanner.

The MRI scanner is equipped with a magnet producing the magnetic field for the imaging procedure. Within the magnet are the gradient coils (controlled/ recorded by a computer through a gradient pulse program/ amplifier) for producing a gradient in the generated magnetic field in the X, Y, and Z directions. Within the gradient coils is the RF coil. The RF coil (controlled by a computer through RF source/ amplifier) produces a second electromagnetic field necessary to rotate the spins by 90^{o}, 180^{o}, or any other value selected by the pulse sequence. The RF coil also detects (the signal is recorded by a computer through RF amplifier/ detector) the signal from the spins within the body. The patient/ biological sample is positioned within the magnet by a computer controlled MRI table. The scan room is surrounded by an RF shield preventing the high power RF pulses from radiating out through the facilities building. It also prevents the various RF signals from television and radio stations from being detected by the imager.

Figure 2.8.: Brains set up for ex vivo MRI- DTI procedure

An example image of the brains set up for ex vivo MRI- DTI scanning.

The brains were put into plastic tubes filled with 4% PFA and labeled tube 1 and tube 2. The brains in tube 1 were consistently labeled 1 and 2. The brains in tube 2 were consistently labeled brain 3 and 4. This was done for experimental "blinding" of the researcher and the subsequent identification of the samples. The animals from the four experimental groups were equally distributed among each batch/ imaging session.

2.9.3. Ex vivo MRI- DTI procedure

Three to four brains were scanned simultaneously per overnight imaging session at RT. The tubes containing the brains were securely positioned in the centre of the RF birdcage coil prior to each imaging session. Contiguous coronal T2- weighted, MTI, and DTI images were all acquired with spin-echo sequences with the following parameters: matrix size 256x128, field of view 24 x 12 mm, slice thickness 0.5 mm, number of slices 52. The repetition time/echo time was 3500/48 ms for the T2-weighted sequence and 2500/30 ms for both the MTI and DTI sequences. For DTI, diffusion-weighted (b = 1800 s/mm^2) volumes were acquired with diffusion gradients (amplitude 25.6 G/cm, duration 4 ms, separation 13 ms) applied in 12 noncollinear directions and 2 volumes without the diffusion gradient applied. The MTI protocol employed two sequences; one acquired with a magnetization transfer pulse applied 3 kHz off resonance (flip angle 900°, duration 8.19 ms). The imaging time was ~12h per session. The ex vivo MRI procedure was developed and performed by Dr Marits Jansen (Medical Physics, University of Edinburgh) and Gavin Merrifield (Medical Physics, University of Edinburgh).

At the completion of the MRI procedure, the brains were transferred into individual 50 ml tubes filled with 0.1% PBS and kept at 4°C for additional 7 days prior to paraffin embedding.

2.9.4. MRI image analysis

The MRI images were analyzed using Image J 1.43o (NIH) software. ROIs were manually delineated on the T2- weighted images in a manner blinded to the experimental treatment and the genotype of the animals using a placement procedure that relied on atlas based reference maps (Franklin and Paxinos, 1997) with morphological landmarks. Special care was taken to avoid any possible contamination by neuroanatomical regions adjacent to the delineated ROI. FA and MTR were measured in areas with known susceptibility to blood flow alterations: the CC (body and horns), EC, IC, and OT as well as in the hippocampus which was selected as a control grey matter ROI. The ROIs delineated on the T2- weighted scans of each mouse were automatically applied to the FA, MTR. The MTR maps were constsructed from the MTI scans with and without the off

resonance pulse allowing the estimation of the magnetization transfer ratio between the free and bound protons in the brain. The generated raw MRI data resulted from the bilateral evaluation of the FA and the MTR on a fixed **n** number of consecutive scans on which a given ROI could be detected: CC (8 scans), EC (7 scans), IC (3 scans), OT (2 scans), hippocampus (2 scans).

2.10. In vitro culture and maturation of oligodendroglial cells

Oligodendroglial progenitor cells (OPCs) were isolated from the cerebral cortices of mice pups (post- natal day 0- 2). Cortices were separated from the rest of the brain under a dissecting microscope and subsequently digested with papain solution (1 ml DMEM (Invitrogen); 40µl papain (Worthington Biochemical); 25µl L-cysteine solution (Sigma); 25µl DNaseI type IV (Sigma) at 37°C for 10min. Following this, cells were further mechanically isolated from the surrounding epithelia by means of a sterile filter. Cell pellets were collected by a centrifugation at 1000 rpm for 5 min (this step was repeated three times and after each centrifugation cells were resuspended into a fresh 10% DMEM solution). Cell pellets were finally resuspended onto a poly- D- lysine coated flasks and cultured into a SATO medium composed of DMEM supplemented with glutamine (Sigma), penicillin and streptomycin (Invitrogen), 10% horse serum (Invitrogen), insulin (Sigma) and transferrin (Sigma), 10ng/ ml fibroblast growth factor (FGF2) (Peprotech), 10ng/ ml platelet derived growth factor (PDGF) (Peprotech). Cells were incubated at 37°C, 7.5% CO_2 for 3 days prior to the first media change. Subsequently, the media was changed every other day. Differentiation was achieved by removal of the growth factors (FGF2 and PDGF) from the SATO media and the cells were cultured for additional 0, 2, 6 DIV to reach a certain maturational stage prior to fixation with 4% PFA (Chapter 2, section 2.12.).

The oligodendroglial cell preparations were kindly provided by Dr Anna Williams and Mr Alasdair Burns (MRC Scottish Centre for Regenerative Medicine, University of Edinburgh).

2.11. In vitro culture of activated and nonactivated microglial cell

Microglia cells were isolated from the cerebral cortices of postnatal day 0- 2 Sprague Dawley rat pups. Following removal of meninges, cortices were mechanically minced then enzymatically digested for 45 min at 37°C in 30u/ml papain (Worthington Biochemical Corporation, USA), 24mg/ml cysteine (Sigma), 4mg/ml DNaseI type IV (Sigma). The cell suspension was incubated with 10% DMEM (with 4.5g/L glucose, L-glutamine, and pyruvate (all purchased from GIBCO) supplemented with 10% FCS (Invitrogen), and 1% penicillin/streptomycin (Sigma)) and centrifuged at 1000 rpm for 5 min. Supernatant was discarded, and the cell suspension was resuspended in 10% DMEM and triturated with 19 and 23 guage syringe needles. Cells were plated on poly-D-lysine (Sigma) coated plastic flasks and grown as mixed glial cultures for 10 days in 10% DMEM with media changed every 2-3 days. Microglia were isolated by collecting the floating fraction in the flasks following 1h on a rotary shaker at 37°C at 250 rpm. Cells were plated on poly-D-lysine coated 16-well glass chamberslides (Lab-TEK, USA) at 50 000 cells per well in 10% DMEM. Microglia were either left untreated or activated by overnight treatment with 20ng/ml IFNγ (Sigma) and 100ng/ml LPS (Sigma). Prior to 5hmC immunocytochemistry, the microglial cells were fixed with 4% PFA as described in Chapter 2, section 2.12.

The microglial cell preparations were kindly provided by Dr Veronique Miron (MRC Scottish Centre for Regenerative Medicine, University of Edinburgh).

2.12. Fixation of oligodendroglial and microglial cells

Prior to fixation with 4% PFA, the culture media was aspirate and the cells were washed 2 x PBS (2min). Subsequently, 4% PFA solution was added to the wells and the cells were left in the fixative for 15min. After 3 x PBS washes (2min/ each), a fresh PBS solution was added to the wells, the plate was covered with parafilm and the cells were stored at 4°C until required for immunocytochemistry.

2.13. Statistics

The applied statistical analysis is described in details in the experimental chapters.

Chapter 3

Effects of chronic cerebral hypoperfusion on white matter integrity and cognitive abilities in mice

3.1. Introduction and aims

Grey matter abnormalities such as synaptic/ dendritic loss and dysfunction are often considered to be the main contributors of cognitive decline during "healthy aging" (Roman and Kalaria, 2006; Esiri, 2007). However, increasing evidence from combined neuroimaging and neuropsychological studies, suggest that white matter disruption or loss of the brains 'connectivity' might be the major neuropathological substrate associated with age- related cognitive decline in "healthy" elderly (O`Sullivan et al., 2001; Deary et al., 2003; Charlton et al., 2006; Grieve et al., 2007; Kennedy and Raz, 2009; Penke et al., 2010). At the microscopic level age- related white matter lesions are characterized by myelin rarefaction, vacuole formation, axonal damage, oligodendroglial apoptosis, increased inflammation, and small vessel pathology (Farkas et al., 2006; Fernando et al., 2006; Ihara et al., 2010). These lesions were initially thought to be 'silent', but a number of studies have since shown that white matter abnormalities contribute to impaired working memory and executive function in "healthy" elderly (O`Sullivan et al., 2001; Charlton et al., 2006; Cook et al., 2007; Grieve et al., 2007; Wright, et al., 2008; Kennedy and Raz, 2009). Working memory is the cognitive ability mediating the learning, memory and recollection of newly learned information over relatively short periods of time, whereas executive function refers to the cognitive ability associated with planning, organization and rapid switching of strategies allowing an adequate behavioural adaptation to the imminent requirements of a constantly changing environment (Baddeley, 1992; Jurado and Rosselli, 2007). Both working memory and executive function are cognitive mechanisms relying on the fast neuronal communication between cortico- cortical and cortico- subcortical regions (Rolls, 2000; Funahashi, 2001; Tekin and Cummings, 2002; Grieve et al., 2007). Therefore, pathological damage to white matter tracts might impact on neuronal connectivity leading to the occurrence of cognitive deficits in the elderly.

The exact etiological causes underlying the development of age- related white matter abnormalities are not well understood mostly due to the existence of comorbidities in elderly such as diabetes, hypertension, cardiac disease, neurodegeneration (Verdelho et al., 2010; Van Swieten et al.; 1991; Lindgren et al., 1994; Ruitenberg et al., 2005). However, age- related changes in the cerebrovasculature are believed to be one of the major

pathophysiological mechanisms associated with white matter lesions in the aging brain. Specifically, chronic cerebral hypoperfusion due to changes in the morphology of the cerebral blood vessels such atherosclerosis, fibrohylinosis, basement membrane thickening and increased vascular inflammation have been related to white matter pathology and cognitive deficits in "healthy" elderly (Kalaria, 1996; Tang et al., 1997; de Leeuw et al., 2000; Farkas et al., 2006; Gold et al., 2007). Chronic cerebral hypoperfusion may be particularly harmful to white matter regions which neuroanatomically are characterized by arterial end and border zones with very limited blood irrigation even under normal physiological conditions (Nonaka et al., 2003) .

In order to study in isolation the effects of chronic cerebral hypoperfusion on the cellular and molecular events leading to the development of age- related white matter abnormalities and cognitive decline in humans, animal models of chronic cerebral hypoperfusion have been initially developed in rats and gerbils (Kudo et al., 1990; Hattori et al., 1992; Kudo et al., 1993; Pappas et al., 1996; de Jong, et al., 1999; Tomimoto et al., 2003; Kim et al., 2008). These two in vivo models consist of the permanent bilateral occlusion of the common carotid artery leading to chronic cerebral hypoperfusion and the development of predominant white matter pathology with concomitant grey matter ischemic injury and increased inflammation (Kudo et al., 1993; Pappas et al., 1996; Kim et al., 2008). At the functional level both chronically hypoperfused rats and gerbils exhibit impaired learning and memory (Kudo et al., 1990; Pappas et al., 1996; Sopala and Danysz, 2001; Kumaran et al., 2008). However, the evaluation of cognitive deficits related to white matter pathology in these two animal models is hampered by the presence of grey matter damage.

Recently, our group and others developed and characterized a new mouse model of chronic cerebral hypoperfusion where piano microcoils are surgically applied to the common carotid arteries leading to mild chronic reductions of the cerebral blood flow, akin to those occurring in the ageing brain where modest reductions in cerebral blood flow occur over many years (Kawamura et al., 1991; Ogawa et al., 1996; Brown et al., 2000; Mathiesen et al., 2004; Fernando et al., 2006; Pardo et al., 2007). The initial characterization of this new animal model has suggested that cerebral hypoperfusion leads

to the development of predominant white matter pathology including increased inflammation in the absence of ischemic neuronal damage (Shibata et al., 2004; Shibata et al., 2007; Nishio et al., 2010; Coltman et al., 2011; Holland et al., 2011). Therefore, this new mouse model seemed to be a suitable in vivo tool for the investigation of functional impairments and associated pathology related to chronic cerebral hypoperfusion relevant to aging. Chronically hypoperfused mice have been previously shown to exhibit a spatial working memory deficit on a radial arm maze task in the absence of spatial reference memory, contextual and fear conditioning deficits (Shibata et al., 2007). However, so far, there has not been a systematic pathological evaluation of behaviourally tested chronically hypoperfused mice, thus rendering difficult any firm conclusions on the effects of hypoperfusion- induced neuropathology on cognitive function in mice.

Building on previous work, the present study tested the hypothesis that hypoperfusion-induced white matter pathology might be associated with the occurrence of working memory and executive function deficits in mice.

On the basis of previous findings on the mouse model of chronic cerebral hypoperfusion, the initial study predictions were that chronic cerebral hypoperfusion would lead to the development of predominant white matter pathology and spatial working memory impairment in mice.

The present study hypothesis challenged the long- lasting dogma (the standard theory) suggesting that grey matter abnormalities are the major neurobiological substrate of age-related cognitive decline

In order to address the study hypothesis, spatial working memory was examined in sham compared with hypoperfused mice one month after surgery using the same radial arm maze paradigm as Shibata et al., 2007. On the basis of previous human findings showing an association between age- related white matter pathology and executive function (Grieve et al., 2007; Kennedy and Raz, 2009), in the present experiment, spatial memory flexibility (executive function) was also examined in a separate cohort of sham and chronically hypoperfused mice using a water maze paradigm one month after surgery. In

this experimental cohort spatial learning capacity, short and long- term recall were simultaneously tested.

Since grey matter abnormalities (e.g. dendritic and synaptic loss) and increased inflammation accompany the development of white matter pathology in alternative animal models of chronic cerebral hypoperfusion as well as in elderly people (Anderson et al., 1983; Kudo et al., 1993; Pappas et al., 1996; Kurumatani et al., 1998; Duan et al., 2003; Tomimoto et al., 2003; Liu et al., 2005; Fernando et al., 2006; Roman and Kalaria, 2006; Esiri, 2007; Kim et al., 2008) in addition to white matter, grey matter integrity and inflammatory levels were also examined in behaviourally tested sham and hypoperfused animals using a standard histological/ immunohistochemichal approach at the completion of the behavioural testing.

The major aims of the present Chapter 3 were to:

- Examine spatial working memory, memory flexibility, learning capacity, short and long term memory recall in sham compared with chronically hypoperfused mice.

- In the same sham and hypoperfused mice which had undergone behavioural testing to examine and compare white and grey matter integrity, inflammation.

- Determine potential associations between white matter integrity and behavioural parameters of working memory/ executive function in chronically hypoperfused mice.

3.2. Materials and methods

3.2.1. Animals and surgery

Three- month old male C57Bl6J mice weighting 25 ± 5gr were used for the experiments presented in Chapter 3 (Chapter 2, section 2.1.1.). The animals were randomly allocated to sham and hypoperfused groups. Initially, 10 sham and 20 hypoperfused mice were included in the radial arm maze experiment. The initial experimental numbers for the water maze experiment were 11 sham and 18 hypoperfused mice. Chronic cerebral hypoperfusion was induced as described in materials and methods (Chapter 2, section 2.2.). Food and water were provided *ad libitum* for the animals tested on the serial spatial water maze task during the whole experimental period. The animals that underwent testing on the radial arm maze task were food- deprived in order to reduce their body weight up to 85-90% from their original one. Only the animals surviving the whole experimental period were included in the final behavioural and pathological analysis.

3.2.1. Behavioural tests

Spatial working memory was challenged on a radial arm maze paradigm in sham and chronically hypoperfused mice (Chapter 2, section 2.3.2.). Additionally, the visual abilities of the animals included in this experiment were examined at three different time points (S.3.1- appendices I; Chapter 2, section 2.3.1.).

Spatial memory flexibility, spatial learning capacity, short and long term memory recall were studied in a separate cohort of sham and chronically hypoperfused mice using a serial spatial learning and memory water maze task (Chapter 2, section 2.3.3.). In addition, as mice are not natural swimmers their ability to swim and perform a water maze task were tested on a cue task paradigm a day prior to surgery and a week prior to the serial spatial and learning task (three weeks post- surgery) (S.3.3- appendices I.; Chapter 2, point 2.3.3.2.1.).

The behavioural training on both the radial arm maze and the water maze tasks was performed one month post- surgery. At the completion of each of the behavioural procedures (~2 months post- surgery) the animals were perfusion- fixed (Chapter 2,

section 2.4.) and their brains were processed for histology and immunohistochemistry (Chapter 2, section 2.5.).

3.2.2. Pathological assessment

The pathological evaluation of white and grey matter structural integrity was performed at the completion of the behavioural training (~ 2 months after surgery) on each of the two behavioural paradigms.

White matter structural integrity and inflammatory activity were examined at -2.12mm bregma neuroanatomical level (Franklin and Paxinos, 1997) as all white matter tracts of interest could be simultaneously studied on the same brain section. A standard immunohistochemical procedure (Chapter 2, section 2.6.1.1.) was applied using antibodies targeted to the neuronal axons (APP), myelin sheath (MAG), and microglia (Iba1). The pathology was assessed by means of a semi- quantitative grading scale (0- normal, 1- mild, 2- moderate, 3- severe pathology) (Chapter 2, section 2.7.4.; Coltman et al., 2011; Holland et al., 2011). A global score of axonal (APP), myelin (MAG) integrity, inflammation (Iba1) in each experimental animal was calculated by a separate summation of the pathological grades across the examined white matter areas (Coltman et al., 2011; Holland et al., 2011). The total biomarker score in white matter areas was considered to be a representative nonquantitative measure of the overall extent and severity of the observed pathological changes (the data and analysis are given in tables S.3.3.1, S.3.3.2., S.3.3.3.- appendices I) and it was used for the correlation analysis with behavioural measures in chronically hypoperfused mice (section 3.2.3.3.).

Grey matter structural integrity and neuronal ischemic damage were evaluated on H&E stained (Chapter 2, section 2.5.3.) coronal brain sections from 0.38mm bregma and -2.12mm bregma neuroanatomical levels (Franklin and Paxinos, 1997) and reported to be present or absent in cortical (the Cx) and subcortical (the striatum and the hippocampus) grey matter regions known to be susceptible to blood flow alterations (Chapter 2, section 2.7.3.).

3.2.3. Statistics

3.2.3.1. Statistical analysis of the behavioural data

3.2.3.1.1. Statistical analysis of the radial arm maze behavioural data

For the radial arm maze behavioural data, statistical comparisons were performed on blocks of data for each animal in which each block comprised the average of two trials conducted on consecutive days of training for each behavioural measure (Shibata et al., 2007, Nishio et al., 2010, Coltman et al., 2011). The experimental group (**n**) numbers included in the statistical analysis were 10 sham and 10 hypoperfused mice. Two-way repeated measures analysis of variance (ANOVA) was applied to statistically compare the average number of revisiting errors and number of novel entries in the first 8 arm choices between sham and hypoperfused groups (Shibata et al., 2007, Nishio et al., 2010 Coltman et al., 2011). A separate two- way ANOVA was performed for each behavioural measure. The same statistical analysis was applied to compare the group average number of total arm entries and trial duration (analysis and data presented in appendices I, S.3.1.2.). When significant main effects of trial block of group x block interactions ($p<0.05$) were indicated by ANOVA, a Tukey`s post- hoc analysis was applied to determine the exact training day(s) when significant group differences in the behavioural performance between sham and hypoperfused mice occurred.

Significant group differences were reported for $p<0.05$.

3.2.3.1.2. Statistical analysis of the water maze behavioural data

Similar to the radial arm maze study, two- way repeated measures ANOVA was applied for the statistical comparisons of the performance on a serial spatial learning and memory water maze task (Chen et al., 2000; Coltman et al., 2011). The experimental group (**n**) numbers included in the statistical analysis were 11 sham and 10 hypoperfused mice. In this particular experiment, the statistical analysis aimed at determining the effects of group (between subjects factor) and task number (platform locations 1-5 – repeated measures factor), and group x task interactions on the following dependent variables: the number of trials to criterion (memory flexibility), percentage of time spent swimming in the training

quadrant during the first 60 sec of the 10min and 3h probe trials (PT) (short and long- term memory recall), and the number of virtual platform crossings, latency to the first platform crossing, and swimming speed to platform for the 10 min and 3h PT data (the analysis is presented in appendices I, table S.3.1.). One-way ANOVA was applied to statistically compare the group average percentage of time spent in the training quadrant during the 10min and 3h probe trials (PTs) with a chance level of performance (determined to be equal to 25% => 100% divided by 4 as the water maze has 4 training quadrants) for each group across the five tasks (Coltman et al., 2011). The average group number of spatial tasks learned in 10 days was statistically analyzed using an unpaired t- test (Coltman et al., 2011).

Significant group differences were reported for $p<0.05$.

3.2.3.2. Statistical analysis of the pathological data

The regional group median pathological grades of axonal and myelin integrity as well as inflammatory activity were compared using Mann- Whitney non- parametric statistics. Only the pathological data from the animals included in the final behavioural analysis of the radial arm maze and the water maze experiments were subjected to a Mann- Whitney statistical analysis. The total group median pathological scores of myelin integrity were also analyzed using Man- Whitney statistics (table S.3.3.3.- appendices I).

Significant group differences were reported for $p<0.05$.

3.2.3.3. Correlation analysis

In an attempt to account for potential associations between white matter integrity and behavioural parameters in hypoperfused mice (the main study hypothesis), a non-parametric Spearman`s correlation analysis was performed between white matter cellular components and behavioural measures of spatial working memory and executive function. The analysis was focused on co- variates relevant to the main study hypothesis in order to avoid performing multiple associations between biomarkers across brain areas and various behavioural parameters inevitably leading to meeting the set criterion of significance ($p<0.05$) purely by chance. Specifically, the correlations between the total pathological scores of axonal (APP), myelin (MAG) integrity and inflammation (tables S.3.3.1,

S.3.3.2.- appendices I) and both the average number of revisiting errors across the 8 training sessions of the radial arm maze task (working memory), and the average number of trials to criterion across the 5 spatial water maze task (executive function) were calculated. The number of revisiting errors and the trials to criterion were selected for behavioural co- variates as these parameters are considered to be robust measures of working memory and memory flexibility (executive function) on a radial arm maze and water maze paradigm, respectively (Olton and Samuelson, 1976; Morris, 1984; Chen et al., 2000; D`Hooge and De Deyn, 2001; Shibata et al., 2007; Nishio et al., 2010; Coltman et al., 2011). A separate Pearson`s analysis was performed between each biomarker and behavioural parameter. In regards to the main study hypothesis suggesting associations between hypoperfusion- induced white matter pathology and spatial working memory and executive function in mice, only the pathological and behavioural data from the hypoperfused animals were used for the correlational analysis with a risk of underpowered statistics (Pappas et al., 1996; Liu et al., 2005). Furthermore, due to the absence of numerical scale for pathological variations (pathological grades equal 0) necessary for the associations between pathology and behaviour, the data from the sham animals could not be used for the correlation analyses.

Significant correlations were reported for ($p<0.05$).

3.3. Results

3.3.1. Post- surgery recovery and physiological status

Five of the initially 20 hypoperfused mice (25%) included in the radial arm maze experiment had a poor post- surgery recovery and were procedure terminated. Unexpectedly, prior to and during the behavioural procedure another 25% (5/20) of the hypoperfused mice exhibited a seizure- like activity consisting of brief (a couple of minutes) uncoordinated body convulsions. These animals were excluded from all subsequent analysis. The remaining 50% (10/20) of the hypoperfused animals and all sham mice (10/10) recovered well after surgery and showed no overt signs of neurological and/or physiological dysfunction for the entire experimental period (figure S.3.1.2. A- appendices I).

From the hypoperfused animals tested on the water maze paradigm, 22.2% (4/18) of the initially included mice had to be procedure terminated prior to or during the behavioural testing due to a poor recovery. The remaining 77.8% (14/18) of the hypoperfused mice survived the entire experimental procedure in the absence of any neurological or physiological dysfunction. Only one of the 14 hypoperfused mice (0.07%) showed seizure- like activity during behavioural testing. This animal was excluded from further analysis. All sham mice (11/11) recovered well after surgery and survived the whole experimental period in the absence of any overt neurological and/ or physiological dysfunction (figure S.3.1.2.B- appendices I)

3.3.2. Effects of chronic cerebral hypoperfusion on spatial working memory, memory flexibility, learning capacity, short- and long- term memory recall in mice

3.3.2.1. Chronic cerebral hypoperfusion leads to spatial working memory impairment

Spatial working memory was tested in food deprived sham and chronically hypoperfused mice using a radial arm maze paradigm in which, on each daily trial, one piece of food reward was available at the end of each arm (Chapter 2, section 2.3.2.). Indications of an intact spatial working memory were considered to be: the absence (or the low number) of

revisiting errors and the high number of novel entries in the first 8 arm choices. The statistical analysis was performed using two- way repeated measures ANOVA (Chapter 3, section 3.2.3.1.1.; Shibata et al., 2007, Nishio et al., 2010, Coltman et al., 2011). The statistical analysis showed that hypoperfused animals (n=10) committed significantly more revisiting errors ($F_{(1, 18)}$= 22.457, p<0.0001) and visited significantly fewer new arms in the first 8 arm choice ($F_{(1, 18)}$= 7.897, p= 0.012) than sham mice (n= 10) (figure 3.1. A, B). There was a significant effect of the training day for both the number of revisiting errors ($F_{(1,18)}$= 25.346, p<0.0001) and the number of novel entries in the first 8 arm choices ($F_{(1,18)}$= 26.136, p<0.0001). Similar significant group differences were observed for the total number of arm entries and the trial duration (S.3.1.3.- appendices I). No significant training day x group interaction was found for any behavioural measure suggesting that the performance of both hypoperfused and sham mice improved with training (overtime): the number of revisiting errors ($F_{(1,18)}$= 1.348, p= 0.288) and the number of novel entries in the first 8 arm choices ($F_{(1,18)}$= 1.981, p=0.176) (the total number of arm entries and the trial duration- S.3.1.3.- appendices I). The post- hoc Tukey`s analysis demonstrated that hypoperfused mice committed significantly more revisiting errors on training day 2 (p= 0.001), day 6 (p=0.011), day 7 (p= 0.003), and day 8 (p=0.031) (figure 3.1. A). They also visited significantly fewer novel arms on training day 4 (p=0.007), day 7 (p=0.043), and day 8 (p=0.019) (figure 3.1. B).

These behavioural results were confirmed by our group in an additional cohort of hypoperfused animals tested on the same radial arm maze spatial working memory task (S.3.2.- appendices I; Coltman et al., 2011) as well as independently by others (Shibata et al., 2007; Nishio et al., 2010).

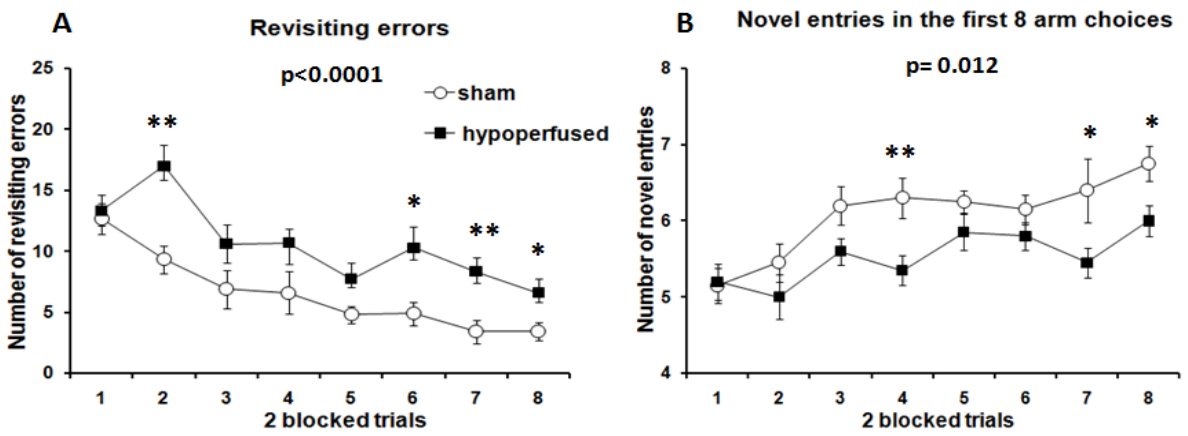

Figure 3.1.: Group performance on a spatial working memory radial arm maze task (group mean ± SE)

Spatial working memory was significantly impaired in chronically hypoperfused mice. Two- way repeated measures ANOVA demonstrated that chronically hypoperfused mice (n=10) committed significantly more revisiting errors (**A**) and entered significantly fewer new arms in the first 8 arm choices (**B**), than sham mice (n=10) on a radial arm maze paradigm ($p<0.05$).

Significant group differences as given by the Tukey`s post- hoc analysis: ($p<0.05$)*, ($p<0.01$)**, ($p<0.001$)***

3.3.2.2. Chronic cerebral hypoperfusion does not affect spatial memory flexibility

Spatial memory flexibility was tested in sham and hypoperfused mice using a water maze protocol where each animal had to learn five separate spatial problems with a set criterion of performance in 10 days (Chapter 2, section 2.3.3.2.2.; Chen et al., 2000; Coltman et al., 2011). Spatial memory flexibility was considered intact when the animals were able to rapidly acquire new spatial problems in a few trials to criterion. The statistical analysis was performed using two- way repeated measures ANOVA (Chapter 3, section 3.2.3.1.2; Chen et al., 2000, Coltman et al., 2011). No significant main effects of task ($F_{(4, 76)}$ = 1.566, p = 0.19), or group ($F_{(1, 19)}$ = 0.035, p = 0.85) and no significant group x task interaction ($F_{(4, 76)}$ = 0.524, p = 0.72) for the number of trials to criterion were evident (figure 3.2. A).

3.3.2.3. Chronic cerebral hypoperfusion does not affect spatial learning capacity

Spatial learning capacity was evaluated by statistically comparing the average number of spatial problems sham and hypoperfused mice managed to learn on the serial spatial learning and memory task in 10 days using an unpaired t- test (Chapter 3, section 3.2.3.1.2; Coltman et al., 2011). This analysis revealed no significant differences between the two experimental groups in the number of spatial tasks learned in 10 days
(t= 0.756, p = 0.459) (figure 3.2.B).

3.3.2.4. Chronic cerebral hypoperfusion does not impact on spatial short and long term memory recall

Spatial short- and long- term memory recall were challenged respectively at 10min and 3h after an animal had reached the learning criterion on each of the five spatial tasks (Chapter 2, section 2.3.3.2.2.2.; Chen et al., 2000; Coltman et al., 2011). Indications of an intact memory recall of the spatial location of the hidden platform were considered to be the high percentage of time spent swimming in the training quadrant (the quadrant where

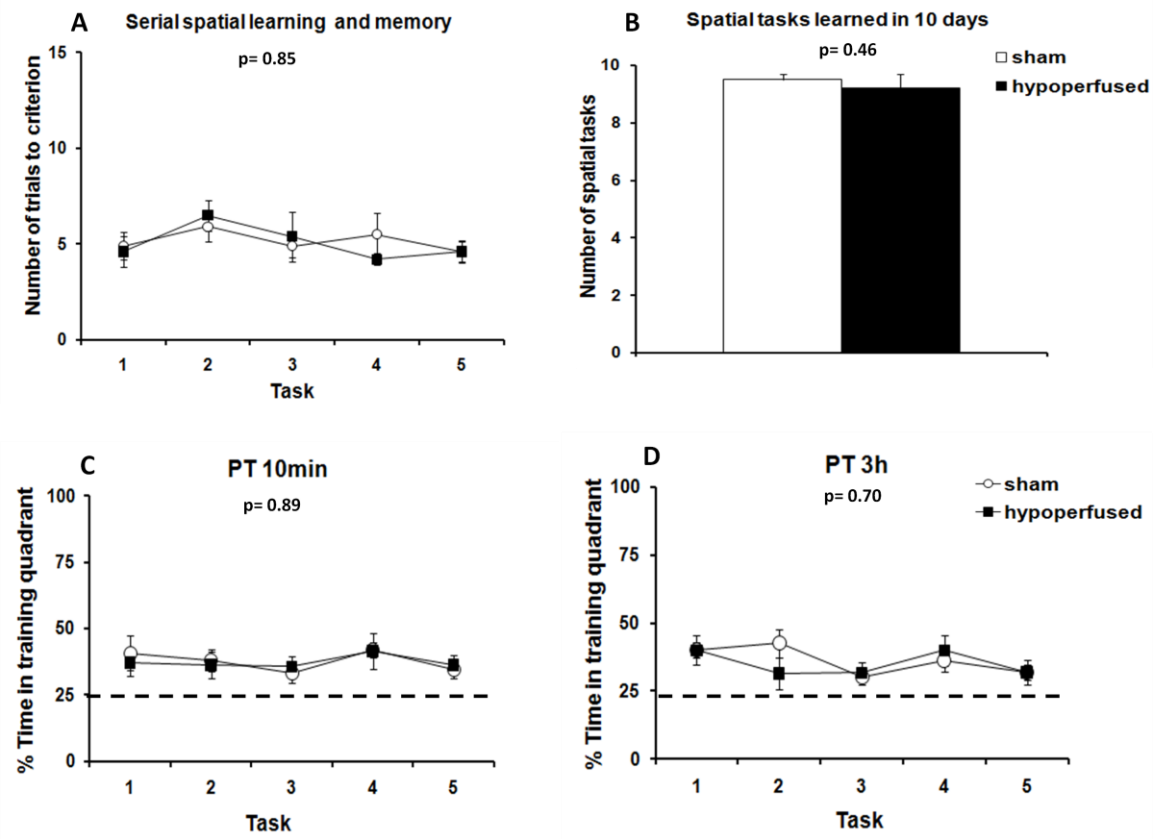

Figure 3.2.: Group performance on a serial spatial learning and memory water maze task

(group mean ± SE)

Spatial memory flexibility (**A**), learning capacity (**B**), short (**C**) and long (**D**) term memory recall were preserved in hypoperfused mice. Two- way repeated measures ANOVA demonstrated an absence of significant differences in the average number of trials to criterion (**A**), the average percentage of time spent swimming in the training quadrant during the 10min (**C**) and 3h (**D**) PT between chronically hypoperfused (n=10) and sham (n=11) mice ($p>0.05$). Both sham and chronically hypoperfused mice performed above chance level (25%) on the 10min and 3h PT ($p>0.05$) (**C, D**). The t- test analysis failed to show significant group differences in the average number of spatial tasks learned in 10 days ($p>0.05$) (**B**).

the platform was situated during the training procedure). The statistical analysis was performed using two- way repeated measures ANOVA (Chapter 3, section 3.2.3.1.2; Chen et al., 2000; Coltman et al., 2011). The statistical analysis on the trials to criterion across the first five platform locations revealed no significant main effects of task ($F_{(4, 76)}$ = 1.566, p = 0.19), or group ($F_{(1, 19)}$ = 0.035, p = 0.85) and no significant group x day interaction ($F_{(4, 76)}$ = 0.524, p = 0.72) (figure 3.2. C, D). These results were confirmed by the statistical analysis of alternative behavioural measures, namely the average number of virtual platform crossings, latency to platform and swimming speed to platform (once the platform reappeared during the last 30 sec of each PT) obtained from the 10 min and 3h PT ($p>0.05$) (table S.3.1- appendices I). One- way ANOVA statistical analysis showed that the percentage of time the animals from the two experimental groups spent searching for the hidden platform in the training quadrant during the first 60 sec for the five spatial tasks was significantly higher than chance (25%) for both the 10min and 3 h PT ($p<.05$) except for the 10min PT for task 1 and the 3h PT for task 5 where no difference from chance performance was evidenced ($p>0.05$).

3.3.3. Effects of chronic cerebral hypoperfusion on white and grey matter integrity, inflammation

3.3.3.1. Chronic cerebral hypoperfusion leads to a significant axonal injury in white and grey matter

Axonal integrity was examined by amyloid precursor protein (APP) immunohistochemistry in white and grey matter ROIs at the completion of the behavioural testing in sham and hypoperfused mice. APP is considered to be a sensitive biomarker of axonal integrity (Stephenson et al., 1992; Selkoe, 1994). Under normal physiological conditions this protein is immunodetected in the neural cell bodies where it is synthesized (Forloni et al., 1992; Palacios et al., 1992). The protein is transported to the axonal terminal via fast axonal transport. APP accumulates in clusters if there is pathological injury to axons (Stephenson et al., 1992).

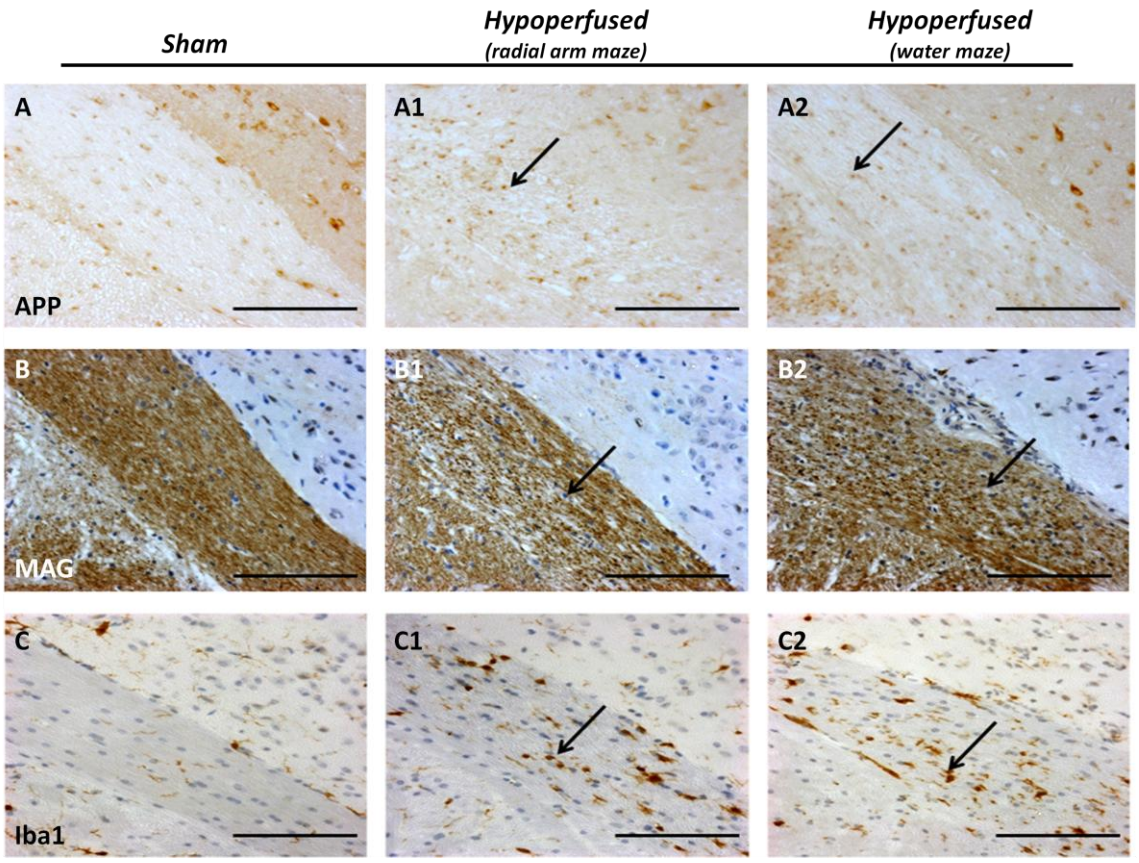

Figure 3.3.: White matter integrity and inflammation in sham and hypoperfused mice

Representative images of immunohistochemically stained axons (**A-A2**), myelin (**B-B2**) and microglia (**C-C2**) from the OT of sham (**A- C**) and chronically hypoperfused mice tested on a radial arm maze (**A1- C1**) and a water maze (**A2- C2**) paradigms. Axonal injury was detected by APP immunoreactivity in swollen and bulbous axons in hypoperfused mice (arrows in **A1**, **A2**). MAG immunostaining revealed myelin abnormalities such as disorganized myelin fibers, vacuoles formations and myelin debris in the two hypoperfused cohorts (arrows in **B1, B2**). Inflammatory levels were increased after chronic cerebral hypoperfusion (arrows in **C1, C2**). Normal axonal (**A**) and myelin (**B**) integrity, inflammatory levels (**C**) were evident in sham animals tested on both the radial arm maze and the water maze paradigms.

Scale bar represents 20µm (magnification x40).

APP immunoreactivity was restricted to cell bodies in all sham operated animals (figure 3.3. A). However, after chronic cerebral hypoperfusion APP was also immunodetected as small dark clusters in swollen/ bulbous axons- an indicative of axonal injury (figure 3.3. A1.A2.- black arrows). The observed hypoperfusion- induced axonal pathology was widespread among examined grey and white matter regions. The statistical analysis comparing the regional and total group pathological grades of axonal integrity was performed using Man- Whitney nonparametric test (Chapter 3, section 3.2.3.2.).

In the radial arm maze experiment, axonal injury with a varying degree of severity was evidenced in 90% (9/10) of the hypoperfused animals (figure 3.3. A1). In this experiment, axonal integrity was significantly compromised in all examined white and grey matter ROIs: the CC ($U= 15.000$, $p= 0.002$), EC ($U= 10.000$, $p= 0.001$), IC ($U= 15.000$, $p= 0.002$), OT ($U= 10.000$, $p<0.0001$), Fx ($U= 15.000$, $p= 0.002$), hippocampus ($U= 10.000$, $p= 0.001$) and Cx ($U= 20.000$, $p= 0.005$), (table 3.1.1.; figure S.3.4.1. A- E, G- H appendices I).

Similarly, axonal injury was also evident in 90% (9/10) of the hypoperfused mice tested on a water maze paradigm (figure 3.3. A2). However, in this particular study, significant hypoperfusion- induced axonal pathology was only observed in the OT ($U= 33.000$, $p= 0.023$) and the hippocampus ($U= 33.000$, $p= 0.023$) (table 3.1.2.; figure S.3.4.2. D, G, appendices I). There was no significant group difference in the axonal integrity in any of the other examined white and grey matter ROIs: the CC ($U= 55.000$, $p= 1.000$), EC ($U= 55.000$, $p= 1.000$), IC ($U= 49.500$, $p= 0.294$), Fx ($U= 49.500$, $p= 0.294$), and Cx ($U= 44.000$, $p= 0.128$) (table 3.1.2.;figure S.3.4.2. A-C, E, H, appendices I).

The regional pathological grades of axonal integrity for each individual mouse are given in tables S.3.2.1. and S.3.2.2., appendices I. The total scores of axonal integrity and the associated statistical analysis are given in table S.3.3.1., S.3.3.2. S.3.3.3.- appendices I.

Biomarker	Regions of interest	Sham (n=10) (median)	Hypoperfused (n=10) (median)
APP	*Corpus callosum (CC)*	0.0	1.0 **
Axonal integrity	*External capsule (EC)*	0.0	1.0 ***
	Internal capsule (IC)	0.0	1.5 **
	Optic tract (OT)	0.0	3.0 ***
	Fimbria fornix (Fx)	0.0	1.0 **
	Hippocampus	0.0	1.5 ***
	Cortex (Cx)	0.0	1.5 **
MAG	*Corpus callosum (CC)*	0.0	1.0 **
Myelin integrity	*External capsule (EC)*	0.0	1.0 **
	Internal capsule (IC)	0.0	2.0 ***
	Optic tract (OT)	0.0	3.0 ***
	Fimbria fornix (Fx)	0.0	1.5 ***
Iba1	*Corpus callosum (CC)*	0.0	0.0 *
Inflammation	*External capsule (EC)*	0.0	1.0 **
	Internal capsule (IC)	0.0	0.5 **
	Optic tract (OT)	0.0	2.0 **
	Fimbria fornix (Fx)	0.0	1.0 **
	Hippocampus	0.0	0.0 *
	Cortex (Cx)	0.0	1.0 **

Table 3.1.1.: Regional group median pathological grades:

Radial arm maze experiment

Chronically hypoperfused mice (n=10) tested on a radial arm maze paradigm exhibited a significant axonal damage (APP), significant myelin abnormalities (MAG) and a significantly increased inflammation (Iba1) compared with sham animals (n=10) in the examined ROIs two months post- surgery.

Significant group differences as given by Mann- Whitney nonparametric statistics: ($p<0.05$)*, ($p<0.01$)**, ($p<0.001$)***

Biomarker	Regions of interest	Sham (n=11) (median)	Hypoperfused (n=10) (median)
APP	*Corpus callosum (CC)*	0.0	0.0
Axonal integrity	*External capsule (EC)*	0.0	0.0
	Internal capsule (IC)	0.0	0.0
	Optic tract (OT)	0.0	0.0 *
	Fimbria fornix (Fx)	0.0	0.0
	Hippocampus	0.0	0.0 *
	Cortex (Cx)	0.0	0.0
MAG	*Corpus callosum (CC)*	0.0	0.5 **
Myelin integrity	*External capsule (EC)*	0.0	1.0 **
	Internal capsule (IC)	0.0	1.0 ***
	Optic tract (OT)	0.0	3.0 ***
	Fimbria fornix (Fx)	0.0	0.0 **
Iba1	*Corpus callosum (CC)*	0.0	0.0
Inflammation	*External capsule (EC)*	0.0	1.0 **
	Internal capsule (IC)	0.0	1.5 ***
	Optic tract (OT)	0.0	2.5 ***
	Fimbria fornix (Fx)	0.0	0.5 **
	Hippocampus	0.0	0.0
	Cortex (Cx)	0.0	0.0

Table 3.1.2.: Regional group median pathological grades:

Water maze experiment

Chronically hypoperfused mice (n=10) tested on a water maze paradigm exhibited minimal axonal injury (APP), a significant myelin pathology (MAG) and increased inflammation (Iba1) compared with sham animals (n=11) in the examined ROIs two months post- surgery.

Significant group differences as given by Mann- Whitney nonparametric statistics: ($p<0.05$)*, ($p<0.01$)**, ($p<0.001$)***

3.3.3.2. Chronic cerebral hypoperfusion leads to a significant myelin pathology

Myelin structural integrity was evaluated in behaviourally tested sham and chronically hypoperfused mice by means of myelin associated glycoprotein (MAG) immunochemistry. MAG is known to be a sensitive biomarker for myelin abnormalities (vacuole formations, fiber disorganization, debris) occurring under mild hypoxic-ischemic conditions (Aboul- Enein et al., 2003).

MAG stained myelin fibers were tightly organized and formed well defined bundle- like structures (tracts), easily detectable in white matter regions of all sham operated animals (figure 3.3. B). However, myelin structural abnormalities with a different degree of severity were evident in white matter regions of all hypoperfused mice (figure 3.3. B1, B2). These white matter pathological changes consisted of vacuole formations in the myelin sheath, deposition of MAG debris (figure 3.3. B1, B2- black arrows). The statistical analysis comparing the regional and total group pathological grades of myelin integrity was performed using Man- Whitney nonparametric test (Chapter 3, section 3.2.3.2.).

In the radial arm maze experiment, hypoperfused mice showed significant myelin abnormalities in all examined white matter ROIs: the CC ($U= 20.000$, $p= 0.004$), EC ($U= 20.000$, $p= 0.004$), IC ($U= 5.000$, $p<0.0001$), OT ($U= 5.000$, $p<0.0001$), and Fx ($U= 5.000$, $p<0.0001$) (figure 3.3. B1) (table 3.1.1.; figure S.3.4.3. A- E, appendices I).

Similar results were observed for the water maze experiment where significant hypoperfusion- induced myelin pathology was observed in the CC ($U= 27.500$, $p= 0.009$), EC ($U= 22.000$, $p= 0.003$), IC ($U= 5.500$, $p<0.0001$), OT ($U= 0.000$, $p<0.0001$), and Fx ($U= 33.000$, $p= 0.023$) (figure 3.3. B2) (table 3.1.2.; figure S.3.4.4. A- E, appendices I).

The regional pathological grades of myelin integrity for each individual mouse are given in table S.3.2.3. and S.3.2.4. appendices I. The total scores of myelin integrity and the associated statistical analysis are given in table S.3.3.1., S.3.3.2. S.3.3.3.- appendices I.

3.3.3.3. Chronic cerebral hypoperfusion leads to a significantly increased inflammation

In the present study, an ionized calcium binding adaptor protein 1 (Iba1) antibody targeted to inflammatory microglia (Ito et al., 1998) was applied to investigate inflammatory processes in white and grey matter ROIs in behaviourally tested sham and hypoperfused mice.

Normal inflammatory levels were evidenced in all sham- operated mice where a few, resident Iba1 positive microglial cells were immunodetected in examined white and grey matter areas (figure 3.3. C). Chronic cerebral hypoperfusion was associated with an increase of Iba1 immunoreactivity in examined grey and white matter ROIs- an indicative of an increased inflammatory activity (figure 3.3. C1, C2- black arrows). The statistical analysis comparing the regional and total group pathological grades of axonal integrity was performed using Man- Whitney nonparametric test (Chapter 3, section 3.2.3.2.).

In the radial arm maze experiment, increased inflammation was observed in 80% (8/10) of the hypoperfused mice (figure 3.3. C1). In this experiment, significant differences in inflammatory levels between sham and chronically hypoperfused mice were reported for all examined ROIs: the CC ($U= 30.000$, $p= 0.030$), EC ($U= 20.000$, $p= 0.005$), IC ($U= 25.000$, $p= 0.013$), OT ($U= 20.000$, $p= 0.005$), Fx ($U= 15.000$, $p= 0.002$), hippocampus ($U= 30.000$, $p= 0.030$) and Cx ($U= 20.000$, $p= 0.005$) (table 3.1.1.; figure S.3.4.5. A-E, G, H, appendices I).

In the water maze experiment, increased inflammatory levels were observed in 90% (9/10) of hypoperfused mice (figure 3.3. C2). However, in this particular study, significant group differences in the inflammatory levels were statistically evidenced only for the EC ($U= 22.000$, $p= 0.003$), IC ($U= 5.500$, $p<0.0001$), OT ($U= 5.500$, $p<0.0001$), Fx ($U= 27.500$, $p= 0.009$). In the CC, inflammatory levels did not change significantly with hypoperfusion ($U= 49.000$, $p= 0.294$) (table 3.1.2.; figure S.3.4.6. A- E, appendices I). In this behavioural cohort, no significant group differences in inflammation were

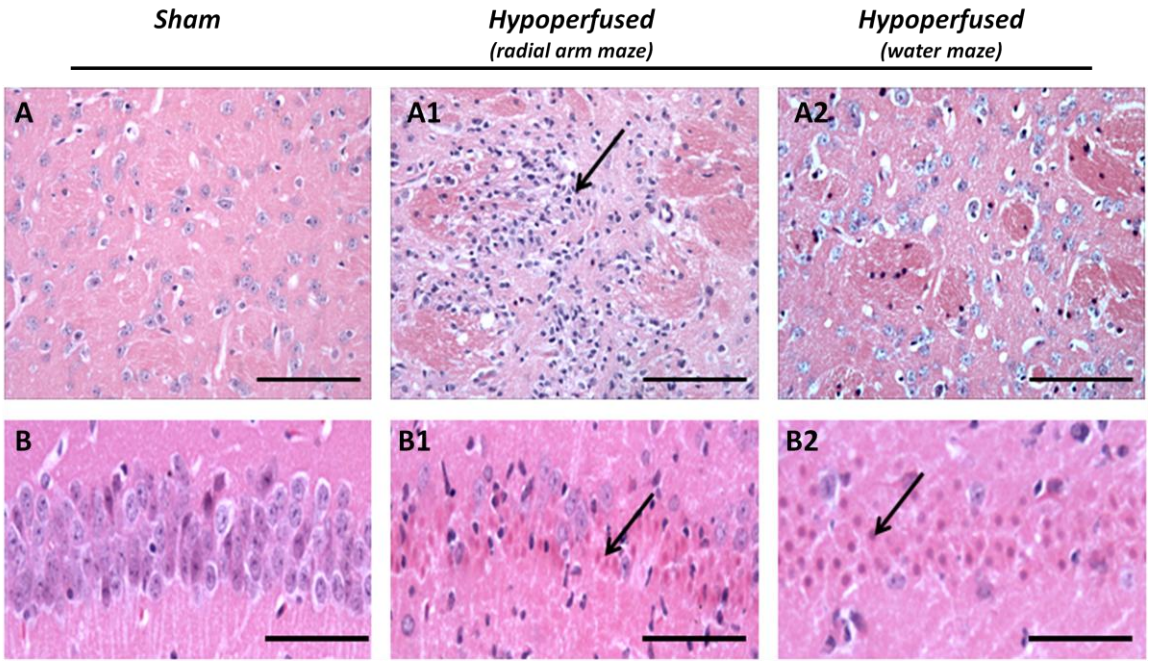

Figure 3.4.: Grey matter integrity in sham and hypoperfused mice

Representative images of H&E staining from the striatum (**A-A2**) and CA1 region of the hippocampus (**B-B2**) of sham (**A, B**) and chronically hypoperfused mice tested on a radial arm maze (**A1, B1**) and water maze (**B1, B2**) paradigms. Neuronal perykaria ischemic injury was observed in examined grey matter areas of hypoperfused mice (arrow in **A1, B1, B2**). Grey matter structural integrity was preserved in all sham mice (**A-B**)

Scale bar represents 15µm (magnification x40) (**A-A2**), 20µm (magnification x60) (**B-B2**).

observed for any of the grey matter ROIs- the hippocampus (U= 49.500, p= 0.294) and Cx (U= 44.000, p= 0.128) (table 3.1.2.; figure S.3.4.6. G, H appendices I).

The regional pathological grades of inflammation for each individual mouse are given in tables S.3.2.5. and S.3.2.6. appendices I. The total scores of inflammation and the associated statistical analysis are given in table S.3.3.1., S.3.3.2. S.3.3.3.- appendices I.

3.3.3.4. Chronic cerebral hypoperfusion leads to neuronal ischemic damage

Previously published studies on chronically hypoperfused mice reported an absence of overt grey matter abnormalities in this animal model (Shibata et al., 2004, Shibata et al., 2007). The present study aimed at independently examining the presence of neuronal ischemic injury in behaviourally tested sham and chronically hypoperfused mice by using a standard H&E histological staining.

In the present study, all sham- operated mice exhibited a healthy neuronal morphology characterized by a large blue nucleus and a light blue cytoplasm observed in cortical (the Cx) and subcortical (the hippocampus, the striatum) areas (figure 3.4. A, B). The overall brain morphology following sham surgery was well preserved and the different brain regions were easily distinguishable on the basis of their specific cellular morphology and layer organization (figure 3.4. A, B).

Unexpectedly, cortical and subcortical grey matter ischemic injury was observed in 70% (7/ 10) of the hypoperfused mice tested on the radial arm maze task and in 28.5% (4/14) of the hypoperfused mice tested on the water maze paradigm (figure 3.4. A1, A2, B1, B2). Ischemic neurons presented a small, shrunken, dark blue, and triangular cellular morphology (figure 3.4. A1, B1- black arrow). In some of the injured cells there was an absence of a clear differentiation between the nucleus and the cytoplasm. “Ghost neuron” formations characterized by the physical disappearance of ischemic neurons were observed among cellular layers as light pink areas (figure 3.4. B1- white arrow). Pallor and vacuolation of the neuropil were also observed in areas of ischemic damage (figure S.3.4., appendices I). The predominantly affected grey matter areas in hypoperfused mice

were regions known for their susceptibility to blood flow alterations: the CA1 area of the hippocampus, the Cx and the striatum. However, as the pathological analysis was performed relatively late after the induction of chronic cerebral hypoperfusion (~ 2 months after the microcoils application), glial scar formations were observed in the majority of the ischemic areas, thus rendering difficult any attempt to quantitatively evaluate the severity of the observed pathological changes (e.g. cell counting was impossible) (figure S.3.4., appendices I). Therefore, in the present study the neuronal ischemic injury was reported only as present/ absent.

At the examined brain levels, an absence of overt neuronal ischemic injury, a preserved grey matter structural integrity and brain morphology were evidenced in only 30% (3/10) of the hypoperfused mice tested on the radial arm maze paradigm and in 71.5 % (10/14) of the hypoperfused mice tested in the water maze experiment.

3.3.4. Inflammation in white matter correlates significantly with working memory, but not executive function in hypoperfused mice.

In order to investigate potential associations between hypoperfusion- induced white matter pathology and behavioural parameters in mice, a Spearman`s correlation analysis was performed between the overall assessment of axonal, myelin integrity, inflammation (tables S.3.3.1 and S.3.3.2- appendices I) in each mouse and their behavioural assessment of working memory (the number of revisiting errors on a radial arm maze paradigm) and executive function (the number of trials to criterion on a water maze task) (Chapter 3, section 3.2.3.3.). The results demonstrated significant associations between working memory and inflammation in white matter ($r= 0.70$, $p= 0.03$), but not between working memory and axonal ($r=0.40$, $p= 0.25$), myelin ($r=-0.19$, $p= 0.58$) integrity in white matter (figure 3.5. A, C, E). An absence of significant associations was evident between executive function (memory flexibility) and all examined white matter components: axonal ($r=0.35$, $p= 0.31$), myelin ($r=-0.18$, $p= 0.61$) integrity and inflammation ($r=-0.01$, $p= 0.97$) (figure 3.5. B, D, F).

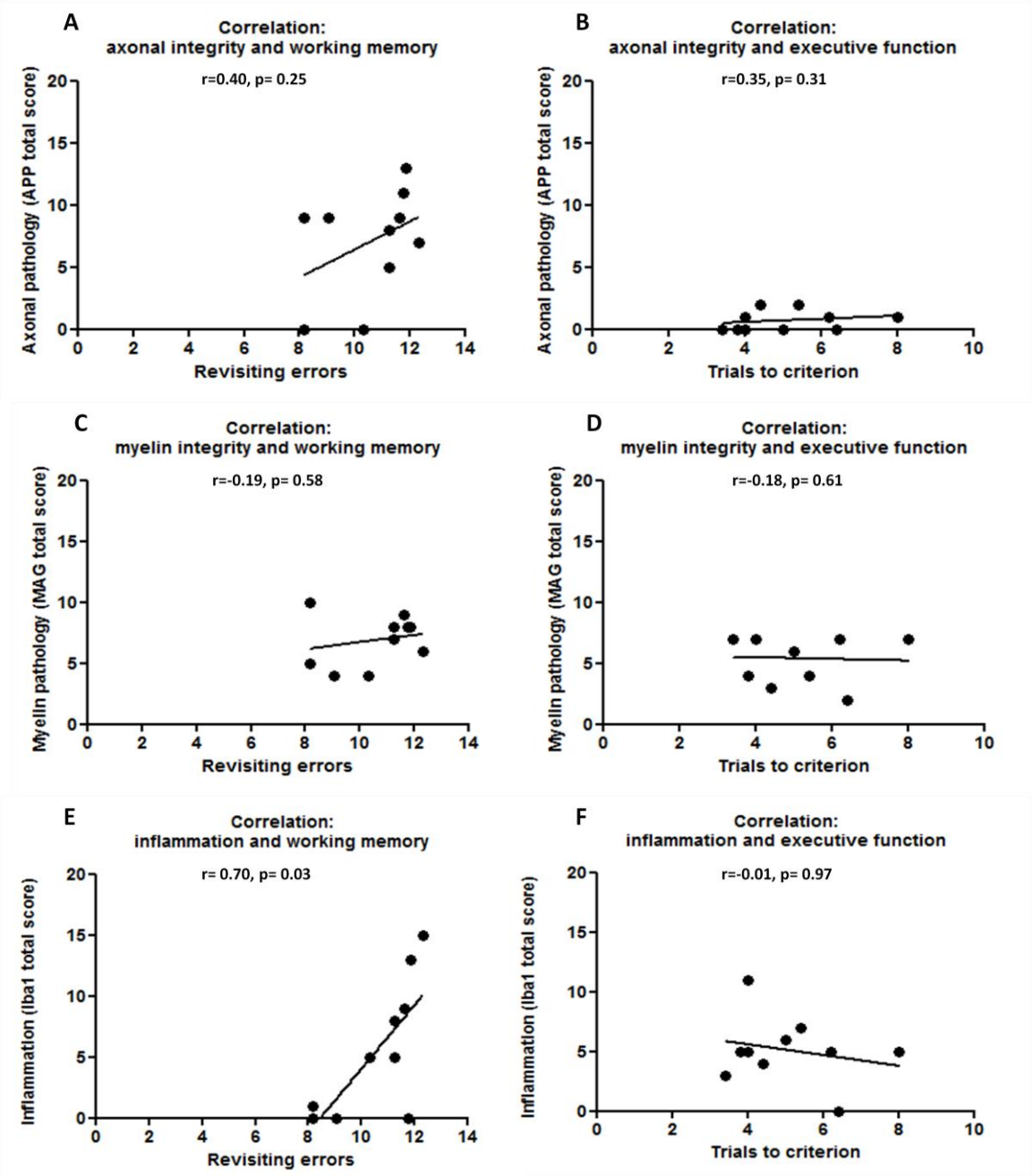

Figure 3.5.: Correlation analysis between white matter cellular components and behavioural parameters of working memory and executive function in hypoperfused mice

The Spearman`s correlation analysis demonstrated significant associations between working memory (revisiting errors) and inflammation in white matter (**E**) ($p<0.05$), in the absence of significant associations between working memory and axonal (**A**)/ myelin (**C**) integrity ($p>0.05$). No significant associations were evident between executive function (trials to criterion) and any of examined white matter cellular components (**B, D, F**) ($p>0.05$).

3.4. Discussion

Building on previous work, the experiments presented in Chapter 3 sought to test the hypothesis that hypoperfusion- induced white matter pathology might be associated with spatial working memory and executive function deficits in mice. In accordance with the existing literature on this animal model, the behavioural data confirmed the existence of spatial working memory impairment in the absence of spatial memory flexibility, learning, short- and long- term memory recall deficits in hypoperfused mice. In contradiction with previously published work on this animal model, a spectrum of white and grey matter abnormalities accompanied by an increased inflammation were evident in behaviourally tested hypoperfused mice. Although there was a significant association only between hypoperfusion- induced inflammation in white matter and performance on a working memory radial arm maze task, the present pathological findings suggest that white matter abnormalities, neuronal ischemia and increased inflammation might be at the basis of hypoperfusion- induced cognitive impairment in mice.

3.4.1. Cognition and memory in chronically hypoperfused mice

3.4.1.1. Spatial working memory impairment in chronically hypoperfused mice

In accordance with previous findings on this animal model (Shibata et al., 2007; Nishio et al., 2010), the present behavioural results confirmed the occurrence of spatial working memory impairment in chronically hypoperfused mice (Coltman et al., 2011). Executive function (memory flexibility), learning capacity, short and long- term memory recall were preserved in hypoperfused mice (Coltman et al., 2011). The absence of visual impairment in the behaviourally tested cohorts suggests that the observed cognitive deficits were due to hypoperfusion- induced neuropathology rather than visual disturbances (data presented in S.3.1.1., S.3.3. appendices I).

The present behavioural data and published work on this animal model suggest that chronic cerebral hypoperfusion results in working memory impairment in mice at early post- surgery time points.

Interestingly, there seem to be species differences in the onset of cognitive impairment following chronic cerebral hypoperfusion in rodents. In rats, chronic cerebral hypoperfusion leads to an initial spatial reference memory impairment on a water maze task (7 days post- surgery) followed by long- term spatial reference and working memory deficits on a radial arm maze task (63 days post surgery) (Pappas et al., 1996; Sopala and Danysz, 2001). In contrast, hypoperfused mice exhibit an early spatial working memory impairment on a radial arm maze task in the absence of spatial reference memory or executive function deficits taxed on radial arm maze and water maze paradigms (Shibata et al., 2007; Coltman et al., 2011). In chronically hypoperfused mice a spatial reference memory deficit is observed 6 months post- surgery (Nishio et al., 2010). The reported differences in the behavioural performance of hypoperfused rats and mice might be due to overall methodological as well as species differences in the response to hypoperfusion. Specifically, in hypoperfused rats, the common carotid arteries are completely ligated leading to severe cerebral blood flow reductions. In hypoperfused mice, the common carotids are only partially obstructed and the cerebral blood flow is modestly reduced. However, at the difference from the majority of rat strains, the C57Bl6J mice have underdeveloped posterior communicating arteries leading to poorer cerebrovascular compensations and a more severe pathological/ functional outcome following cerebrovascular challenges (e.g. cerebral ischemia) in this mouse strain (Yang et al., 1997; Kitagawa et al., 1998). Therefore, it is possible that differences inherent to the surgical procedure and the underlying cerebrovasculature might differentially impact on the spatio-temporal onset of neuropathology in hypoperfused rats and mice resulting in differential temporal onset of cognitive impairment in these animal models. However, in both hypoperfused mice and rats the severity of cognitive deficits seems to increase overtime in consistency with the chronic nature of the surgical intervention.

In the alternative gerbil model of chronic cerebral hypoperfusion impaired learning capacity was evidence on a fear- conditioning task (Kudo et al., 1990). These behavioural data were also confirmed in hypoperfused rats which exhibited a learning impairment on a similar paradigm- the passive avoidance step task one month post- surgery (Kumaran et al., 2008). However, at the same post- surgical time point chronically hypoperfused mice

performed a fear- conditioning task as well as sham- operated counterparts (Shibata et al., 2007; Nishio et al., 2010). It is unknown whether working memory and executive function are impaired in hypoperfused gerbils and whether the observed learning deficits worsen proportionally with the post- surgery time point in this animal model of chronic cerebral hypoperfusion. This is due to the fact that it is difficult to train this rodent species on standard behavioural paradigms such as the water maze and the radial arm maze.

Overall, the behavioural data from the existing rodent models indicate the existence of certain species differences in the functional outcome following chronic cerebral hypoperfusion. This is important for preclinical (animal) data interpretation and extrapolation to humans. Specifically, when working with animal models one should be aware of the fact that animal models do not replicate the human condition in its entire complexity, but do mimic some of its pathophysiological, neuropathological and functional aspects and therefore by their nature they do present certain limitations (Hainsworth and Markus, 2008; Jiwa et al., 2010).

The present animal data support clinical findings on elderly people with artery stenosis exhibiting working memory impairment (Derdeyn et al., 1994; Mathiesen et al., 2004; Ruitenberg et al., 2005). However, at the difference from elderly people, chronically hypoperfused mice have preserved executive function (memory flexibility) at least at early post- surgery time points (1-2 months after surgery). Future behavioural experiments on this animal model would allow to investigate alternative memory and cognitive processes such as for instance processing speed (reaction time) which are known to be impaired in "healthy" elderly (Kennedy and Raz, 2009; Madden et al., 2009; Sullivan et al., 2010). From a methodological point of view this could be achieved by comparing the performance of sham and hypoperfused mice on existing behavioural paradigms such as operant and serial choice paradigms (Moore et al., 1992; Young et al., 2010). Further detailed time- course behavioural studies would allow to examine the temporal evolution of cognitive impairment in this chronic animal model (discussed in section 3.4.4.3.).

3.4.2. Spectrum of white and grey matter pathology in chronically hypoperfused mice

3.4.2.1. Axonal injury in white and grey matter of chronically hypoperfused mice

Pathological damage to axons is associated with a disruption of axonal cytoarchitecture and disturbances of fast axonal transport. Following axonal damage, the anterogradely transported APP accumulates proximal to the disrupted segment in swollen and bulbous axons forming immunodetectable protein clusters occurring before conventional morphological evidence of axonal damage (e.g. in the form of axonal end bulbs) (Stephenson et al., 1992). Therefore, APP immunochemistry is considered to be more sensitive technique than routinely used histological methods for detecting axonal damage such as for example Bodian or Bielschowsky's silver impregnation (Switzer, 2000).

The results from the present study demonstrated that axonal integrity was intact in sham-operated mice as evidenced by restricted APP immunoreactivity to cell bodies in white and grey matter areas. However, axonal injury with a varying degree of severity was observed in white and grey matter regions of behaviourally tested, chronically hypoperfused mice. Specifically, in the radial arm maze experiment, a significant widespread axonal damage was evidenced in white matter tracts (CC, EC, IC, Fx, and OT), cortical (Cx) and subcortical (hippocampus) grey matter regions of the hypoperfused brain. In the water maze experiment, chronic cerebral hypoperfusion was associated with relatively preserved axonal integrity in the majority of the examined white matter areas (CC, EC, IC, Fx) and the Cx. In this particular experiment, a significant hypoperfusion-induced axonal injury was observed only in the OT and hippocampus. The more widespread axonal injury observed in the hypoperfused cohort tested on a radial arm maze paradigm is in consistency with the more pronounced grey matter pathology in these animals (discussed in section 3.4.2.3.).

The present pathological findings are in contradiction with previous studies on hypoperfused mice suggesting the existence of selective white matter pathology with minimal axonal injury in this animal model (Holland et al., 2011; Reimer et al., 2011).

In particular, two recent publications from our group have demonstrated using scanning-confocal and electron microscopy (Reimer et al., 2011) as well as in vivo MRI (Holland et al., 2011) an absence of and/ or a minimal axonal injury in *ad libitum* fed and non-behaviourally tested chronically hypoperfused mice at both early (3 days) and late (1 month) post- surgery time points. The observed discrepancies with the present pathological findings could be explained by differences in the applied methodological approach. From a technical point of view, both Holland et al., 2011 and Reimer et al., 2011 used much more sophisticated imaging tools allowing quantification of the observed axonal pathology, which could not be achieved by means of the presently applied semi-quantitative grading scale used to differentiate among variations in APP immunoreactivity. Further, at the difference from the present study, in Holland et al., 2011, Reimer et al., 2011, the animals were not food deprived and/ or behaviourally tested (discussed in section 3.4.4.). Also, the time point used for the pathological analysis was 1 month post- surgery for Holland et al., 2011, Reimer et al., 2011, whereas in the present study the pathology was examined ~2 months post- surgery (discussed in section 3.4.4.).

The presently observed significant axonal injury in white and grey matter areas of chronically hypoperfused mice is substantiated by animal and human studies. Specifically, hypoperfusion- induced axonal injury was reported in chronically hypoperfused rats and gerbils even in the absence of behavioural training (Kurumatani et al., 1998; Wakita et al., 2002). In the rat model of chronic cerebral hypoperfusion APP clusters were immunodetected in white and grey matter areas as soon as 14 days post- surgery and the severity of the observed axonal pathology was reported to increase gradually from 1 to 30 days after artery ligation (Wakita et al., 2002). In chronically hypoperfused gerbils, significant changes in axonal cytoarchitecture were evidenced by applying a Western blot analysis to one of the major axonal neurofilaments- neurofilament H, two months after chronic cerebral hypoperfusion (Kurumatani et al., 1998). In the present experiments on chronically hypoperfused mice, axonal neurofilaments and microtubules were not examined, but future studies should aim at gaining a better understanding of the precise hypoperfusion- induced alterations in axonal cytoarchitecture in relation to other white/ grey matter cellular components (neurons, glia, myelin) by using a combined

immunochemical and biomolecular (e.g. Western blot and/ or (q)PCR) approach to visualize as well as to quantitatively detect protein levels and/ or mRNA expression of neurofilaments, microtubules, synaptic terminals.

Clinical studies demonstrated axonal pathology in "healthy" and demented elderly on MRI/ DTI scans (e.g. reductions in axial diffusivity) and post- mortem as immunochemically- evident axonal swellings and bulbs (Syde et al., 2005; Gunning-Dixon et al., 2009; Madden et al., 2009; Salehi et al., 2009). In regards to the overall literature on white matter pathology, it seems that axonal abnormalities are more likely to be "the rule" than "the exception". For instance, an extensive axonal loss has been reported in grey and white matter areas of multiple sclerosis patients and animal models of this condition (Davie et al., 1995; Trapp et al., 1998; Bitsch et al., 2000; Mancardi et al., 2001; Lassmann, 2003; Craner et al., 2004; Fischer et al., 2009). These findings are interesting as multiple sclerosis is primarily regarded as an autoimmune, demyelinating disorder. Axonal injury is also a common pathological hallmark in spinal cord and traumatic brain injury (Park et al., 2004; Buki and Povlishok, 2006; Yi and Hazell, 2006). It is believed that axonal injury is at the basis of functional impairment (cognitive, memory and motor deficits) associated with white matter damage in different neurological/ neurodegenerative conditions as well as in elderly (Medana and Esiri, 2003). This is not surprising considering the fact that axonal degeneration could lead to synaptic loss, dendritic abnormalties and disruption of broad neural connections (Medana and Esiri, 2003; Buki and Povlishok, 2006; Fields, 2008).

Although, there are discrepancies between the present findings of axonal injury in chronically hypoperfused mice and already published work on this model (Holland et al., 2011; Reimer et al., 2011), the overall existing literature supports the existence of axonal abnormalities following hypoperfusion.

3.4.2.2. Myelin pathology in chronically hypoperfused mice

In the present study, myelin associated glycoprotein (MAG) immunochemistry was applied for the pathological evaluation of myelin structural integrity in behaviourally tested sham and chronically hypoperfused mice.

MAG is a minor myelin protein (2% of total myelin protein) with periaxonal localization (Quarles, 2007). Functionally, MAG is involved in axon- glial interactions and it is a well established molecular factor inhibiting axonal regeneration following brain injury by its involvement in the NOGO signaling system (Liu et al., 2002; Quarles, 2007).

MAG has been shown to be preferentially lost under hypoxic- ischemic like conditions such as stroke (Aboul- Enein et al., 2003). Therefore, MAG immunohistochemistry is considered to be a sensitive pathological tool for the detection of mild structural abnormalities in the myelin sheath such as fibers disorganizations, vacuoles and accumulations of MAG debris which could not be detected using standard histological tools such as Kluver- Barrera and Luxol fast blue staining (Kluver and Barrera, 1953; Goto, 1987). This immunohistochemical approach has been previously applied by our group and has been shown to be sensitive to myelin abnormalities in chronically hypoperfused mice (Coltman et al., 2011; Holland et al., 2011; Reimer et al., 2011).

In the present experiments, all sham- operated mice exhibited preserved myelin integrity in examined white matter areas. In accordance with previous findings in this model (Shibata et al., 2004, Shibata et al., 2007; Nishio et al., 2010; Coltman et al., 2011; Holland et al., 2011; Reimer et al., 2011), myelin abnormalities such as fibers disorganizations, vacuole formations and an accumulation of myelin debris in examined white matter tracts (the CC, EC, IC, OT, Fx) were evidenced in all hypoperfused animals tested on both the radial arm maze and the water maze tasks. These data suggest that myelin pathology assessed by MAG immunoreactivity is inherent to the hypoperfused condition regardless of any additional environmental factors (e.g. behavioural paradigm, food deprivation).

In regards to previous findings on this animal model, it seems that pathological changes in MAG and the associated axon- glial interactions might be an early pathological

phenomenon occurring as soon as 3 days following microcoils surgery (Reimer et al., 2011). These myelin abnormalities increase in severity proportionally with the post-surgery time period indicating cumulative pathological changes in the myelin sheath of chronically hypoperfused mice (Reimer et al., 2011). Interestingly, MAG protein levels remain intact in white matter areas of the chronically hypoperfused mouse brain at both early (3 days) and late (1 month) post- surgery time points. The reason(s) for the steady protein levels are unknown, but they might be related to preserved oligodendroglial protein synthesis as demonstrated by an absence of oligodendroglial apoptosis in this animal model (Reimer et al., 2011; Chapter 5). However, in MAG null mice, oligodendroglial apoptosis is reported to occur with chronological aging suggesting that following MAG loss in chronically hypoperfused mice, oligodendroglial apoptosis could occur at later post- surgical time points (Weiss et al., 2000). These in vivo results are supported by in vitro findings showing increased survival rate and myelin production by oligodendrocytes cultured in MAG supplemented media suggesting that MAG signaling is important for oligodendroglial biology (Gard et al.1996). Future long- term studies on chronically hypoperfused mice would allow to determine oligodendroglial fate in relation to MAG. Alternatively, it would be interesting to apply the microcoils surgery on MAG null mutants in order to determine the effects of deficient MAG signaling on oligodendroglia and myelin integrity in this model. Since MAG is involved in axon- glial interactions, one could suppose that an absence of MAG might also impact on the severity of axonal injury following chronic cerebral hypoperfusion. This hypothesis is supported by the existence of late- onset axonopathy in aging MAG null mutants characterized by axonal swellings, spheroids, as well as decreases in neurofilaments associated with nerve conduction abnormalities (Weiss et al., 2001; Loers et al. 2004). Further, compact myelin was reported to remain intact in chronically hypoperfused mice as shown by preserved MBP immunohistochemical distribution and protein levels between 3 days and 1 month post- surgery (Reimer et al., 2011). These observations are in accordance with findings in MAG null mutants where the absence of MAG does not affect compact myelin (PLP and MBP) protein levels (Weiss et al. 2000). However, in chronically hypoperfused rats, significant MBP decreases were evidenced by means of immunohistochemical analysis and protein assays (Farkas et al., 2004). Using a specific MBP isoform- degraded MBP

(dMBP) which selectively labels degraded myelin (Matsuo et al., 1997), myelin pathology was evidenced in various white matter regions of the hypoperfused mouse brain 1- 2 months post- surgery using a standard immunohistochemical approach (Coltman et al., 2011; Holland et al., 2011). These data were confirmed in the presence (Coltman et al., 2011) and absence (Holland et al., 2011) of behavioural training suggesting that myelin pathology is an inherent pathological hallmark of the hypoperfused mouse brain. In addition to changes at the peri-axonal space evidenced by MAG immunohistochemistry, Reimer et al., 2011 demonstrated concomitant changes at the paranodes by Caspr-Neurofascin (Nfasc155) immunoreactivity. Caspr is located at the axonal paranode, and Nfasc155 is contained at the opposing paranodal loops of the myelin sheath. These proteins function as a diffusion barrier for the nodal Nav1.6. channels and are essential for the integrity of nodes of Ranvier. With hypoperfusion, there were significant reductions in Nfasc155 immunoreactivity suggesting paranodal abnormalities. It is unknown whether and/ or how MAG abnormalities might influence on the occurrence of paranodal pathology following chronic cerebral hypoperfusion and future studies should elucidate this question.

Overall, the experimental data so far suggest the occurrence of paranodal- peri-axonal abnormalities in chronically hypoperfused mice at least at early post- surgery time points (1- 2 months following microcoils application).

Chronological age is associated with pathological changes in myelin structure such as vacuole formations, cytoplasm- filled ballons, fibers disorganization and accumulation of myelin debris in white matter areas accompanied by alterations in myelin lipid and protein content (Knox et al., 1989; Tang et al., 1997; Peters et al., 2000; Peters and Sethares, 2002; Bartzokis, 2004). These myelin abnormalities are observed in elderly humans, aged rats, and non- human primates and they are supposed to contribute to age- related cognitive decline (Knox et al., 1989; Tang et al., 1997; Peters et al., 2000; Peters and Sethares, 2002; Bartzokis, 2004). Additionally, MAG pathology is evidenced in several central nervous system disorders such as schizophrenia (Aberg et al. 2006; Mcinnes and Lauruat 2006), multiple sclerosis (Johnson et al. 1986; Rodriguez and Scheithauer 1994), cuprizone toxicity (Ludwin and Johnson 1981), progressive multifocal

leukoencephalopathy (Itoyama et al. 1982), hypoxic- ischemic conditions (Aboul- Enein et al., 2003). However, the functional implication of MAG abnormalities in humans remains unknown. In mice, MAG null mutantion is not associated with any major functional deficits (at least during early and mid- adulthood) when compared with aged matched WT controls (Montag et al., 1994). These animal data suggest that MAG abnormalities might not be crucial for sustaining normal cognitive and motor function.

3.4.2.3. Neuronal ischemic injury in chronically hypoperfused mice

In the present experiments, a standard histological H&E staining was used to investigate the overall brain morphology and detect potential neuronal ischemic injury in the examined behavioural cohorts. Similar to other histological techniques, H&E is a crude method of pathological evaluation and lacks a sufficient sensitivity as to the mechanisms leading to neuronal cell death (apoptosis vs. necrosis), the damaged cellular compartments (dendrites, axons, soma, axonal terminals, synapses), the functional changes (protein synthesis, neurotransmission, gene expression, neuronal action potential firing) as well as the phenotype of the injured neurons.

In the present experiments, an extensive neuronal ischemic loss was evidenced in examined cortical (the Cx) and subcrotical (the striatum, the hippocampus) grey matter areas of hypoperfused mice. The observed grey matter pathology was characterized by areas of pyknotic neural cells accompanied by regional disorganizations of structural layer morphology, pallor of neuropil. These pathological changes were primarily observed in food- deprived hypoperfused animals tested on a radial arm maze paradigm. The same results were observed for the replica of the radial arm maze experiment presented in appendices I confirming the presence of neuronal ischemic injury in the majority of hypoperfused mice (~70%) following behavioural training on a radial arm maze task.

The present findings of neuronal ischemic injury in chronically hypoperfused mice tested on a radial arm maze task were surprising in regards to a previously published work on this model suggesting an absence of overt grey matter abnormalities at early post- surgery time points (1- 2 months post- coiling) (Shibata et al., 2004; Shibata et al., 2007; Coltman

et al., 2011; Holland et al, 2011). Specifically, Shibata et al. 2007 tested spatial working memory in chronically hypoperfused mice one month after surgery using the same behavioural paradigm (the radial arm maze task). However, this group never examined the pathological profile of the behaviourally tested cohort reporting no overt grey matter ischemic injury on the basis of pathological data from a simultaneously examined non-behaviourally challenged and *ad libitum* fed cohort of hypoperfused mice. Therefore, it is possible that grey matter ischemia was not detected by Shibata et al., 2007 as the neuropathology was not examined in the behaviourally tested chronically hypoperfused mice.

Neuronal ischemic injury as well as morphological changes in neurons have been reported to occur in chronically hypoperfused rats and gerbils (Kudo et al., 1993; Ni et al., 1995; Pappas et al., 1996; Kim et al., 2008). Specifically, changes in MAP-2- a cytoskeletal phosphoprotein associated with dendritic microtubules and synaptophysin- a marker of synaptic vesicles, have been shown to decrease in both hypoperfused rats and gerbils (Kudo et al., 1993; Kurumatani et al., 1998; Liu et al., 2005). MAP-2 is regarded as a sensitive marker for ischemic brain injury and MAP- 2 mRNA and protein concentrations are significantly decreased at both early (1 month) and late (5 months) time points in the hypoperfused rat brain, indicating dendritic loss with hypoperfusion. Further, using an ethanolic phosphotungstic acid electron microscopy Hai et al., 2012 demonstrated a significant increase in the post- synaptic density proteins in the rat model of chronic cerebral hypoperfusion three months after surgery. In the same study, Western blot analysis identified significant changes in the protein levels of various kinases involved in signal transduction pathways Ca2+-calmodulin-dependent protein kinase II (CaMKII), phospho-CaMKII (p-CaMKII), phospho-extracellular regulated kinase (p-ERK), in the CA1 region of the hypoperfused hippocampus.

The present data showing neuronal ischemia in chronically hypoperfused mice as well as data from alternative animal models indicates the existence of important cellular and molecular changes occurring in grey matter areas following hypoperfusion and supports to a certain extent the validity of the alternative to the present hypothesis suggesting a role of

grey matter pathology in cognitive deficits associated with chronic cerebral hypoperfusion in mice (discussed in section 3.4.3.).

In humans, neuronal loss is evidenced in various neurological conditions. Specifically, neuronal injury following cerebrovascular challenge is observed in patients with ischemic stroke, vascular dementia, cerebral amyloid angiopathy observed in Alzheimer`s disease, CADASIL (Garcia et al., 1996; Kalaria, 1996; Grinberg and Thal, 2010). Interestingly, to a lesser extent, grey matter pathology (neuronal cell loss) is also observed in different white matter conditions (Liu et al., 1997; Clark et al., 2000; Volpe, 2001; Dutta and Trapp, 2007; Fischer et al., 2009; Geurts and Barkhof, 2008). Clinical and preclinical studies have demonstrated the presence of neuronal loss in multiple sclerosis patients and animal models of this condition (Meyer et al., 2001; Dutta and Trapp, 2007; Fischer et al., 2009; Geurts and Barkhof, 2008). In multiple sclerosis, grey matter pathology is believed to contribute to the occurrence of permanent disability (Meyer et al., 2001; Dutta and Trapp, 2007).

3.4.2.4. Increased inflammation in white and grey matter of chronically hypoperfused mice

Previous findings on chronically hypoperfused rats, gerbils and mice (Kudo et al., 1990; Pappas et al., 1996; Tomimoto et al., 2003; Shibata et al., 2004; Coltman et al., 2011; Holland et al, 2011; Kitamura et al., 2012) suggest increased inflammatory levels in these animal models. Recently using a microarray analysis, Reimer et al., 2011, demonstrated significant alterations in inflammation associated genes following chronic cerebral hypoperfusion in mice. The present results support these previous data by demonstrating significant hypoperfusion- induced increases in Iba1 immunoreactivity in major white matter tracts (EC, IC, OT and Fx) in behaviourally tested mice. In consistency with the overall more severe pathological profile, only the hypoperfused animals tested on the radial arm maze paradigm presented significantly increased inflammation in the CC, Cx and hippocampus. Inflammatory levels in examined white and grey matter areas were considered normal in all sham- operated mice.

From a mechanistic point of view, microglia might have contributed to the development and severity of both white and grey matter pathology observed in the present experiments on chronically hypoperfused mice. Previous studies on hypoperfused mice and rats showed selective white matter- related increases in microglial cells/ inflammatory agents associated with the predominant white matter injury in these animal models (Tomimoto et al., 2003; Farkas et al., 2004; Shibata et al., 2004; Coltman et al., 2011; Holland et al., 2011). These data are substantiated by in vitro, animal and clinical studies demonstrating that the myelin- producing oligodendroglial cells are particularly vulnerable to inflammation (Otero and Merrill, 1994; McLaurin et al., 1995; Vartanian et al., 1995; Merrill and Scolding, 1999). This is due to the fact that oligodendroglial cells express receptors for IL, cytokines and chemokines- inflammatory factors known to play an important role during oligodendroglial maturation, proliferation, migration and axonal myelination during neurodevelopment (Otero and Merrill, 1994; Dopp et al., 1997; Diemel et al., 1998; Vela et al., 2002). However, these signaling molecules could also be harmful to oligodendrocytes when synthesized in relatively high quantities as in the case of various neurodegenerative conditions (e.g. multiple sclerosis). For instance, in vitro studies have demonstrated that high concentrations of TNFα, IL-2 and IFNγ are lethal to oligodendroglia (Otero and Merrill, 1994; McLaurin et al., 1995; Vartanian et al., 1995). In transgenic mice overexpressing TNFα there are chronic inflammatory demyelination and degeneration of oligodendroglia. Further, TNFα levels have been shown to increase in chronically hypoperfused rats (Tomimoto et al., 2003) and to be associated with oligodendroglial apoptosis suggesting a role of this inflammatory factor in the development of hypoperfusion- induced neuropathology. In order to test the effects of the potential involvement of TNFα in the development of neuropathology following chronic cerebral hypoperfusion in mice, one could apply the microcoil surgery in TNFα mutants (Pasparakis et al., 1996) and compare axonal structure, myelin integrity in white and grey matter areas.

The inflammatory response associated with hypoperfusion is sustained, occurring during the early post- surgery time points and detected up to 13 weeks after hypoperfusion in rats (Tomimoto et al., 2003; Farkas et al., 2004). However, little is known about the dynamics

of the inflammatory reaction following hypoperfusion in mice and how the observed spatio- temporal microglial activity might be associated with the development of neuropathology. Therefore, future studies should examine microglia at different post-surgery time points and determine the potential contribution of these cells to the observed pathological changes in chronically hypoperfused mice. These future experiments might be useful for the identification of cellular and molecular mechanisms involved in the development of neuropathology following chronic cerebral hypoperfusion (discussed in Chapter 6, section 6.1.3.).

Microglia release free radicals such as NO which are known to be harmful to cellular mitochondrias. Damage to mitochondrias is associated with an increased synthesis of pro-apoptotic signals (caspase- 3, cytochrom- c) initiating molecular pathways leading to cellular death (Kroemer et al., 1998; Ricci et al., 2004). NO concentration increases substantially in chronically hypoperfused rats 2 weeks after artery ligation (de la Torre et al., 2003). Elevated NO levels following hypoxic- ischemic events in vivo have been related to neuronal and glial cell loss (Eliasson et al., 1999; Haynes et al., 2003). In vitro studies have confirmed these data by demonstrating that microglia secreted NO leads to neuronal and glial apoptosis (Kim and Kim, 1991; Boje and Arora, 1992; Chao et al., 1992; Cazevieille et al., 1993; Mitrovic et al., 1995). These data suggest that microglia activity following chronic cerebral hypoperfusion in mice might be impacting on the development of both white and grey matter injury. This is not surprising in regards to the existing literature. For instance, neuronal cells loss is observed in multiple sclerosis patients presenting elevated microglial activity accompanied by increased inflammatory and oxidative levels (Fischer et al., 2009). Further, microglia obtained from brain autopsy material of vascular or Alzheimer`s dementia patients were immunoreactive to major histocompatibility complex class I and II MHC-II, matrix metalloprotease-3 (MMP-3), and pro- inflammatory cytokines suggesting a role of these signaling cues in the development of age- related neuropathology (Wakita et al., 1994 ; de Groot et al., 2001; Lue et al., 2001). In order to investigate the role of microglia in the development of white and grey matter injury following chronic cerebral hypoperfusion in mice one could use different approaches (discussed in Chapter 6, section 6.1.3.3.). For instance, the

application of adriamycin- a known chemotherapeutic drug (Neuwelt et al., 1981) has been shown to inhibit microglial activation/ proliferation (Graeber et al., 1989). Future in vivo experiments might consider blocking microglial proliferation by intraventricular administration of adriamycin in sham and chronically hypoperfused mice at different post-surgery time points to determine the effects of microglia and the associated inflammatory agents on neuropathology and functional impairment in this animal model. However, this experiment would require the performance of two surgical procedures on the same animal- intraventricular cannulae implantation for the adriamycin as this drug does not normally diffuse through the blood brain barrier and the microcoils surgery to induce hypoperfusion which might be problematic from an ethical and regulatory point of view in the UK. Therefore, one could consider applying the microcoils surgery on microglia mutants (Gowing et al., 2008) where these cells are genetically ablated and then study the effects of this mutation on the neuropathological and functional outcome following hypoperfusion in mice.

Further the astrocytic response following hypoperfusion was not examined in the present experiments. Astrocytes are known to be important cellular players during the processes of neurodegeneration/ neuroregeneration secreting pro- inflammatory agents and growth factors, buffering extracellular glutamate and participating in concert with microglia in the formation of glial scars (Volterra and Meldolesi, 2005). Previous studies on chronically hypoperfused rats, gerbils and mice demonstrated increased numbers of astroglial cells suggesting an important role of astrocytes in the cellular and molecular processes following experimental chronic cerebral hypoperfusion (Pappas et al., 1996; Kurumatani et al., 1998; Farkas et al., 2004; Shibata et al., 2004; Farkas et al., 2007).

In humans, increased inflammatory levels were associated with grey and white matter pathology in multiple sclerosis patients (Fischer et al., 2009). Further increased inflammation seems to accompany the development of neuropathology in elderly people, aged nonhuman primates and rodents (Sloane et al., 1999; Ye and Johnson, 1999; Abraham and Lazar, 2000; Rosenberg et al., 2001; Fernando et al., 2006; Gold et al., 2007; Ihara et al., 2010).

Overall, the observed increases in inflammatory microglia in both white and grey matter areas of the chronically hypoperfused mouse brain rise again the question of the validity of the main hypothesis under test. The observed inflammation affected both white and grey matter suggesting a spectrum of complex hypoperfusion- induced cellular and molecular disturbances affecting various cortical, subcortical regions and white matter tracts potentially contributing in concert to the observed cognitive deficits in chronically hypoperfused mice.

3.4.3. Is hypoperfusion- induced white matter pathology associated with cognitive impairment in mice? An unresolved question.

The present experiments sought to test the hypothesis suggesting that hypoperfusion-induced white matter pathology may impact on working memory and executive function in mice. This hypothesis was based on data from clinical and preclinical studies suggesting that white matter abnormalities with cerebrovascular origin are related to working memory and executive function impairment (O`Sullivan et al., 2001; Charlton et al., 2006; Cook et al., 2007; Grieve et al., 2007; Shibata et al., 2007; Wright, et al., 2008; Kennedy and Raz, 2009; Nishio et al., 2010; Coltman et al., 2011).

To investigate this, a potential association was tested between white matter cellular components (axonal, myelin integrity, inflammation) and behavioural parameters of working memory (the number of revisiting errors) and executive function (the number of trials to criterion) in hypoperfused mice (section 3.2.3.3.). Since in the present study, the pathological analysis was limited to certain neuroanatomical levels, it was difficult to estimate the overall extent and severity of pathology throughout the brain, but the cumulative score represented an overall estimation of the observed axonal, myelin pathology, inflammation across the examined white matter areas (Coltman et al., 2011; Holland et al., 2011). The total pathological score was considered more appropriate for the correlation analysis as it gives larger numerical scale for potential variations than the regional pathological grades which were numerical restricted between 0- 3. The number of revisiting errors and trials to criterion were chosen for behavioural co- variates as they are suggested to be robust measures of working memory and executive function on a radial

arm maze and a water maze paradigm, respectively (Olton and Samuelson, 1976; Morris, 1984; Chen et al., 2000; D`Hooge and De Deyn, 2001; Shibata et al., 2007; Nishio et al., 2010; Coltman et al., 2011).

A significant positive association was evident between the severity of inflammation in white matter and working memory deficits, but not executive function in hypoperfused mice. This is in consistency with the observed working memory deficits in hypoperfused animals. Executive function (memory flexibility) remained intact following hypoperfusion in mice at least at the examined post- surgery time point. The present data are supported by animal and human reports demonstrating the existence of significant associations between inflammatory levels and cognitive deficits. Specifically, increases in GFAP positive cells in the hippocampus of hypoperfused rats correlated significantly with the number of revisiting errors (working memory) on a radial arm maze task, but not with spatial learning capacity taxed on a water maze paradigm (Pappas et al., 1996). LPS-treated aged mice presented significant correlations between mRNA expression of cytokines (IL-1b, IL-6, and TNFa) in grey matter (e.g. hippocampus) and working memory assessed on a radial arm maze task (Chen et al., 2008) and a T- maze paradigm (Murray et al., 2012). One of the major methodological differences between the present study and these previous reports relies in the brain areas where inflammation was examined. The present associations were focused on hypoperfusion- induced inflammation across white matter areas. However, significant hypoperfusion- induced inflammation was also evident in grey matter regions, especially in mice tested on a radial arm maze paradigm (discussed in section 3.4.2.4.). Therefore, it is possible that inflammation in grey matter might have contributed to the observed working memory impairment in hypoperfused mice. In elderly people, peripheral inflammation (e.g. cytokines) was found to be associated with the occurrence of cognitive deficits (Marsland et al., 2006; Wright et al., 2006) and dementia (Trollor et al., 2010).

Previous clinical reports suggest the existence of significant associations between age-related axonal pathology in white matter and cognitive deficits in the elderly (Morris and Price, 2001; Chalrton et al., 2006). However, in the present study an absence of significant

associations was observed between axonal integrity in white matter and working memory/ executive function in hypoperfused mice. This is surprising with regards to the observed widespread hypoperfusion- induced axonal pathology suggesting the existence of important neural disconnections among various cortico- cortical, cortical subcortical areas supporting working memory and executive function. Similarly, myelin integrity did not correlate significantly with cognitive function following hypoperfusion in mice. These findings are supported by previous reports on MAG null mutants showing an absence of functional impairment in the absence of MAG (at least during early and mid- adulthood) (Montag et al., 1994). MAG might not be crucial for sustaining normal cognitive and motor function and compact myelin proteins (e.g. MBP, PLP) might compensate for MAG deficiency in the rodent brain supporting cognition and memory. However, the present data is in contradiction with the existing literature on elderly people and aged nonhuman primates. Specifically, Bartzokis, 2004 suggested that age- related myelin breakdown is the major neurobiological determinant of cognitive decline and dementia in humans. Significant reductions of MBP protein were observed post- mortem in "healthy" and demented elderly and they correlated significantly with performance scores on cognitive and memory tests (Wang et al., 2004). Similarly, Peters and Sethares, 2002 observed significant associations between myelin pathology and cognitive dysfunction in aged macaque monkeys.

Alternatively, it is possible that pathological damage to axons and myelin affecting specific white and grey matter regions might have contributed to the occurrence of cognitive deficits in hypoperfused mice, but these regional associations remained undetected by the presently applied analysis which focused on the overall scores of axonal and myelin integrity in white matter. For instance, age- related white matter abnormalities in the CC were associated with working memory and executive function impairment in both elderly humans and aged non- human primates (Clarke and Zaidel, 1994; Peters and Sethares, 2002; Meguro et al., 2003; Teipel et al., 2003; Jokinen et al., 2007; Paul et al., 2007; Sullivan et al., 2010). Additionally, lesions to the IC and EC have been associated with working memory, executive function, reaction time and processing speed deficits in elderly people (Kenedy and Raz, 2009).

Since the correlation analysis was underpowered (focused on the hypoperfused group- n=10), it is possible that significant associations between axonal, myelin integrity in white matter and behavioural parameters in hypoperfused mice existed, but remained presently undetected. It was impossible to perform a separate correlation analysis for the sham group due to the limited numerical pathological variation for this experimental group (all grades were equal 0) (section 3.2.3.3.).

Further, hypoperfusion- induced damage to specific grey matter areas, namely major neuroanatomical components of the working memory circuit (e.g. the striatum, thalamus, hippocampus and prefrontal cortex) might have contributed to the occurrence of cognitive deficits in hypoperfused mice (Herrero et al., 2002, Ergorul and Eichenbaum, 2004). However, in the absence of any quantification/ categorization of the severity of grey matter pathology in hypoperfused mice, it was difficult to perform any association analysis between grey matter integrity and behavioural performance. This is an important methodological drawback as it prevents experimental test of the alternative to the main study hypothesis suggesting neuronal involvement in hypoperfusion- induced cognitive deficits in mice. This alternative hypothesis is supported by previous findings in animal models of chronic cerebral hypoperfusion where changes in synaptic (synaptophysin) and dendritic (MAP2) protein levels correlated significantly with spatial memory recall on a water maze task (Liu et al., 2005). These results suggest that even subtle abnormalities in neuronal cytoarchitecture could impact on cognitive function under hypoperfused conditions.

Overall, the evidence of neuronal ischemic injury (grey matter loss) in hypoperfused mice challenges the validity of the main study hypothesis. The presently observed pathological profile in hypoperfused mice suggests that widespread neuropathology affecting both white and grey matter areas might be at the basis of cognitive deficits in this animal model. In addition, nonexamined brain processes such as blood brain barrier integrity, neurotransmission might have been affected by the microcoils surgery and might have contributed to the observed pathology and cognitive deficits in hypoperfused mice (discussed in Chapter 6, section 6.1.1.).

Only future experimental work with an improved methodological design and increased experimental groups (**n**) would allow to make any firm conclusions on the role of hypoperfusion- induced neuropathology on cognition and memory in mice (discussed in section 3.4.4.3.).

At the completion of the experimental work presented in this thesis a new rat model of chronic cerebral hypoperfusion has been developed by Kitamura et al., 2012. This new model consists of the bilateral application of an ameroid constrictor device to the common carotids allowing regulated blood flow reductions associated with the development of white matter pathology in the absence of grey matter ischemia. Chronically hypoperfused rats exhibited a spatial working memory impairment one- month post- surgery. In the future, one could consider using this new animal model to experimentally study the effects of hypoperfusion- induced white matter pathology on cognition and memory. However, although, this new model represents an inventive experimental tool, due to its recent development, it requires a more detailed behavioural and pathological characterization. Addtionally, the presently limited availability of transgenic rat lines prevents the wide application of the ameroid constrictor device surgery on a variety of genetically modified animals. This is not the case for the microcoils surgery which has been specifically optimized on C57Bl6J mice- the mouse strain on which the majority of currently available genetically modified mice are backcrossed to.

3.4.4. Methodological strengths, limitations and future behavioural and pathological experiments on chronically hypoperfused mice

3.4.4.1. Strengths of the applied behavioural and pathological approach

In the present study spatial working memory and executive function were evaluated using two of the most widely employed behavioural paradigms, namely the radial arm maze and the water maze tasks (Olton and Samuelson, 1976; Morris, 1984; Chen et al., 2000; D`Hooge and De Deyn, 2001; de Wilde et al., 2002; Shibata et al., 2007; Nishio et al., 2010; Coltman et al., 2011). These behavioural paradigms provide a good estimation of cognition and memory in rodents. and they have been largely employed to evaluate the

functional outcome in chronically hypoperfused rats and mice (Pappas et al., 1996; Sopala and Danysz, 2001; de Wilde et al., 2002; Shibata et al., 2007; Nishio et al., 2010; Coltman et al., 2011). This allowed to confirm and expand previous behavioural findings on chronically hypoprefused mice as well as to compare the present results with existing data from alternative animal models (rats).

The strengths of the present pathological analysis relate to the sensitivity of the applied immunochemical procedure to specific white matter cellular components- axons (APP), myelin (MAG) and inflammatory microglia (Iba1). This represents an important advantage considering that previously white matter abnormalities in hypoperfused mice were described using basic histological techniques (e.g. Kluver- Barrera) (Shibata et al., 2004; Shibata et al., 2007; Nishio et al., 2010). The present pathological data provide a more detailed characterization of the cellular changes underlying hypoperfusion- induced white matter pathology in mice. In contrast to previous reports on this animal model, the present study examined for the first time grey matter integrity by means of a standard H&E histological staining which gives a good, overall indication of brain morphology and allows to identify neuronal ischemic injury.

Lastly, the applied systematic evaluation of behaviour and pathology in the same cohorts of chronically hypoperfused mice allowed to reveale a previously undetected spectrum of white and grey matter pathology in this animal model.

3.4.4.2. Limitations of the applied behavioural and pathological approach

The present study also presented certain limitations in its experimental design which constituted an important drawback for hypothesis test.

Performing behavioural training in rodents using available paradigms (e.g. radial arm maze and water maze) involves stress- related, aversive factors such as: 1) handling and daily contact with humans**;** 2) food- deprivation, swimming (particularly aversive for mice who are not natural swimmers)**;** 3) extra- cage physical and exploratory activity. These, additional to the microcoils surgery factors, might have contributed to the overall functional and pathological profile of chronically hypoperfused mice. In the present study a poorer physiological post- surgery outcome was observed in the food- deprived

hypoperfused cohort tested on a radial arm maze paradigm. These animals exhibited pronounced post- surgical neurological dysfunction such as seizing activity, sickness and even death leading to an important loss of experimental (**n**) numbers in this hypoperfused group. The remaining hypoperfused animals exhibited a spectrum of white and grey matter abnormalities accompanied by an increased inflammation. At the functional level, these animals presented impaired working memory. The hypoperfused mice tested on a water maze task recovered relatively well after surgery and exhibited predominant white matter pathology. At the functional level, this hypoperfused cohort presented intact cognition and memory (memory flexibility, learning, short and long term memory recall). It is unknown whether and/ or to what extent the behavioural procedure impacted on the functional outcome in the two cohorts of hypoperfused mice and future studies should examine the effects of the behavioural procedure and its associated factors on both neuropathology and functional outcome in this animal model (discussed in section 3.4.4.3).

The applied pathological approach presented important limitations, namely related to the restricted number of examined brain levels/ regions, the limited number of applied biomarkers, the nonquantitative nature of the obtained data (pathological grades) and the specific time- point when the pathological changes were examined. This limited spatio-temporal and biomarker analysis might have omitted pathological changes as 1) they might have been present on non- examined brain levels/ areas and/ or 2) not detected by the applied antibody, and/ or 3) occurring at later post- surgery time points especially in regards to the chronic nature of the cerebrovascular challenge and the cumulative severity of the observed neuropathology and cognitive impairment in chronically hypoperfused mice (Nishio et al 2010; Reimer et al., 2011). Further, the observed pathology was not quantitatively measured in the experimental cohorts limiting all observations in a restricted numerical range from 0- 3. This semi- quantitative pathological approach could not account for potentially subtle inter- individual differences in the severity of the pathological profile. Further, the non- quantitative nature of the obtained results presented certain limitations in regards to the experimental test of the main and alternative study hypotheses (discussed in section 3.4.3.).

A good scientific practice usually requires the application of more than one methodological strategies to support any given result. In the present experiment, white and grey matter integrity, inflammation were examined only be means of standard histology/ immunohistochemistry in the absence of any additional biomolecular (e.g. protein levels, gene expression) and/ or structural analysis (e.g. electron microscopy).

3.4.4.3. Future behavioural and pathological studies on chronically hypoperfused mice

With regards to the limitations of the present methodology discussed in the previous section, future behavioural and pathological experiments on chronically hypoperfused mice should apply an improve experimental design to address the study hypothesis as well as to determine the specific effects of factors which were presently suspected to affect on neuropathology and functional outcome in this animal model.

Future experiments on chronically hypoperfused mice should systematically evaluate white and grey matter integrity as well as alternative brain processes (e.g. cerebrovasculature, neurotransmission- discussed in Chapter 6, section 6.3.1.) in behaviourally tested chronically hypoperfused mice using a combination of experimental techniques This would allow to obtain a detailed spatio- temporal characterization of neuropathology and the associated behavioural deficits in chronically hypoperfused mice. Further, a quantitative pathological assessment would allow to account for potentially subtle inter- individual pathological differences which could not be detected by the presently applied semi- quantitative approach. The obtained quantitative pathological data would be more suitable for correlational analyses with behavioural parameters in this animal model due to the larger spectrum of numerical inter- individual pathological variations necessary to more accurately address the present study hypothesis (discussed in section 3.4.3.).

Depending on the scientific question(s) neuropathology could be examined and/ or measured using different in vitro and in vivo strategies. For instance, by using double/ triple immunochemistry with compatible, fluorescent antibody probes one could study on

the same brain samples axonal (e.g. APP, SMI312R), myelin (e.g. MAG, MBP, PLP) integrity in relation to neuronal (e.g. NeuN, MAP-2)/ glial (e.g. MBP, PLP, MAG, GFAP) cells. The subsequent confocal (or immunofluorescence detecting) microscopy would allow to quantitatively measure the respective biomarker fluorescence levels. Alternatively, one could examine structural white matter integrity using electron microscopy on semi- thin toluidine blue stained brain sections. Additionally, modern neuroimaging approaches such as MRI- DTI exist and allow to quantify both in vivo as well as in vitro (brain samples) changes in white matter integrity (Chapter 4). Axons and myelin could be quantitatively evaluated by analyzing axial (axons) and radial (myelin) diffusivity respectively on MRI- DTI scans. Western blot (protein levels) and/ or (q)PCR (mRNA expression) analysis would allow to quantitatively determine potential biomolecular changes occurring in white and grey matter areas of the chronically hypoperfused mouse brain. One could also consider developing in vitro procedures mimicking the hypoperfused conditions, by culturing brain slices under low glucose and oxygen levels allowing to reduce the number of experimental animals. However, this in vitro approach presents certain limitations such as an absence of active circulation which might impact on neuropathology. Further, although functional experiments (e.g. action potential propagation) could be performed in vitro, it is impossible to test specific alterations in cognitive and memory function (e.g. processing speed, working memory, memory flexibility, attention, memory recall).

In the present study, the behavioural and pathological evaluation of sham and hypoperfused mice was performed at a relatively short post- surgery time point (1- 2 months post- surgery). A recent study suggests more severe behavioural deficits (both spatial working and reference memory impairment) and pathological pattern (white and grey matter injury) in hypoperfused mice 6 months after microcoils application (Nishio et al. 2010). Future detailed timecourse behavioural and pathological analyses of this animal model would allow to better assess the temporal dynamics of hypoperfusion- induced neurobiological alterations and the associated functional impairment in mice (Nishio et al., 2010). For instance, future behavioural experiments could examine working memory and/ or references memory in the same cohorts of sham and chronically hypoperfused mice at different time points after surgery using a radial arm maze and/ or water maze paradigm

and/ or alterantive behavioural paradigms (e.g. as reaction time and serial choice tasks). However, this longitudinal approach presents the drawback of cumulative effects of the repeated training on the performance of both sham and chronically hypoperfused animals and could also affect on neuropathology. An alternative experimental strategy, would consists of applying a cross- group approach, comparing simultaneously the performance of experimental cohorts at a different post- surgery time points- e.g. 1 month vs. 6 months post- surgery and their pathological profile. The cross- group approach would allow to control for the cumulative effects of training on cognition and neuropathology associated with the above mentioned longitudinal approach. However, the cross- group approach would not allow to determine the progression of cognitive impairment and neuropathology within the same cohorts of animals.

In the present study, environmental factors associated with the behavioural training such as the feeding pattern (food deprivation vs. *ad libitum*) seem to have impacted on the pathological and functional outcome following hypoperfusion in behaviourally tested, young, adult mice. It is unknown whether and/ or how the feeding pattern interacted with the behavioural training and whether the resulting pathological and behavioural profile was due to the effects of a single factor and/ or a combination of factors. It is important that future experiments try to determine the individual as well as combined effects of the three major experimental factors in the present study: 1) surgical procedure (sham vs, hypoperfused), 2) feeding pattern (food deprivation vs. *ad libitum*), and 3) behavioural training (absence vs. presence of behavioural training) in order to gain a better understanding of the etiological causes associated with neuropathology and functional outcome in hypoperfused mice. This could be done by simply comparing sham vs. chronically hypoperfused mice under different experimental conditions (mentioned above) allowing to evaluate the individual as well as interactive effects of the above mentioned 3 experimental factors on the pathological profile as well as behavioural performance of sham and chronically hypoperfused mice.

Inter- individual differences could exist among experimental animals as well as batches of animals which may account for the presently observed pathological and functional

differences between the two hypoperfused cohorts. In the present study, the cerebral blood flow was not measured in the behaviourally tested animals. It is possible that differences in the perfusion rate existed between the two behaviourally tested hypoperfused cohorts due to variations in the artery size, the exact placement of the microcoils, the skills of the surgeon, the used anesthetic leading to the observed pathological and functional differences. It is important, that future studies using this animal model measure the perfusion rates in all experimental animals. This could be done, in vivo, non- invasively by means of Laser- Doppler flowmetry or by means of PET imaging for rodents. However, introducing these additional experimental factors could also aversively (e.g. stress- related) affect the functional as well as pathological outcome. Alternatively, one could measure the cerebral blood flow and metabolism post- mortem by means of autoradiographic techniques employing I-iodo-antipyrine and "C-deoxyglucose (Mies et al., 1981).

Further, the present study did not examine alternative brain processes (e.g. cerebral metabolism, cerebrovasculature, neurotransmission) that could be affected in the chronically hypoperfused brain and by consequence could impact on both the neuropathological and functional outcome in this model (discussed in Chapter 6, section 6.1.1.).

Additionally, the present experiments, at the exception of inflammation, did not address the pathophysiological mechanisms (e.g. excitotoxicity, oxidative stress) underlying the development of neuropathology and cognitive impairment in chronically hypoperfused mice. Therefore, it is important that future mechanistic studies address this question as discussed in Chapter 6, sections 6.1.3..

Lastly, in regards to the relevance of this animal model to the aging process in humans, it is necessary that future experimental work addresses the effects of chronic cerebral hypoperfusion on neuropathology and cognition in the context of aging (discussed in Chapter 6, section 6.1.2.).

Future research directions on chronically hypoperfused mice are discussed in details in Chapter 6.

3.4.5. Implications of the new mouse model of chronic cerebral hypoperfusion and future directions

The major interest of the new mouse model of chronic cerebral hypoperfusion is that it allows to study in isolation the effects of chronic cerebral hypoperfusion on neuropathology and cognitive function in mice. As previously discussed in the present thesis, in clinical settings it is extremely difficult to examine in isolation the effects of single etiological entities on neuropathology and cognitive function due to ethical issues and the presence of comorbidities in the elderly.

Further development and characterization of the new mouse model of chronic cerebral hypoperfusion would allow the future application of the microcoils surgery on genetically modified rodents. This would allow to investigate the individual and combined effects of cerebrovascular (e.g. hypoperfusion) and molecular (e.g. APOE) factors on the development of neuropathology and cognitive deficits in experimental settings (Chapter4; Chapter 6, section 6.1.5.). Further analysis of the underlying pathophysiological mechanisms (e.g. excitotoxicity, oxidation) in this animal model would potentially reveal new biological targets for the future pre- clinical development of therapeutic strategies for the treatment of age- related neuropathology and cognitive decline (Chapter 6, section 6.1.3.).

However, this animal model also presents certain limitations. Specifically, the observed pathological profile in chronically hypoperfused mice is heterogeneous- certain hypoperfused mice exhibit predominant white matter pathology whereas others present a spectrum of grey and white matter abnormalities. Therefore, in order to obtain meaningful conclusions on potential associations between a certain pathological profile (e.g. white matter pathology) and functional impairment in chronically hypoperfused mice, for future experiments, one should use larger hypoperfused cohorts.

3.5. Summary

The present study confirmed the existence of white matter pathology, increased inflammation and spatial working memory impairment in hypoperfused mice. However, at the difference from previous findings on this model, grey matter ischemic injury was evidenced in the majority of the hypoperfused animals tested on a radial arm maze paradigm. Due to the observed spectrum of white and grey matter pathology as well as to certain methodological limitations it was difficult to accurately test the main study hypothesis suggesting that hypoperfusion- induced white matter pathology is associated with cognitive impairment in mice.

Chapter 4

Effects of APOE on white matter integrity under normal physiological and chronically hypoperfused conditions in mice

4.1. Introduction and aims

MRI techniques developed for the noninvasive investigation of white matter integrity are largely employed in clinical settings. These neuroimaging techniques revealed the prevalence of white matter abnormalities associated with chronic cerebral hypoperfusion in the elderly (Farkas and Luitent, 2001; O`Sullivan et al., 2001; Deary et al., 2003; Charlton et al., 2006; Fernando et al., 2006; Grieve et al., 2007; Kennedy and Raz, 2009; Penke et al., 2010) FA and MTR are MRI parameters accounting for white matter structural integrity and reductions in their values are indicative for white matter pathology (Moseley et al., 1990; Wolff and Balaban, 1989; Basser, 1995; Beaulieu, 2002; Harsan et al., 2006; Blezer et al., 2007; Holland et al., 2011). Both FA and MTR have been shown to decrease with increasing age in humans (O` Sullivan et al., 2001; Deary et al., 2003; ; Charlton et al., 2006; Grieve et al., 2007; Kennedy and Raz, 2009; Bastin et al., 2009; Penke et al., 2010). The broad application of MRI for clinical diagnosis and the existing uncertainty in regards to its underlying biological substrates have urged the validation and further development of neuroimaging techniques using animal models (Benveniste and Blackband, 2002). Recently, our group demonstrated the sensitivity of in vivo MRI to detect widespread white matter pathology occurring in chronically hypoperfused mice (Holland et al., 2011).

Recent clinical studies suggest that human APOE allelic variation differentially impacts on white matter integrity and cerebrovasculature in cognitively intact adults- the APOE4 allele being associated with white matter pathology and cerebrovascular abnormalities (Kalmijn et al., 1996; Skoog et al., 1998; Reiman et al., 1996; Reiman et al., 2004; Bartzokis et al., 2007; Filippini et al., 2009; Heise et al., 2010; Ryan et al., 2011).

Human APOE allelic variation also differentially affects grey matter integrity. Specifically, the APOE4 allele is the major, known genetic risk factor for the development of age- related neurodegeneration and dementia (e.g. Alzheimer`s disease) (Saunders et al., 1993; Schuff et al., 2009b). Additionally, APOE4 carriers show poorer pathological and functional outcome following injury to the central nervous system compared with non- APOE4 carriers (Nicoll et al., 1995; Gromadzka et al., 2007; Wagle et al., 2009). Similarly, APOE deficient and human APOE4 transgenic mice exhibit an early onset

neurodegeneration, cerebrovascular pathology and poor outcome following injury to the brain when compared with WT and APOE3 counterparts (Piedrahita et al. 1992; Gordon et al., 1995; Masliah et al., 1995; Masliah et al., 1997; Sheng et al., 1998; Buttini et al., 1999; Sheng et al., 1999; Buttini et al., 2000; Fullerton et al., 2001; Methia et al., 2001; Kitagawa et al., 2002; Hafezi- Moghadam et al., 2006). APOE effects on grey matter integrity have been largely studied and characterized in both clinical and preclinical settings (Saunders et al., 1993; Gordon et al., 1995; Masliah et al., 1995; Masliah et al., 1997; Buttini et al., 1999; Sheng et al., 1998; Sheng et al., 1999; Buttini et al., 2000; Schuff et al., 2009b).

However, little is known about APOE effects on white matter It is possible that APOE affects on white matter integrity under both normal physiological and pathological conditions (e.g. chronic cerebral hypoperfusion) via an impaired turnover of myelin lipids and cholesterol, increased inflammation, lipid peroxidation, protein oxidation and excitotoxicity (Van Ree et al., 1994; Laskowitz et al., 1997a; Laskowitz et al., 1998; Horsburgh et al., 2000a; Laskowitz et al., 2000; Ramassamy et al., 2001; Aono et al., 2002; Han et al., 2003; Horsburgh et al., 2003; Choi et al., 2004; Champagne et al., 2005; Bartzokis et al., 2006).

Further, little is known about the concomitant effects of genetic (APOE) and cerebrovascular (chronic cerebral hypoperfusion) mechanisms on white matter integrity. This question is particularly important especially with regards to the multifactorial etiology of white matter pathology in elderly people.

Building on previous work, the present study sought to test the hypothesis that APOE deficiency might be associated with white matter anomalies under normal physiological conditions and the development of more severe hypoperfusion- induced white matter pathology in mice.

Mouse APOE deficiency was also expected to impact on grey matter integrity and/ or the cerebrovasculature under both normal physiological and chronically hypoperfused conditions as previously demonstrated in this animal model (Piedrahita et al. 1992; Gordon et al., 1995; Masliah et al., 1995; Masliah et al., 1997; Laskowitz et al., 1997;

Hosrburgh et al., 1999; Sheng et al., 1999; Fullerton et al., 2001; Methia et al., 2001; Kitagawa et al., 2002; Hafezi- Moghadam et al., 2006).

To detect potentially subtle genetic differences in white matter integrity, an ex vivo MRI was applied to compare regional MRI parameters of white matter integrity (FA and MTR) between age and sex- matched WT and APOEKO mice subjected to sham surgery or hypoperfusion. Ex vivo MRI allows longer imaging times in the absence of physiological artifacts and the generation of images with a very good spatial resolution. The sensitivity of ex vivo MRI to detect white matter integrity was verified at the microstructural level using a standard immunohistochemistry with antibodies targeted to the neuronal axons (APP) and myelin sheath (MAG, dMBP). With regards to previously reported early occurring neurodegeneration and more severe neuropathology (e..g infarctions) following cerebrovascular challenge in APOEKO mice (Gordon et al., 1995; Masliah et al., 1995; Masliah et al., 1997; Laskowitz et al., 1997; Hosrburgh et al., 1999; Sheng et al., 1999; Buttini et al., 2000; Kitagawa et al., 2002), in addition to white matter, grey matter integrity was also examined on T2- weighted scans and corresponding H&E stained brain sections in all experimental animals. Inflammation was evaluated by Iba1 immunochemistry as 1) APOE is known to exert immunomodulatory function (Laskowitz et al., 1997a; Laskowitz et al., 2000; Champagne et al., 2005), 2) inflammation increases after chronic cerebral hypoperfusion (Shibata et al., 2004; Coltman et al., 2011), 3) inflammation could impact on MRI metrics (Blezer et al., 2007; Wu et al., 2008). To control for any naturally occurring cerebrovascular abnormalities (e.g. atherosclerosis) in APOEKO mice which could affect on the perfusion rate in these animals, relatively young WT and APOEKO mice (5 months old) were used in the present study.

The major aim of the present thesis chapter was to:

- Determine the effects of APOE on white and grey matter integrity, inflammation under normal physiological conditions as well as one month after chronic cerebral hypoperfusion in WT compared with APOE deficient mice.

4.2. Materials and methods

4.2.1. Animals and surgery

Five months old male C57Bl6J (WT) (n= 19) (31±3gr) and APOE deficient (APOEKO) (n= 18) (30±4gr) mice were used for the experimental purposes of Chapter 4 (Chapter 2, section, 2.1.1.; section 2.1.2.). The animals from both genotypes were randomly allocated to a sham or a microcoils surgery. Eleven WT and 10 APOEKO mice were subjected to chronic cerebral hypoperfusion. The rest of the WT (n= 8) and APOEKO (n= 8) mice underwent sham surgery. The surgical procedure is described in details in Chapter 2, section 2.2. Food and water were provided *ad libitum* during the whole experimental period. All animals were sacrificed a month after surgery for ex vivo MRI and immunohistological analysis. Animals not surviving the entire experimental period were excluded from any further analysis.

4.2.2. Ex vivo MRI procedure

Ex vivo MRI was performed on perfusion- fixed WT and APOEKO mouse brains one month after microcoils or sham surgery as described in Chapter 2, section 2.9. The generated ex vivo MRI images had a good spatial resolution allowing the delineation of ROIs on T2- weighted scans with a minimal contamination by adjacent brain regions (figure 4.1. A, B, C). Regional FA and MTR analysis were used to examine white matter integrity in selected ROIs (the CC, EC, IC, OT) (Chapter 2, section 2.9.4.). Additionally, FA and MTR were examined in the hippocampus which was selected as a control grey matter region. The overall brain morphology and grey matter structural integrity were visually examined on four T2- weighted MRI scans from the following neuroanatomical levels: 0.74 mm, 0.38 mm, -0.94 mm, -2.12 mm bregma (Franklin and Paxinos, 1997). Grey matter pathology usually appears as dark hypointense regions on T2- weighted scans. The grey matter ROIs were cortical (the Cx) and subcortical (the striatum and the hippocampus) regions known to be susceptible to cerebral blood flow alterations

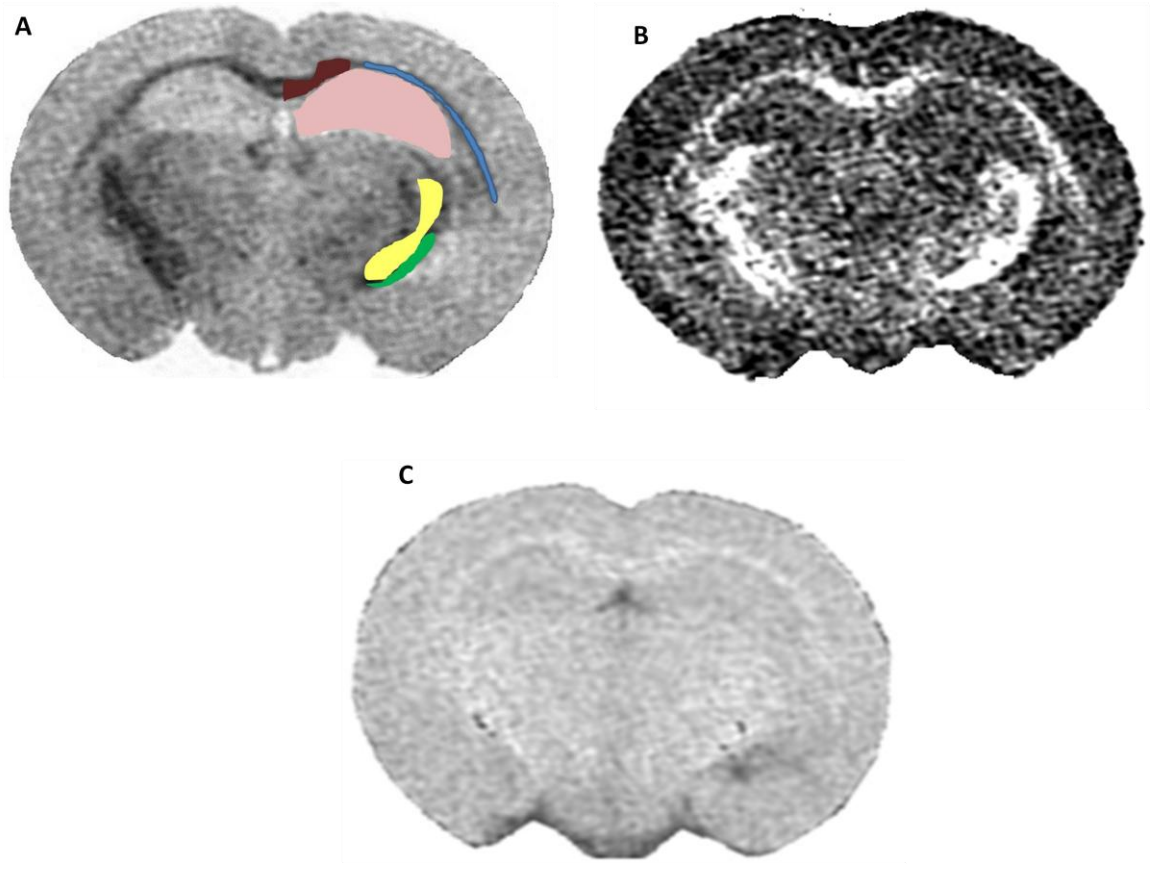

Figure 4.1.: Representative ex vivo MRI generated T2- weighted, FA, and MTR scans

MRI images with a good spatial resolution were generated using a new ex vivo MRI procedure for multiple brains imaging. In (**A**) is presented a T2-weighted scan with the examined ROIs delineated in colour on the left hemisphere: CC (brown), EC (blue), IC (yellow), OT (green), hippocampus (pink). In (**B**) is shown a representative FA scan with an example of a MTR map presented in (**C**). All images are representative of the same neuroanatomical level from the same WT sham animal.

4.2.3. Pathological assessment

The pathological assessment of white and grey matter integrity, inflammation was performed at the completion of the ex vivo MRI procedure (one month after surgery) using standard histological and immunohistochemical procedures (Chapter 2, section 2.5., section 2.6.1.).

Axonal (APP) and myelin (MAG, dMBP) integrity, inflammation (Iba1) were examined on 6μm thin coronal brain sections from -2.12mm bregma neuroanatomical level (Franklin and Paxinos, 1997) using a standard immunohistochemical procedure (Chapter 2, section 2.6.1.). The applied biomarkers were studied in the same white matter ROIs as those examined for the MRI analysis, namely the CC, EC, IC, and OT. Additionally, axonal integrity (APP), degraded myelin (dMBP), and inflammatory activity (Iba1) were also examined in the hippocampus. The severity of the observed pathological changes was semi- quantitatively evaluated by means of a pathological grading scale (Chapter 2, section 2.7.4.; Coltman et al., 2011; Holland et al., 2011).

The overall grey matter integrity and the presence of neuronal ischemic injury were examined on 6μm H&E stained coronal brain sections from neuroanatomical levels 0.74 mm; 0.38 mm; -0.94 mm; -2.12 mm bregma (Franklin and Paxinos, 1997) corresponding to each of the four T2- weighted scans (figure S.4.3.- appendices II). The grey matter ROIs were cortical (the Cx) and subcortical (the striatum, the hippocampus) regions known to be susceptible to blood flow alterations.

4.2.4. Statistics

The experimental group (**n**) numbers included in the statistical analysis were: 8 WT sham, 8 APOEKO sham, 10 WT hypoperfused and 8 APOEKO hypoperfused animals.

4.2.4.1. Statistical analysis of the ex vivo MRI (FA and MTR) data

The regional average MRI biomarkers (FA and MTR) were statistically compared among the four experimental groups using two- way multifactorial analysis of variance (MANOVA, Hotelling`s trace multivariate test) with the regional MRI data (FA and MTR in the CC, EC, IC, OT and hippocampus) as the dependent variable and genotype (WT vs.

APOEKO) and surgery (sham vs. hypoperfusion) as the experimental factors. The surgery x genotype interaction was simultaneously analyzed. MANOVA is used for data analysis in neuroimaging studies to correct for the issue of multiple intercorrelated MRI voxels, thus minimizing the risk of committing type I statistical error (Madden et al., 2007; de Weijer et al., 2011; Holland et al., 2011). Multiple intercorrelated voxels, or multicollinearity, can arise as the MRI biomarkers are related (e.g. changes in FA could affect MTR as measured on the same biological samples). Furthermore, it is possible that adjacent voxels (e.g. regional FA and MTR voxels in the CC and EC) may influence each other due to averaging across the spatial resolution. The Hotelling`s trace multivariate test was selected for the present MANOVA analysis as it is considered to be appropriate for group comparisons when the experimental (**n**) numbers are relatively small and/ or uneven. In the case of significant differences indicated by MANOVA, group differences for each dependent variable (regional FA and MTR) were tested using Tukey`s post- hoc analysis.

Significance was accepted for $p < 0.05$.

4.2.4.2. Statistical analysis of the pathological data

Kruskal-Wallis nonparametric statistics followed by Dunn`s multiple comparisons post-hoc analysis were applied for the statistical comparison of the regional group median pathological grades of axonal (APP), myelin (MAG, dMBP) integrity and inflammation (Iba1). The Kruskal- Wallis nonparametric statistics were applied as the pathological data was not a quantitative measure (semi- quantitative grades). The group differences were considered significant for $p<0.05$.

4.3. Results

4.3.1. Post- surgery recovery and physiological status

All sham animals from both genotypes recovered well after the surgical procedure. One of the 11 WT (0.09%) and 2 of the 10 APOEKO (20%) hypoperfused animals did not survive the post- surgery recovery period and were excluded from the subsequent MRI and pathological analysis. The remaining 99.1% WT (10/11) and 80% APOEKO (8/10) hypoperfused mice recovered well after surgery and did not show any overt signs of neurological dysfunction. In the final analysis were included: 8 WT sham, 8 APOEKO sham, 10 WT hypoperfused and 8 APOEKO hypoperfused animals (figure S.4.1.- appendices II).

4.3.1. Ex vivo MRI results

4.3.1.1. APOE deficiency and chronic cerebral hypoperfusion impact on MRI parameters of white matter integrity

The regional average MRI biomarker values (FA and MTR) were statistically compared among the four experimental groups using two- way MANOVA, Hotelling`s trace multivariate test (Chapter 4, section 4.2.4.2.; Madden et al., 2007; de Weijer et al., 2011; Holland et al., 2011). The Hotelling's Trace multivariate test of overall differences among groups for FA and MTR was statistically significant for the CC, EC and IC ($p<0.05$) where there was a significant effect of genotype (CC, $F_{(3, 26)}= 5.264$, $p=0.006$; EC, $F_{(3, 26)}= 3.597$, $p=0.028$; IC $F_{(3, 26)}= 5.844$, $p=0.004$) and surgery (CC, $F_{(3, 26)}= 61.750$, $p=0.000$; EC, $F_{(3, 26)}= 59.343$, $p=0.000$; IC, $F_{(3, 26)}= 69.409$, $p=0.000$) as well as a significant interaction between surgery x genotype (CC, $F_{(3, 26)}= 6.804$, $p=0.002$; EC, $F_{(3, 26)}= 5.315$, $p=0.006$; IC, $F_{(3, 24)}= 4.440$, $p=0.013$). In the OT and the hippocampus there was a significant effect of surgery (OT, $F_{(3, 26)}= 31.286$, $p=0.000$; hippocampus, $F_{(3, 26)}= 11.105$, $p=0.000$), but an absence of significant effect of genotype (OT, $F_{(3, 26)}= 0.729$, $p=0.545$; hippocampus, $F_{(3, 26)}= 3.022$, $p=0.05$) or interaction between surgery and genotype (OT, $F_{(3, 26)}= 0.507$, $p=0.681$; hippocampus, $F_{(3, 26)}= 1.896$, $p= 0.157$).

4.3.1.1.1. APOE deficiency is associated with significant FA reductions in white, but not grey matter after chronic cerebral hypoperfusion

FA is an MRI- DTI parameter of white matter integrity (Basser, 1995; Beaulieu, 2002) and a decrease in FA is associated with white matter pathology (Harsan et al., 2006; Holland et al., 2011). Significant group differences in FA were evident in the CC ($F_{(3, 26)}$= 35.71, p= 0.000), EC ($F_{(3, 26)}$= 29.56, p= 0.000), IC ($F_{(3, 26)}$= 33.91, p= 0.000) and OT ($F_{(3, 26)}$= 15.40, p= 0.000). An absence of significant group difference in FA was observed in the control grey matter ROI- the hippocampus ($F_{(3,26)}$= 1.94, p= 0.147). The post- hoc Tukey`s analysis showed that WT and APOEKO hypoperfused animals had a significantly reduced FA in the CC, EC, IC, and OT in comparison with WT and APOEKO sham groups ($p<0.05$) (table 4.1., figure S.4.2.1- A-D- appendices II). Interestingly, APOEKO hypoperfused mice presented a significantly decreased FA in the CC, EC and IC when compared with WT hypoperfused group ($p<0.05$) (table 4.1., figure S.4.2.1. A-C- appendices II). FA did not differ significantly in any of the ROIs between WT and APOEKO sham mice ($p>0.05$) (table 4.1.; figure S.4.2.1. A-E- appendices II).

4.3.1.1.2. APOE deficiency is associated with significant MTR reductions in white, but not grey matter after chronic cerebral hypoperfusion

MTR accounts for changes in white matter integrity by measuring the alterations in energy transfer between the free and the macromolecules (lipids)- bound pools of water molecules in the brain (Wolff and Balaban, 1989). MTR was significantly different among the groups in all examined white matter ROIs: the CC ($F_{(3, 26)}$= 47.99, p= 0.000), EC ($F_{(3, 26)}$= 55.29, p=0.000), IC ($F_{(3, 26)}$= 36.48, p= 0.000), and OT ($F_{(3, 26)}$= 22.14, p= 0.000). Significant group differences in MTR were also observed in the control grey matter ROI- the hippocampus ($F_{(3, 26)}$= 13.53, p= 0.000). The post- hoc Tukey`s analysis revealed that WT and APOEKO hypoperfused mice had significantly reduced MTR values in all ROIs when compared with WT and APOEKO sham groups ($p<0.05$) (table 4.1.; figure S.4.2.2. A-E- appendices II). However, only in the CC was MTR found to be significantly decreased in APOEKO hypoperfused mice compared with WT hypoperfused animals ($p<0.05$) (table 4.1.; figure S.4.2.2. A- appendices II).

MRI parameter	Region of interest	WT (n=8) *Sham*	WT (n=10) *Hypoperfused*	APOEKO (n=8) *Sham*	APOEKO (n=8) *Hypoperfused*
FA	*CC*	0.54 ± 0.01	0.45 ± 0.12$^{\Delta\square}$	0.56 ± 0.02	0.33 ± 0.01$^{\Delta\square\circ}$
	EC	0.53 ± 0.01	0.43 ± 0.02$^{\Delta\square}$	0.56 ± 0.02	0.32 ± 0.01$^{\Delta\square\circ}$
	IC	0.59 ± 0.02	0.48 ± 0.01$^{\Delta\square}$	0.58 ± 0.02	0.36 ± 0.02$^{\Delta\square\circ}$
	OT	0.76 ± 0.02	0.50 ± 0.03$^{\Delta\square}$	0.71 ± 0.04	0.44 ± 0.04$^{\Delta\square}$
	Hippocampus	0.33 ± 0.007	0.35 ± 0.01	0.35 ± 0.01	0.32 ± 0.005
MTR	*CC*	57.47 ± 1.11	48.56 ± 0.83$^{\Delta\square}$	57.35 ± 0.87	44.20 ± 1.22$^{\Delta\square\circ}$
	EC	58.25 ± 0.68	48.77 ± 1.24$^{\Delta\square}$	58.35 ± 0.55	44.25 ± 1.07$^{\Delta\square}$
	IC	59.25 ± 1.23	49.64 ± 1.23$^{\Delta\square}$	58.93 ± 1.11	46.18 ± 0.90$^{\Delta\square}$
	OT	58.82 ± 1.22	45.24 ± 1.94$^{\Delta\square}$	58.86 ± 1.42	44.44 ± 2.36$^{\Delta\square}$
	Hippocampus	50.47 ± 0.35	46.54 ± 1.29$^{\Delta\square}$	49.95 ± 0.70	42.50 ± 1.26$^{\Delta\square}$

Table 4.1.: Regional MRI biomarker values (group mean ± SE)

Significant group differences in FA and MTR were evident by two- way MANOVA in examined white matter ROIs ($p<0.05$). In the hippocampus significant group differences were observed in MTR ($p<0.05$), but not FA ($p>0.05$). Tukey`s post- hoc analysis revealed significant reductions in MRI metrics (FA and MTR) in major white matter tracts with hypoperfusion in both WT and APOEKO mice ($p<0.05$). APOEKO hypoperfused mice exhibited significant reductions in FA and MTR in the CC when compared with WT hypoperfused mice ($p<0.05$). Additionally, following hypoperfusion FA was significantly reduced in the EC and IC of APOEKO mice compared with WT counterparts ($p<0.05$). In the hippocampus, although there were significant decreases in MTR with hypoperfusion ($p<0.05$), they were not associated with the APOE genotype ($p>0.05$). No significant differences in MRI metrics were evident in all examined ROIs between WT and APOEKO sham mice ($p>0.05$).

Significant group differences as given by the Tukey`s post- hoc analsysis if $p<0.05$ from:

WT shamΔ, APOEKO sham□, WT hypoperfused○

There was no significant difference in MTR in any of the examined ROIs between WT and APOEKO sham mice ($p>0.05$) (table 4.1.; figure S.4.2.2. A-E- appendices II).

4.3.1.1.3. APOE deficiency does not affect grey matter structural integrity under normal physiological and chronically hypoperfused conditions: T2-weighted scans

The overall brain morphology was visually examined on T2- weighted scans in all four experimental groups. No overt grey matter abnormalities and preserved brain morphology were evident in examined cortical and subcortical areas of all experimental animals (figure S.4.3.- appendices II).

4.3.2. Pathological data

4.3.2.1. APOE deficiency does not impact on axonal integrity under normal physiological and chronically hypoperfused conditions

In the present study, axonal integrity was studied by means of APP immunohistochemistry (Chapter 2, section 2.7.4.1.; Coltman et al., 2011; Holland et al., 2011). APP is localized to cell bodies under normal physiological conditions, but it accumulates in injured axons (Forloni et al., 1992; Palacios et al., 1992; Stephenson et al., 1992; Selkoe, 1994).

Axonal integrity was preserved in all WT (8/8) and APOEKO (8/8) sham mice where APP immunoreactivity was restricted to cellular somas (figure 4.2. A1, A3). However, APP clusters- inducative of axonal injury were evident in 7 WT hypoperfused (7/10) and in 7 APOEKO hypoperfused (7/8) mice (figure 4.2. A2, A4).

The Kruskal- Wallis nonparametric analysis demonstrated significant group differences in axonal integrity in all white matter ROIs: the CC ($\chi^2= 14.42$, $p= 0.0061$), EC ($\chi^2= 14.42$, $p= 0.0061$), IC ($\chi^2= 14.53$, $p= 0.0023$), and OT ($\chi^2 = 17.20$, $p= 0.0006$), but not in the control grey matter region- the hippocampus ($\chi^2 = 6.58$, $p= 0.0866$) (table 4.2., figure S.4.3.1. A- E- appendices II). The subsequent Dunn`s post- hoc analysis showed that for all white matter ROIs (the CC, EC, IC, and OT) only APOEKO hypoperfused mice ($p<0.05$), but not WT hypoperfused animals ($p>0.05$) presented a significantly more severe axonal injury in comparison with WT and APOEKO sham groups (table 4.2.,

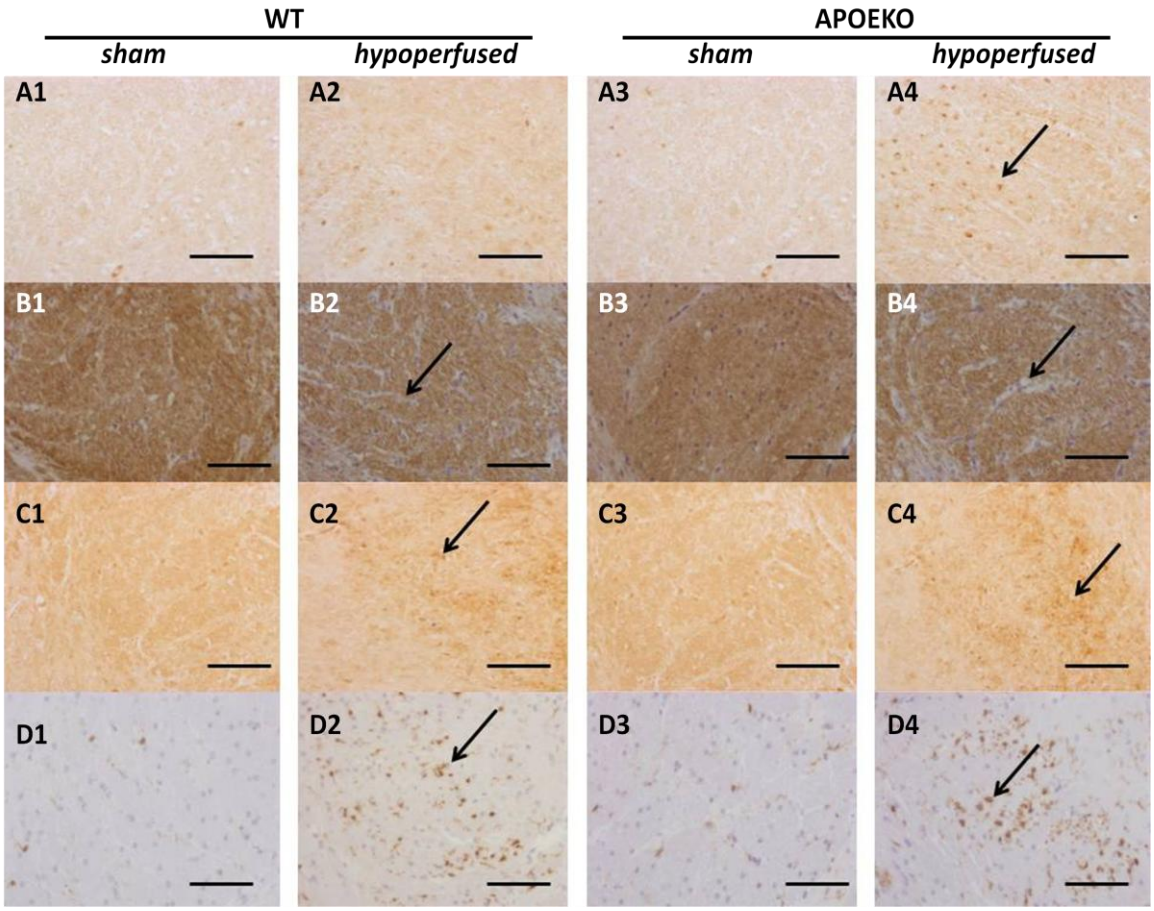

Figure 4.2.: White matter integrity in WT and APOEKO sham and hypoperfused mice

Representative images of immunohistochemically stained axons (**A1- A4**), myelin (**B1-B4**), degraded myelin (**C1- C4**), and microglia (**D1- D4**) from the IC of WT sham (**A1-D1**), WT hypoperfused (**A2-D2**), APOEKO sham (**A3-D3**), APOEKO hypoperfused mice (**A4-D4**). Myelin structural abnormalities (arrows in **B2, B4**), degraded myelin (arrows in **C2, C4**), increased inflammation (arrows in **D2, D4**) were observed in both WT and APOEKO hypoperfused mice one month after chronic cerebral hypoperfusion. Axonal, myelin integrity and inflammation were considered normal in both WT (**A1-D1**) and APOEKO (**A3- D3**) sham mice.

Scale bar represents 20µm (magnification x40).

Biomarker	Region of interest	WT (n=8) Sham	WT (n=10) Hypoperfused	APOEKO (n=8) Sham	APOEKO (n=8) Hypoperfused
APP	*Corpus callosum (CC)*	0.0	0.5	0.0	$1.0^{\Delta\square}$
Axonal integrity	*External capsule (EC)*	0.0	0.5	0.0	$1.0^{\Delta\square}$
	Internal capsule (IC)	0.0	0.5	0.0	$1.0^{\Delta\square}$
	Optic tract (OT)	0.0	$1.5^{\Delta\square}$	0.0	$1.0^{\Delta\square}$
	Hippocampus	0.0	0.0	0.0	0.0
MAG	*Corpus callosum (CC)*	0.0	0.0	0.0	0.0
Myelin integrity	*External capsule (EC)*	0.0	$1.0^{\Delta\square}$	0.0	0.5
	Internal capsule (IC)	0.0	$1.5^{\Delta\square}$	0.0	$1.0^{\Delta\square}$
	Optic tract (OT)	0.0	$2.5^{\Delta\square}$	0.0	$2.5^{\Delta\square}$
dMBP	*Corpus callosum (CC)*	0.0	1.0	0.0	0.5
Degraded myelin	*External capsule (EC)*	0.0	$1.0^{\Delta\square}$	0.0	$1.0^{\Delta\square}$
	Internal capsule (IC)	0.0	$1.0^{\Delta\square}$	0.0	$1.0^{\Delta\square}$
	Optic tract (OT)	0.0	0.0	0.0	$1.0^{\Delta\square}$
	Hippocampus	0.0	$1.0^{\Delta\square}$	0.0	$1.0^{\Delta\square}$
Iba1	*Corpus callosum (CC)*	0.0	0.0	0.0	$1.0^{\Delta\square}$
Inflammation	*External capsule (EC)*	0.0	$1.5^{\Delta\square}$	0.0	1.0
	Internal capsule (IC)	0.0	$2.0^{\Delta\square}$	0.0	$1.5^{\Delta\square}$
	Optic tract (OT)	0.0	$3.0^{\Delta\square}$	0.0	$3.0^{\Delta\square}$
	Hippocampus	0.0	$2.0^{\Delta\square}$	0.0	$1.5^{\Delta\square}$

Table 4.2.: Regional group median pathological grades

Chronic cerebral hypoperfusion led to a significant axonal and myelin pathology, an increased inflammation in both WT and APOEKO hypoperfused mice ($p<0.05$). Only APOEKO hypoperfused mice showed a significantly more severe axonal injury in white matter regions than the two sham groups ($p<0.05$). There was no difference in the pathological profile between WT and APOEKO sham as well as between WT and APOEKO hypoperfused mice ($p>0.05$).

The post hoc Dunn`s analysis is indicated to be significantly different ($p<0.05$) from: WT shamΔ, APOEKO sham$\square$

figure S.4.3.1. A- D- appendices II). There was no significant difference in the axonal integrity in any of the ROIs between WT and APOEKO sham as well as between WT and APOEKO hypoperfused mice ($p>0.05$) (table 4.2., figure S.4.3.1.- A- E- appendices II).

The individual pathological grades of axonal integrity for each mouse are given in table S.4.1.1., appendices II.

4.3.2.2. APOE deficiency does not impact on myelin integrity under normal physiological and chronically hypoperfused conditions

Myelin integrity was examined using MAG immunohistochemistry which is a sensitive biomarker to hypoxia- ischemia- induced myelin pathology (Chapter 2, section 2.7.4.2.; Aboul- Enein et al., 2003; Coltman et al., 2011; Holland et al., 2011).

The pathological analysis demonstrated that myelin integrity was preserved in all WT (8/8) and all APOEKO (8/8) sham mice where myelin fibers were tightly organized in bundles forming the white matter ROIs (the CC, EC, IC, and OT) (figure 4.2. B1, B3). Myelin pathology consisting of disorganized myelin fibers, vacuole formations, and myelin debris was pathologically evidenced in all WT (10/10) and all APOEKO (8/8) hypoperfused animals (figure 4.2. B2, B4).

The nonparametric Kruskal- Wallis analysis demonstrated significant group differences in myelin integrity in the EC ($\chi^2 = 12.15$, $p= 0.0069$) where the Dunn`s post- hoc analysis indicated that WT hypoperfused mice ($p< 0.05$), but not APOEKO hypoperfused ($p> 0.05$) mice presented significantly more severe myelin abnormalities in comparison with WT and APOEKO sham animals (table 4.2., figure S.4.3.2. B- appendices II). Significant group differences in myelin integrity were also observed in the IC ($\chi^2 = 21.12$, $p<0.0001$) and OT ($\chi^2 = 24.14$, $p<0.0001$) where both WT and APOEKO hypoperfused mice showed significant myelin abnormalities when compared with WT and APOEKO sham groups ($p<0.05$) (table 4.2., figure S.4.3.2.C, D- appendices II). Myelin integrity did not differ significantly in any of the ROIs between WT and APOEKO sham mice as well as between WT and APOEKO hypoperfused mice ($p> 0.05$) (table 4.2., figure 4.3.2. A-D- appendices II). There was no significant group difference in myelin integrity in the CC ($\chi^2 = 24.14$, $p= 0.1118$) (table 4.2., figure S.4.3.2. A- appendices II).

The individual pathological grades of myelin structural integrity (MAG) for each mouse are given in table S.4.1.2., appendices II.

4.3.2.3. APOE deficiency does not impact on myelin degradation under normal physiological and chronically hypoperfused conditions

In addition to MAG immunochemistry in the present experiment, myelin pathology was also examined by using an alternative immunostaining for degraded myelin basic protein (dMBP). dMBP is a MBP isoform expressed only under pathological conditions and it is associated with myelin abnormalities (Matsuo et al., 1997). dMBP is usually not immunodetected under normal physiological conditions.

The pathological analysis demonstrated an absence of dMBP immunoreactivity in WT and APOEKO sham- operated animals in all examined ROIs (figure 4.3. C1, C3). Degraded myelin was immunodetected in 9 WT (9/10) and in all APOEKO (8/8) hypoperfused animals (figure 4.2. C2, C4).

The Kruskal- Wallis nonparametric analysis demonstrated significant group differences in the extent of degraded myelin in the EC ($\chi^2 = 19.96$, $p= 0.0002$), IC ($\chi^2 = 20.36$, $p= 0.0001$), OT ($\chi^2 = 11.68$, $p= 0.0086$) and hippocampus ($\chi^2 = 17.31$, $p= 0.0006$) (table 4.2., figure S.4.3.3. B- E- appendices II). The post- hoc analysis showed that both WT and APOEKO hypoperfused animals presented a significant myelin degradation in the EC, IC and hippocampus than WT and APOEKO sham mice ($p< 0.05$) (table 4.2., figure S.4.3.3. B, C- appendices II). In the OT, only WT hypoperfused mice ($p< 0.05$), but not APOEKO hypoperfused ($p> 0.05$) animals showed significantly more degraded myelin than the two sham groups (table 4.2., figure S.4.3.3. D- appendices II). The extent of degraded myelin did not differ significantly in any of the ROIs between WT and APOEKO sham mice as well as between WT and APOEKO hypoperfused groups ($p> 0.05$) (table 4.2., figure S.4.3.3. A-_ E- appendices II). In the CC, although there was an overall significant group difference in the extent of degraded myelin ($\chi^2 = 11.94$, $p= 0.0076$), the post- hoc analysis failed to show any significant differences among the four experimental groups ($p>0.05$) (table 4.2. figure S.4.3.3. A- appendices II).

The individual pathological grades of myelin structural integrity (dMBP) for each mouse are given in table S.4.1.3., appendices II.

4.3.2.4. APOE deficiency does not impact on inflammatory levels under normal physiological and chronically hypoperfused conditions

Inflammatory activity was examined by means of an Iba1 immunohistochemistry (Ito et al.,1998).

The inflammatory levels were considered normal in both WT (8/ 8) and APOEKO (8/ 8) sham mice where only a few Iba1 immunopositive microglia were evidenced in examined white and grey matter areas (figure 4.2. D1, D3). Increased levels of inflammation translated by an increase in Iba1 positive microglia were observed in 9 WT hypoperfused animals (9/ 10) and in 7 APOEKO hypoperfused mice (7/ 8) (figure 4.2. D2, B4).

The Kruskal- Wallis nonparametric analysis demonstrated significant group differences in inflammatory activity in all examined ROIs: the CC ($\chi^2 = 13.92$, $p= 0.0030$), EC ($\chi^2 = 13.43$, $p= 0.0038$), IC ($\chi^2 = 17.03$, $p= 0.0007$), OT ($\chi^2 = 21.69$, $p<0.0001$), and hippocampus ($\chi^2 = 15.23$, $p= 0.0016$) (table 4.2., figure S.4.3.4. A_ E- appendices II). The post- hoc Dunn`s analysis showed that in the CC, only APOEKO hypoperfused ($p<0.05$), but not WT hypoperfused ($p>0.05$) mice presented a significantly increased inflammation compared with WT and APOEKO shams (table 4.2., figure S.4.3.4. A- appendices II). In contrast, in the EC, WT hypoperfused ($p<0.05$), but not APOEKO hypoperfused ($p>0.05$) animals had a significantly increased microglial response compared with the two sham groups (table 4.2., figure S.4.3.4. B- appendices II). In the IC, OT and hippocampus both WT and APOEKO hypoperfused animals showed a significantly more severe inflammation than WT and APOEKO sham mice ($p<0.05$) (table 4.2., figure S.4.3.4. C, D- appendices II). The inflammatory levels did not differ significantly in any of the ROIs between WT and APOEKO sham mice as well as between WT and APOEKO hypoperfused groups ($p>0.05$) (table 4.2., figure S.4.3.4. A- E- appendices II)

The individual pathological grades of inflammation for each mouse are given in table S.4.1.4., appendices II.

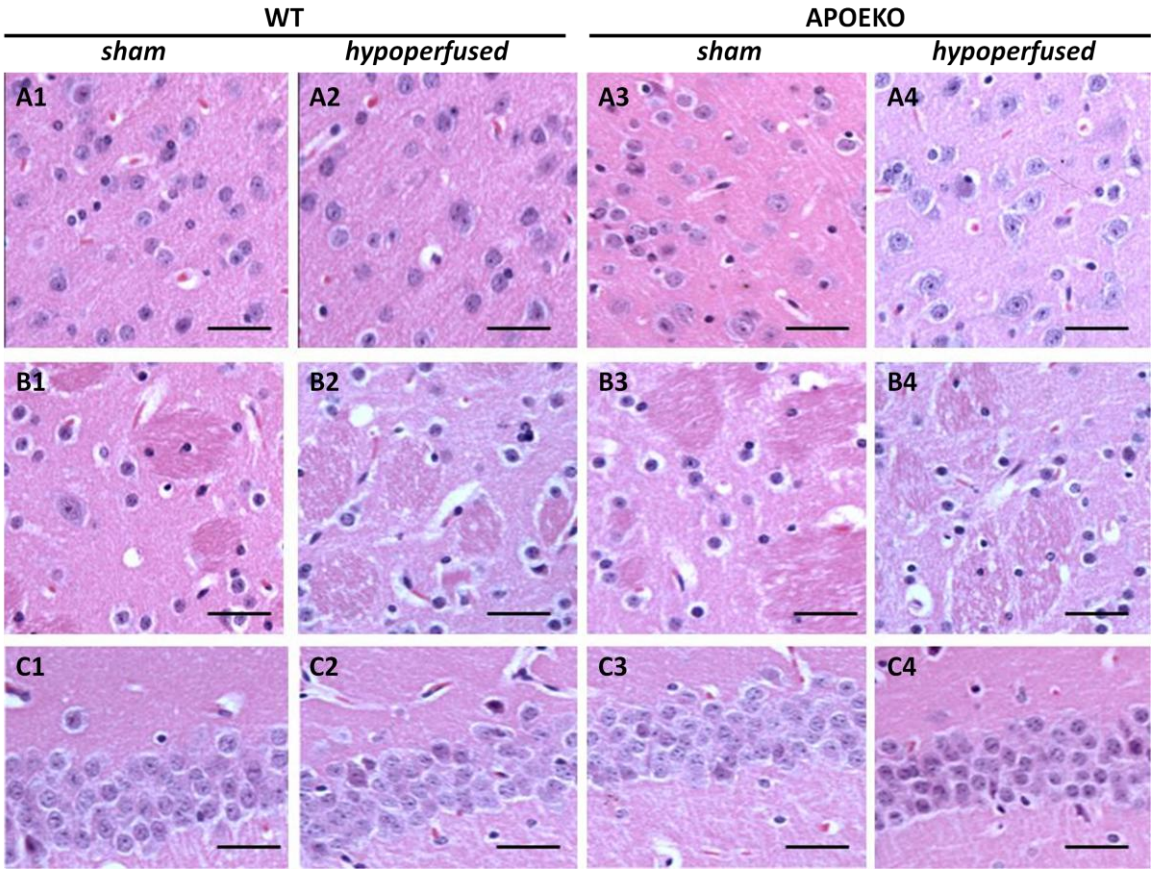

Figure 4.3.: Grey matter integrity in WT and APOEKO sham and hypoperfused mice

Representative H&E images of the Cx (**A1- A4**), the striatum (**B1- B4**), and the CA1 region of the hippocampus (**C1- C4**) of WT sham (**A1- C1**), WT hypoperfused (**A2-C2**), APOEKO sham (**A3- C3**), and APOEKO hypoperfused animals (**A4- C4**). The visual analysis revealed an absence of overt neuronal perikarya ischemic injury and preserved grey matter integrity in all experimental groups.

Scale bar represents 15µm (magnification x60).

4.3.2.5. APOE deficiency does not affect grey matter integrity under normal physiological and chronically hypoperfused conditions

Grey matter integrity was study in selected cortical (the Cx) and subcortical (the hippocampus, striatum) brain areas of WT and APOEKO mice in the presence and absence of experimentally induced chronic cerebral hypoperfusion.

The pathological examination of grey matter integrity and neuronal perikarya showed an absence of overt neuronal ischemic damage and grey matter infarctions in all experimental animals at least in the examined brain regions. In the present experiment, the neuronal cells in cortical and subcortical areas in the four experimental groups presented healthy cellular morphology consisting of light blue stained cytoplasm and well distinguishable nuclei. The examined grey matter areas showed preserved layer- specific morphology (figure 4.3.).

4.4. Discussion

The study presented in Chapter 4 sought to test the hypothesis that mouse APOE deficiency might be associated with white matter anomalies under normal physiological conditions and the development of more severe hypoperfusion- induced white matter pathology. In an attempt to translate this research to human subjects, a combined ex vivo neuroimaging/ histological approach was applied to compare white and grey matter integrity between WT and APOEKO mice under normal physiological conditions as well as one month after hypoperfusion. The ex vivo MRI findings, but not the immunohistochemical analysis partially validated the main study hypothesis suggesting a role of APOE in the development of hypoperfusion- induced white matter pathology in mice. Further, the present neuroimaging and pathological findings suggest that mouse APOE deficiency might not impact on grey matter integrity and inflammation under normal physiological and chronically hypoperfused conditions.

4.4.1. APOE effects on white matter integrity under normal physiological and chronically hypoperfused conditions in mice

4.4.1.1. APOE does not affect white matter integrity under normal physiological conditions in mice

The ex vivo MRI results demonstrated that under normal physiological conditions white matter was preserved in the absence of endogenous mouse APOE. Specifically, no significant differences in FA and MTR values in major white matter tracts- the CC, EC, IC, OT were evident between WT and APOEKO sham groups. The neuroimaging findings were confirmed at the microstructural level where intact myelin and neuronal axons were immunochemically revealed in examined white matter regions of APOEKO sham animals.

In contrast to the main study hypothesis, the present neuroimaging and immunohistochemical data suggest that mouse APOE may not be essential for the maintenance of white matter integrity under normal physiological conditions.

These results are surprising with regards to clinical data suggesting the existence of white matter abnormalities in cognitively intact APOE4 carriers (Bartzokis et al., 2006;

Bartzokis et al., 2007). The myelin sheath is particularly enriched in lipids and cholesterol composing~75% of its total dry mass (de Vries and Hoekstra, 2000; Dietschy et al., 2001). Previous studies on naïve APOEKO mice demonstrated an impaired cholesterol metabolism, an increased lipid peroxidation, a deficient phospholipids and sulfatides content in this animal model (Piedrihta et al., 1992; Van Ree et al., 1994; Montine et al., 1999; Han et al., 2003; Elosua et al., 2004).

Taken together the existing literature suggests a potential APOE involvement in regulating myelin lipid content in white matter. It is possible that genotype differences in white matter lipids existed between the two sham groups, but they were not examined in the present study (discussed in section 4.4.6.2.3).

In the absence of concomitant pathology, it is possible that alternative mechanisms of lipid turnover such as APOA-I or APOA- J compensate for APOE deficiency in the brain and are sufficient to maintain myelin lipid homeostasis. For instance, the myelin- producing oligodendrocytes express the liver- X receptor- a nuclear oxysterol receptor activated by both APOE and APOA-I (Nelissen et al., 2012). Exogenous treatment of oligodendrocytes with the liver- X- receptor agonist T0901317 induces an enhanced cholesterol efflux in the presence of APOA-I or high-density lipoprotein particles. These data suggest the existence of alternative pathways which may sustain cholesterol levels in APOE deficient oligodendrocytes necessary for myelin production.

Although MAG and dMBP are sensitive biomarkers to myelin pathology occurring following mild hypoxic- ischemic events (Matsuo et al., 1997; Aboul- Enein et al., 2003; Coltman et al., 2011; Holland et al., 2011; Reimer et al., 2011), they might not be sensitive to potentially subtle genotype differences in myelin integrity affecting for instance, other myelin proteins (e.g. PLP, CNPase). This hypothesis is substantiated by previous studies on naive APOEKO mice demonstrating the existence of an increased grey matter protein oxidation in this animal model (Ramassamy et al., 2001; Choi et al., 2004). It is unknown whether APOE affects white matter (myelin) protein content. Future experiments following previously established protocols for myelin proteins purification (Bellini et al., 1986; Heape et al., 1999) and identification of oxidized proteins (Ramassamy et al., 2001;

Choi et al., 2004) would allow to determine the levels of protein oxidation in white matter areas of APOEKO mice (discussed in section 4.4.6.2.3).

In contradiction with the present pathological findings, previous studies on naïve APOEKO mice have demonstrated the early occurrence of axonal pathology in this animal model characterized by decreases in α and β tubulin (Masliah et al., 1995). In the present study, the immunochemical analysis revealed preserved axonal integrity and APP transport in WT and APOEKO sham mice. This might be partially explained by the preservation of kinesin microtubules in APOEKO animals (Masliah et al., 1995) and their support of the fast axonal APP transport. It is important that future experiments examine in details axonal cytoarchitecture in APOEKO mice as changes in microtubules, neurofilaments might have existed in these animals, but remained undetected by the presently applied APP immunochemistry (discussed in section 4.4.6.2.3.).

Additionally, it is possible that the ex vivo MRI procedure was unable to detect subtle genotype differences in white matter integrity. To selectively assess axonal and myelin integrity on the same biological sample, one should consider applying more sophisticated neuroimaging analysis taking into consideration the axial ($\lambda_{\parallel}$; axonal integrity) and radial ($\lambda_{\perp}$; myelin integrity) diffusivity (discussed in sections 4.4.4., 4.4.6.1.3).

Further, it is possible that APOEKO sham animals were too young (5 months) to exhibit white matter pathology which might occur later during their lifespan (discussed in section 4.4.6.3.).

4.4.1.2. APOE affects hypoperfusion- induced white matter pathology in mice

Chronic cerebral hypoperfusion was associated with significant reductions in MRI metrics of white matter integrity (FA and MTR) in the CC, EC, IC, OT of both WT and APOEKO hypoperfused mice one month after surgery. Additionally, the MTR analysis demonstrated significant hypoperfusion- induced abnormalities in the control grey matter region- the hippocampus. APOEKO hypoperfused mice exhibited more severe white matter abnormalities in the CC where both FA and MTR were significantly reduced when compared with WT hypoperfused mice. In the IC and EC, FA, but not MTR was also

significantly decreased in APOEKO hypoperfused compared with WT hypoperfused animals.

The present neuroimaging findings partially confirmed the main study hypothesis that APOE deficiency may impact on the severity of hypoperfusion- induced white matter abnormalities in mice.

These results are not surprising in regards to previous experimental work suggesting a role of APOE in the endogeneous processes of myelination/ remyeliantion (Boyles et al., 1989; Stoll et al., 1989; Zhao et al., 2007; Chaerkady et al., 2011; Gan et al., 2011). Specifically, APOE has been identified as one of the molecular factors controlling adult and embryonic neural stem cells survival and differentiation towards the oligodendroglial lineage in vitro (Chaerkady et al., 2011; Gan et al., 2011). Experimental findings from an in vivo model of optic nerve injury suggest that oligodendroglial cells, but not astrocytes upregulate APOE after injury which may be associated with the processes of cholesterol synthesis and remyelination (Stoll et al., 1989). APOE levels increase significantly with a peak at the time of active remyelination in a rat model of sciatic nerve injury (Boyles et al., 1989). It has been shown that APOE plays an important role in the delivery of newly synthesized cholesterol to damaged cells and actively participates in the clearance of cellular debris promoting neuroregeneration and remyelination. On the basis of these in vitro and in vivo findings one could hypothesize that APOE deficiency may impact on oligodendroglial number, survival, functionality (e.g. cholesterol synthesis, myelin production) and indirectly may influence the processes of remyelination by 1) an impaired production of sterols and fatty acids by mature oligodendrocytes necessary for remyelination of demyelinated axons and/ or 2) a deficient differentiation of the endogenous neural stem cells pool towards the oligodendroglial lineage following hypoperfusion in mice. Future experiments should examine oligodendroglial cell differentiation, survival and functionality in relation to APOE under normal physiological as well as chronically hypoperfused conditions in mice (discussed in section 4.4.6.3).

APOE may influence the severity of neuropathology via alternative pathways such as modulation of excitotoxicity, oxidative stress and inflammation (Laskowitz et al., 1998; Horsburgh et al., 2000b; Horsburgh et al., 2003). For instance, in vitro exposure of primary neural culture and a neuronal cell line to a human recombinant APOE prior to NMDA- induced excitotoxic challenge partially reduces cell death (Aono et al., 2002). In vivo, intracerebral infusion of recombinant APOE in APOE deficient mice significantly reduces free radical levels following global ischemia (Horsburgh et al., 2000a). In vitro, recombinant APOE and APOE conditioned media prevent peroxide free radical induced cytotoxicity (Miyata and Smith, 1996). These in vivo and in vitro findings suggest that APOE deficiency might lead to the presently MRI- evidenced more severe white matter pathology in APOEKO hypoperfused mice via an impaired anti- excitotoxic and anti-oxidative function (discussed in section 4.4.6.3.). Further APOE deficiency might mediate its effects on white matter integrity in hypoperfused mice via an impaired immunomodulation (discussed in section 4.4.3.).

Additionally, previous studies have demonstrated that APOE affects the integrity of the blood brain barrier under both normal physiological as well as pathological conditions and it is associated with the formation of atherosclerotic plaques (Piedrihta et al., 1992; Nakashima et al., 1994; Van Ree et al., 1994; Fullerton et al., 2001; Methia et al., 2001; Meir and Leitersdorf, 2004 Hafezi- Moghadam et al., 2006). It is possible that cerebrovascular anomalies in APOEKO hypoperfused mice might have impacted on their neuropathological profile (discussed in section 4.4.6.3.).

The present neuroimaging findings are in consistency with clinical data demonstrating the existence of white matter pathology in APOE4 adults (Persson et al., 2006; Filippini et al., 2009; Smith et al., 2010; Heise et al., 2010; Ryan et al., 2011).. These white matter abnormalities occur relatively early during lifespan and they are not directly associated with cognitive impairment. However, it is possible that APOE associated white matter abnormalities increase the risk of age- related neurodegeneration and the occurrence of dementia in APOE4 carriers (Strittmatter et al., 1993). Further, cognitively intact APOE4 adults exhibit impaired cerebrovasculature and cerebral metabolism suggesting that

cerebrovascular factors might contribute to the development of white matter pathology in these individuals (Kalmijn et al., 1996; Skoog et al., 1998; Reiman et al., 1996; Reiman et al., 2004).

At the microstructural level axonal and myelin pathology was evidenced in both WT and APOEKO hypoperfused mice in consistency with previous findings on the hypoperfused model (Coltman et al., 2011; Holland et al., 2011; Reimer et al., 2011). However, in the present study, the neuroimaging findings suggesting significant APOE differences in hypoperfusion- induced white matter pathology were not supported by the pathological data. Specifically, the semi-quantitative pathological grading scale was unable to detect significant genotype differences in the severity of hypoperfusion- induced axonal and myelin abnormalities. The observed discrepancy between the ex vivo MRI data and the pathological analysis could be partially explained by differences in the sensitivity of the two techniques (discussed in section 4.4.5).

Overall, the pathological analysis failed to confirm the neuroimaging findings rising questions as to validity of the main study hypothesis.

4.4.2. APOE effects on grey matter integrity under normal physiological and chronically hypoperfused conditions in mice

An absence of mouse APOE effects on grey matter integrity was observed in sham and hypoperfused mice using T2- weighted neuroimaging and H&E histological analysis.

These findings are in consistency with previous studies on chronically hypoperfused mice suggesting an absence of overt grey matter pathology in this animal model (Shibata et al., 2004; Shibata et al., 2007; Nishio et al., 2010; Coltman et al., 2011; Holland et al., 2011).

However, the present results are in controversy with data from alternative animal models where grey and white matter abnormalities develop following artery ligation (Kudo et al., 1993; Ni et al., 1995; Pappas et al., 1996; Kim et al., 2008).

Further, naïve APOEKO mice have been shown to exhibit synapto- dendritic abnormalities and an early onset neurodegeneration (Gordon et al., 1995; Masliah et al., 1995; Masliah et al., 1997; Sheng et al., 1999; Buttini et al., 2000). In addition, following experimental global and focal ischemia, APOEKO mice develop more severe neuropathology (e.g. infarctions) compared with WT counterparts (Laskowitz et al., 1997; Hosrburgh et al., 1999; Sheng et al., 1999; Kitagawa et al., 2002).

In humans, the APOE4 allele is associated with the development of age- related neurodegeneration and dementia (Saunders et al., 1993; Moffat et al., 2000; Cohen et al., 2001; Schuff et al., 2009b). Human APOE4 carriers show poorer recovery after stroke exhibiting more severe infarctions than APOE3 carriers (Gromadzka et al., 2007; Wagle et al., 2009).

The observed discrepancy between the present pathological data on APOEKO hypoperfused mice and the existing human and animal literature on APOE might be partially explained by cerebrovascular and methodological differences. For instance, during focal and global ischemia the cerebral blood flow reductions are severe leading to the development of neuronal ischemic injury (infarctions) and white matter pathology, whereas during chronic cerebral hypoperfusion, the cerebral blood flow is mildly but chronically reduced leading to the development of predominant white matter pathology (at least in non- food deprived and behaviourally tested mice). Further, it is possible that the applied pathological approach, namely the visual examination of T2- weighted scans and H&E stained brain samples was not sensitive to detect subtle grey matter abnormalities (e.g. dendritic/ synaptic loss). Interestingly, in the present study significant MTR reductions were evident in the hypoperfused hippocampus in the absence of significant APOE effects. Pathologically, significant dMBP accumulations were observed in the hippocampus of both WT and APOEKO hypoperfused mice.

On the basis of the present findings and the existing literature, one could suppose the existence of presently non- detected grey matter abnormalities on T2- weighted scans and H&E stained brain sections in APOEKO sham and hypoperfused animals (Gordon et al., 1995; Masliah et al., 1995; Laskowitz et al., 1997; Masliah et al., 1997; Hosrburgh et al., 1999; Sheng et al., 1999; Buttini et al., 2000; Kitagawa et al., 2002). Additionally, it is

possible that WT hypoperfused mice also exhibited grey matter pathology, especially with regards to the pathological findings presented in Chapter 3 and data from alternative animal models (Kudo et al., 1993; Ni et al., 1995; Pappas et al., 1996; Kim et al., 2008).

4.4.3. APOE effects on inflammation under normal physiological and chronically hypoperfused conditions in mice

In contrast to previous findings on naïve APOE deficient mice (Laskowitz et al., 2000; Lynch et al., 2001), the present pathological analysis revealed that the baseline inflammatory levels were similar in WT and APOEKO sham mice. The inflammatory activity increased significantly after chronic cerebral hypoperfusion as previously shown in this animal model (Shibata et al., 2004; Coltman et al., 2011; Holland et al., 2011). However, the APOE genotype was not related to the severity of the observed inflammatory response in white and grey matter areas of hypoperfused mice.

These results are in contradiction with previous reports showing an impaired immune response in APOEKO mice under different pathological conditions (Ophir et al., 2003; Champagne et al., 2005). In a previous in vivo study on APOE deficient mice, a stereological quantification of GFAP positive astrocytes demonstrated APOE genotype differences in the astroglial response following experimental entorhinal cortex lesion (Champagne et al., 2005). Similar results were evidenced after LPS treatment where APOEKO and human APOE4 transgenic mice exhibited an impaired astroglial and microglial activation associated with the development of more pronounced white matter pathology in these animals compared with WT and APOE3 counterparts (Ophir et al., 2003). In this particular study, inflammatory levels were examined by means of a standard immunohistochemical procedure followed by a quantitative, stereological assessment of GFAP- positive astroglial processes length and the number of F4/80- positive microglia. Further, by using an immunohistochemical approach for interleukins (IL-6; IL-1β; IL-18) and CD45 (marker of inflammatory cells) accompanied by a subsequent cell counting procedure, Rahman et al., 2005 demonstrated increased inflammatory levels in APOE deficient mice maintained on a high cholesterol diet.

With regards to the observed discrepancy between the present pathological findings suggesting an absence of APOE differences in the immune response following chronic cerebral hypoperfusion and previously published work demonstrating APOE immunomodulatory role following injury to the brain (Ophir et al., 2003; Champagne et al., 2005; Rahman et al., 2005), one should consider applying quantitative pathological techniques (similar to the ones presented in peer- reviewed publications) in order to verify the present findings. Further, astrocytes are glial cells constituting the blood brain barrier and exerting various physiological functions in the central nervous system (e.g. secretion of neurotrophic factors, buffering of extracellular glutamate, immunomodulation) (Hertz and Zielke, 2004; Hawkins and Davis, 2005; Volterra and Meldolesi, 2005; Magistretti, 2006). APOEKO mice have been shown to exhibit blood brain barrier abnormalities under normal physiological conditions and increases in blood brain barrier permeability in the presence of neuropathology (Fullerton et al., 2001; Methia et al., 2001; Hafezi-Moghadam et al., 2006). To gain a better understanding of the cellular and molecular mechanisms mediating APOE effects on neuropathology, it would be interesting to examine the astroglial response in APOEKO mice under normal physiological and chronically hypoperfused conditions compared with WT counterparts. From a methodological point of view, this could be achieved by the application of astroglial specific biomarkers such as GFAP for immunohistochemical and/ or Western blot analysis (previously discussed experimental strategies are given in Chapter 3 sections 3.4.2.4., 3.4.4.3.)

In humans, significantly increased inflammatory levels are evidenced in APOE4 carriers with Alzheimer`s dementia corresponding with the accelerated disease progression in these individuals compared with non- APOE4 demented adults (Fazekas et al., 2005).

4.4.4. Sensitivity of ex vivo MRI to white matter integrity

Postmortem MRI was previously used to study white matter integrity in human, primate and rodent brain under normal physiological and pathological conditions (Nagara et al., 1987; Grafton et al., 1991; Bronge et al., 2002; Guilfoyle et al., 2003; Sun et al., 2003; Song et al., 2003; Englund et al., 2004; Larsson et al., 2004; Pfefferbaum et al., 2004; Schmierer et al, 2004; Song et al., 2005; Sun et al., 2005; Dhenain et al., 2006; Harms et

al., 2006; Sun et al., 2006b; Blezer et al., 2007; D`Arceuil et al., 2007; Ou et al., 2009; Augustinack et al., 2010).

Ex vivo MRI differs from in vivo MRI as the tissue samples are drained from the circulating blood, their temperature is below the normal body temperature of the living animal/ human and a fixative reagent is usually applied to ensure the perseveration of protein connections and sample morphology. All this could alter MRI measures as the procedure relies on the temperature driven diffusion of water molecules in the brain and applying MRI on postmortem samples has to overcome certain issues. This is done by adjusting the ex vivo imaging protocol by applying stronger magnet gradients and excitation frequencies to the sample (Larsson et al., 2004; Pfefferbaum et al., 2004). Some groups also use additional sample treatments with enhancing contrast agents (Blezer et al., 2007; D`Arceuil et al., 2007; Augustinack et al., 2010) or agar embedding (Bronge et al., 2002; Pfefferbaum et al., 2004; Dhenain et al., 2006) to improve image quality.

Ex vivo MRI presents some obvious advantages compared to in vivo MRI procedure. Ex vivo MRI allows longer imaging times in the absence of anesthesia and physiological artifacts inherent to all in vivo MRI, the application of stronger magnets gradients and the subsequent generation of high quality images which are valuable tool for the detailed study of neuroanatomy. Furthermore, in contrast to in vivo MRI where only one animal (one brain) is scanned per imaging session, ex vivo MRI allows the simultaneous scanning of multiple samples (3- 4 brains in the present study) per imaging session thus leading to significant reductions in the experimental cost related to the MRI procedure. Although tissue fixation prior to ex vivo MRI has been shown to decrease the apparent water diffusivity, it does not affect the overall anisotropy compared with in vivo imaging procedures (Guilfoyle et al., 2003; Sun et al., 2003; Sun et al., 2005). Up to 10h after death in fixative solution the anisotropy values in the brain have been shown to remain the same as in the living animal (Kim et al., 2007). To avoid any potential bias related to an overfixation of the tissue material and/ or long postmortem delays, in the present study, ex vivo MRI was performed relatively shortly after death (~24h) in the absence of additional enhancing contrast agents and embedding substances.

From a neurobiological perspective, FA is determined by both myelin and axonal integrity (Basser, 1995; Beaulieu, 2002). Pathological damage to one or both of these white matter components leads to a reduction in FA measured using both in vivo (Filippi et al., 2001; Bozzali et al., 2002; Deary et al., 2003; Harsan et al., 2006; Penke et al., 2010; Holland et al., 2011) as well as ex vivo (Song et al., 2003; Song et al., 2005; Dhenain et al., 2006; Harms et al., 2006; Sun et al., 2006a; Gouw et al., 2008) MRI settings.

MTR has slightly different neurobiological basis (Wolff and Balaban, 1989; Grossman et al., 1994), but damage to the myelin sheath and/ or the neuronal axons can impact on the pool of bound water molecules in the brain and therefore could lead to reductions in MTR (McGowan et al., 1999; Blezer et al., 2007; Ou et al., 2009; Holland et al., 2011).

Interestingly, in the present study, although FA and MTR detected with the same sensitivity pathological changes in white matter tracts, they differed in their sensitivity to detect subtle white matter changes in grey matter. In the hippocampus, only MTR decreased significantly after chronic cerebral hypoperfusion and correlated with myelin (dMBP), but not axonal pathology (S.4.1.- appendices II). This is in accordance with previous findings showing that MTR is particularly sensitive to myelin pathology as in the case of multiple sclerosis (Schmierer et al., 2004; Blezer et al., 2007). Although there were no APOE genotype differences in MRI parameters in the hippocampus, the correlation data suggest that MTR, but not FA is sensitive to pathological changes affecting both grey and white matter (S.4.1.- appendices II).

To distinguish between axonal and myelin pathology using MRI- DTI (Beaulieu, 2002), it is necessary to apply more sophisticated DTI analysis focused on the axial ($\lambda\parallel$; axons) and radial ($\lambda\perp$; myelin) diffusivities (discussed in section 4.4.6.1.3.).

In vivo DTI has been shown to differentiate between axonal and myelin pathology in a cuprizone mouse model of demyelination (Sun et al., 2006a) and in mice with retinal ischemia (Song et al., 2003) where increases in radial diffusivity were associated with myelin loss and reductions in axial diffusivity were indicative of axonal injury.

Similar results were obtained using ex vivo MRI in mice with middle cerebral carotid artery occlusion (Sun et al., 2005), on cuprizone- treated mice (Song et al., 2005) and on

mice with induced retinal ischemia (Sun et al., 2006b). Furthermore, Sun et al., 2006b showed differential sensitivity of in vivo and ex vivo MRI to axonal and myelin pathology in mice with retinal ischemia. Although DTI sensitivity to myelin pathology was similar for in vivo and ex vivo MRI settings, ex vivo DTI failed to detect axonal pathology observed in vivo, pointing to the necessity of a further development and validation of ex vivo DTI techniques. In the present ex vivo MRI study, $\lambda\parallel$ and $\lambda\perp$ were not measured and future in vivo and ex vivo experiments on the same hypoperfused mice should elucidate the respective contribution of axonal and myelin pathology to the observed white matter structural changes observed on MRI scans (discussed in section 4.4.6.1.3.).

Using an in vivo MRI approach on chronically hypoperfused mice, our group previously reported that both FA and MTR are sensitive metrics of diffuse white matter abnormalities occurring in this animal model (Holland et al., 2011). In vivo, FA decreased significantly following hypoperfusion in the CC and EC, whereas MTR reductions were evidenced in all white matter ROIs (the CC, IC, OT, Fx). In the present ex vivo MRI study, both FA and MTR detected with the same sensitivity white matter integrity (the CC, EC, IC, OT) and were able to account for significant genotype differences in hypoperfusion- induced white matter pathology (the CC). The hippocampal (grey matter) FA and MTR in vivo did not change significantly in chronically hypoperfused mice. However, in the present ex vivo MRI experiment on the same animal model, MTR was found to be significantly reduced in the hypoperfused hippocampus in the absence of significant APOE effects.

4.4.5. Differential sensitivity of ex vivo MRI and immunohistochemistry to APOE genotype differences in white matter integrity in mice

In the present study ex vivo MRI was found to be more sensitive to APOE genotype differences in white matter integrity than a standard immunohistochemistry. This discrepancy could be explained by differences in the nature of the two techniques as well as in the total volume of examined brain tissue. FA and MTR quantitatively measured alterations in white matter structural integrity occurring in tracts throughout the brain (section thickness 0.5mm), whereas axonal and myelin integrity was semi- quantitatively categorized on brain sections from only one neuroanatomical level (-2.12mm bregma, Franklin and Paxinos, 1997) (section thickness 6μm). Similar results showing differences

in the sensitivity of ex vivo MRI and histology in detecting white matter pathology were reported by other groups. Ex vivo MRI was found to be either more (Grafton et al., 1991) or less (Bronge et al., 2002) sensitive than standard histological techniques in identifying white matter abnormalities. This discrepancy in the existing literature is most likely due to differences in the employed MRI and histological techniques, the strength of the MRI magnet, the total imaging time, the type of fixative and the postmortem delay. However, similar to the present study, Grafton et al., 1991 found ex vivo MRI to be more sensitive to white matter pathology in human brains than a semi- quantitative pathological grading scale. In the present study, the microstructural changes in white matter integrity were evaluated by means of a semi- quantitative grading scale because of 1) its shown sensitivity to detect white matter pathology in chronically hypoperfused mice (Coltman et al., 2011; Holland et al., 2011) and 2) its broad application in human neuropathological studies (Grafton et al., 1991; Dickson et al., 1991; Curtis et al., 2003). Further development and characterization of ex vivo MRI might be of particular interest for the elucidation of the microstructural basis of diffuse white matter pathology evidenced in different neuropathological conditions and associated with cognitive impairment. Ex vivo MRI might become a useful complementary tool to basic histological techniques allowing a detailed whole brain anatomy examination which otherwise would be an expensive histological venture.

4.4.6. Strengths and limitations of the applied methodology and future experimental work

4.4.6.1. Strengths and limitations of ex vivo MRI and future experiments to further develop and characterize this newly developed neuroimaging procedure

4.4.6.1.1. Strengths of the ex vivo MRI procedure

One of the major advantages of the newly developed ex vivo MRI procedure consists of the important reductions of the experimental costs associated with neuroimaging. In contrast to in vivo MRI, ex vivo MRI allows to image more than 1 biological sample per imaging session which leads to ~1 /4 reductions in the cost of performing pre- clinical neuroimaging studies (discussed in section 4.4.4.).

Further, ex vivo MRI allows longer imaging times in the absence of anesthetic agents, movement and physiological artifacts leading to the generation of images with a very good spatial resolution facilitating the subsequent regional image analysis (discussed in section 4.4.4.). In the present study, a significant technical achievement was accomplished by optimizing ex vivo MRI without applying any additional contrast agents/ embedding substances which could impact on the subsequent pathological analysis by changing the tissue morphology.

Another interest of the ex vivo neuroimaging approach relies in its translational nature to clinics and the extrapolation of experimental (animal) findings to humans.

Lastly, the applied ex vivo MRI analysis allows to quantitatively assess white matter integrity throughout the mouse brain. This would be difficult to achieve by using standard immunohistochemical procedures, especially in regards to the implicated costs associated with whole brain immunostaining.

4.4.6.1.2. Limitations of the ex vivo MRI procedure

In the present study, the neuroimaging procedure was performed post- mortem in conditions which were different from the natural, physiological environment of the living animal (discussed in section 4.4.4.). For instance, there are important differences in the brain sample temperature in vivo (~37°C) compared with ex vivo (~20°C) which might impact on the water molecule diffusivity and by consequence on the MRI metrics (Sun et al., 2003). Additionally, at the difference from the living animal the perfused brain is characterized by an absence of active circulation and neurotransmission. It is unknown whether and/ or to what extent the present ex vivo MRI findings recapitulated the actual pathology in the living animal (discussed in section 4.4.6.1.3.).

In addition, the ex vivo MRI procedure was associated with a prolonged samples conservation in fixative solution (> 24h) under an increased ambient temperature (>4°C). This might have overfixed the tissue material and by consequence impacted on the immunohistochemical analysis. Previous studies demonstrated that up to 10h after death in fixative solution does not affect anisotropy in ex vivo MRI samples (Kim et al., 2007) (discussed in 4.4.4.). However, the effects of prolonged tissue fixation (>24h) on mean

diffusivity, anisotropy and neuropathology are unknown. Potential artifectual alterations in ex vivo MRI parameters due to tissue overfixation might have led to wrong study conclusions (e.g. not detected group differences in white matter integrity when present or vice- versa) (discussed in section 4.4.6.1.3.).

Another limitation of the presently applied ex vivo MRI procedure relates to the obtained data and its subsequent analysis. Specifically, although the applied FA and MTR analysis is sensitive to overall pathological changes in white matter integrity, it does not allow to distinguish between axonal and myelin pathology. Therefore, this neuroimaging analysis does not provide any information on the cellular (microstructural) determinants of the MRI- evidenced white matter abnormalities in WT and APOEKO hypoperfused mice. Further, the present MRI analysis might not have been sensitive to subtle white matter abnormalities in APOEKO sham mice (discussed in sections 4.4.1.1.).

In the present study, grey matter integrity was not quantitatively measured on T2-weighted scans. The MRI scans are designed to detect white matter integrity and they are not suited to grey matter. Therefore, although, the visual examination of T2- weighted scans allows to determine the potential presence/ absence of overt grey matter pathology it does not provide quantitative assessment of grey matter integrity. This nonquantitative approach risks of omitting important pathological changes in grey matter potentially present in some of the experimental animals (Chapter 3; Gordon et al., 1995; Masliah et al., 1995; Laskowitz et al., 1997; Masliah et al., 1997; Hosrburgh et al., 1999; Sheng et al., 1999; Buttini et al., 2000; Kitagawa et al., 2002) (discussed in section 4.4.2.).

4.4.6.1.3. Future experiments to further develop and characterize ex vivo MRI

To test the sensitivity and biological significance of post- mortem MRI, it is important to measure FA and MTR in vivo and subsequently perform the same measures ex vivo in the same sham and hypoperfused mice in order to determine the existence of any potential in vivo/ ex vivo “within” and “between” group differences in the regional FA and MTR values. The results from this analysis would allow to validate and further refine the sensitivity of ex vivo MRI.

To determine the effects of the prolonged time in fixative under an increased ambient temperature inherent to post- mortem MRI, future experiments should compare MRI/ immunochemical data from the living animal with the same measures in brain samples kept for different periods in fixative (e.g. 0h vs. 12h vs. 24h. vs. > 24h). This would allow to determine whether the prolonged time in fixative solution (>24h) affects on MRI measures and neuropathology.

To selectively detect axonal and myelin integrity using MRI, one should consider applying more sophisticated neuroimaging analyses such as assessment of axial ($\lambda\parallel$; axonal integrity) and radial ($\lambda\perp$; myelin integrity) diffusivity (Song et al., 2003; Song et al., 2005; Sun et al., 2006a; Sun et al., 2006b; Blezer et al., 2007). Under normal physiological conditions, the water molecules in the brain diffuse preferentially along the neuronal axons and this physical phenomenon is translated into an increased axial diffusivity. In the absence of pathology, the water molecules could hardly diffuse perpendicular to the neuronal axons being hindered by the myelin sheath and the axonal cytoarchitecture (e.g. microtubules, neurofilaments). Therefore, under normal physiological conditions, the radial diffusivity is low. Axonal pathology results in decreases in axial diffusivity. Inversely, pathological damage to the myelin sheath results in an increased radial diffusivity. Thus, by measuring axial and radial diffusivity one could get a better understanding of the cellular determinants of white matter integrity on MRI scans. Further, it is important to compare axial and radial diffusivity in vivo vs. ex vivo as previous studies on a mouse model of retinal ischemia suggest that ex vivo MRI might not be sensitive to in vivo MRI evidenced axonal pathology (Sun et al., 2006b). Future combined in vivo and ex vivo MRI analysis of axial and radial diffusivity in sham and hypoperfused animals would allow to determine whether the newly developed ex vivo MRI procedure is sensitive to pathological changes in axonal and myelin integrity and whether the ex vivo MRI metrics are comparable with in vivo findings in the same groups of animals. This would allow to further refine and develop neuroimaging approaches for both pre- clinical and clinical application.

4.4.6.2. Strengths and limitations of the immunochemical pathological approach and future experiments

4.4.6.2.1. Strengths of the immunochemical approach

The strengths of the immunohistochemical procedure are discussed in details in Chapter 3, section 3.4.4.1 Briefly, the major advantage of this approach relates to the selective examination of specific white matter cellular components by the application of antibody probes targeted to the neuronal axons (APP), myelin sheath (dMBP, MAG) and inflammatory microglia (Iba1) allowing more detailed characterization of white matter abnormalities in this animal model. The applied H&E histological staining gives a good overall indication of grey matter morphology and the existence of neuronal ischemic injury.

4.4.6.2.2. Limitations of the immunohistochemical approach

The major drawbacks of the applied immunohistochemical approach are discussed in details in Chapter 3, section 3.4.4.2. Briefly, the limitations of the pathological analysis are associated with the limited number of applied white and grey matter- specific biomarkers, the single brain level pathological analysis, as well as the semi- quantitative nature of the obtained data. Overall, this pathological approach risks of omitting neuropathology affecting alternative white and grey matter cellular components not immunodetected by the applied antibodies and/ or present on non- examined brain levels. This is of particular importance especially in regards to the presently observed discrepancy between the immunohistochemical and ex vivo MRI findings (discussed in section 4.4.5.).

4.4.6.2.3. Future pathological studies

Future experiments should perform a quantitative pathological characterization in this animal model especially with regards to the presently observed discrepancy between the immunochemical (single brain level) and ex vivo (whole brain) MRI analysis (discussed in section 4.4.5.). This could be achieved by 1) the application of a wider range of white and grey matter specific biomarkers, 2) the examination of additional neuroanatomical

levels (corresponding to the MRI- DTI analysis) and 3) the application of laboratory techniques allowing quantitative neuropathological evaluation (discussed in Chapter 3, section 3.4.4.3.). Additionally, an electron microscopy structural analysis would allow to better characterize APOE effects on white matter integrity in the presence and absence of chronic cerebral hypoperfusion in mice.

In regards to 1) the important role of APOE in regulating brain cholesterol and lipid homeostasis (Mahley and Innerarity, 1983; Han et al., 2003; Bartzokis et al., 2003; Bartzokis et al., 2007), 2) the high lipid and cholesterol content of the myelin sheath (~75% of its dry mass) (de Vries and Hoekstra, 2000; Dietschy et al., 2001) as well as 3) previously demonstrated impaired cholesterol metabolism, increased lipid peroxidation, deficient phospholipids and sulfatides content in naïve APOEKO mice (Piedrihta et al., 1992; Van Ree et al., 1994; Montine et al., 1999; Han et al., 2003; Elosua et al., 2004), future experiments should examine the individual and combined effects of the surgical procedure (sham vs. hypoperfused) and genotype (APOEKO vs.WT) on myelin cholesterol and lipid levels using for example HPLC (e.g. myelin lipids) and/ or Western blot analysis (e.g. myelin proteins).

4.4.6.3. Other methodological limitations and future experiments to examine APOE effects on white matter integrity under normal physiological and hypoperfused conditions in mice

The present study presented other methodological limitations not directly related to the ex vivo MRI and immunohistochemical procedures.

All pathological analysis was performed one- month post- surgery. It is unknown whether APOE- associated differences in white and grey matter integrity occur or not at later post-surgery time points. Future experiments should examine white and grey matter integrity at different post- surgery time points in APOEKO and WT animals in the presence and absence of chronic cerebral hypoperfusion. This is important in regards to 1) previously demonstrated cumulative pathology in chronically hypoperfused animals (Farkas et al., 2007; Nishio et al., 2010; Reimer et al., 2011) and 2) the natural effects of aging on neuropathology (Arnsten and Goldman- Rakic, 1985; Olendorf, 1987; de Jong et al., 1990;

Miguez et al., 1990; McEntee and Crook, 1991; Ni et al.,1995; Kondo et al., 1996; Egashira et al., 1996; Tanaka et al., 1996; Tang et al., 1997; Ouchi et al., 1998; Bimonte et al., 2003; Blesch, 2006; Choy et al., 2006; Farkas et al., 2006; Fernando et al., 2006; Gold et al., 2007) which might impact on their neuropathological profile. On the basis of these previous data, it is possible that a more severe neuropathology develops at later post-surgery time points and these pathological changes might be more pronounced in APOEKO hypoperfused animals.

Further, the cerebral blood flow was not measured in the experimental groups. This is an important methodological drawback especially in regards to previously reported naturally occurring cerebrovascular anomalies (e.g. atherosclerosis, blood brain barrier leakage) in APOE deficient mice (Piedrihta et al., 1992; Nakashima et al., 1994; Van Ree et al., 1994; Fullerton et al., 2001; Methia et al., 2001; Meir and Leitersdorf, 2004; Hafezi- Moghadam et al., 2006). These pathological changes are exacerbated in the presence of neuropathology (Methia et al., 2001). Although, in the present study, an attempt was made to limit these effects by using relatively young adult mice, it is possible that early atherosclerotic plaques existed in the APOEKO mice impacting on the overall perfusion rates in these animals. Future experiments on APOEKO mice should take into consideration the existence of potential differences in the hypoperfusion rates between APOEKO and WT mice which might impact on neuropathology and functional outcome. Methodological strategies to measure the cerebral blood flow are discussed in Chapter 3, section 3.4.4.3.

The present study focused on relatively young, adult WT and APOEKO mice. However, in regards to the relevance of the hypoperfused model and APOE to the aging process in humans, it is important to examine the individual and combined effects of surgery (sham vs. hypoperfusion) and genotype (APOEKO vs. WT) on neuropathology and functional outcome in the context of aging (Chapter 6, section 6.1.2.).

Although the present study provides an interesting insight into APOE effects on white matter integrity following chronic cerebral hypoperfusion, it does not inform on the functional significance of the observed genotype differences in white matter integrity. Previous studies on APOEKO deficient mice with experimentally induced injury to the

central nervous system have reported more severe pathological and functional outcome in these animals in comparison with WT counterparts (Chen et al., 1997; Laskowitz et al., 1997a; Lomnitski et al., 1997; Horsburgh et al., 1999; Lomnitski et al., 1999; Sheng et al., 1999; Lynch et al., 2002; Kitagawa et al., 2002; Champagne et al., 2005). These findings suggest that APOEKO mice might exhibit more severe neuropathology associated with more pronounced functional impairment following chronic cerebral hypoperfusion. Future experiments should examine the individual and combined effects of surgery (sham vs. hypoperfusion) and genotype (APOEKO vs. WT) on cognition and memory using behavioural paradigms. In vitro experimental strategies would allow to determine whether these experimental factors affect on action potential propagation using electrophysiology (e.g. action potential propagation measured in brain slice preparation) These functional experiments would allow to determine whether the presently MRI- evidenced APOE differences in hypoperfusion- induced white matter pathology are relevant at the functional level.

Further, at the exception of inflammation, the exact molecular and/ or cellular mechanism(s) via which APOE might modulate the development of hypoperfusion-induced white matter pathology in mice remain(s) unknown. Future experiments should examine possible pathophysiological pathways (e.g. impaired lipid and cholesterol metabolism, excitotoxic levels, oxidation, pre- existing cerebrovascular abnormalities) associated with hypoperfusion- induced neuropathology in APOEKO mice using experimental strategies discussed in Chapter 6, section 6.1.3.. Briefly, the application of anti- excitotoxic, anti- oxidative, anti- inflammatory agents would allow to determine whether these pathways influence on the development of white matter pathology and whether and/ or how they are modulated by APOE. Alternative strategy would consist of the intracerebral infusion of synthetic APOE vs. control (saline) into APOEKO sham and hypoperfused mice and their respective controls followed by a subsequent evaluation of excitotoxic levels, oxidative stress and inflammation in these animals (discussed in Chapter 6, section 6.1.4.2.).

Future studies would allow to determine the potential cellular substrates of the MRI-evidenced APOE genotype differences in the severity of hypoperfusion- induced white

matter pathology. Recent experiments suggest that APOE might impact on the myelin producing oligodendroglia and by consequence could affect the endogenous processes of remyelination (Chaerkady et al., 2011; Gan et al., 2011; Nelissen et al., 2012) (discussed in section 4.4.1.2.). Methodologically this question could be addressed by comparing the proportions of mature oligodendrocytes (e.g. MBP, PLP) and OPC (e.g. NG2, O4) (DAPI for cell nuclei) in WT and APOEKO sham and hypoperfused mice using for instance a combined immunochemical/ confocal imaging approach.

Another major methodological limitation of the present study relates to the small group (**n**) numbers on which the analyses were based. This was due to a slow breeding in the APOEKO colony and the difficulty to gather simultaneously sufficient numbers of sex, age, and genotype- matched animals. The alternative commercial purchase of large numbers of genetically modified animals involved important costs. However, with regards to the heterogeneous nature of the hypoperfused model one should consider using larger groups of WT and APOEKO hypoperfused animals as this would allow 1) a more precise pathological evaluation, 2) an increased statistical power and by consequence 3) firmer study conclusions.

In an attempt to approach the human condition and an additional step towards translation of this research, future experiments should also investigate the effects of the human APOE isoforms (APOE 3 vs. APOE4) on neuropathology (white matter integrity) and functional outcome comparing human APOE3 vs. APOE4 transgenic mice under normal physiological and chronically hypoperfused conditions.

4.4.7. Implications of the study and future directions

The present study provides a preclinical insight into the individual and combined effects of genetic (APOE) and cerebrovascular (chronic cerebral hypoperfusion) factors on the development of neuropathology. This question has a direct relevance to clinics where human APOE allelic variation and chronic cerebral hypoperfusion have been associated with the development of age- related white matter pathology (Kalaria, 1996; Tang et al., 1997; de Leeuw et al., 2000; Farkas et al., 2006; Gold et al., 2007; Bartzokis et al., 2007; Filippini et al., 2009; Heise et al., 2010; Ryan et al., 2011).

The present neuroimaging findings suggest that APOE may not be essential for the maintenance of white matter integrity under normal physiological conditions, but it may impact on the severity of hypoperfusion- induced white matter pathology at least in the mouse.

Although a substantial future development of the ex vivo MRI procedure, immunochemical evaluation and overall study design is required, the present data are interesting and would serve as a basis for future research into the pathophysiological mechanism(s) underlying APOE effects on hypoperfusion- induced white matter pathology. This future work would potentially lead to the identification of biological targets for the pre- clinical development of therapeutic strategies for the treatment of age-related cognitive decline in APOE4 carriers who are at a higher risk of dementia.

Future experiments on human APOE3 and APOE4 transgenic mice would allow to better approach the human condition and would facilitate the translation of the obtained pre-clinical findings to clinics.

4.5. Summary

The neuroimaging findings presented in Chapter 4 suggest that mouse APOE deficiency may not impact on white matter integrity under normal physiological conditions, but it may be associated with the development of more severe hypoperfusion- induced white matter abnormalities. However, these neuroimaing findings were not supported by the applied immunochemical (microstructural) analysis showing an absence of APOE differences in the severity of axonal and myelin integrity in examined hypoperfused white matter tracts. An absence of APOE effects on grey matter and inflammation were evidenced under normal physiological and chronically hypoperfused conditions in mice.

Chapter 5

Characterization of methylation and hydroxymethylation in white matter under normal physiological and chronically hypoperfused conditions in mice

5.1. Introduction and aims

5- Methylcytosine (5mC) is a major form of epigenetic DNA modification involving methylation of the 5' carbon of cytosine in a CpG dinucleotide context in gene promoters (Bird, 2002). Methylation is associated with regulation of gene expression (e.g. transcriptional silencing) modulating cellular function during lifespan and disease.

With aging there are dynamic global and gene-specific changes in 5mC distribution in cortical and subcortical grey matter regions of the mammalian brain which are associated with neurodegeneration and cognitive impairment (West et al., 1995; Mehler, 2008; Zawai et al., 2009; Chouliaras et al., 2010; Penner et al., 2010). Several mechanisms have been proposed to impact on DNA methylation with increasing age including cerebrovascular conditions (e.g. stroke, chronic cerebral hypoperfusion) and the resulting hypoxic-ischemic environment accompanied by increased excitotoxicity, oxidative stress, inflammation (Endres et al., 2000; Westberry et al., 2008). Severe reductions of cerebral blood flow as a result of experimental stroke and focal ischemia are known to reduce brain genomic methylation (Endres et al., 2000; Westberry et al., 2008).

This is particularly relevant with regard to a newly discovered oxygen- dependent modification of 5mC- 5- hydroxymethylcytosine (5hmC) catalyzed by the Ten- eleven translocation proteins (TET1, TET2, TET3) (Kriaucionis and Heintz., 2009; Tahiliani et al., 2009; Ito et al., 2010). 5hmC is detected in a range of mammalian tissues at different developmental stages, but it is particularly enriched in the early mammalian embryo as well as in the developing and adult brain where it is abundant in neurons (Kriaucionis and Heintz., 2009; Li and Liu, 2011; Ruzov et al.., 2011). From a functional perspective, recent genome- wide studies using human brain tissue (Jin et al., 2011) and mouse embryonic stem cells (Ficz et al., 2011) have demonstrated that in contrast to 5mC which is predominantly located at heterochromatic regions, 5hmC is abundant in euchromatin suggesting that this epigenetic DNA modification is most likely to be involved in facilitating gene expression. In the adult mouse cerebellum, increases in intragenic 5hmC have been associated with age- related neuropathology (Song et al., 2010). However, the exact functional significance of 5hmC in the healthy and diseased central nervous system remains unclear.

White matter abnormalities linked to hypoxic environment occurring with cerebrovascular disease (e.g. chronic cerebral hypoperfusion) are suggested to contribute to cognitive decline in "healthy" elderly (Farkas and Luiten, 2001; O`Sullivan et al., 2001; Roman et al., 2002; Deary et al., 2003; Charlton et al., 2006; Fernando et al., 2006; Grieve et al., 2007; Kennedy and Raz, 2009; Ihara et al., 2010; Penke et al., 2010).

At the outset of this thesis, there was minimal information on methylation and hydroxymethylation dynamics in white matter under normal physiological and chronically hypoperfused conditions. Although, more than 90% of the existing age- related neuropathologies are not inherited (absence of DNA alterations), changes in gene expression are known to occur in the aging brain most likely due to epigenetic dysregulations (Penner et al., 2010; Marques et al., 2011). Using a microarray analysis, Reimer et al., 2011, demonstrated alterations in the expression of 129 genes in white matter following chronic cerebral hypoperfusion in mice of which some were associated with oxidative stress.

The present study aimed at investigating methylation and hydroxymethylation in white matter using the mouse model of chronic cerebral hypoperfusion outlined in previous chapters within the thesis. On the basis of previous studies on alternative animal models (Endres et al., 2000; Westberry et al., 2008) and clinical conditions in which TETs mutations were associated with perturbations in hydroxy/ methylation (myeloid cancer- Ko et al., 2010), the initial study predictions were that chronic cerebral hypoperfusion might impact on 5hmC in the brain either as a direct consequence of hypoperfusion-induced perturbations in 5mC and/ or via an impaired TETs enzymatic activity. Since the major pathological changes in this animal model occur in white matte tracts, the expectations at the outset of this study were that epigenetic alterations might appear in hypoperfused white matter areas.

The study hypothesis was that in mice, chronic cerebral hypoperfusion and the resulting mild reductions of the cerebral blood flow might impact on the oxidative production of 5hmC in white matter by modification of brain methylation dynamics and/ or the disruption of TETs machinery responsible for the oxidation of 5mC.

However, since little was known about the cellular distribution and functional significance of 5hmC in the brain at the outset of this experiment, the alternative hypothesis that 5hmC might not be altered with chronic cerebral hypoperfusion was also considered. Alternatively, with regards to grey matter abnormalities observed in some hypoperfused mice in this thesis (Chapter 3) as well as in alternative animal models (Kudo et al., 1993; Ni et al., 1995; Pappas et al., 1996; Kim et al., 2008), epigenetic alterations were also expected to occur in grey matter areas following chronic cerebral hypoperfusion. Therefore, in the present study 5mC, 5hmC and one of the TETs members- TET2 were also examined in cortical and subcortical grey matter areas.

In order to experimentally address the present study hypothesis, methylation, hydroxymethylation and TET2 were investigated by a standard immunohistochemistry in white and grey matter areas under normal physiological conditions compared with one month after chronic cerebral hypoperfusion in mice. To account for observed specific hypoperfusion- induced hydroxymethylation increases in white matter, 5hmC was studied in relation to 5mC and TET2 in vivo. To determine the potential cellular basis of 5hmC in white matter, 5hmC was examined in relation to mature and progenitor oligodendroglia (OPC) in vivo. Based on previous findings suggesting that 5hmC is high in progenitor cells and neurons (Kriaucionis and Heintz., 2009; Li and Liu, 2011; Ruzov et al.., 2011) the initial study predictions were that 5hmC would be high in all neural cells at different stages of maturation. Additionally, since inflammatory cells increase in white matter tracts of chronically hypoperfused mice (Shibata et al., 2004; Coltman et al., 2011) and inflammatory agents have been shown to affect methylation under different pathological conditions (Zhang et al., 2007; Wilson, 2008; Backdahl et al., 2009), hydroxymethylation in white matter was studied in relation to inflammatory microglia in vivo. To verify the in vivo findings and further examine hydroxymethylation in relation to glia, 5hmC immunochemical distribution was examined using in vitro systems of oligodendroglial maturation and microglial activation.

The aims of the present thesis chapter were to:

- Investigate methylation, hydroxymethylation and TET2 in white and grey matter areas of the adult mouse brain under normal physiological conditions compared with one month after chronic cerebral hypoperfusion in mice.

- In the event of significant group differences in epigenetic dynamics in the brain, determine potential associations between epigenetic marks (5hmC, 5mC and TET2).

- In the event of significant group differences in epigenetic dynamics in the brain, determine their potential cellular determinants.

5.2. Materials and methods

5.2.1. Animals and surgery

For the experimental purposes of the present Chapter 5, I used the remaining brain tissue material from 8 WT (C57Bl6J) sham and 9 WT (C57Bl6J) hypoperfused mice that were previously used for the experiment presented in Chapter 4. One of the original 10 WT hypoperfused mice (mouse number 800940) from Chapter 4 was not included in the present study due to a lack of sufficient number of brain sections.

5.2.2. In vivo evaluation of the proportion of 5mC, 5hmC and TET2 immunopositive cells in the mouse brain under normal physiological and chronically hypoperfused conditions

5mC, 5hmC and TET2 immunoreactivity was examined on semi- adjacent coronal brain sections from -2.12mm bregma neuroanatomical level (Franklin and Paxinos, 1997) in white (the CC, IC, EC) and grey matter regions (the CA1 and Cx) of sham and chronically hypoperfused mice one month after surgery. 5mC, 5hmC, TET2 positive cells as well as ssDNA positive cells (for the 5hmC and 5mC immunostaining), DAPI stained cells (for the TET2 immunostaining) were manually counted on five random fields imaged from each ROI. The regional proportion of 5mC, 5hmC, TET2 positive cells was calculated as described in the materials and methods (Chapter 2, section 2.8.).

5.2.3. In vivo evaluation of the proportion of CC1, NG2, Iba1 immunopositive cells in the mouse brain under normal physiological and chronically hypoperfused conditions

CC1, NG2, Iba1 immunoreactivity was examined on semi- adjacent coronal brain sections from -2.12mm bregma neuroanatomical level (Franklin and Paxinos, 1997) in sham and chronically hypoperfused mice one month after surgery. CC1, NG2, Iba1 positive cells were studied in major white matter tracts (the CC, EC, IC). CC1, NG2, Iba1 positive cells were manually counted on five random fields imaged from a given ROI as well as the total number of cells (DAPI stained cells for CC1 and NG2; haemotoxylin stained cells for

Iba1). The regional proportion of CC1, NG2, and Iba1 positive cells was calculated as described in Chapter 2, section 2.8.

5.2.4. In vitro evaluation of 5hmC immunochemical distribution in oligodendroglial cells at different stages of maturation (0, 2, 6 DIV), in IFNγ/ LPS activated and nonactivated microglia in vitro

5hmC immunoreactivity was studied using an in vitro system of oligodendroglial maturation (Chapter 2, section 2.10.). Oligodendroglial cells at 0, 2, 6 DIV were immunocytochemically stained for 5hmC. Additionally, in vitro, 5hmC immunoreactivity was studied in IFNγ and LPS activated and nonactivated microglia cells (Chapter 2, section 2.11.). These in vitro experiments were performed in triplicates.

5.2.5. Statistics

5.2.5.1. Statistical analysis of the regional group proportions of biomarker positive cells

The group average regional proportion of 5mC, 5hmC, TET2, CC1, NG2, and Iba1 positive cells were statistically compared using an unpaired t- test.

Significant group differences were reported for $p<0.05$.

5.2.5.2. Correlation analyses

Due to the relatively small (**n**) group numbers the correlation analyses were performed on data from both sham and chronically hypoperfused mice. In order to avoid performing multiple correlations among epigenetic marks as well as between epigenetic marks and glia across brain regions inevitably leading to meeting the set criterion of significance ($p<0.05$) purely by chance, the analysis was focused on relevant epigenetic and cellular markers in a major white matter tract (the CC) where hypoperfusion- induced changes in 5hmC were observed in the present study.

5.2.5.2.1. Correlation analysis among epigenetic marks (5mC, 5hmC and TET2)

To account for specific hypoperfusion- induced variations in 5hmC observed in the CC and to address the main study hypothesis, the regional proportions of 5hmC positive cells were correlated with the regional proportions of 5mC and TET2 positive cells in the CC using a parametric Pearson`s correlation analysis. A separate Pearson`s correlation analysis was performed between each pair of epigenetic marks (e.g. 5hmC/ 5mC, 5hmC/ TET2).

5.2.5.2.2. Correlation analysis between hydroxymethylation and cells composing the cerebral white matter

To determine the potential cellular basis underlying the presently observed 5hmC dynamics in white matter, the proportion of 5hmC positive cells in the CC was correlated with the proportion of mature oligodendrocytes (CC1), OPC (NG2), and microglia (Iba1) in the same white matter tract by using a parametric Pearson`s correlation analysis. A separate correlation analysis was performed between 5hmC and each glial marker (e.g. 5hmC/ CC1, 5hmC/ NG2, 5hmC/ Iba1).

For all correlational analyses, significance was reported for p values ($p < 0.05$).

5.3. Results

5.3.1. Chronic cerebral hypoperfusion leads to the development of white matter pathology

Significant axonal (APP) and myelin (MAG, dMBP) pathology was evident in examined white matter tracts in chronically hypoperfused mice, but not sham- operated animals a month after surgery. An absence of overt grey matter abnormalities in cortical and subcortical areas was observed in all experimental animals. These results are presented in S.5.1.- appendices III.

5.3.2. Chronic cerebral hypoperfusion does not affect brain 5mC distribution

The proportion of 5mC positive cells was identified by means of a double 5mC/ ssDNA nuclear immunoreactivity in grey and white matter regions of the brain. Under both normal physiological and chronically hypoperfused conditions, 5mC was identified in cell nuclei as evidenced by its co- localization with ssDNA in all cells composing white and grey matter areas (figure 5.1. A- A1; figure S.5.2.1. appendices III). The t- test statistical analysis demonstrated that chronic cerebral hypoperfusion did not affect the regional distribution of 5mC in the brain as shown by the absence of significant group differences in the proportion of 5mC/ ssDNA positive cells in examined white and grey matter ROIs: the CC ($t= 0.68$, $p= 0.51$), EC ($t= 0.12$, $p= 0.90$), IC ($t= 0.01$, $p= 0.99$), CA1 ($t= 0.31$, $p= 0.76$), and Cx ($t= 0.15$, $p= 0.88$) (table 5.1.). Further, there was an absence of significant group differences in the number of 5mC positive cells and the total number of ssDNA positive cells in all examined brain areas ($p>0.05$) (table S.5.2.- appendices III).

5.3.3. Chronic cerebral hypoperfusion leads to significant white matter tract- specific changes in brain 5hmC distribution

The proportion of 5hmC positive cells was identified by means of a double 5hmC/ ssDNA nuclear immunoreactivity in grey and white matter regions of the brain. Under both normal physiological and chronically hypoperfused conditions, 5mC was identified in cell nuclei as evidenced by its co- localization with ssDNA in cells composing white

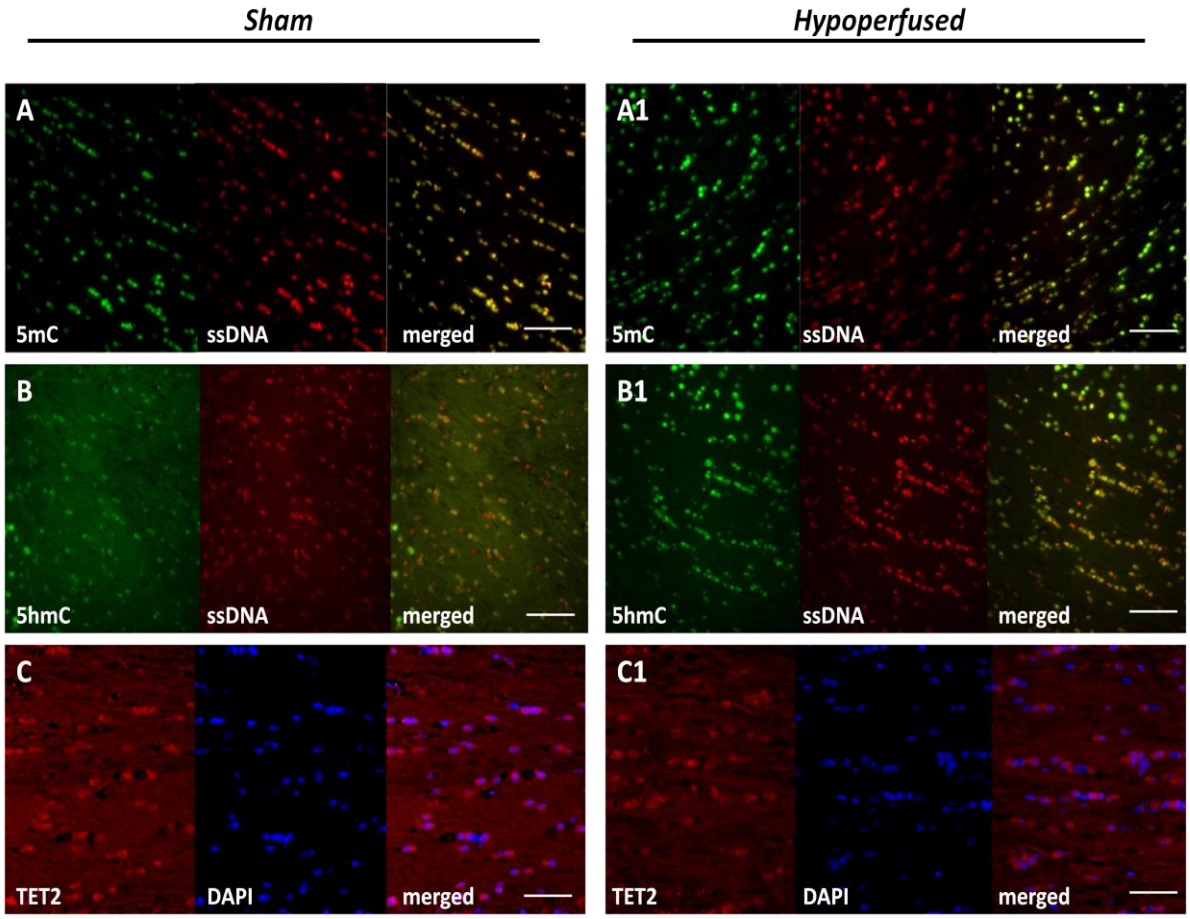

Figure 5.1.: Methylation, hydroxymethylation and TET2 immunochemically evidenced distribution in the CC of sham and chronically hypoperfused mice

Representative images of 5mC (**A-A1**), 5hmC (**B-B1**) and TET2 (**C-C1**) immunoreactivity in the CC of sham (**A-C**) and chronically hypoperfused (**A1-C1**) mice. Under both normal physiological and chronically hypoperfused conditions, 5mC (**A-A1**) and 5hmC (B-B1) were evidenced in the nuclei of cells situated in the CC (predominantly glia) as evidenced by immunochemical co- localization of these biomarkers with ssDNA (**A1-B1**). TET2 immunoreactivity was evidenced in both the cellular nuclei and cytoplasm of cells composing the cerebral white matter (predominantly glia) in sham and chronically hypoperfused mice (**C-C1**). Chronic cerebral hypoperfusion did not impact on 5mC (**A1**) and TET2 (**C1**) immunochemical distribution in white matter, but led to significant increases in the proportion of 5hmC immunopositive cells in the CC (**B1**).

Scale bar represents 20µm (magnification x40).

Biomarker	Region of interest	Proportion of biomarker positive cells (mean ± SE)	
		Sham (n=8)	*Hypoperfused (n=9)*
5mC	*Corpus callosum (CC)*	0.78 ± 0.1	0.83 ± 0.0
	External capsule (EC)	0.77 ± 0.1	0.76 ± 0.1
	Internal capsule (IC)	0.88 ± 0.1	0.84 ± 0.0
	CA1	0.96 ± 0.0	0.99 ± 0.0
	Cortex (Cx)	0.91 ± 0.0	0.90 ± 0.0
5hmC	*Corpus callosum (CC)*	0.50 ± 0.1	0.84 ± 0.0*
	External capsule (EC)	0.51 ± 0.1	0.60 ± 0.1
	Internal capsule (IC)	0.86 ± 0.1	0.74 ± 0.1
	CA1	0.79 ± 0.1	0.89 ± 0.1
	Cortex (Cx)	0.89 ± 0.0	0.92 ± 0.0
TET2	*Corpus callosum (CC)*	0.31 ± 0.1	0.31 ± 0.1
	External capsule (EC)	0.29 ± 0.1	0.28 ± 0.1
	Internal capsule (IC)	0.49 ± 0.1	0.46 ± 0.1
	CA1	0.58 ± 0.0	0.57 ± 0.0
	Cortex (Cx)	0.30 ± 0.0	0.40 ± 0.0*

Table 5.1.: Regional mean proportions of 5mC, 5hmC, TET2 immunopositive cells

(group mean ±SE)

Chronic cerebral hypoperfusion did not impact on the regional distribution of 5mC and TET2 in the CC ($p>0.05$), but was associated with a significant increase in the proportion of 5hmC immunopisitive cells in the CC ($p<0.05$). The proportion of TET2 immunopositive cells was significantly increased in the hypoperfused Cx. In the rest of the examined white and grey matter areas, no significant group differences in the proportion of biomarker positive cells (5mC, 5hmC, TET2) were evidenced by the t- test statistical analysis for all biomarkers ($p>0.05$).

Significant group differences as given by the t- test statistical analysis: ($p<0.05$)*

and grey matter areas (figure 5.1. B- B1; figure S.5.2.2.- appendices III). Interestingly, under normal physiological conditions, not all cells in white matter were 5hmC immunopositive (figure S.5.2.2. A, D- appendices III). There was a significant increase in the proportion of 5hmC/ ssDNA positive cells in the hypoperfused CC ($t= 2.21$, $p= 0.04$) (figure 5.1. B; figure S.5.2.2. A1, D1- appendices III). The majority of cells in the hypoperfused CC were 5hmC immunoreactive (figure 5.1. B1; figure S.5.2.2. A1, D1, appendices III). There were no statistically significant alterations in the proportion of 5hmC/ ssDNA positive cells in any of the other ROIs: the IC ($t= 1.31$, $p= 0.21$), EC ($t= 0.23$, $p= 0.82$), CA1 ($t= 1.15$, $p= 0.27$), Cx ($t= 1.48$, $p= 0.16$) (table 5.1.). Additionally, there was also an absence of significant group differences in the number of 5hmC positive cells and the total number of ssDNA positive cells in all examined brain areas ($p>0.05$) (table S.5.2.- appendices III).

5.3.4. Chronic cerebral hypoperfusion leads to significant grey matter- specific changes in TET2 distribution

The proportion of TET2 positive cells was identified by double TET2/ DAPI staining in grey and white matter regions. TET2 immunoreactivity showed a differential cellular localization in cells situated in grey and white matter areas under both normal physiological and chronically hypoperfused conditions. Specifically, in grey matter cells (predominantly neurons), TET2 immunoreactivity was restricted to the cellular cytoplasm, whereas TET2 was immunodetected in both the cytoplasm and the nucleus of white matter cells (predominantly glia) (figure 5.1. C- C1; figure S.5.2.3- appendices III). The cellular identity of TET2 immunopositive cells was determined on the basis of their regional localization (grey matter regions or white matter tracts) as well as on the relative size of their nucleus. There were no significant differences in the proportion of TET2/ DAPI positive cells between hypoperfused and sham mice in any of the examined white matter tracts- the CC ($t= 0.07$, $p= 0.94$), EC ($t= 0.08$, $p= 0.93$), IC ($t= 0.44$, $p= 0.66$) as well as in the CA1 region ($t= 0.23$, $p= 0.82$) (table 5.1). However, the proportion of TET2/ DAPI positive cells increased significantly in the Cx of chronically hypoperfused mice in comparison with sham animals ($t= 2.190$, $p= 0.04$) (table 5.1.; figure S.5.2.3. C-C1, F-F1- appendices III). There was an absence of significant group differences in the

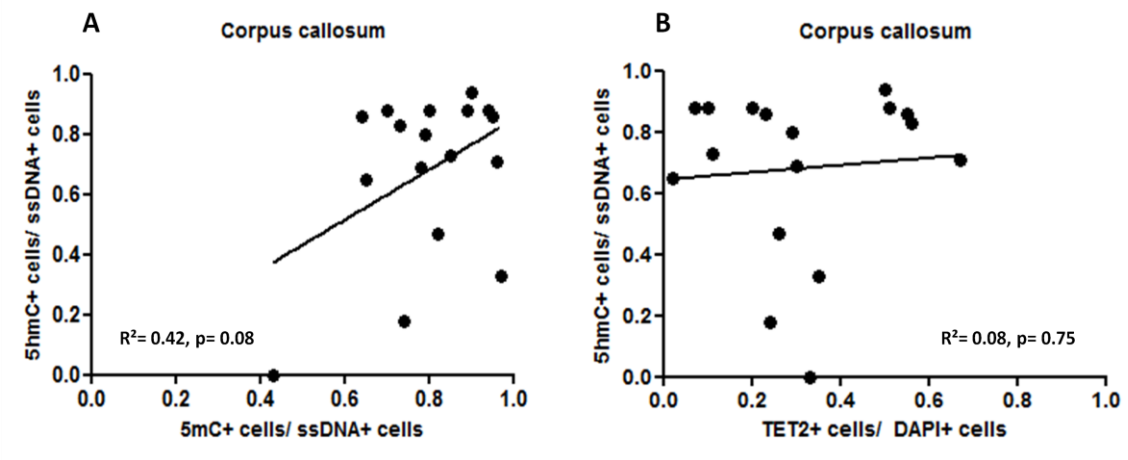

Figure 5.2.: Hydroxymethylation does not correlate significantly with methylation and TET2 in the CC

The Pearson`s correlation analysis demonstrated an absence of significant associations between the proportion of 5hmC/ ssDNA positive cells with the proportion of 5mC/ ssDNA as well as TET2/ DAPI positive cells in the CC ($p>0.05$)

number of TET2 positive cells and the total number of DAPI positive cells in all examined brain areas ($p>0.05$) (table S.5.2.- appendices III).

5.3.5. Hydroxymethylation does not correlate significantly with methylation and TET2 in white matter (the CC)

In order to account for the observed hypoperfusion- induced significant increases in 5hmC in the CC and to determine the existence of potential association(s) between hydroxymethylation and methylation, TET2 in white matter of the adult mouse brain (the main study hypothesis), the regional proportions of these epigenetic biomarkers in the CC were correlated using Pearson`s statistical analysis (Chapter 5, section 5.2.5.2.1.). There was no significant correlation between hydroxymethylation and methylation ($R^2= 0.42$, $p= 0.08$) as well as between hydroxymethylation and TET2 ($R^2= 0.08$, $p= 0.75$) in the CC (figure 5.2. A, B).

5.3.6. Chronic cerebral hypoperfusion does not affect the proportion of mature oligodendrocytes

The proportion of mature oligodendroglia was revealed by double CC1/ DAPI staining restricted to white matter tracts in the brain (figure 5.3. A-A1). There was not a significant difference in the proportion of mature oligodendrocytes between hypoperfused and sham mice in any of the examined white matter tracts: the CC ($t= 1.35$, $p= 0.19$), EC ($t= 0.51$, $p= 0.62$), IC ($t= 1.55$, $p= 0.14$) (table 5.2., figure 5.3. A-A1). Further, there was an absence of significant group differences in the number of CC1 positive mature oligodendroglia and the total number of DAPI positive cells in all ROIs ($p>0.05$) (table S.5.3.- appendices III).

5.3.7. Chronic cerebral hypoperfusion is associated with a significant increase in the proportion of OPC

The proportion of OPC was identified by double NG2/ DAPI staining in white matter ROIs (figure 5.3. B-B1). A significant increase in the proportion of OPC was evident in the CC ($t= 3.22$, $p= 0.006$) and the IC ($t= 2.19$, $p= 0.04$) of hypoperfused mice compared with sham animals (table 5.2., figure 5.3. B-B1). In the EC ($t= 1.66$, $p= 0.12$) there were

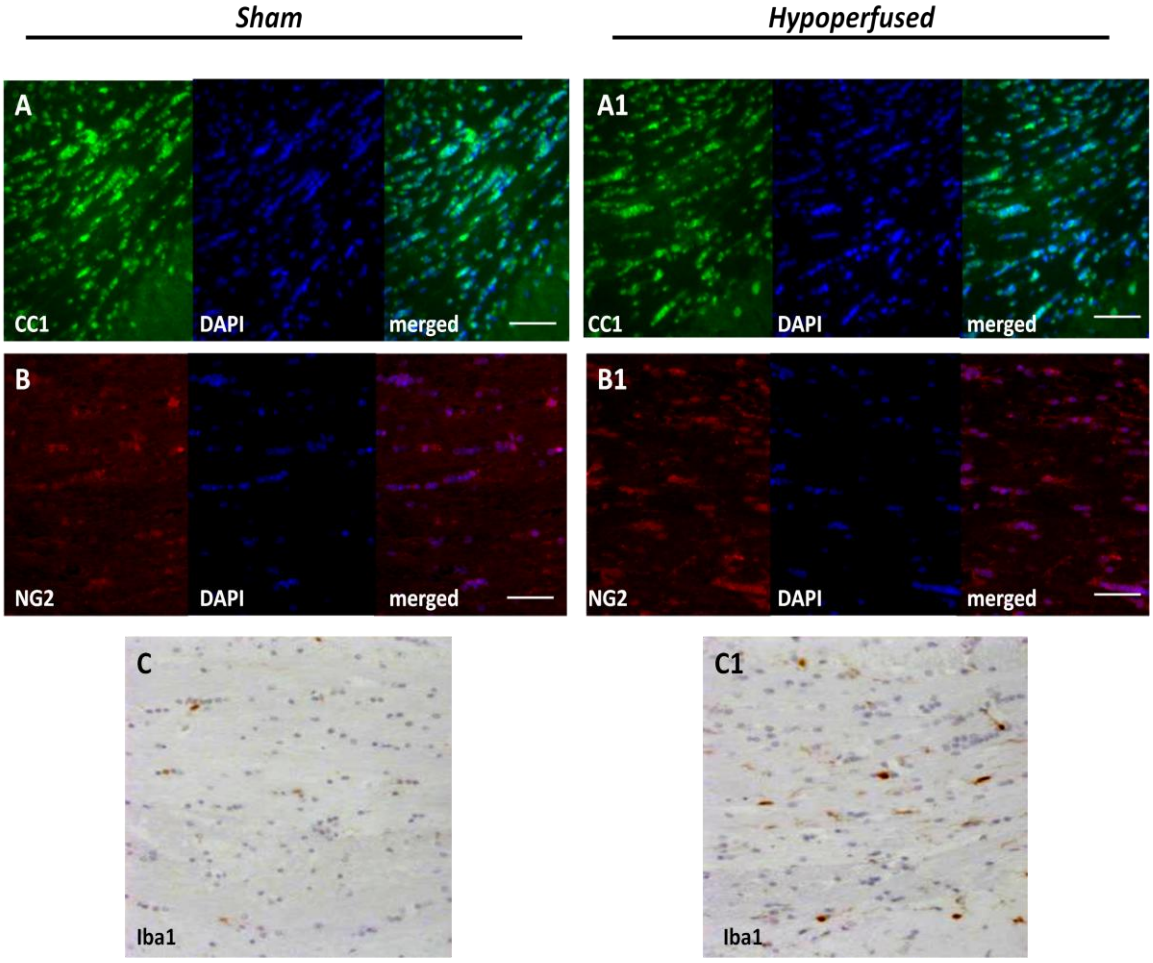

Figure 5.3.: Mature oligodendrocytes (CC1), OPC (NG2) and microglia (Iba1) immunoreactivity in the CC of sham and chronically hypoperfused mice

Representative images of mature oligodendrocytes (CC1) (**A- A1**), OPC (NG2) (**B-B1**) and microglia (Iba1) (**C-C1**) in the CC of sham (**A-C**) and chronically hypoperfused (**A1-C1**) mice. Cellular nuclei were counterstained with DAPI for CC1 and NG2 immuoreactive cells (**A-A1; B-B1**). Haemotoxylin was used to counterstain cellular nuclei for Iba1 immunoreactive cells (**C-C1**). Chronic cerebral hypoperfusion did not affect the proportion of mature oligodendrocytes in the CC (**A1**), but led to significant increases in the proportions of OPC and microglia in the same white matter tract (**B1, C1**).

Scale bar represents 20µm (magnification x40).

Biomarker	Region of interest	Proportion of biomarker positive cells (mean ± SE)	
		Sham (n=8)	***Hypoperfused (n=9)***
CC1	*Corpus callosum (CC)*	0.68 ± 0.1	0.51 ± 0.1
	External capsule (EC)	0.55 ± 0.1	0.49 ± 0.1
	Internal capsule (IC)	0.74 ± 0.0	0.61 ± 0.1
NG2	*Corpus callosum (CC)*	0.16 ± 0.1	0.42 ± 0.1**
	External capsule (EC)	0.42 ± 0.1	0.57 ± 0.1
	Internal capsule (IC)	0.19 ± 0.1	0.37 ± 0.1*
Iba1	*Corpus callosum (CC)*	0.08 ± 0.0	0.14 ± 0.0*
	External capsule (EC)	0.08 ± 0.0	0.09 ± 0.0
	Internal capsule (IC)	0.06 ± 0.0	0.12 ± 0.0*

Table 5.2.: Regional mean proportions of mature oligodendrocytes (CC1), OPC (NG2), and microglia (Iba1)

(group mean ±SE)

No significant hypoperfusion- induced changes were evidenced in the proportion of CC1 positive mature oligodendroglia in all examined white matter tracts ($p>0.05$). The proportion of NG2 positive OPC and Iba1 positive microglia increased significantly in the CC and IC ($p<0.05$), but not in the EC ($p<0.05$) as shown by the t- test statistical analysis.

Significant group differences as given by the t- test statistical analysis: ($p<0.05$)*, ($p<0.01$)**

no significant group differences in the proportion of OPC (table 5.2.). Further, there were significant group differences in the number of NG2 positive OPC ($p<0.05$) in the absence of significant group differences in the regional total number of DAPI positive cells ($p>0.05$) in all examined white matter areas (table S.5.3.- appendices III).

5.3.8. Chronic cerebral hypoperfusion leads to a significant increase in the proportion of microglia

The proportion of microglia was revealed by Iba1 immunoreactivity with haemotoxylin counterstaining for identification of cellular nuclei and the regional total number of cells (figure 5.3. C-C1). There was a significant increase in the proportion of microglia in the CC ($t= 2.54$, $p= 0.02$) and the IC ($t= 2.83$, $p= 0.013$) of hypoperfused mice compared with sham animals (table 5.2., figure 5.3. C-C1). In the EC ($t= 0.57$, $p= 0.58$) there were no significant group differences in the proportion of inflammatory cells (table 5.2.). There were significant group differences in the number of Iba1 positive microglia in the CC and the IC ($p<0.05$), but not in the rest of the ROIs. Further, there were no significant group differences in the regional total number of cells ($p>0.05$) (table S.5.3.- appendices III).

5.3.9. Hydroxymethylation significantly correlates with microglia in the CC

In order to determine the potential cellular basis of 5hmC in white matter, the proportion of 5hmC positive cells was correlated with the proportion of mature oligodendroglia (CC1), OPC (NG2), and microglia (Iba1) in the CC using Pearson`s analysis (Chapter 5, section 5.2.5.2.2.). The results demonstrated that hydroxymethylation correlated significantly with inflammatory microglia ($R^2= 0.60$, $p= 0.01$), but not with mature oligodendroglia ($R^2= -0.17$, $p= 0.52$) and OPC ($R^2= 0.37$, $p= 0.14$) in the CC (figure 5.4. A-C).

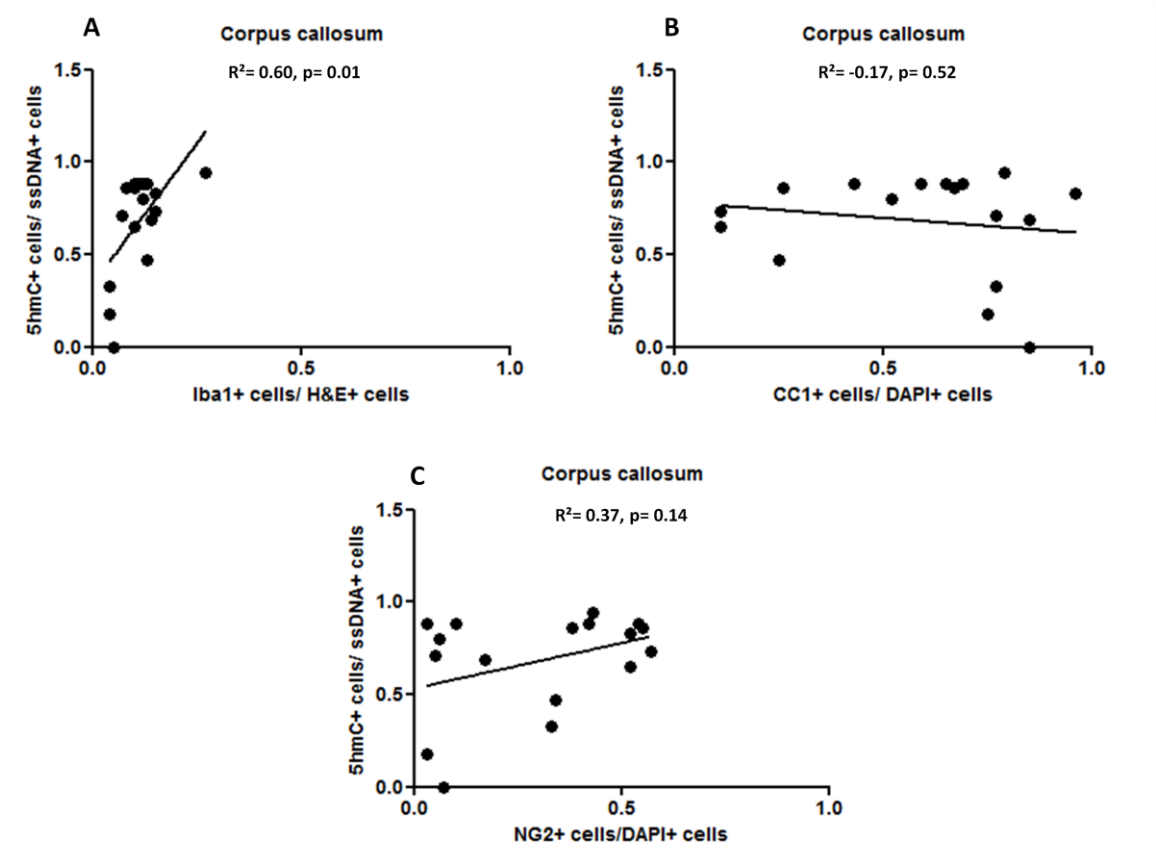

Figure 5.4.: Hydroxymethylation correlates significantly with inflammatory microglia, but not with mature and progenitor oligodendroglia in the adult mouse CC

The Pearson`s correlation analysis demonstrated the existence of a significant association between the proportions of 5hmC/ ssDNA positive cells and Iba1/ H&E positive microglia in the adult mouse CC ($p<0.05$) (**A**). No significant associations were evidenced between the proportions of 5hmC/ ssDNA positive cells and CC1/ DAPI positive mature oligodendrocytes (**B**) as well as NG2/ DAPI positive OPC (**C**) in the same white matter tract ($p>0.05$).

5.3.10. In vitro 5hmC immunochemical distribution decreases with oligodendroglial maturation and it is abundant in both activated and non activated microglia

To verify the in vivo findings and further examine hydroxymethylation in relation to glia, 5hmC immunochemical distribution was studied using in vitro systems of oligodendroglial maturation and microglial activation. 5hmC immunoreactivity was found to decrease with oligodendroglial maturation in vitro. High 5hmC immunoreactivity was observed in the oligodendroglial cell preparations at 0 DIV and it subsequently decreased progressively with the in vitro maturation of these cells from 2 to 6 DIV (figure 5.5. A-A2). Both nonactivated and IFNγ/ LPS activated microglial cells were strongly 5hmC immunopositive (figure 5.5. B-B1).

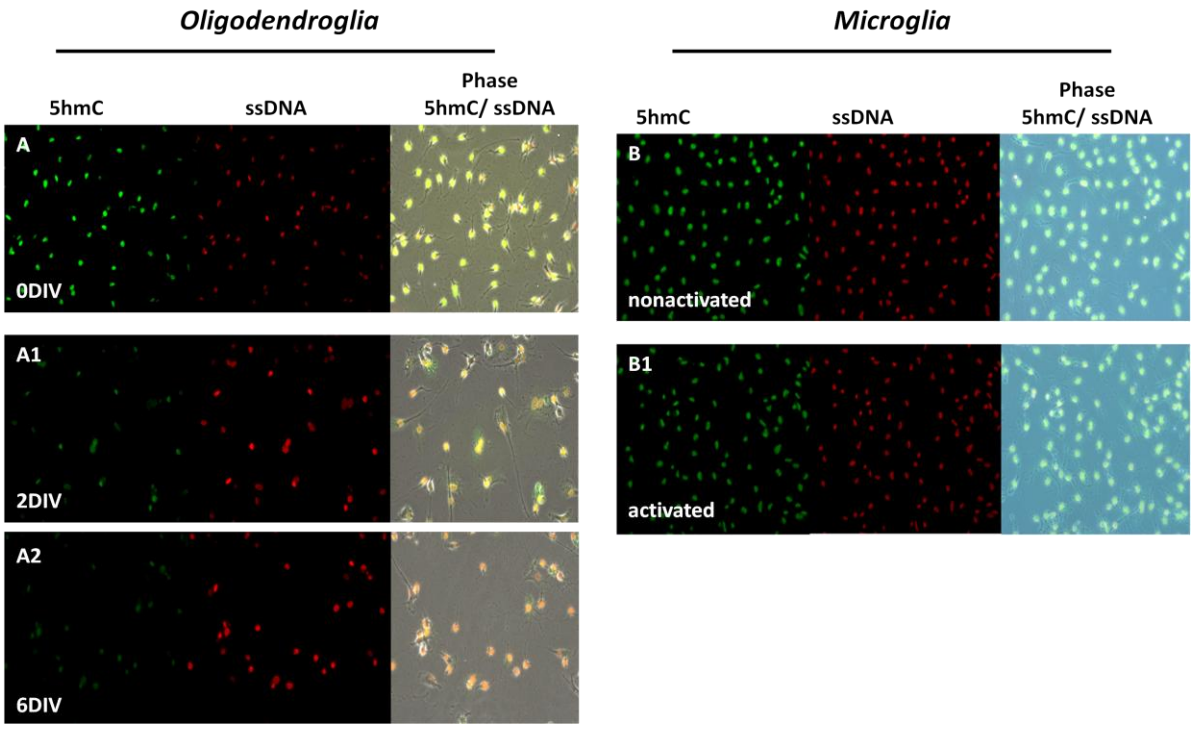

Figure 5.5.: In vitro 5hmC immunochemical distribution in oligodendroglia at different stages of maturation (0-6DIV), in IFNγ/ LPS activated and nonactivated microglia

Representative images of 5hmC immunochemical distribution in oligodendroglia cultures at different stages of maturation (**A-A2**) and in vitro nonactivated and IFNγ/ LPS activated microglia (**B-B1**). In vitro, 5hmC decreased with oligodendroglia maturation from 0- 6DIV (**A-A2**). 5hmC was high in both activated and nonactivated microglia (**B-B1**).

Scale bar represents 20μm (magnification x40).

5.4. Discussion

The experimental work presented in Chapter 5 sought to test the hypothesis that chronic cerebral hypoperfusion might affect the oxidative production of 5hmC in white matter by modification of methylation dynamics and/ or by disruption of TETs enzymatic machinery. 5mC, 5hmC and one of the TETs members- TET2 were immunochemically examined in white and grey matter areas of the adult mouse brain under normal physiological conditions compared with one month after chronic cerebral hypoperfusion. In contrast to the main study hypothesis, the results demonstrated significant alterations in 5hmC in the absence of changes in 5mC and TET2 in the hypoperfused CC (white matter). These data and a subsequent correlation analysis suggest that hydroxymethylation might be an epigenetic mechanism occurring independently from 5mC and TET2 in white matter. In vivo and in vitro investigation of the cellular determinants of 5hmC in white matter points to a potential role of microglia in the processes of hydroxymethylation. In regards to the alternative hypothesis suggesting epigenetic perturbations in grey matter following cerebrovascular challenge, in the present study significant increases in TET2 were observed in the hypoperfused Cx in the absence of hypoperfusion- induced alterations in 5mC and 5hmC in any of the examined grey matter areas.

5.4.1. Methylation dynamics in white and grey matter under normal physiological conditions and one month after chronic cerebral hypoperfusion in mice

Under both normal physiological and chronically hypoperfused conditions 5mC was found to be restricted to cell nuclei in white and grey matter areas as demonstrated by an immunochemical co- localization of this epigenetic mark with single stranded DNA (ssDNA). Methylation was found to be abundant in all cells composing white and grey matter areas in both sham and chronically hypoperfused mice.

In contrast to the main study hypothesis, chronic cerebral hypoperfusion did not impact on 5mC distribution in white matter areas (the CC, EC, and IC) in mice. These findings suggest that methylation might be a stable epigenetic mechanism in white matter and subtle alterations in the cerebral blood supply such as those occurring with hypoperfusion might not affect the distribution of this epigenetic mark in the mouse brain.

In contradiction with the alternative prediction suggesting potential hypoperfusion-induced alterations in 5mC in grey matter, in the present study methylation was found to remain unchanged in the hypoperfused Cx and hippocampus (the CA1). This alternative prediction was based on clinical and pre- clinical work. In alternative animal models of focal ischemia brain methylation dynamics are significantly altered via increased oxidative stress, free radicals and excitotoxicity in grey matter. In mice, focal ischemia was associated with a global brain hypermethylation (Endres et al., 2000). Experimental stroke in rats significantly altered methylation of the ERα in the brain (Westberry et al., 2008). The differences in the observed methylation patterns in experimental focal ischemia (stroke) and chronic cerebral hypoperfusion might be partially explained by the severity of the cerebrovascular challenge. During focal ischemia the blood flow reductions are temporary, but severe leading to the occurrence of both grey and white matter ischemic injury (Mao et al., 1999), whereas during chronic cerebral hypoperfusion the blood flow is only partially, but permanently restricted leading to very mild cerebral perfusion and the development of a predominant white matter pathology (Shibata et al., 2004; Shibata et al 2007; Nishio et al., 2010; Coltman et al., 2011, Holland et al., 2011; Reimer et al., 2011). It is also possible that during mild hypoperfusion, damaged DNA is efficiently repaired by alternative mechanisms such as hydroxymethylation (Surani and Hajkova, 2010). Therefore, no changes in methylation are observed in hypoperfused mice.

The present results are also in contradiction with human data. For instance clinical studies on monozygous twins with discordant Alzheimer`s disease showed a significantly decreased 5mC immunoreactivity in grey matter areas of the affected twin compared with the cognitively intact twin brother (Mastroeni et al., 2009). Similar results were reported in Alzheimer`s patients exhibiting a significant global DNA hypomethylation in subcortical grey matter areas (e.g. entorhinal cortex) in comparison with healthy controls (Mastroeni et al., 2010). These findings suggest that changes in methylation dynamics might play a role in the development of age- related neuropathology. The discrepancies with the present preclinical data on chronically hypoperfused mice might be due to a variety of factors such as species differences in epigenetic marks, etiological differences (e.g. cerebrovascular challenge vs. age- related neurodegeneration), age (elderly people (>70 years) vs. young adult mice (3 months)) and others (e.g. environmental factors).

Little is known about methylation dynamics in elderly people exhibiting white matter abnormalities with cerberovascular etiology. On the basis of the present pre- clinical findings showing an absence of hypoperfusion- induced 5mC alterations in white matter, it is possible that this epigenetic mark may not be involved in the development of white matter pathology in the elderly. However, in regards to the limitations of animal models no firm conclusions based on data extrapolations could be made at the present time.

Alternatively, it is possible that changes in methylation occur in the hypoperfused brain, but following a different spatio- temporal dynamics. Specifically, alterations in methylation might occur in presently non- examined brain areas as well as at earlier and/ or later post- surgical time points and these methylation dynamics might be differentially associated with neuropathology. This is particularly true in regards to the chronic nature of the cerebrovascular challenge in this animal model and the cumulative hypoperfusion-induced neuropathology (Nishio et al, 2010; Reimer et al., 2011) (discussed in sections 5.4.6.2., 5.4.6.3.).

Further, it is also possible that the applied immunochemistry could not detect potentially subtle changes in genomic methylation occurring in the hypoperfused mouse brain. Future applications of quantitative techniques for genomic 5mC detection such as bisulfite DNA sequencing might be more sensitive to subtle changes in brain methylation occurring with hypoperfusion in mice (discussed in section 5.4.6.2.).

The recent discovery of 5hmC- an oxygen dependent modification of 5mC particularly enriched in the central nervous system, initiated a debate as to the sensitivity of the currently applied techniques to selectively assess brain methylation and hydroxymethylation. Specifically, the majority of the standard molecular techniques cannot distinguish 5mC from its oxidative derivative- 5hmC (Nestor et a., 2010). By consequence, there is a current reappraisal of previous publications on methylation and a necessity to clarify whether and/ or to what extent these studies account for actual methylation and not hydroxymethylation dynamics.

5.4.2. Hydroxymethylation in white and grey matter under normal physiological conditions and one month after chronic cerebral hypoperfusion in mice

Similar to 5mC, 5hmC was found to be restricted to cellular nuclei in both white and grey matter as demonstrated by an immunochemical co- localization of this epigenetic mark with ssDNA under normal physiological as well as hypoperfused conditions in mice. Interestingly, under normal physiological conditions, not all cells in white matter were 5hmC immunopositive (discussed in section 5.4.3.)

Chronic cerebral hypoperfusion was associated with white matter tract- specific changes in 5hmC. Specifically, a significant 5hmC up- regulation was observed in the hypoperfused CC where most cells were found to be 5hmC immunoreactive. In the rest of the examined white and grey matter ROIs, 5hmC distribution was not altered by chronic cerebral hypoperfusion. The reasons for this differential regional regulation of 5hmC after chronic cerebral hypoperfusion remain unknown. However, from a cerebrovascular and neuroanatomical perspective, the CC is situated just beneath the highly vascularized Cx having much higher oxygen supply necessary for oxidation of 5mC in comparison with subcortical white matter tracts characterized by a very limited cerebrovascular irrigation and low oxygen levels even under normal physiological conditions (Nonaka et al., 2003).

The present findings are partially in accordance with the study predictions suggesting 5hmC alterations in white matter following chronic cerebral hypoperfusion in mice. However, in contrast to the initial study hypothesis these hypoperfusion- induced changes in 5hmC in white matter occurred independently from alterations in 5mC and TET2 (discussed in section 5.4.5.).

Interestingly, changes in 5hmC dynamics were only observed in white matter regions where the major pathological abnormalities occur in the hypoperfused model (at least in the absence of food deprivation and behavioural training) (the pathological data is presented in S.5.1.- appendices III; Chapter 4). These findings suggest a potential role for 5hmC in the development of neuropathology in chronically hypoperfused mice. This idea is supported by a recently published work suggesting intragenic 5hmC increases in the

brain under different conditions including Alzheimer`s disease, hypoxia and chronological aging (Song et al., 2010; Chen et al., 2012).

The exact molecular mechanism(s) via which 5hmC up- regulation might impact on neuropathology are unknown, but a recent review suggests a role of 5hmC in the processes of DNA repair and more particularly in base excision mechanisms via a specific 5hmC DNA glycosylase activity (Cannon et al., 1988; Surani and Hajkova, 2010). It is possible that during pathological events an increase in damaging oxidative, inflammatory, and excitotoxic agents affects DNA integrity and 5hmC up- regulation might help rescuing the genetic material and by consequence modulate the pathological outcome. With regards to the euchromatic genomic 5hmC localization, it is also possible that this epigenetic mark promotes the transcription of genes necessary for cell survival such as growth factors and natural anti- oxidants (Jin et al., 2011).

However, due to the semi- quantitative immunochemical evaluation of 5hmC and the relatively small (**n**) numbers on which the statistical analysis was based as well as the observed absence of significant group differences in the proportion of 5hmC positive cells in the rest of the examined ROIs, one should consider the alternative explanation for the present findings, namely that the observed statistically significant group differences in 5hmC in this particular white matter tract (the CC) might not represent actual biological phenomena, but instead were due to chance. Only future studies applying quantitative techniques (e.g. deep- genome sequencing) to assess the regional 5hmC content in the brain under normal physiological and chronically hypoperfused conditions in mice would allow to verify the present immunochemical findings suggesting significant 5hmC increases in the hypoperfused CC. Further future experiments would allow to gain a better understanding of the biological significance of this newly discovered epigenetic mark, its involvement in neuropathology, as well as the underlying molecular and cellular mechanisms associated with hydroxymethylation in the brain (discussed in sections 5.4.6.2., 5.4.6.3.).

In relation to humans, it is difficult to speculate on any particular role of 5hmC in age-related neuropathology and functional impairment based on the present preclinical

findings. However, the present results are interesting and they could potentially constitute the basis for a future experimental and clinical work focused on 5hmC in the context of "healthy" and pathological aging.

5.4.3. In search of the cellular basis of 5hmC in white matter. An unresolved question.

In order to account for specific 5hmC dynamics observed in white matter following hypoperfusion in mice, hydroxymethylation was examined in relation to some of the cells composing the cerebral white matter, namely mature oligodendroglia, OPC and inflammatory microglia in a series of in vivo and in vitro experiments. Given that it was technically impossible to perform double immunochemistry on 5hmC stained biological samples (discussed in section 5.4.6.2.), separate immunochemical analyses were performed for mature oligodendroglia (CC1), OPC (NG2) and microglia (Iba1) in sham and chronically hypoperfused mice on semi- adjacent brain sections. Subsequently, the obtained regional proportions of these cells were correlated with the proportion of 5hmC positive cells in the CC. The CC was selected for a white matter tract of interest for the correlation analysis as 1) clinical and preclinical studies suggest important age- related neuropathology in this white matter region associated with cognitive and memory deficits (Clarke and Zaidel, 1994; Peters and Sethares, 2002; Meguro et al., 2003; Teipel et al., 2003; Jokinen et al., 2007; Paul et al., 2007; Sullivan et al., 2010), 2) hypoperfusion-induced abnormalities have been evidenced in the CC in mice (Shibata et al., 2004; Shibata et al., 2007; Nishio et al., 2010; Holland et al., 2011; Reimer et al., 2011), 3) in the present study a significant hydroxymethylation upregulation was evident in the hypoperfused CC. The data from all sham and hypoperfused animals were included in the correlation analysis due to the limited **n** numbers per experimental group and the potential bias due to a loss of statistical power if the correlation were to be performed separately for the two experimental groups (Chapter 5, sections 5.2.5.2.; 5.2.5.2.2.).

The in vivo experiments revealed that chronic cerebral hypoperfusion did not affect the proportion of mature oligodendroglia, but led to significant increases in the proportion of NG2 positive OPC in the CC and IC.

The presently observed absence of changes in the proportion of mature oligodendroglia one month after hypoperfusion is in accordance with recent observations of an absence of significant caspase- 3 immunoreactivity in white matter areas of chronically hypoperfused mice (Reimer et al., 2011).

Significant increases in OPC are observed in various white matter disorders where these cells are believed to contribute to the endogenous brain repair mechanisms by replacing injured/ dying oligodendrocytes and/ or by contributing to the remyelination of demyelinated axons (Chang et al., 2000; Reynolds et al., 2002).

The applied parametric correlation analysis failed to demonstrate significant associations between 5hmC and oligodendroglia at different stages of maturation in vivo which might be related to the nature of the used data (proportions of cells counted on semi- adjacent sections) (discussed in section 5.4.6.2.).

To overcome some of the limitations associated with the in vivo analysis, 5hmC immunoreactivity was further examined using in vitro systems of oligodendroglial maturation.

The results demonstrated that 5hmC immunoreactivity decreased with the in vitro maturation of oligodendroglia. The present in vitro findings showing high 5hmC content in OPC are supported by previous studies from our and other laboratories suggesting that this epigenetic mark is particularly enriched in embryonic stem cells and multipotent progenitors, but it is low in most of the differentiated somatic cells (Ito et al., 2010; Ficz et al., 2011; Jin et al., 2011; Li and Liu, 2011; Kinney et al., 2011; Ruzov et al. 2011). In contrast to a previously demonstrated high 5hmC distribution in mature neurons, the present in vitro immunochemical analysis suggests that 5hmC is low in mature oligodendroglia (Kriaucionis and Heintz., 2009; Li and Liu, 2011; Ruzov et al.., 2011). These in vitro findings support the present in vivo data showing that not all cells in white matter are 5hmC immunopositive under normal physiological conditions. It is possible that in the absence of pathology, mature oligodendroglia are 5hmC negative in vivo. However, it is also possible that, in the living animal, under pathological conditions (e.g. chronic cerebral hypoperfusion), the mature oligodendrocytes up- regulate 5hmC as part

of their endogenous cell survival program, namely repair of damaged DNA thus contributing to the presently observed significant increases in 5hmC in the hypoperfused CC.

The differential 5hmC dynamics observed in oligodendroglia at different maturational stages might be related to the ability of these cells to produce and maintain myelin (myelinating and non- myelinating oligodendrocytes). Additionally, the observed 5hmC differences between mature and progenitor oligodendroglia might be associated with a differential activity of other epigenetic mechanisms such as HDAC1 and methylation regulating gene expression in these cells. For instance, it is known that histone deacetylation (HDAC1), a marker of gene silencing is highly increased in mature oligodendrocytes, but not in other neural cells (e.g. progenitors, neurons) (Martin-Husstege et al., 2002; Liu et al., 2007). Further, a differential methylation pattern of the GFAP promoter determines neural stem cells differentiation towards neuronal vs. glial phenotype. Specifically, hypermethylation of the GFAP promoter is associated with predominantly neuronal cell fate, whereas hypomethylation of the GFAP promoter triggers glial differentiation (Okada et al., 2008). On the basis of these previous findings, one could hypothesize that decreases in 5hmC might be necessary for supporting alternative epigenetic mechanisms differentiating OPC form their mature derivatives expressing genes associated with myelin production (e.g. MBP, PLP).

In the present study, 5hmC was also examined in relation to inflammation as inflammatory activity has been shown to impact on epigenetic marks such as methylation (Zhang et al., 2007; Wilson, 2008; Backdahl et al., 2009) and to increase after chronic cerebral hypoperfusion (Shibata et al., 2004; Coltman et al., 2011). The results confirmed previous findings on the hypoperfused model showing a significant increase in the proportion of inflammatory cells in white matter one month after chronic cerebral hypoperfusion in mice (Shibata et al., 2004; Coltman et al., 2011). Interestingly, a significant correlation between the proportion of inflammatory cells and the proportion of 5hmC positive cells was evidenced in the CC, suggesting a role of inflammatory processes in 5hmC up- regulation in white matter after chronic cerebral hypoperfusion.

The in vivo results were confirmed using an in vitro system where both IFNγ/ LPS activated and nonactivated microglia were found to be highly 5hmC immunopositive.

On the basis of these in vivo and in vitro findings, it is possible that inflammatory microglia modulate the production of 5hmC from 5mC in white matter. These findings are not surprising in regards to the existing literature demonstrating a role of inflammation in epigenetic regulation under various pathological conditions (Zhang et al., 2007; Wilson, 2008; Backdahl et al., 2009). Recently, using a microarray analysis, Reimer et al., 2011 reported significant alterations in the expression of 129 genes in white matter areas of chronically hypoperfused mice. Subsequent analysis indicated alterations in biological pathways, including inflammatory responses and cytokine- cytokine receptor interactions. It is possible that the presently observed associations between hydroxymethylation and microglia in white matter account for the previously observed hypoperfusion- induced alterations in inflammatory gene expression. Therefore, it would be interesting to further examine the exact associations between 5hmC and inflammatory microglia in vivo. For instance, one could examine hydroxymethylation dynamics under normal physiological and chronically hypoperfused conditions in microglia mutant mice compared with WT controls (Gowing et al., 2008). The obtained data would help understanding whether 5hmC is regulated by inflammatory microglia in vivo as well as whether the 5hmC-inflammatory pathway have any biological significance at the neuropathological and functional levels.

In regards to the present in vivo results, it is difficult to assume that microglia are the only cell type up- regulating 5hmC in the hypoperfused CC due to obvious differences in the proportion of microglia (0.14) and 5hmC (0.84) positive cells in this white matter tract. It is possible that other cells (e.g. OPC and/ or astrocytes) contribute to hydroxymethylation in white matter.

The present study did not address 5hmC distribution in astrocytes in the experimental groups. Astrocytes contribute to the inflammatory response following injury to the central nervous system and participate in the processes of neurodegeneration/ neuroregeneration (Hertz and Zielke, 2004; Hawkins and Davis, 2005; Volterra and Meldolesi, 2005; Magistretti, 2006). Future experiments should therefore examine 5hmC distribution in

astroglia under normal physiological and chronically hypoperfused conditions in mice using a combination of experimental techniques such as for instance immunochemistry and a deep genome sequencing.

5.4.4. TET2 in white and grey matter under normal physiological conditions and one month after chronic cerebral hypoperfusion in mice

TET2 immunoreactivity exhibited a differential cellular localization in white and grey matter areas under normal physiological and chronically hypoperfused conditions in mice. TET2 was abundant in the cytoplasm of cortical and subcortical cells (predominantly neurons), but was essentially absent from their nuclei. In white matter regions, TET2 immunoreactivity was evident in both the cytoplasm and nucleus of cells (predominantly glia) (figure S.5.2.3.- appendices III). These data suggest that TET2 might fulfill differential gene regulatory function in white and grey matter.

Chronic cerebral hypoperfusion did not impact significantly on TET2 distribution in subcortical (the CA1) and white matter (the CC, EC, and IC) regions. Interestingly, a significant increase in TET2 was evidenced in the Cx of hypoperfused mice.

These findings support the study initial predictions suggesting possible alterations in TET2 dynamics in the brain following chronic cerebral hypoperfusion in mice. However, in contrast to the study hypothesis, these changes were not directly related to hypoperfusion- induced alterations in 5hmC (discussed in section 5.4.5.).

The molecular mechanism(s) and functional significance of TET2 upregulation in the hypoperfused Cx remain unknown. However, limited or no cortical damage is usually observed in *ad libitum* fed and non- behaviourally tested hypoperfused mice at early post-surgery time points (Shibata et al., 2004; Holland et al., 2011; Reimer et al., 2011). It is possible that TET2 up- regulation is necessary for the survival program of neurons under hypoxic conditions protecting these cells from harmful agents. Due to the cytoplasmic localization of this protein in cells composing grey matter areas (predominantly neurons), its function is most likely trophic and/ or antioxidative rather than gene regulatory.

Alternatively, similar to the present 5hmC findings, it is possible that the observed hypoperfusion- induced alterations in cortical TET2 do not have any particular functional (biological) significance and these significant results could be explained by chance (discussed in section 5.4.2.).

It has been shown that each TET member has a tissue specific spatial and temporal pattern of expression, TET2 being most widely expressed in mouse tissues (Langemeijer et al., 2009). This suggests that TET proteins might fulfill different biological functions in distinct somatic contexts. Recently, our and other groups discovered that 5hmC is differentially distributed among adult organs, essentially 5hmC was absent or very low in the majority of examined adult tissues except in the brain and bone marrow where 5hmC was highly enriched (Globisch et al., 2010; Li and Liu, 2011; Kinney et al., 2011; Ruzov et al., 2011). As TET proteins are involved in the production of 5hmC, it is possible that they follow similar tissue distribution patterns in adult mammalian organisms. Using an in vitro system for neural differentiation of human embryonic stem cells, TET1, TET2, and TET3 were detected in neural progenitor cells at least at the mRNA level (Ruzov et al., 2011). However, so far, the biological significance of TET members especially in regards to neural cells and 5hmC production during neurodevelopment as well as in the healthy and diseased adult brain remains to be elucidated (discussed in sections, 5.4.6.2, 5.4.6.3.).

5.4.5. Is hydroxymethylation associated with methylation and TET2 in white matter?

The present study sought to test the hypothesis that chronic cerebral hypoperfusion might affect the oxidative production of 5hmC in white matter by modification of brain methylation dynamics and/ or by disruption of TETs machinery. This hypothesis was based on previous studies demonstrating that cerebral blood flow reductions are associated with alterations in methylation patterns in the brain (Endres et al., 2000; Westberry et al., 2008). Further, a pathological disruption of the TETs enzymatic pathway might affect 5mC oxidation processes especially in the case of reduced oxygen levels to the brain (e.g. chronic cerebral hypoperfusion) and by consequence might impact indirectly on 5hmC. This was recently demonstrated in the case of myeloid cancers where TET2 mutation was found to reduce the hydroxylation of 5mC (Ko et al., 2010). In order to account for any potential associations between hydroxymethylation and 5mC, TET2 in white matter, a non

parametric correlation analysis was performed between the proportion of 5hmC positive cells and the proportion of 5mC, TET2 positive cells in the CC, respectively (Chapter 5, sections 5.2.5.2.; 5.2.5.2.1.; 5.4.3.).

The results demonstrated an absence of significant associations between 5mC and 5hmC in the CC. These data suggest that either 1) brain methylation and hydroxymethylation are two independent epigenetic phenomena and changes in hydroxymethylation occur as a distinct regulatory mechanism and/ or 2) the employed immunochemical approach lacked sufficient sensitivity to accurately determine 5mC and 5hmC levels and therefore the subsequent correlation analysis failed to show any links between these two epigenetic marks in the adult mouse CC and/ or 3) nondetected associations existed between these two epigenetic marks in nonexamined brain areas and/ or occurred at different post-surgical time points.

However, it is difficult to assume that methylation and hydroxymethylation would be exclusively independent processes in the brain at least in regards to findings in the early mammalian embryo. Recently, our and other groups reported that the process of active demethylation of the paternal pronucleus of the zygote constitutes an active hydroxymethylation (Iqbal et al., 2011; Ruzov et al., 2011; Wossidlo et al., 2011). Alternatively, it is also possible that in the adult organism these two epigenetic processes are less interdependent and 5hmC might represent a separate epigenetic mechanism fulfilling an entirely different function from what is known in the zygote. This is supported by a recent study on aged animals showing significant increases in hydroxymethylation in grey matter in the absence of alterations in methylation and TETs mRNA expression (Chen et al., 2012). From a functional perspective, this is not surprising since 5mC and 5hmC exhibit differential genomic localization suggesting that these two epigenetic marks might antagonistically regulate gene silencing/ transcription (Bird, 2002; Ficz et al., 2011; Jin et al., 2011) Furthermore, it has been recently shown that transcriptional repressors known to bind methylated DNA such as MeCP2, MBD1, MBD2, and MBD4 do not recognize 5hmC (Jin et al., 2010). Future studies should determine the respective functional roles of 5mC and 5hmC in the brain (e.g. white

matter) as well as the potential interplay between these two epigenetic phenomena in health and disease (discussed in sections 5.4.6.2., 5.4.6.3.).

Methylation and hydroxymethylation should also be examined in relation to other epigenetic marks such as histone acetylation (HAT) and deacetylation (HDAC) as possible interactions among these mechanisms might regulate gene expression in the normal and diseased brain (Wu and Zhang, 2010). In regards to published studies suggesting an important role of HDAC in oligodendrocytes and remyelination following experimental demyelination of the CC in the aging brain (Shen et al., 2008), it would be interesting to examine potential associations between histone deacetylation and hydroxy/methylation dynamics in white matter areas of hypoperfused mice. This is important as to the presently observed specific 5hmC increases in the hypoperfused CC and the differential distribution of this epigenetic mark in glial cells (discussed in sections 5.4.6.2., 5.4.6.3.).

In the present study, hydroxymethylation was also examined in relation to TET2 in the CC. The correlation analysis failed to show any significant links between TET2 and hydroxymethylation in this white matter tract. These results suggest that TET2 may not be directly involved in the production of 5hmC from 5mC in the adult mouse brain which is in consistency with its cytoplasmic localization at least in cells composing the cerebral grey matter (predominantly neurons). However, in cells located in white matter tracts (predominantly glia) TET2 immunoreactivity was also detected in nuclei suggesting a potential involvement of TET2 in gene regulatory processes. Alternatively, it is possible that TET1 and/ or TET3 (presently non- examined), but not TET2 catalyze the hydroxylation of 5mC in the brain under normal physiological and chronically hypoperfused conditions (discussed in sections 5.4.6.2., 5.4.6.3.).

Overall, in relation to the main study hypothesis the present results suggest that hypoperfusion induces selective alterations in 5hmC in white matter (the CC), but these changes in 5hmC dynamics seem to be independent from 5mC and TET2.

5.4.6. Methodological strengths, limitations and future epigenetic experiments in chronically hypoperfused mice

5.4.6.1. Strengths of the applied methodology to examine epigenetic marks in the mouse brain under normal physiological and chronically hypoperfused conditions

The methodological strengths of the present study relate to the immunochemical visualization of 5mC, 5hmC, TET2 cellular localization in white and grey matter areas of the adult mouse brain under normal physiological and chronically hypoperfused conditions using previously validated, sensitive antibody probes (Ruzov et al., 2011). This could not be achieved by means of standard biomolecular techniques such as for example, bisulfite DNA sequencing unable to differentiate methylation from its oxidative derivative- hydroxymethylation (Nestor et al., 2010).

5.4.6.2. Limitations of the applied methodology to examine epigenetic marks in the mouse brain under normal physiological and chronically hypoperfused conditions

The major methodological drawback of the present study relates to the technical difficulty to perform a double/ triple immunochemistry on 5mC, 5hmC stained samples due to the severe HCL treatment required for nuclear DNA immunostaining. This methodological limitation prevented the direct immunochemical co- localization among epigenetic marks (5mC, 5hmC and TET2) and glial specific biomarkers. By consequence, the exact cellular identity of these epigenetic marks in white matter remains unclear. The in vitro experiments using relatively pure oligodendroglia and microglia cell preparations were also methodologically limited. The absence of immunocolocalization between epigenetic and glial specific biomarkers did not rule out the presence of fibrobalsts and astrocytes known to be frequent contaminators in neural preparations. Further, the in vitro environment does not recapitulate the cellular and molecular complexity of the in vivo central nervous system which is an important drawback in regards to the sensitivity of epigenetic phenomena to environmental factors (e.g. inflammation, free radicals) (Cerda and Weitzan, 1997; Duan et al., 2002; Kruman et al., 2002; Zhang et al., 2007; Wilson, 2008; Backdahl et al., 2009). Thus, it is difficult to extrapolate without certain reservations the in vitro findings to the in vivo situation.

In the present study, the immunohistochemical analysis was performed at a specific post-surgery time point (1 month after surgery) as well as on a single brain level due to the expenses associated with a whole brain immunohistochemistry. By consequence, all conclusions on the regional distribution of 5mC, 5hmC, TET2 as well as CC1, NG2 and Iba1 positive cells in sham and hypoperfused mice are spatio- temporally limited. Pathological and epigenetic alterations might have occurred at earlier/ later post- surgery time points and/ or might have been present on non- examined brain areas/ levels.

The present immunochemical evaluation was not supported by any additional biomolecular, quantitative analysis (e.g. deep genome sequencing (5mC and 5hmC) and Western blot analysis (TETs protein levels)). By consequence, it is possible that the observed group differences in 5hmC did not represent the actual, whole brain 5hmC genomic content in the CC. Further, the functional significance of the examined epigenetic processes remains largely unknown.

The present study examined only TET2 immunoreactivity and it did not address the cellular distribution of other TET family members (TET1 and TET3) due to the absence of available antibody probes at the time when the experiments were performed. It is possible that TET1 and TET3 in the brain present a differential cellular localization and fulfill different function under normal physiological and chronically hypoperfused conditions when compared with TET2. This hypothesis is based on recent findings suggesting differential distribution of these proteins in somatic tissues where each TET member exhibits a tissue specific spatial and temporal pattern of expression (Langemeijer et al., 2009). In regards to the presently observed absence of significant associations between TET2 and hydroxymethylation in white matter it is possible that hydroxymethylation in the brain is catalyzed by TET1 and/ or TET3 (discussed in section 5.4.5.).

With the exception of methylation, TET2, and inflammatory microglia the present study did not examine any other potential pathways which might impact on 5hmC content in the brain following hypoperfusion in mice. Therefore, it is unknown whether and/ or how hydroxy/ methylation dynamics relate to alternative epigenetic marks (e.g. TET1 and TET3; HDAC) as well as whether/ how 5mC and 5hmC are modulated by

pathophysiological mechanisms (e.g. excitotoxicity, oxidative stress, inflammation) in the adult mammalian brain (discussed in section 5.4.6.3.).

5.4.6.3. Future experiments to examine epigenetic mechanism in the mouse brain under normal physiological and chronically hypoperfused conditions

Although, a significant progress has been made in optimizing double 5mC and 5hmC immunochemistry after the completion of this thesis, further optimization is still required for the performance of 5mC/ 5hmC immunochemistry with neural specific biomarkers on the same biological sample. The major methodological difficulty relies in the currently used HCL treatment required for nuclear DNA immunostaining (e.g. 5mC, 5hmC). Methodologically, one could reduce the incubation time in HCL, currently performed at 37°C for 30min which might allow a better preservation of membrane epitopes.

Since little is known about TETs in the central nervous system (discussed in section 5.4.4., 5.4.6.2.), future molecular studies should examine these proteins in white and grey matter areas of sham compared with hypoperfused mice using for instance a combination of laboratory techniques such as immunochemistry, (q)PCR and/ or Western blot analysis. Further, to determine the potential TETs functional significance in the brain, one could proceed by a selective genetic ablation or pharmacological inhibition of one (or a combination) of TETs followed by a subsequent examination of brain hydroxy/ methylation dynamics, neuropathology and functional outcome in sham compared with hypoperfused mice.

To test potential (presently undetected) associations between brain hydroxymethylation and methylation, one could investigate the effects of perturbation in methylation patterns on brain hydroxymethylation in the presence and absence of chronic cerebral hypoperfusion. Methodologically, one could use DNMT deficient mice exhibiting perturbed methylation dynamics (Okano et al., 1998; Bird and Wolffe, 1999; Okano et al., 1999) and their respective WT controls to compare the regional brain 5hmC content in the presence and absence of chronic cerebral hypoperfusion. A subsequent investigation of neuropathology and functional outcome in this animal model would allow to determine the potential biological importance of these epigenetic marks.

With regards to published studies suggesting an important role of HDAC in oligodendroglial biology and the implication of this epigenetic mark in the processes of remyelination following experimental demyelination of the CC in the aging brain (Shen et al., 2008), it would be interesting to examine potential associations between histone deacetylation and hydroxymethylation dynamics in the hypoperfused white matter. From a methodological point of view, this could be achieved by comparing 5hmC content in white matter of sham and chronically hypoperfused mice treated with valporic acid (HDAC antagonist) vs. saline (control). This study would allow to determine whether an absence of active histone deacetylation impacts on hydroxymethylation in white matter in the presence and absence of chronic cerebral hypoperfusion and what the potential functional consequence (e.g. neuropathological and functional outcome) might be.

Additionally, methylation and hydroxymethylation dynamics might be modulated by environmental factors such as for example increased excitotoxicity, oxidative stress and inflammation under hypoperfused conditions (Cerda and Weitzan, 1997; Duan et al., 2002; Kruman et al., 2002; Zhang et al., 2007; Wilson, 2008; Backdahl et al., 2009). Future mechanistic studies examining for instance the effects of pharmacological inhibition of these pathophysiological mechanisms in chronically hypoperfused mice (discussed in Chapter 6, section 6.1.3., 6.1.4.3.) would allow to determine whether they affect on epigenetic marks in the presence and absence of chronic cerebral hypoperfusion and what the potential neuropathological and functional consequences might be.

It is known that epigenetic patterns are not stable and they vary under different physiological conditions as well as naturally during lifespan (Bird, 2002; Mehler, 2008; Penner et al., 2010; Song et al., 2010; Hernandez et al., 2011; Chen et al., 2012; Dzitoyeva et al., 2012; Szulwach et al., 2012). Therefore, with regards to the chronic nature of the hypoperfused mouse model, future time- course studies should examine methylation and hydroxymethylation dynamics at different post- surgery time points in sham and hypoperfused mice. These experiments would allow to determine the associations of potential temporal and regional variations in brain methylaiton and hydroxymethylation with the observed neuropathological and functional outcome in this animal model.

Further in regards to the relevance of the hypoperfused model to the aging processes in humans, it would be interesting to compare epigenetic marks in the brains of aged vs. young animals in the presence vs. absence of chronic cerebral hypoperfusion (discussed in Chapter 6, section 6.1.2.)

5.4.7. Implications of the study and future directions

The major implication of the present study relies in the experimental investigation of emerging epigenetic phenomena such as methylation and hydroxymethylation in the normal and diseased (e.g. chronic cerebral hypoperfusion) mammalian brain. Both methylation and hydroxymethylation have been associated with age- related neuropathology (Post et al., 1999; Tohgi et al., 1999; Wang et al., 2008; Kriaucionis and Heintz., 2009; Mastroeni et al., 2009; Mastroeni et al., 2010; Song et al., 2010; Szulwach et al., 2011; Chen et al., 2012). However, little is known about 1) the specific distribution of methylation and hydroxymethylation in cells composing the cerebral white and grey matter, 2) the dynamics of these epigenetic phenomena in the central nervous system under normal physiological and pathological conditions, 3) the association between methylation and hydroxymethylation as well as their relations to other epigenetic marks, 4) whether and/ or how changes in 5mC and 5hmC dynamics under pathological conditions might impact on neuropathology and functional outcome, 5) whether the TET proteins are important regulators of hydroxylation of 5mC in the brain and whether/ how pathological alterations in TETs- associated pathways could impact on 5mC and 5hmC distribution in the brain.

The present study addressed some of the above mentioned questions. Specifically, it 1) provided the first detailed, immunochemical characterization of methylation, hydroxymethylation and TET2 in white and grey matter areas of the adult mouse brain under normal physiological conditions and one month after chronic cerebral hypoperfusion, 2) examined potential associations between these epigenetic marks in white matter (5mC, 5hmC, TET2), 3) attempted to determine the cellular basis of 5hmC in white matter using in vivo and in vitro strategies.

The present findings would potentially constitute the basis for future studies examining the molecular and functional significance of epigenetic mechanisms in the development of age- related neuropathology and cognitive decline. Understanding the functional significance of distinct epigenetic marks in the brain, their interplay and how they could be exogenously regulated would potentially allow the identification of new molecular targets for the treatment of age- related neuropathology and cognitive decline.

5.5. Summary

The experimental findings presented in Chapter 5 suggest that chronic cerebral hypoperfusion alters significantly hydroxymethylation in the CC in the absence of changes in methylation and TET2 in white matter. Significant TET2 alterations were evidenced in the hypoperfused Cx. A subsequent correlation analysis demonstrated that hydroxymethylation in white matter might occur independently from 5mC and TET2. Further in vivo and in vitro investigation of the potential cellular basis of 5hmC suggests that microglia might be the cells associated with hydroxymethylation in white matter.

Chapter 6

Discussion

In the present thesis a new mouse model of chronic cerebral hypoperfusion was further developed and characterized. The obtained data would potentially constitute the basis for future research leading to the pre- clinical identification of new biological targets for the development of therapies for age- related cognitive decline.

6.1. Future research directions using the new mouse model of chronic cerebral hypoperfusion

6.1.1. Effects of chronic cerebral hypoperfusion on alternative (non- examined) brain processes in mice

Chronic cerebral hypoperfusion might affect presently non- examined brain processes potentially contributing to the pathological and behavioural profile in this animal model.

6.1.1.1. Effects of chronic cerebral hypoperfusion on the cerebral metabolism in mice

Age- related alterations in the cerebral hemodynamics are associated with carotid stenosis (e.g. chronic cerebral hypoperfusion) and cognitive impairment (Derdeyn et al., 1994; Ogawa et al., 1996; Pardo et al., 2007).

Hypoperfusion- induced alterations in the cerebral hemodynamics might impact on the cerebral metabolism in mice by affecting the glucose turnover, the ATPase activity, the ATP and lactate concentrations as shown in alternative animal models (Plaschke et al., 2005; Shang et al., 2005). Specifically, in chronically hypoperfused rats a sudden ATP depletion is observed in the minutes following artery ligation (5-10 mins post- surgery) (Plaschke et al., 2005). These ATP reductions persist for two weeks and ATP concentrations are restored to normal (baseline level) 8 weeks post- surgery. (Plaschke et al., 2005). Importantly, the ATPase activity was found to be decreased, whereas the lactate concentrations and utilization were 2.5 fold increased in grey matter areas (the Cx and hippocampus) in chronically hypoperfused rats (Shang et al., 2005). By using 18F-

fluorodeoxyglucose positron emission tomography (PET), which measures cerebral glucose transport across the blood- brain barrier, Nishio et al., 2010 demonstrated that the glucose utilization in the hippocampus of chronically hypoperfused mice remains impaired 6 months post- surgery. Similar findings were observed in clinical studies on elderly people using the same experimental approach (18F-fluorodeoxyglucose PET). In particular, reductions in the cerebral glucose uptake were evident in individuals with mild cognitive impairment or probable and possible Alzheimer`s disease (Drzezga et al., 2003; Hunt et al., 2007). A longitudinal FDG-PET study revealed hippocampal reductions in glucose uptake during normal aging (Mosconi et al., 2006; Samuraki et al., 2007). Further, by using the same neuroimaging technique, Reiman et al., 1996 and Reiman et al., 2004 demonstrated low rates of glucose metabolism in young and middle aged, cognitively intact APOE4 carriers in the same regions of the brain where such metabolic abnormalities are usually evident in Alzheimer`s patients (e.g. prefrontal, parietal, temporal and posterior cingulate regions). Taken together these clinical data suggest that decreases in the cerebral metabolism might be a predictive factor of neurodegeneration and cognitive decline with increasing age.

Further, the discussed animal and human data are important considering the more pronounced neuronal ischemic injury observed in the food deprived, behaviourally tested hypoperfused cohorts in the present thesis (Chapter 3). It is possible that undetected hypoglycaemia due to the experimental diet led to more pronounced metabolic perturbations in the brains of food deprived hypoperfused animals impacting on neuronal function and survival.

However, the cerebral blood metabolism was not examined in any of the studies in the present thesis. Future experiments measuring the cerebral metabolism (e.g. ATP, ATPase activity, glucose, lactate) at different post- surgery time points under different experimental conditions (e.g. presence vs. absence of behavioural training; food diet vs. *ad libitum* feeding or a combination of these) comparing sham and chronically hypoperfused mice would help to get a better understanding of the effects of potential hypoperfusion- induced cerebral hemodynamic changes on the neuropathological and

functional outcome in this model over time. Additionally, one could suspect that hypoperfusion- induced metabolic abnormalities might be more pronounced in APOEKO deficient and human APOE4 transgenic mice due to naturally occurring cerebrovascular abnormalities in these animals (Piedrahita et al. 1992; Buttini et al., 1999; Sheng et al., 1999; Buttini et al., 2000; Fullerton et al., 2001; Methia et al., 2001; Kitagawa et al., 2002; Fryer et al., 2005 Hafezi- Moghadam et al., 2006).

6.1.1.2. Effects of chronic cerebral hypoperfusion on the cerebrovasculature in mice

The observed cerebral blood flow restoration in all animal models of chronic cerebral hypoperfusion suggests the existence of compensatory mechanisms occurring overtime following surgery. Compensatory blood flow might be provided through artery dilation, nonperfused capillaries and veins, angiogenesis. This idea is supported by existing data from chronically hypoperfused rats and recent findings on chronically hypoperfused mice. In the rat model of chronic cerebral hypoperfusion compensatory mechanisms such as enlargement of the posterior arteries at the base of the brain and the arteries emanating from the circle of Willis were evident between 4- 6 months after artery ligation. Further, in this model, an increased capillary diameter, neovascularization, and an increase in vascular endothelial growth factor (VEGF) were found in grey matter areas after 4 weeks of artery stenosis (de Wilde et al., 2002; Ohtaki et al., 2006). A recent microarray study in chronically hypoperfused mice revealed alterations in blood vessels development genes in white matter (Reimer et al., 2011). These data are suggestive of potential cerebrovascular, compensatory mechanisms taking place in the hypoperfused mouse brain.

Further, microcerebrovascular pathology (e.g. small arteries and arterioles abnormalities) is observed in both elderly people and hypoperfused rats (Olendorf, 1987; Tang et al., 1997; de Jong et al., 1999; Choy et al., 2006; Farkas et al., 2006; Fernando et al., 2006; Gold et al., 2007). Therefore, microcerebrovascular pathology might contribute to the pathological and behavioural profile following hypoperfusion in mice.

Future experiments on chronically hypoperfused mice should examine the morphology of cerebral blood vessels and angiogenesis in this animal model using a standard histological approach (e.g. H&E) and/ or sensitive biomarkers targeted to endothelial cells (e.g. BMEC), pericytes (e.g. CD31), pericytes progenitors (e.g. Angiopoietin-1), VEGF. Further these future experiments should take into consideration the potential effects of additional factors such as APOE which might affect the microcerebrovascular integrity under both normal physiological and chronically hypoperfused conditions. Specifically, APOE deficient mice exhibit reduced VEGF expression and impaired collateral vessel development following experimental ischemic injury which impacts negatively on pathology and functional outcome (Couffinhal et al., 1999). Human APOE4 carriers with Alzheimer`s disease exhibit more severe microvascular pathology consisting of Aβ accumulation in the cerebral blood vessels and small vessels artheriosclerosis in white and grey matter areas of the brain (Premkumar et al., 1996; Yip et al.,2005).

The blood brain barrier plays an important role in protecting the brain from potentially harmful molecules coming from the peripheral circulation. The blood brain barrier is particularly vulnerable to hypoxic- ischemic events and its rupture could exacerbate both the observed pathological and functional outcome (Lenzser et al., 2005; Preston and Foster, 1997). Morphological abnormalities in the blood brain barrier such as basement membrane thickening, fibrous collagen deposit have been reported to occur in both "healthy" and demented elderly potentially affecting the normal transport of nutrients to the brain (Farkas and Luiten, 2001; Bell and Zlokovic, 2009). In accordance with these human findings, naive aged rats (30 months) exhibit capillary basement membrane pathology (de Jong et al., 1990). The possible associations between the observed blood brain barrier abnormalities in elderly people and aged rats were tested in chronically hypoperfused adult rats. In this animal model, microvascular basement membrane thickening and collagen deposits similar to those observed in clinical studies were reported 14 months after artery ligation (de Jong et al., 1999). These experimental data suggest a role of chronic cerebral hypoperfusion in the occurrence of blood brain barrier abnormalities in the aging mammalian brain.

At the present time, little is known about the blood brain barrier integrity in chronically hypoperfused mice and whether and/ or how potential blood brain barrier abnormalities could affect the pathological and functional outcome in this animal model. This is important as to the future identification of pathophysiological mechanisms influencing the development of neuropathology and cognitive deficits in chronically hypoperfused mice (discussed in section 6.1.3.).Future experiments should focus on examining the blood brain barrier integrity in this animal model for instance, by using previously described methods such as venous administration of Evans blue dye that does not cross the blood brain barrier under normal physiological conditions, but accumulates in the brain parenchyma when the blood brain barrier is pathologically disrupted. Investigation of Evans blue in the brain parenchyma of sham compared with chronically hypoperfused mice would allow to determine the potential existence of blood brain barrier abnormalities in this animal model (Fullerton et al., 2001). Further, it is unknown how potential hypoperfusion- induced blood brain barrier abnormalities could be modulated by additional molecular factors such as APOE. Previous studies demonstrated the existence of blood brain barrier abnormalities in naïve APOEKO mice which increase in severity in the presence of pathology (Fullerton et al., 2001; Methia et al., 2001; Hafezi- Moghadam et al., 2006) suggesting that blood brain barrier integrity might be modulated by the APOE genotype in the presence of chronic cerebral hypoperfusion.

6.1.1.3. Effects of chronic cerebral hypoperfusion on neurotransmission in mice

Impaired neurotransmission, namely disturbances in the cholinergic system are one of the hallmarks of dementia (Minger et al., 2000; Fong et al., 2011). Age- related cerebrovascular abnormalities have been proposed to play a role in the occurrence of cholinergic dysfunction and associated cognitive impairment in patients with Alzheimer`s and vascular dementia (Roman and Kalaria, 2006). A recent clinical study suggests a potential association between a state of chronic cerebral hypoperfusion and an impaired cholinergic function in Alzheimer`s patients (Fong et al., 2011) exhibiting significantly

more pronounced losses of choline acetyltransferase (ChAT) activity in the presence of the APOE4 allele (Lai et al., 2006).

Experimental cerebral hypoperfusion, in a similar way, leads to memory impairment with alterations in the cholinergic parameters such as muscarinic, nicotinic receptors, ChAT and decreased acetylcholine levels in the hippocampus of chronically hypoperfused rats (Ni et al., 1995; Kondo et al., 1996; Egashira et al., 1996; Tanaka et al., 1996; Ouchi et al., 1998). In chronically hypoperfused mice a recent study by Nishio et al., 2010 suggested reduced levels of acetylcholine esterase in cortical and subcortical grey matter areas. Both clinical and experimental studies have proven that a cholinergic agonist based therapy mitigates memory dysfunctions in Alzheimer`s patients and hypoperfused rats (Nanri et al., 1998; Murakami et al., 2000). In regards to the important role of the cholinergic system in mediating learning and memory processes as well as in the development of dementia (Van der Zee et al., 2011), future studies in chronically hypoperfused mice should determine to what extent hypoperfusion- induced alterations in the acetylcholine levels could impact on cognitive and memory function in mice.

Disturbances in the cholinergic system are often accompanied by alterations in other neurotransmitter systems (e.g. catecholamines) and future studies should also get a better understanding of the effects of the microcoils surgery on catecholamines, gabaergic and glutamatergic synthesis in mice. Little is known about the effects of hypoperfusion on catecholamines in both humans and animal models of chronic cerebral hypoperfusion. Catecholamines are known to play a role in the modulation of prefrontal executive function, in particular the dopamine system (Arnsten, 1998). Experimental evidence from aged rats, nonhuman primates and elderly people suggests a role of the catecholamine (e.g. dopamine and serotonine) and noradrenaline systems in age- related cognitive decline (Adolfsson et al., 1979; Arnsten and Goldman- Rakic, 1985; Miguez et al., 1990; McEntee and Crook, 1991; Reeves et al., 2002).

Future experiments on chronically hypoperfused mice should determine if there are any alterations in the brain neurotransmitter systems and if they impact on the pathological and

functional outcome in this animal model. Methodologically, one could use HPLC and/ or a standard immunohistochemical approach to measure neurotransmitters in the brains of behaviourally tested sham compared with chronically hypoperfused mice. Subsequent association analysis between neurotransmitter levels (e.g. acetylcholine) with neuropathological and behavioural measures would allow to determine whether potential hypoperfusion- induced alterations in neurotransmission are functionally relevant. Further, one should consider the effects of additional factors such as APOE that could potentiate the effects of hypoperfusion on neurotransmission. For instance, naïve APOE deficient mice exhibit reduced numbers in muscarinic acetylcholine receptors in grey matter (the hippocampus) and impaired performance on a 5-choice serial reaction time tasks (executive function) (Siegel et al., 2011). Therefore, potential hypoperfusion- induced alterations in neurotransmitters systems might be more pronounced in APOEKO mice.

6.1.2. Effects of chronic cerebral hypoperfusion on neuropathology and cognitive impairment in the context of aging

Reduced neurotrophic levels, neuronal abnormalities (e.g. synaptic/ dendritic loss and dysfunction), impaired neurotransmission, cerebrovascular pathology occur with chronological age and may impact on the pathological and functional profile of aged sham and hypoperfused animals compared with young treatment- matched counterparts (Arnsten and Goldman- Rakic, 1985; Olendorf, 1987; de Jong et al., 1990; Miguez et al., 1990; McEntee and Crook, 1991; Ni et al.,1995; Kondo et al., 1996; Egashira et al., 1996; Tanaka et al., 1996; Tang et al., 1997; Ouchi et al., 1998; Bimonte et al., 2003; Blesch, 2006; Choy et al., 2006; Farkas et al., 2006; Fernando et al., 2006; Gold et al., 2007).

Aged rodents, dogs and nonhuman primates exhibit cognitive deficits even in the absence of surgical/ phramacological intervention when compared with young counterparts. For instance, relative to young controls, aged dogs exhibit worse cognitive scores in object recognition, reversal learning and spatial learning tasks (Head et al. 1995; Cummings et al. 1996). Similar results are observed in aged monkeys presenting memory flexibility, working memory and processing speed deficits when compared with young counterparts

(Herndon et al., 1997; Luebke et al., 2004). However, some behavioural studies on aged animals suggest differential effects of aging on cognition and memory. Specifically, an inter- animal variability in the severity of age- related cognitive impairment exists among aged rodents. Some aged animals present intact cognitive and memory function, whereas others exhibit an age- related deterioration in cognition and memory (Matzel et al., 2008).

In regards to the relevance of the hypoperfused model to the aging process in humans, future experiments comparing aged vs. young cohorts of sham vs. chronically hypoperfused mice would allow to determine the effects of aging alone as well as in combination with experimentally induced cerebrovascular challenge (e.g. chronic hypoperfusion) on the development of cognitive decline and neuropathology. However, for these particular studies one should consider the above mentioned inter- animal variability in cognitive function in naïve aged mice.

Age- related pathological alterations seem to be more pronounced in APOE4 human carriers, APOE deficient mice and human APOE 4 transgenic animals (Piedrihta et al., 1992; Van Ree et al., 1994; Gordon et al., 1995; Masliah et al, 1995; Premkumar et al., 1996; Reiman et al., 1996; Masliah et al., 1997; Sheng et al., 1999; Buttini et al., 2000; Fullerton et al., 2001; Methia et al., 2001; Han et al., 2003; Reiman et al., 2004; Hafezi-Moghadam et al., 2006; Beeri et al., 2006; Persson et al., 2006; Filippini et al., 2009; Smith et al., 2010; Heise et al., 2010; Ryan et al., 2011). In the present thesis APOE deficiency was found to impact on the development of hypoperfusion- induced white matter pathology on MRI scans of relatively young, adult mice (Chapter 4). It is possible that white matter abnormalities develop naturally, at a later time point during the lifespan of APOEKO mice even under normal physiological conditions due to previously demonstrated increased lipid peroxidaiton, protein oxidation and impaired cholesterol transport, cerebrovascular abnormalitites in this animal model leading to the development of more severe neuropathology following chronic cerebral hypoperfusion in aged APOEKO mice (Piedrahita et al. 1992; Van Ree et al., 1994; Fullerton et al., 2001; Methia et al., 2001; Ramassamy et al., 2001; Han et al., 2003; Choi et al., 2004; Hafezi-Moghadam et al., 2006). Future experiments should examine the individual and combined

effects of the surgical procedure (sham vs. hypoperfusion), genotype (WT vs. APOEKO; APOE3 vs. APOE4) and age (young vs. old) on neuropathology and functional impairment in this animal model.

Previous reports suggest age- related epigenetic alterations associated with neuropathology and cognitive decline (Post et al., 1999; Tohgi et al., 1999; Wang et al., 2008; Kriaucionis and Heintz., 2009; Mastroeni et al., 2009; Mastroeni et al., 2010; Song et al., 2010; Szulwach et al., 2011; Chen et al., 2012). In the present thesis methylation and hydroxymethylation dynamics were investigate under normal physiological and hypoperfused conditions in white and grey matter areas of relatively young adult mice. Hypoperfusion was found to increase significantly 5hmC, but not 5mC in white matter, most likely related to increases in inflammatory microglia (Chapter 5). It is possible that age- related changes in the brain microenvironment such as increases in inflammation, excitotoxicity, oxidative stress, neurodegeneration could impact on the processes of hydroxylation of 5mC (Arnsten and Goldman- Rakic, 1985; Olendorf, 1987; de Jong et al., 1990; Miguez et al., 1990; McEntee and Crook, 1991; Ni et al.,1995; Kondo et al., 1996; Egashira et al., 1996; Tanaka et al., 1996; Tang et al., 1997; Ouchi et al., 1998; Bimonte et al., 2003; Blesch, 2006; Choy et al., 2006; Farkas et al., 2006; Fernando et al., 2006; Gold et al., 2007; Baltan et al., 2008). Future experimental work should investigate using sensitive techniques methylation and hydroxymethylaiton dynamics in the brains of aged sham vs. chronically hypoperfused mice compared with treatment- matched young counterparts. Subsequent associations of epigenetic marks with neuropathology and functional outcome under normal physiological and chronically hypoperfused conditions in young vs. aged animals would allow to reveal the potential biological significance of these molecular mechanisms in the central nervous system during lifespan and disease.

6.1.3. Pathophysiological mechanisms in chronically hypoperfused mice

Although in the present thesis the inflammatory response was partially examined in chronically hypoperfused mice, the pathophysiological mechanism(s) in this animal model remain(s) largely unknown. It is important that future research identifies cellular and molecular pathways underlying hypoperfusion- induced neuropathology and functional impairment in mice. Considering the chronic nature of the cerebrovascular challenge, it is

possible that at different post- surgery time points, different pathophysiological mechanisms modulate neuropathology and functional impairment in hypoperfused mice. These mechanistic studies would potentially constitute the basis for future pre- clinical development of therapeutic strategies for age- related cognitive decline. As previously discussed in this thesis (Chapter 1, section 1.6.) APOE could modulate excicotoxic, oxidative and inflammatory levels therefore determining the pathophysiological environment in the hypoperfused mouse brain.

6.1.3.1. A role of excitotoxicity in hypoperfusion- induced neuropathology and cognitive deficits in mice?

Excitotoxic brain injury is associated with disturbances in brain ionic homeostasis occurring following excessive glutamate synthesis under pathological conditions such as hypoxic- ischemic events (Hazell, 2007; Tekkok et al., 2007). Excitotoxicity is associated with an overactivation of glutamatergic receptors present on glia and neurons leading to the occurrence of white and grey matter pathology (Choi, 1990; Sattler and Tymianski, 2001; Karadottir and Attwell, 2007; Bakiri et al., 2009).

Nonselective Na+ channels blockers such as tetrodoxin (TTX), lidocaine and flecainide as well as glutamatergic receptor antagonists (e.g. NBQX) reduce pathological damage to white and grey matter in experimental models of hypoxia- ischemia (e.g. stroke, periventricular leukomalacia), multiple sclerosis, spinal cord and traumatic brain injury (Zafonte et al., 1999; Schwartz and Fehlings, 2001; Bechtold et al., 2004; Follet et al., 2004; Sfaello et al., 2005; Waxman, 2006). For instance, BW61 9C89, a blocker of voltage- gated Na+ receptors inhibits glutamate release in a rat model of middle cerebral artery occlusion and exerts neuroprotection (Graham et al., 1994). Intraperitoneal administration of riluzole, a Na+ blocker is associated with an improved neuropathology and functional outcome following spinal cord injury in the rat (Schwartz and Fehlings, 2001). Intracerebral infusion of topiramate, reduces excitotoxic white matter injury following intracerebral administration of ibotanate- a glutamatergic agonist acting via the NMDA, AMPA receptors, in newborn mice (Sfaello et al., 2005).

Pathological changes at the paranodal structure and the nodes of Ranvier have been reported to occur in white matter as soon as 3 days following chronic cerebral hypoperfusion in mice and these morphological abnormalities seem to increase in severity overtime (Reimer et al., 2011). Specifically, progressive paranodal breakdown and increases in the length of the nodes of Ranvier characterized by spreading of $Na_v1.6$. channels along the axolemma were evident in white matter tracts of hypoperfused mice between 3 days and 1 month after surgery. $Na_v1.6$. is the major Na+ channel at the nodes of Ranvier (Caldwell et al., 2000) and these receptors might be essential molecular players mediating excitotoxic damage to white matter (Stys, 1998; Stys, 2005). Nav1.6. receptors are also present on neuronal dendrites and synapses (Caldwell et al., 2000). In alternative animal models of chronic cerebral hypoperfusion significant alterations in synapses and dendrites are reported to occur in hypoperfused grey matter areas (Kudo et al., 1993; Kurumatani et al., 1998; Liu et al., 2005). Changes in the paranodal structure of the axolemma have been reported to occur in both aged animals and humans. For instance, Sugiyama et al., (2002) reported age-dependent alterations in the paranodal structure, illustrating paranodal loops that fail to reach the axon in white matter of 31 month old rats. An increase in paranodal profiles and the presence of short, thin internodal lengths of myelin in cortical areas 17 and 46 have been evident in aged rhesus monkey (Peters and Sethares, 2003). In humans, changes in the axolemma at the nodal regions seem to occur with chronological age (Lasiene et al., 2009).

It is possible that excitotoxic mechanisms mediate the development of both white and grey matter pathology in chronically hypoperfused mice via Nav1.6. receptors. From a methodological point of view, it might be challenging to test this hypothesis due to the current lack of specific Nav1.6 blockers. However, Nav1.6.KO mouse line exists (Levin and Meisler, 2004) and the microcoils surgery could be applied on Nav1.6. KO and WT control mice to test the effects of Nav1.6. receptors on neuropathology and functional outcome in this animal model. The absence of Nav1.6. receptors might be associated with a better neuropathological and functional outcome following hypoperfusion in mice due to limited excitotoxicity. Alternatively, to reduce the cost of using genetically modified animals, one could intracerebrally administer Na+ blockers (e.g. TTX) or glutamatergic

antagonists (e.g. NBQX) vs. saline in C57BlJ6 hypoperfused mice and compare the effects of these treatments on neuropathology and functional outcome. However, there are a few considerations concerning this pharmacological approach. The cerebrovascular challenge in this animal model is chronic and it is necessary to determine when to apply Na+/ glutamatergic blockers in hypoperfused mice. The long- term administration of pharmacological inhibitors of Na+/ glutamatergic- dependent cellular activity risks of perturbing non- affected neural circuits leading to additional neuropathology and functional deficits.

6.1.3.2. A role of oxidative stress in hypoperfusion- induced neuropathology and cognitive deficits in mice?

Oxidative stress has been reported to occur in various neuropathological conditions, characterized by increased excitotoxic and inflammatory levels (e.g. hypoxic- ischemic insults) (Auten and Davis, 2009). Oxidative stress is defined as a disturbance in the pro-oxidant- antioxidant balance in favour of the former, leading to cellular injury, molecular dysfunction, cell death (Auten and Davis, 2009). Excitotoxic and inflammatory processes might influence the development of neuropathology following chronic cerebral hypoperfusion in mice and their effects might be potentiated and/ or partially mediated via the formation of reactive oxygen species such as NO. For instance, hypoxia- ischemia increases the expression of NO synthases- the enzymes catalyzing the production of NO during the initial hours following the insult (Iadecola et al., 1997). NO concentration has been shown to increase 2 weeks following artery ligation in chronically hypoperfused rats (de la Torre et al., 2003). An excess of NO is known to be harmful to cellular mitochondrias initiating the release of pro- apoptotic signals such as cytochrome- C and caspase- 3 resulting in an increased cell death and neuropathology (Kroemer et al., 1998; Ricci et al., 2004). Elevated NO levels following hypoxic- ischemic events in vivo have been shown to cause neuronal and glial cell death (Eliasson et al., 1999; Haynes et al., 2003). In vitro studies have confirmed these data by demonstrating that microglia secreted NO leads to neuronal and glial apoptosis (Kim and Kim, 1991; Boje and Arora, 1992; Chao et al., 1992; Cazevieille et al., 1993; Mitrovic et al., 1995). It is possible that hypoperfusion- induced increases in reactive oxygen species contribute to the

development of white and grey matter pathology in this animal model (Chapter 3, section 3.4.2.4.). Previous experimental work has demonstrated beneficial effects of anti-oxidative agents on neuropathological and functional outcome in different central nervous system disorders. For instance, the antioxidants N-acetyl-cysteine, a-lipoic acid, and a-tocopherol (vitamin E) prevent axonal degeneration in a mouse model of x-adrenoleukodystrophy (Lopez- Erauskin et al., 2011). Intaperitoneal injection of the anti-oxidant peroxiredoxin 5 is neuroprotective in new born mice with experimentally- induced excitotoxic brain lesions (Plaisant et al., 2003). In a rat model of middle cerebral artery occulusion, oral administration of the anti- oxidant ebselen reduces significantly the volume of brain infarcts (Takagaso et al., 1997).

Future experimental work on chronically hypoperfused mice could examine the potential effects of anti-oxidative agents (e.g. N-acetyl-cysteine, a-lipoic acid, a-tocopherol vitamin A, C, and/ or E, peroxiredoxin 5) on neuropathology and functional outcome in this animal model potentially revealing new molecular targets for the preclinical development of therapeutic strategies for age- related cognitive decline. Similar to the discussed in the previous section, experimental modulation of brain oxidative levels in chronically hypoperfused mice should overcome certain issues associated with the chronic nature of the cerebrovascular challenge in this animal and potentially adverse effects associated with nonselective modulation of reactive oxygen species in the brain. Specifically, previous studies have demonstrated that although high concentrations of oxidative species are harmful to neuronal and glial cells, reactive oxygen species also play an important role in modulating cellular function. For instance, NO promotes vasodilatation, inhibition of platelet aggregation, modulation of neurotransmission, promotion of synaptogenesis, synaptic remodelling, and exerts antimicrobial toxicity- all important for neuroprotection and functional recovery following hypoxic- ischemic injury to the brain (Love, 1999).

6.1.3.3. A role of inflammation in hypoperfusion- induced neuropathology and cognitive deficits in mice?

As previously discussed within the present thesis increased inflammatory levels following chronic cerebral hypoperfusion could impact on the development of white and grey matter

abnormalities observed in this animal model. Inflammatory cells such as microglia and astrocytes play an important role during the endogenous processes of brain repair by buffering extracellular glutamate, secreting neurotrophic factors (e.g. BDNF, IGF-1), pro-inflammatory agents (e.g. cytokines, chemokines, matrix metalloproteinase), interleukins (IL1- 10) and oxidative species (e.g. NO) (Lakhan et al., 2009). The balance among these glial- produced molecular factors could modulate the severity of neuropathology and functional outcome following injury to the central nervous system.

To test the effects of immunomodulatory interventions on neuropathology and functional impairment in chronically hypoperfused mice one could consider different experimental strategies (some experimental strategies were previously discussed within the thesis). For instance, a potential inhibition of presently observed hypoperfusion- induced microglial activation in mice, could be achieved by the application of naloxone- a nonselective antagonist of the G-protein linked opioid receptors that are widely expressed on cells of the central nervous system (CNS) (Liu and Hong, 2003). Previous in vitro studies demonstrated that naloxone was capable of reducing the LPS-stimulated production of cytokines and NO in glial cultures (Das et al., 1995; Kong et al., 1997). In vivo naloxone exerts neuroprotective effects in LPS animal models of Parkison`s disease by inhibiting microglial secretion of pro- inflammatory substances (Liu et al., 2000, Lu et al., 2000). Further, corticosteroids have recognized anti- inflammatory properties in different pathological conditions with a certain effect on neuropathology and functional recovery such as in the case of spinal cord and traumatic brain injury, stroke, multiple sclerosis (Limbourg et al., 2002; He et al., 2004; Kwon et al., 2004; Garay et al., 2008). Alternatively, nonsteroidal drugs such as aspirin have been suggested to modulate the inflammatory response under pathological conditions and exert neuroprotective function by inhibiting glial secreted proinflammatory cyclooxygenase enzymes, which have been implicated in neurodegenerative pathways (Wahner et al., 2007). These nonsteroidal compounds seem to be particularly promising for future clinical application as most of them are already marketed (approved by regulatory agencies) and easy to administer (oral intake).

Future research work on chronically hypoperfused mice could consider examining the effects of the above mentioned immunomodulatory substances on neuropathology and functional outcome in this animal model.

6.1.4. Preclinical development of therapeutic strategies for the treatment of age-related cognitive decline using chronically hypoperfused mice

In addition to modulation of potential hypoperfusion- associated pathophysiological mechanisms, future experimental work could consider developing alternative therapeutic strategies in this animal model.

6.1.4.1. Cerebral reperfusion

Since hypoperfusion- induced neuropathology and cognitive impairment in mice are associated with microcoils- mediated partial obstruction of the common carotids resulting in mild cerebral hypoprefusion, a potential strategy to restore brain structure- function in this animal model might consist of the surgical removal of the microcoils followed by restoration of cerebral blood flow (e.g. reperfusion). In alternative cerebrovascular models (e.g. focal ischemia) and human patients with stroke, the processes of cerebral perfusion-reperfusion involve complex cellular and molecular pathways persisting even after the reperfusion phase (D`Ambrosio et al., 2001; Fiehler et al., 2004). However, with the restoration of cerebral irrigation, there is a progressive normalization of the cerebral microenvironment (e.g. decreases in inflammation) followed by a long- term restoration of function by neuroregeneration of injured areas and/ or by compensatory brain mechanisms (Hossmann, 2008). The immediate hours (up to 6 hours) following reperfusion have been shown to represent a therapeutic window to reduce brain damage and improve functional outcome after hypoxic- ischemic events (Baron et al., 1995; Molina and Saver, 2005).

It is unclear whether the removal of the microcoils in chronically hypoperfused mice would be beneficial (e.g. improvement of working memory). Although, technically challenging (e.g. risk of potential arterial damage; a second surgical intervention on the same animal), future experimental work should address this question by characterizing the processes of cerebral perfusion- reperfusion in hypoperfused mice at both the

neuropathological and functional levels. Due to the chronic nature of the cerebrovascular challenge in this animal model, this future work would require the identification of the optimal post- surgery time point for reperfusion (e.g. microcoils removal) associated with any beneficial pathological and/ or functional outcome. This intervention (e.g. removal of microcoils) might be less efficient at later post- hypoperfusion time points characterized by more severe neurodegeneration and cognitive impairment in mice (Nishio et al., 2010; Reimer et al., 2011).

6.1.4.2. APOE modulation

Human APOE allelic polymorphism has been shown to modulate the person`s susceptibility to recover following injury to the brain as well as to develop dementia and cerebrovascular pathology with increasing age (Saunders et al., 1993; Kalmijn et al., 1996; Skoog et al., 1998; Reiman et al., 1996; Reiman et al., 2004; Schuff et al., 2009b; Nicoll et al., 1995; Gromadzka et al., 2007; Wagle et al., 2009). Recent clinical reports associated the APOE4 allele with the occurrence of white matter abnormalities in cognitively intact adults which at a higher risk of dementia (Bartzokis et al., 2007; Filippini et al., 2009; Heise et al., 2010; Ryan et al., 2011).

In the present thesis, ex vivo MRI analysis revealed that APOE may impact on the severity of hypoperfusion- induced white matter pathology in mice. Specifically, an absence of endogenous APOE was associated with more severe reductions in MRI parameters of white matter integrity in APOEKO hypoperfused mice compared with WT hypoperfused counterparts (Chapter 4). Although, the neuroimaging data were not supported by the applied pathological analysis (discussed in Chapter 4, section 4.4.5.), they are interesting and if confirmed in the future, they could constitute the basis for future investigation of APOE effects on neuropathology and functional outcome in this animal model. Results from previous studies suggest that restoring and/or increasing APOE levels can promote neuroprotection in the injured brain. For instance, an amelioration of neurological and pathological deficits in APOE deficient mice was achieved by intracerebral administration of recombinant APOE. Infusion of human recombinant APOE3 and APOE4 reversed cognitive deficits and participated in restoration of neuronal

structure in APOEKO mice (Masliah et al., 1997). The neuroprotective effects of APOE were also observed in WT mice following global ischemia (Horsburgh et al., 2000c). Increasing APOE levels in the brain would therefore appear to be a tempting therapeutic strategy to pursue in chronically hypoperfused mice. Several approaches could be used to augment endogenous APOE levels in the brain: (1) direct intrathecal administration of APOE in lipid-conjugated form (Horsburgh et al., 2000c) (2) intrathecal or systemic administration of APOE mimetic peptides (that could cross the blood-brain barrier) (Aono et al., 2003); (3) administration of agents that can increase APOE expression levels. A key consideration of any approach, however, would be the potential systemic side effects of increasing APOE levels given the fundamental role of APOE in lipid and cholesterol homeostasis, especially in the periphery. In this regard, restricting increased APOE expression to the brain would be an important advantage. Since there is no clear evidence that APOE crosses the blood-brain barrier, direct intrathecal administration/viral vector-mediated delivery of APOE could achieve brain-specific increases in APOE. However, even with these approaches, blood-brain barrier disruption in the injured brain could result in leakage of APOE into the systemic circulation. Another key issue, especially in regards to translation of this research to clinics relates to human APOE polymorphism. Although the precise mechanism(s) responsible for APOE genotype dependent responses to brain injury are not fully understood, there is evidence that differences may be due to beneficial properties of the APOE3 (and APOE2) isoform (that are absent in the APOE4 isoform) but also to direct toxic properties of APOE4 (Marques et al., 1997). In regards to clinics, these divergent effects of human APOE isoforms could preclude development of a single drug that would benefit patients with chronic cerebral hypoperfusion of all APOE genotypes. For example, a drug that indiscriminately enhances APOE expression in the brain may be beneficial in APOE3 (and APOE2) carriers (promotes beneficial APOE3/E2 effects), but have mixed effects in APOE4 carriers (compensates for effects due to APOE4 deficiency but also promotes toxic APOE4 effects). In view of the above pharmacogenomic issues, specifically enhancing APOE3 effects could be advantageous. A third consideration with an APOE-based therapeutic approach would be the duration of APOE expression that could be achieved. The ability to mediate prolonged APOE

expression in the brain under chronic conditions (e.g. chronic cerebral hypoperfusion) might provide more long-term benefits than a transient period of expression.

Future experiments on this animal model should therefore examine the effects of APOE-based therapy in mice taking into account the above mentioned considerations.

6.1.4.3. Epigenetic modulation

Modulation of epigenetic mechanisms might constitute a promising new therapeutic alternative for age- related cognitive decline. The sporadic nature of 90% of dementia cases, the differential susceptibility to and course of the illness, as well as the relatively late onset of functional impairment suggest that epigenetic and environmental components play a role in the pathogenesis of age- related cognitive decline (Mehler, 2008; Zawai et al., 2009; Chouliaras et al., 2010; Penner et al., 2010). This idea is supported by clinical studies on monozygotic twins where both genomic 5mC content and the acetylation levels of histone 3 (H3) and H4 were significantly different in each twin and these epigenetic differences were more pronounced with increasing age (Fraga et al., 2005). Additionally, studies on monozygous twins with discordant Alzheimer`s disease demonstrated decreases in grey matter methylation in the affected twin compared with the cognitively intact twin brother (Mastroeni et al., 2009). In recent years, it has become increasingly clear that, besides stochastic changes in the epigenome that occur throughout life, environmental factors such as nutrition, diet, drugs, hormones, and infections modulate a person's phenotype and susceptibility to dementia via epigenetic mechanisms (Abdolmaleky et al., 2004; Poulsen et al., 2007; Liu et al., 2008). For instance, epigenetic changes occur following cerebrovascular challenge most likely induced by increases in excitotoxicity, oxidative stress and inflammation (Endres et al., 2000; Westberry et al., 2008). Epigenetic changes might be associated with the occurrence of white matter abnormalities with cerebrovascular etiology in elderly people (Farkas and Luiten, 2001; O`Sullivan et al., 2001; Roman et al., 2002; Deary et al., 2003; Charlton et al., 2006; Fernando et al., 2006; Grieve et al., 2007; Kennedy and Raz, 2009; Ihara et al., 2010; Penke et al., 2010).

The results from this thesis suggest significant hypoperfusion- induced alterations in 5hmC in white matter in the absence of 5mC alterations in mice. Significant increases in cortical TET2- one of the enzymes catalyzing the hydroxylation of 5mC were also evident in hypoperfused mice (Chapter 5). The functional significance of these epigenetic alterations in the hypoperfused mouse brain remains unclear. If, in the future, the present results are confirmed, modulation of epigenetic phenomena in hypoperfused mice should be considered as a potential therapeutic strategy in this animal model.

Currently, there is an absence of identified compounds which specifically modulate 5hmC due to the recent discovery of this epigenetic mark (Kriaucionis and Heintz., 2009; Tahiliani et al., 2009; Ito et al., 2010). Hydroxymethylation could be targeted via alternative molecular pathways such as methylation, TETs and potentially HDAC which might influence neuropathology and functional outcome in hypoperfused mice. One of the major considerations of exogenous (e.g. pharmacological) epigenetic modulation relies in the high inter- dependence among epigenetic mechanisms and the possibility of undesired alterations in associated epigenetic marks having deleterious rather than beneficial effects on neuropathology and functional outcome such as in the case of cancer (Ptak and Petronis, 2008). The majority of currently applied compounds for epigenetic modulation are nonspecific and by consequence not always safe for clinical application. However, experimental studies have demonstrated that pharmacological modulation of methylation and HDAC in animal models of stroke could be neuroprotective. For instance, intracerebroventricular administration of a methyltransferase inhibitor (5-aza-29-deoxycytidine) and a deacetylation inhibitor (trichostatin A) increased gene expression and conferred neuroprotection in WT mice following focal ischemia (Enders et al., 2000). Intraperitoneal administration of suberoylanilide hydroxamic acid- an HDAC inhibitor induced an increased expression of the neuroprotective proteins Hsp70 and Bcl-2 within the ischemic mouse parenchyma (Faraco et al., 2006).

Alternatively, there are currently marketed compounds shown to modulate epigenetic marks in the brain. For instance, the psychotropic valporate induces gene expression via inhibition of HDACs and its ability to perform DNA demethylation (Milutinovic et al.,

2007). The antidepressant fluoxetine, a selective serotonin reuptake inhibitor, induces expression of genes encoding MeCP2 and MBD1 (proteins associated with maintenance of methylation- Chapter 1, section 1.7.1.) by continuously activating the serotonergic system in the adult rat brain suggesting that fluoxetine might affect on methylation dynamics (Cassel et al., 2006).

Future experimental work on chronically hypoperfused mice could investigate the effects of compounds known to modulate epigenetic mechanisms on hypoperfusion- induced neuropathology and functional outcome. However, it is important to take into consideration the fact that these substances are not selective to the examined molecular mechanisms and their application could be potentially associated with disturbances in alternative brain processes (e.g. neurotransmission) impacting on neuropathology and cognition in hypoperfused mice.

Since hydroxymethylation results from the oxidation of 5mC catalyzed by the TETs- another strategy to modulate 5hmC in the brain would potentially reside in modifying TETs activity. Although, in the present thesis, a correlation analysis suggested an absence of associations between 5hmC and TET2 in white matter, it is unknown whether/ how the other TET members- TET1 and TET3 regulate hydroxylation of 5mC in the brain under normal physiological and chronically hypoperfused conditions (Chapter 5, sections 5.4.5., 5.4.6.3.). Future experimental work should investigate the catalysis of hydroxymethylation in the brain. If, as shown in stem, cancer cells and the early mammalian embryo (Tahiliani et al., 2009; Ito et al., 2010; Ko et al., 2010; Ficz et al., 2011; Ruzov et al., 2011), TETs participate in this molecular pathway, then one could modulate 5hmC in the brain via modulation of TETs activity. Methodologically, this could be achieved by comparing the effects of exogenously administered pharmacological agents (TETs inhibitors/ agonists) and/ or infusion of synthetic TETs (one or a combinations of these proteins) in the brains of hypoperfused mice and compare the effects of this experimental intervention with saline treatment on 5hmC, neuropathology and functional outcome (other strategies to study TETs in the brain are discussed in Chapter 5 section 5.4.6.3.).

6.1.4.4. Alternative therapeutic interventions

There is evidence that alternative compounds could be neuroprotective and promote functional recovery following hypoperfusion in clinical and preclinical settings. For instance, Choto-san, a Kampo (traditional medicine of Japan) formula was shown to improve cognitive impairment in stroke patients and spatial learning deficits in chronically hypoperfused rats via stimulation of muscarinic receptor M1 (Terasawa et al., 1997; Murakami et al., 2005). High fish consumption (a source of long chain n- 3 polyunsaturated fatty acids) has been associated with a reduced risk of cognitive decline in elderly people (Kalmijn et al., 1997; Terano et al., 1999). In hypoperfused rats n- 3 polyunsaturated fatty acids supplemented diet compared with three other diets (i.c. normal chow) improved behavioural performance on a water maze paradigm and better preserved blood brain barrier integrity via decreases in the number of endothelial mitochondria, as well as the ratio of microvessels with degenerative pericytes (de Wilde et al., 2002).

These alternative therapeutic strategies are interesting to explore in chronically hypoperfused mice especially in regards to their relatively easy adaptation to humans.

6.1.4.5. Cellular therapies

In principle stem cells constitute a promising resource for the development of allogeneic cellular therapies for incurable diseases characterized by the loss of one or more cell type owing to their broad capacity for growth and to be specified into functional derivatives. In practice, this potential has already been demonstrated in animal models of neuropathological conditions, such as spinal cord injury, stroke, periventricular leukomlalacia and many others (Lindvall et al., 2004; Keirstead et al., 2005; England et al., 2009; Titomanlio et al., 2011; Abe et al., 2012). However, the broad clinical application of exogenous stem- cells based therapies is still restricted in Europe and North America due to safety (e.g. tumorigenesis), ethical (e.g. human embryonic stem cells) and regulatory issues. Furthermore, there are important considerations concerning 1) the type of the cellular implant (e.g. embryonic/ fetal/ adult/ induced stem cells, in vitro predifferentiated, nondifferentiated progenitors), 2) the time for the intervention (e.g. early or late post- injury time point), 3) the route of administration (e.g. venously vs.

intracerebrally), 4) the location (e.g. near vs. far from the lesion- this is particularly challenging in the case of widespread pathologies such as multiple sclerosis), 5) the promotion of the graft survival especially under pathological conditions, 6) the time when a certain outcome should be expected (e.g. neuroregeneraion, functional recovery).

An interesting alternative to allogenic cellular therapies for neuropathological conditions may reside in the stimulation of the endogenous neural stem cell pool in the brain promoting neuroregeneration and functional recovery (Lie et al., 2004). This could be achieved by exogenous administration of substances (e.g. growth factors- BDNF, EGF, PDGF) known to play a role in neural stem cells proliferation, survival and differentiation during neurodevelopment and under pathological conditions (Picard- Riera et al., 2004; Calza et al., 2010; Guerra- Crespo et al., 2012)

The present thesis as well as a recently published work by Reimer et al., 2011 suggest significant increases in OPC in white matter areas of hypoperfused mice- an indicative of active cellular proliferation in this animal model. However, neuropathology and cognitive deficits occur in hypoperfused mice suggesting that the endogenous brain repair mechanisms are insufficient to prevent brain injury and promote functional recovery (e.g. working memory impairment).

In the future, it would be interesting to examine the effects of exogenous stimulation of neural repair in this animal model by infusion of compounds stimulating the endogenous neural stem cell pool or by implantation of exogenous progenitors.

However, there are important considerations to take into account before developing a cellular therapy in chronically hypoperfused mice.

Specifically, the first challenge resides in the chronic nature of the model raising questions as to when to intervene (e.g. immediately after the microcoils surgery or at later post-surgery time points). To determine the most beneficial time point for the application of cellular therapy in chronically hypoperfused mice, an initial strategy might involve the comparison of the therapeutic efficacy (e.g. brain repair, functional recovery) at different time- points following microcoils implication. Second, the pathology in this animal model is widespread affecting both white and grey matter areas. This raises questions as to what

type of progenitors to administer/ what type of substances to infuse. An administration of nondifferentiate neural progenitors might be a better strategy than application of pre-differentitated oligodendrocytes/ neurons. Further, the alternative pharmacological simulation of progenitors would require a cocktail of substances promoting differentiation towards multiple neural lineages. In addition, the widespread nature of the observed pathology in this animal model might constitute a problem as to the location of the implant/ infusion of substances. In regards to the literature in this case, the lateral ventricles are in general the preferred location for exogenous cellular application/ pharmacological intervention (Lindvall et al., 2004). Third, under chronically hypoperfused conditions there are increases in inflammation, oxidative species and excicotoxicity which might compromise the survival of the cellular implant or counteract the effects of the applied substances. This could be overcome by treating chronically hypoperfused mice with anti- inflammatory, anti- oxidative and/ or anti- excitotoxic agents prior to any other intervention (e.g. cellular graph/ pharmacological stimulation of endogenous stem cells). However, blocking these molecular processes, might impact on the proliferation capacity of both exogenously applied and endogenous progenitor cells as inflammatory, oxidative and neutrotransmitter signals have been shown to regulate neural migration and differentiation during neurodevelopment as well as in the presence of pathology.

Fourth, there are inter- individual differences in the observed pathological profile in chronically hypoperfused mice. For this type of heterogenous pathology, it is particularly challenging to develop universal cellular therapies and a patient- specific approach might be more appropriate.

Therefore, although promising, cellular therapies might be difficult to optimize and apply in this animal model as well as in human patients with chronic cerebral hypoperfusion at least in the near future.

6.1.5. Future application of the microcoils surgery on genetically modified mice

One of the major advantages of the new mouse model of chronic cerebral hypoperfusion compared with the alternative rat and gerbil models consists of the potential application of

the microcoils surgery on genetically modified animals allowing to address in pre- clinical settings the individual and combined effects of cerebrovasculr (e.g. chronic cerebral hypoperfusion) and molecular (e.g. APOE) factors on neuropathology and functional outcome.

There is increasing evidence suggesting the presence of cerebrovascular pathology in Alzheimer`s dementia (Iadecola, 2010). The neurovascular hypothesis of Alzheimer`s disease (Zlokovic, 2005; Roman and Kalaria, 2006; Bell and Zlokovic, 2009) suggests that faulty clearance of Aβ across the blood brain barrier, aberrant angiogenesis and senescence of the cerebrovascular system could initiate neurovascular uncoupling, vessel regression, brain hypoperfusion and neurovascular inflammation. Ultimately, this would lead to blood brain barrier disruption accompanied by chemical imbalance in the neuronal environment and to synaptic and neuronal dysfunction, injury and loss.

A few groups have recently applied the microcoils surgery on APP transgenic mice to address the role of cerebral hypoperfusion in familial Alzheimer`s dementia. Kitaguchi et al., 2009 demonstrated that chronic cerebral hypoperfusion accelerates the deposition of Aβ in APP transgenic mice bearing both the Swedish and Indiana familial human APP mutations. In these mice, Yamada et al., 2011 showed that the microcoils surgery impairs performance on a Barnes maze and is associated with impaired Aβ metabolism. Taken together these animal findings suggest that chronic cerebral hypoperfusion might accelerate the development of familial Alzheimer`s disease in humans. However, future research is required to further characterize the molecular and cellular pathways leading to the observed neuropathology and functional impairment in this animal model of dementia.

As previously discussed in this thesis, human APOE allelic polymorphism is the major known genetic risk factor for the occurrence of age- related neurodegeneration, cerebrovascular pathology and cognitive impairment (Saunders et al., 1993; Kalmijn et al., 1996; Skoog et al., 1998; Reiman et al., 1996; Reiman et al., 2004; Schuff et al., 2009b; Nicoll et al., 1995; Gromadzka et al., 2007; Wagle et al., 2009). The present thesis partially addressed APOE effects on neuropathology following chronic cerebral hypoperfusion in mice (Chapter 4). However, in order to better approach the human condition, future research should focus on comparing the effects of human APOE3 and

APOE4 isoforms on neuropathology and functional outcome under normal physiological and chronically hypoperfused conditions in transgenic mice (Sheng et al., 1998; Buttini et al., 1999; Buttini et al., 2000; Fryer et al., 2005). Based on previous reports, the initial expectations are that the presence of the human APOE4 allele would be associated with the development of more severe neuropathology and cognitive deficits in hypoperfused mice (Sheng et al., 1998; Buttini et al., 2000; Fryer et al., 2005).

Further, cerebral blood flow reductions and white matter pathology are also evident in other non age- related neurodegenerative and psychiatric disorders (e.g. Huntington` s disease, schizophrenia) (Goldberg et al., 1990; Lim et al., 1999; Rosas et al., 2006) and the microcoils surgery could be applied on existing mouse models of these conditions in order to examine the effects of hypoperfusion on neuropathology and functional outcome.

6.2. Summary

The present thesis provided a behavioural, neuropathological, genetic and epigenetic characterization of a new mouse model of chronic cerebral hypoperfusion opening novel directions for future experimental work leading to the potential development of therapeutic strategies for age- related cognitive decline.

References

Abdolmaleky, H.M., Smith, C.L., Faraone, S.V., Shafa, R., Stone, W., Glatt, S.J., Tsuang, M.T., (2004). Methylomics in psychiatry: modulation of gene–environment interactions may be through DNA methylation. *Am. J. Med. Genet. B: Neuropsychiatr. Genet.* **127B,** 51–59.

Abe, K., Yamashita, T., Takizawa, S., Kuroda, S., Kinouchi, H., Kawahara, N. (2012). Stem cell therapy for cerebral ischemia: from basic science to clinical applications. *J. Cereb. Blood Flow Metab.* **32**, 1317–1331.

Aberg, K., Saetre, P., Jareborg N., Jazin, E. (2006). Human QKI, a potential regulator of mRNA expression of human oligodendrocyte- related genes involved in schizophrenia. *Proc. Natl. Acad. Sci.USA.* **103**, 7482–7487.

Aboul- Enein, F., Rauschka, H., Kornek, B., Stadelmann, C., Stefferl, A., Bruck, W., Lucchinetti, C., Schmidbauer, M., Jellinger, K., Lassmann, H. (2003). Preferential loss of myelin-associated glycoprotein reflects hypoxia-like white matter damage in stroke and inflammatory brain diseases. *J. Neuropathol. Exp. Neurol.* **62**, 25-33.

Abraham, H., Lazar, G. (2000). Early microglial reaction following mild forebrain ischemia by common carotid artery occlusion in rats. *Brain Res.* **862**, 63-73.

Adelmann, G., Deller, T., Frotscher, M. (1996). Organization of identified fiber tracts in the rat fimbria-fornix: an anterograde tracing and electron microscopic study. *Anat. Embryol*. **193**, 491-493.

Adolfsson, R., Gottfries,C.G., Roos, B.E., Winblad, B. (1979). Changes in the brain catecholamines in patients with dementia of Alzheimer type. *B. J. Psychiatr.* **135**, 216-223.

Alafuzoff, I., Helisalmi, S., Mannermaa, A., Soininen, H. (2000). Severity of cardiovascular disease, apolipoprotein E genotype, and brain pathology in aging and dementia. *Annal. NY Acad. Sci.* **903**, 244-251.

Allegretta, M., Nicklas, J.A., Sriram, S., Albertini, R.J. (1990). T cells responsive to myelin basic protein in patients with multiple sclerosis. *Science.* **247**, 718-721.

Amir, R.E., Van den Veyver, I.B., Wan, M., Tran, C.Q., Francke, U., Zoghbi, H.Y. (1999). Rett syndrome is caused by mutations in X- linked MECP2, encoding methyl-CpG- binding protein 2. *Nat. Genet.* **23**, 185-188.

Anderson, J.M., Hubbard, B.M., Coghill, G.R., Slidders, W. (1983). The effect of advanced old age on the neuron content of the cerebral cortex. Observations with an automatic image analyser point counting method. *J. Neurol. Sci.* **58**, 235-246.

Andrews, T.J., Halpern, S.D., Purves, D. (1997). Correlated size variations in human visual cortex, lateral geniculate nucleus, and optic tract. *J. Neurosci.* **17**, 2859-2868.

Aono, M., Lee, Y., Grant, E.R., Zivin, R.A., Pearlstein, R.D., Warner, D.S., Bennett, E.R., Laskowitz, D.T. (2002). Apolipoprotein E protects against NMDA excitotoxicity. *Neurobiol Dis.* **11**, 214-220.

Aono, M., Bennett, E.R., Kim, K.S., Lynch, J.R., Myers, J., Pearlstein, R.D., Warner, D.S., Laskowitz, D.T. (2003). Protective effect of apolipoprotein E-mimetic peptides on N-methyl-D-aspartate excitotoxicity in primary rat neuronal-glial cell cultures. *Neurosci.* **116**, 437-445.

Ariza, M., Pueyo, R., del M Martin, M., Junque, C., Mataro, M., Clemente, I., Moral, P., Poca, M.A., Garnacho, A., Sahuquillo, J. (2006). Influence of APOE polymorphism on cognitive and behavioural outcome in moderate and severe traumatic brain injury. *J. Neurol. Neurosurg. Psychiatry*. **77**, 1191-1193.

Arnsten, A.F.T., Goldman- Rakic, P.S. (1985). Catecholamines and cognitive decline in aged nonhuman primates. *Ann. N.Y. Acad. Sci.* 218-234.

Arnsten, A.F.T. (1998). Catecholamine modulation of prefrontal cortical cognitive function. *Trends Cogn. Sci.* **2**, 436-447.

Augustinack, J.C., Helmer, K., Huber, K.E., Kakunoori, S., Zoller, L., Fischl, B. (2010). Direct visualization of the perforant pathway in the human brain with ex vivo diffusion tensor imaging. *Front. Hum. Neurosci.* **24**, 1-13.

Auten, R.L., Davis, J.M. (2009). Oxygen toxicity and reactive oxygen species: the devil is in the details. *Pediatr. Res.* **66**, 121-127.

Backdahl, L., Bushell, A., Beck, S. (2009). Inflammatory signaling as mediator of epigenetic modulation in tissue- specific chronic inflammation. *Int. J. Biochem. Cell Biol.* **41**, 176-184.

Bacskai, B.J., Xia, M.Q., Strickland, D.K., Rebeck, G.W., Hyman, B.T. (2000). The endocytic receptor protein LRP also mediates neuronal calcium signaling via N-methyl-D-aspartate receptors. *Proc. Natl. Acad. Sci .USA.* **97**, 11551-11556.

Baddeley, A. (1992). Working memory. *Science.* **31**, 556- 559.

Bakiri, Y., Burzomato, V., Frugier, G., Hamilton, N.B., Karadottir, R., Attwell, D. (2009). Glutamatergic signaling in the brain` s white matter. *Neurosci.* **158**, 266-274.

Baltan, S., Besancon, E.F., Mbow, B., Ye, Z.C., Hammer, M.A., Ransom, B.R. (2008). White matter vulnerability to ischemic injury increases with age because of enhanced excitotoxicity. *Neurobiol. Dis.* **28**, 1479-1489

Baron, J.C., von Kummer, R., del Zoppo, G.J. (1995). Treatment of acute ischemic stroke challenging the concept of a rigid and universal time window. *Stroke.* **26**, 2219-2221.

Bartzokis, G. (2003). White matter structural integrity in healthy aging adults and patients with Alzheimer`s disease. *Arch. Neurol.* **60**, 393-398.

Bartzokis, G. (2004). Age-related myelin breakdown: a developmental model of cognitive decline and Alzheimer's disease. *Neurobiol. Aging.* **25**, 5–18.

Bartzokis, G., Lu, P.H., Geschwind, D.H., Edwards, N., Mintz, J., Cummings, J.L. (2006). Apolipoprotein E genotype and age- related myelin breakdown in healthy individuals. *Arch. Gen. Psychiatry.* **63**, 63-72.

Bartzokis, G., Lu, P.H., Geschwind, D.H., Tingus, K., Huang, D., Mendez, M.F., Edwards, N., Mintz, J. (2007). Apolipoprotein E affects both myelin breakdown and cognition: implication for age- related trajectories of decline into dementia. *Biol. Psychiatry.* **62**, 1380-1387.

Basser, P.J. (1995). Inferring microstructural features and the pathophysiological state of tissues from diffusion- weighted images. *NMR Biomed.* **18**, 333-344.

Bastin, M.E., Clayden, J.D., Pattie, A., Gerrish, I.F., Wardlaw, J.M., Deary, I.J. (2009). Diffusion tensor and magnetization transfer MRI measurements of periventricular white matter hyperintensities in old age. *Neurobiol. Aging.* **30**, 125-136.

Baumann, N., Pham- Dihn, D. (2001). Biology of oligodendrocytes and myelin in the mammalian central nervous system. *Physiol. Rev.* **81**, 871-926.

Beaulieu, C. (2002) The basis of anisotropic water diffusion in the nervous system—a technical review. *NMR Biomed.* **15**, 435–455.

Bechtold, D.A., Kapoor, R., Smith, K.J. (2004). Axonal protection using flecainide in experimental autoimmune encephalomyelitis. *Ann. Neurol.* **55**, 607–616.

Beeri, M.S., Rapp, M., Silverman, J.M., Schmeidler, J., Grossman, H.T., Fallon, J.T., Purohit, D.P., Perl, D.P., Siddiqui, A., Lesser, G., Rosendorff, C., Haroutunian, V. (2006). Coronary artery disease is associated with Alzheimer disease neuropathology in APOE4 carriers. *Neurology.* **66**, 1399- 1404.

Bell, R.D., Zlokovic, B.V. Neurovascular mechanisms and blood–brain barrier disorder in Alzheimer's disease. *Acta Neuropathol.* **118**, 103–113.

Bellini, T, Rippa, M., Matteuzzi, M., Dallocchio, F. (1986). A rapid method for purification of myelin basic protein. *J. Neurochem.* **46,** 1644-1646.

Bimonte, H.A., Nelson, M.E., Granholm, A.C.E. (2003). Age-related deficits as working memory load increases: relationships with growth factors. *Neurobiol. Aging.* **24**, 37–48.

Bird, A.P., Wolffe, A.P. (1999). Methylation- induced repression- belts, braces, and chromatin. *Cell.* **99**, 451-454.

Bird, A. (2002). DNA methylation patterns and epigenetic memory. *Genes Dev.* **16**, 6-21.

Bitsch, A., Schuhardt, J., Bunkowski, S., Kuhlmann, T., Bruck, W. (2000). Acute axonal injury in multiple sclerosis. Correlation with demyelination and inflammation. *Brain.***123**, 1174-1183.

Bjorkhem, I., Heverin, M., Leoni, V., Meaney, S., Diczfalusy, U. (2006). Oxysterols and Alzheimer`s disease. *Acta Neurol. Scand. Suppl.* **185**, 43- 49.

Blesch, A. (2006). Neurotrophic factors in neurodegeneration. *Brain Pathol.* **16**, 295–303.

Blezer, E.L.A., Bauer, J., Brok, H.P.M., Nicolay, K., Hart, BA`t (2007). Quantitative MRI- pathology correlations of brain white matter lesions developing in a non- human primate model of multiple sclerosis. *NMR Biomed.* **20,** 90-103.

Bloom, J.S., Hynd, G.W. (2005). The role of the corpus callosum in the interhemispheric transfer of information: excitation or inhibition? *Neuropsych. Rev.* **15**, 59-71.

Boje, K.M., Arora, P.K. (1992). Microglial-produced nitric oxide and reactive nitrogen oxides mediate neuronal cell death. *Brain Res.* **587**, 250-256.

Bookheimer, S.Y., Strojwas, M.H., Cohen, M.S., Saunders, A.M., Pericak- Vance, M.A., Mazziotta, J.C., Small, G.W. (2000). Patterns of brain activation in people at risk for Alzheimer`s disease. *N. Engl. J. Med.* **343**, 450-456.

Boschert, U., Merlo-Pich, E., Higgins, G., Roses, A.D., Catsicas, S. (1999). Apolipoprotein E expression by neurons surviving excitotoxic stress. *Neurobiol. Dis.* **6**, 508-514.

Boyles, J.K., Pitas, R.E., Wilson, E., Mahley, R.W., Taylor, J.M. (1985). Apolipoprotein E associated with astrocytic glia of the central nervous system and with non- myelinating glia of the peripheral nervous system. *J. Clin. Invest.* **76**, 1501-1513.

Boyles, J.K., Zoeliner, C.D., Anderson, L.J., Kosik, L.M., Pitas, R.E., Weisgraber, K.H., Hui, D.Y., Mahley, R.W., Gebicke- Haerter, P.J., Ignatius, M.J., Shooter, E.M. (1989). A role of apolipoprotein E, apolipoprotein A-I, and low density lipoprotein receptors in cholesterol transport during regeneration and remyelination of the rat sciatic nerve. *J. Clin. Invest.* **83**, 1015-1031.

Bozzali, M., Falini, A., Franceschi, M., Cercignani, M., Zuffi, M., Scotti, G., Comi, G., Filippi, M. (2002). White matter damage in Alzheimer's disease assessed in vivo using diffusion tensor magnetic resonance imaging. *J. Neurol. Neurosurg. Psych.* **72**, 742-746.

Braughler, J.M., Duncan, L.A., Chase, R.L. (1986). The involvement of iron in lipid peroxidation. *J. Biol. Chem.* **261**, 10282-10289.

Bronge, L., Bogdanovic, N., Wahlund, L-O. (2002). Postmortem MRI and histopathology of white matter changes in Alzheimer brains. *Dement. Geriatr. Cogn. Disord.* **13**, 205-212.

Brown, W.R., Moody, D.M., Thore, C.R., Challa, V.R. (2000). Cerebrovascular pathology in Alzheimer's disease and leukoaraiosis. *Annal. NY Acad. Sci.* **903**, 39-45.

Buki, A., Povlishock, J.T. (2006). All roads lead to disconnection? – Traumatic axonal injury revisited. *Acta Neurochir. (Wien).* **148**, 181–194.

Buttini, M., Orth, M., Bellosta, S., Akeefe, H., Pitas, R.E., Wyss- Coray, T., Mucke, L., Mahley, R.W. (1999). Expression of human apolipoprotein E3 or E4 in the brains of *Apoe*-/- mice: isoform-specific effects on neurodegeneration. *J. Neuroscie.* **19**, 4867-4880.

Buttini, M., Akeefe, H., Lin, C., Mahley, R.W., Pitas, R.E., Wyss- Coray, T., Mucke, L. (2000). Dominant negative effects of apolipoprotein E4 revealed in transgenic models of neurodegenerative disease. *Neurosci.* **97**, 207–210.

Calabrese, P. (2006). Neurpsychology of multiple sclerosis. *J. Neurol.* **253**, i10-i15.

Caldwell, J.H., Schaller, K.L., Lasher, R.S., Peles, E., Levinson, S.R. (2000). Sodium channel Nav1.6 is localized at nodes of Ranvier, dendrites, and synapses. *Proc. Nat. Acad. Sci.* **97**, 5616-5620.

Calza, L., Fernandez, M., Giardino, L. (2010). Cellular approaches to central nervous system remyelination stimulation: thyroid hormone to promote myelin repair via endogenous stem and precursor cells. *J. Mol. Endocrinol.* **44**, 13–23.

Cannon, S.V., Cummings, A. Teebor, G.W. (1988). 5- Hydroxymethylcytosine DNA glycosylase activity in mammalian tissue. *Biochem. Biophys. Res. Commun.* **151**, 1173-1179.

Cassel, S., Carouge, D., Gensburger, C., Anglard, P., Burgun, C., Dietrich, J-B., Aunis, D., Zwiller, J. (2006). Fluoxetine and cocaine induce the epigenetic factors MeCP2 and MBD1 in adult rat brain. *Mol. Pharmacol.* **70**, 487–492.

Cazevieille, C., Muller, A., Meynier, F., Bonne, C. (1993). Superoxide and nitric oxide cooperation in hypoxia/reoxygenation- induced neuron injury. *Free Radical Biol. Med.* **14**, 389-395.

Cerda, S., Weitzman, S.A. (1997). Influence of oxygen radical injury on DNA methylation. *Mut. Res.* **386**, 141-152.

Chaerkady, R., Letzen, B., Renuse, S., Sahasrabuddhe, N.A., Kumar P., All, A.H., Thakor, N.V., Delanghe, B., Gearhart, J.D., Pandey, A., Kerr, C.L. (2011). Quantitative temporal proteomic analysis of human embryonic stem cell differentiation into oligodendrocyte progenitor cells. *Proteomics.* **11**, 4007–4020.

Champagne, D., Rochford, J., Poirier, J. (2005). Effect of apolipoprotein deficiency on reactive sprouting in the dentate gyrus of the hippocampus following entorhinal cortex lesion: role of the astroglial response. *Exp. Neurol.* **194**; 31-42.

Chang, A., Nishiyama, A., Peterson, J., Prineas, J., Trapp, B.D. (2000). NG2- positive oligodendrocyte progenitor cells in adult human brain and multiple sclerosis lesions. *J. Neurosci.* **20**, 6404-6412.

Chao, C.C., Hu, S., Molitor, T.W., Shaskan, E.G., Peterson, P.K. (1992). Activated microglia mediate neuronal cell injury via nitric oxide mechanism. *J. Immunol.* **149**, 2736-2741.

Charlton, R.A., Barrick, T.R., McIntyre, D.J., Shen, Y., O`Sullivan, M., Howe, F.A., Clark, C.A., Morris, R.G., Markus, H.S. (2006). White matter abnormalities on diffusion tensor imaging correlates with age-related cognitive decline. *Neurology*. **66**, 217-222.

Chaturvedi, S., Bruno, A., Feasby, T., Holloway, R., Benavente, O., Cohen, S.N., Cohen, S.N., Cote, R., Hess, D., Saver, J., Spence, J.D., Stern, B., Wilterdink, J. (2005). Therapeutics and Technology Assessment Subcommittee of the American Academy of Neurology. Carotid endarterectomy- an evidence- based review: report of the Therapeutics and Technology Assessment Subcommittee of the American Academy of Neurology. *Neurology*. **65**, 794-801.

Chen, Y., Lomnitski, L., Michaelson, D.M., Shohami, E. (1997). Motor and cognitive deficits in apolipoprotein E-deficient mice after closed head injury. *Neuroscience* **80**, 1255–1262.

Chen, G., Chen, K.S., Knox, J., Inglis, J., Bernard, A., Martin, S.J., Justice, A., McConlogue, L., Games, D., Freedman, S.B., Morris, R.G.M. (2000). A learning deficit related to age and β- amyloid plaques in a mouse model of Alzheimer` s disease. *Nature.* **408,** 975- 979.

Chen, J., Buchanan, J.B., Sparkman, N.L., Godbout, J.P., Freund, G.G., Johnson, R.W. (2008). Neuroinflammation and disruption in working memory in aged mice after acute stimulation of the peripheral innate immune system. *Brain Behav. Immunity.* **22**, 301–311.

Chen, H., Dzitoyeva, S., Manev, H. (2012). Effect of aging on 5-hydroxymethylcytosine in the mouse hippocampus. *Restor. Neurol. Neurosci.* **30**, 237–245.

Chiang, M-F., Chang, J-G., Hu, C-J. (2003). Association between apolipoprotein E genotype and outcome of traumatic brain injury. *Acta Neuropathol.* **145**, 649-654.

Choi, D.W. (1990). The role of glutamate neurotoxicity in hypoxic- ischemic neuronal death. *Annu. Rev. Neurosci.* **13**, 171-182.

Choi, J., Foster, M.J., McDonald, S.R., Weintraub, S.T., Carroll, C.A., Gracy, R.W. (2004). Proteomic identification of specific oxidized proteins in ApoE-knockout mice: relevance to alzheimer's disease. *Free Radical Biol. Med.* **36,** 1155-1162.

Chouliaras, L., Rutten, B.P.F., Kenis, G., Peerbooms, O., Visser, P.J., Verhey, F., van Os, J., Steinbusch, H.W.M., van den Hove, D.L.A. (2010). Epigenetic regulation in the pathophysiology of Alzheimer's disease. *Prog.Neurobiol.* **90**, 498–510.

Choy, M., Ganesan, V., Thomas, D.L., Thornton, J.S., Proctor, E., King, M.D., van der Weed, L., Gadian, D.G., Lythgoe, M.F. (2006). The chronic vascular and haemodynamic response after permanent bilateral common carotid occlusion in newborn and adult rats. *J. Cereb. Blood Flow Metab.* **26**, 1066-1075.

Clark, R.S.B., Kochanek, P.M., Watkins, S.C., Chen, M., Dixon, C.E., Seidberg, N.A., Melick, J., Loeffert, J.E., Nathaniel, P.D., Jin, K.L., Graham, S.H. (2000). Caspase-3 mediated neuronal death after traumatic brain injury in rats. *J. Neurochem.* **74,** 740–753.

Clarke, J.M., Zaidel, E. (1994). Anatomical-behavioral relationships: corpus callosum morphometry and hemispheric specialization. *Behav. Brain Res.* **64**, 185-202.

Coetzee, T., Fujita, N., Dupree, J., Shi, R., Blight, A., Suzuki, K., Suzuki, K., Popko, B. (1996). Myelination in the absence of galactocerebroside and sulfatide: normal structure with abnormal function and regional instability. *Cell.* **86**, 209-219.

Cohen, R.M., Small, C., Lalonde, F., Friz, J., Sunderland, T. (2001). Effect of apolipoprotein E genotype on hippocampal volume loss in aging healthy women. *Neurol*. **57**, 2223- 2228.

Coltman, R., Spain, A., Tsenkina, Y., Fowler, J.H., Smith, J., Scullion, G., Allerhand, M., Scott, F., Kalaria, R.N., Ihara, M., Daumas, S., Deary, I.J., Wood, E., McCulloch, J., Horsburgh, K. (2011). Selective white matter pathology induces selective impairment in spatial working memory. *Neurobiol Aging.* **32**. 2324.e7–2324.e12.

Colton, C.A., Brown, C.M., Cook, D., Needham, L.K., Xu, Q., Czapiga, M., Saunders, A.M., Schmechel, D.E., Rasheed, K., Vitek, M.P. (2002). APOE and the regulation of microglial nitric oxide production a link between genetic risk and oxidative stress. *Neurobiol. Aging.* **23**, 777-785.

Cook, I.A., Bookheimer, S.Y., Mickes, L., Leuchter, A.F., Kumar, A. (2007). Aging and brain activation with working memory tasks: an fMRI study of connectivity. *Int. J. Geriatr. Psychiatry.* **22**, 332-342.

Cooper, J.A., Howell, B.W. (1999). Lipoprotein receptors: signaling functions in the brain? *Cell.* **97**, 671-674.

Corbin, J.G., Kelly, D., Rath, E.M., Baerwald, K.D., Suzuki, K., Popko, B. (1996). Targeted CNS expression of interferon- γ in transgenic mice leads to hypomyelination, reactive gliosis, and abnormal cerebellar development. *Mol. Cell Neurosci.* **7**, 354-370.

Couffinhal, T., Silver, M., Kearney, M., Sullivan, A., Witzenbichler, B., Magner, M., Annex, B., Peters, K., Isner, J.M. (1999). Impaired collateral vessel development associated with reduced expression of vascular endothialial growth factor in ApoE-/- mice. *Circulation.* **99**, 3188-3198.

Craner, M.J., Hains, B.C., Lo, A.C., Black, J.A., Waxman, S.G. (2004). Co-localization of sodium channel Nav1.6 and the sodium±calcium exchanger at sites of axonal injury in the spinal cord in EAE. *Brain.* **127**, 294-303.

Cummings, B. J., Head, E., Ruehl, W., Milgram N. W., Cotman C. W. (1996). The canine as an animal model of human aging and dementia. *Neurobiol. Aging.* **17**, 259–268.

Curtis, M.A., Penney, E.B., Pearson, A.G., van Roon- Mom, W.M.C., Butterworth, N.J., Dragunow, M., Connor, B., Faull, R.L.M. (2003). Increased cell proliferation and neurogenesis in the adult human Huntington's disease brain. *Proc. Natl. Acad. Sci. USA.* **100**, 9023-9027.

D`Ambrosio, A.L., Pinsky, D.J., Connolly, E.S. (2001). The role of the complement cascade in ischemia/reperfusion injury: implications for neuroprotection. *Mol. Med.* **7**, 367–382.

D`Arceuil, H.E., Westmoreland, S., de Crespigny, A.J. (2007). An approach to high resolution diffusion tensor imaging in fixed primate brain. *NeuroImage.* **35**, 553-565.

Das, K.P., McMillian, M.K., Bing, G., Hong, J.S. (1995). Modulatory effects of [Met5]-enkephalin on interleukin-1 secretion from microglia in mixed brain cell cultures. *J Neuroimmunol.* **62,** 9–17.

Davie, C.A., Barker, G.J., Webb, S., Tofts, P.S., Thompson, A.J., Harding, A.E., McDonald, W.I., Miller, D.H. (1995). Persistent functional deficit in multiple sclerosis and autosomal dominant cerebellar ataxia is associated with axon loss. *Brain.* **118,** 1583-1592.

Davis, P.S., Mirra, S.S., Alazraki, N. (1994). The brain in older persons with and without dementia: findings on MR, PET, and SPECT images. *AJR.* **162**, 1267-1278.

Deary, I.J., Leaper, S.A., Murray, A.D., Staff, R.T., Whalley, L.J. (2003). Cerebral white matter abnormalities and lifetime cognitive change: a 67-year follow-up of the Scottish Mental Survey of 1932. *Psychol. Aging*. **18**; 140-148.

de Bortoli, V.C., Tangrossi Junior, H., de Aguiar Correa, F.M., Almeida Side, S., de Oliviera, A.M. (2005). Inhibitory avoidance memory retention in the elevated T-maze is impaired after perivascular manipulation of the common carotid arteries. *Life Sci.* **76**, 2103-2114.

de Groot, C.J., Hulshof, S., Hoozemans, J.J., Veerhuis, R. (2001) Establishment of microglial cell cultures derived from postmortem human adult brain tissue: immunophenotypical and functional characterization. *Microsc. Res. Tech.* **54**, 34–39.

de Jong, G.I., de Weerd, H., Schuurman, T., Traber, J., Luiten, P.G.M. (1990). Microvascular changes in aged rat forebrain. Effects of chronic nimodipine treatment. *Neurobiol. Aging.* **11**, 381–389.

de Jong, G.I., Farkas, E., Stienstra, C.M., Plass, J.R.M., Keuser, J.N., de la Torre, J.C., Luiten, P.G.M. (1999). Cerebral hypoperfusion yields capillary damage in the hippocampal CA1 area that correlates with spatial memory impairment. *Neuroscience.* **91**, 203-210.

de la Torre, J.C., Pappas, B.A., Prevot, V., Emmerling, M.R., Mantione, K., Fortin, T., Watson, M.D., Stefano, G.B., (2003). Hippocampal nitric oxide upregulation precedes memory loss and A beta 1–40 accumulation after chronic brain hypoperfusion in rats. *Neurol. Res.* **25**, 635–641.

de Leeuw, F-E., de Groot, J.C., Bots, M.L., Witteman, J.C.M., Oudkerk, M,., Hofman, A., van Gijn, J., Breteler, M.M.B. (2000). Carotid atherosclerosis and cerebral white matter lesions in a population based magnetic resonance imaging study. *J. Neurol.* **247**, 291-296.

Derdeyn, C.P., Videen, T.O., Fritsch, S.M., Carpenter, D.A., Grubb Jr, R.L., Powers, W.J. (1999). Compensatory mechanisms for chronic cerebral hypoperfusion in patients with carotid occlusion. *Stroke.* **30**, 1019-1024.

de Vries, H., Hoekstra, D. (2000). On the biogenesis of the myelin sheath: Cognate polarized trafficking pathways in oligodendrocytes. *Glycoconj. J.* **17**, 181-190.

de Weijer, A.D., Mandl, R.C.W., Diederen, K.M.J., Neggers, S.F.W., Kahn, R.S., Hulshoff Pol, H.E., Sommer, I.E.C. (2011). Microstructural alterations of the arcuate fasciculus in schizophrenia patients with frequent auditory verbal hallucinations. *Schizophrenia Res.* **130**, 68–77.

de Wilde, M.C., Farkas, E., Gerrits, M., Kiliaan, A.J., Luiten, P.G.M. (2002). The effect of n-3 polyunsaturated fatty acid-rich diets on cognitive and cerebrovascular parameters in chronic cerebral hypoperfusion. *Brain Res.* **947**, 166–173.

Dhenain, M., Delatour, B., Walczac, C., Volk, A. (2006). Passive staining: a novel ex vivo MRI protocol to detect amyloid deposits in mouse models of Alzheimer's disease. *Magn. Res. Med.* **55**, 687-693.

D`Hooge, R., De Deyn, P.P. (2001). Applications of the Morris water maze in the study of learning and memory. *Brain Res. Rev.* **36**, 60–90.

Dickson, D.W., Crystal, H.A., Mattiace, L.A., Masur, D.M., Blau, A.D., Davies, P., Yen, S-H., Aronson, M.K. (1991). Identification of normal and pathological aging in prospectively studied nondemented elderly humans. *Neurobiol. Aging.* **13**, 179- 189.

Diemel, L.T., Copelman, C.A., Cuzner, M.L. (1998). Macrophages in CNS remyelination : friends or foe? *Neurochem. Res.* **23**, 341-347.

Dietschy, J.M., Turley, S.D. (2001). Cholesterol metabolism in the brain. *Curr. Opin. Lipidol.* **12**, 105- 112.

Dopp, J.M., Mackenzie- Graham, A., Otero, G.C., Merrill, J.E. (1997). Differential expression, cytokine modulation, and specific functions of type- 1 and type- 2 tumor necrosis factor receptors in rat glia. *J. Neuroimmunol.* **75**, 104-112.

Dougherty, K.D., Dreyfus, C.F., Black, I.B. (2000). Brain- derived neurotrophic factor in astrocytes, oligodendrocytes, and microglia/ macrophages after spinal cord injury. *Neurobiol. Dis.* **7**, 574-585.

Drzezga, A., Lautenschlager, N., Siebner, H., Riemenschneider, M., Willoch, F., Minoshima, S., Schwaiger, M., Kurz, A. (2003) Cerebral metabolic changes accompanying conversion of mild cognitive impairment into Alzheimer's disease: a PET follow-up study. *Eur. J. Nucl. Med. Mol. Imaging.* **30**, 1104–1113.

Duan, W., Ladenheim, B., Cutler, R.G., Kruman, I.I., Cadet, J.L., Mattson, M.P. (2002). Dietary folate deficiency and elevated homocysteine levels endanger dopaminergic neurons in Parkinson`s disease. *J. Neurochem.* **80**, 101-110.

Duan, H., Wearne, S.L., Rocher, A.B., Macedo, A., Morrison, J.H., Hof, P.R. (2003). Age-related dendritic and spine changes in corticocortically projecting neurons in macaque monkeys. *Brain.* **13**, 950-961.

Dupouey, P., Jacque, C., Bourre, J.M., Cesselin, F., Privat, A., Baumann, N. (1979). Immunochemical studies of myelin basic protein in shiverer mouse devoid of major dense line of myelin. *Neurosci. Lett.* **12**, 113-118.

Dutta, R., Trapp, B.C. (2007). Pathogenesis of axonal and neuronal damage in multiple sclerosis. *Neurol.* **68**, S22-S31.

Dzitoyeva, S., Chen, H., Manev, H. (2012). Effect of aging on 5-hydroxymethylcytosine in brain mitochondria. *Neurobiol. Aging.* (in press)

Egashira, T., Takayama, F., Yamanaka, Y. (1996). Effects of bifemelane on muscarinic receptors and choline acetyltransferase in the brains of aged rats following chronic cerebral hypoperfusion induced by permanent occlusion of bilateral carotid arteries. *Jpn. J. Pharmacol.* **72**, 57–65.

Eliasson, M.J.L., Huang, Z., Ferrante, R.J., Sasamata, M., Molliver, M.E., Snyder, S.H., Moskowitz, M.A. (1999). Neuronal nitric oxide synthase activation and peroxynitrite formation in ischemic stroke linked to neural damage. *J. Neurosci.* **19**, 5910–5918.

Elosua, R., Ordovas, J.M., Cupples, L.A., Fox, C.S., Polak, J.F., Wolf, P.A., D`Agostino, R.A., O`Donnell, C.J. (2004). Association of APOE genotype with carotid atherosclerosis in men and women: The Farmingham Heart Study. *J. Lipid Res.* **45**, 1868-1875.

Elshourbagy, N.A., Liao, W.S., Mahley, R.W., Taylor, J.M. (1985). Apolipoprotein E mRNA is abundant in the brain and adrenals, as well as in the liver, and is present in other peripheral tissues of rats and marmosets. *Proc. Natl. Acad. Sci. USA.* **83,** 203-207.

Endres, M., Meisel, A., Biniszkiewicz, D., Namura, S., Prass, K., Ruscher, K., Lipski, A., Jaenisch, R., Moskowitz, M.A., Dirnagl, U. (2000). DNA methylatransferase contributes to delayed ischemic brain injury. *J. Neurosci.* **20**, 3175-3181.

Endres, M., Fan, G., Meisel, A., Dirnagl, U., Jaenisch, R. (2001). Effects of cerebral ischemia in mice lacking DNA methyltransferase I in post- mitotic neurons. *Clin. Neurosci. Neuropath*. **12**, 3763-3766.

England, T., Martin, P., Bath, P.M.W. (2009). Stem cells for enhancing recovery after stroke: a review. *Int. J. Stroke*. **4**, 101–110.

Englund, E., Sjobeck, M., Brockstedt, S., Latt, J., Larsson, E-M. (2004). Diffusion tensor MRI post mortem demonstrated cerebral white matter pathology. *J. Neurol.* **251**, 350-352.

Ergorul, C., Eichenbaum, H. (2004). The hippocampus and memory for "What", "Where", and "When". *Learning Mem.* **11**, 397-405.

Esiri, M.M. (2007). Aging and the brain. *J. Pathol.* **211**, 181–187.

Faraco, G., Pancani, T., Formentini, L., Mascagni, P., Fossati, G., Leoni, F., Moroni, F., Chiarugi, A. (2006). Pharmacological Inhibition of Histone Deacetylases by Suberoylanilide Hydroxamic Acid Specifically Alters Gene Expression and Reduces Ischemic Injury in the Mouse Brain. *Mol. Pharmacol.* **70**, 1876-1884.

Farkas, E., Luiten, P.G.M., (2001). Cerebral microvascular pathology in aging and Alzheimer's disease. *Prog. Neurobiol.***64**, 575–611.

Farkas, E., Donka, G., de Vos, R.A.I., Mihaly, A., Bari, F., Luiten, P.G.M. (2004). Experimental cerebral hypoperfusion imposes white matter injury and microglial activation in the rat brain. *Acta Neuropathol. (Berl.).* **108**, 57-64.

Farkas, E., de Vos, R.A.I., Donka, G., Steur, E.N.J., Mihaly, A., Luiten, P.G.M. (2006). Age- related microvascular degeneration in the human cerebral periventricular white matter. *Acta Neuropathol.* **111**, 150-157.

Farkas, E., Luiten, P.G.M., Bari, F. (2007). Permanent, bilateral common carotid artery occlusion in the rat: a model for chronic cerebral hypoperfusion- related neurodegenerative disease. *Brain Res. Rev.* **54**, 162-180.

Fazekas, F., Enzinger, C., Ropele, S., Schmidt, H., Schmidt, R., Strasser- Fuchs, S. (2005). The impact of our genes: c.onsequences of the apolipoprotein E polymorphism in Alzheimer disease and multiple sclerosis. *J. Neurol. Sci.* **245**, 35-39.

Fernando, M.S., Simpson, J.E., Matthews, F., Brayne, C., Lewis, C.E., Barber, R., Kalaria, R.N., Forster, G., Esteves, F., Wharton, S.B., Shaw, P.J., O' Brien, J.T., Ince, P.G. (2006). White matter lesions in an unselected cohort of the elderly: molecular pathology suggests origin from chronic hypoperfusion injury. *Stroke.* **37**, 1391-1398.

Ficz, G., Branco, M.R., Seisenberger, S., Santos, F., Krueger, F., Hore, T.A., Marques, C.J., Andrews, S., Reik, W. (2011). Dynamic regulation of 5-hydroxymethylcytosine in mouse ES cells and during differentiation. *Nature.* **473**, 398-402.

Fiehler, J., Knudsen, K., Kucinski, T., Kidwell, C.S., Alger, J.R., Thomalla, G., Eckert, B., Wittkugel, O., Weiller, C., Zeumer, H., Röther, J. (2004). Predictors of apparent diffusion coefficient normalization in stroke patients. *Stroke*. **35**, 514-519.

Fields, R.D. (2008). White matter in learning, cognition and psychiatric disorders. *Trends Neursci*. **31**, 361-370.

Filippi, M., Cercignani, M., Inglese, M., Horsfield, M.A., Comi, G. (2001). Diffusion tensor magnetic resonance imaging in multiple sclerosis. *Neurology*. **56**, 304-311.

Filippini, N., Zarei, M., Beckmann, C.F., Galluzzi, S., Borsci, G., Testa, C., Bonetti, M., Beltramello, A., Ghidoni, R., Benussi, L., Binetti, G., Frisoni, G.B. (2009). Regional atrophy of transcallosal prefrontal connections in cognitively normal APOE ε4 carriers. *J. Mag. Res. Imag.* **29**, 1021-1026.

Fischer, J.M., Bramow, S., Dal- Bianco, A., Luchinetti, C.F., Rauschka, H., Schmidbauer, M., Laursen, H., Sorensen, P.S., Lassmann, H. (2009). The relation between inflammation and neurodegeneration in multiple sclerosis brains. *Brain.* **132**, 1175-1189.

Follet, P.L., Deng, W., Dai, W., Talos, D.M., Massillon, L.J., Rosenberg, P.A., Volpe, J.J., Jensen, F.E. (2004). Glutamate receptor-mediated oligodendrocyte toxicity in periventricular leukomalacia: a protective role for topiramate. *J. Neurosci.* **24**, 4412-4420.

Fong, T. G., Inouye, S.K., Dai, W., Press, D.Z., Alsop, D.C. (2011). Association cortex hypoperfusion in mild dementia with Lewy bodies: a potential indicator of cholinergic dysfunction? *Brain Imaging Behav.* **5**, 25–35.

Forloni, G., Demicheli, F., Giorgi, S., Bendotti, C., Angeretti, N. (1992). Expression of amyloid precursor protein mRNAs in endothelial, neuronal, and glial cells: modulation by interleukin- 1. *Mol. Brain Res.* **16**, 128-134.

Fraga, M.F., Ballestar, E., Paz, M.F., Ropero, S., Setien, F., Ballestar, M.L., Heine-Suner, D., Cigudosa, J.C., Urioste, M., Benitez, J., Boix-Chornet, M., Sanchez-Aguilera, A.,

Ling, C., Carlsson, E., Poulsen, P., Vaag, A., Stephan, Z., Spector, T.D., Wu, Y.Z., Plass, C., Esteller, M., (2005). Epigenetic differences arise during the lifetime of monozygotic twins. *Proc. Natl. Acad. Sci. U.S.A.* **102**, 10604–10609.

Franklin, W., Paxinos, G. (1997) The mouse brain in stereotaxic coordinates. New York: Academic Press.

Friede, R.L. (1972). Control of myelin formation by axon caliber (with a model of the control mechanism). *J. Comp. Neurol.* **144**, 233-252.

Fryer, J.D., Simmons, K., Parsadanian, M., Bales, K.R., Paul, S.M., Sullivan, P.M., Holtzman, D.M. (2005). Human apolipoprotein E4 alters the amyloid-β40:42 ratio and promotes the formation of cerebral amyloid angiopathy in an amyloid precursor protein transgenic model. *J. Neurosci.* **25**, 2803–2810.

Fullerton, S.M., Shirman, G.A., Strittmatter, W.J., Matthew, W.D. (2001). Impairment of the blood- nerve and the blood- brain barriers in apolipoprotein E knockout mice. *Exp. Neurol.* **169**, 13-22.

Funahashi, S. (2001). Neuronal mechanisms of executive control by the prefrontal cortex. *Neurosci. Res.* **39**, 147-165.

Gan, H.T., Tham, M., Hariharan, S., Ramasamy, S., Yu, Y.H., Ahmed, S. (2011). Authentication of APOE as an autocrine/ paracrine factor that stimulates neural stem cells survival via MAPK/ ERK signalling pathway. *J. Neurochem.* **117**, 565-578.

Garay, L., Gonzalez Deniselle M.C., Gierman, L., Meyer, M., Lima, A., Roig, P., De Nicola, A.F. (2008). Steroid protection in the experimental autoimmune encephalomyelitis model of multiple sclerosis. *Neuroimmunomodul.* **15**, 76–83.

Garbern, J.Y., Yool, D.A., Moore, G.J., Wilds, I.B., Faulk, M.W., Klugmann, M., Nave, K-A., Sistermans, E.A., van der Knaap, A.S., Bird, T.D., Shy, M.E., Kamholz, J.A., Griffiths, I.R. (2002). Patients lacking the major CNS myelin protein, proteolipid protein

1, develop length- dependent axonal degeneration in the absence of demyelination and inflammation. *Brain.* **125**, 551-561.

Garcia, J.H., Lassen, N.A., Weiller, C., Sperling, B., Nakagawara, J. (1996). Ischemic stroke and incomplete infarction. *Stroke.* **27,** 761-765.

Gard, A. L., Maughon, R. H., Schachner, M. (1996). In vitro oligodendrogliotrophic properties of cell adhesion molecules in the immunoglobulin superfamily: myelin-associated glycoprotein and N-CAM. *J. Neurosci. Res.* **46**, 415–426.

Geurts, J.J.G., Barkhof, F. (2008). Grey matter pathology in multiple sclerosis. *Lancet Neurol.* **7**, 841-851.

Globisch, D., Munzel, M., Muller, M., Michalakis, S., Wagner, M., Koch, S., Bruckl, T., Biel, M., Carell, T. (2010). Tissue distribution of 5- hydroxymethylcytosine and search for active demethylation intermediates. *PloSone.* **5**, e15367

Gold, G., Kovari, E., Hof, P.R., Bouras, C., Giannakopoulos, P. (2007). Sorting out the clinical consequences of ischemic lesions in brain aging: a clinicopathological approach. *J. Neurol. Sci.* **257**, 17-22.

Goldberg, T.E., Berman, K.F., Mohr, E., Weinberg, D.R. (1990). Regional cerebral blood flow and cognitive function in Huntington's disease and schizophrenia. *Arch. Neurol.* **47**, 418-422.

Gootjes, L., Teipel, S.J., Zebuhr, Y., Schwarz, R., Leinsinger, G., Scheltens, P., Moller, H.J., Hampel., H. (2004). Regional distribution of white matter hyperintensities in vascular dementia, Alzheimer` s disease and healthy aging. *Dement. Geriatr. Cog. Dis.* **18**, 180-188.

Gordon, I., Grauter, E., Genis, I., Sehayek, E., Michaelson, D.M. (1995). Memory deficit and cholinergic impairments in apolipoprotein E-deficient mice. *Neurosci. Lett.* **199**, 1–4.

Goritz, C., Mauch, D.H., Nagler, K., Pfrieger, F.W. (2002). Role of glia- derived cholesterol in synaptogenesis: new revelations in the synapse- glia affaire. *J. Physiol. Paris.* **96**, 257- 263.

Goto, N. (1987). Discriminative staining methods for the nervous system: Luxol fast blue–periodic acid-schiff– hematoxylin triple stain and subsidiary staining methods. *Biotech. Histochem.* **62**, 305-315.

Gowing, G., Philips, T., Van Wijmeersch, B., Audet, J-N., Dewil, M., Van Den Bosch, L., Billiau, A.D., Robberecht, W., Julien, J-P. (2008). Ablation of proliferating microglia does not affect motor neuron degeneration in amyotrophic lateral sclerosis caused by mutant superoxide dismutase. *J. Neurosci.* **28**, 10234 –10244.

Gouw, A.A., Seewann, A., Vrenken, H., van der Flier, W.M., Rozemuller, J.M., Barkhof, F., Scheltens, P., Geurts, J.J.G. (2008). Heterogeneity of white matter hyperintensities in Alzheimer` s disease: post- mortem quantitative MRI and neuropathology. *Brain.* **131**, 3286-3298.

Graeber, M.B., Streit, W.J., Kreutzberg, G.W. (1989). Formation of microglia-derived brain macrophages is blocked by adriamycin. *Acta Neuropathol.* **78**, 348- 358.

Grafton, S.T., Sumi, S.M., Stimae, G.K., Alvord, E.C., Shaw, C-M., Nochlin, D. (1991). Comparison of postmortem magnetic resonance imaging and neuropathological findings in the cerebral white matter. *Arch. Neurol.* **48**, 293-298.

Graham, S.H., Chen, J., Lan, J., Leach, M.J., Simon, R. P. (1994). Neuroprotective effects of a use- dependent blocker of voltage- dependent sodium channels, BW61 9C89, in rat middle cerebral artery occlusion. *J. Pharmacol. Exp. Therap.* **269**, 854-859.

Grieve, S.M., Williams, L.M., Paul, R.H., Clark, C.R., Gordon E. (2007) Cognitive aging, executive function, and fractional anisotropy: a diffusion tensor MR imaging study. *Am. J. Neuroradiol.* **28**, 226- 235.

Griffiths, I., Klugmann, M., Anderson, T., Yool, D., Thomson, C., Schwab, M.H., Schneider, A., Zimmermann, F., McCulloch, M., Nadon, N., Nave, K-A. (1998). Axonal

swellings and degeneration in mice lacking the major proteolipid of myelin. *Science.* **280**, 1610-1613.

Grinberg, L.T., Thal, D.R. (2010). Vascular pathology in the aged human brain. *Acta Neuropathol.* **119**, 277–290.

Gromadzka, G., Baranska-Gieruszczak, M., Sarzynska-Dlugosz, I., Ciesielska, A., Czlonkowska, A. (2007). The APOE polymorphism and 1-year outcome in ischemic stroke: genotype–gender interaction. *Acta Neurol. Scand.* **116**, 392–398.

Grossman, R.I., Gomori, J.M., Ramer, K.N., Lexa, F.J., Schnall, M.D. (1994). Magnetization transfer: theory and clinical applications in neuroradiology. *RadioGraphics.* **14**, 279-290.

Guilfoyle, D.N., Helpern, J.A., Lim, K.O. (2003). Diffusion tensor imaging in fixed brain tissue at 7.0T. *NMR Biomed.* **16**, 77-81.

Gunning- Dixon, F.M., Brickman, A.M., Cheng, J.C., Alexopoulos, G.S. (2009). Aging of cerebral white matter: a review of MRI findings. *Int. J. Geriatr. Psychiatry.* **24**, 109-117.

Guerra-Crespo, M., De la Herrán-Arita, A.K., Boronat-García, A., Maya-Espinosa, G., García-Montes, J.R., Fallon, J.H., Drucker-Colín, R. (2012). Neural stem cells: exogenous and endogenous promising therapies for stroke, neural stem cells and therapy. ISBN: 978-953-307-958-5.

Hafezi- Moghadam, A., Thomas, K.L., Wagner, D.D. (2006). ApoE deficiency leads to a progressive age-dependent blood-brain barrier leakage. *Am. J. Physiol. Cell Physiol.* **292**, C1256–C1262.

Hai, J., Yu, F., Lin, Q., Su, S-H. (2012). The changes of signal transduction pathways in hippocampal regions and postsynaptic densities after chronic cerebral hypoperfusion in rats. *Brain Res.* **1429**, 9-17.

Hainsworth, A.H., Markus, H.S. (2008). Do in vivo experimental models reflect human cerebral small vessel disease? A systematic review. *J. Cereb. Blood Flow Metabol.* **28**, 1877–1891.

Han, S.H., Einstein, G., Weisgraber, K.H., Strittmatter, W.J., Saunders, A.M., Pericak-Vance, M., Roses, A.D., Schmechel, D.E. (1994). Apolipoprotein E is localized to the cytoplasm of human cortical neurons: a light and electron microscopic study. *J. Neuropathol. Exp. Neurol.* **153,** 535-544.

Han, X., Cheng, H., Fryer, J.D., Fagan, A.M., Holtzman, D.M. (2003). Novel role for apolipoprotein E in the central nervous system: modulation of sulfatide content; *J. Bio. Chem.* **278**, 8043-8051.

Hanlon, C.S., Rubinsztein, D.C. (1995). Arginine residues at codons 112 and 158 in the apolipoprotein E gene correspond to the ancestral state in humans. *Atheroclerosis***. 112,** 85-90.

Harms, M.P., Kotyk, J.J., Merchant, .KM. (2006). Evaluation of white matter integrity in ex vivo brains of amyloid plaque- bearing APPsw transgenic mice using magnetic resonance diffusion tensor imaging. *Exp. Neurol.* **199**, 408-415.

Harsan, L.A., Poulet, P., Guignard, B., Steibel, J., Parizel, N., de Sousa, P.L., Boehm, N., Grucker, D., Ghandour, M.S. (2006). Brain dysmyelination and recovery assessment by noninvasive in vivo diffusion tensor magnetic resonance imaging. *J. Neuroscie. Res.* **83**, 392-402.

Hartline, D.K., Colman, D.R. (2007). Rapid conduction and the evolution of giant axons and myelinated fibers. *Curr. Biol.* **17**, R29-R35.

Hattori, H., Takeda, M., Kudo, T., Nishimura, T., Hashimoto, S. (1992). Cumulative white matter changes in the gerbil brain under chronic cerebral hypoperfusion. *Acta Neuropathol.* **84**, 437-442.

Hawkins, B.T., Davis, T.P. (2005). The blood- brain barrier/ neurovascular unit in health and disease. *Pharmacol. Rev.* **57**, 173-185.

Haynes, R.L., Folkerth, R.D., Keefe, R.L., Sung, I., Swezda, L.I., Rosenberg, P.A., Volpe, J.J., Kinney, H.C. (2003). Nitrosative and oxidative injury to premyelinating oligodendrocytes in periventricular leukomalacia. *J. Neuropathol. Exp. Neurol.* **62**, 441 450.

Hazell, A.S. (2007). Excitotoxic mechanisms in stroke: an update of concepts and treatment strategies. *Neurochem. Inter.* **50**, 941–953.

He, J., Evans, C-O., Hoffman, S., Oyesiku, N.M., Stein, D.G. (2004). Progesterone and allopregnanolone reduce inflammatory cytokines after traumatic brain injury. *Exp.Neurol.* **189**, 404– 412.

Head, E., Mehta, R., Hartley, J., Kameka, M., Cummings, B. J., Cotman, C.W., Ruehl, W.W., Milgram, N.W. (1995). Spatial learning and memory as a function of age in the dog. *Behav. Neurosci.* **109**, 851–858.

Head, D., Buckner, R.L., Shimony, J.S., Williams, L.E., Akbudak, E., Conturo, T.E., McAvoy, M., Morris, J.C., Snyder, A.Z. (2004). Differential vulnerability of anterior white matter in nondemented aging with minimal acceleration in dementia of Alzheimer type: evidence from diffusion tensor imaging. *Cerebral. Cortex.* **14**, 410-423.

Heape, A.M., Lehto, V-P., Kursula, P. (1999). The expression of recombinant large myelin-associated glycoprotein cytoplasmic domain and the purification of native myelin-associated glycoprotein from rat brain and peripheral nerve. *Protein Expres. Purific.* **15,** 349–361.

Hedden, T., Gabrielli, J.D. (2004). Insights into the aging mind: a view from a cognitive neuroscience. *Nature Rev. Neurosci.* **5**, 87-96.

Heise, V., Fillipini, N., Ebmeier, K.P., Mackay, C.E. (2010). The APOE ε4 allele modulates brain white matter integrity in healthy adults. *Mol. Psychiatry.* 1-9.

Hernandez, D.G., Nalls, M.A., Gibbs, J.R., Arepalli, S., van der Burg, M., Chong, S., Moore, M., Longo, D.L., Cookson, M.R., Traynor, B.J., Singleton, A.B. (2011). Distinct DNA methylation changes highly correlated with chronological age in the human brain. *Hum. Mol. Genet.* 1-9.

Herndon, J.G., Moss, M.B., Rosene, D.L., Killiany, R.J. (1997). Patterns of cognitive decline in aged rhesus monkeys. *Behav. Brain Res.* **87**, 25-34.

Herrero, M-T., Barcia, C., Navarro, J.M. (2002). Functional anatomy of thalamus and basal ganglia. *Child's Nerv. Syst.* **18**, 386–404.

Hertz, L., Zielke, H.R. (2004). Astrocytic control of glutamatergic activity: astrocytes as stars of the show. *Trends. Neurosci.* **27**, 735-743.

Holland, R.H., Bastin, M.E., Jansen, M.A., Merrifield, G.D., Coltman, R.B., Scott, F., Nowers, H., Khallout, K., Marshall, I., Wardlaw, J.M., Deary, I.J., McCulloch, J., Horsburgh, K. (2011). MRI is a sensitive marker of subtle white matter pathology in hypoperfused mice. *Neurobiol Aging.* **32.** 2325.e1–2325.e6.

Holliday, R., Pugh, J.E. (1975). DNA modification mechanisms and gene activity during development. *Science.* **187**, 226-232.

Horsburgh, K. & Nicoll, J.A. (1996). Selective alterations in the cellular distribution of apolipoprotein E immunoreactivity following transient cerebral ischaemia in the rat. *Neuropathol. Appl. Neurobiol.* **22**, 342-349.

Horsburgh, K., Fitzpatrick, M., Nilsen, M., Nicoll, J.A. (1997). Marked alterations in the cellular localisation and levels of apolipoprotein E following acute subdural haematoma in rat. *Brain Res.* **763**, 103-110.

Horsburgh, K., Kelly, S., McCulloch, J., Higgins, G.A., Roses, A.D., Nicoll, J.A. (1999). Increased neuronal damage in apolipoprotein E-deficient mice following global ischaemia. *Neuroreport.* **10**, 837-841.

Horsburgh, K., McCulloch, J., Nilsen, M., McCracken, E., Large, C., Roses, A.D., Nicoll, J.A. (2000a). Intraventricular infusion of apolipoprotein E ameliorates acute neuronal damage after global cerebral ischemia in mice. *J Cereb Blood Flow Metab.* **20**, 458-462.

Horsburgh, K., McCarron, M.O., White, F., Nicoll, J.A.R. (2000b). The role of apolipoprotein E in Alzheimer` s disease, acute brain injury and cerebrovascular disease: evidence of common mechanisms and utility of animal models. *Neurobiol. Aging.* **21**, 245-255.

Horsburgh, K., McCulloch, J., Nilsen, M., McCracken, E., Large, C., Roses, A.D., Nicoll, J.A. (2000c). Intraventricular infusion of apolipoprotein E ameliorates acute neuronal damage after global cerebral ischemia in mice. *J. Cereb. Blood Flow Metab.* **20**, 458-462.

Horsburgh, K., McColl, B.W., White, F., McCulloch, J. (2003).Apolipoprotein E influences neuronal death and repair. *Int. Cong. Series.* **1252**, 171-178.

Hortega, R. (1928). Tercera aportacion al conocimiento morfologico e interpretacion funcional de la oligodendroglia. *Memor. Real Soc. Esp. Hist .Nat.* **14**, 5–122.

Hossmann, K-A. (2008). Cerebral ischemia: models, methods and outcomes. *Neuropharmacol.* **55**, 257- 270.

Hotchkiss, R.D. (1948). The quantitative separation of purines, pyrimidines, and nucleosides by paper chromatography. *J. Biol. Chem.* **175**, 315-332.

Hsu, S.M., Raine, L., Fanger, H. (1981). The use of antiavidin antibody and avidin-biotin-peroxidase complex in immunoperoxidase technics. *Am J Clin Pathol.* **75**, 816-821.

Hu, W., Lucchinetti, C.F. (2009). The pathological spectrum of CNS inflammatory demyelinating disease. *Semin. Immunopathol.* **31**, 439-453.

Hunt, A., Schonknecht, P., Henze, M., Seidl, U., Haberkorn, U., Schroder, J. (2007). Reduced cerebral glucose metabolism in patients at risk for Alzheimer's disease. *Psychiatry Res.* **155**, 147–154.

Iadecola, C., Zhang, F., Casey, R., Nagayama, M., Ross, M.E. (1997). Delayed reduction of ischemic brain injury and neurological deficits in mice lacking the inducible nitric oxide synthase gene. *J. Neurosci.* **17**, 9157-9164.

Iadecola, C. (2010). The overlap between neurodegenerative and vascular factors in the pathogenesis of dementia. *Acta Neuropathol.* **120**, 287–296.

Ihara, M., Polviskoski, T.M., Hall, R., Slade, J.Y., Perry, R.H., Oakley, A.E., Englund, E., O`Brien, J.T., Ince, P.G., Kalaria, R.N. (2010). Quantification of myelin loss in frontal lobe white matter in vascular dementia, Alzheimer` s disease, and dementia with lewy bodies. *Acta Neuropathol.***119**, 579-589.

Iqbal, K., Jin, S.G., Pfeifer, G.P., Szabo, P.E. (2011). Reprogramming of the paternal genome upon fertilization involves genome-wide oxidation of 5-methylcytosine. *Proc. Natl. Acad. Sci. U S A.* **108**, 3642-3647.

Ito, D., Imai, Y., Oshawa, K., Nakajima, K., Fukuuchi, Y., Kohsaka, S. (1998). Microglia-specific localisation of a novel calcium binding protein, Iba1. *Mol. Brain Res.* **57**, 1-9.

Ito, S., D`Alessio, A.C., Taranova, O.V., Hong, K., Sowers, L.C., Zhang, Y. (2010). Role of Tet proteins in 5mC to 5hmC conversion, ES- cell self renewal and inner cell mass specification. *Nature.* **466**, 1129-1133.

Itoyama, Y., Webster, H. D., Sternberger, N. H., Richardson, E. J., Walker, D. L., Quarles, R. H., Padgett, B. L. (1982). Distribution of papovavirus, myelin-associated glycoprotein, and myelin basic protein in progressive multifocal leukoencephalopathy lesions. *Ann. Neurol.* **11**, 396–407.

Jahn, O., Tenzer, S., Werner, H.B. (2009). Myelin proteomics: molecular anatomy of an insulating sheath. *Mol. Neurobiol.* **40**, 55-72.

Jin, S-G., Kadam, S., Pfeifer, G.P. (2010). Examination of the specificity of DNA methylation profiling techniques towards 5- methylcytosine and 5-hydroxymethylcytosine. *Nucleic Acids Res.* **38**, e125.

Jin, S-G., Wu, X., Li, A.X., Pfeifer, G.P. (2011). Genomic mapping of 5-hydroxymethylcytosine in the human brain. *Nucleic Acids Res.* 1-10.

Jiwa, N.S., Garrad, P., Hainsworth, A.H. (2010). Experimental models of vascular dementia and vascular cognitive impairment: a systematic review. *J. Neurochem.* **115**, 814-828.

Johnson, D., Sato, S., Quarles, R. H., Inuzuka, T., Brady R. O., Tourtellotte, W. W. (1986). Quantitation of the myelin-associated glycoprotein in human nervous tissue from controls and multiple sclerosis patients. *J. Neurochem.* **46**, 1086–1093.

Johnson, A.B. (2002). Alexander disease: a review and the gene. *Int. J. Dev. Neurosci.* **20**, 391-394.

Jokinen, H., Ryberg, C., Kalska, H., Ylkoski, R., R., Rostrup, E., Stegmann, M.B., Waldermar, G., Madureira, S., Ferro, J.M., van Straaten, E.C.W., Scheltens, P., Barkhof, P., Fazekas, F., Schmidt, R., Carlucci, G., Pantoni, L., Inzitari, D., Erkinjuntti, T, on behalf of the LADIS group. Corpus callosum atrophy is associated with mental slowing and executive deficits in subjects with age-related white matter hyperintensities: the LADIS Study. *J. Neurol. Neurosurg. Psychiatry.* **78**, 491–496.

Jolivalt, C., Leininger- Muller, B., Bertrand, P., Herber, R., Christen, Y., Siest, G. (2000). Differential oxidation of apolipoprotein E isoforms and interaction with phospholipids. Free *Radicals Biol. Med.* **28**, 129-140.

Jurado, M.B., Rosselli, M (2007). The elusive nature of executive functions: a review of our current understanding. *Neuropsychol. Rev.* **17**, 213- 233.

Kalaria, R.N. (1996). Cerebral vessels in aging and Alzheimer`s disease. *Pharmacol. Ther.* **72**, 193-214.

Kalback, W., Esch, C., Castano, E.M., Rahman, A., Kokjohn, T., Luehrs, D.C., Sue, L., Cisneros, R., Gerber, F., Richardson, C., Bohmann, B., Walker, D.G., Beach, T.G., Roher,

A.E. (2004). Atherosclerosis, vascular amyloidosis and brain hypoperfusion in the pathogenesis of sporadic Alzheimer's disease. *Neurol. Res.* **26**, 525-539.

Kalmijn, S., Feskens, E.J.M., Launer, L.J., Kromhout, D. (1996). Cerebrovascular disease, the apolipoprotein e4 allele, and cognitive decline in a community-based study of elderly men. *Stroke.* **27**, 2230-2235.

Kalmijn, S., Launer, L.J., Ott, A., Witteman, J.C., Hofman, A.M. Br, Breteler, M.M. (1997). Dietary fat intake and the risk of incident dementiain the Rotterdam Study. *Ann. Neurol.* **42**, 776–782.

Karadottir, R., Attwell, D. (2007). Neurotransmitter receptors in the life and death of oligodendrocytes. *Neurosci.* **148**, 1426-1238.

Karadottir, R., Hamilton, N.B., Bakiri, Y., Attwell, D. (2008) Spiking and non spiking classes of oligodendrocyte precursor glia in CNS white matter. *Nat. Neurosci.* **11**, 450-456.

Kassmann, C.M., Lappe- Siefke, C., Baes, M., Brugger, B., Mildner, A., Werner, H.B., Natt, O., Michaelis, T., Prinz, M., Frahm, J., Nave, K-A. (2007). Axonal loss and neuroinflammation caused by peroxisome- deficient oligodendrocytes. *Nat. Genet.* **39**, 969-976.

Kawamura, J., Meyer, J.S., Terayama, Y., Weathers, S. (1991). Leukoarosis correlates with cerebral hypoperfusion in vascular dementia. *Stroke.* **22**, 609-611.

Kennedy, K.M. and Raz, N. (2009). Aging white matter and cognition: differential effects of regional variations in diffusion properties on memory, executive functions, and speed. *Neuropsychologia.* **47**, 916–927.

Keirstead, H.S., Nistor, G., Bernal, G., Totoiu, M., Cloutier, F., Sharp, K., Steward, O. (2005). Human embryonic stem cell-derived oligodendrocyte progenitor cell transplants remyelinate and restore locomotion after spinal cord injury. *J. Neurosci.* **25**, 4694-4705.

Kim, Y.S., Kim, S.U. (1991). Oligodendroglial cell death induced by oxygen radicals and its protection by catalase. *J. Neurosci. Res.* **29**, 100-106.

Kim, J.H., Trinkaus, K., Ozcan, A., Budde, M.D., Song, S- K. (2007). Postmortem delay does not change regional diffusion anisotropy characteristics in mouse spinal cord white matter. *NMR Biomed.* **20,** 352- 3359.

Kim, S-K., Cho, K-O., Kim, S.Y. (2008). White matter damage and hippocampal neurodegeneration induced by permanent bilateral occlusion of common carotid artery in the rat: comparison between Wistar and Sprague- Dawley strain. *Korean J. Physiol. Pharamcol.* **12**, 89-94.

Kinney, S.M., Chin, H.G., Vaisvila, R., Bitinaite, J., Zheng, Y., Esteve, P-O., Feng, S., Stroud, H., Jacobsen, S.E., Pradhan, S. (2011). Tissue-specific distribution and dynamic changes of 5-hydroxymethylcytosine in mammalian genomes. *J. Biol. Chem*. **286**, 24685–24693.

Kirkpatrick, L.L., Witt, A.S., Payen, H.R., Shine, H.D., Brady, S.T. (2001). Changes in microtubule stability and density in myelin-deficient shiverer mouse CNS axons. *J. Neurosci.* **21**, 2288-2297.

Kitagawa, K., Matsumoto, M., Yang, G., Mabuchi, T., Yagita, Y., Hori, M., and Yanagihara, T. (1998). Cerebral ischemia after bilateral carotid artery occlusion and intraluminal suture occlusion in mice: evaluation of the patency of the posterior communicating artery. *J. Cereb. Blood Flow Metab.* **18**, 570–579.

Kitaguchi, H., Tomimoto, H., Ihara, M., Shibata, M., Uemura, K., Kalaria, R.N., Kihara, T., Asada-Utsugi, M., Kinoshita, A., Takahashi, R. (2009). Chronic cerebral hypoperfusion accelerates amyloid β deposition in APPSwInd transgenic mice. *Brain Res.* **1294**, 202-210.

Kitamura, A., Fujita, Y., Oishi, N., Kalaria, R.N., Washida, K., Maki, T., Okamoto, Y., Hase, Y., Yamada, M., Takahashi, J., Ito, H., Tomimoto, H., Fukuyama, H., Takahashi, R., Ihara, M. (2012). Selective white matter abnormalities in a novel rat model of vascular dementia. *Neurobio Aging.* **33**, 1012.e25–1012.e35.

Klugmann, M., Schwab, M.H., Puhlhofer, A., Schneider, A., Zimmermann, F., Griffiths, I.R., Nave, A-K. (1997). Assembly of CNS myelin in the absence of proteolipid protein. *Neuron.* **18**, 59-70.

Kluver, H., Barrera, E. (1953). A method for the combined staining of cells and fibers in the nervous system. *J. Neuropath. Exp. Neurol*. **12**, 400-403.

Knox, C.A., Kokmen, E., Dyck, P.J. (1989). Morphometric alteration of rat myelinated fibers with aging. *J. Neuropathol. Exp. Neurol.* **10**, 2817-2821.

Ko, M., Huang, Y., Jankowska, A.M., Pape, U.J., Tahiliani, M., Bandukwala, H.S., An, J., Lamperti, E.D., Koh, K.P., Ganetzky, R., Liu, X.S., Aravind, L., Agarwai, S., Maciejewski, J.P., Rao, A. (2010). Impaired hydroxylation of 5- methylcytosine in myeloid cancers with mutant TET2. *Nature.* **468**, 839-843.

Kondo, Y., Ogawa, N., Asanuma, M., Matsuura, K., Nishibayashi, K., Iwata, E. (1996). Preventive effects of bifemelane hydrochloride on decreased levels of muscarinic acetylcholine receptor and its mRNA in a rat model of chronic cerebral hypoperfusion. *Neurosci. Res.* **24**, 409–414.

Kong, L.Y., McMillian, M.K., Hudson, P.M., Jin, L., Hong, J.S. (1997). Inhibition of lipopolysaccharide- induced nitric oxide and cytokine production by ultralow concentrations of dynorphins in mixed glia cultures. *J. Pharmacol. Exp. Ther.* **280,** 61–66.

Kothari, R.M., Shankar, V. 5- Methylcytosine content in the vertebrate deoxyribonucleic acids: species specificity. *J. Mol. Evol.* **3**, 325- 329.

Kriaucionis, S., Heintz, N. (2009). The nuclear DNA base 5- hydroxymethylcytosine is present in Purkinje neurons and the brain. *Science.* **324**, 929-930.

Kroemer, G., Dallaporta, B., Resche- Rigon, M. (1998). The mitochondrial death/ life regulator in apoptosis and necrosis. *Annu. Rev. Physiol.* **60**, 619-642.

Kruman, I.I., Kumaravel, T.S., Lohani, A., Pedersen, W.A., Cutler, R.G., Kruman, Y., Haughey, N., Lee, J., Evans, M., Mattson, M.P. (2002). Folic acid deficiency and homocysteine impair DNA repair in hippocampal neurons and sensitize them to amyloid toxicity in experimental models of Alzheimer` s disease. *J. Neurosci.* **22**, 1752-1762.

Kudo, T., Tada, K., Takeda, M., Nishimura, T. (1990). Learning impairment and microtubule- associated protein 2 decrease in gerbils under chronic cerebral hypoperfusion. *Stroke.* **21**, 1205-1209.

Kudo, T., Takeda, M., Tanimukai, S., Nishimura, T. (1993). Neuropathological changes in the gerbil brain after chronic hypoperfusion. *Stroke.* **24**, 259-264.

Kumaran, D., Udayabanu, M., Kumar, M., Aneja, R., Katyal, A. (2008). Involvement of angiotensin converting enzyme in cerebral hypoperfusion induced anterograde memory impairment and cholinergic dysfunction in rats. *Neurosci.* **155.** 626 – 639.

Kurumatani, T., Kudo, T., Ikura, Y., Takeda, M., Kontos, H.A. (1998). White matter changes in the gerbils brain under chronic cerebral hypoperfusio. Editorial comments. *Stroke.* **29**, 1059-1062.

Kwon, B.K., Tetzlaff, W., Grauer, J.N., Beiner, J., Vaccaro, A.R. (2004). Pathophysiology and pharmacologic treatment of acute spinal cord injury. *Spine J.* **4**, 451–464.

Lai, M.K.P., Tsang, S.W.Y., Garcia-Alloza, M., Minger, S.L., Nicoll, J.A.R., Esiri,M.M., Wong, P.T.H., Chen, C.P.L.H., Ramı´rez, M.A., Francis, P.T. (2006). Selective effects of the APOE (4 allele on presynaptic cholinergic markers in the neocortex of Alzheimer's disease. *Neurobiol. Dis.* **22**, 555 – 561.

Lakhan, S.E., Kirchgessner, A., Hofner, M. (2009). Inflammatory mechanisms in ischemic stroke: therapeutic approaches. *J. Transl. Med.* **7**, 1-11.

Larocca, J.N., Farooq, M., Norton, W.T. (1997). Induction of oligodendrocyte apoptosis by C_2- ceramide. *Neurochem. Res.* **22**, 529-534.

Larsson, E-M., Englund, E., Sjobeck, M., Latt, J., Brockstedt, S. (2004). MRI with diffusion tensor imaging post- mortem at 3.0T in a patient with a frontotemporal dementia. *Dement. Geriatr. Cogn. Disord.* **17**, 316-319.

Lasiene, J., Matsui, A., Sawa, Y., Wong, F., Horner, P.J. (2009). Age-related myelin dynamics revealed by increased oligodendrogenesis and short internodes. *Aging Cell.* **8**, 201–213.

Laskwoitz, D.T., Sheng, H., Bart, R.D., Joyner, K.A., Roses, A.D., Warner, D.S. (1997a). Apolipoprotein E- deficient mice have increased susceptibility to focal cerebral ischemia. *J. Cer. Blood. Flow. Met.* **17**, 753-758.

Laskowitz, D.T., Goel, S., Bennett, E.R., Mathew, W.D. (1997b). Apolipoprotein E suppresses glia cell secretion of TNFα. *J. Neuroimmunology* **76**, 70-74.

Laskowitz, D.T., Horsburgh, K., Roses, A.D. (1998). Apolipoprotein E and the CNS response to injury. *J. Cereb. Blood Flow Met.* **18**, 465-471.

Laskowitz, D.T., Lee, D.M., Schmechel, D., Staats, H.F. (2000). Altered immune responses in apolipoprotein E- deficient mice. *J. Lipid Res.* **41**, 613- 620.

Lassmann, H. (2003). Axonal injury in multiple sclerosis. *J. Neurol. Neurosur. Psychiatry*. **74**, 695-697.

Lauterber, P.C. (1973). Image formation by induced local interactions: examples of employing nuclear magnetic resonance. *Nature*. **242**, 190–191.

Lebel, C., Walker, L., Leemans, A., Phillips, L., Beaulieu, C. (2008). Microstructural maturation of the human brain from childhood to adulthood. *NeuroImage*. **40**, 1044-1055.

Lenzsér, G., Kis, B., Bari, F., Busija, D.W. (2005). Diazoxide preconditioning attenuates global cerebral ischemia-induced blood–brain barrier permeability. *Brain Res.* **1051**, 72–80.

Levin, S.I., Meisler, M.H. (2004). Floxed allele for conditional inactivation of the voltage-gated sodium channel Scn8a [Na(v)1.6]. *Genesis.* **39**, 234–239.

Li, W., Liu, M. (2011). Distribution of 5- hydroxymethylcytosine in different human tissues. *J. Nuc. Acids.* doi:10.4061/2011/870726

Lie, D.C., Song, H., Colamarino, S.A., Ming, G.L., Gage, F.H. (2004). Neurogenesis in the adult brain: new strategies for central nervous system diseases. *Annu. Rev. Pharmacol. Toxicol.* **44**, 399–421.

Lim, K.O., Hedehus, M., Moseley, M., de Crespigny, A., Sullivan, E.V., Pfefferbaum, A. (1999). Compromised white matter tract integrity in schizophrenia inferred from diffusion tensor imaging. *Arch. Gen. Psyhciatry*. **56**, 367-374.

Limbourg, F.P., Huang, Z., Plumier, J-C., Simoncini, T., Fujioka, M., Tuckermann, J., Schütz, G., Moskowitz, M.A., Liao, J.K. (2002). Rapid nontranscriptional activation of endothelial nitric oxide synthase mediates increased cerebral blood flow and stroke protection by corticosteroids. *J. Clin. Invest.* **110**, 1729–1738.

Lindgren, A., Roijer, A., Rudling, O., Norrving, B., Larsson, E.M., Eskilsson, J., Wallin, L., Olsson, B., Johansson, B.B. (1994). Cerebral lesions on magnetic resonance imaging, heart disease, and vascular risk factors in subjects without stroke. A population-based study. *Stroke*. **25**, 929-934.

Lindvall, O., Kokaia, Z., Martinez- Sorrano, A. (2004). Stem cell therapies for human neurodegenerative disorders- how to make it work. *Nat. Med.Rev.* S42-S50.

Liu, X-Z., Xu, X.M., Hu, R., Du, C., Zhang, S.X., McDonald, J.W., Dong, H.X., Wu, Y.J., Fan, G.S., Jacquin, M.F., Hsu, C.Y., Choi, D.W. (1997). Neuronal and glial apoptosis after traumatic spinal cord injury. *J. Neurosci.* **17**, 5395–5406.

Liu, B., Jiang, J.W., Wilson, B., Du, L., Yang, S.N., Wang, J.Y., Wu, G.C., Cao, X.D., Hong, J..S (2000) .Systemic infusion of naloxone reduces degeneration of rat substantia nigral dopaminergic neurons induced by intranigral injection of lipopolysaccharide. *J. Pharmacol. Exp. Ther.* **295,** 125–132.

Liu, B.P., Fournier, A., GrandPre, T., Strittmatter, S.M. (2002). Myelin- associated glycoprotein as a functional ligand for the Nogo- 66 receptor. *Science.* **297**, 1190-1193.

Liu, B., Hong J.S. (2003). Role of microglia in inflammation- mediated neurodegenerative diseases: mechanisms and strategies for therapeutic intervention. *J. Pharmacol. Exp. Therap.* **304**, 1-7.

Liu, H-X., Zhang, J-J., Zheng, P., Zhang, Y. (2005). Altered expression of MAP-2, GAP-43, and synaptophysin in the hippocampus of rats with chronic cererbral hypoperfusion correlates with cognitive impairment. *Mol. Brain Res.* **139**, 169-177.

Liu, A., Han, Y.R., Li, J., Sun, D., Ouyang, M., Plummer, M.R., Cassaccia-Bonnefil, P. (2007). The glial or neuronal fate choice of oligodendrocyte progenitors is modulated by their ability to acquire an epigenetic memory. *J. Neurosci.* **27**, 7339-7343.

Liu, L., Li, Y., Tollefsbol, T.O., (2008). Gene–environment interactions and epigenetic basis of human diseases. *Curr. Issues Mol. Biol.* **10**, 25–36.

Loers, G., Aboul-Enein, F., Bartsch, U., Lassmann, H., Schachner, M. (2004) Comparison of myelin, axon, lipid, and immunopathology in the central nervous system of differentially myelin-compromised mutant mice: a morphological and biochemical study. *Mol. Cell. Neurosci.* **27**, 175–189.

Lomnitski, L., Kohen, R., Chen, Y., Shohami, E., Trembovler, V., Vogel, T., Michaelson, D.M. (1997). Reduced levels of antioxidants in brains of apolipoprotein E-deficient mice following closed head injury. *Pharmacol Biochem Behav.* **56**, 669-673.

Lomnitski, L., Chapman, S., Hochman, A., Kohen, R., Shohami, E., Chen, Y., Trembovler, V., Michaelson, D.M. (1999). Antioxidant mechanisms in apolipoprotein E deficient mice prior to and following closed head injury. *Biochim Biophys Acta.* **1453**, 359-368.

Lorpez-Erauskin, J., Fourcade, S.P., Galino, J., Ruiz, M., Schluter, A., Naudi, A., Jove, M., Portero-Otin, M., Pamplona, R., Ferrer, I., Pujol, A. (2011). Antioxidants halt axonal degeneration in a mouse model of X-adrenoleukodystrophy. *Ann. Neurol.* **70**, 84–92.

Lorent, K., Overbergh, L., Moechars, D., De Strooper, B., Van Leuven, F., Van den Berghe, H. (1995). Expression in mouse embryos and in adult mouse brain of three members of the amyloid precursor protein family, of the alpha-2-macroglobulin receptor/low density lipoprotein receptor-related protein and of its ligands apolipoprotein E, lipoprotein lipase, alpha-2-macroglobulin and the 40,000 molecular weight receptor-associated protein. *Neurosci.* **65,** 1009-1025.

Love, S. (1999). Oxidative stress in brain ischemia. *Brain Pathol.* **9**, 119-131.

Lu, X., Bing, G., Hagg, T. (2000). Naloxone prevents microglia-induced degeneration of dopaminergic substantia nigra neurons in adult rats. *Neurosci.* **97,** 285–291.

Ludwin, S. K., Johnson, E. S. (1981). Evidence for a ‘‘dying-back’’ gliopathy in demyelinating disease. *Ann. Neurol.* **9**, 301–305.

Lue, L.F., Rydel, R., Brigham, E.F., Yang, L.B., Hampel, H., Murphy, G.M. Jr, Brachova, L., Yan, S.D., Walker, D.G., Shen, Y., Rogers, J. (2001). Inflammatory repertoire of Alzheimer’s disease and nondemented elderly microglia in vitro. *Glia.* **35**, 72–79.

Luebke, J.I., Chang, Y.M., Moore, T.L., Rosene, D.L. (2004). Normal aging results in decreased synaptic excitation and increased synaptic inhibition of layer 2/3 pyramidal cells in the monkey prefrontal cortex. *Neurosci.* **125**, 277-288.

Lutjohann, D., Papassotiropoulos, A., Bjorkhem, I., Locatelli, S., Bagli, M., Oehring, R.D., Schlegel, U., Jessen, F., Rao, M.L., von Bergman, K., Heun, R. (2000). Plasma 24S-hydroxycholesterol (cerebrosterol) is increased in Alzheimer and vascular demented patients. *J. Lipid Res.* **41**, 195- 198.

Lynch, J.R., Morgan, D., Mance, J., Matthew, W.D., Laskowitz, D.T. (2001). Apolipoprotein E modulates glial activation and the endogenous central nervous system inflammatory response. *J. Neuroimmunol.* **114**, 107-113.

Lynch, J.R., Pineda, J.A., Morgan, D., Zhang, L., Warner, D.S., Benveniste, H., Laskowitz, D.T. (2002). Apolipoprotein E affects the central nervous system response to injury and the development of cerebral edema. *Ann. Neurol.* **51**, 113-117.

Madden, D.J., Spaniol, J., Whiting, W.L., Bucur, B., Provenzale, J.M., Cabeza, R., White, L.E., Huettel, S.A. (2007). Adult age differences in the functional neuroanatomy of visual attention: A combined fMRI and DTI study. *Neurobiol. Aging.* **28**, 459–476.

Madden, D.J., Bennett, I.J., Song, A.W. (2009). Cerebral white matter integrity and cognitive aging: contributions from diffusion tensor imaging. *Neurpsychol. Rev.* **19**, 415-435.

Magistretti, P.J., (2006). Neuron- glia metabolic coupling and plasticity. *J. Exp. Biol.* **209**, 2304-2311.

Mahley, R.W., Innerarity, T.L. (1983). Lipoprotein receptors and cholesterol homeostasis. *Biochim. Biophys. Acta.* **737,** 197-222.

Mahley, R.W., Weisgraber, K.H., Huang, Y. (2006). Apolipoprotein E4: a causative factor and therapeutic target in neuropathology, including Alzheimer`s disease. *Proc. Natl. Acad. Sci. USA.* **103**, 5644-5651.

Maloney, B., Ge, Y-W., Alley, G.M., Lahin, D.K. (2007). Important differences between human and mouse APOE gene promoters: limitation of mouse APOE models in studying Alzheimer`s disease. *J. Neurochem.* **103**, 1237-1257.

Mancardi, M., Hart, B-t., Roccatagliata, L., Brok, H., Giunti, D., Bontrop, R., Massaceci, L., Capello, E., Uccelli, A. (2001). Demyelination and axonal damage in a non-human primate model of multiple sclerosis. *J. Neurol. Sci.* **184**, 41-49.

Mao, Y., Yang, G-Y., Zhou, L-F., Stern, J.D., Betz, A.L. (1999). Focal cerebral ischemia in the mouse: description of a model and the effects of permanent and temporary occlusion. *Mol. Brain Res.* **63**, 366-370.

Marcus, J., Honigbaum, S., Shroff, S., Honke, K., Rosenbluth, J., Dupree, J.L. (2006). Sulfatide is essential for the maintenance of CNS myelin and axon structure. *Glia.* **53**, 372-381.

Marques, M.A., Tolar, M., Crutcher, K.A. (1997). Apolipoprotein E exhibits isoform-specific neurotoxicity. *Alzheimer's Res.* **3,** 1-6.

Marques, S.C.F., Oliveira, C.R., Pereira, C.M.F., Outeiro, T.F. (2011). Epigenetics in neurodegeneration: A new layer of complexity. *Prog. Neuro-psychopharm. Biol. Psychiatry*. **35**, 348-355.

Marret, S., Mukendi, R., Gadisseux, J.F., Gressens, P., Evrard, P. (1995). Effect of ibotenate on brain development: an excitotoxic mouse model of microgyria and posthypoxic-like lesions. *J. Neuropathol. Exp. Neurol.* **54**, 358- 370.

Marsland, A.L., Petersen, K.L., Sathanoori, R., Muldoon, M.F., Neumann, S.A., Ryan, C., Flory, J.D., Manuck, S.B. (2006). Interleukin-6 covaries inversely with cognitive performance among middle-aged community volunteers. *Psychosom. Med.* **68**, 895–903.

Martin- Husstege, M., Muggironi, M., Liu, A., Casaccia- Bonnefil, P. (2002). Histone deacetylase activity is necessary for oligodendrocyte lineage progression. *J. Neurosci.* **22**, 10333-10345.

Masliah, E., Mallory, M., Ge, N., Alford, M., Veinbergs, I., Roses, A.D. (1995). Neurodegeneration in the central nervous system of apoE-deficient mice. *Exp. Neurol.* **136**, 107–122.

Masliah, E., Samuel, W., Veinbergs, I., Mallory, M., Mante, M., Saitoh, T. (1997). Neurodegeneration and cognitive impairment in apoE-deficient mice ameliorated by infusion of recombinant apoE. *Brain.* **751**, 307–314.

Mastroeni, D., McKee, A., Grover, A., Rogers, J., Coleman, P.D. (2009). Epigenetic differences in cortical neurons from a pair of monozygotic twins discordant for Alzheimer`s disease. *PLoS One.* **4**, e6617.

Mastroeni, D., Grover, A., Delvaux, E., Whiteside, C., Coleman, P.D., Rogers, J. (2010). Epigenetic changes in Alzheimer`s disease: decrements in DNA methylation. *Neurobiol. Aging.* **31**, 2025-2037.

Mathiesen, E.B., Waterloo, K., Joakimsen, O., Bakke, S.J., Jacobsen, E.A., Benaa, K.H. (2004). Reduced neuropsychological test performance in asymptomatic carotid stenosis: the Tromso Study. *Neurology.* **62**, 695-701.

Matsuo, A., Lee, G.C., Terai, K., Takami, K., Hickey, W.F., McGeer, E.G., McGeer, P.L. (1997). Umasking of an unusual myelin basic protein epitope during the process of myelin degeneration in humans. *Am. J. Pathol.* **150**, 1253-1266.

Matute, C., Alberdi, E., Domercq, M., Perez- Cerda, F., Perez- Samartin, A., Sanchez-Gomez, M.V. (2001). The link between excitotoxic oligodendroglial death and demyelinating diseases. *Trends Neurosci.* **24**, 224-230.

Matzel, L.D., Grossman, H., Light, K., Townsend, D., Kolata, S. (2008). Age-related declines in general cognitive abilities of Balb/C mice are associated with disparities in working memory, body weight, and general activity. *Learn. Mem.* **15**, 733-746.

Mauch, D.H., Nagler, K., Schumacher, S., Goritz, C., Muller, E-C., Otto, A., Pfrieger, F.W. (2001). CNS synaptogenesis promoted by glia- derived cholesterol. *Science.* **294**, 1354- 1357.

McEntee, W.J., Crook, T.H. (1991). Serotonin, memory, and the aging brain. *Psychopharmacol.* **103**, 143-149.

McGowan, J.C., McCormack, T.M., Grossman, R.I., Mendonca, R., Chen, X-H., Berlin, J.A., Meaney, D.F., Xu, B-H., Cecil, K.M., McIntosh, T.K., Smith, D.H. (1999). Diffuse axonal pathology detected with magnetization transfer imaging following brain injury in the pig. *Mag. Res. Med.* **41**, 727- 733.

McLaurin, J., D`Souza, S., Stewart, J., Blain, M., Beaudet, A., Nalbantoglu, J., Antel, J.P. (1995). Effect of tumor necrosis factor α and β on human oligodendrocytes and neurons in culture. *Int. J. Dev. Neurosci.* **13**, 369-381.

Medana, I.M., Esiri, M.M. (2003). Axonal damage: a key predictor of outcome in human CNS disease. *Brain.* **126**, 515-530.

Meguro, K., Constans, J-M., Shimada, M., Yamaguchi, S., Ishizaki, J., Ishi, H., Yamadori, A., Sekita, Y. (2003). Corpus callosum atrophy, white matter lesions, and frontal executive dysfunction in normal aging and Alzheimer's disease. A community-based study: The Tajiri project. *Inter. Psychoger.***15**, 9-25.

Mehler, M.F. (2008). Epigenetic principles and mechanisms underlying central nervous system functions in health and disease. *Prog. Neurobiol.* **86**, 305-341.

Meir, K.S., Leitersdorf, E. (2004). Atherosclerosis in the apolipoprotein E-deficient mouse : a decade of progress. *Arterioscler Thromb Vasc Biol.* **24**, 1006-1014.

Merrill, J.E., Scolding, N.J. (1999). Mechanisms of damage to myelin and oligodendrocytes and their relevance to disease. *Neuropathol. Appl. Neurobiol.* **25**, 435–458.

Methia, N., Andre, P., Hafezi- Moghadam, A., Economopoulos, M., Thomas, K.L., Wanger, D.D. (2001). ApoE deficiency compromises the blood brain barrier especially after Injury. *Mol. Med.* **7**, 810- 815.

Metzger, R.E., LaDu, M.J., Pan, J.B., Getz, G.S., Frail, D.E., Falduto, M.T. (1996). Neurons of the human frontal cortex display apolipoprotein E immunoreactivity: implications for Alzheimer's disease. *J. Neuropathol. Exp. Neurol.* **55,** 372-380.

Meyer, R., Weissert, R., Diem, R., Storch, M.K., de Graaf, K.L., Kramer, B., Bahr, M. (2001). Acute neuronal apoptosis in a rat model of multiple sclerosis. *J. Neurosci.* **21**, 6214–6220.

Mies, G., Niebuhr, I., Hossmann, K-A. (1981). Simultaneous measurement of blood flow and glucose metabolism by autoradiographic techniques. *Stroke.* **12**, 581-588.

Miguez, J.M., Aldegunde, M., Paz-Valinaz, L., Recio, J., Sanchez- Barcelo, E. (1999). Selective changes in the contents of noradrenaline, dopamine and serotonin in rat brain areas during aging. *J. Neural. Transm.* **106**, 1089-1098.

Milutinovic, S., D'Alessio, A.C., Detich N.,, Szyf, M. (2007). Valproate induces widespread epigenetic reprogramming which involves demethylation of specificgenes. *Carcinogenesis.* **28**, 560–571.

Minagar, A., Shapshak, P., Fujimura, R., Ownby, R., Heyes, M., Eisdorfer, C. (2002). The role of macrophage/microglia and astrocytes in the pathogenesis of three neurologic disorders: HIV-associated dementia, Alzheimer disease, and multiple sclerosis. *J. Neurol. Sci.* **202**, 13-23.

Minger, S.L., Esiri, M.M., McDonald, B., Keene, J., Carter, J., Hope, T., Francis, P.T. (2000). Cholinergic deficits contribute to behavioral disturbance in patients with dementia. *Neurol.* **55**, 1460–1467.

Mitrovic, B., Ignarro, L.J., Vinters, H.V., Akers, M-A., Schmid, I., Uittenbogaarts, C., Merrill, J.E. (1995). Nitric oxide induces necrtotic, but not aopoptotic cell death in oligodendrocytes. *Neurosci.* **65**, 531-539.

Miyata, M., Smith, J.D. (1996). Apolipoprotein E allele-specific antioxidant activity and effects on cytotoxicity by oxidative insults and beta-amyloid peptides. *Nat. Genet.* **14**, 55-61.

Moffat, S.D., Szekely, C.A., Zonderman, A.B., Kabani, N.J., Resnick, S.M. (2000). Longitudinal change in hippocampal volume as a function of apolipoprotein E genotype. *Neurol.* **55**, 134–136.

Molina, C.A., Saver, J.L. (2005). Extending reperfusion therapy for acute ischemic stroke emerging pharmacological, mechanical, and imaging strategies. *Stroke.* **36**, 2311-2320.

Montag, D., Glese, P.K., Bartsch, U., Martini, R., Lang, Y., Bluthmann, H., Karthigasan, J., Kirschner, D.A., Wintergerst, E.S., Nave, K-A., Zielasek, J., Toyka, K.V., Lipp, H-P., Schachner, M. (1994). Mice deficient for the myelin- associated glycoprotein show subtle abnormalities in myelin. *Neuron.* **13**, 229-246.

Montine, T.J., Montine, K.S., Olson, S.J., Graham, D.G., Roberts II, L.J., Morrow, J.D., Linton, M.F., Fazio, S., Swift, L.L. (1999). Increased cerebral cortical lipid peroxidation and abnormal phospholipids in aged homozygous apoE- deficient C57BL/6J mice. *Exp. Neurol.* **158**, 234- 241.

Montpied, P., de Bock, F., Lerner-Natoli, M., Bockaert, J., Rondouin, G. (1999). Hippocampal alterations of apolipoprotein E and D mRNA levels in vivo and in vitro following kainate excitotoxicity. *Epilepsy Res.* **35**, 135-146.

Moore, H., Dudchenko, P., Bruno, J.P., Sarter, M (1992). Toward modeling age-related changes of attentional abilities in rats: Simple and choice reaction time tasks and vigilance. *Neurobiol. Aging.* **13**, 759-772.

Moore, K.J., Tabas, I. (2011). Macrophages in the pathogenesis of atherosclerosis. *Cell.* **145**, 341-355.

Morris, R.G.M. (1984). Development of a watermaze procedure for studying spatial learning in the rat. *J. Neurosci. Methods.* **11,** 47- 60.

Morris, J.C., Price, J.L. (2001). Pathologic correlates of nondemented aging, mild cognitive impairment, and early-stage Alzheimer's disease. *J. Mol. Neurosci.* **17**, 101-118.

Mosconi, L., Sorbi, S., de Leon, M.J., Li, Y., Nacmias, B., Myoung, P.S., Tsui, W., Ginestroni, A., Bessi, V., Fayyazz. M., Caffarra, P., Puppi, A. (2006). Hypometabolism exceeds atrophy in presymptomatic early-onset familial Alzheimer's disease. *J. Nucl. Med.* **47**, 1778–1786.

Moseley, M.E., Cohen, Y., Mintorovitch, J., Chileuitt, L., Shimizu, H., Kucharczyk, J., Wendland, M.F., Weinstein, P.R. (1990). Early detection of regional cerebral ischemia in cats: comparison of diffusion- and T_2-weighted MRI and spectroscopy. *Magn. Reson. Med.* **14**, 330–346.

Murakami, Y., Ikenoya, M., Matsumoto, K., Li, H.B., Watanabe, H. (2000). Ameliorative effect of tacrine on spatial memory deficit in chronic two-vessel occluded rats is reversible and mediated by muscarinic M1 receptor stimulation. *Behav. Brain Res.* **109**, 83–90.

Murakami, Y., Zhao, Q., Harada, K., Tohda, M., Watanabe, H., Matsumoto, K. (2005). Choto-san, a Kampo formula, improves chronic cerebral hypoperfusion-induced spatial learning deficit via stimulation of muscarinic M1 receptor. *Pharmacol. Biochem. Behav.* **81**, 616 – 625.

Murray, C., Sanderson, D.J., Barkus, C., Deacon, R.M.J., Rawlins, J.N.P., Bannerman, D.M., Cunningham. C. (2012). Systemic inflammation induces acute working memory deficits in the primed brain: relevance for delirium. *Neurobiol. Aging.* **33**, 603–616.

Nagara, H., Inoue, T., Koga, T., Kitaguchi, T., Tateishi, J., Goto, I. (1987). Formalin fixed brains are useful for magnetic resonance imaging (MRI) study. *J. Neurol. Sci.* **81**, 67-77.

Nakashima, Y.., Plump, A.S., Raines, E.W., Breslow, J.L., Ross, R. (1994). ApoE-deficient mice develop lesions of all phases of atherosclerosis throughout the arterial tree. *Arterioscler. Thromb. Vasc. Biol.* **14**, 133-140.

Nan, X., Ng, H-H., Johnson, C.A., Laherty, C.D., Turner, B.M., Eisenman, R.N., Bird, A.P. (1998). Transcriptional repression by the methyl-CpG-binding protein MeCP2 involves a histone deacetylase complex. *Nature*. **393**, 386-389.

Nanri M, Miyake H, Murakami Y, Matsumoto K, Watanabe H. GTS-21, a nicotinic agonist, attenuates multiple infarctions and cognitive deficit caused by permanent occlusion of bilateral common carotid arteries in rats. *Jpn. J. Pharmacol.* **78**, 463–469.

Nave, K.A., Lai, C., Bloom, F.E., Milner, R.J. (1986). Jimpy mutant mouse : a 74- base deletion in the mRNA for myelin proteolipid protein and evidence for a primary defect in RNA splicing. *Proc. Natl. Acad. Sci. USA*. **83**, 9264-9268.

Nave, K-A., Trapp, B.D. (2008). Axon- glial signaling and the glial support of axon function. *Annu. Rev. Neurosci.* **31**, 535-561.

Nelissen, K., Mulder, M., Smets, I., Timmermans, S., Smeets, K., Ameloot, M., Hendriks, J.J.A. (2012). Liver X receptors regulate cholesterol homeostasis in oligodendrocytes. *J. Neurosci. Res.* **90**, 60–71.

Nestor, C., Ruzov, A., Meehan, R.R., Dunican, D.S. (2010). Enzymatic approaches and bisulfite sequencing cannot distinguish between 5-methylcytosine and 5-hydroxymethylcytosine in DNA. *BioTechn.* **48**, 317-319.

Neuwelt, E.A., Paguel, M., Barnett, P., Glassberg, M., Frenkel, E.P. (1981). Pharmacology and toxicity of intracarotid adriamycin administration following osmotic blood- brain barrier modification. *Cancer Res.* **41**, 4466-4470.

Ni, J-W., Matsumoto, K., Li, H-B., Murakami, Y., Watanabe, H. (1995). Neuronal damage and decrease of central acetylcholine level following permanent occlusion of bilateral common carotid arteries in rat. *Brain Res.* **673**, 290-296.

Nicoll, J.A.R., Roberts, G.W., Graham, D.I. (1995). Apolipoprotein E ε4 allele is associated with deposition of amyloid β- protein following head injury. *Nat. Med.* **1**, 135-137.

Nishio, K., Ihara, M., Yamasaki, N., Kalaria, R.N., Maki, T., Fujita, Y., Ito, H., Oishi, N., Fukuyama, H., Miyakawa, T., Takahashi, R., Tomimoto, H. (2010). A mouse model characterizing features of vascular dementia with hippocampal atrophy. *Stroke.* **41**, 1278-1284.

Nonaka, H., Akima, M., Hatori, T., Nagayama, T., Zhang, Z., Ihara, F. (2003). Microvasculature of the human cerebral white matter: arteries of the deep white matter. *Neuropathol.* **23**, 111-118.

O`Brien, J.S., Sampson, E.L. (1965). Lipid composition of the normal human brain: gray matter, white matter, and myelin. *J. Lipid Res.* **6**, 537-544.

Ogawa, M., Fukuyama, H., Ouchi, Y., Yamauchi, H., Kimura, J. (1994). Altered energy metabolism in Alzheimer` s disease. *J. Neurol. Sci.* **139**, 78-82.

Ohtaki, H., Fujimoto, T., Sato, T., Kishimoto, K., Fujimoto, M., Moriya, M., Shioda, S. (2006). Progressive expression of vascular endothelial growth factor (VEGF) and angiogenesis after chronic ischemic hypoperfusion in rat. *Acta Neurochir. Suppl*. **96**, 283–287.

Okada, Y., Matsumoto, A., Shimazaki, T., Enoki, R., Koizumi, A., Ishii, S., Itoyama, Y., Sobue, G., Okano, H. (2008). Spatiotemporal recapitulation of central nervous system development by murine embryonic stem cell-derived neural stem/progenitor cells. *Stem Cells*. **26**, 3086-3098.

Okano, M., Xie, S., Li, E. (1998). Dnmt2 is not required for de novo and maintenance methylation of viral DNA in embryonic stem cells. *Nucleic Acids Res.* **26**, 2536-2540.

Okano, M., Bell, D.W., Haber, D.A., Li, E. (1999). DNA methyltransferases Dnmt3a and Dnmt3b are essential for de novo methylation and mammalian development. *Cell.* **99**, 247-257.

O`Leary, D.H., Polak, J.F., Kronmal, R.A., Kittner, S.J., Bond, G.M., Wolfson, Jr. S.K., Bommer, W., Price, T.R., Gardian, J.M., Savage, P.J. (1992). Distribution and correlates of sonographically detected carotid artery disease in the Cardiovascular Health Study. The CHS Collaborative Research Group. *Stroke.* **23**, 1752-1760.

Olendorf, W.H. (1989). Trophic changes in the arteries at the base of the brain in response to bilateral common carotid ligation. *J. Neuropathol. Exp. Neurol.* **48**, 534-547.

Olton, D.S., Samuelson, R.J. (1976). Remembrance of places passed: spatial memory in rats. *J. Exp. Psychol.* **2,** 97- 116.

Ophir, G., Meilin, S., Efrati, M., Chapman, J., Karussis, D., Roses, A., Michaelson, D.M. (2003). Human apoE3 but not apoE4 rescues impaired astrocyte activation in apoE null mice. *Neurobiol. Dis*. **12**, 56- 64.

O` Sullivan, M., Jones, D.K., Summers, P.E., Morris R.G., Williams, S.C.R., Markus, H.S. (2001). Evidence for cortical "disconnection" as a mechanism of age- related cognitive decline. *Neurology.* **57**, 632-638.

Otero, G.C., Merrill, J.E. (1994). Cytokine reseptors on glial cells. *Glia.* **11**, 117-128.

Otori, T., Katsumata, T., Muramatsu, H., Kashiwagi, F., Katayama, Y., Terashi, A. (2003). Long- term measurement of cerebral blood flow and metabolism in a rat chronic hypoperfusion model. *Clin. Exp. Pharmacol. Physiol.* **30**, 266-272.

Ou, X., Sun, S-W., Liang, H-F., Song, S-K., Gochberg, D.F. (2009). The MT pool size ratio and the DTI radial diffusivity may reflect the myelination in shiverer and control mice. *NMR Biomed.* **22**, 480-487.

Ouchi, Y., Tsukada, H., Kakiuchi, T., Nishiyama, S., Futatsubashi, M. (1998). Changes in cerebral blood flow and postsynaptic muscarinic cholinergic activity in rats with bilateral carotid artery ligation. *J. Nucl. Med.* **39**, 198–202.

Palacios, G., Palacios, J.M., Mengod, G., Frey, P. (1992). β-Amyloid precursor protein localization in the Golgi apparatus in neuron and oligodendrocytes. An immunocytochemical structural and ultrastructural study in normal and axotomized neurons. *Mol. Brain Res.* **15,** 195-206.

Pappas, B.A., de la Torre, J.C., Davidson, C.M., Keyes, M.T., Fortin, T. (1996). Chronic reduction of cerebral blood flow in the adult rat: late- emerging CA1 cell loss and memory dysfunction. *Brain Res.* **708**, 50-58.

Pardo, J.V., Lee, J.T., Sheikh, S.A., Surerus- Johnson, C., Shah, H., Munch, K.R., Carlis, J.V., Lewis, S.M., Kuskowski, M.A., Dysken, M.W. (2007). Where the brain grows old: decline in anterior cingulated and medial prefrontal function with normal aging. *NeuroImage.* **35**, 1231-1237.

Park, E., Velumian, A.A., Fehlings, M.G. (2004). The role of excitotoxicity in secondary mechanisms of spinal cord injury: a review with an emphasis on the implications for white matter degeneration. *J. Neurotrauma.* **21**, 754-774.

Parkhurst, C.N., Gan, W-B. (2010). Microglia dynamics and function in the CNS. *Curr. Opin. Neurobiol.* **20**, 595-600.

Pasparakis, M., Alexopoulou, L., Episkopou, V., Kollias, G. (1996). Immune and inflammatory responses in TNFα-deficient mice: a critical requirement for TNFα in the formation of primary B cell follicles, follicular dendritic cell networks and germinal centers, and in the maturation of the humoral immune response. *J. Exp. Med.* **184,** 1397-1411.

Paul, L.K., Brown, W.S., Adolphs, R., Tyszka, J.M., Richards, L.J., Mukherjee, P., Sherr, E.H. (2007). Agenesis of the corpus callosum: genetic, developmental and functional aspects of connectivity. *Nat. Rev. Neurosci.* **8**, 287-299.

Penke, L., Maniega, S.M., Houlihan, L.M., Murray, C., Gow, A.J., Clayden, J.D., Bastin, M.E., Wardlaw, J.M., Deary, I.J. (2010). White matter integrity in the splenium of the corpus callosum is related to successful cognitive aging and partly mediates the protective effects of an anscestral polymorphism in ADRB2. *Behav. Genet.* **40**, 146-156.

Penn, N.W., Suwalski, R., O`Riley, C., Bojanowski, K., Yura, R. (1972). The presence of 5- hydroxymethylcytosine in animal deoxyribonucleic acid. *Biochem. J.* **126**, 781-790.

Penner, M.R., Roth, T.L., Barnes, C.A., Sweatt, J.D. (2010). An epigenetic hypothesis of aging- related cognitive dysfunction. *Front. Aging Neurosci.* **2**, 1-11.

Persson, J., Lind, J., Larsson, A., Ingvar, M., Cruts, M., Van Broeckhoeven, C., Adolfsson, R., Nilsson, L-G., Nyberg, L. (2006). Altered brain white matter integrity in healthy carriers of the APOE ε4 allele: a risk for AD? *Neurology.* **66**, 1029-1033.

Peters, A. (1966). The node of Ranvier in the central nervous system. *Quart. J. Exp. Physiol*. **51**, 229-236.

Peters, A., Moss, M.B., Sethares, C. (2000). Effects of aging on myelinated nerve fibers in the monkey primary visual cortex. *J. Comp. Neurol.* **419**, 364- 376.

Peters, A., Sethares, C. (2002). Aging and the myelinated fibers in the prefrontal cortex and corpus callosum of the monkey. *J. Comp. Neurol.* **442**, 277- 291.

Pfefferbaum, A., Sullivan, E.V., Adalsteinsson, E., Garrick, T., Harper, C. (2004). Postmortem MR imaging of formalin- fixed human brain. *NeuroImage.* **21**, 1585-1595.

Picard-Riera, N., Nait-Oumesmar, N., Baron-Van Evercooren, A. (2004). Endogenous adult neural stem cells: limits and potential to repair the injured central nervous system. *J. Neurosci. Res*. **76**, 223–231.

Piedrahita, J.A., Zhang, S.H., Hagaman, J.R., Oliver, P.M., Maeda, N. (1992). Generation of mice carrying a mutant apolipoprotein E gene inactivated by gene targeting in embryonic stem cells. *Proc. Natl. Acad. Sci. USA.* **89**, 4471-4475.

Plaisant, F., Clippe, A., Stricht, D.V., Knoops, B., Gressens, P. (2003). Recombinant peroxiredoxin 5 protects against excitotoxic brain lesions in newbron mice. *Free Rad. Biol. Med.* **34**, 862–872.

Plaschke, K. (2005). Aspects of ageing in chronic cerebral oligaemia. Mechanisms of degeneration and compensation in rat models. *J. Neural. Transm.* **112**, 393-413.

Poduslo, S.E., Miller, K. (1985). Levels of sulfatides synthesis distinguish oligodendroglia in different stages of maturation. *Neurochem. Res.* **10**, 1285-1297.

Poirier, J., Baccichert, A., Dea, D., Gauthier, S. (1993). Cholesterol synthesis and lipoprotein reuptake during synaptic remodeling in hippocampus in adult rats. *Neurosci.* **55**, 81- 90.

Post, W.S., Goldschmidt-Clermont, P.J., Wilhide, C.C., Heldman, A.W., Sussman, M.S., Ouyang, P., Milliken, E.E., Issa, J.J.P. (1999). Methylation of the estrogen receptor gene is associated with aging and atherosclerosis in the cardiovascular system. *Cardiovas. Res.* **43**, 985-991.

Poulsen, P., Esteller, M., Vaag, A., Fraga, M.F. (2007). The epigenetic basis of twin discordance in age-related diseases. *Pediatr. Res.* **61**, 38R–42R.

Pratico, D., Rockach, J., Tangilara, R.K. (2002). Brains of aged apolipoprotein E-deficient mice have increased levels of F_2-Isoprostanes, in vivo markers of lipid peroxidation. *J. Neurochem.* **73**, 736- 741.

Premkumar, D.R.D., Cohen, D.L., Hedera, P., Friedland, R.P., Kalaria, R.N. (1996). Apolipoprotein E- ε4 alleles in cerebral amyloid angiopathy and cerebrovascular pathology Associated with Alzheimer's Disease. *Am. J. Pathol.* **148**, 2083-2095.

Preston, E., Foster, D.O. (1997). Evidence for pore-like opening of the blood–brain barrier following forebrain ischemia in rats. *Brain Res.* **761**, 4–10.

Ptak, C., Petronis, A. (2008). Epigenetics and complex disease: from etiology to new therapeutics. *Annu. Rev. Pharmacol. Toxicol.* **48**, 257–276.

Quarles, R.H. (2007). Myelin- associated glycoprotein (MAG): past, present and beyond. *J. Neurochem.* **100**, 1431-1448.

Qiu, Z., Strickland, D.K., Hyman, B.T., Rebeck, G.W. (2002). alpha 2-Macroglobulin exposure reduces calcium responses to N-methyl-D-aspartate via low density lipoprotein receptor-related protein in cultured hippocampal neurons. *J. Biol. Chem.* **277**, 14458-14466.

Raffai, R.L., Dong, L.M., Farese, R.V., Weisgraber, K.H. (2001). Introduction of human apolipoprotein E4 "domain interaction" into mouse apolipoprotein E. *Proc. Natl. Acad. Sci. USA.* **98,** 11587-11591.

Rahman, S.M.A., Van Dam, A-M., Schultzberg, M., Crisby, M. (2005). High cholesterol diet results in increased expression of interleukin-6 and caspase-1 in the brain of apolipoprotein E knockout and wild type mice. *J. Neuroimmunol*. **169**, 59 – 67.

Ramakrischnan, H., Hedayati, K.K., Lullmann- Rauch, R., Wessig, C., Fewou, S.N., Maier, H., Goebel, H- H., Gieselmann, V., Eckhardt, M. (2007). Increasing sulfatide synthesis in myelin-forming cells of arylsulfatase A-deficient mice causes demyelination and neurological symptoms reminiscent of human metachromatic leukodystrophy. *J. Neurosci.* **27**, 9482–9490.

Ramassamy, C.**,** Krzywkowski, P., Averill, D., Lussier-Cacan, S., Theroux, L., Christen, Y., Davignon, J., Poirier, J. (2001). Impact of apoE deficiency on oxidative insults and antioxidant levels in the brain. *Mol. Brain. Res.* **31**, 76- 83.

Ravera, S., Panfoli, I., Galzia, D., Aluigi, M.G., Bianchini, P., Diaspro, A., Mancardi, G., Morelli, A. (2009). Evidence for aerobic ATP synthesis in isolated myelin vesicles. *Int. J. Biochem. Cell Biol.* **41**, 1581-1591.

Raz, N., Gunning, F.M., Head, D., Dupuis, J.H., McQuain, J., Briggs, S.D., Loken, W.J., Thornton, A.E., Acker, J.D. (1997). Selective aging of the human cerebral cortex observed *in vivo*: differential vulnerability of the prefrontal gray matter. *Cereb. Cortex.* **7**, 268–282.

Readhead, C., Hood, R. (1990). The dymyelinating mouse mutation shiverer (*shi*) and the myelin deficient (*shi*^{mld}). *Behav. Genet.* **20**, 213-234.

Redford, E.J., Hall, S.M., Smith, K.J. (1995). Vascular changes and demyelination induced by the intraneuronal injection of tumor necrosis factor. *Brain*. **118**, 869-878.

Reeves, S., Bench, C., Howard, R. (2002). Ageing and the nigrostriatal dopaminergic system. *Int. J. Geriatr. Psychiatr.* **17**, 359–370.

Reiman, E.M., Caselli, R.J., Yun, L.S., Chen, K., Bandy, D., Minoshima, S., Thibodeau, S.N., Osborne, D. (1996). Preclinical evidence of Alzheimer's disease in persons homozygous for the epsilon 4 allele for apolipoprotein E. *N. Eng. J. Med.* **334**, 752- 758.

Reiman, E.M., Chen, K., Alexander, G.E., Caselli, R.J., Bandy, D., Osborne, D., Saunders, A.M., Hardy, J. (2004). Functional brain abnormalities in young adults at the genetic risk for late- onset Alzheimer`s disease. *Proc. Natl. Acad. Sci. USA.* **101**, 284-289.

Reimer, M.M., McQueen, J., Searcy, L., Scullion, G., Zonta, B., Desmazieres, A., Holland, P.R., Smith, J., Gliddon, C., Wood, E.R., Herzyk, P., Brophy, P.J., McCulloch, J., Horsburgh, K. (2011). Rapid disruption of axon- glial integrity in response to mild cerebral hypoperfusion. *J. Neurosci.* **31**, 18185–18194.

Reynolds, R., Dawson, M., Papadopoulos, D., Polito, A., Cenci Di Bello, I., Pham-Dinh, D., Levine, J. (2002). The response of NG2- expressing oligodendrocyte progenitors to demyelination in MOG-EAE and MS. *J. Neurocytol.* **31**, 523-536.

Ricci, J-E., Munoz- Pinedo, C., Fitzgerald, P., Bailly-Maitre, B., Perkins, G.A., Yadava, N., Scheffer, I.E., Ellisman, M.H., Green, D.R. (2004). Disruption of mitochondrial

function during apoptosis is mediated by caspase cleavage of the p75 subunit of complex I of the electron transport chain. *Cell.* **117**, 773-786.

Riggs, A.D. (1975). X inactivation, differentiation, and DNA methylation. *Cytogenet. Cell Genet.* **14**, 9-25.

Rinholm, J.E., Hamilton, N.B., Kessaris, N., Richardson, W.D., Bergeresen, L.H., Attwell, D. (2011). Regulation of oligodendrocyte development and myelination by glucose and lactate. *J. Neurosci*. **31**, 538-548.

Rodriguez, M., Scheithauer, B. (1994). Ultrastructure of multiple sclerosis. *Ultrastruct. Pathol*. **18**, 3–13.

Rolls, E.T. (2000). Hippocampo- cortical and cortico- cortical backprojections. *Hippocampus.* **10**, 380-388.

Roman, G.C., Kalaria, R.N. (2006). Vascular determinants of cholinergic deficits in Alzheimer disease and vascular dementia. *Neurobiol. Aging.* **27**, 1769–1785.

Rosas, H.D., Tuch, D.S., Hevelone, N.D., Zaleta, A.K., Vangel, M., Hersch, S.M., Salat, D.H. (2006). Diffusion tensor imaging in presymptomatic and early Huntington's disease: selective white matter pathology and its relationship to clinical measures. *Move. Disor.* **21**, 1317–1325.

Rosenberg, G.A., Sullivan, N., Esiri, M.M., Sobel, R.A. (2001). White matter disease is associated with matrix metalloproteinases in vascular dementia. Editorial comments: Matrix metalloproteinases and diffuse white matter injury. *Stroke.* **32**, 1162-1168.

Ruitenberg, A., den Heijer, T., Bakker, S.L.M., van Swieten, J.C., Koudstaal, P.J., Hofman, A., Breteler, M.M.B. (2005). Cerebral hypoperfusion and clinical onset of dementia: The Rotterdam study. *Ann. Neurol.* **57**, 789-794.

Ruzov, A., Tsenkina, Y., Serio, A., Dudnakova, T., Fletcher, J., Chebotareva, T., Pells, Hannoun, Z., Sullivan, G., Chandran, S., Hay, D., Bradley, M., Wilmut, I., De Sousa, P.

(2011). Lineage specific distribution of high levels of genomic 5-hydroxymethylcytosine in mammalian development. *Cell Res.* **21**,1332-1342.

Ryan, L., Walther, K., Bendlin, B.B., Lue, L-F., Walker, D.G., Glisky, E.L. (2011). Age-related differences in white matter integrity and cognitive function are related to APOE status. *NeuroImage*. **54**, 1565-1577.

Saher, G., Brugger, B., Lappe- Siefke, C., Mobius, W., Tozawa, R-I., Wehr, M.C., Wieland, F., Ishibashi, S., Nave, K-A. (2005). High cholesterol level is essential for myelin membrane growth. *Nature*. **8**, 468-475.

Salat, D.H., Tuch, D.S., Greve, D.N., van der Kouwe, A.J.W., Hevelone, N.D., Zaleta, A.K., Rosen, B.R., Fischl, B., Corkin, S., Rosas, H.D., Dale, A.M. (2005). Age- related alterations in white matter microstructure measured by diffusion tensor imaging. *Neurobiol. Aging.* **26**, 1215-1227.

Salehi, A., Wu, C., Zhan, K., Mobley, W.C. (2009). Axonal transport of neurotrophic signals. An Achille`s heel for neurodegeneration? *Res. Pers. Alzh. Dis.* 87-101, DOI: 10.1007/978-3-540-87941-1_7.

Samuraki, M., Matsunari, I., Chen, W.P., Yajima, K., Yanase, D., Fujikawa, K., Takeda, N., Nishimura, S., Matsuda, H., Yamada, M. (2007). Partial volume effect-corrected FDG PET and grey matter volume loss in patients with mild Alzheimer's disease. *Eur J Nucl Med. Mol. Imaging.* **34**, 1658–1669.

Sanchez- Abarca, L.I., Tabernero, A., Medina, J.M. (2001). Oligodendrocytes use lactate as a source of energy and as a precursor of lipids. *Glia.* **36**, 321-329.

Sattler, R., Tymianski, M. (2001). Molecular mechanisms of glutamate receptor-mediated excitotoxic neuronal cell death. *Mol. Neurobiol.* **24**, 107-129.

Saunders, A.M., Strittmatter, W.J., Schmechel, D., George-Hyslop, P.H., Pericak-Vance, M.A., Joo, S.H., Rosi, B.L., Gusella, J.F., Crapper-MacLachlan, D.R., Alberts, M.J.

(1993). Association of apolipoprotein E allele epsilon 4 with late-onset familial and sporadic Alzheimer's disease. *Neurology*. **43**, 1467-1472.

Saugier- Veber, P., Munnich, A., Bonneau, D., Rozet, J.M., Le Merrer, M. (1994). X-linked spastic paraplegia and Pelizaeus- Merzbacher disease are allelic disorders at the proteolipid protein locus. *Nat. Genet.* **6**, 257-262.

Saunders, A.M., Strittmatter, W.J., Schmechel, D., George-Hyslop, P.H., Pericak-Vance, M.A., Joo, S.H., Rosi, B.L., Gusella, J.F., Crapper-MacLachlan, D.R., Alberts, M.J. (1993). Association of apolipoprotein E allele epsilon 4 with late-onset familial and sporadic Alzheimer's disease. *Neurology*. **43**, 1467-1472.

Schachner, M. (1994). Mice deficient for the myelin- associated glycoprotein show subtle abnormalities in myelin. *Neuron*. **13**, 229-246.

Schmierer, K., Scaravilli, F., FRCPath, Dphil, D.R.A., Barker, G.J., Miller, D.H., FRCP. (2004). Magnetization transfer ratio and myelin in postmortem multiple sclerosis brain.*Ann. Neurol.* **56**, 407- 415.

Schuff, N., Matsumoto, S., Kmiecik, J., Studholme, C., Du, A., Ezekiel, F., Miller, B.L., Kramer, J.H., Jagust, W.J., Chui, H.C., Weiner, M.W. (2009a). Cerebral blood flow in ischemic vascular dementia and Alzheimer` s disease, measured by arterial spin- labeling magnetic resonance imaging. *Alzh. Dem.* **5**, 454-462.

Schuff, N., Woerner, N., Boreta, L., Kornfield, T., Shaw, L.M., Trojanowski, J.Q., Thompson, P.M., Jack Jr, C.R., Weiner, M.W., the Alzheimer`s Disease Neuroimaging Initiative (2009b). MRI of hippocampal volume loss in early Alzheimer's disease in relation to ApoE genotype and biomarkers. *Brain.* **132**, 1067–1077.

Schwartz, G., Fehlings, M.G. (2001). Evaluation of the neuroprotective effects of sodium channel blockers after spinal cord injury: improved behavioral and neuroanatomical recovery with riluzole. *J. Neurosurg. (Spine 2).* **94,** 245–256.

Selden, N.R., Gitelman, D.R., Salamon- Murayama, N., Parrish, T.B., Mesulam, M.M. (1998). Trajectories of cholinergic pathways within the cerebral hemispheres of the human brain. *Brain.* **121**, 2249-2257.

Selkoe, D. (1994). Normal and abnormal biology of the beta- amyloid precursor protein. *Ann. Rev. Neurosci.* **17**, 489-517.

Sfaello, I., Baud, O., Arzimanoglou, A., Gressens, P. (2005). Topiramate prevents excitotoxic damage in the newborn rodent brain. *Neurobiol. Dis.* **20**, 837 – 848.

Shang, Y., Cheng, J., Oi, J., Miao, H., (2005). Scutellaria flavonoid reduced memory dysfunction and neuronal injury caused by permanent global ischemia in rats. *Pharmacol. Biochem. Behav*. **82**, 67–73.

Shen, S., Sandoval, J., Swiss, V.A., Li, J., Dupree, J., Franklin, R.J., Casaccia-Bonnefil, P. (2008). Age-dependent epigenetic control of differentiation inhibitors is critical for remyelination efficiency. *Nat. Neurosci*. **11**, 1024-101034.

Sheng, H., Laksowitz, D.T., Bennett, E., Schmechel, D.E., Bart, R.D., Saunders, A.M., Pearlstein, R.D., Roses, A.D., Warner, D.S. (1998). Apolipoprotein E isoform-specific differences in outcome from focal ischemia in transgenic mice. *J. Cereb. Blood Flow Metab.* **18**, 361-366.

Sheng, H., Laskowitz, D.T., Mackensen, G.B., Kudo, M., Pearlstein, R.D., Warner, D.S. (1999). Apolipoprotein E deficiency worsens outcome from global cerebral ischemia in the mouse. *Stroke*. **30**, 1118 –1124.

Sherman, D.L., Brophy, P.J. (2005).Mechanisms of axon ensheathment and myelin growth. *Nat. Rev. Neurosci*. **6**, 683-690.

Shibata, M., Ohtani, R., Ihara, M., Tomimoto, H. (2004). White matter lesions and glia activation in a novel mouse model of chronic cerebral hypoperfusion. *Stroke.* **35**, 2598-2603.

Shibata, M., Yamasaki, N., Miyakawa, T., Kalaria, R.N., Fujita, Y., Ohtani, R., Ihara, M., Takahashi, R., Tomimoto, H. (2007). Selective impairment of working memory in a mouse model of chronic cerebral hypoperfusion. *Stroke.* **38**, 2826- 2932.

Shore, V.G., Shore, B. (1973). Heterogeneity of human plasma very low density lipoproteins. Separation of species differing in protein components. *Biochemistry.* **12**, 502-507.

Siegel, J.A., Benice, T.S., Van Meera, P., Park, B.S., Raber, J. (2011). Acetylcholine receptor and behavioral deficits in mice lacking apolipoprotein E. *Neurobiol. Aging.* **32**, 75–84.

Siesjo, B.K., Zhao, Q., Pahlmark, K., Siesjo, P., Katsura, K-I., Folbregrova, J. (1995). Glutamate, calcium, and free radicals as mediators of ischemic brain damage. *Ann. Thor. Surg.* **59**, 1316-1320.

Skoog, I., Hesse, C., Aevarsson, O., Landahl, S., Wahlstrom, J., Fredman, P., Blennow, K. (1998). A population study of apoE genotype at the age of 85: relation to dementia, cerebrovascular disease, and mortality. *J. Neurol. Neurosurg. Psychiatry.* **64**, 37-43.

Sloane, J.A., Hollander, W., Moss, M.B., Rosene, D.L., Abraham, C.R. (1999). Increased microglial activation and protein nitration in white matter of the aging monkey. *Neurobiol. Aging.* **20**, 395–405.

Smith, C.D., Chebrolu, H., Andersen, A.H., Powell, D.A., Lovell, M.A., Xiong, S., Gold, B.T. (2010). White matter diffusion alterations in normal women at risk of Alzheimer's disease. *Neurobiol. Aging.* **31**, 1122-1131.

Song, H., Stevens, C.F., Gage, F.H. (2002). Astroglia induce neurogenesis from adult neural stem cells. *Nature.* **417**, 39-44.

Song, S-K., Sun, S-W., Ju, W-K., Lin, S-J., Cross, A.H., Neurfeld, A.H. (2003). Diffusion tensor imaging detects and differentiates axon and myelin degeneration in mouse optic nerve after retinal ischemia. *NeuroImage.* **20**, 1714-1722.

Song, S-K., Yoshito, J., Le, T.Q., Lin, S-J., Sun, S-W., Cross, A.H., Armstrong, R.C. (2005). Demyelination increases radial diffusivity in corpus callosum of mouse brain. *NeuroImage.* **26,** 132-140.

Song, C-X., Szulwach, K.E., Fu, Y., Dai, Q., Yi, C., Li, X., Li, Y., Chen, C-H., Zhang, W., Jian, X., Wang, J., Zhang, L., Looney, T.J., Zhang, B., Godley, L.A., Hicks, L.M., Lahn, B.T., Jin, P., He, C. (2010). Selective chemical labeling reveals the genome- wide distribution of 5- hydroxymethylcytosine. *Nat. Biotech.* **29**, 68-72.

Sopala, M., Danysz, W. (2001). Chronic cerebral hypoperfusion in the rat enhances age-related deficits in spatial memory. *J. Neural. Transm.* **108**, 1445-1456.

Spooner, R.I., Thomson, A., Hall, J., Morris, R.G., Salter, S.H. (1994). The Atlantis platform: a new design and further developments of Buresova`s on- demand platform for the water maze. *Learn. Mem.* **1,** 203- 211.

Stephenson, D.T., Rash, K., Clemens, J.A. (1992). Amyloid precursor protein accumulates in regions of neurodegeneration following focal cerebral ischemia in the rat. *Brain Res.* **593**, 128-135.

Stoll, G., Muller, H.W., Trapp, B.D., Griffin, J.W. (1989). Oligodendrocytes, but not astrocytes express apolipoprotein E after injury of rat optic nerve. *Glia.* **2**, 170-176.

Strittmatter, W.J., Saunders, A.M., Schmechel, D., Pericak-Vance, M., Enghild, J., Salvesen, G.S., Roses, A.D. (1993). Apolipoprotein E, high-avidity binding to beta-amyloid and increased frequency of type 4 allele in late-onset familial Alzheimer disease. *Proc. Natl. Acad. Sci. USA.* **90**, 1977-1981.

Stys, P.K. (1998). Anoxic and ischemic injury of myelinated axons in CNS white matter: from mechanistic concepts to therapeutics. *J. Cer. Blood Flow Metab.* **18**, 2-25.

Stys, P.K. (2005). General mechanisms of axonal damage and its prevention. *J. Neurol. Sci.* **233**, 3 – 13.

Sugiyama, I., Tanaka, K., Akita, M., Yoshida, K., Kawase, T., Asou, H. (2002O. Ultrastructural analysis of the paranodal junction of myelinated fibers in 31-month-old rats. *J. Neurosci. Res.* **70**, 309–317.

Sullivan, E.V., Zahr, N.M., Rohlfing, T. Pfefferbaum, A. (2010). Fiber tracking functionally distinct components of the internal capsule. *Neuropsychologia.* **48**, 4155–4163.

Sun, S-W., Neil, J.J., Song, S-K. (2003). Relative indices of water diffusion anisotropy are equivalent in live and formalin- fixed mouse brains. *Magn. Res. Med.* **50**, 743-748.

Sun, S-W., Neil, J.J., Liang, H-F., He, Y.Y., Schmidt, R.E., Hsu, C.Y., Song, S-K. (2005). Formalin fixation alters water diffusion coefficient magnitude but not anisotropy in infracted brain. *Magn. Res. Med.* **53**, 1447-1451.

Sun, S-W., Liang, H-F., Trinkaus, K., Cross, A.H., Armstrong, R.C., Song, S-K. (2006a). Noninvasive detection of cuprizone induced axonal damage and demyelination in the mouse corpus callosum. *Mag. Res. Med.* **55**, 302-308.

Sun, S-W., Liang, H-F., Le, T.Q., Armstrong, R.C., Cross, A.H., Song, S-K. (2006b). Differential sensitivity of in vivo and ex vivo diffusion tensor imaging to evolving optic nerve injury in mice with retinal ischemia. *NeuroImage.* **32**, 1195- 1204.

Surani, M.A., Hajkova, P. (2010). Epigenetic reprogramming of mouse germ cells toward totipotency. *Cold Spring Harb. Symp. Quant. Biol.* 1-8.

Svennerholm, L., Bostrom, K., Jungbjer, B., Olsson, L. (1994). Membrane lipids of adult human brain: lipid composition of frontal and temporal lobe in subjects of age 20 to 100 years. *J. Neurochem.* **63**, 1802-1811.

Switzer, R.C. (2000). Morphologic approaches for evaluating nervous system injury. *Toxicol. Pathol.* **28**, 70-83.

Syde, A.B., Armstrong, R.A., Smith, C.U.M. (2005). A quantitative analysis of optic nerve axons in elderly control subjects and patients with Alzheimer's disease. *Folia Neuropathol.* **43**, 1-6.

Szulwach, K.E., Li, X., Li, Y., Song, C-X., Wu, H., Dai, Q., Irier, H., Upadhyay, A.K., Gearing, M., Levey, A.I., Vasanthakumar, A., Godley, L.A., Chang, Q., Cheng, X., He, C., Jin, P. (2011). 5-hmC–mediated epigenetic dynamics during postnatal neurodevelopment and aging. *Nat. Neurosci.* **14,** 1607-1616.

Tahiliani, M., Koh, K.P., Shen, Y., Pastor, W.A., Bandukwala, H., Brudno, Y., Agarwal, S., Iyer, L.M., Liu, D.R., Aravind, L., Rao, A. (2009). Conversion of 5- methylcytosine to 5- hydroxymethylcytosine in mammalian DNA by MLL partner TET1. *Science.* **324**, 930-935.

Takasago, T., Peters, E.E., Graham, D.I., Masayasu, H., Macrae, I.M. (1997). Neuroprotective efficacy of ebselen, an anti-oxidant with anti- inflammatory actions, in a rodent model of permanent middle cerebral artery occlusion. *B. J. Pharmacol.* **122**, 1251-1256.

Tanaka, K., Ogawa, N., Asanuma, M., Kondo, Y., Nomura, M. (1996). Relationship between cholinergic dysfunction and discrimination learning disabilities in Wistar rats following chronic cerebral hypoperfusion. *Brain Res.* **729**, 55–65.

Tang, Y., Nyengaard, J.R., Pakkenberg, B., Gundersen, H.J.G. (1997). Age- induced white matter changes in the human brain: a stereological investigation. *Neurobiol. Aging.* **18**, 609-615.

Teipel, S.J., Bayer, W., Alexander, G.E., Bokde, A.L.W., Zebuhr, Y., Teichberg, D., Muller- Spahn, F., Schapiro, M.B., Moller, H-J., Rapoport, S.I., Hampel, H. (2003). Regional pattern of hippocampus and corpus callosum atrophy in Alzheimer's disease in relation to dementia severity: evidence for early neocortical degeneration. *Neurobiol. Aging.* **24**, 85-94.

Tekin, S., Cummings, J.L. (2002). Frontal–subcortical neuronal circuits and clinical neuropsychiatry: An update. *J. Psychosom. Res.* **53**, 647– 654.

Tekkok, S.B., Goldberg, M.P. (2001). AMPA/ kainate receptor activation mediates hypoxic oligodendrocyte death and axonal injury in cerebral white matter. *J. Neurosci.* **21**, 4237-4248.

Tekkok, S.B., Ye, Z., Ransom, B.R. (2007). Excitotoxic mechanisms of ischemic injury in myelinated white matter. *J. Cereb. Blood Flow Metab.* **27**, 1540–1552.

Terano, T., Fujishiro, S., Ban, T., Yamamoto, K., Tanaka, T., Noguchi, Y., Tamura, Y., Yazawa, K., Hirayama, T. (1999). Docosahexaenoic acid supplementation improves the moderately severe dementia from thrombotic cerebrovascular diseases, *Lipids.* **34**, (Suppl.). S345–S346.

Terasawa, K., Shimada, Y., Kita, T., Yamamoto, T., Tosa, H., Tanaka, N., Saito, Y., Kanaki, E., Goto, S., Mizushima, N., Fujioka, M., Takase, S., Seki, S., Kimurn, I., Ogawa, T., Nakamura, N., Araki, G., Maruyama, I., Maruyama, Y., Takaori, S. (1997). Choto-san in the treatment of vascular dementia: a double-blind, placebo-controlled study. *Phytomed.* **4**, 15– 22.

Thaung, C., Arnold, K., Jackson, I.J., Coffey, P.J. (2002). Presence of visual head tracking differentiates normal sighted from retinal degenerate mice. *Neurosci. Lett.* **325**, 21- 24.

Thelen, K.M., Falkai, P., Bayer, T.A., Lutjohann, D. (2006). Cholesterol synthesis rate in human hippocampus declines with aging. *Neurosci. Lett.* **403**, 15- 19.

Thorburne, S.K., Juurlink, B.H. (1996). Low glutathione and high iron govern the susceptibility of oligodendroglial precursors to oxidative stress. *J. Neurochem.* **67**, 1014-1022.

Titomanlio, L., Bouslama, M., Le Verche, V., Dalous, J., Kaindl, A., Tsenkina, Y., Lacaud, A., Peineau, S., Elghouzzi, V., Lelievre, V., Gressens, P. (2011). Implanted neurosphere- derived precursors promote recovery after neonatal excitotoxic brain injury. *Stem cells Dev.* **20**, 865-879.

Todorich, B., Pasquini, J.M., Garcia, C.I., Paez, P.M., Connor, J.R. (2009). Oligodendrocytes and myelination: the role of iron. *Glia.* **57**, 467-478.

Tohgi, H., Utsugisawa, K., Nagane, Y., Yoshimura, M., Ukitsu, M., Genda, Y. (1999). The methylation status of cytosines in a tau gene promoter region alters with age to dowregulate transcriptional activity in human cerebral cortex. *Neurosci. Lett.* **275**, 89-92.

Tomimoto, H., Ihara, M., Wakita, H., Ohtani, R., Lin, J-X., Akiguchi, I., Kinoshita, M., Shibasaki, H. (2003). Chronic cerebral hypoperfusion induces white matter lesions and loss of oligodendroglia with DNA fragmentation in the rat. *Acta Neuropathol.* **106**, 527-534.

Trapp, B.D., Peterson, J., Ransohoff, R.M., Rudik, R., Mork, S., Bo, L. (1998). Axonal transection in the lesions of multiple sclerosis. *N. Eng. J. Med.* **338**, 278-285.

Trollor, J.N., Smith, E., Baune, B.T., Kochan, N.A., Campbell, L., Samaras, K., Crawford, J., Brodaty, H., Sachdev, P. (2010). Systemic inflammation is associated with MCI and its subtypes: the Sydney memory and aging study. *Dement. Geriatr. Cogn. Disord.* **30,** 569–578.

Ueno, M., Tomimoto, H., Akiguchi, I., Wakita, H., Sakamoto, H. (2001). Blood- brain barrier disruption in white matter lesions in a rat model of chronic cerebral hypoperfusion. *J. Cereb. Blood Flow Metab.* **22**, 97-104.

Utermann, G., Hees, M., Steinmetz, A. (1977). Polymorphism of apolipoprotein E and occurrence of dysbetalipoproteinaemia in man. *Nature.* **269**, 604-607.

Valinluck, V., Tsai, H.H., Rogstad, D.K., Burdzy, A., Bird, A., Sowers, L.C. (2004). Oxidative damage to methyl- CpG- sequences inhibits the binding of the methyl- CpG binding domain (MBD) of methyl- CpG binding protein 2 (MeCP2). *Nucleic Acids Res.* **32**, 4100- 4108.

Van Der Zee, E.A., Platt, B., Riedel, G. (2011). Acetylcholine: Future research and perspectives. *Behav. Brain Res.* **221**, 583–586.

Van Ree, J.H., van den Broek, W.J., Dahlmans, V.E., Groot, P.H., Vidgeon-Hart, M., Frants, R.R., Wieringa, B., Havekes, L.M., Hofker, M.H. (1994). Diet-induced hypercholesterolemia and atherosclerosis in heterozygous apolipoprotein E-deficient mice. *Atherosclerosis.* **111**, 25-37.

Van Reempts, J., Haseldockx, M., van Deuren, B., Wouters, L., Borgers, M. (1986). Structural damage to the ischemic brain: involvement of calcium and effects of postischemic treatment with calcium entry blockers. *Drug Dev. Res.* **8**, 387-395.

Van Swieten, J.C., Geyskes, G.G., Derix, M.M.A., Peeck, B.M., Ramos, M.P., van Latum, J.C., van Gijn, J. (1991). Hypertension in the elderly is associated with white matter lesions and cognitive decline. *Ann. Neurol.* **30**, 825-830.

Vartanian, T., Li, Y., Zhao, M., Stefansson, K. (1995). Interferron gamma- induced oligodendrocyte cell death: implications for the pathogenesis of multiple sclerosis. *Mol. Med.* **1**, 732-743.

Vela, J.M., Molina- Holgado, E., Arevalo- Martin, A., Almazan, G., Guaza, C. (2002). Interleukin-1 regulates proliferation and differentiation of oligodendrocyte progenitor cells. *Mol. Cell. Neurosci.* **20**, 489-502.

Verdelho, A., Madureira, S., Moleiro, C., Ferro, J.M., Santos, C.O., Erkinjuntti, T., Pantoni, L., Fazekas, F., Visser, M., Waldemar, G., Wallin, A., Hennerici, M., Inzitari, D. and on behalf of the LADIS Study (2010). White matter changes and diabetes predict cognitive decline in the elderly The LADIS Study. *Neurology.* **75**, 160-167.

Vesalius, A. (1543). De humanis corporis fabrica libri septem, in Andreae Vesalii Bruxellensis, scholae medicorum Patauinae professoris De humani corporis fabrica libri septem. Basileae (Basel). *Ex officina Joannis Oporini*

Virchow, R. (1854). Über das ausgebreitete Vorkommen einer dem Nervenmark analogen Substanz in den tierischen Geweben". *Virchows Arch. Pathol. Anat.* **6**, 562–572.

Volpe, J.J. (2001). Neurobiology of periventricular leukomalacia in the premature infant. *Pediatr. Res.* **50**, 553-562.

Volterra, A., Meldolesi, J. (2005). Astrocytes, from brain glue to communication elements: the revolution continues. *Nat. Rev. Neurosci.* **6**, 626-640.

Waddington, C.H. (1942). The epigenotype. *Endeavour.* **1**, 18–20.

Wahner, A.D., Bronstein, J.M., Bordelon, Y.M., Ritz, B. (2007). Nonsteroidal anti-inflammatory drugs may protect against Parkinson disease. *Neurol.* **69**, 1836- 1842.

Wagle, J., Farner, L., Flekkшy K., Wyller, T.B., Sandvik L., Eiklid, K.L., Fure, B., Stensrшd, B., Engedal, K. (2009). Association between ApoE ε4 and cognitive impairment after stroke. *Dement. Geriatr. Cogn. Disord.* **27**, 525–533.

Wakita, H., Tomimoto, H., Akiguchi, I., Kimura, J. (1994) Glial activation and white matter changes in the rat brain induced by chronic cerebral hypoperfusion: an immunohistochemical study. *Acta Neuropathol. (Berl).* **87**, 484–492.

Wakita, H., Tomimoto, H., Akiguchi, I., Matsuo, A., Lin, J-X., Ihara, M., McGeer, P- L. (2002). Axonal damage and demyelination in the white matter after chronic cerebral hypoperfusion in the rat. *Brain Res.* **924.** 63-70.

Wang, D-S., Bennett, D.A., Mufson, E.J., Mattila, P., Cochran, E., Dickson, D.W. (2004). Contribution of changes in ubiquitin and myelin basic protein to age-related cognitive decline. *Neurosci. Res.* **48**, 93-100.

Wang, S.C., Oelze, B., Schumacher, A. (2008). Age- specific epigenetic drift in late-onset Alzheimer`s disease. *PLoS One.* **3**, e2698.

Waxman, S.G. (2006). Axonal conduction and injury in multiple sclerosis: the role of sodium channels. *Nat. Neurosci. Rev.* **7**, 932-941.

Weisgraber, K.H. (1994). Apolipoprotein E: structure-function relationships. *Adv. Protein Chem.* **45**, 249-302.

Weiss, M. D., Hammer, J., Quarles, R. H. (2000). Oligodendrocytes in aging mice lacking myelin-associated glycoprotein are dystrophic but not apoptotic. *J. Neurosci. Res.* **62**, 772–780.

Weiss, M. D., Luciano, C. A., Quarles, R. H. (2001). Nerve conduction abnormalities in aging mice deficient for myelin-associated glycoprotein. *Muscle Nerve.* **24**, 1380–1387.

West, R.L., Lee, J.M., Maroun, L.E. (1995). Hypomethylation of the amyloid precursor protein gene in the brain of an Alzheimer`s disease patient. *J. Mol. Neurosci.* **6**, 141-146.

Westberry, J.M., Prewitt, A.K., Wilson, M.E. (2008). Epigenetic regulation of the estrogen receptor alpha promoter in the cerebral cortex following ischemia in male and female rats. *Neurosci.* **152**, 982-989.

Wilkins, A., Majed, H., Layfield, R., Compston, A., Chandran, S. (2003). Oligodendrocytes promote neuronal survival and axonal length by distinct intracellular mechanisms: a novel role for oligodendrocyte- derived glial cell line- derived neurotrophic factor. *J. Neurosci.* **23**, 4967-4974.

Wilson, A. G. (2008). Epigenetic regulation of gene expression in the inflammatory response and relevance to common diseases. *J. Periodontol.* **79**, 1514-1519.

Wishart, H.A., Saykin, A.J., Rabin, L.A., Santulli, R.B., Flashman, L.A., Guerin, S.J., Mamourian, A.C., Belloni, D.R., Rhodes, C.H., McAllister, T.W. (2006). Increased brain activation during working memory in cognitively intact adults with the APOE ε4 allele. *Am. J. Psychiatry.* **163**, 1603-1610.

Witting, P.K., Pettersson, K., Letters, J., Stocker, R. (2000). Anti-atherogenic effect of coenzyme Q10 in apolipoprotein E gene knockout mice. *Free Radical Biol. Med.* **29**, 295-305.

Wolff, S.D., Balaban, RS. (1989). Magnetization transfer contrast (MTC) and tissue water proton relaxation in vivo. *Magn. Res.Med.* **10,** 135-144.

Wossidlo M, Nakamura T, Lepikhov K, Marques CJ, Zakhartchenko V, Boiani M, Arand J, Nakano T, Reik W, Walter J. (2011). 5-Hydroxymethylcytosine in the mammalian zygote is linked with epigenetic reprogramming. *Nat .Commun.* **2**, 241.

Wright, C.B., Sacco, R.L., Rundek,T.R., Delman, J.B., Rabbani, L.E., Elkind, M.S.V. (2006). Interleukin-6 is associated with cognitive function: the Northern Manhattan study. *J. Stroke Cerebrovas. Dis.* **15**, 34-38.

Wright, C.B., Festa, J.R., Paik, M.C., Schmiedigen, A., Brown, T.R., Yoshita, M., DeCarli, C., Sacco, R., Stern, Y. (2008). White matter hyperintensities and subclinical infarction: associations with psychomotor speed and cognitive flexibility. *Stroke.* **39**, 800-805.

Wu, Q-Z., Yang, Q., Cate, H.S., Kemper, D., Binder, M., Wang, H-X., Fang, K., Quick, M.J., Marriott, M., Kilpatrick, T.J., Egan, G.F. (2008). MRI identification of the rostral-caudal pattern of pathology within the corpus callosum in the cuprizone mouse model. *J. Mag. Res. Imag*. **27**, 446-453.

Wu, S.C., Zhang, Y. (2010). Active DNA demethylation: many roads lead to Rome. *Nat. Rev. Mol. Cellular Biol.* **11**, 607- 620.

Wyatt, G.R. (1951). Recognition and estimation of 5-methylcytosine in nucleic acids. *Biochem. J.* **48**, 581-584.

Wyatt, G.R., Cohen, S.S. (1952). A new pyramidine base from bacteriophage nucleic acid. *Nature.* **170**, 1072-1073.

Xi, M- C., Liu, R- H., Engelhardt, K.K., Morales, F.R., Chase, M.H. (1999). Changes in the axonal conduction velocity of pyramidal tract neurons in the aged cat. *Neurosci.* **92**, 219- 225.

Yamada, M.,Ihara, M., Okamoto, Y., Maki, T., Washida, K., Kitamura, A., Hase, Y., Ito, H., Takao, K., Miyakawa, T., Kalaria, R.N., Tomimoto, H., Takahashi, R. (2011). The influence of chronic cerebral hypoperfusion on cognitive function and amyloid b metabolism in APP overexpressing mice. *PloSOne.* **6**, e16567.

Yang, G., Kitagawa, K., Matsushita, K., Mabuchi, T., Yagita, Y., Yanagihara, T., and Matsumoto, M. (1997). C57BL/6 strain is most susceptible to cerebral ischemia following bilateral common carotid occlusion among seven mouse strains: selective neuronal death in the murine transient forebrain ischemia. *Brain Res.* **752**, 209–218.

Yanagisawa, K. (2002). Cholesterol and pathological processes in Alzheimer` s disease. *J. Neurosci. Res.* **70**, 361- 366.

Ye, S-M., Johnson, R.W. (1999). Increased interleukin-6 expression by microglia from brain of aged mice. *J. Neuroimmunol.* **93**, 139–148.

Yi, J-H., Hazell, A.S. (2006). Excitotoxic mechanisms and the role of astrocytic glutamate transporters in traumatic brain injury. *Neurochem. Int.* **48**, 394-403.

Yip, A.G., McKee, A.C., Green, R.C., Wells, J., Young, H., Cupples, L.A., Farrer, L.A. (2005). APOE, vascular pathology, and the AD brain. *Neurol.* **65**, 259- 265.

Yoder, J.A., Soman, N.S., Verdine, G.L., Bestor, T.H. (1997). DNA (cytosine- 5)-methyltransferases in mouse cells and tissues. Studies with a mechanism- based probe. *J. Mol. Biol.* **270**, 385-395.

Yonezawa, M., Back, S.A., Gan, X., Rosenberg, P.A., Volpe, J.J. (1996). Cystine deprivation induces oligodendroglial death: rescue by free radical scavengers and by a diffusible glial factor. *J. Neurochem.* **67**, 566-573.

Young, J.W., Powell, S.B., Geyer, M.A., Jeste, D.V., Risbrough, V.B. (2010). The mouse attentional- set- shifting task: a method for assaying successful cognitive aging. *Cogn. Affect. Beh. Neurosci.* **10**, 243-251.

Zafonte, R.D., Giap, B.T., Coplin, W.M., Pangilian, P. (1999). Traumatic brain injury and spinal cord injury: pathophysiology and acute therapeutic strategies. *Top. Spinal Cord Inj. Rehabil.* **5**, 21–40.

Zannis,V.I., Just, P.W., Breslow, J.L. (1981). Human apolipoprotein E isoprotein subclasses are genetically determined. *Am. J. Hum. Genet.* **33**, 11-24.

Zawia, N.H., Lahiri, D.K., Cardozo-Pelaez, F. (2009). Epigenetics, oxidative stress, and Alzheimer disease. *Free Rad. Biol.Med.* **46**, 1241–1249.

Zhang, K., Sejnowski, T.J. (2000). A universal scaling law between gray matter andwhite matter of cerebral cortex. *Proc. Natl. Acad. Sci. USA*. **97**, 5621–5626.

Zhang, Z-Y., Zhang, Z., Fauser, U., Schluesener, H.J. (2007). Clobal hypomethylation defines a sub-population of reactive/ macrophages in experimental traumatic brain injury. *Neurosci. Letters.* **429**, 1-6.

Zhao, S., Hu, X., Park, J., Zhu, Y., Qiang, Z., Hong, L., Luo, C., Han, R., Cooper, N., Qiu, M. (2007). Selective expression of LDLR and VLDLR in myelinating oligodendrocytes. *Dev. Dynamics.* **236**, 2708- 2712.

Zhu, B., Zheng, Y., Angliker, H., Schwartz, S., Thiry, S., Siegmann, M., Jost, J-P. (2000). 5- Methylcytosine DNA glycosylase activity is also present in the human MBD4 (G/T mismatch glycosylase) and in a related avian sequence. *Nucleic Acid Res*. **28**, 4157-4165.

Zhu, J-K. (2009). Active DNA demethylation mediated by DNA glycosylases. *Ann. Rev. Genetics.* **43**, 143-166.

Zlokovic, B.V. (2005). Neurovascular mechanisms of Alzheimer's neurodegeneration. *Trends Neursci.* **28**, 202-208.

ELSEVIER

Neurobiology of Aging 32 (2011) 2324.e7–2324.e12

NEUROBIOLOGY OF AGING

www.elsevier.com/locate/neuaging

Brief communication

Selective white matter pathology induces a specific impairment in spatial working memory

Robin Coltman[a,1], Aisling Spain[a,1], Yanina Tsenkina[a,1], Jill H. Fowler[a], Jessica Smith[a], Gillian Scullion[a], Mike Allerhand[b], Fiona Scott[a], Rajesh N. Kalaria[c], Masafumi Ihara[d], Stephanie Daumas[a], Ian J. Deary[a,b], Emma Wood[a], James McCulloch[a], Karen Horsburgh[a,*]

[a] *Centre for Cognitive Ageing and Cognitive Epidemiology and Centre for Cognitive and Neural Systems, University of Edinburgh, Edinburgh, UK*
[b] *Department of Psychology, University of Edinburgh, Edinburgh, UK*
[c] *Institute for Ageing and Health, Campus for Ageing and Vitality, University of Newcastle, Newcastle-upon-Tyne, UK*
[d] *Department of Neurology, Faculty of Medicine, Kyoto University, Kyoto, Japan*

Received 26 November 2009; received in revised form 20 August 2010; accepted 5 September 2010

Abstract

The integrity of the white matter is critical in regulating efficient neuronal communication and maintaining cognitive function. Damage to brain white matter putatively contributes to age-related cognitive decline. There is a growing interest in animal models from which the mechanistic basis of white matter pathology in aging can be elucidated but to date there has been a lack of systematic behavior and pathology in the same mice. Anatomically widespread, diffuse white matter damage was induced, in 3 different cohorts of C57Bl/6J mice, by chronic hypoperfusion produced by bilateral carotid stenosis. A comprehensive assessment of spatial memory (spatial reference learning and memory; cohort 1) and serial spatial learning and memory (cohort 2) using the water maze, and spatial working memory (cohort 3) using the 8-arm radial arm maze, was conducted. In parallel, a systematic assessment of white matter components (myelin, axon, glia) was conducted using immunohistochemical markers (myelin-associated glycoprotein [MAG], degraded myelin basic protein [dMBP], anti-amyloid precursor protein [APP], anti-ionized calcium-binding adapter molecule [Iba-1]). Ischemic neuronal perikarya damage, assessed using histology (hematoxylin and eosin; H&E), was absent in all shams but was present in some hypoperfused mice (2/11 in cohort 1, 4/14 in cohort 2, and 17/24 in cohort 3). All animals with neuronal perikaryal damage were excluded from further study. Diffuse white matter damage occurred, throughout the brain, in all hypoperfused mice in each cohort and was essentially absent in sham-operated controls. There was a selective impairment in spatial working memory, with all other measures of spatial memory remaining intact, in hypoperfused mice with selective white matter damage. The results demonstrate that diffuse white matter pathology, in the absence of gray matter damage, induces a selective impairment of spatial working memory. This highlights the importance of assessing parallel pathology and behavior in the same mice.

Keywords: Cognitive decline; Axonal damage; Myelin damage; Hypoperfusion

1. Introduction

Cognitive performance declines with advancing age and a number of measures are especially impaired such as processing speed, executive function, and episodic memory. These measures are increasingly linked to pathological changes in white matter in vivo using diffusion tensor imaging (Bucur et al., 2008; Deary et al., 2003). White matter lesions, at postmortem, are defined by a loss of white matter integrity and an inflammatory response, often associated with chronic cerebral hypoperfusion resulting from small vessel pathology (Fernando et al., 2006). Although there is a statistical association between the white matter pathology and age-related cognitive decline (Bucur et al., 2008), a causal relationship remains to be established. This is further confounded by the presence of other vascular factors such

* Corresponding author at: Centre for Cognitive and Neural Systems, School of Biomedical Sciences, University of Edinburgh, 1 George Square, Edinburgh, EH8 9JZ, UK. Tel.: +44 0131 650 6940; fax: +44 0131 651 1835.
E-mail address: karen.horsburgh@ed.ac.uk (K. Horsburgh).
[1] Each of these authors contributed equally to the work.

0197-4580/$ – see front matter © 2011 Published by Elsevier Inc.
doi:10.1016/j.neurobiolaging.2010.09.005

as atherosclerosis, hypertension, and diabetes which influence the presence of white matter lesions.

Experimental animal models have been developed in which white matter pathology is precipitated in response to chronic cerebral hypoperfusion. They allow the study of hypoperfusion, in isolation, on the development of white matter lesions and cognitive abilities, and provide a powerful tool to study the neurobiological basis of white matter lesions occurring in human brain in the absence of other confounding factors such as hypertension and diabetes. In rat models of chronic hypoperfusion (induced by permanent carotid ligation), deficits in spatial reference learning and memory are observed, although the presence of ischemic neuronal perikaryal damage complicates interpretation of the behavioral data (see Farkas et al., 2007). A mouse model of chronic cerebral hypoperfusion, produced by carotid stenosis using microcoils, has been developed (Shibata et al., 2004) which produces selective and delayed damage to the white matter. Separate behavioral studies of this mouse model demonstrated an impairment of spatial working memory, with intact spatial reference memory, and intact contextual and cued fear conditioning (Shibata et al., 2007). Thus, this model could provide a basis to define whether selective white matter pathology parallels cognitive decline. However, as yet, there has been no parallel assessment of cognition and pathology in the same animals. To address this we assessed spatial learning and memory in parallel with a systematic assessment of white and gray matter pathology in the same animals in the mouse model of chronic cerebral hypoperfusion.

2. Methods

2.1. Animals and experimental design

Chronic cerebral hypoperfusion was induced as previously described (Shibata et al., 2004) by applying microcoils (0.18-mm internal diameter) to both common carotid arteries in male 3–4-month-old C57Bl/6J mice (25–30 g) under isoflurane anesthesia. Sham mice underwent an identical surgical procedure to hypoperfused mice except the microcoils were not placed on the arteries. Mice were coded and randomized for surgery, and subsequent behavioral and pathological studies were conducted with investigators blind to the surgical status of the mice. Following behavioral testing, the mice were sacrificed under deep isoflurane anesthesia by transcardiac perfusion fixation, and the brains removed and processed for paraffin embedding. In cohort 1, cued learning and spatial reference learning and memory were assessed using a water maze task, and the subsequent pathological examination was conducted at 1 month after the onset of hypoperfusion. In cohort 2, cued learning and serial spatial learning and memory were assessed, also in a water maze, and the subsequent pathological examination was conducted at 2 months after the onset of hypoperfusion. In cohort 3, spatial working memory was assessed using an 8-arm radial arm maze and pathological examination was conducted at 2 months after the onset of hypoperfusion.

2.2. Pathological assessment of white matter integrity

Sections were stained with hematoxylin and eosin to determine the presence of neuronal perikarya damage. Adjacent sections were immunostained using standard techniques with different antibodies to visualize the cellular components of white matter. The loss of myelin integrity, assessed using anti-myelin-associated glycoprotein (MAG, Santa Cruz Biotechnologies, Santa Cruz, CA, USA), was identified by the presence of disorganized white matter fibers and myelin debris and graded from 0–3 (none–extensive). Degraded myelin, assessed using anti-dMBP (Millipore, Watford, UK), was identified by the presence of intensely stained irregular myelin sheaths which were graded from 0–3 (none–extensive). Axonal damage, visualized using antiamyloid precursor protein (APP, Millipore), was identified as intense APP immunoreactivity in swollen or bulbous axons and graded as 0–3 (none–extensive). Microglial activation was assessed using anti-ionized calcium-binding adapter molecule (Iba-1, Menarini, Wokingham, UK) and activated cells per mm^2 defined. Cellular changes were assessed in corpus callosum, external capsule, internal capsule, fimbria hippocampus, optic tract, and the fiber bundles of the caudate nucleus and the grading score summated from these 6 regions.

2.3. Cue task

The motivation and ability to swim were assessed using a cued task in the water maze for 1 day before surgery and at 3 weeks after surgery for 5 days (cohort 1) or 4 days (cohort 2).

2.4. Spatial reference learning and memory task

Animals from cohort 1 were trained to find a hidden platform over 5 days with 4 trials per day (10-minute intertrial interval [ITI]), beginning 3 days after the cue task ended. The platform location remained constant throughout testing. To test memory retention, probe trials were run 10 minutes and 24 hours after the final training trial.

2.5. Serial spatial learning and memory task

Animals from cohort 2 were trained on this task as described previously (Chen et al., 2000; Daumas et al., 2008) beginning 3 days after the cue task ended. Each animal was first trained to swim to a hidden platform for up to 8 trials per day (10-minute intertrial interval [ITI]; maximum of 32 trials), to a criterion of 3 successive trials with an escape latency of less than 20 seconds. The platform location remained the same on each trial. Once this criterion was achieved, the platform was moved to a new location on the following day, and the mouse commenced training on the second location, again until it reached criterion. This

procedure was repeated for at least 5 different platform locations, and for at least 10 days. The number of trials taken to reach criterion for each of the first 5 platform locations (trials to criterion), and the number of platform locations learned within 10 days (learning capacity) were analyzed. To assess memory for each platform location, 2 probe tests were conducted 10 minutes and 3 hours after reaching criterion on each of the first 5 platform locations.

2.6. Spatial working memory

Animals from cohort 3 were trained on this task as described previously (Shibata et al., 2007). Mice were trained over 16 days on an 8-arm radial arm maze in which, on each daily testing session, each arm was baited with a single reward. Each animal was placed in the center of the maze, and allowed to explore the maze until it retrieved all 8 rewards. Between arm choices each mouse was confined to the central platform for 5 seconds. The number of entries into baited arms during the first 8 arm choices, and the number of visits into unbaited arms during the whole session (revisiting errors) were analyzed. Full details of all behavioral methods are available in the supplementary methods.

2.7. Statistics

Statistical comparisons of myelin and axonal damage between sham and hypoperfused groups were made using Fisher's exact test. Microglial activation was analyzed with Student *t* test. Behavioral data were analyzed using 2-way analysis of variance (ANOVA) with the Greenhouse-Geisser correction. Student *t* test with Bonferroni adjustment for multiple comparisons was used post hoc. Learning capacity data in the serial spatial task were analyzed using an unpaired Student *t* test.

3. Results

3.1. Pathology

There was no evidence of neuronal perikaryal damage in any brain region in any of the sham-operated mice. Ischemic neuronal perikaryal damage was seen in 2 out of 11 hypoperfused animals in cohort 1, in 4 out of 14 hypoperfused mice in cohort 2, and in 17 out of 24 hypoperfused mice in cohort 3. The mice in cohort 3 were food-deprived for the radial arm maze task which may contribute to the higher frequency of ischemic neuronal damage in this cohort compared with cohorts 1 and 2. Mice exhibiting ischemic neuronal damage were excluded from the subsequent analysis of white matter pathology and behavior (Fig. 1A and B). In sham operated mice, minimal damage to the myelin or axons was detected in each region examined (corpus callosum, external capsule, internal capsule, fimbria, optic tract, and myelinated tracts within the caudate nucleus, Fig. 1K). In contrast, in hypoperfused animals, marked anatomically widespread damage to myelinated fibers was observed.

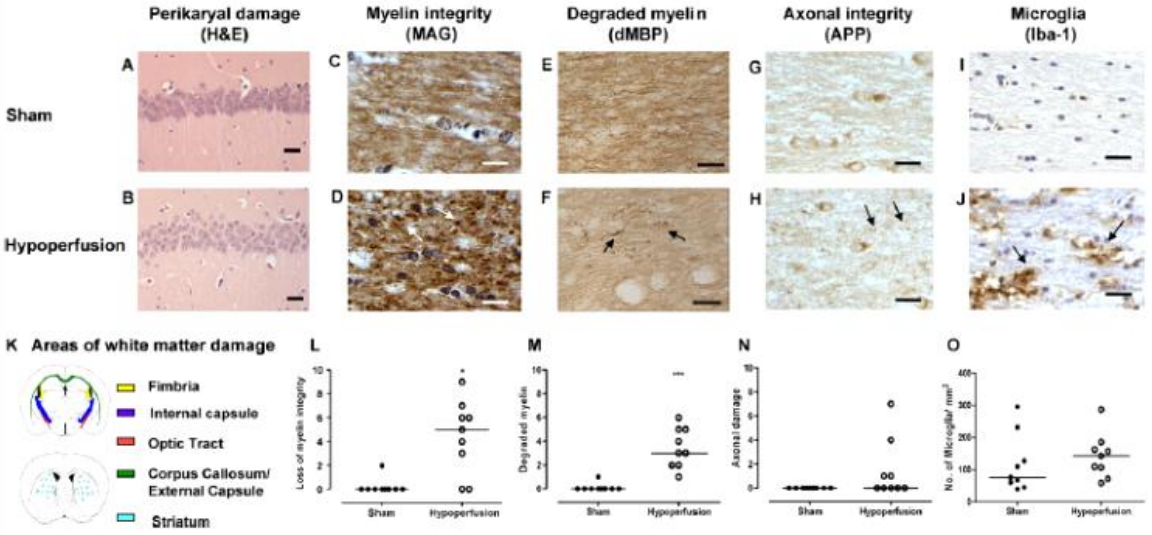

Fig. 1. Representative images to illustrate the integrity of the neuronal perikarya (CA1 region of the hippocampus; A,B) and white matter integrity (optic tract) of myelin (C, D), degraded myelin (E, F), axons (G, H), and microglia (I, J) in sham and hypoperfused mice. (K) The regions that were examined for white matter pathology. The grade of pathology or number of microglia from these regions was summated and analyzed between the groups. Data are shown from cohort 1 which is representative of the 3 cohorts as there was no significant difference in the extent of white matter damage between the cohorts. There was no neuronal perikarya damage in any of the sham (A) or the hypoperfused mice that were used for behavioral analysis (B). Myelin debris (D, arrows), and vacuolation, indicative of a loss of myelin integrity and damage, was significantly increased in hypoperfused animals (L) and there was also a significant increase in the extent of degraded myelin (dMBP) (M, see arrows F). There was evidence of axonal damage in hypoperfused mice (N, see arrows H), and the number of activated microglia was also increased after hypoperfusion (O, see arrows J). Scale bar represents 15 μm (A, B) and 30 μm (C–J).

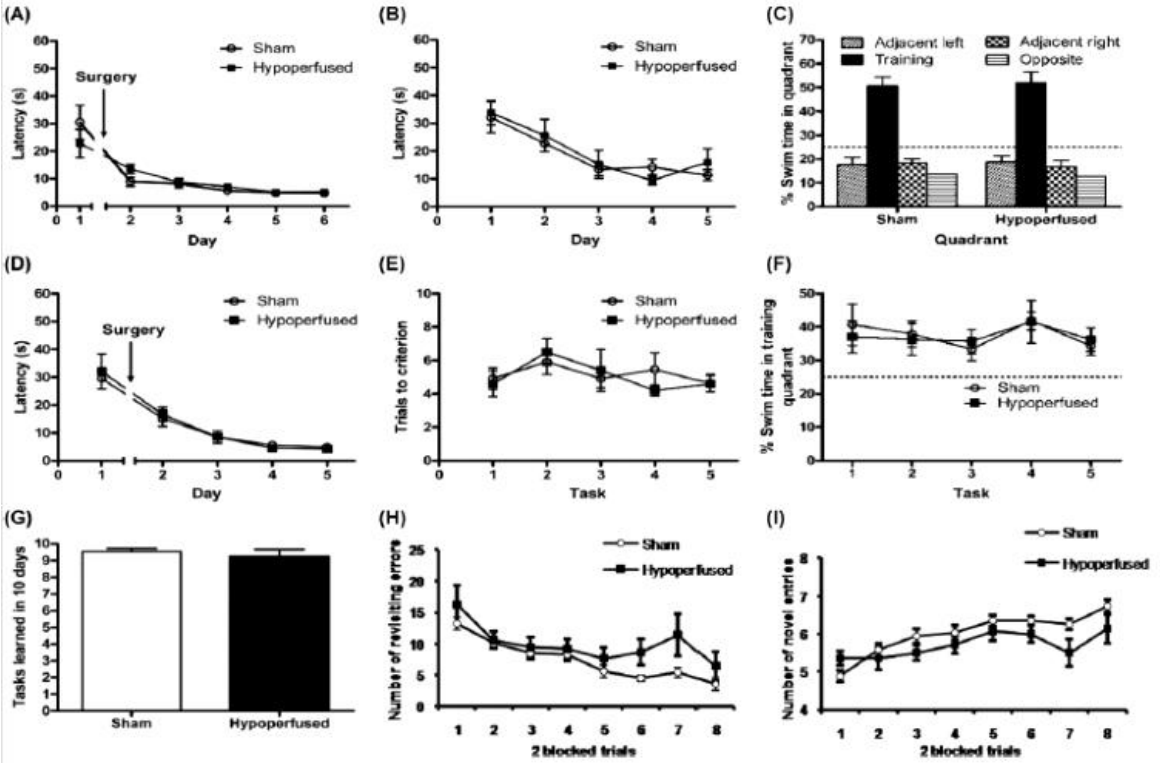

Fig. 2. Three different cohorts of mice underwent either a spatial reference learning and memory task (A–C), a serial spatial learning and memory task in the water maze (D–G), or a spatial working memory task in an 8-arm radial maze (H and I). In an initial cued platform task in the water maze, hypoperfused and sham groups in cohorts 1 and 2 showed similar learning and asymptotic levels of performance, indicating intact motor ability and motivation (A and D). The ability to learn the location of a hidden platform by cohort 1 was not affected by chronic cerebral hypoperfusion (B). Both groups of animals showed the same degree of preference for the quadrant in which they had been trained to find the platform when memory was probed 10 minutes after the task (C). In the serial spatial task (cohort 2), both sham and hypoperfused groups took a similar number of trials to reach criterion on each of the 5 platform locations (E). Both groups of animals showed the same degree of preference for the most recently learned platform location when memory was probed 10 minutes after each task (F). The number of platform locations the animals learned in 10 days was not statistically different between the shams and hypoperfused mice (G). In the spatial working memory task, hypoperfused mice exhibited significantly more revisiting errors in the 8-arm radial maze than sham mice [$F(1,22) = 6.981$; $p = 0.015$] (H). They also visited significantly fewer new arms in the first 8 arm entries than shams [$F(1,22) = 5.619$; $p = 0.027$] (I).

There was no difference in the extent of white matter damage between the 3 cohorts ($p < 0.05$, Kruskal-Wallis). In each cohort, there was extensive damage to the myelin (myelin debris, vacuolation, disorganization of fibers) (Fig. 1C, D, and L) in addition to an increased presence of degraded myelin after hypoperfusion compared with sham (Fig. 1E, F, and M). Axonal damage was observed in some hypoperfused mice but absent in shams (Fig. 1G, H, and N). Upregulation of microglia was also observed in response to hypoperfusion (Fig. 1I, J, and O).

3.2. Spatial learning and memory

3.2.1. Cue task

In the cued navigation task, there were no significant differences in performance between hypoperfused and sham groups in either cohort 1 (sham $n = 9$ and hypoperfused $n = 9$, $p = 0.97$; Fig. 2A) or cohort 2 (sham $n = 11$; hypoperfused $n = 10$, $p = 0.82$; Fig. 2D). In both cohorts, performance improved significantly across days (cohort 1 $p < 0.001$; cohort 2 $p < 0.001$) and escape latencies averaged less than 10 seconds in all groups by the end of training. Swim speeds did not differ significantly between the groups (supplementary data).

3.2.2. Spatial reference learning and memory task

There were no significant differences between hypoperfused ($n = 9$) and sham ($n = 9$) mice in the latency to reach the platform across training ($p = 0.66$; Fig. 2B). Both groups improved significantly over the training period ($p < 0.001$). Both groups also showed a similar preference for the quadrant in which they had been trained when memory for the platform location was probed at 10 minutes ($p = 0.97$; Fig. 2C) and 24 hours ($p = 0.53$; Supplementary Fig. 1A) after the end of training.

3.2.3. Serial spatial learning and memory task

There were no significant effects of hypoperfusion on any measure on this task. Sham ($n = 11$) and hypoperfused ($n = 10$) mice took a similar number of trials to reach criterion on the first 5 platform locations ($p = 0.85$; Fig. 2E). There were also no significant differences between the groups on the 10 minute ($p = 0.89$; Fig. 2F) and 3 hours ($p = 0.70$; Supplementary Fig. 1B) probe trials. The learning capacity, defined as the number of platform locations learned in 10 days, did not differ significantly between the groups ($p = 0.46$; Fig. 2G).

3.2.4. Spatial working memory

The hypoperfused mice ($n = 7$) committed significantly more revisiting errors than the sham group ($n = 17$) ($p = 0.015$; Fig. 2H). In addition, the hypoperfused mice visited significantly fewer new arms in the first 8 arm entries compared with shams ($p = 0.027$; Fig. 2I). There was a significant improvement in learning across days, with the number of errors committed by both groups decreasing significantly over the training period ($p < 0.001$) and the number of new arms visited in the first 8 arm entries increasing significantly over the same period ($p < 0.001$). Full details of statistical analyses and additional behavioral data are provided in the supplementary results.

4. Discussion

The development of a mouse model of chronic cerebral hypoperfusion has provided a powerful tool to study the effects of hypoperfusion, in isolation, on the development of white matter lesions and their impact on cognition. In human disease this type of study has been limited by the presence of multiple factors such as hypertension, atherosclerosis and diabetes, which may influence the development of white matter lesions. The present study provides a robust demonstration that diffuse white matter pathology, 1–2 months after chronic hypoperfusion, selectively impairs spatial working memory and does not affect a number of other different measures of spatial memory. Analysis of the behavioral consequences of white matter damage in rat models of chronic cerebral hypoperfusion are often limited by the presence of neuronal ischemic perikaryal damage (Farkas et al., 2007). In the mouse model of chronic cerebral hypoperfusion, in which selective white matter pathology occurs in a subset of animals, there has been an absence of parallel pathology and behavioral analysis in the same animals. Behavioral analysis, conducted in isolation, has indicated that chronic hypoperfusion results in deficits in spatial working memory in the absence of changes in spatial reference memory, or in contextual and cued fear conditioning (Shibata et al., 2007). Although separate cohorts of hypoperfused mice revealed the presence of selective white matter pathology in this model it is impossible to directly correlate pathology to behavior between different cohorts. Miki et al. (2009) recently addressed the impact of the severity of white matter abnormalities, as a result of hypoperfusion, on cognitive and motor abilities. They found a significant association between white matter integrity and performance on a probe test in a spatial reference memory task in the water maze and concluded that the deficits in spatial memory were caused by white matter lesions. However, all of the hypoperfused mice in their study exhibited a degree of hippocampal perikaryal damage which could have contributed to the behavioral deficit. In the present study we measured a range of spatial memory abilities. We hypothesised that the white matter lesions, as a result of cerebral hypoperfusion, would lead to disconnection and impair spatial learning and memory. We were able to demonstrate that selective white matter pathology is sufficient to impair spatial working memory. However, mice with the same degree of selective white matter pathology were able to learn the spatial reference memory task and demonstrated a similar degree of improvement over the period of training as shams. They also showed intact short (10 minute) and long term (24 hour) memory for the platform location. These data are consistent with those of Shibata et al. (2007) who reported no deficits on a spatial reference memory task conducted on a radial arm maze in hypoperfused mice at 1 month. In aging humans, there are clear links between white matter integrity and episodic memory and task switching (Bucur et al., 2008; Deary et al., 2003). Studies in aging monkeys have also revealed that spatial reversal memory is impaired and associated with white matter volume (Lyons et al., 2004). A novel behavioral task has been developed to investigate serial spatial learning and memory in mice (Chen et al., 2000). This task, which is sensitive to aging and Alzheimer pathology (Chen et al., 2000; Daumas et al., 2008), is a form of serial spatial memory in which mice are required to learn a series of different platform locations successively. Thus, once an animal has learned 1 location, the platform is moved to a novel location, and so on. Successful learning and recall of the successive platform locations requires the ability to encode changes in the spatial representation of the environment, and also the selective recall of the appropriate platform location (which requires memory flexibility — an element of episodic-like memory). We found that the spatial memory flexibility, memory retention, and learning capacity of the hypoperfused mice with selective white matter damage all remained intact in this task. Taken together, the behavioral data indicate an impairment only in the spatial task that requires the most behavioral flexibility, as the spatial working memory task requires constant updating of memory regarding which arms have been visited within a session, whereas the serial spatial learning task requires updating only across days, and the spatial reference memory task requires a consistent response to 1 rewarded location. Similar to previous studies, we determined that the mouse model of hypoperfusion is characterised by a predominantly white matter pathology (Miki et al., 2009; Shibata et al., 2004, 2007). Extending previous studies, we assessed the cellular vulnerability of white matter components using sensitive immunohistochemical approaches. In particular we found that the cellular distribution of MAG immunoreactivity is altered and that there is a significant

increase in degraded myelin in hypoperfused mice as compared with shams. Interestingly, MAG, which may function in glia-axon interactions, when deficient in MAG null mice does not affect spatial learning and memory assessed in the water maze (Montag, 1994). Thus in the present model, disruption of components of the white matter are able to induce a deficit in spatial working memory but may be insufficient to cause a detectable impairment of less challenging measures of spatial learning and memory.

Disclosure statement

All authors certify that they do not have any actual or potential conflicts of interest, including any financial, personal or other relationships with other people or organizations within 3 years of beginning this work, that could inappropriately influence (bias) this work.

All experiments were performed under an appropriate Home Office License with the approval of the University of Edinburgh Ethical Review Panel and subject to the Animals (Scientific Procedures) Act 1986.

Acknowledgements

The work was undertaken by the University of Edinburgh Centre for Cognitive Ageing and Cognitive Epidemiology, part of the cross council Lifelong Health and Wellbeing Initiative. The authors gratefully acknowledge the support of Age UK to which "The Disconnected Mind" project contributes. The support of the Alzheimer Research Trust, Alzheimer's Society, and Lloyd's TSB Foundation/ Royal Society of Edinburgh is also gratefully acknowledged. The studies in Newcastle are supported by the Medical Research Council, UK.

Appendix: A. Supplementary data

Supplementary data associated with this article can be found, in the online version, at doi:10.1016/j.neurobiolaging.2010.09.005.

References

Bucur, B., Madden, D.J., Spaniol, J., Provenzale, J.M., Cabeza, R., White, L.E., Huettel, S.A., 2008. Age-related slowing of memory retrieval: contributions of perceptual speed and cerebral white matter integrity. Neurobiol. Aging 29, 1070–1079.

Chen, G., Chen, K.S., Knox, J., Inglis, J., Bernard, A., Martin, S.J., Justice, A., McConlogue, L., Games, D., Freedman, S.B., Morris, R.G., 2000. A learning deficit related to age and beta-amyloid plaques in a mouse model of Alzheimer's disease. Nature 408, 975–979.

Daumas, S., Sandin, J., Chen, K.S., Kobayashi, D., Tulloch, J., Martin, S.J., Games, D., Morris, R.G., 2008. Faster forgetting contributes to impaired spatial memory in the PDAPP mouse: deficit in memory retrieval associated with increased sensitivity to interference? Learn. Mem. 15, 625–632.

Deary, I.J., Leaper, S.A., Murray, A.D., Staff, R.T., Whalley, L.J., 2003. Cerebral white matter abnormalities and lifetime cognitive change: a 67-year follow-up of the Scottish Mental Survey of 1932. Psychol. Aging 18, 140–148.

Farkas, E., Luiten, P.G., Bari, F., 2007. Permanent, bilateral common carotid artery occlusion in the rat: a model for chronic cerebral hypoperfusion-related neurodegenerative diseases. Brain Res. Rev. 54, 162–180.

Fernando, M.S., Simpson, J.E., Matthews, F., Brayne, C., Lewis, C.E., Barber, R., Kalaria, R.N., Forster, G., Esteves, F., Wharton, S.B., Shaw, P.J., O'Brien, J.T., Ince, P.G., 2006. White matter lesions in an unselected cohort of the elderly: molecular pathology suggests origin from chronic hypoperfusion injury. Stroke 37, 1391–1398.

Lyons, D.M., Yang, C., Eliez, S., Reiss, A.L., Schatzberg, A.F., 2004. Cognitive correlates of white matter growth and stress hormones in female squirrel monkey adults. J. Neurosci. 24, 3655–3662.

Miki, K., Ishibashi, S., Sun, L., Xu, H., Ohashi, W., Kuroiwa, T., Mizusawa, H., 2009. Intensity of chronic cerebral hypoperfusion determines white/gray matter injury and cognitive/motor dysfunction in mice. J. Neurosci. Res. 87, 1270–1281.

Montag, D., Giese, K.P., Bartsch, U., Martini, R., Lang, Y., Blüthmann, H., Karthigasan, J., Kirschner, D.A., Wintergerst, E.S., Nave, K.A., Zielasek, J., Toyka, K.V., Lipp, H.-P., Schachner, M., 1994. Mice deficient for the myelin-associated glycoprotein show subtle abnormalities in myelin. Neuron 13, 229–246.

Shibata, M., Ohtani, R., Ihara, M., Tomimoto, H., 2004. White matter lesions and glial activation in a novel mouse model of chronic cerebral hypoperfusion. Stroke 35, 2598–2603.

Shibata, M., Yamasaki, N., Miyakawa, T., Kalaria, R.N., Fujita, Y., Ohtani, R., Ihara, M., Takahashi, R., Tomimoto, H., 2007. Selective impairment of working memory in a mouse model of chronic cerebral hypoperfusion. Stroke 38, 2826–2832.

STEM CELLS AND DEVELOPMENT
Volume 20, Number 5, 2011

DOI: 10.1089/scd.2010.0302

Implanted Neurosphere-Derived Precursors Promote Recovery After Neonatal Excitotoxic Brain Injury

Luigi Titomanlio,[1–4] Myriam Bouslama,[1–3,*] Virginia Le Verche,[1–3,*] Jérémie Dalous,[1–3] Angela M. Kaindl,[1–3,5] Yanina Tsenkina,[6] Adrien Lacaud,[6] Stéphane Peineau,[1,2,7] Vincent El Ghouzzi,[1–3] Vincent Lelièvre,[1–3,6] and Pierre Gressens[1–3]

Brain damage through excitotoxic mechanisms is a major cause of cerebral palsy in infants. This phenomenon usually occurs during the fetal period in human, and often leads to lifelong neurological morbidity with cognitive and sensorimotor impairment. However, there is currently no effective therapy. Significant recovery of brain function through neural stem cell implantation has been shown in several animal models of brain damage, but remains to be investigated in detail in neonates. In the present study, we evaluated the effect of cell therapy in a well-established neonatal mouse model of cerebral palsy induced by excitotoxicity (ibotenate treatment on postnatal day 5). Neurosphere-derived precursors or control cells (fibroblasts) were implanted into injured and control brains contralateral to the site of injury, and the fate of implanted cells was monitored by immunohistochemistry. Behavioral tests were performed in animals that received early (4 h after injury) or late (72 h after injury) cell implants. We show that neurosphere-derived precursors implanted into the injured brains of 5-day-old pups migrated to the lesion site, remained undifferentiated at day 10, and differentiated into oligodendrocyte and neurons at day 42. Although grafted cells finally die there few weeks later, this procedure triggered a reduction in lesion size and an improvement in memory performance compared with untreated animals, both 2 and 5 weeks after treatment. Although further studies are warranted, cell therapy could be a future therapeutic strategy for neonates with acute excitotoxic brain injury.

Introduction

Brain injury in the context of preterm birth is a major health problem worldwide: the incidence of preterm birth has increased, and improvements in survival rates have outpaced a concomitant decrease in long-term neurodevelopmental disability rates [1–4]. Excitotoxicity is a key factor contributing to the evolution of encephalopathy of prematurity, defined as white and gray matter damage to the premature brain [5–7]. Periventricular white matter damage (PWMD) is characterized by the formation of focal necrotic lesions within the white matter surrounding the lateral ventricles and/or the subsequent appearance of more widespread, diffuse lesions [8] involving the apoptotic death of late oligodendrocyte progenitors [9]. The main neuropathological finding of PWMD is substantial hypomyelination [10]. In addition, it is now acknowledged that white matter damage is accompanied by gray matter abnormalities, including neuronal loss and impaired neuronal guidance [7]. These findings support the view that some of the dysfunctions seen in preterm infants reflect a reduction in connectivity, needed for the integration of information arriving from different areas of the brain [11,12].

When survivors of preterm birth are assessed years later, they often perform less well in tests of cognition, attention, executive function, and perception than children born at term [13]. Despite the prevalence of perinatal brain damage and the personal as well as the economic burdens of long-term neurological morbidity, there is to date no effective treatment [14].

Cell therapy appears to be a promising neuroprotective and/or neuroregenerative strategy in various models of brain injury or disease (for a few examples, see [15–19]). Over the last couple of decades, numerous studies have attempted

[1]Inserm, U676; Hopital Robert Debré, Paris, France.
[2]Faculté de Médecine Denis Diderot, IFR02 and IFR25, Paris, France.
[3]Université Paris 7, Paris, France.
[4]Pediatric Emergency Department, AP-HP, Hopital Robert Debré, Paris, France.
[5]Department for Pediatric Neurology, Charité—Universitätsmedizin Berlin, Berlin, Germany.
[6]Institut des Neurosciences Cellulaires et Intégratives, UPR3212 CNRS, Université de Strasbourg, Strasbourg, France.
[7]MRC Centre for Synaptic Plasticity, Department of Anatomy, School of Medical Sciences, Bristol, United Kingdom.
*These authors (MB and VLV) contributed equally to this work.

to determine the efficacy and/or feasibility of transplanting stem cells or progenitor cells, including cells of both neural and non-neural origin, such as embryonic or mesenchymal stem cells, into the injured neonatal brain, to replace lost cells or to prevent damaged cells from dying [20,21]. Among these, neural stem cells (NSCs), self-renewing multipotent cells capable of generating the 3 main components of the nervous system—neurons, astrocytes, and oligodendrocytes—are present in the brain both during development and to a lesser extent in adulthood (for a review, see [22,23]), and have the advantage of being easy to isolate from mouse embryos and to propagate in culture in the form of multicellular aggregates called neurospheres [24]. However, despite the wide availability and use of these cells in animal models of injury, few studies have focused on their protective/regenerative effect in models of perinatal brain damage [25,26], and reports on functional recovery of the injured brain are practically nonexistent. Because clinical application of such cells as potential source of therapeutic cells in human is still impossible, it is of high importance to evaluate in adequate animal models the therapeutical potentiality of NSCs in vivo.

In the present study, we evaluated whether the implantation of neurosphere-derived precursors (NDPs) has a beneficial effect on the histopathological and behavioral outcome of ibotenate excitotoxicity in a neonatal mouse model of cerebral palsy. In this well-characterized model, ibotenate activates NMDA and metabotropic glutamate receptors and induces white matter cysts as well as cortical necrosis, similar to the lesions seen in newborns [27–29].

Materials and Methods

All experimental protocols involving animals or human patients were carried out in accordance with local ethics guidelines after approval by the institutional review committee.

Animals

Wild-type mouse pups and embryos were obtained from pregnant Swiss mice (Janvier) housed at 24°C with a 12 h light/dark cycle and free access to food and water. To obtain green fluorescent protein (GFP)-positive NDPs, embryos were taken from *C57BL/6* mice expressing GFP under an actin promoter (generously provided by Olaf Ninnemann, Institute of Cell Biology and Neurobiology, Charité, Berlin). Initial data were obtained using NDPs isolated from Swiss embryos and labeled with DiI staining. Because DiI is known to fade out, we have replicated the data with NDPs prepared from actin-GFP mice and extended the studies to longer time points (i.e P42). Animals used in the present study are detailed in Table 1.

Isolation and culture of NDPs

Forebrains were dissected from E10.5 Swiss mouse or GFP mouse embryos as described previously [30,31] (Fig. 1). Cells were cultured in 10 mL Neurobasal medium (Gibco) supplemented with 20 ng/mL human recombinant fibroblast growth factor 2 (FGF2) (Sigma). The resulting neurospheres were dissociated into single cells by trypsinization and replated every 7 days. After dissociation, cell count and viability (>92%) were assessed by trypan blue exclusion. Culture media were supplemented with 10 nM pituitary adenylyl cyclase-activating polypeptide (PACAP; Calbiochem) and 1 ng/μL triiodothyronine (T3; Sigma) for 3 consecutive days before cells were harvested on in vitro day (DIV) 18 for implantation (see Supplementary Fig. S1; Supplementary Data are available online at www.liebertonline.com/scd). To analyze the in vitro phenotype of NDPs, real-time polymerase chain reaction (PCR) was performed on DIV18 cells, and immunocytochemistry was carried out on DIV34 (corresponding to the behavioral evaluation of 3-week-old mice).

RNA extraction and quantification of gene expression by real-time PCR

Total RNA was extracted on DIV18 according to a protocol previously described in detail [30]. Genes of interest were (1) the neuronal markers βIII-tubulin, nuclear receptor regulated 1 protein Nurr1 (dopaminergic neurons) and tryptophan hydroxylase (serotonergic neurons), (2) the astrocytic markers glial fibrillary acidic protein (GFAP) and S100, (3) the following markers for oligodendrocytes: 2′,3′-cyclic nucleotide 3′phosphodiesterase and platelet-derived growth factor receptor, alpha polypeptide, 2 transcripts specific to oligodendrocyte precursors; Notch and Delta1, known to promote the oligodendrocyte lineage; myelin proteolipid protein and myelin basic protein (MBP), expressed in mature oligodendrocytes, and (4) certain morphogens and neurotrophic (Table 2). Primer sets were designed using Oligo6.0 (Molecular Biology Insights Inc.) and M-fold software [32] (Table 2). The standard housekeeping gene used to normalize mRNA levels was glyceraldehyde-3-phosphate dehydrogenase (primer sequences in Table 2). Real-time PCR was set up using SYBR green-containing Supermix™ (Biorad) for 45 cycles of a 3-step procedure: a 20 s denaturation step at 96°C, a 20 s annealing step at 60°C, and a 20 s extension step at 72°C. Amplification specificity was assessed by melting curve and subsequent amplicon sequencing after subcloning into the TOPO-II vector (Invitrogen). Quantification was carried out using standard curves made from serial dilutions of control RNA samples, and transcript levels expressed as the ratio of the gene or interest to the housekeeping gene/genes.

Immunocytochemistry

On DIV18, neurospheres were dissociated into single cells by trypsinization and replated on glass coverslips coated with polyornithine. Sixteen days later (DIV34), cells were fixed with prewarmed 4% paraformaldehyde (PFA) for 20 min at room temperature. Fixed cells were identified/characterized by immunocytochemistry using the following primary antibodies: (1) NSCs: rabbit anti-Nestin (1:2,000; Sigma), (2) neurons: mouse anti-microtubule-associated protein 2 (MAP2, 1:10,000; Sigma), and mouse anti- neuron-specific nuclear protein [neuronal nuclei (NeuN), 1:1,000; Chemicon] (3) astrocytes: rabbit anti-GFAP (1:500; Sigma), (4) oligodendrocytes: mouse anti-NG2 (1:500; Sigma), mouse anti-O4 (1:500; Sigma). Cells were incubated in the appropriate primary antibody combinations overnight, and immunolabeling revealed with the following secondary antibodies for 2 h: Alexa Fluor 488 donkey anti-mouse IgG (1:500) or Alexa

Fluor 488 donkey anti-rabbit IgG (1:500) (both from Invitrogen). Cells were then counterstained with DAPI (Boehringer) at room temperature for 1 min. Cell types were quantified by counting stained cells in 10 random fields per coverslip, and at least 3 coverslips per group, from 3 independent experiments.

Fibroblast culture

Cultured fibroblasts used as controls in our experiment were kindly provided by V. Paupe (Inserm U676, Paris, France) and originally derived from a forearm skin biopsy of a healthy male patient after written informed consent. Fibroblasts were cultured in Dulbecco's modified Eagle's medium (Gibco) supplemented with 10% bovine calf serum (Gibco) until they reached 80% confluency. Cells were then harvested by trypsinization and resuspended in 3–5 mL of phosphate-buffered saline (PBS) at a concentration of 3×10^5/mL.

DiI staining

NDP and fibroblasts not derived from actin-GFP mice were labeled with the red fluorescent dye DiI on DIV18 before infusion into the brain for later in vivo tracing. Cells were exposed to 7.5 mM DiI (Vybrant SE Cell Tracer DiI; Molecular Probes, Invitrogen) in their normal culture medium for 20 min at 37°C and then resuspended in PBS. The viability of NDPs after staining was evaluated by trypan blue exclusion in each experiment.

Excitotoxic lesions

Excitotoxic brain lesions were induced by a single intracerebral injection of 10 µg of the glutamate analogue ibotenate (5 µg/µL; Sigma) on postnatal day 5 (P5) isoflurane-anesthetized pups, as described previously [33,34] (Supplementary Fig. S2). This dose has been shown to consistently cause brain damage in P5 mice [35]. Ibotenate was injected into the neopallial parenchyma with a 26-gauge beveled needle adapted on 50 µL Hamilton syringe (Hamilton) and mounted on a calibrated microdispenser attached to a mechanically rigid holder. The needle was inserted 2 mm under the external surface of the scalp in the frontoparietal area of the right hemisphere, 2 mm from the midline in the mediolateral plane, and 3 mm from the junction between the sagittal and lambdoid sutures in the rostrocaudal plane. Histological analysis of brain tissue from 1,500 animals injected in our laboratory has previously confirmed that these visual coordinates result in highly reproducible injections that reach the periventricular white matter (P. Gressens, pers. comm.). Two pulses of 1 µL each were injected at an interval of 30 s. The needle was left in place for an additional 30 s. The correct positioning of the needle was verified by injecting some animals with toluidine blue. After the injections, pups were allowed to recover from anesthesia and were returned to their dams. Lesion induction by ibotenate was confirmed in a subset of pups ($n=5$, see lesion size determination below).

Cell implantation

Within each litter, pups were first tattooed on the tail and then were randomly assigned to 1 of the following 6 treatment groups (see Fig. 3 and Table 1): (1) intracerebral ibotenate injection + DIV18 NDPs implantation ($n=12$), (2) intracerebral ibotenate injection + fibroblasts implantation ($n=10$), (3) intracerebral ibotenate injection + PBS injection (no cells implanted, $n=13$), (4) intracerebral PBS injection + DIV18 NDP implantation ($n=12$), (5) intracerebral PBS injection + fibroblasts implantation ($n=9$), and (6) intracerebral PBS injection + PBS injection (no cells implanted; $n=8$). At the given time, cells were implanted or PBS injected (negative control) 4 h after the ibotenate or first PBS (control) injection, intracerebroventricularly into the lateral ventricle contralateral to the ibotenate lesion, that is, the left lateral ventricle (A-P: 1 mm caudal to bregma, 0.5 mm left of the midline, and 2 mm below the surface of the scalp of isoflurane-anesthetized animals). The contralateral side was chosen to determine whether the implanted cells were capable of migrating toward the lesion site, rather than merely filling up the lesion when injected locally. For each pup, about 3×10^5 cells were slowly infused with a controlled flow of 100,000 cell/min using a NANOmite™ syringe pump (Harvard Apparatus), and the 26-gauge needle was slowly withdrawn after an additional 2 min. To evaluate the effect of later treatment initiation, pups were similarly treated on P8, that is, 72 h after ibotenate/vehicle injection, in the following groups: PBS + PBS ($n=10$), ibotenate + PBS ($n=9$), and ibotenate + NDP ($n=10$).

Tissue processing

Injected mice were sacrificed by isoflurane inhalation followed by transcardiac perfusion of PBS (0.12 M TPO4, pH 7.4) before whole body fixation with 4% PFA in PBS. Brains were removed, postfixed overnight in 4% PFA in 0.12 M PBS at 4°C, and then cryoprotected in 10% sucrose in 0.12 M PBS for 2 days. Subsequently, brains were immersed in 10% sucrose and 7.5% gelatine in 0.12 M PBS for 1 h at 37°C, embedded in a block of the same solution for 1 h at 4°C, or flash-frozen in isopentane at −70°C, and stored at −80°C until further use. Ten-µm-thick parasagittal sections were cut using a cryostat, mounted on Superfrost Plus slides, and stored at −80°C. Brains dedicated to the determination of lesion size (see below) were fixed in 4% formaldehyde for 5 days and embedded in paraffin, and coronal sections of 16 µm were cut.

Lesion size determination

Lesion size was determined in randomly chosen pups from the ibotenate + PBS ($n=5$), ibotenate + fibroblasts ($n=5$), and ibotenate + NDP ($n=6$) groups. Pups were sacrificed on P10, that is, 5 days after treatment, by transcardiac perfusion with 4% PFA, and the brains removed. After postfixation in the same solution for an additional 24 h at 4°C, the brains were dehydrated in alcohol and embedded in paraffin. Each brain was completely and serially sectioned from the frontal pole to the occipital lobes at 15 µm intervals in the coronal plane. Coronal sections were chosen because of the difficulty in accurately evaluating lesion extent along the radial axis, given the neuronal damage in the neocortical layers at the epicenter of the lesion, and our previous findings regarding the high level of correlation that exists between the maximal diameter of ibotenate-induced lesions along the radial and fronto-occipital axes [29]. An index of

TABLE 1. OVERVIEW ON ANIMAL GROUP USED IN THE WHOLE STUDIES

Experiments	*Age*	*P5*	*P6*	*P7*	*P8*	*P9*	*P10*	*P21*	*P42*	*P180*
4 h	DiI +GFP series									
implantation	-PBS+PBS	7 (6)						7 (6)	7 (6)	
	-PBS+fibroblast	8 (6)						8 (6)		
	-PBS+NDP	12 (6)+8 (4)	2 (2)	2 (2)	2 (2)	2 (2)		12 (10)		
	-ibotenate+PBS	13 (6)+4 (4)					5 (4)	12 (10)	12 (10)	
	-ibotenate+fibroblast	10 (6)+13 (4)	2 (2)	2 (2)	2 (2)	2 (2)	5 (4)	10 (5)		
	-ibotenate+NDP	12 (6)+21 (4)	3 (3)	3 (3)	3 (3)	3 (3)	16 (14)	11 (10)	10 (9)	5 (5)
72 h	GFP series									
implantation	-PBS+PBS				10 (3)			10 (3)		
	-ibotenate+PBS				9 (3)			9 (3)		
	-ibotenate+fibroblast									
	-ibotenate+NDP				10 (3)			10 (3)		
		Cell implantation	Cell migration	Cell migration	Cell migration + cell implantation	Cell migration	Lesion size + cell phenotype	Behavioral studies	Behavioral studies + cell phenotype	Tumor transformation

Sizes of the different animal groups used in individual experiments performed at a given time are herein summarized. Numbers in parentheses indicate the different litters used to compose a given group.

GFP, green fluorescent protein; NDP, neurosphere-derived precursor; PBS, phosphate-buffered saline. Grey color indicated the infection time and therefore recapitulated the total number of animals used.

lesion volume was obtained after cresyl violet staining by multiplying the maximal diameter of the lesion along the fronto-occipital and sagittal axes by the number of sections in which the lesion was present and the thickness per section [28,36]. The size of the lesion in each brain was determined independently by 2 investigators blind to the treatment group.

NDP distribution and phenotype within the brain

To control the ability of NDPs to migrate toward the lesion, a subset of implanted animals was randomly chosen for brain analysis using either DiI or GFP to observe grafted cells on postinjury days 1, 2, 3, and 4.

To determine (1) the distribution of NDPs within the brain of ibotenate-lesioned and control pups and (2) the phenotype of NDPs at the level of the lesion, mice were sacrificed at 2 time points: at P10 ($n = 10$) and following behavioral assessment, at 6 weeks ($n = 10$) (see below). The following antibodies were used for immunohistochemical staining: (1) rabbit anti-Nestin (1:1,000; Sigma) for NSCs, (2) mouse anti-MAP2 (1:10,000; Sigma) and mouse anti-NeuN (1:1,000; Chemicon) for neurons, (3) rabbit anti-GFAP (1:500 dilution; Sigma) for astrocytes, and (4) mouse anti-NG2 (1:500 dilution; Sigma), mouse anti-MBP (1:500 dilution; Sigma) and mouse anti-O4 (1:500 dilution; Sigma) for oligodendrocytes, and (5) rabbit anti-caspase-3 (1:1,000; Sigma). Sections were incubated in the appropriate primary antibodies overnight, exposed to the secondary antibodies Alexa Fluor 488 donkey anti-mouse IgG (1:500) and Alexa Fluor 488 donkey anti-rabbit IgG (1:500) (Invitrogen), and stained with DAPI (Roche) at room temperature for 2 min. To assess transplanted mice for tumor formation, we autopsied the brain of the 2 transplanted females that died naturally before sacrifice, as well as the brains of 3 randomly chosen mice (1 female and 2 males) 6 months after transplantation. To evaluate abnormal proliferation of implanted cells, we also performed staining with rabbit anti-Ki67 (Invitrogen) on these and on randomly chosen younger mice (3 P10 and 3 P42).

Confocal microscopy

Confocal microscopy was performed using an oil-immersion objective (Plan-Apochromat 63x/1.4) on a Zeiss Observer inverted microscope equipped with an LSM 5 Exciter confocal scanning system (Carl Zeiss) and 488 and 543 nm lasers to observe the DiI or GFP signal (red and green, respectively) displayed by NDPs and the red signal displayed by various markers for stem cells, neurons, astrocytes, and oligodendrocytes. Images were processed using Adobe Photoshop CS software.

Behavioral assessment

The behavior of mice from the following groups was evaluated in an open field test [37,38] once per mouse at 3 weeks of age (Fig. 3): (1) intracerebral ibotenate injection + NDP implantation ($n = 11$), (2) intracerebral ibotenate injection + fibroblast implantation ($n = 10$), (3) intracerebral ibotenate injection + PBS injection (no cells implanted, $n = 12$), (4) intracerebral PBS injection + NDP implantation ($n = 12$), (5) intracerebral PBS injection + fibroblast implantation ($n = 8$), and (6) intracerebral PBS injection + PBS injection (no cells implanted; $n = 7$). The number of rears and contacts

TABLE 2. PRIMERS USED FOR IDENTIFICATION OF NEUROSPHERE-DERIVED PRECURSOR PHENOTYPES AND NEUROTROPHIC FACTORS EXPRESSED IN NEUROSPHERE-DERIVED PRECURSORS BY REAL-TIME POLYMERASE CHAIN REACTION

Gene	*Sequence (5′ and 3′, respectively)*	*Gene*	*Sequence (5′ and 3′, respectively)*
GFAP	TGGAGAGAATTGAATCGC CCGGAGTTCTCGAACTTCCTC	BMP6	CCTGGTGGAGTACGACAAGGA CCTCAGGAATCTGGGATAGGT
S100b	ATGGAGACGCTGGACGAAGAT ACGAAGGCCATGAACTCCTG	BMP7	TGAGCTTCGTCAACCTCGTGG TCAAACCGGAACTCTCGATGG
BIII-tubulin	CTACAACGCCACCCTGTCC GCAGATGTCGTAGAGGGCTTC	IGF1	GCAGCCTTCCAACTCAATTAT GCCAGGTAGAAGAGGTGTGA
Nurr1	CGCCGAAATCGTTGTCAGTAC CTCCGGCCTTTTAAACTGTCC	IGF2	CTTGTGCTGCATCGCTGCTTA GCGGTCCGAACAGACAAACTG
Tryptophan Hydroxylase	GTGCACACAGTACATCCGTCA AGCCAACATGGGTACGTGTC	NRG2	GGGAAGCTGAGACCACGTTC CTCCACGTGTGGCTCTCATGT
Notch (1)	TGACTATCTCGGCGGCTTTT GACAGGCAGTCGTTGATCTCC	NRG3	CCACCCCAGAAACTAGCACCA CGCCAGGTCCTTGTCTCGAC
PDGFRa	GACGTTCAAGACCAGCGAGTT CAGTCTGGCGTGCGTCC	LIF	CAACGTGGAAAAGCTATGTGC GTATGCGACCATCCGATACAG
delta 1	CGGCTTCTATGGCAAGGTCT GTGTAGCCTCCGTCAGGGTTA	PDGF	TCTCACTGAGATCACCACCGA CGCTGTCTTCTTCCTTAGCC
CNPase	AGACAGCGTGGCGACTAGACT GGGCTTCAGCTTCTTCAGGT	NGF	CACAGACATCAAGGGCAAGGA GCTCGGCACTTGGTCTCAAA
PLP	GCAAGGTTTGTGGCTCCAAC CGCAGCAATAAACAGGTGGAA	CNTF	GCCTCTCATCCTGGACCAAT ATGTATTCCTTCCCTGCGTAG
MBP	CCTGCCCCAGAAGTCGC CTTGGGATGGAGGTGGTGTTC	GDNF	GTGTTGCTCCACACCGCGTCT GGTCTTCAGCGGGCGCTTC
artemin	CCTGGTGGCCAACCCTAGC GGACATTGGGTCCAGGGAAGC	TGFb	CGCTGAATGGCTGTCTTTCG GGGCTGAAAGGTGTGACATGG
persephin	GGCAGATAAGCTCTCATTTGG AGACGGACATGGTTGTTACCC	NT3	AAGTCCTCAGCCATTGACATT TGTTTCACAGGAGAGTTACCG
neurturin	TTGCCCCGCTACGACGCCCTC TCGGGGGCGCCCTGGAGCAGA	NT4/5	CTCCCTCGCCACTCCTGTTCT GGGGCAGGGTGGAGGATG
BDNF	AACAATGTGACTCCACTGCC ACCGAAGTATGAAATAACCAT	Shh	ACGGCCATCATTCAGAGGAGT GCCAGGCGAGCCAGCAT
BMP2	GCGCTTCTTCTTCAATTTAAG AAGCTTCCTGTATCTGTTCCC	VIP	TTTCACCAGCGATTACAGCAG GCTGATTCGTTTGCCAATGAG
BMP4	TAGCAAGAGTGCCGTCATTCC TTCCTCCTCCTCCCCAGACT	PACAP	TGGTGTATGGGATAATAATGC GTCGTAAGCCTCGTCTTCT
BMP5	ATCAGAGGAGGCATTACAAAG ATGGTTTCCCTTGTCCTTAT	GAPDH	GGCCTTCCGTGTTCCTAC TGTCATCATACTTGGCAGGTT

with objects as well as the total number of crossed squares and inside and outside crossings were scored. Motor activity included the number of rears and contacts with objects (testing exploratory behavior and sensorimotor activity, respectively) as well as the total number of crossed squares (motor activity) and the ratio of inside to outside crossings (inversely related to anxious behavior).

Memory function was studied in the same mice using the novel object recognition (NOR) test [39]. Indeed, under control conditions, mice explore a novel object more than a familiar object, and the degree of their preference for the new object is an indication of their memory of the familiar one [40–42]. Tests were performed as described [39,43] with several modifications. Mice were allowed to habituate to an open field arena for 2 days (5 min per day) preceding the test. Two objects (A and B) were placed diagonally in the open field on day 3, and each mouse was allowed to explore them for 5 min. The time spent exploring each object individually and both objects were recorded, to evaluate levels of motivation, curiosity, and interest in exploring objects. Exploration of an object was defined as pointing the nose toward the object at a distance of <1 cm and/or touching it with the nose. Turning around, climbing, or sitting on an object was not considered exploration. After 30 min, object A was replaced by a replica (R: same shape but novel odor) and object B was replaced with a novel object, C, to test temporal memory. Alternatively, object B was replaced with a replica (R′) that was moved from its original position to test spatial memory. The mouse was again allowed to explore the objects for 5 min. Object recognition was scored by preferential exploration of the novel object using a discrimination index (DI) (novel object interaction/total interaction with both objects, ranging from 0 to 1; 0.5 = no preference) [39].

A subset of mice from the PBS + PBS ($n = 7$), ibotenate + PBS ($n = 12$), and ibotenate + NDP ($n = 11$) groups were retested with the NOR at 6 weeks of age to exclude the possibility that any recovery of behavioral function seen at 3 weeks was temporary. Pups included in the 72 h implantation procedure [PBS + PBS ($n = 10$), ibotenate + PBS ($n = 9$), ibotenate + NDP ($n = 10$)] were tested at 3 weeks of age. All

behavioral assessments were carried out by 2 independent investigators blind to the treatment group.

Statistics

Data (mean ± standard error of the mean) were evaluated using the Student's *t*-test or standard analyses of variance with treatment as the between-subject factor. Statistical analyses revealed no significant influence of the litter of origin, gender, and weight of the animals on the results. The main within-subject effects and interactions are reported, together with *P* values based on the adjusted degrees of freedom.

Results

Phenotype of NDPs in vitro

The mouse embryonic forebrain NDPs used in this study presented the cardinal features of NSCs: (1) proliferation in FGF2 supplemented medium to form neurospheres, (2) differentiation into the different neural phenotypes (neurons, oligodendrocytes, and astrocytes), and (3) generation of secondary neurospheres after dissociation. After 2 weeks in culture, 55.8% ± 7.5% of the NDPs were NG2-positive cells, suggesting a high proportion of oligodendrocyte precursors. Neuroblasts (MAP2+ cells, 16.4% ± 4%) and astrocytes (GFAP+ cells, 27.8% ± 7.8%) were also detected (Fig. 1A–J). Quantitative PCR analysis confirmed the presence of the following mRNAs: (1) GFAP and S100 (astrocytes); (2) βIII-tubulin, Nurr1, and Tryptophan Hydroxylase (neurons); and (3) Notch, Delta1, 2′,3′-cyclic nucleotide 3′phosphodiesterase, platelet-derived growth factor receptor, alpha polypeptide, myelin proteolipid protein, and MBP (oligodendrocytes at various stages of differentiation; Supplementary Fig. S3).

NDPs migrate to the site of brain injury

NDPs were implanted into injured and control brains, contralateral to the site of injury (Fig. 2). As negative controls, fibroblasts or PBS solution were similarly injected. The fate of implanted cells was monitored 1, 2, 3, and 4 days after the ibotenate injury or control injection to analyze whether implanted cells were able to reach the lesion site. One day after implantation, cells had already migrated from the site of injection toward the contralateral hemisphere. Three days later, about 66% of the implanted cells were visible at the lesion site. In contrast, implanted fibroblasts were found only at the injection site and showed no evidence of migration (not shown).

NDP therapy reduces the size of the excitotoxic brain lesion

To study whether implanted NDPs reduced/attenuated ibotenate-induced brain damage, we determined lesion size in untreated and treated P7 and P10 mice. Mouse pups injected with ibotenate on P5 and treated with PBS or fibroblasts developed cortical and periventricular white matter lesions. The cortical lesion was typical, with dramatic neuronal loss in all neocortical layers and the almost complete disappearance of neuronal cell bodies along the ibotenate injection track (Fig. 3A, B). On the other hand, pups injected with ibotenate on P5 and implanted with NDPs showed a significantly smaller gray and white matter lesion than those treated with PBS or fibroblasts, both at P10, the usual time point for lesion size evaluation in this model (Fig. 3D), and, even earlier, at P7 (Fig. 3C), that is, 48 h after ibotenate injection, when the lesion was almost fully developed in control mice [36]. However, at this earlier time point, NDPs had not

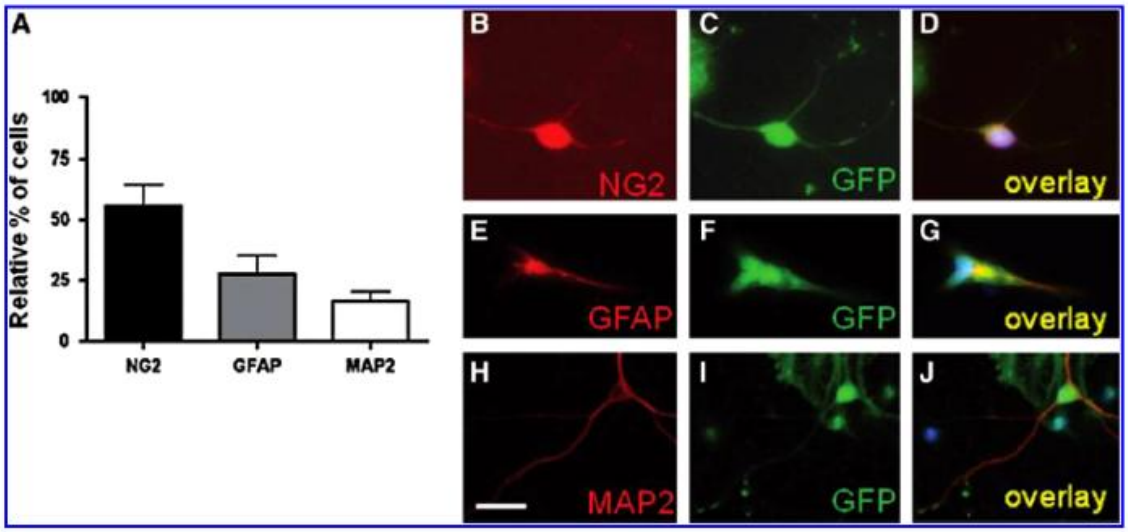

FIG. 1. In vitro phenotype of neurosphere-derived precursors (NDPs) injected into ibotenate-lesioned brains. **(A–J)** After pituitary adenylyl cyclase-activating polypeptide (PACAP) and triiodothyronine (T3) treatments in vitro, a high proportion of oligodendrocyte precursors are obtained (NG2-positive cells: 55.8% ± 7.5%; **A–D**). Astrocytes [glial fibrillary acidic protein (GFAP)-positive cells: 27.8% ± 7.8%; **E–G**] and neuroblasts [microtubule-associated protein 2 (MAP2)-positive cells: 16.4% ± 4%; **H–J**] are also detected **(A)**. Scale bar: 20 μm. Color images available online at www.liebertonline.com/scd

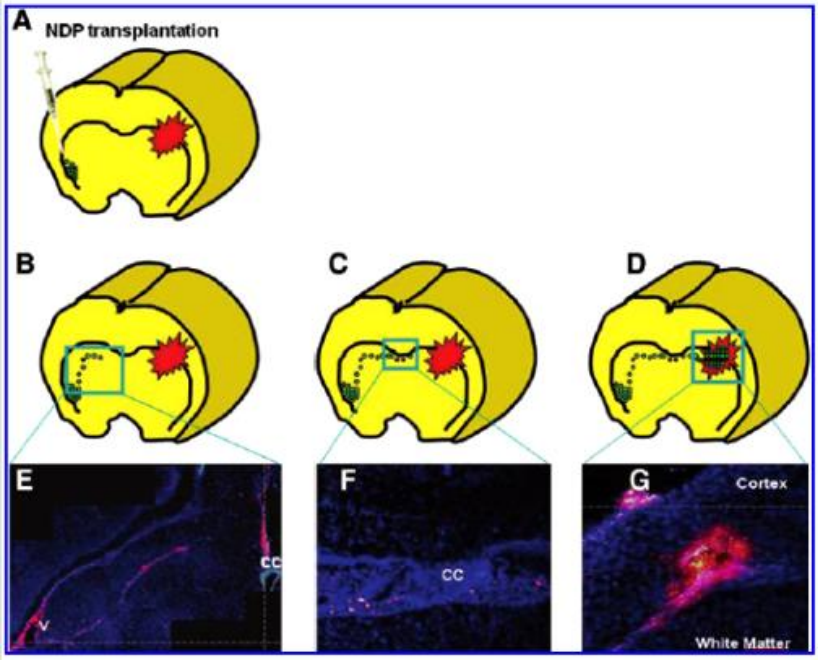

FIG. 2. In vivo fate of NDPs injected into ibotenate-lesioned brains. Injected NDPs migrate rapidly to the lesion site **(A–D)**. One day after ibotenate administration and NDP infusion, DiI-positive cells (red) are mostly located in the injected ventricle, and individual cells can be detected in the cerebrospinal fluid. Some NDPs are juxtaposed to the ventricular wall, whereas others are already migrating away from the injected ventricle. On day 2, DiI-positive cells migrate toward the lesion **(B, E)**. Migrating NDPs reach the corpus callosum on day 3 **(C, F)**. On day 4, DiI-positive cells are visible at the level of the lesion **(D, G)**. Blue staining, DAPI; red staining, DiI; V, ventricle; CC, corpus callosum. Color images available online at www.liebertonline.com/scd

yet reached the lesion site, suggesting a significant and cell specific long-range effect of the implanted precursor cells, when compared with non- or fibroblast-implanted brains.

To determine the fate of NDPs at the lesion site, we studied their phenotype using immunohistochemistry. Implanted DiI-positive or GFP-positive NDPs were localized at the level of the lesion in P10 mice (5 days after implantation). They were positive for Nestin (marker for NSCs or precursors) but not for GFAP, NG2, O4, MAP2, NeuN, or activated caspase-3, indicating that the NDPs reaching the lesion were still undifferentiated.

Improvement of memory performance through NDP implantation

To test the hypothesis that implanted cells could play a role in reducing the behavioral deficits caused by an ibotenate-induced brain injury, we performed behavioral tests in NDP-implanted and control 3- and 6-week-old mice (Fig. 4). Motor activity as evaluated by the open field test did not differ between the experimental groups. We further evaluated memory performance in our mice using the NOR test. In our study, the total amount of time spent exploring object A or B at time 0 did not differ significantly between control mice, lesioned NDP-implanted mice, and lesioned untreated mice. This indicates that mice had the same level of motivation, curiosity, and interest in exploring objects. Next, we compared the amount of time spent exploring the novel object as a fraction of the total object-exploration time (DI). All the ibotenate-lesioned mice injected with saline or fibroblasts showed a significant deficit in memory function (spatial and temporal) at 3 weeks (Fig. 4A). This deficit was not observed in mice implanted with NDP that performed as good as control PBS injected animals in memory tasks (Fig. 4A).

To determine whether or not the beneficial effect of NDPs was transient, NOR evaluations were repeated with 6-week-old mice. Similar to our observations at 3 weeks, ibotenate-lesioned mice implanted with NDPs performed significantly better than those infused with PBS (Fig. 4B), suggesting that the behavioral improvement persisted throughout the developmental period. We observed a significant improvement in memory performance even when NDP implantation was delayed, that is, when cells were implanted 72 h after the excitotoxic lesion. The improvement in spatial memory in these animals was partial (DI = 0.78; Fig. 4C) and limited to the DIV18 PACAP + T3-treated NDPs, whereas the control DIV18 NDPs failed to improve the spatial memory defects (DI = 0.54, data not shown).

NDPs undergo cell death at the lesion site

To evaluate the long-term fate of implanted NDP, we determined their cellular phenotype in 6-week-old mice after behavioral evaluation. At this time point, the majority of the NDPs that had migrated to the lesion site were positive for neuronal (MAP2 and NeuN) or oligodendrocytic markers (NG2 and MBP). We were unable to find any NDP-derived GFAP-positive astrocytes (Fig. 5). Similar results were obtained when NDPs derived from actin-GFP mice were implanted (not shown). Since cell-type markers stained the entire cell rather than being localized in their respective antibody-specific compartments, we asked whether the implanted cells had retained their integrity. Activated caspase-3 staining did indeed show that all the DiI-labeled cells surrounding the lesion site were actively dying (Fig. 6G–L). Similar results were obtained with GFP-positive implanted cells (Fig. 6M–R). However, no actin-GFP cells were found positive for activated caspase at P10 when still in the vicinity of the ventricular zone where they have been originally

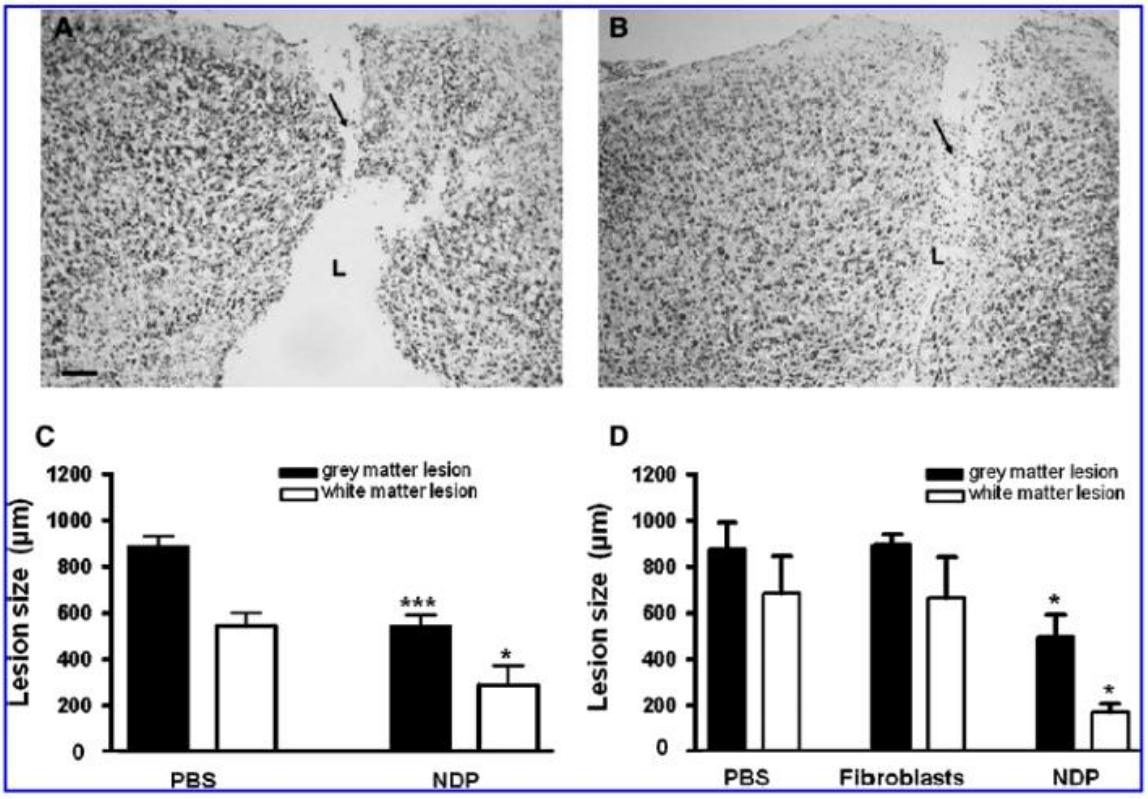

FIG. 3. NDP implantation reduces the size of the ibotenate-induced gray and white matter. **(A, B)** Gray and white matter lesions in representative cresyl violet-stained brain sections from fibroblast-implanted **(A,** $n = 5$**)**, and NDP-injected **(B,** $n = 6$**)** mice on P10, that is, 5 days after ibotenate injection (scale bar: 40 µm), showing typical neuronal loss in cortical layers II–VI (*arrows*) and a white matter lesion (L). Sham-operated mice ($n = 5$) show brain lesions similar to mice implanted with fibroblasts. **(C, D)** Quantitative analysis of lesion diameter in the sagittal plane on P7 **(C)** and on P10 **(D)**. NDP implant reduces both gray and white matter lesion size when compared with treatment with fibroblasts or phosphate-buffered saline (PBS) [bar: mean ± standard error of the mean (SEM), $^{***}P < 0.001$ or $^{*}P < 0.05$, analyses of variance with Dunnett's multiple comparison test].

grafted (Fig. 6A–F). The results indicate that the grafted cells retain their integrity until they have reached the lesion site where they finally undergo cell death.

No tumor formation was observed at the macroscopic or microscopic level in tested mice. Staining with anti-Ki67 antibodies did not detect any abnormal cellular proliferation (data not shown).

Grafted cells may produce a wide range of neurotrophic factors that could actively participate in functional recovery

Since implanted NDP cells did not survive after their migration to the injury site, we hypothesized that they could deliver neurotrophic factors, which in turn would enhance the recovery of endogenous cells after excitoxic brain injury. To test this, we cultured NDPs under medium conditions similar to those used for cell engrafting (FGF2 vs. PACAP+T3), before extracting total RNA and performing quantitative PCR to analyze the expression levels of several trophic factors that could promote recovery of the injured brain. Our results reveal that NDPs express several morphogenetic factors such as BMPs and shh; the neurotrophins NT3, NT4/5, and BDNF; neuropeptides, including VIP and PACAP (Fig. 7 and Table 3); and many other neurotrophic factors, including IGFs, NGF, GDNF, and CNTF (not shown). In addition, we observed that differences in culture conditions (FGF2 vs. PACAP+T3) resulted in a variation in expression levels of a few of them, including an increase in transcripts coding for the morphogens BMP6 and 7, the neuropeptide VIP, and the neurotrophic factors artemin, persephin, GDNF, and PDGF in the presence of PACAP+T3 (Fig. 7). Conversely, neurturin and LIF levels were found to be significantly decreased under these culture conditions. This indicates that NDPs express many growth factor transcripts in vitro and show that PACAP+T3 treatment is able to enhance this phenomenon. Although further experiments are required to fully demonstrate that implanted cells secreted recovery-promoting trophic factors in vivo, these results suggest that the implanted cells likely produce a wide range of neurotrophic factors that could actively participate in functional recovery.

Discussion

In the present study, we evaluated the therapeutic potential of NDPs in acute excitotoxic injury of the neonatal

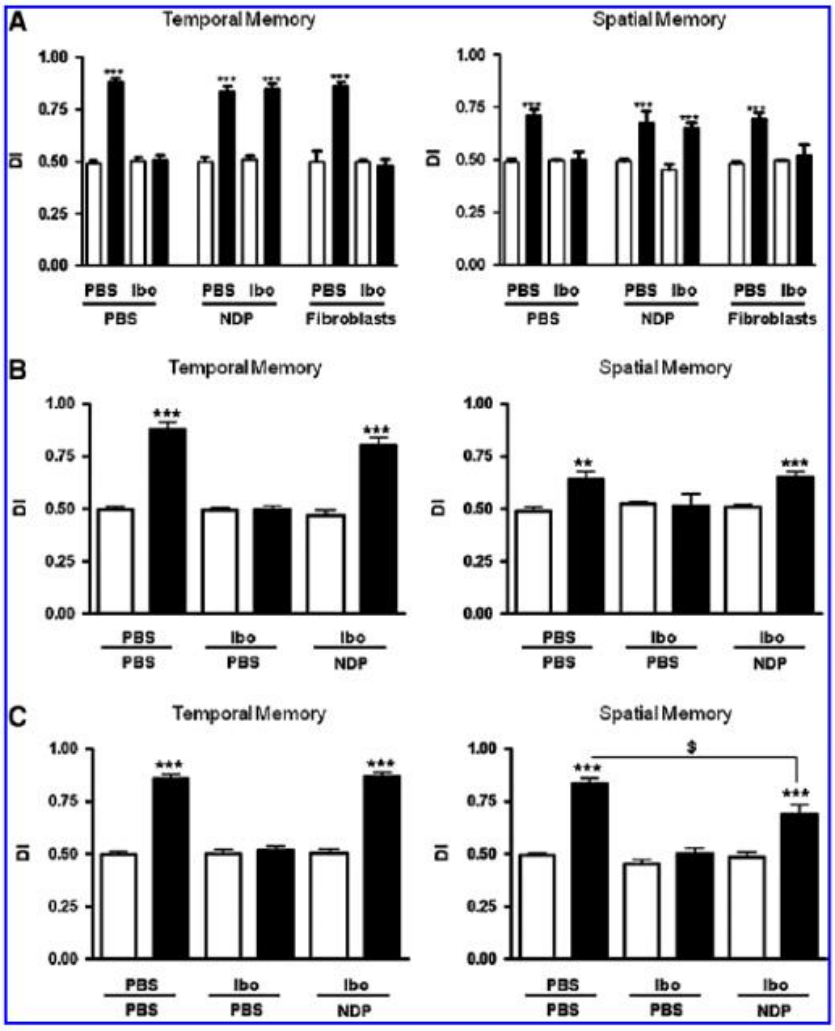

FIG. 4. Improvement of memory performance after NDP implantation in ibotenate-lesioned mice. **(A, B)** Behavioral tests for temporal and spatial memory in mice given NDP implants 4 h after ibotenate injection, at 3 weeks **(A)** and 6 weeks of age **(B)**. **(C)** Memory assessment at 3 weeks of age in mice treated with NDPs 72 h after ibotenate injection. Data (mean ± SEM) are presented as a discrimination index (DI, see main text). White and black columns represent DI at baseline and 30 min later, respectively ($^{**}P < 0.01$, $^{***}P < 0.0001$, $^{\$}P < 0.05$ using analyses of variance with Bonferroni's multiple comparison test). Ibo, ibotenate-lesioned mice.

mouse brain. The ibotenate-lesioned infant mouse is a classic excitotoxic injury model for the study of white and gray matter damage in humans, a major characteristic of cerebral palsy. The ibotenate-induced white matter lesion progressively increases in size during the first 24 h after the insult and then remains stable for 3–4 weeks, eventually being replaced by a glial scar [36]. Excitotoxicity-induced inflammation plays a central role in the formation of this lesion. Indeed, there is a significant increase in the density of activated microglia at the level of the lesion as soon as 4 h after ibotenate injection, before detectable cell death or axonal degeneration [36]. In addition, blockade of this microglial activation leads to significant neuroprotection [44]. The ibotenate-induced lesion mimics several key aspects of human perinatal brain damage, including its periventricular location, the initial cystic appearance, the secondary evolution of PWMD toward a glial scar, the associated appearance of gray matter damage, the deleterious effect of inflammatory cytokines, and the discrete ontogenetic window of sensitivity of the brain to damage [35,36]. These gray and white matter abnormalities tend to go hand in hand [7,12]: preterm infants who develop magnetic resonance imaging (MRI)-defined focal and diffuse white matter damage tend to have smaller cerebral cortical and deep gray volumes [45] than their preterm peers who do not have white matter damage. Expression of Nestin, a cytoskeletal protein involved in normal development and a marker for NSCs, is often reduced in the cortical gray matter during the subacute stage of PWMD but is increased at later stages, suggesting acute impairment with subsequent compensation leading to repair and plasticity [46].

We found that early (4-h) and late (72-h) NDP implantation significantly reduces the extent of the brain lesion after an acute excitotoxic injury to the neonatal mouse brain. Moreover, these cells are capable of migrating across the midline [47] toward the lesion site even when implanted contralateral to the lesion, similar to the long-distance migration of NSCs seen in a hypoxic-ischemic model of brain injury [48]. At the lesion site, they undergo transient differentiation into neurons and oligodendrocytes but not astrocytes. This strongly suggests that fate specification toward

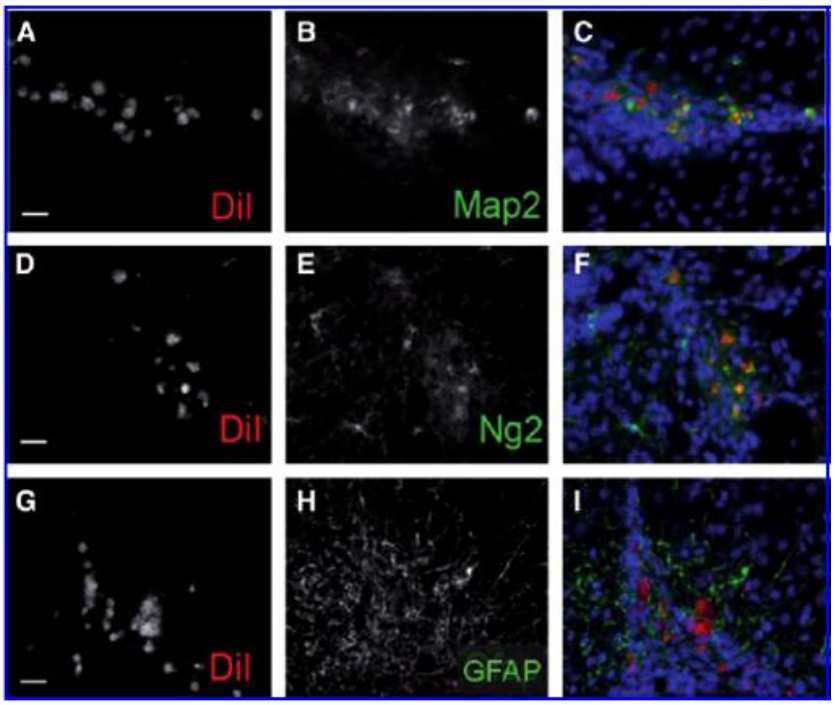

FIG. 5. Phenotype of NDPs in vivo in 6-week-old ibotenate-lesioned mice. Cellular fate of NDPs at the lesion site determined using immunohistochemistry 5 weeks after implantation: DiI-positive NDPs (red) are immunopositive for the neuroblast marker MAP2 **(A–C)** and the oligodendrocyte marker NG2 **(D–F)**, but there was no significant overlay with the astrocyte marker GFAP **(G–I)**. Cellular morphology resembles that of immature or dying cells (see also Fig. 6). Similar results are obtained with green fluorescent protein (GFP)-positive NDPs. Scale bar: 20 μM, DAPI, blue staining. Color images available online at www.liebertonline.com/scd

oligodendrocytic lineage is achieved by the culture conditions. Various protective and/or regenerative mechanisms by which NSCs could exert their effects have been described, and several of these could be involved in our model [49–53]. Such mechanisms include, but are not limited to, an attenuation of central nervous system inflammation, the secretion of survival-promoting neurotrophic factors, the stimulation of the plastic response or neural activity in the damaged host tissue, and the restoration of synaptic transmitter release by providing/promoting local re-innervation. The latter mechanism that refers to the integration of NDPs into existing neural and synaptic networks to re-establish functional afferent and efferent connections is obviously impracticable in our model.

Therefore, our data address the legitimate question whether NDP implantation improves cognitive defects through a neuroprotective or a neuroregenerative mechanism or again through a simpler mechanism of wound healing. In this context, lesion can first be identified under the microscope as early as 4 h after injection, and the lesion size remains stable from P6 to P30 [36]. In our study, at P7, the lesion was already smaller in NDP-treated mice than in controls, and remained so at P10. At the latter time point, NDPs were still undifferentiated, suggesting that wound healing is a plausible mechanism to reduce brain lesion size. In addition, implanted NSCs have been reported to remain undifferentiated in other brain injury models (eg, for 30 days in ref. [53]). At P42, corresponding to the last behavioral evaluation (ie, in 6-week-old mice), implanted cells were undergoing cell death. Our data thus support the hypothesis that in this model, NDPs exert their beneficial effect through wound repair and neuroprotection rather than neuron and oligodendrocyte regeneration. However, in absence of any therapeutic intervention, the wound is known to heal but also to result in cognitive defects, suggesting that wound healing per se is not sufficient for full recovery.

This effect is probably mediated by a non-local immunomodulatory or trophic mechanism, since NDPs need about 9 days to reach the lesion site. For instance, a decrease in microglial activity has previously been shown to be induced by grafted stem cells (for review, see [54]). The active secretion of neurotrophic factors by NDPs (as shown in Fig. 7) may also play a key role in the present study. Indeed, we demonstrate expression of mRNAs for several morphogens and neurotrophic factors known to be associated with neuroprotection, such as BMPs, members of the neurotrophin family, GDNF, CNTF, and VIP [33,35,55–57], or reported to be beneficial to oligodendrocyte development, such as PDGF, PACAP, IGF1, and GDNF [58–61]. In addition, we observed that preconditioning medium containing PACAP+T3 further enhanced expression of VIP, BMP6, artemin, persephin, and GDNF compared with medium containing FGF2. This may have played a role in the improved neuroprotective activity of NDPs when grafted 72 h after injury.

In parallel with the reduction in lesion size, injured mice implanted with NDPs displayed a persistent and marked improvement in temporal and spatial memory, performing significantly better in the open field and NOR tests at 3 and 6 weeks of age than littermates that received intracerebroventricular injections of PBS or fibroblasts. The behavioral impairment seen in control mice was no longer apparent at 3 weeks in injured mice that were implanted with NDP, even when the implantation was delayed to 72 h after ibotenate injection. This result is quite intriguing because memory performance in adult mice is mainly controlled by adult neurogenesis occurring in dentate gyrus. Because we did not

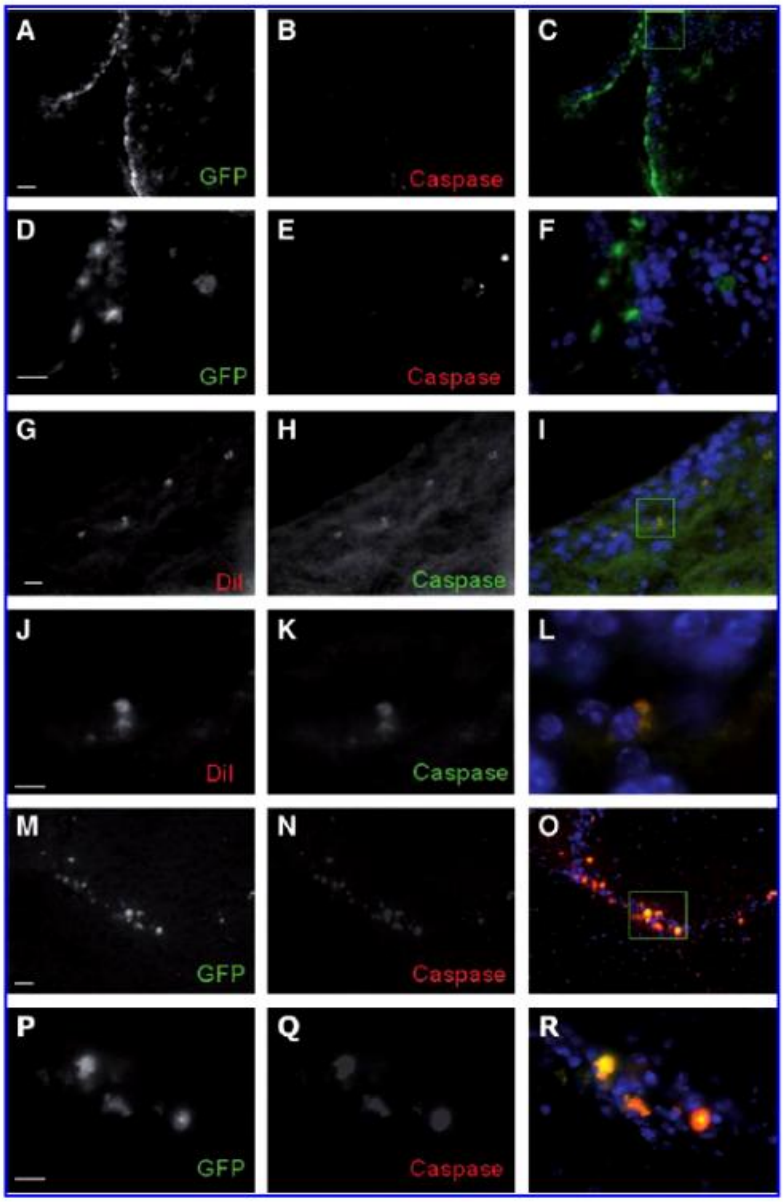

FIG. 6. NDPs undergo cell death at the lesion site. Confocal microscopy shows no activated caspase-3 in the GFP-positive **(A–F)** NDPs at P10 in ventricular zone vicinity, whereas at the lesion site most of DiI-positive **(G–L)** and GFP-positive **(M–R)** NDPs of 6-week-old mice (P42) were found positive for activated caspase after ibotenate injection on P5 and early cell injection. Scale bar: 20 μm. DAPI, blue staining. High magnification pictures (shown in row **D-F**; **J-L** and **P-R**) were focused on the areas marked in green boxes. Color images available online at www.liebertonline.com/scd

observe changes in adult neurogenesis in both P10 and P42 mice after NDPs implantation (using Ki67 immunostaining; data not shown), we have no further explanation for such a phenomenon, although 2 recent reports using a different experimental brain damage paradigm have described similar behavioral improvements in 9-day-old mouse pups and 7-day-old rat pups when subjected to intracerebral implantation of mesenchymal stem cells [62,63]. Our results suggest that even in the absence of the survival or differentiation of implanted cells or enhanced adult neurogenesis in NDPs implanted P10 and P42 mice (data not shown), the functional impact of brain injury in neonates can be modified.

The use of preorientated neural progenitors such as oligodendrocyte precursors for the treatment of neurological diseases characterized mainly by myelin loss is slowly becoming a realistic option [64,65]. At 6 weeks, implanted NDPs expressed neuronal and oligodendrocytic markers but were also undergoing cell death, as shown by their immunoreactivity for activated caspase-3. Our current data do not allow us to state conclusively whether the in vitro exposure of NDPs to PACAP and T3 modifies their in vivo fate or whether this plays a role in the behavioral improvement shown by implanted mice. This supplement cocktail was chosen because previous studies have shown that both PACAP [30,58] and T3 [66,67] are important extrinsic cues

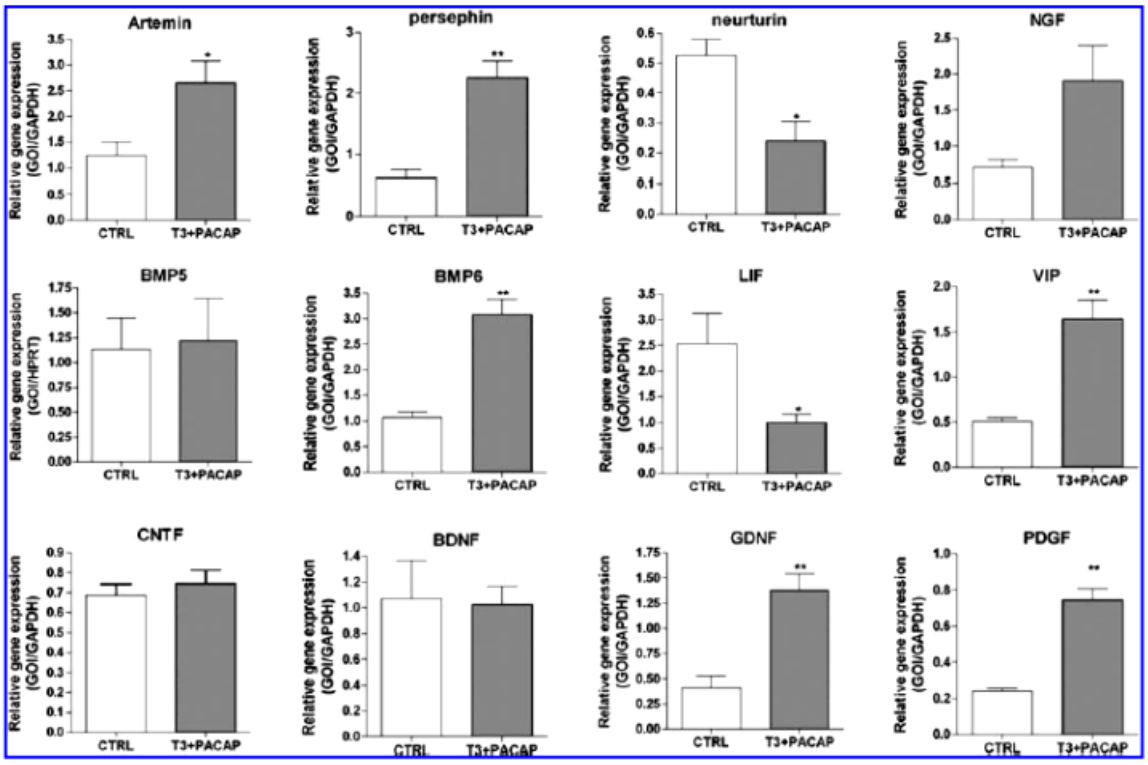

FIG. 7. NDPs express a wide range of morphogenetic/neurotrophic factors in vitro. Gene expression (see Table 3 for details) in NDP cultures under standard conditions or with PACAP and T3 supplementation (see Supplementary Fig. S1) was quantified by real-time polymerase chain reaction (PCR) using total RNAs from cellular extracts. Data are presented as means ± SEM of the ratio of the gene of interest (GOI) to *GAPDH*. $^{*}P < 0.05$, $^{**}P < 0.01$, $^{***}P < 0.001$; Student's *t*-test.

regulating the proliferation and differentiation of oligodendrocyte progenitors in vitro and in vivo.

Both embryonic stem cell and mesenchymal stem cell implants from various sources have been shown to reduce lesion size in animal models of neonatal brain damage, but few if any of these cells differentiate into neural cells in vivo [21]. Besides, tumor development remains a serious concern with regard to embryonic stem cell use [68]. We did not observe tumor formation in a subset of our treated mice, although more animals will need to be analyzed to confirm these data.

From a clinical and ethical point of view, treating infants suffering from brain insults using NSCs is still highly questionable. However, in view of future therapeutic interventions, we also chose to implant NDPs 3 days after lesion induction as a proof of concept. The efficacy of a therapeutic intervention is directly related to the rapidity with which it is implemented in acute human brain disorders such as stroke [69]. Mice receiving NDPs 72 h after the ibotenate injury showed a partial recovery of impaired memory function. This suggests that intervention at a later time point after an acute excitotoxic injury could also be effective. A better definition of this therapeutic window, as well as the pathophysiological mechanisms involved, could lead to optimal behavioral improvement.

In this study, we have demonstrated the occurrence of functional recovery induced by precursor cell therapy in a

TABLE 3. SCHEMATIC OVERVIEW OF REAL-TIME QUANTITATIVE POLYMERASE CHAIN REACTION DATA FOR TROPHIC FACTORS

Gene	*Control vs. PACAP+T3*
Artemin	↗
Persephin	↗↗
neurturin	↘
NGF	↗
BMP5	0
BMP6	↗↗
LIF	↘
VIP	↗↗
CNTF	0
GDNF	↗↗
BDNF	0
PDGF	↗↗

Data obtained in fibroblast growth factor 2 or in PACAP+T3 culture conditions shown on Fig. 6 are summarized using the following symbols: minor increase (↗) or decrease (↘); major increase (↗↗); no change (0).

PACAP, pituitary adenylyl cyclase-activating polypeptide; T3, triiodothyronine.

neonatal model of cerebral palsy. In humans, the potential benefits of such an approach could extend to other neurological disorders of childhood, glutamate excitotoxicity being the final common pathway for many diseases such as hypoxic-ischemic encephalopathy, stroke, herpes virus encephalitis, and shaken baby syndrome [70]. However, further studies are needed to fully understand the mechanisms involved in stem cell-mediated neuroprotection before cell therapy can be considered for acute diseases of the developing human brain.

Acknowledgments

This work was supported by INSERM, Université Paris-7, Fondation pour la Recherche Médicale, the ELA foundation (ELA 2007-02414), APHP (Interface contract to P. Gressens), the Niemann-Pick Association—Italy, and the PremUp Foundation. The authors thank Olaf Ninnemann and Robert Nitsch, Institute for Cell Biology and Neurobiology, Charité, Berlin, for providing the actin promoter GFP mice. We are very grateful to Gap Junction for their proficient English editing service and useful comments (www.gap-junction.com).

Author Disclosure Statement

No competing financial interests exist.

References

1. Allen MC. (2008). Neurodevelopmental outcomes of preterm infants. Curr Opin Neurol 21:123–128.
2. Robertson CM, MJ Watt and Y Yasui. (2007). Changes in the prevalence of cerebral palsy for children born very prematurely within a population-based program over 30 years. JAMA 297:2733–2740.
3. Vincer MJ, AC Allen, KS Joseph, DA Stinson, H Scott and E Wood. (2006). Increasing prevalence of cerebral palsy among very preterm infants: a population-based study. Pediatrics 118:e1621–e1626.
4. Wilson-Costello D, H Friedman, N Minich, B Siner, G Taylor, M Schluchter and M Hack. (2007). Improved neurodevelopmental outcomes for extremely low birth weight infants in 2000–2002. Pediatrics 119:37–45.
5. Deng W, J Pleasure and D Pleasure. (2008). Progress in periventricular leukomalacia. Arch Neurol 65:1291–1295.
6. Johnston MV. (2005). Excitotoxicity in perinatal brain injury. Brain Pathol 15:234–240.
7. Volpe JJ. (2005). Encephalopathy of prematurity includes neuronal abnormalities. Pediatrics 116:221–225.
8. Volpe JJ. (2001). Neurobiology of periventricular leukomalacia in the premature infant. Pediatr Res 50:553–562.
9. Craig A, N Ling Luo, DJ Beardsley, N Wingate-Pearse, DW Walker, AR Hohimer and SA Back. (2003). Quantitative analysis of perinatal rodent oligodendrocyte lineage progression and its correlation with human. Exp Neurol 181:231–240.
10. Inder TE, PS Huppi, S Warfield, R Kikinis, GP Zientara, PD Barnes, F Jolesz and JJ Volpe. (1999). Periventricular white matter injury in the premature infant is followed by reduced cerebral cortical gray matter volume at term. Ann Neurol 46:755–760.
11. Kesler SR, B Vohr, KC Schneider, KH Katz, RW Makuch, AL Reiss and LR Ment. (2006). Increased temporal lobe gyrification in preterm children. Neuropsychologia 44:445–453.
12. Leviton A and P Gressens. (2007). Neuronal damage accompanies perinatal white-matter damage. Trends Neurosci 30:473–478.
13. Marlow N, D Wolke, MA Bracewell and M Samara; EPICure Study Group. (2005). Neurologic and developmental disability at six years of age after extremely preterm birth. N Engl J Med 352:9–19.
14. O'Shea M. (2008). Cerebral palsy. Semin Perinatol 32:35–41.
15. Cao Q, RL Benton and SR Whittemore. (2002). Stem cell repair of central nervous system injury. J Neurosci Res 68:501–510.
16. Conti L, T Cataudella and E Cattaneo. (2003). Neural stem cells: a pharmacological tool for brain diseases? Pharmacol Res 47:289–297.
17. Pluchino S, L Zanotti, B Rossi, E Brambilla, L Ottoboni, G Salani, M Martinello, A Cattalini, A Bergami, R Furlan, G Comi, G Constantin and G Martino. (2005). Neurosphere-derived multipotent precursors promote neuroprotection by an immunomodulatory mechanism. Nature 436:266–271.
18. Pluchino S, L Zanotti, E Brini, S Ferrari and G Martino. (2009). Regeneration and repair in multiple sclerosis: the role of cell transplantation. Neurosci Lett 456:101–106.
19. Neri M, C Maderna, D Ferrari, C Cavazzin, AL Vescovi and A Gritti. (2010). Robust generation of oligodendrocyte progenitors from human neural stem cells and engraftment in experimental demyelination models in mice. PLoS ONE 5:e10145.
20. Kim SU and J de Vellis. (2009). Stem cell-based cell therapy in neurological diseases: a review. J Neurosci Res 87:2183–2200.
21. Pimentel-Coelho PM and R Mendez-Otero. (2010). Cell therapy for neonatal hypoxic-ischemic encephalopathy. Stem Cells Dev 19:299–310.
22. Alvarez-Buylla A and S Temple. (1998). Stem cells in the developing and adult nervous system. J Neurobiol 36:105–110.
23. Gage FH. (2000). Mammalian neural stem cells. Science 287:1433–1438.
24. Reynolds BA and S Weiss. (1992). Generation of neurons and astrocytes from isolated cells of the adult mammalian central nervous system. Science 255:1707–1710.
25. Sato Y, K Nakanishi, M Hayakawa, H Kakizawa, A Saito, Y Kuroda, M Ida, Y Tokita, S Aono, F Matsui, S Kojima and A Oohira. (2008). Reduction of brain injury in neonatal hypoxic-ischemic rats by intracerebroventricular injection of neural stem/progenitor cells together with chondroitinase ABC. Reprod Sci 15:613–620.
26. Zheng T, GP Marshall Ii 2nd, KA Chen and ED Laywell. (2009). Transplantation of neural stem/progenitor cells into developing and adult CNS. Methods Mol Biol 482:185–197.
27. Dommergues MA, J Patkai, JC Renauld, P Evrard and P Gressens. (2000). Proinflammatory cytokines and interleukin-9 exacerbate excitotoxic lesions of the newborn murine neopallium. Ann Neurol 47:54–63.
28. Husson I, B Mesples, P Bac, J Vamecq, P Evrard and P Gressens. (2002). Melatoninergic neuroprotection of the murine periventricular white matter against neonatal excitotoxic challenge. Ann Neurol 51:82–92.
29. Marret S, R Mukendi, JF Gadisseux, P Gressens and P Evrard. (1995). Effect of ibotenate on brain development: an excitotoxic mouse model of microgyria and posthypoxic-like lesions. J Neuropathol Exp Neurol 54:358–370.
30. Lelievre V, Z Hu, JY Byun, Y Ioffe and JA Waschek. (2002). Fibroblast growth factor-2 converts PACAP growth action on embryonic hindbrain precursors from stimulation to inhibition. J Neurosci Res 67:566–573.
31. Tropepe V, M Sibilia, BG Ciruna, J Rossant, EF Wagner and D van der Kooy. (1999). Distinct neural stem cells proliferate

in response to EGF and FGF in the developing mouse telencephalon. Dev Biol 208:166–188.
32. Zuker M. (2003). Mfold web server for nucleic acid folding and hybridization prediction. Nucleic Acids Res 31:3406–3415.
33. Gressens P, S Marret, JM Hill, DE Brenneman, I Gozes, M Fridkin and P Evrard. (1997). Vasoactive intestinal peptide prevents excitotoxic cell death in the murine developing brain. J Clin Invest 100:390–397.
34. Olney JW, C Ikonomidou, JL Mosinger and G Frierdich. (1989). MK-801 prevents hypobaric-ischemic neuronal degeneration in infant rat brain. J Neurosci 9:1701–1704.
35. Husson I, CM Rangon, V Lelievre, AP Bemelmans, P Sachs, J Mallet, BE Kosofsky and P Gressens. (2005). BDNF-induced white matter neuroprotection and stage-dependent neuronal survival following a neonatal excitotoxic challenge. Cereb Cortex 15:250–261.
36. Tahraoui SL, S Marret, C Bodenant, P Leroux, MA Dommergues, P Evrard and P Gressens. (2001). Central role of microglia in neonatal excitotoxic lesions of the murine periventricular white matter. Brain Pathol 11:56–71.
37. Walsh RN and RA Cummins. (1976). The Open-Field Test: a critical review. Psychol Bull 83:482–504.
38. Karl T, R Pabst and S von Horsten. (2003). Behavioral phenotyping of mice in pharmacological and toxicological research. Exp Toxicol Pathol 55:69–83.
39. Bevins RA and J Besheer. (2006). Object recognition in rats and mice: a one-trial non-matching-to-sample learning task to study "recognition memory". Nat Protoc 1:1306–1311.
40. Dere E, JP Huston and MA De Souza Silva. (2007). The pharmacology, neuroanatomy and neurogenetics of one-trial object recognition in rodents. Neurosci Biobehav Rev 31:673–704.
41. Rampon C, YP Tang, J Goodhouse, E Shimizu, M Kyin and JZ Tsien. (2000). Enrichment induces structural changes and recovery from nonspatial memory deficits in CA1 NMDAR1-knockout mice. Nat Neurosci 3:238–244.
42. Soderling SH, LK Langeberg, JA Soderling, SM Davee, R Simerly, J Raber and JD Scott. (2003). Loss of WAVE-1 causes sensorimotor retardation and reduced learning and memory in mice. Proc Natl Acad Sci U S A 100:1723–1728.
43. Dulawa SC, DK Grandy, MJ Low, MP Paulus and MA Geyer. (1999). Dopamine D4 receptor-knock-out mice exhibit reduced exploration of novel stimuli. J Neurosci 19:9550–9556.
44. Dommergues MA, F Plaisant, C Verney and P Gressens. (2003). Early microglial activation following neonatal excitotoxic brain damage in mice: a target for neuroprotection. Neuroscience 121:619–628.
45. Inder TE, SK Warfield, H Wang, PS Hüppi and JJ Volpe. (2005). Abnormal cerebral structure is present at term in premature infants. Pediatrics 115:286–294.
46. Okoshi Y, M Mizuguchi, M Itoh, A Oka and S Takashima. (2007). Altered nestin expression in the cerebrum with periventricular leukomalacia. Pediatr Neurol 36:170–174.
47. Modo M, RP Stroemer, E Tang, S Patel and H Hodges. (2002). Effects of implantation site of stem cell grafts on behavioral recovery from stroke damage. Stroke 33:2270–2278.
48. Imitola J, K Raddassi, KI Park, Mueller FJ, M Nieto, YD Teng, D Frenkel, J Li, RL Sidman, CA Walsh, EY Snyder and SJ Khoury. (2004). Directed migration of neural stem cells to sites of CNS injury by the stromal cell-derived factor 1alpha/CXC chemokine receptor 4 pathway. Proc Natl Acad Sci U S A 101:18117–18122.
49. Aharonowiz M, O Einstein, N Fainstein, H Lassmann, B Reubinoff and T Ben-Hur. (2008). Neuroprotective effect of transplanted human embryonic stem cell-derived neural precursors in an animal model of multiple sclerosis. PLoS ONE 3:e3145.
50. Ben-Hur T. (2008). Immunomodulation by neural stem cells. J Neurol Sci 265:102–104.
51. Einstein O and T Ben-Hur. (2008). The changing face of neural stem cell therapy in neurologic diseases. Arch Neurol 65:452–456.
52. Locatelli F, A Bersano, E Ballabio, S Lanfranconi, D Papadimitriou, S Strazzer, N Bresolin, GP Comi and S Corti. (2009). Stem cell therapy in stroke. Cell Mol Life Sci 66:757–772.
53. Bacigaluppi M, S Pluchino, L Peruzzotti Jametti, E Kilic, U Kilic, G Salani, E Brambilla, MJ West, G Comi, G Martino and DM Hermann. (2009). Delayed post-ischaemic neuroprotection following systemic neural stem cell transplantation involves multiple mechanisms. Brain 132:2239–2251.
54. Mathieu P, D Battista, A Depino, V Roca, M Graciarena and F Pitossi. (2010). The more you have, the less you get: the functional role of inflammation on neuronal differentiation of endogenous and transplanted neural stem cells in the adult brain. J Neurochem 112:1368–1385.
55. Hampton DW, RA Asher, T Kondo, JD Steeves, MS Ramer and JW Fawcett. (2007). A potential role for bone morphogenetic protein signalling in glial cell fate determination following adult central nervous system injury in vivo. Eur J Neurosci 26:3024–3035.
56. Lee CS, LY Tee, S Dusenbery, T Takata, JP Golden, BA Pierchala, DI Gottlieb, EM Johnson Jr., DW Choi and BJ Snider. (2005). Neurotrophin and GDNF family ligands promote survival and alter excitotoxic vulnerability of neurons derived from murine embryonic stem cells. Exp Neurol 191:65–76.
57. Beurrier C, M Faideau, KE Bennouar, C Escartin, L Kerkerian-Le Goff, G Bonvento and P Gubellini. (2010). Ciliary neurotrophic factor protects striatal neurons against excitotoxicity by enhancing glial glutamate uptake. PLoS ONE 5:e8550.
58. Lee M, V Lelievre, P Zhao, M Torres, W Rodriguez, JY Byun, S Doshi, Y Ioffe, G Gupta, AE de los Monteros, J de Vellis and J Waschek. (2001). Pituitary adenylyl cyclase-activating polypeptide stimulates DNA synthesis but delays maturation of oligodendrocyte progenitors. J Neurosci 21:3849–3859.
59. Iannotti C, H Li, P Yan, X Lu, L Wirthlin and XM Xu. (2003). Glial cell line-derived neurotrophic factor-enriched bridging transplants promote propriospinal axonal regeneration and enhance myelination after spinal cord injury. Exp Neurol 183:379–393.
60. Barres BA, MC Raff, F Gaese, I Bartke, G Dechant and YA Barde. (2004). A crucial role for neurotrophin-3 in oligodendrocyte development. Nature 120:1097–1108.
61. Zeger M, G Popken, J Zhang, S Xuan, QR Lu, MH Schwab, KA Nave, D Rowitch, AJ D'Ercole and P Ye. (2007). Insulin-like growth factor type 1 receptor signaling in the cells of oligodendrocyte lineage is required for normal in vivo oligodendrocyte development and myelination. Glia 55:400–411.
62. Van Velthoven CT, A Kavelaars, F van Bel and CJ Heijnen. (2010). Mesenchymal stem cell treatment after neonatal hypoxic-ischemic brain injury improves behavioral outcome and induces neuronal and oligodendrocyte regeneration. Brain Behav Immun 24:387–393.
63. Lee JA, BI Kim, CH Jo, CW Choi, EK Kim, HS Kim, KS Yoon and JH Choi. (2010). Mesenchymal stem-cell transplantation for hypoxic-ischemic brain injury in neonatal rat model. Pediatr Res 67:42–46.
64. Sher F, V Balasubramaniyan, E Boddeke and S Copray. (2008). Oligodendrocyte differentiation and implantation:

new insights for remyelinating cell therapy. Curr Opin Neurol 21:607–614.
65. Kondo Y and ID Duncan. (2009). Transplantation of oligodendrocyte progenitor cells in animal models of leukodystrophies. Methods Mol Biol 549:175–185.
66. Barres BA, MA Lazar and MC Raff. (1994). A novel role for thyroid hormone, glucocorticoids and retinoic acid in timing oligodendrocyte development. Development 120: 1097–1108.
67. Jones SA, DM Jolson, KK Cuta, CN Mariash and GW Anderson. (2003). Triiodothyronine is a survival factor for developing oligodendrocytes. Mol Cell Endocrinol 199: 49–60.
68. Comi AM, E Cho, JD Mulholland, A Hooper, Q Li, Y Qu, DS Gary, JW McDonald and MV Johnston. (2008). Neural stem cells reduce brain injury after unilateral carotid ligation. Pediatr Neurol 38:86–92.
69. Adams HP Jr., G del Zoppo, MJ Alberts, DL Bhatt, L Brass, A Furlan, RL Grubb, RT Higashida, EC Jauch, C Kidwell, PD Lyden, LB Morgenstern, AI Qureshi, RH Rosenwasser, PA Scott and EF Wijdicks. (2007). Guidelines for the early management of adults with ischemic stroke: a guideline from the American Heart Association/American Stroke Association Stroke Council, Clinical Cardiology Council, Cardiovascular Radiology and Intervention Council, and the Atherosclerotic Peripheral Vascular Disease and Quality of Care Outcomes in Research Interdisciplinary Working Groups: the American Academy of Neurology affirms the value of this guideline as an educational tool for neurologists. Stroke 38:1655–1711.
70. Moritani T, WR Smoker, Y Sato, Y Numaguchi and PL Westesson. (2005). Diffusion-weighted imaging of acute excitotoxic brain injury. Am J Neuroradiol 26:216–228.

Address correspondence to:
Dr. Vincent Lelièvre
Institut des Neurosciences Cellulaires et Intégratives
UPR3212 CNRS Université de Strasbourg
5 rue Blaise Pascal
Strasbourg Cedex 67084
France

E-mail: lelievre@inci-cnrs.unistra.fr

Received for publication July 29, 2010
Accepted after revision October 22, 2010
Prepublished on Liebert Instant Online October 22, 2010

Open
ORIGINAL ARTICLE

Cell Research (2011) 21:1332-1342.

www.nature.com/cr

Lineage-specific distribution of high levels of genomic 5-hydroxymethylcytosine in mammalian development

Alexey Ruzov[1, 2], Yanina Tsenkina[2], Andrea Serio[3], Tatiana Dudnakova[4], Judy Fletcher[2], Yu Bai[2], Tatiana Chebotareva[2], Steve Pells[2], Zara Hannoun[2], Gareth Sullivan[2], Siddharthan Chandran[3], David C Hay[2], Mark Bradley[5], Ian Wilmut[2], Paul De Sousa[2, 6]

[1]Wolfson Centre for Stem Cells, Tissue Engineering and Modelling, Centre for Biomolecular Sciences, University of Nottingham, University Park, Nottingham NG7 2RD, UK; [2]MRC Centre for Regenerative Medicine, University of Edinburgh, 49 Little France Crescent, Edinburgh EH16 4SB, UK; [3]Euan MacDonald Centre for Motor Neurone Disease Research, University of Edinburgh, 49 Little France Crescent, Edinburgh EH16 4SB, UK; [4]MRC Human Genetics Unit, Western General Hospital, Crewe Road, Edinburgh EH4 2XU, UK; [5]School of Chemistry, University of Edinburgh, West Mains Road, Edinburgh EH9 3JJ, UK; [6]Roslin Cells, Roslin Biocentre, Roslin, Midlothian, EH25 9PS, Edinburgh, UK

Methylation of cytosine is a DNA modification associated with gene repression. Recently, a novel cytosine modification, 5-hydroxymethylcytosine (5-hmC) has been discovered. Here we examine 5-hmC distribution during mammalian development and in cellular systems, and show that the developmental dynamics of 5-hmC are different from those of 5-methylcytosine (5-mC); in particular 5-hmC is enriched in embryonic contexts compared to adult tissues. A detectable 5-hmC signal appears in pre-implantation development starting at the zygote stage, where the paternal genome is subjected to a genome-wide hydroxylation of 5-mC, which precisely coincides with the loss of the 5-mC signal in the paternal pronucleus. Levels of 5-hmC are high in cells of the inner cell mass in blastocysts, and the modification colocalises with nestin-expressing cell populations in mouse post-implantation embryos. Compared to other adult mammalian organs, 5-hmC is strongly enriched in bone marrow and brain, wherein high 5-hmC content is a feature of both neuronal progenitors and post-mitotic neurons. We show that high levels of 5-hmC are not only present in mouse and human embryonic stem cells (ESCs) and lost during differentiation, as has been reported previously, but also reappear during the generation of induced pluripotent stem cells; thus 5-hmC enrichment correlates with a pluripotent cell state. Our findings suggest that apart from the cells of neuronal lineages, high levels of genomic 5-hmC are an epigenetic feature of embryonic cell populations and cellular pluri- and multi-lineage potency. To our knowledge, 5-hmC represents the first epigenetic modification of DNA discovered whose enrichment is so cell-type specific.

Keywords: epigenetics; 5-hydroxymethylcytosine; 5-methylcytosine; CpG-methylation; stem cells; mammalian development; pluripotency

Cell Research (2011) **21**:1332-1342. doi:10.1038/cr.2011.113; published online 12 July 2011

Introduction

The methylation of cytosines in a CpG context is a common modification in mammalian genomes, and is generally associated with gene repression *in vivo* and *in vitro* [1]. Alteration of 5-methylcytosine (5-mC) patterns during development contributes to the regulation of gene expression and cell specification [1-3]. In addition to 5-mC, a novel cytosine modification, 5-hydroxymethylcytosine (5-hmC), has recently been found in mouse brain and murine embryonic stem cells (mESCs) [4, 5]. The conversion of 5-mC to 5-hmC is catalysed by *Tet* (Ten-eleven translocation) oncogene family member proteins [4, 6]. Notably, as 5-hmC is interpreted as 5-mC

Correspondence: Alexey Ruzov[a], Paul De Sousa[b]
[a]Tel: +44(0)1158231234
E-mail: Alexey.Ruzov@nottingham.ac.uk
[b]Tel: +44(0)1312426646
E-mail: paul.desousa@ed.ac.uk
Received 4 March 2011; revised 9 May 2011; accepted 26 May 2011; published online 12 July 2011

in bisulphite sequencing [7-10], the routine method of mC identification, these two cytosine modifications are indistinguishable from each other in the vast majority of currently available experimental results. Therefore, there is a need to re-evaluate many DNA methylation data, taking into account the existence of this novel cytosine modification with its (probable) distinct functional role. Since it has been already reported that methyl-CpG binding proteins do not interact with 5-hmC-containing DNA substrates [7, 11], these two modifications are likely to play distinct roles in biological systems. Although a recent report suggested the importance of Tet1 in mESC self-renewal and inner cell mass (ICM) specification in early embryos [6], the biological functions and developmental distribution of genomic 5-hmC levels have not been studied. Here we assessed 5-hmC distribution throughout mammalian development, and in adult tissues *in vivo* and in *in vitro* cell systems using immunochemical methods.

Results

Genomic 5-hmC is enriched in embryonic and induced pluripotent stem cells compared to differentiated cells

We used two commercially available anti-5-hmC antibodies produced by Diagenode and Active Motif for our analysis. Since the Diagenode antibody has not been characterised in immunochemistry previously, we first confirmed its specificity in dot blot assays using PCR-produced DNA fragments with all of the cytosines replaced by either 5-hmC or 5-mC, and total genomic human ESC and human dermal fibroblast (HDF) DNA (Supplementary information, Figure S1A). The anti-5-hmC antibody specifically recognised the 5-hmC-enriched PCR fragment and hESC genomic DNA, but not 5-mC-containing or unmodified PCR fragments or HDF DNA. The dot blot assay exhibited relatively low sensitivity, and only the equivalent of 500 ng of total genomic DNA produced a detectable signal with the anti-5-hmC antibody. Since the estimated genomic proportion of 5-hmC in mESCs is relatively low (<1% total cytosine content) [4], we used a peroxidase-conjugated secondary antibody coupled with a tyramide signal enhancement system for 5-hmC detection in subsequent immunochemical staining experiments. Under these conditions, the anti-5-hmC antibody produced distinctive nuclear staining patterns on mESCs and hESCs (Figure 1A and Supplementary information, Figure S1B), but not on human and mouse cancer and immortalised cell lines (Supplementary information, Figure S1C). These results were consistent with previously reported data obtained by thin layer chromatography (TLC) [4, 5] and with our dot blot results (Supplementary information, Figure S1A). We obtained essentially identical results using the Active Motif anti-5-hmC antibody, which has been successfully used in dot blots, immunochemistry and other applications previously [6, 9, 12, 13]. In our experiments 5-hmC was strongly enriched in hESCs, compared to a very weak 5-hmC signal in HDFs (Supplementary information, Figure S2). Both antibodies also behaved similarly in all further experiments. We concluded that the Diagenode anti-5-hmC antibody specifically recognises 5-hmC, but not 5-mC, in immunocytochemical assays. Notably, the distribution of 5-hmC staining in ESCs was strikingly different from that of 5-mC. The intensity of the 5-hmC signal was strong in the cells forming the colonies of ESCs, and was considerably weaker in surrounding differentiating fibroblast-like "stromal" cells, whereas 5-mC was detectable in both cell types at similar levels (Figure 1B and Supplementary information, Figure S1D). This is consistent with the observation that 5-hmC content decreases upon differentiation of murine ESCs, as reported previously [4, 14]. We decided to examine the dynamics of this process using a protocol to differentiate hESCs to hepatic endoderm [15]. The 5-hmC signal dropped significantly following a 3-day treatment with Wnt3A and Activin to induce definitive endoderm, and was virtually undetectable after an additional 2 days of differentiation (Figure 1C). Concurrent analysis of transcriptome changes by global quantitative deep sequencing revealed a parallel reduction in the number of *Oct4* and *Nanog* transcripts (Figure 1D). Unexpectedly, we observed an increase in the numbers of transcripts of all three *Tet* genes at 3 days post-induction at the time point where the 5-hmC signal dropped significantly (Figure 1D). Possible explanations for this discrepancy include the presence of mechanisms regulating Tet proteins at either the post-transcriptional/post-translational levels, or the inhibition of their oxygenase enzymatic activity. Over 5 days of differentiation, the numbers of *Tet1*, *Tet2* and *Tet3* transcripts also decreased (Figure 1D). To determine the correspondence of 5-hmC with acquisition of a pluripotent state we carried out 5-hmC immunostaining on human induced pluripotent stem cells (iPSCs) [16] and their parental somatic cell lines. hiPSC lines generated from both normal and Huntington's disease tissues (Supplementary information, Figure S3), but not from their parental HDFs, exhibited a strong 5-hmC signal (Figure 1E and Supplementary information, Figure S1D). In summary, our screening of *in vitro* cell systems for the presence of immunochemically detectable levels of 5-hmC revealed a strong correlation of high levels of this modification with a pluripotent stem cell state.

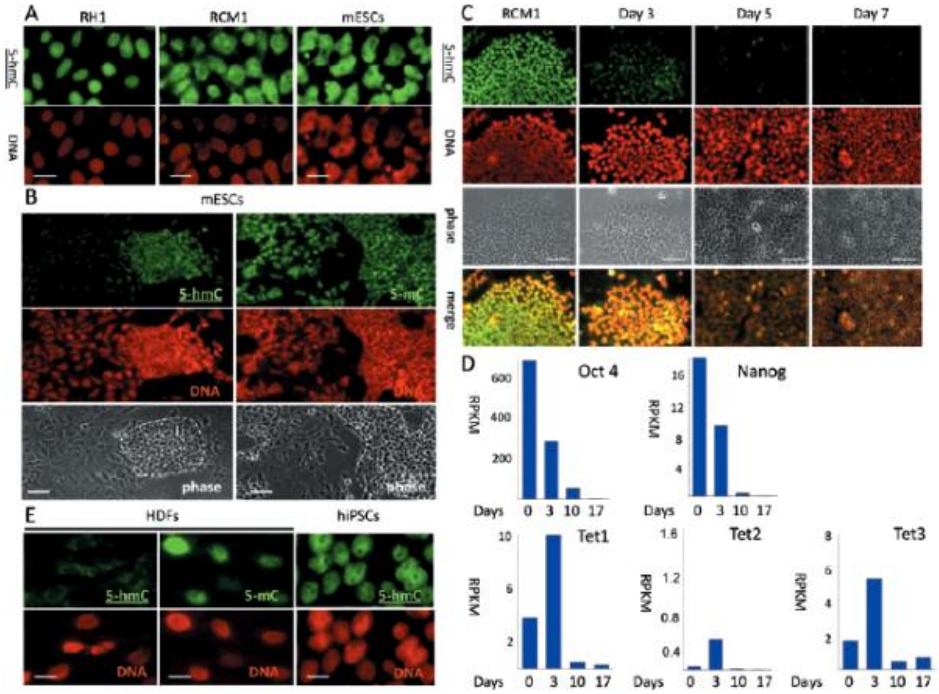

Figure 1 The presence of immunochemically detectable 5-hydroxymethylcytosine (5-hmC) levels correlates with pluripotency in mammalian cells. 5-hmC is detectable in mouse and human (RH1 and RCM1) ESCs. **(A)** Lines stained with 5-hmC antibody. **(B)** 5-hmC and 5-mC staining of mouse ESC colonies (defined morphologically on the basis of phase images and indicated by dotted lines) and surrounding fibroblast-like differentiating cells. 5-hmC Immunostaining **(C)** and quantitative transcriptome deep sequencing (Solexa) data for Oct4, Nanog, Tet1, 2 and 3 **(D)** of RCM1 cells differentiating towards hepatic endoderm. Identical exposure times were used for different time points. Days post-induction are shown. RPKM – reads per kilobase per million reads. **(E)** High levels of 5-hmC are detectable in human iPSCs but not in human dermal fibroblasts (HDFs). DNA signal is indicated. Scale bars are 20 μm in A and E, 50 μm in B and 100 μm in C. The experiments were performed using the Diagenode antibody.

Global hydroxymethylation of the paternal genome coincides with the loss of 5-methylcytosine signal in zygote

Several hours after fertilisation, chromatin of both maternal and paternal pronuclei of the mammalian zygote is subjected to extensive genome-wide reprogramming as the embryo makes a transition from a germ cell to a somatic developmental programme [2, 17]. One notable reprogramming event is a dramatic loss of the 5-mC signal detectable by immunochemistry only in the paternal pronucleus after fertilisation [18]. It has been suggested that conversion of 5-mC to 5-hmC may represent an intermediate step in the process of cytosine demethylation [4]. In agreement with a recent study [19], we could not detect any 5-hmC staining in the embryos before 2.5 h post-fertilisation, when a weak 5-hmC signal started to appear in the paternal pronucleus (Figure 2A, PN_{1-2}, PN_{2-3}). The intensity of the 5-hmC signal increased dramatically during the next 2 h (Figure 2A, PN_{3-4}, PN_4), peaking at 5-8 h post-fertilisation (Figure 2A, PN_5, syngamy) coincident with a significant decrease and subsequent loss of 5-mC staining in the male pronucleus. The majority of embryos exhibited a strong 5-hmC signal, exclusively in the paternal pronucleus, whereas the maternal pronuclear 5-hmC staining was weak or undetectable (Figures 2A, Supplementary information, S4A, S4B). This corresponded to a strong 5-mC signal in the maternal pronucleus and its loss in the paternal pronucleus. Some embryos (11.4% at PN_{4-5}) showed comparable levels of strong 5-hmC staining in both male and female pronuclei concurrently with equally low or absent 5-mC signals in both pronuclei (Supplementary information, Figure S4A, S4B). Nonparametric statistical analysis showed a significant

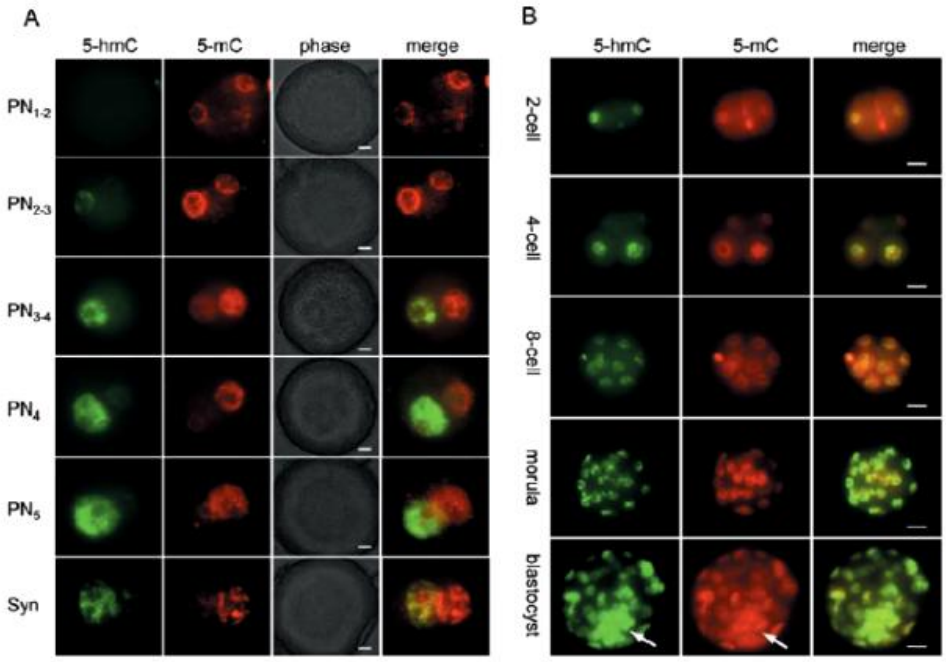

Figure 2 5-Hydroxymethylcytosine (5-hmC) distribution in mouse pre-implantation development. **(A)** Distribution of 5-hmC and 5-mC during indicated pronuclear stages in mouse zygote. Merged and phase views, where pronuclei are distinguishable at PN_3-PN_4 stages, are shown. The exposure times were identical for each channel. 5-hmC antibodies produced by Active Motif were used. Scale bar, 10 μm. **(B)** 5-hmC Distribution at the indicated later stages of mouse pre-implantation development. 5-hmC Antibodies produced by Active Motif were used. 5-mC signal and merge view are indicated. ICM is arrowed. Scale bar, 10 μm.

negative correlation ($r = -0.9834$, $p < 0.0001$) between 5-hmC and 5-mC immunostaining scores (Supplementary information, Figure S4A-S4C), suggesting that a decrease in 5-mC staining intensity is related to an increase in 5-hmC content in the mouse zygote at PN_{4-5}. This most likely represents genome-wide 5-mC conversion into 5-hmC. Since 5-hmC is not detectable using an anti-5-mC antibody [4] and accumulates in the paternal genome at significant levels during the embryo's first cell cycle, together with a previous report, [19] these results suggest that the loss of 5-mC signal in the zygote at least partially represents a consequence of genome-wide 5-mC conversion into 5-hmC. 5-hmC-Independent demethylation of several genes has indeed been detected using bisulphate sequencing in the zygote [20], but bisulphite sequencing has never been performed on a genome-wide scale in preimplantation embryos. It is most likely that hydroxylation-independent demethylation of certain genome regions and global 5-mC hydroxylation occurs simultaneously in mouse embryos after fertilisation.

High levels of 5-hmC colocalise with the ICM in blastocysts and with nestin-expressing cell populations in post-implantation mouse embryos

To determine the dynamics of 5-hmC content in later mammalian development, we carried out whole-mount immunostaining of pre-implantation and sections of post-implantation mouse embryos. A detectable 5-hmC signal was present throughout all the stages of pre-implantation development, slightly decreasing by the 8-cell stage (Figure 2B). Strong 5-hmC staining started to appear at the morula stage and was observed in mouse blastocysts with the maximum signal intensity in the ICM (Figure 2B and Supplementary information, Figure S5A). In contrast, the 5-mC signal showed less perceptible variation between the ICM and trophoblast cells of blastocysts than did the 5-hmC signal (Figure 2B and Supplementary information, Figure S5B).

The 5-hmC enrichment in the ICM of mouse blastocysts is consistent with our immunochemical detection of 5-hmC in mESCs and previous TLC data [4, 5]. It is

also consistent with the expression of Tet proteins in both mESCs and the blastocyst ICM [4, 6]. Interestingly, the study of murine post-implantation embryos revealed a pattern of regional enrichment of 5-hmC nuclear staining correlated with the presumptive location of multi-potent progenitor or stem cells, becoming increasingly restricted with development (Figure 3A). At 10.5 days post-coitum (dpc) most embryonic tissues were highly enriched for 5-hmC (Figure 3A). At 12.5 dpc, mouse embryos exhibited intense 5-hmC staining in a range of embryonic tissues. Significantly higher levels of 5-hmC were observed in the brain, spinal cord, tailbud and liver but not in heart, skin or mesenchymal tissue (Figure 3A and 3B, Supplementary information, Figure S5C-S5G, Figure 4A-4D). By 15.5 dpc, 5-hmC staining was generally less intense and limited to the brain and peripheral neural tissue (Figure 3A and 3B). According to 5-hmC signal quantification, the intensity of 5-hmC staining gradually decreased in brain tissue over time and fell dramatically in embryonic tongue between 12.5 dpc and 15.5 dpc

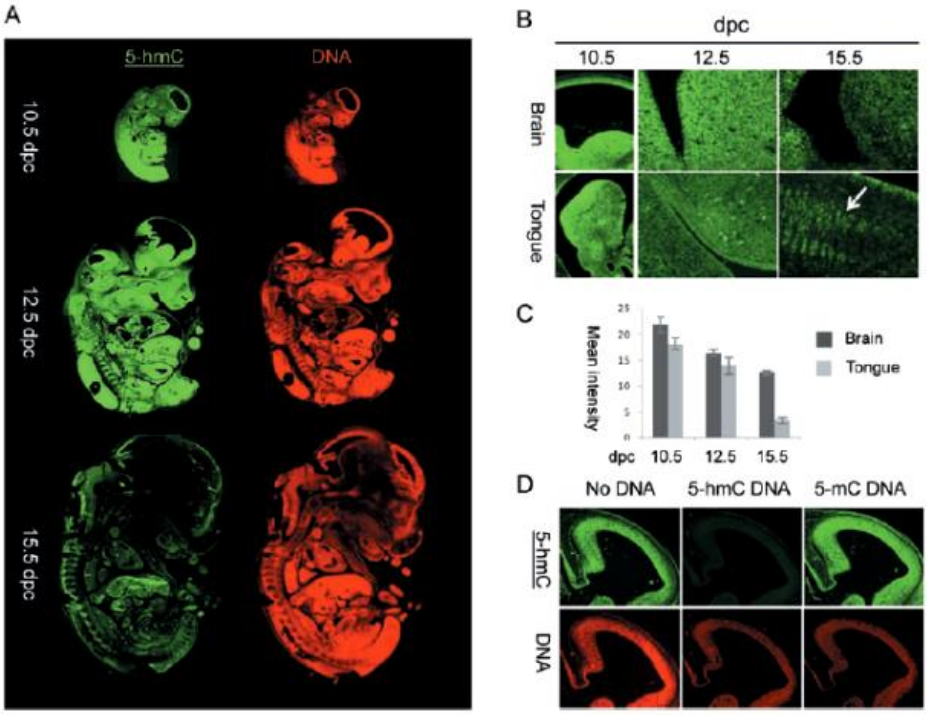

Figure 3 The dynamics of 5-hydroxymethylcytosine (5-hmC) in mouse post-implantational embryonic development. **(A)** Sagital sections of 10.5 days post coitum (dpc), 12.5 dpc and 15.5 dpc mouse embryos stained with Diagenode antibody to 5-hmC. Immunostaining for single-stranded DNA is shown in red. **(B)** Fragments of brain and tongue (indicated) embryonic sagital sections at 10.5 dpc, 12.5 dpc and 15.5 dpc stages (indicated). Corresponding slides were immunostained for 5-hmC in parallel with identical conditions and imaged with the same exposure times. Cell populations of embryonic tongue enriched in 5-hmC at 15.5 dpc are arrowed. **(C)** A schematic showing of the results of quantification of 5-hmC signal in embryonic brain and tongue at 10.5 dpc, 12.5 dpc and 15.5 dpc. Corresponding slides were immunostained for 5-hmC in parallel and imaged with the same exposure times. Mean values for mean signal intensities of 10 random measurements of parts of images shown in B are presented. The same central part of developing brain was quantified for all the stages analysed. Error is expressed as s.e.m. **(D)** The results of 5-hmC immunostaining of 3 adjacent sections of 12.5 dpc embryo brain region using primary antibody mix pre-incubated with PCR-produced DNA fragments where all the cytosines were replaced with either 5-hmC (5-hmC DNA) or 5-mC (5-mC DNA). Control staining without pre-incubation with any DNA is shown (no DNA). The 5-hmC immunostaining is specifically competed by 5-hmC- but not by 5-mC-containing DNA. Genomic DNA was visualised using single-stranded DNA antibody (indicated) used at a high titre. The experiments were performed using the Diagenode antibody.

(Figure 3B and 3C). Whereas high levels of 5-hmC were detected in most of the cells of embryonic tongue at 10.5 dpc and 12.5 dpc, 5-hmC distribution in this organ at 15.5 dpc was limited to certain cell populations (Figure 3B). As expected, over the same period of development, the global level of DNA methylation was not restricted to any particular embryonic cell populations and did not vary significantly between embryonic stages (Supplementary information, Figures S5C-S5G, S6).

To identify these 5-hmC-rich cell populations, we performed immunostaining for nestin, an established marker of multi-potent progenitors and stem cells [21, 22], in 12.5 dpc mouse embryos. Adjacent serial sections were used for nestin and 5-hmC or 5-mC staining, as immunodetection of 5-hmC and 5-mC requires treatment of tissues with 4 N HCl, which is incompatible with the preservation of most protein epitopes. We observed that nestin staining closely correlates with the intense 5-hmC signal in brain, peripheral neural tissue and the tailbud, suggesting that a high genomic content of 5-hmC is a feature of nestin-expressing multi-potent fetal cells (Figure 4E and 4F). Consistent with our observed association of high levels of 5-hmC with multi-lineage potency, we also observed a highly localised 5-hmC signal in the olfactory epithelium of 17.5 dpc mouse embryos (Supplementary information, Figure S7). The olfactory epithelium is known to contain multi-potent stem cells constantly differentiating into supporting and olfactory cells in the embryo and adult [23].

The presence of high 5-hydroxymethylcytosine levels is restricted to neuronal tissue and bone marrow in adult human and mouse

Finally, we evaluated adult murine and human tissues for genomic 5-hmC distribution. In agreement with previously reported data obtained by TLC [5], we could

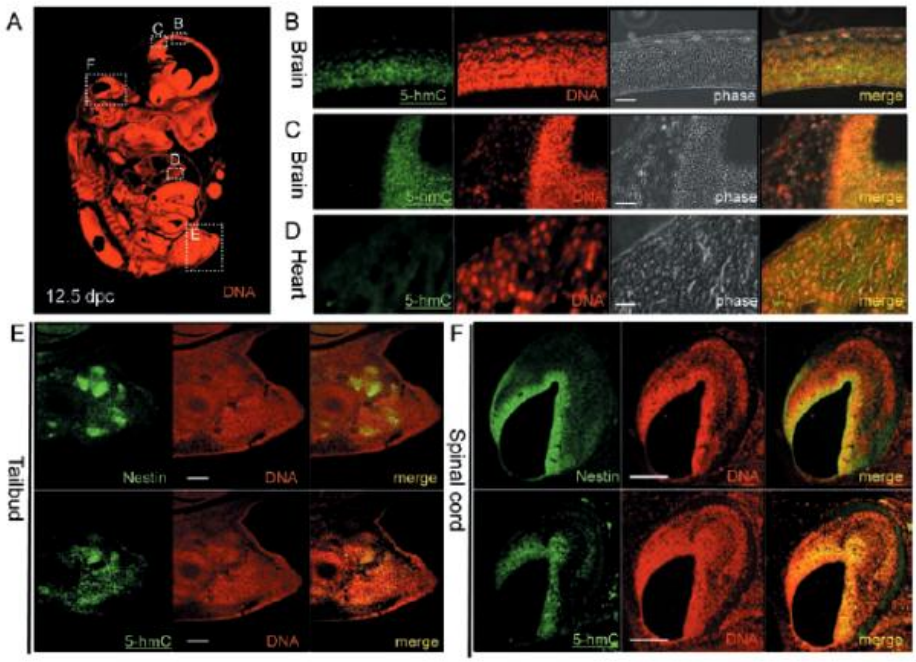

Figure 4 5-Hydroxymethylcytosine (5-hmC) localises with nestin-expressing stem cell populations in 12.5 dpc mouse embryos. **(A)** Sagital section of 12.5 dpc mouse embryo with DNA visualised and B, C, D, E and F views indicated with dotted squares. Immunohistochemical detection of 5-hmC in sagital sections of mouse embryonic brain (B, C) and heart (D). Localisation of 5-hmC and nestin in the sagital adjacent sections of tailbud (E) and a part of the spinal cord (F). DAPI signal in nestin immunostaining was colourised as red. Anti-single-stranded DNA antibody was used for DNA visualisation in 5-hmC immunostaining experiments. Scale bars are 150 μm in B, C and D and 300 μm in E and F. The experiments were performed using the Diagenode antibody.

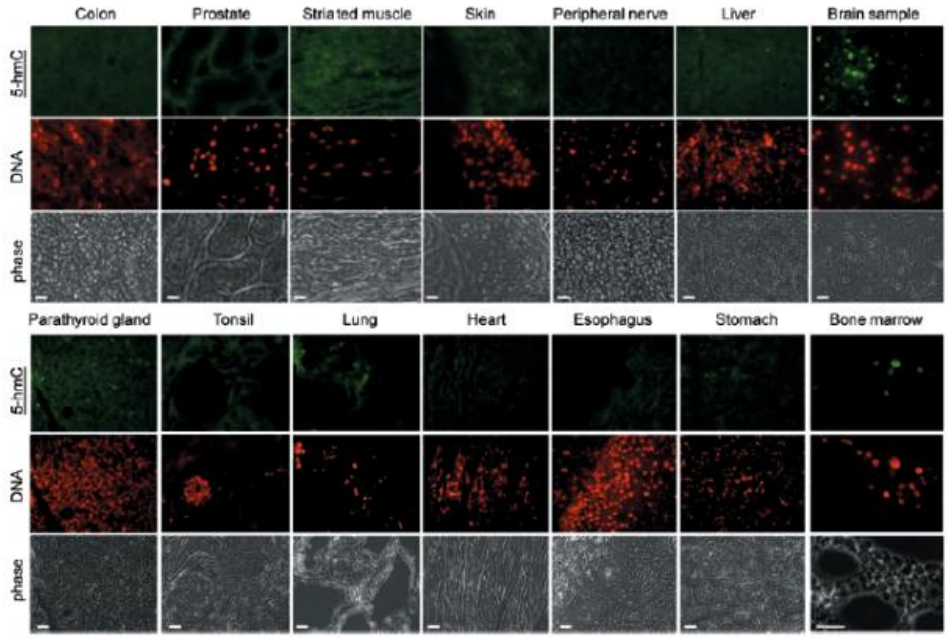

Figure 5 The presence of immunochemically detectable 5-hydroxymethylcytosine (5-hmC) levels is restricted to bone marrow and neuronal tissues in adult mammals. A range of indicated normal adult human tissues from a Folio histological tissue array were immunostained with anti-5-hmC antibody. Phase views are shown. An identical maximal exposure of the images made using the 488 nm (5-hmC, tyramide) filter is shown for all the samples, except brain and bone marrow, to illustrate the pattern of background staining, which does not correspond to the DNA signal (indicated) in the majority of tissues. All the triplicate tissue samples on the array exhibited identical staining patterns. Six different bone marrow specimens were tested and gave essentially the same results. Representative views are shown. Scale bars are 20 μm, except 30 μm in bone marrow sample. Essentially the same results were obtained with samples of ovary, testis, kidney, small intestine, salivary gland, uterus, uterine cervix, mesothelium, eye muscle, adrenal gland, pancreas and breast tissue (see Supplementary information, Figure S9). The experiments were performed using the Diagenode antibody.

not detect any significant 5-hmC signal in mouse liver, skin, ovary, spleen or heart (Supplementary information, Figure S8), nor in any human tissue tested, except for brain and bone marrow (Figure 5 and Supplementary information, Figure S9). In mouse brain, strong 5-hmC nuclear staining was found not only in the hippocampal region and subventricular zone, which have previously been reported as regions of active neurogenesis containing populations of neural stem cells (NSCs) and neural progenitors [24-28], but also in the neuronal tissue of the cortex and other parts of the brain and cerebellum (Figure 6A-6C, Supplementary information, Figure S8B). In particular, in the hippocampus, higher levels of 5-hmC were observed in the dentate gyrus than the adjacent pyramidal layer (Figure 6A), but this difference may be due to the relatively higher cell density of the former. Brain white matter did not display an intense 5-hmC signal (Figure 6A, 6B and Supplementary information, Figure S8B). Consistent with these results and in agreement with already published data [29], NSC derived *in vitro* from hESCs also exhibit strong 5-hmC staining, which does not disappear or decline after 18 days of neuronal differentiation (Figure 6D and 6E), but differentiation of progenitors towards oligodendrocyte lineages is characterised by the progressive loss of 5-hmC staining (data not shown). Notably, the transcripts of all 3 *Tet* genes are highly expressed in human NSCs, which make them distinct from human ES cells where only *Tet1* and *Tet3* transcripts are present at significant levels (Figure 6F).

Discussion

Our study shows a correlation between high levels of genomic 5-hmC and multi-lineage-potential during mam-

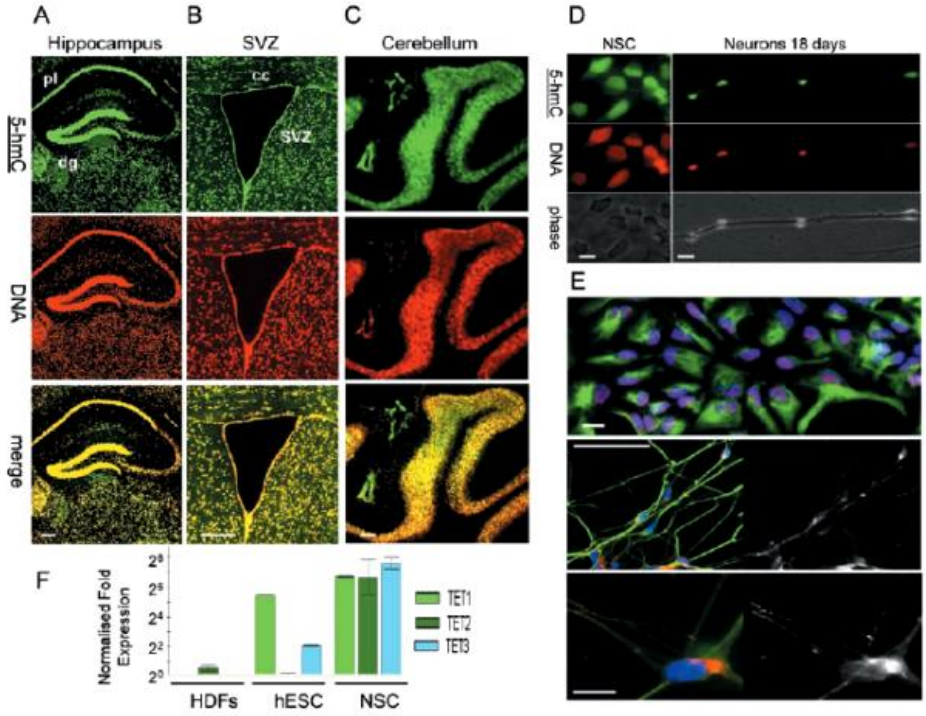

Figure 6 5-Hydroxymethylcytosine (5-hmC) is dramatically enriched in both neuronal progenitors and differentiated post-mitotic cells of neuronal lineages. **(A)** 5-hmC Is visualised by immunochemistry in hippocampal **A** and ventricular **(B)** regions of mouse brain and cerebellar folia **(C)**. Pyramidal layer (pl), dentate gyrus (dg), subventricular zone (svz) and corpus colossum (cc) are indicated. Scale bars are 250 μm. The experiments were performed using the Diagenode antibody. **(D)** Human neural stem cells (NSCs) exhibit high levels of 5-hmC staining, which does not disappear after 18 days of differentiation into neurons. hESC-derived NSCs (indicated) and neurons derived from them after 18 days (neurons 18 days) of differentiation were immunostained for 5-hmC. 5-hmC, DNA and phase views are indicated. Scale bars are 20 μm. The experiments were performed using the Diagenode antibody. **(E)** The upper panel shows a representative field of human NSC culture used for 5-hmC immunostaining in D stained for Sox1 (red nuclear signal), DAPI (blue) and nestin (green cytoplasmic signal). The majority of cells co-express both markers. Scale bar is 50 μm. The middle panel shows a representative field of the neuronal culture obtained after 18 days of differentiation and used for 5-hmC immunostaining in D, stained for β-III tubulin (green), Synapsin I (red in the colour image and presented as single channel in the grayscale image on the right) and DAPI (blue). The majority of cells co-express β-III tubulin and Synapsin (scale bar is 50 μm). The lower panel shows the same stained population at a higher magnification (scale bar is 10 μm). **(F)** The results of real-time RT-PCR analysis of *Tet1/2/3* transcripts (indicated) in HDFs, human H1 ES cells and obtained from them human NSCs (indicated). The transcripts of all three *Tet* genes are highly expressed in human NSCs. The data were normalised with relative to GAPDH. Error is expressed as s.e.m.

malian development and in a number of adult tissues. High 5-hmC level is a feature of induced or embryonic pluripotent stem cells. Nestin-expressing fetal stem cells in post-implantation development, and stem cell-rich tissues including adult bone marrow and nasal epithelium of the late development mouse embryo also exhibit high 5-hmC levels, whereas the actively proliferating unipotent cells of adult mammalian skin or liver do not. Sometimes it appears that a strong 5-hmC signal coincides with stronger DNA staining (SVZ, olfactory epithelium), but it is worth noting that a higher DNA content is an expected feature of some rapidly proliferating stem cell populations, wherein a significant proportion of cells is present in the S-phase of the cell cycle. A more detailed analysis will be required to determine if high 5-hmC is being utilised by other adult tissue-specific stem cells. According to our study, neuronal lineages seem to be exceptional in their maintenance of high 5-hmC levels

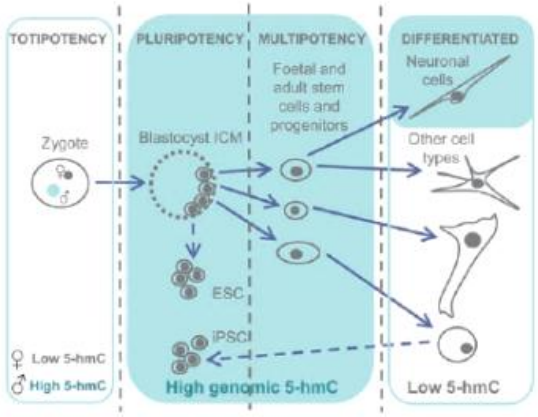

Figure 7 A graphical summary illustrating 5-hydroxymethylcytosine (5-hmC) distribution in mammalian development. High levels of 5-hmC are marked with green shading.

in differentiated, post-mitotic cells. In agreement with this finding it has been previously reported that differentiation of mESCs into neuronal progenitors and subsequently into mature neurons has been shown to be accompanied by relatively few changes in DNA methylation, most of which occur during the first stage of differentiation [30, 31]. Thus, neurons may represent a unique mammalian post-mitotic differentiated cell type, with a chromatin organisation similar in some aspects (5-hmC enrichment) to that of stem cells. Our analysis of 5-hmC distribution in adult mouse tissues is supported by other reports on 5-hmC tissue quantification showing that 5-hmC is strongly enriched in the central nervous system, compared to other adult organs [5, 12, 14]. Our data are also generally in agreement with TLC-based data [5], an isotope-based chromatographic method for quantification of 5-hmC [12], and with immunolocalisation of 5-hmC in mouse brain presented in the same study [12]. In contrast to Globisch and colleagues, our results do not reveal immunochemically detectable 5-hmC in adult mouse liver and kidney, but the resolution of the corresponding figures in that report does not allow us to draw conclusions on the specificity of the observed staining in these tissues. It is also important to note that there is a slight discrepancy between the study of enzymatic quantification of genomic 5-hmC [14], where its levels in mouse lung and, especially, in kidney were similar to those in brain, and both our immunochemical data and the other published data, based on biochemical methods [5, 12], where the 5-hmC content of lung and kidney was reported to be much lower than that of neural tissues. It is possible that these differences stem from the nature and sensitivity of the methods used to quantify genomic 5-hmC in the corresponding reports.

Previous studies have established that 5-mC- and 5-hmC-containing DNAs have different protein binding properties; for example, the interaction of MBD proteins with 5-mC is abolished by hydroxymethylation [7, 11]. This implies that these two epigenetic modifications perform distinct biological functions. It is possible that an elevated genomic content of 5-hmC could contribute both to the general "openness" of the chromatin in stem cell and neuronal nuclei, and to the regulation of expression of specific target genes during stem cell self renewal and differentiation. Further work is necessary to reveal the identity and roles of any 5-hmC binding proteins, and identify genes affected by hydroxymethylation of cytosine residues in tissue-specific contexts.

In conclusion, we show that unlike 5-mC, genomic 5-hmC is significantly enriched in embryonic contexts, cells with multi-lineage potency and neurons in mammals (Figure 7). To our knowledge, 5-hmC is the first epigenetic modification shown to possess such a cell-type-specific enrichment in its distribution.

Materials and Methods

ES cell culture and iPSC generation

RH1 and RCM1 hESCs have been described previously [32, 33]. Mouse HM1 ESCs were maintained on gelatin-coated dishes in Glasgow's Minimum Essential medium (GIBCO), supplemented with 15% fetal bovine serum, 55 μM β-mercaptoethanol (GIBCO), 2 mM L-glutamine, 0.1 mM MEM non-essential amino acids, 5 000 units ml^{-1} penicillin/streptomycin and 1 000 units ml^{-1} of murine LIF (Chemicon) under feeder-free conditions. hESCs and hiPSCs were cultured on matrigel-coated plates and slides in feeder-free mTeSR1 medium (STEMCELL Technologies). Cells were passaged using collagenase IV (200 units ml^{-1} in DMEM, GIBCO) and mechanical dissociation. hESC differentiation to hepatic endoderm was performed according to the published protocol [15]. hiPSCs were produced as described previously [16] and validated by flow cytometry, embryoid body formation, differentiation into endoderm, mesoderm and ectoderm and RT-PCR as described [32].

Immunocytochemistry, immunohistochemistry, pre-implantation embryo culture, imaging and dot blot assay

For immunocytochemistry, cells were fixed in 4% formaldehyde for 15 min. Paraffin-embedded formaldehyde-fixed sections of wild-type CD1 mouse embryos and adult tissues were used for immunohistochemistry. A normal human tissue histological array (Folio) was used for 5-hmC detection in human tissues. Tissue sections were de-waxed according to standard procedures. Cells and tissue sections were permeabilised for 15 min with PBS containing 0.5% Triton X-100. For 5-hmC and 5-mC staining, permeabilised cells and tissue sections were incubated in 4 N HCl for 1 h at 37 °C and then neutralised in 100 mM Tris-HCl (pH 8.5) for 10 min,

followed by a standard immunostaining protocol.

Anti-5-hmC (Diagenode, 1:1 000 dilution; Active Motif, 1:5 000; 1:50 000 dilutions), anti-5-mC (Eurogentec) and anti-nestin clone 401 (DSHB) primary antibodies were used. DNA was visualised using an anti-single-stranded DNA antibody (Zymo research). Peroxidase-conjugated anti-rat secondary antibody (Dako) and the tyramide signal enhancement system (Perkin Elmer) were employed for 5-hmC detection.

Mouse embryos were produced by mating superovulated F1 females with CD1 males, and cultured according to standard procedures. Anti-5-hmC (Active Motif, 1:5 000 dilution) and anti-5-mC (Eurogentec, 1:200 dilution) antibodies were used for immunochemistry. Pre-implantation embryos were immunostained as described [34] with the use of peroxidase-conjugated secondary antibody and the additional tyramide (Perkin-Elmer) signal enhancement step for 5-hmC staining. Control staining without primary antibody produced no detectable signal. Images were acquired using a Zeiss Axiovert 200 immunofluorescence microscope and Axiovision software. Dot blot assays were performed as reported previously [10].

Image quantification

Image quantification was performed using Fiji software. Corresponding slides were processed in identical conditions and were imaged at the same exposure settings. Mean intensities were measured for 10 random squares on each region of interest for each sample. The 5-hmC signal was standardised to the total DNA signal. Mean values of the mean intensities are presented. Experimental error is expressed as s.e.m.

Statistical analysis

We used a numerical grading system 0 (absent), 1 (low) and 2 (high) to account for differences in 5-hmC and 5-mC staining intensities in maternal and paternal pronuclei of the mouse zygotes (the examples of the categories are arrowed on Supplementary information, Figure S4A). The statistical analysis was performed using GraphPad Prism software. The individual 5-hmC and 5-mC immunostaining scores (total number of *xy* pairs = 70) of both maternal ($n = 35$) and paternal pronuclei ($n = 35$) were correlated using Spearman's nonparametric test. The P value was considered significant for $P < 0.05$.

Solexa deep sequencing

Total RNA was isolated from hESCs at the times indicated after induction of differentiation and sequenced directly using a Solexa 1G system. The Solexa results were normalised as follows: the raw count reads of each gene were first divided by the total number of aligned reads multiplied by 1 million to take into account the depth of sequencing. The results were then divided by the length of each gene multiplied by 1 000 to get an RPKM value (read per kilo bases per million reads).

Neural stem cells

Neural stem cells were generated from p57 H9 hESCs and cultured as described [35]. NSCs' identity was confirmed by immunostaining for Pax6, Sox2, Sox1 and Nestin. H9 hESCs were cultured on Matrigel with TeSR2 (STEMCELL Technologies) medium. Differentiation was performed in Neurobasal medium (N2 supplement 1:100).

Real time RT-PCR

Total RNA was extracted with TriReagent (Sigma). Samples were reverse transcribed using random primers (Promega) and Superscript II RT (Invitrogen). Products were detected using SYBR Green PCR Mastermix (Applied Biosystems) and a PTC-200 cycler with a Chromo-4 detection system (MJ Research). Data were normalised with relative to GAPDH. Error is expressed as s.e.m. Primer sequences for human Tet proteins are available upon request.

Immunostaining competition experiment

Immunostaining competition experiments were performed as described [12] using PCR-produced 100-bp DNA fragments, where all the cytosines were replaced with either 5-hmC or 5-mC.

Acknowledgments

We thank Adrian Bird (University of Edinburgh) for encouragement, Paz Freile, Sebastian Greenhough, Sharmin Haideri, Heidi Mjoseng, Jane Taylor (MRC Centre for Regenerative Medicine, University of Edinburgh) and Britt Tye (Roslin Cells) for technical support; the Histology team of MRC Human Reproductive Sciences Unit for excellent service and John Iredale (MRC Centre for Regenerative Medicine, University of Edinburgh) for access to Solexa data. DH is an RCUK fellow.

References

1 Bird A. DNA methylation patterns and epigenetic memory. *Genes Dev* 2002; **16**:6-21.
2 Reik W, Dean W, Walter J. Epigenetic reprogramming in mammalian development. *Science* 2001; **293**:1089-1093.
3 Surani MA, Hayashi K, Hajkova P. Genetic and epigenetic regulators of pluripotency. *Cell* 2007; **128**:747-762.
4 Tahiliani M, Koh KP, Shen Y, *et al*. Conversion of 5-methylcytosine to 5-hydroxymethylcytosine in mammalian DNA by MLL partner TET1. *Science* 2009; **324**:930-935.
5 Kriaucionis S, Heintz N. The nuclear DNA base 5-hydroxymethylcytosine is present in Purkinje neurons and the brain. *Science* 2009; **324**:929-930.
6 Ito S, D'Alessio AC, Taranova OV, *et al*. Role of Tet proteins in 5mC to 5hmC conversion, ES-cell self-renewal and inner cell mass specification. *Nature* 2010; **466**:1129-1133.
7 Jin SG, Kadam S, Pfeifer GP. Examination of the specificity of DNA methylation profiling techniques towards 5-methylcytosine and 5-hydroxymethylcytosine. *Nucleic Acids Res* 2010; **38**:e125.
8 Hayatsu H, Shiragami M. Reaction of bisulfite with the 5-hydroxymethyl group in pyrimidines and in phage DNAs. *Biochemistry* 1979; **18**:632-637.
9 Huang Y, Pastor WA, Shen Y, *et al*. The behaviour of 5-hydroxymethylcytosine in bisulfite sequencing. *PLoS One* 2010; **5**:e8888.
10 Nestor C, Ruzov A, Meehan R, Dunican D. Enzymatic approaches and bisulphite sequencing cannot distinguish between 5-methylcytosine and 5-hydroxymethylcytosine in DNA. *Biotechniques* 2010; **48**:317-319.
11 Valinluck V, Tsai HH, Rogstad DK, Burdzy A, Bird A, Sowers LC. Oxidative damage to methyl-CpG sequences inhibits the

binding of the methyl-CpG binding domain (MBD) of methyl-CpG binding protein 2 (MeCP2). *Nucleic Acids Res* 2004; **32**:4100-4108.
12 Globisch D, Münzel M, Müller M, *et al.* Tissue distribution of 5-hydroxymethylcytosine and search for active demethylation intermediates. *PLoS One* 2010; **5**:e15367.
13 Ko M, Huang Y, Jankowska AM, *et al.* Impaired hydroxylation of 5-methylcytosine in myeloid cancers with mutant TET2. *Nature* 2010; **468**:839-843.
14 Szwagierczak A, Bultmann S, Schmidt CS, Spada F, Leonhardt H. Sensitive enzymatic quantification of 5-hydroxymethylcytosine in genomic DNA. *Nucleic Acids Res* 2010; **38**:e181.
15 Hay DC, Fletcher J, Payne C, *et al.* Highly efficient differentiation of hESC to functional hepatic endoderm requires ActivinA and Wnt3a signalling. *Proc Natl Acad Sci USA* 2008; **105**:12301-12306.
16 Takahashi K, Tanabe K, Ohnuki M, *et al.* Induction of pluripotent stem cells from adult human fibroblasts by defined factors. *Cell* 2007; **131**:861-872.
17 Feng S, Jacobsen SE, Reik W. Epigenetic reprogramming in mammalian development. *Science* 2010; **330**:622-627.
18 Mayer W, Niveleau A, Walter J, Fundele R, Haaf T. Demethylation of the zygotic paternal genome. *Nature* 2000; **403**:501-502.
19 Iqbal K, Jin SG, Pfeifer GP, Szabó PE. Reprogramming of the paternal genome upon fertilization involves genome-wide oxidation of 5-methylcytosine. *Proc Natl Acad Sci USA* 2011; **108**:3642-3647.
20 Oswald J, Engemann S, Lane N, *et al.* Active demethylation of the paternal genome in the mouse zygote. *Curr Biol* 2000; **10**:475-478.
21 Wislet-Gendebien S, Wautier PF, Leprince B. Astrocytic and neuronal fate of mesenchymal stem cells expressing nestin. *Brain Res Bull* 2005; **68**:95-102.
22 Wiese C, Rolletschek A, Kania G, *et al.* Nestin expression-a property of multi-lineage progenitor cells? *Cell Mol Life Sci* 2004; **61**:2510-2522.
23 Murrell W, Féron F, Wetzig A, *et al.* Multipotent stem cells from adult olfactory mucosa. *Dev Dyn* 2005; **233**:496-515.
24 Merkle FT, Tramontin AD, Garcia-Verdugo JM, Alvarez-Buylla A. Radial glia give rise to adult neural stem cells in the subventricular zone. *Proc Natl Acad Sci USA* 2004; **101**:17528-17532.
25 Merkle FT, Alvarez-Buylla A. Neural stem cells in mammalian development. *Curr Opin Cell Biol* 2006; **18**:704-709.
26 Doetsch F, Caille I, Lim DA, García-Verdugo JM, Alvarez-Buylla A. Subventricular zone astrocytes are neural stem cells in the adult mammalian brain. *Cell* 1999; **97**:703-716.
27 Seri JM, García-Verdugo BS, McEwen A, Alvarez-Buylla A. Astrocytes give rise to new neurons in the adult mammalian hippocampus. *J Neurosci* 2001; **21**:7153-7160.
28 Deng W, Aimone JB, Gage FH. New neurons and new memories: how does adult hippocampal neurogenesis affect learning and memory? *Nat Rev Neurosci* 2010; **11**:339-350.
29 Song CX, Szulwach KE, Fu Y, *et al.* Selective chemical labeling reveals the genome-wide distribution of 5-hydroxymethylcytosine. *Nat Biotechnol* 2011; **29**:68-72.
30 Meissner A, Mikkelsen TS, Gu H, *et al.* Genome-scale DNA methylation maps of pluripotent and differentiated cells. *Nature* 2008; **454**:766-770.
31 Mohn F, Weber M, Rebhan M, *et al.* Lineage-specific polycomb targets and *de novo* DNA methylation define restriction and potential of neuronal progenitors. *Mol Cell* 2008; **30**:755-766.
32 Fletcher JM, Ferrier PM, Gardner JO, *et al.* Variations in humanized and defined culture conditions supporting derivation of new human embryonic stem cell lines. *Cloning Stem Cells* 2006; **8**:319-334.
33 De Sousa PA, Gardner J, Sneddon S, *et al.* Clinically failed eggs as a source of normal human embryo stem cells. *Stem Cell Res* 2009; **2**:188-197.
34 Beaujean N, Taylor J, Gardner J, *et al.* Effect of limited DNA methylation reprogramming in the normal sheep embryo on somatic cell nuclear transfer. *Biol Reprod* 2004; **71**:185-193.
35 Koch P, Opitz T, Steinbeck JA, Ladewig J, Brüstle O. A rosette-type, self-renewing human ES cell-derived neural stem cell with potential for *in vitro* instruction and synaptic integration. *Proc Natl Acad Sci USA* 2009; **106**:3225-3230.

(**Supplementary information** is linked to the online version of the paper on the *Cell Research* website.)

Brain Struct Funct
DOI 10.1007/s00429-012-0419-0

ORIGINAL ARTICLE

Lesions of the anterior thalamic nuclei and intralaminar thalamic nuclei: place and visual discrimination learning in the water maze

Pierre-Henri Moreau · Yanina Tsenkina · Lucas Lecourtier · Joëlle Lopez · Brigitte Cosquer · Mathieu Wolff · John Dalrymple-Alford · Jean-Christophe Cassel

Received: 6 January 2012 / Accepted: 14 April 2012

Abstract Medial thalamic damage produces memory deficits in humans (e.g., Korsakoff's syndrome) and experimental animals. Both the anterior thalamic nuclei (ATN) and rostral intralaminar plus adjacent lateral thalamic nuclei (ILN/LT) have been implicated. Based on the differences in their main connections with other neural structures, we tested the prediction that ATN lesions would selectively impair acquisition of spatial location discrimination, reflecting a hippocampal system deficit, whereas ILN/LT lesions would impair acquisition of visual pattern discrimination, reflecting a striatal system deficit. Half the rats were first trained in a spatial task in a water maze before switching to a visual task in the same maze, while the remainder were tested with the reverse order of tasks. Compared with sham-operated controls, (1) rats with ATN lesions showed impaired place learning, but normal visual discrimination learning, (2) rats with ILN/LT lesions showed no deficit on either task. Rats with ATN lesions were also hyperactive when their home cage was placed in a novel room and remained more active than ILN/LT or SHAM rats for the subsequent 21 h, especially during the nocturnal phase. These findings confirmed the influence of ATN lesions on spatial learning, but failed to support the view that ILN/LT lesions disrupt striatal-dependent memory.

Keywords Anterior thalamic nuclei · Hippocampus · Intralaminar thalamic nuclei · Spatial memory · Striatum · Visual pattern memory · Water maze

P.-H. Moreau and Y. Tsenkina contributed equally to the work.

P.-H. Moreau · Y. Tsenkina · L. Lecourtier · J. Lopez · B. Cosquer · J.-C. Cassel (✉)
Laboratoire d'Imagerie et Neurosciences Cognitives, UMR 7237, Université de Strasbourg, CNRS, IFR 37 Neurosciences, GDR CNRS 2905, 12 Rue Goethe, 67000 Strasbourg, France
e-mail: jcassel@unistra.fr

M. Wolff
University of Bordeaux, INCIA, UMR 5287, 33400 Talence, France

M. Wolff
CNRS, INCIA, UMR 5287, 33400 Talence, France

J. Dalrymple-Alford
New Zealand Brain Research Institute, Christchurch 8011, New Zealand

J. Dalrymple-Alford
Department of Psychology, University of Canterbury, Christchurch 8140, New Zealand

J. Dalrymple-Alford
Department of Medicine, University of Otago, Christchurch, New Zealand

Introduction

Injury to the medial thalamus is a major cause of severe memory dysfunction in humans (Kopelman 2002; van der Werf et al. 2003). The specific thalamic substrates of this diencephalic amnesia are uncertain, with some clinical studies attributing memory deficits in a non-specific manner to many medial thalamic nuclei (Gold and Squire 2006), others that focus on particular thalamic nuclei (Harding et al. 2000), and some on the possibility that separate nuclei primarily influence different aspects of cognition beyond memory (van der Werf et al. 2000; Jodar et al. 2011). Variability in lesion locus and close proximity of the thalamic nuclei and their related pathways permit only tentative conclusions from the clinical evidence. Experimental animal lesion studies to address this issue,

Published online: 29 April 2012

however, have also generated conflicting views (Aggleton et al. 2011; Mair et al. 1998; Bailey and Mair 2005; Savage et al. 1998). The anterior thalamic nuclei (ATN) and the rostral intralaminar thalamic nuclei plus the adjacent lateral thalamic region (ILN/LT) have been most frequently emphasised, but evidence for their relative influence on memory after injury is mixed, with many (Lopez et al. 2009; Mair et al. 2003; Mitchell and Dalrymple-Alford 2005; Mitchell and Dalrymple-Alford 2006; Wolff et al. 2008a) but not all studies (Gibb et al. 2006; Savage et al. 1998) suggesting dissociations. The need to clarify the relative role of these thalamic nuclei is emphasised by recent evidence that thiamine deficiency in the rat, a model for the Wernicke–Korsakoff syndrome, depletes neurones in both of these thalamic regions (Anzalone et al. 2010).

It is possible that ATN and ILN/LT nuclei each influence different memory processes and that impairments associated with their injury vary as a function of the memory task (Lopez et al. 2009; Mitchell and Dalrymple-Alford 2005, 2006; Wolff et al. 2008a). One promising perspective is that the influence of each thalamic region reflects its involvement in different neural systems and, by implication, an involvement in different memory systems in the brain. An influential view in the literature is that the ATN are an important part of an extended hippocampal memory system (Aggleton 2008; Aggleton and Brown 1999; Vann and Albasser 2009). There is ample evidence that selective ATN lesions often impair performance on many, although not all, hippocampal-dependent memory tasks (Aggleton et al. 2009, 2011; Byatt and Dalrymple-Alford 1996; Mair et al. 2003; Moran and Dalrymple-Alford 2003; Sziklas and Petrides 1999, 2007; Warburton et al. 2001; Wolff et al. 2006, 2008b). In contrast, the rostral ILN/LT region has prominent connections with the dorsal striatum (Berendse and Groenewegen 1991; van der Werf et al. 2002), so that this thalamic region may influence memory processes that depend on the functional integrity of the dorsal striatum and its network interactions with other brain structures, especially the prefrontal cortex (Mair et al. 1998).

Some support for this dissociation comes from evidence that ATN, but not ILN/LT lesions impair acquisition of allocentric spatial memory in both the radial arm maze and water maze (Bailey and Mair 2005; Mair et al. 2003; Mitchell and Dalrymple-Alford 2005, 2006; Wolff et al. 2008a). Stronger support was provided by evidence of a double dissociation between the effects of ATN and ILN/LT lesions on two memory tasks. Mitchell and Dalrymple-Alford (2006) reported that ILN/LT, but not ATN lesions impaired a preoperatively acquired egocentric working memory task, while only ATN lesions impaired allocentric spatial memory. Egocentric spatial memory impairments have often been reported after dorsal striatum lesions (Cook and Kesner 1988; DeCoteau and Kesner 2000; Kesner et al. 1993; McDonald and White 1993, 1994; Mitchell and Hall 1988; Packard and Teather 1998). A recent study, however, failed to observe an egocentric spatial reference memory deficit in a radial-arm water maze after ILN/LT lesions, which questions the degree of overlap between the effects of ILN/LT and striatal lesions (Wolff et al. 2008a).

The separation between the effects of ATN and ILN/LT lesions was extended here by comparing their effects on the classic water maze tasks designed by Packard and McGaugh (1992). These authors demonstrated a double dissociation between the effects of fornix lesions and dorsal caudate lesions, in which only fornix lesions impaired acquisition of a spatial reference memory task for locations tagged by irrelevant visual cues, whereas only dorsal caudate lesions impaired acquisition of a visual pattern discrimination task between cues tagged by irrelevant spatial location. It was predicted that the effects of ATN and ILN/LT lesions on these tasks would correspond to the previous effects of fornix and dorsal caudate lesions, respectively. The comparable nature of the two tasks means that any differential deficit between them would be unlikely to be due to differences in motivational, sensory or motor characteristics. Visual discrimination learning is relatively spared in Korsakoff's amnesia (e.g., Oscar-Berman and Zola-Morgan 1980), so a dissociation across these two tasks after ATN and rostral ILN lesions in rats would support the suggested importance of ATN dysfunction in human amnesic cases (Harding et al. 2000; van der Werf et al. 2003).

Based on their anatomical connections, an additional comparison between the two thalamic lesions examined their effects on home cage activity measured in a novel room over a 24-h period. Indeed, hippocampal lesions consistently increase this measure of home cage activity (e.g., Galani et al. 1997). Moreover, the intralaminar nuclei may influence arousal and one study has suggested that striatal lesions increase nocturnal locomotor activity (Mena-Segovia et al. 2002; Van der Werf et al. 2002).

Methods

Subjects and housing conditions

Fifty-eight adult male Long Evans rats (3 months old at the time of surgery; Centre d'Elevage R Janvier, Le Genest-St-Isles, France) were used. They were housed individually in opaque Makrolon cages (42 × 26 × 15 cm) under controlled temperature (21 °C) and 12/12 h light/dark cycle (light on at 7:00 h). Food and water were provided ad libitum. The study adhered to the regulations specified by the

European Committee Council Directive of November 24, 1986 (86/609/EEC) and the French Department of Agriculture (personal authorization license no. 67-215 for J-C.C. with co-authors operating under his authority).

Surgery

Surgeries were conducted under aseptic conditions by authorized personnel. Rats received either ATN ($n = 22$) or ILN/LT ($n = 21$) lesions after being anaesthetized with sodium pentobarbital (50 mg/ml i.p., 20 min after 0.15 mg/ml atropine at 1.5 ml/kg, i.p.). The lesions were made via slow infusions of sub-microlitre volumes of *N*-methyl-D-aspartate using coordinates adapted to different Bregma-to-Lambda distances (see Table 1 for coordinates) and the incisor bar set at −7.5 mm. The needle was left in place for 3 min after each infusion before being slowly retracted. A third group (controls, $n = 15$) received sham lesions with the infusion needle lowered to the ATN (about half of the group) or the ILN/LT sites.

Water maze, apparatus

The Morris water maze (diameter 160 cm, height 60 cm) was filled 32 cm deep with 22 °C water made opaque by the addition of powdered milk. The pool was located in the colony/experimental room and contained numerous extra maze cues (e.g., cages and racks; a desk; lights; two pillars; pictures on the wall, etc). The pool was divided into four virtual quadrants with four start points identified as north (N), east (E), south (S), and west (W). Following Packard and McGaugh (1992), the visual cues were provided by rubber balls (8 cm in diameter) that were painted with one of two different visual patterns. One pair of rubber balls was painted white with three black horizontal stripes (1 cm width) while the second pair was painted with three black vertical stripes (1 cm width). One of each pair was attached to a 5 cm round Plexiglas support that rested 1 cm below the water surface (i.e., fake platform) and one of each pair provided an escape because it was attached to one corner of a rectangular platform (11 × 14 × 0.6 cm; Fig. 1). About half of the rats from each surgery group were chosen randomly and tested first on the spatial discrimination task followed 3 days later by training on the visual pattern discrimination task, whereas the remaining rats were tested with the reverse order of tasks.

Spatial discrimination task

In the place learning task, rats had to swim to the appropriate location to escape the water on to a platform, with the correct location and one of the three remaining locations cued by the irrelevant visual cues. On the morning, before training, the rats were placed on a platform with no cue, positioned in one quadrant (NW or SE), and replaced on the platform if it failed to remain there for 10 s (unless 60 s in total had elapsed). On the afternoon, before training, the rat was released from the opposite quadrant and allowed to find the platform and climb onto it. When a rat failed to find the platform within 60 s, it was gently guided to it by the experimenter's hand and allowed to stay there for 10 s.

For training, an escape platform was located at the centre of the "NE" quadrant, regardless of the horizontal or vertical striped cue used to mark that location (see Fig. 2). For any three successive trials, one of the two cues marked the location of the escape platform while the alternate cue (with no escape) was located in the centre of one of the three other quadrants, using one of each position for the three trials. The particular cue associated with the correct

Table 1 Infusion volumes, infusion rates and coordinates for the NMDA lesions of the anterior (ATN) or lateral (ILN/LT) thalamic aggregates

ATN			ILN/LT		
	Ant	Post	Ant	Ant	Post
AP coordinates for B–L distance (cm)			AP coordinates for B–L distance (cm)		
0.60–0.63	−0.22	−0.20	−0.31	−0.31	−0.35
0.64–0.66	−0.23	−0.21	−0.32	−0.32	−0.36
0.67–0.72	−0.24	−0.22	−0.33	−0.33	−0.37
ML distance	±0.15	±0.08	±0.13	±0.13	±0.13
DV distance	−0.45	−0.45	−0.54	−0.56	−0.55
Volume (µl, 0.12 M)	0.09	0.11	0.06	0.06	0.06
Infusion rate (µl/min)	0.03	0.03	0.03	0.03	0.03

Ant anterior site, *Post* posterior site, *AP* anterior–posterior coordinates from Bregma, at three B–L (Bregma–Lambda, see Paxinos and Watson 1998) distances, *ATN* anterior thalamic aggregate comprising the anterodorsal, anteromedial, and anteroventral thalamic nuclei, *DV* dorsal–ventral distance from dura, *ILN/LT* lateral medial thalamic aggregate comprising the intralaminar nuclei (centrolateral, paracentral, and rostral central medial nuclei) and lateral mediodorsal thalamic nuclei (lateral and paralamellar nuclei), *ML* medial-lateral distance from midline, *Post* posterior AP site

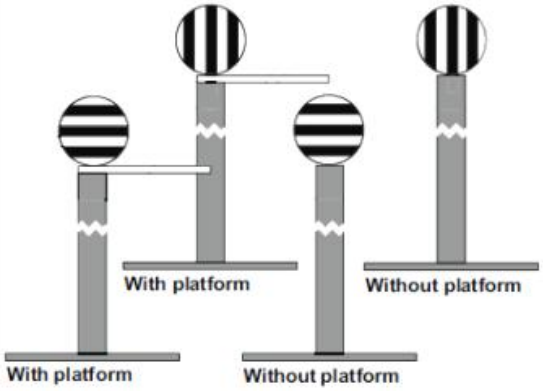

Fig. 1 Drawing showing the real (*left*) and fake (*right*) escape platforms used for the spatial and visual versions of the water maze learning tasks. The size of the escape platform associated with the cue (*left*) was 11 × 14 × 0.6 cm. The height of the pedestal was 31 cm. The diameter of the rubber ball was 8 cm. The cues (the white rubber ball painted with *black vertical* or *horizontal stripes*) protruded 7 cm above the water surface. The rubber ball with the *vertical stripes* was used as the cues in the visual discrimination task

(escape) location remained the same for either one or two trials on a pseudo-random basis. Across every four trials, the rat was placed into the pool, facing the wall, at one starting point designated pseudo-randomly among four possibilities (N, E, S or W) and given a maximum of 60 s to reach the correct platform, with guidance after 60 s. When the rat had climbed onto the platform, it was allowed to stay there for 10 s. A random half of every four trials used a start point that was close to the platform location. As per Packard and McGaugh (1992), the primary-dependent measure was the number of errors made (when a rat touched the incorrect target). The latency to reach the correct location (i.e., the escape platform) was also recorded.

The rats that were tested first for spatial learning were trained over 10 blocks of 8 trials each. These rats were given two trials per day for the first 2 days and four trials on day 3. These eight trials were considered the first block. For the subsequent 9 days (i.e., days 4–12), they were given eight consecutive daily trials. The rats that were first tested in the visual discrimination learning task (see below) were already familiarised to the general water maze procedures and were thus given eight trials per day from day 1 onwards for the spatial discrimination task, using the same methods.

Visual pattern discrimination task

Rats that began first with the visual discrimination task were given the same pretraining familiarisation as those starting with the spatial task. For the visual discrimination task, rats had to swim to the correct visual pattern

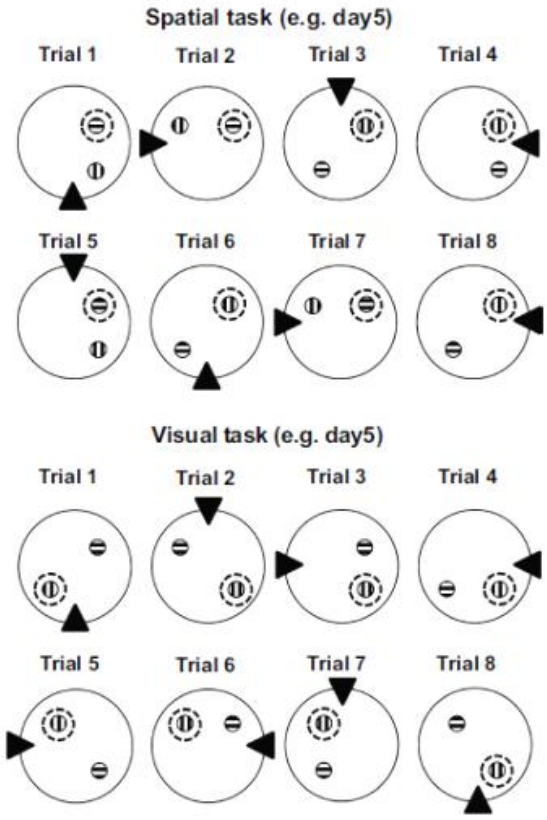

Fig. 2 Training protocol in the water maze used on day 5 of either the spatial learning (*top*) or the visual discrimination tasks (*bottom*). The *solid triangles* indicate the location from where the rats were released on each trial (1–8). The *two circles* with *horizontal* or *vertical stripes* indicate the location of the cues in the pool. For each trial, the *stippled circle* surrounding one of the four cue locations points to the cue associated with the escape platform. In the spatial task, rats had to swim to a constant location regardless of the cue (*horizontal* or *vertical stripes*). In the visual discrimination task, rats had to swim to the correct cue (*vertical stripes*) regardless of its location

(i.e. vertical stripes), which was consistently associated with the escape platform regardless of its location in the pool, and ignore the alternate visual cue (i.e., horizontal stripes) with no escape platform located at the centre of one of the other quadrants (see Fig. 2). The general methodology was the same as that used for the spatial learning task, with four different start positions used randomly across every four trials, and the same measures were collected. From the first trial onwards, the location of the correct cue remained in the same position for three consecutive trials and was changed on every fourth trial to a new randomly designated location; the incorrect cue was placed in one of the three other quadrants on each of the three consecutive trials. Each of the four possible locations

for the correct cue was used across every 12 trials. The rats that were tested first on the visual discrimination task received two trials per day for the first 2 days and four trials for day 3, followed by eight trials per day for the remaining eight blocks of eight trials. The rats that had been tested first for spatial learning (see above) received eight daily trials from the start of training over seven blocks of trials when trained on the visual discrimination task.

Home cage locomotor activity

Spontaneous locomotor activity was assessed for 24 h 2 weeks after the end of the water maze experiments. Clean transparent Perspex home cages were placed on shelves located in a new room. Two photocells outside each cage, located 4.5 cm above floor level and 28 cm apart, recorded horizontal locomotor activity. As per Galani et al. (2001), the first 3 h "habituation" period is the time when rats generally adapt to the novelty of the test situation. The remaining 21 h provided a diurnal period of 9 h and a nocturnal period of 12 h.

Histology

Rats were deeply anaesthetized with an overdose of sodium pentobarbital (200 mg/kg, i.p.) and perfused transcardially with 4 % paraformaldehyde (PFA, in 0.1 M PBS; 4 °C). The brains were post-fixed for 2 h in 4 % PFA (4 °C), cryoprotected by a 48-h immersion (at 4 °C) in a 20 % sucrose solution (in PBS), snap-frozen in isopentane (−40 °C) and kept at −80 °C until coronal sections (30 µm) were made (Reichert Jung cryostat and Frigocut 2800 microtome). Verification of the location and extent of thalamic damage was performed as described previously (Mitchell and Dalrymple-Alford 2005; Wolff et al. 2008a) using sections stained with cresyl violet. Briefly, the area covered by the lesions in each rat was replicated on electronic copies of the Paxinos and Watson (1998) atlas, which were then used to generate automated pixel counts of the percent damage and hence lesion volume of the brain region of interest. Additional sections through the dorsal and ventral hippocampus were stained for acetylcholinesterase (AChE) histochemistry and optical density (OD) was used to examine the cholinergic innervation of the hippocampus.

Statistical analyses

All data were analyzed by a mixed factor analysis of variance (ANOVA)—(Group: SHAM, ATN, ILN/LT vs. within subject: trial blocks for water maze performance, hours for habituation in the activity test). Newman–Keuls tests provided post hoc comparisons (Winer 1971). The association between lesion extent and performance was examined using Spearman's correlation.

Results

Lesion analysis

Representative lesions are shown in Fig. 3. Lesion extent and location are illustrated in Figs. 4 and 5. Five ATN and three ILN/LT rats had minor damage and were discarded from the statistical analysis. The rats retained for behavioral analyses exhibited highly selective, but subtotal damage, comparable to previous work (Mitchell and Dalrymple-Alford 2006; Wolff et al. 2008a). Rats first tested for spatial learning and those first tested for visual learning exhibited comparable lesion extents. Lesions in the ATN group (median of 75.8 %; range 50.0–94.5 %) produced little damage in the ILN/LT region (9.9 %; range 1.3–29.4 %) or the remaining mediodorsal (MD) region (3.8 %; range 0.6–13.7 %; the MD region is of interest because damage to this region may give rise to some memory impairments; Mitchell and Dalrymple-Alford 2005). Lesions in the ILN/LT group were also highly selective (median of 63.7 %; range 50.8–74.3 %), with minor ATN damage (3.3 %; range 0.0–20.0 %) and little MD region damage (22.2 %; range 5.2–33.5 %). The damage to other thalamic structures including midline nuclei was generally minimal to modest, with the exception of the interanteromedial nucleus (in ATN rats: median 24 %, range 1.7–90.3 %; in ILN/LT rats: median 0.0 %, range 0.0–35.8 %) and the parataenial nucleus (in ATN rats: median 34.4 %, range 9.9–70.8 %; in ILN/LT rats: median 0.0 %, range 0.0–25.0 %). Little damage occurred to the laterodorsal nucleus: ATN rats, 5.9 % (range 1.4–13.2 %) and ILN/LT rats, 4.7 % (range 0.2–18.4 %). The median damage was <1.0 % in both groups for each of the following: paraventricular and posterior paraventricular nuclei, anterior paraventricular nucleus, reuniens nucleus, and rhomboid nuclei. The maximum value for any of these regions was just below 20.0 % (anterior paraventricular nucleus in both groups).

Visual inspection of the other AChE-stained slides did not reveal obvious cholinergic denervation. Owing to a technical problem, sections from three rats did not show sufficient AChE stain for reliable optical density (OD) measurements. OD measurements showed a weak, but significant lesion-induced AChE reduction, irrespective of hemisphere, in the ventral hippocampus (lesion effect, $F(2,45) = 3.7$, $p < 0.05$; Table 2), with reduced OD (−23.3 %) in ATN when compared with either ILN/LT or SHAM rats ($p < 0.05$), which did not differ from each other. The group differences on AChE measures for the

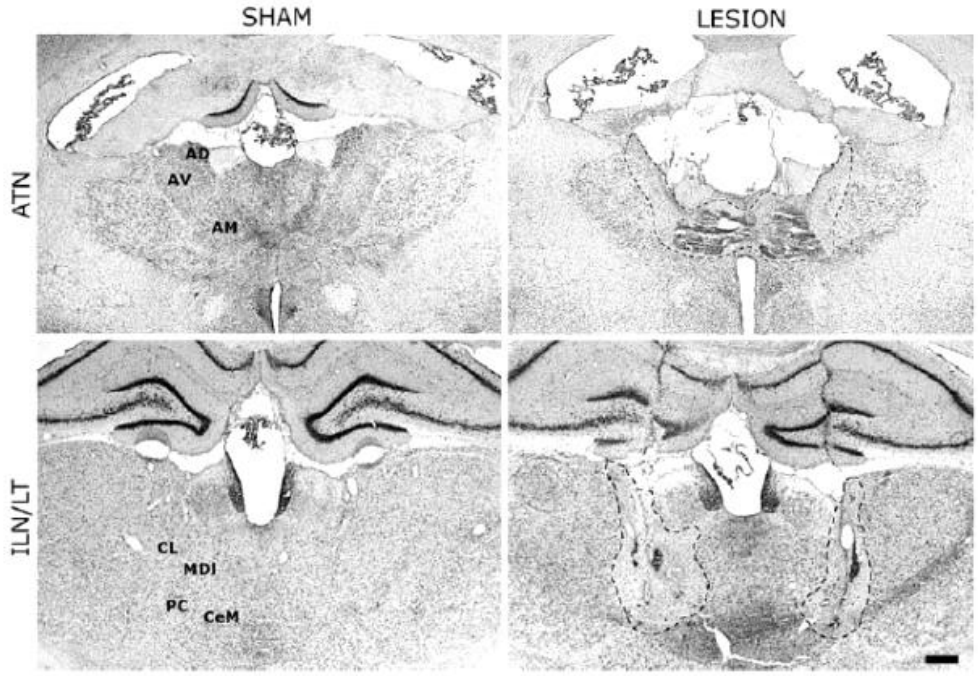

Fig. 3 Photomicrographs showing a representative example of an ATN lesion (*top*, *right*) and an ILN/LT lesion (*bottom*, *right*) on coronal brain sections stained with cresyl violet. The lesion is delimited by the interrupted line in each case. This ATN lesion encroached onto 75.9 % of the ATN, 15 % of the ILN/LT and 3 % of the medial thalamus. This ILN/LT lesion encroached onto 63.4 % of the ILN/LT, 0 % of the ATN and 19.4 % of the medial thalamus (compare with data shown in Fig. 5). Note that the lesion, especially in the ATN case, has caused shrinkage of the tissue. Comparative locations of the main nuclei targeted by each lesion are shown on the corresponding left sections, illustrating two sham controls. *AD* anterodorsal nucleus, *AM* anteromedial nucleus, *AV* anteroventral nucleus (the AD, AM and AV constitute the ATN, i.e. anterior thalamic nuclei); *CL* central lateral nucleus, *MDl* lateral mediodorsal nucleus, *PC* paracentral nucleus, *CeM* central median nucleus (the CL, MDl, PC and rostral CeM constitute the rostral ILN/LT, i.e., intralaminar/lateral thalamic nuclei; the caudal part of CeM are regarded as posterior ILN; van der Werf et al. 2002). *Scale bar* 500 μm

dorsal hippocampus did not reach significance, both in the anterior ($F(2,45) = 2.6$, $p = 0.087$) and posterior regions ($F(2,45) = 2.5$, $p = 0.096$).

Groups trained on spatial learning, followed by visual discrimination learning

The SHAM and ILN/LT groups showed acquisition of the spatial task, whereas there was little evidence of spatial learning in the ATN group (Fig. 6a, left panel). There were significant overall Lesion ($F(2,23) = 13.0$, $p < 0.001$) and Block ($F(9,207) = 9.6$, $p < 0.001$) effects, but the interaction between the two factors was not significant ($F(18,207) = 1.41$, $p > 0.10$). Newman–Keuls tests confirmed that ATN rats produced significantly more errors than both SHAM ($p < 0.001$) and ILN/LT groups ($p < 0.01$); there was no significant difference between the two latter groups. The analysis of the latencies to reach the correct platform (data not shown) also produced a significant Block effect in the spatial learning task ($F(9,207) = 74.0$, $p < 0.001$), due to improvement over the six first test days primarily, and a significant Lesion effect ($F(2,23) = 6.1$, $p < 0.01$), due to longer latencies in the ATN group as compared to SHAM ($p < 0.01$) and ILN/LT ($p < 0.05$) rats. The Lesion by Block interaction for latency was not significant.

The switch to the visual discrimination task resulted in an increase of the number of errors in all groups. Subsequently, there was a marked improvement of performance in all three groups, resulting in a significant Block effect ($F(6,138) = 14.9$, $p < 0.001$; Fig. 6a, right panel) irrespective of lesion status (Lesion effect, $F(2,23) < 1.0$, $p > 0.75$; Lesion × Block interaction, $F(6,138) = 1.52$, $p > 0.10$). The analysis of latencies to reach the correct platform led to the same conclusions, with a reduction in latencies over time (data not shown) being the only significant effect (Block, $F(6,138) = 9.6$, $p < 0.001$).

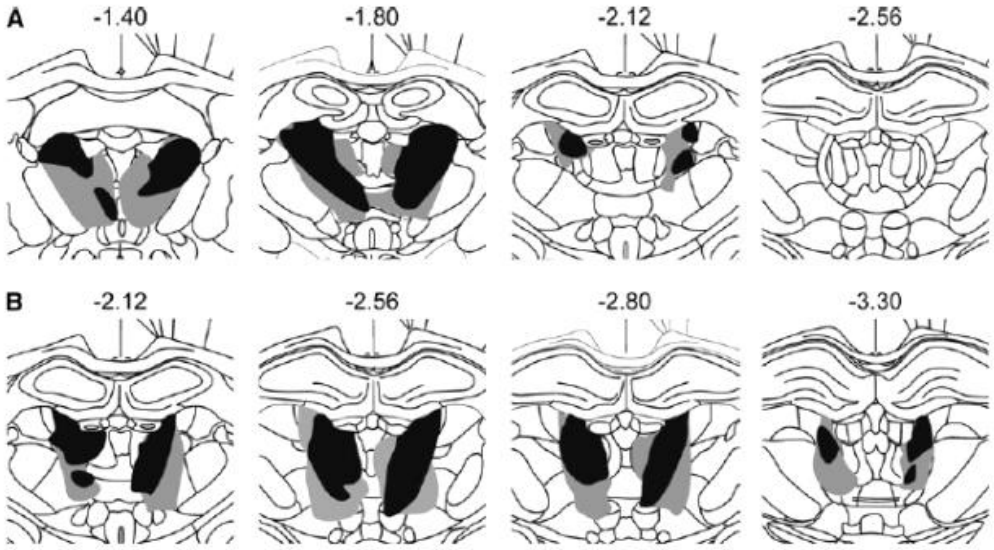

Fig. 4 Schematic representation of the smallest (*black*) and largest (*gray*) thalamic lesion extents in the rats retained for statistical analyses. a Anterior thalamic nuclei group (ATN), b intralaminar nucleus/lateral thalamic lesion group (ILN/LT). *Numbers above the drawings* indicate the distance (mm) of each section from bregma (according to Paxinos and Watson 1998)

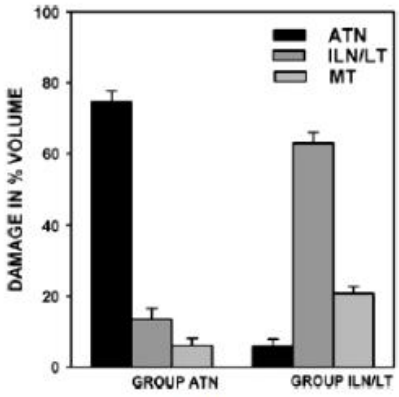

Fig. 5 Mean lesion extent +SEM for the two lesion groups (expressed as a percent bilateral volume of damage) in three regions of the medial thalamus: ATN (anterodorsal, anteromedial and anteroventral nuclei), the ILN/LT (centrolateral, rostral centromedian, lateral mediodorsal, paralamellar and paracentral nuclei) and MT (intermediodorsal, mediodorsal, central mediodorsal and medial mediodorsal nuclei)

Groups trained on visual discrimination learning, followed by spatial learning

The pattern of results found in the groups that were trained with the reverse order of tasks replicated the previous findings. In the visual discrimination task (Fig. 6b, left panel), all rats acquired the task, irrespective of group (Block effect, $F(8,176) = 15.2$, $p < 0.001$; Lesion, $F(2,22) = 1.5$, $p > 0.20$); Lesion × Block interaction, $F(16,176) < 1.0$, $p > 0.85$). The analysis of the latencies for the visual task (not shown) also produced only a significant Block effect ($F(8,176) = 60.0$, $p < 0.001$).

The switch to the spatial task resulted in an increase in the number of errors in all groups (Fig. 6b, right panel). As before, the Lesion ($F(2,22) = 7.1$, $p < 0.01$) and Block ($F(7,154) = 12.0$, $p < 0.001$) effects were significant, but not the interaction ($F(14,154) < 1.0$, $p > 0.95$). Once again, ATN rats were significantly impaired as compared to SHAM ($p < 0.001$) and ILN/LT ($p < 0.01$) rats, which did not differ. Similarly, the ANOVA of the latencies (not shown) produced significant Block ($F(7,154) = 25.2$, $p < 0.001$) and Lesion effects ($F(2,22) = 6.9$, $p < 0.01$).

Correlations between lesion extent and performance

No association was evident between ATN or LTN lesion extent and behavioral performance on either the spatial or visual water maze tasks (ATN lesion extent: respectively, $r = 0.13$ and -0.24; LTN lesion extent: respectively, $r = 0.10$ and -0.13). Thus, the minimal acceptable ATN lesions were sufficient to impair spatial memory acquisition. Similarly, there was no evidence that the extent of damage to adjacent nuclei influenced the level of impairment found in ATN rats (no correlation approached significance).

Table 2 Optic density measurements (±SEM) of ATN and ILN/LT rats expressed as a percentage of the average density measured in controls (SHAM)

Lesion	Anterior dorsal hippocampus (Bregma −2.8 mm)	Posterior dorsal hippocampus (Bregma −3.6 mm)	Ventral hippocampus (Bregma −4.8 mm)
SHAM	100.0 ± 6.9	100.0 ± 6.8	100.0 ± 6.3
ATN	80.7 ± 5.9	78.0 ± 7.1	76.7 ± 7.4 *
ILN/LT	85.8 ± 5.9	94.0 ± 7.0	97.1 ± 5.8

Values given between brackets are levels of anteriority defined according to Bregma (Paxinos and Watson 1998). Statistics: * $p < 0.05$ versus SHAM

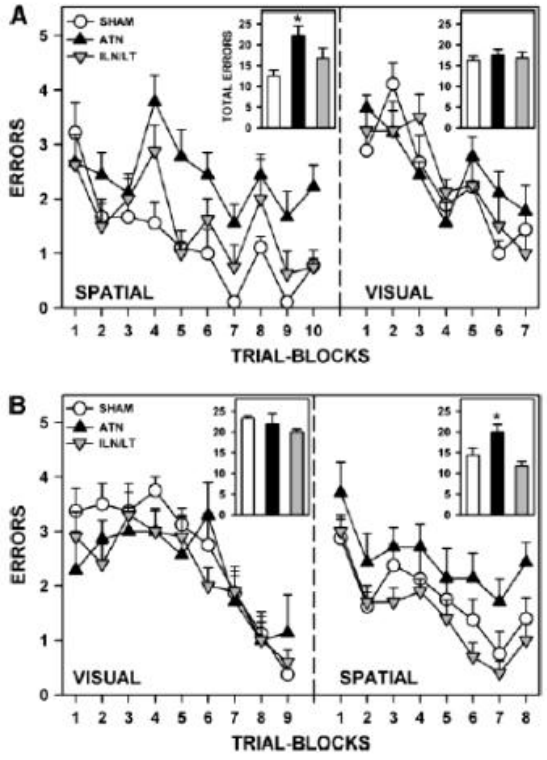

Fig. 6 Effect of ATN and ILN/LT lesions on the acquisition of the spatial task and of the visual discrimination task in the water maze. a Rats were first trained in the spatial task and, after ten 8-trial blocks, in the visual discrimination one for seven additional 8-trial blocks. b The order of testing was inversed: these rats were first trained for visual discrimination over nine 8-trial blocks, then for spatial learning over eight additional 8-trial blocks. All data are mean +SEM. In the *inserts*, the *bar graphs* indicate the average total number of errors (+SEM) found in each group, illustrating the overall Group effects. Statistics: *asterisks* significantly different from SHAM, $p < 0.05$

Home cage locomotor activity

As shown in Fig. 7, ATN lesions produced hyperactivity, which was particularly marked during the first hour of the habituation period and during the nocturnal phase of the cycle. The ANOVA of the activity scores recorded during the habituation period showed significant Lesion ($F(2,48) = 11.4$, $p < 0.001$), Hour ($F(2,96) = 27.9$, $p < 0.001$), and Lesion × Hour interaction ($F(4,96) = 12.0$, $p < 0.001$) effects. Newman–Keuls tests confirmed that the activity recorded in ATN rats over the first hour was significantly higher than in both other groups ($p < 0.001$). Nocturnal hourly activity was about four times higher than activity during the diurnal phase ($p < 0.001$, irrespective of group). The Lesion effect was also significant across the whole diurnal and nocturnal phases ($F(2,48) = 4,7$ and 10,3, respectively, $p < 0.05$ and 0.001). In both phases, the ATN group once again showed significantly higher activity levels than the ILN/LT group ($p < 0.01$) and the SHAM group ($p < 0.05$), which did not differ.

Discussion

The current findings did not confirm the expected double dissociation of the effects of ATN and ILN/LT lesions

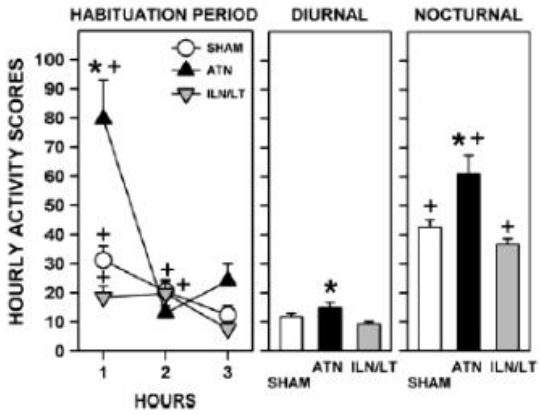

Fig. 7 Effect of ATN and ILN/LT lesions on locomotor activity recorded in the rats' home cages during a 3-h habituation period (*left*), the remaining 9-h diurnal phase (*middle*) and the entire, uninterrupted 12-h nocturnal phase (*right*) of a 24-h cycle. All data are hourly mean +SEM. Statistics: *asterisks* significantly different from SHAM, $p < 0.05$; *plus* significantly larger than the average hourly diurnal activity found in each group, $p < 0.05$

across the two water maze tasks. As expected, however, ATN lesions severely disrupted the ability of rats to learn the allocentric spatial task when the correct location was tagged with an irrelevant visual cue, but had no effect on the acquisition of the visual discrimination task when spatial location was irrelevant. ILN/LT lesions had no effect on either task. Thus, a single dissociation was demonstrated on one task only.

Evidence that ATN lesions impaired acquisition of the allocentric spatial learning task, but not the visual discrimination task used here, adds further support considering that the ATN constitute an important region of an extended hippocampal memory system (Aggleton 2008; Aggleton and Brown 1999; Vann and Albasser 2009). In addition, the pattern of increased activity in the home cage is also consistent with similar findings using the same conditions in rats with hippocampal lesions (e.g., Cassel et al. 1998; Galani et al. 1997). It would be interesting to know whether the activity changes after ATN lesions are, like after hippocampal lesions (e.g., Wilkinson et al. 1993), the consequence of an increased dopaminergic activity in the basal ganglia due to a reduced inhibitory influence on the nucleus accumbens.

The selective deficit exhibited by ATN rats in the water maze cannot be explained by differences in motivational or sensory-motor demands as they were similar in the two tasks (spatial vs. visual discrimination). In addition, this deficit did not reflect proactive (or any other kind of) interference between the two memory procedures, as it was found regardless of the order in which the two tasks were performed. It is possible, however, that reduced cholinergic activity in the ventral hippocampus contributed to this deficit (see Table 2). The reduced AChE staining was not a consequence of mechanical damage to the fornix or adjacent regions by the infusion needle used to make the ATN lesions, because sham rats also had similar surgery. Related studies have demonstrated an alteration of ventral hippocampal cholinergic function in the pyrithiamine-induced thiamine deficiency model of diencephalic amnesia (Anzalone et al. 2010; Savage et al. 2007). It seems unlikely, however, that the weak ventral hippocampal cholinergic depletion observed played a major role in the deficits found after ATN lesions because rats with an almost complete cholinergic denervation of the hippocampus are still able to acquire a spatial task (e.g., Lehmann et al. 2002; Parent and Baxter 2004). Furthermore, non-specific functional blockade of the ventral hippocampus by lidocaine infusions before acquisition of a spatial version of the water maze task does not prevent spatial learning (Loureiro et al. 2011).

The hypothesis that the effects of rostral ILN/LT lesions generally mimic those of dorsal caudate lesions appears thus far to have limited predictive utility (Mitchell and Dalrymple-Alford 2005, 2006). The current prediction was based on the neuroanatomical data that the central lateral thalamic nucleus projects densely to the dorsolateral striatum and the paracentral and rostral central medial nuclei to the dorsomedial region (Berendse and Groenewegen 1991; Van der Werf et al. 2002), which overlap with the same site of dorsal caudate lesions that severely impair the visual pattern discrimination used in the current study (Packard and McGaugh 1992). The current failure to find visual discrimination learning deficits after rostral ILN/LT lesions adds to other evidence that these lesions did not produce an egocentric spatial memory deficit (Wolff et al. 2008a) or increased visuospatial reaction time (Hembrook and Mair 2011), both of which would be expected if disruption occurred to critical striatal pathways (Bailey and Mair 2006; Mitchell and Hall 1988; Packard and McGaugh 1992; White and McDonald 2002, review). It is nevertheless worth mentioning that Kato et al. (2011) recently reported that mice that received recombinant immunotoxic lesions of the parafascicular nucleus, depleting the primary caudal ILN projections to the lateral and dorsolateral striatum, showed impaired visually guided attention. Functional heterogeneity within the striatum and across ILN regions is, however, one complication that is neglected by a simple ILN-striatal perspective (Mair et al. 2002). Thus far, the primary evidence for a striatal-like effect after rostral ILN/LT lesions relies on impaired egocentric working memory (Mitchell and Dalrymple-Alford 2006). It is clear that working memory per se is not impaired after ILN/LT lesions, because allocentric working memory is only transiently affected by these lesions (Mitchell and Dalrymple-Alford 2006).

Nonetheless, other evidence supports the idea that the rostral ILN/LT region and the prefrontal cortex functionally interact to influence several different functions, including memory consolidation, motor planning, temporal coding, and motor working memory (Kesner 2000; Bailey and Mair 2004; Bailey and Mair 2007; Harrison and Mair 1996; Koger and Mair 1994; Lopez et al. 2009; Mair et al. 1988, 2011; Mitchell and Dalrymple-Alford 2005). The extent to which these latter effects require an involvement of the striatum, or conversely that the lack of some expected effects of ILN/LT lesions such as the visual discrimination task examined here can be supported sufficiently by cortico-striatal pathways alone, will require investigation in future studies, perhaps using a unilateral lesion-disconnection approach. The extent of the rostral ILN/LT lesion may also be an issue, because it is difficult to make large selective lesions without encroaching onto other adjacent nuclei. Indeed, the use of large rostral ILN lesions and their encroachment onto the ATN nuclei or other central nuclei in particular seems likely to be responsible for earlier reports of working memory or

acquisition deficits in allocentric memory in rats with ILN injury (Savage et al. 1998; Hembrook and Mair 2011).

In conclusion, based on the neural connectivity and evidence from existing behavioral studies, we expected that ATN lesions would impair allocentric, but not egocentric memory functions and that rostral ILN/LT lesions would yield an opposite picture. We could not establish such a double dissociation. Our current data, however, consolidate the existing evidence showing that the ATN constitute a crucial node in an extended hippocampal system subserving spatial memory processes in particular. They also confirm that the ILN/LT, which in previous studies has been shown to contribute to egocentric working memory and remote memory processes, and is not implicated in visual discrimination memory and thus may not be crucial to striatum-dependent functions. Therefore, it seems that damage to the ATN is the major contributor to the classical neuropsychological symptoms of diencephalic amnesia.

Acknowledgments The authors are grateful to O. Bildstein, G. Edomwony and O. Egesi for their help in animal care. They also acknowledge research funds from the University of Strasbourg and the CNRS. J.C.D-A. has been supported during his stay in Strasbourg as an invited professor by University of Strasbourg. M.W. was supported by a Lavoisier post-doctoral fellowship from the French Government (when he was at Christchurch) and a 1-year fellowship by the Fondation pour la Recherche Médicale. A 3-year PhD fellowship was awarded to J.L. from the French Ministère de l'Enseignement Supérieur et de la Recherche. Finally, L.L. contributed to the current work while being a post-doctoral fellow supported by the French A.N.R. (ANR-06-NEURO-027-04).

References

Aggleton JP (2008) Understanding anterograde amnesia: disconnections and hidden lesions. Q J Exp Psychol 61:1441–1471

Aggleton JP, Brown MW (1999) Episodic memory, amnesia, and the hippocampal-anterior thalamic axis. Behav Brain Sci 22(3):425–444

Aggleton JP, Dumont JR, Warburton EC (2011) Unraveling the contributions of the diencephalon to recognition memory: a review. Learn Mem 18(6):384–400

Aggleton JP, Poirier GL, Aggleton HS, Vann SD, Pearce JM (2009) Lesions of the fornix and anterior thalamic nuclei dissociate different aspects of hippocampal-dependent spatial learning: Implications for the neural basis of scene learning. Behav Neurosci 123(3):504–519

Anzalone S, Vetreno RP, Ramos RL, Savage LM (2010) Cortical cholinergic abnormalities contribute to the amnesic state induced by pyrithiamine-induced thiamine deficiency in the rat. Eur J Neurosci 32(5):847–858

Bailey KR, Mair RG (2004) Dissociable effects of frontal cortical lesions on measures of visuospatial attention and spatial working memory in the rat. Cereb Cortex 14(9):974–985

Bailey KR, Mair RG (2005) Lesions of specific and nonspecific thalamic nuclei affect prefrontal cortex-dependent aspects of spatial working memory. Behav Neurosci 119(2):410–419

Bailey KR, Mair RG (2006) The role of striatum in initiation and execution of learned action sequences in rats. J Neurosci 26(3):1016–1025

Bailey KR, Mair RG (2007) Effects of frontal cortex lesions on action sequence learning in the rat. Eur J Neurosci 25(9):2905–2915

Berendse HW, Groenewegen HJ (1991) Restricted cortical termination fields of the midline and intralaminar thalamic nuclei in the rat. Neuroscience 42(1):73–102

Byatt G, Dalrymple-Alford JC (1996) Both anteromedial and anteroventral thalamic lesions impair radial-maze learning in rats. Behav Neurosci 110(6):1335–1348

Cassel JC, Cassel S, Galani R, Kelche C, Will B, Jarrard L (1998) Fimbria-fornix vs selective hippocampal lesions in rats: effects on locomotor activity and spatial learning and memory. Neurobiol Learn Mem 69(1):22–45

Cook D, Kesner RP (1988) Caudate nucleus and memory for egocentric localization. Behav Neural Biol 49(3):332–343

DeCoteau WE, Kesner RP (2000) A double dissociation between the rat hippocampus and medial caudoputamen in processing two forms of knowledge. Behav Neurosci 114(6):1096–1108

Galani R, Duconseille E, Bildstein O, Cassel JC (2001) Effects of room and cage familiarity on locomotor activity measures in rats. Physiol Behav 74(1–2):1–4

Galani R, Jarrard LE, Will BE, Kelche C (1997) Effects of postoperative housing conditions on functional recovery in rats with lesions of the hippocampus, subiculum, or entorhinal cortex. Neurobiol Learn Mem 67(1):43–56

Gibb SJ, Wolff M, Dalrymple-Alford JC (2006) Odour-place paired-associate learning and limbic thalamus: comparison of anterior, lateral and medial thalamic lesions. Behav Brain Res 172(1):155–168

Gold JJ, Squire LR (2006) The anatomy of amnesia: neurohistological analysis of three new cases. Learn Mem 13(6):699–710

Harding A, Halliday G, Caine D, Kril J (2000) Degeneration of anterior thalamic nuclei differentiates alcoholics with amnesia. Brain 123:141–154

Harrison LM, Mair RG (1996) A comparison of the effects of frontal cortical and thalamic lesions on measures of spatial learning and memory in the rat. Behav Brain Res 75(1–2):195–206

Hembrook JR, Mair RG (2011) Lesions of reuniens and rhomboid thalamic nuclei impair radial maze win-shift performance. Hippocampus 21(8):815–826

Jodar M, Martos P, Fernández S, Canovas D, Rovira A (2011) Neuropsychological profile of bilateral paramedian infarctions: three cases. Neurocase 17(4):345–352

Kato S, Kuramochi M, Kobayashi K, Fukabori R, Okada K, Uchigashima M, Watanabe M, Tsutsui Y, Kobayashi K (2011) Selective neural pathway targeting reveals key roles of thalamostriatal projection in the control of visual discrimination. J Neurosci 31(47):17169–17179

Kesner RP (2000) Behavioral analysis of the contribution of the hippocampus and parietal cortex to the processing of information: interactions and dissociations. Hippocampus 10(4):483–490

Kesner RP, Bolland BL, Dakis M (1993) Memory for spatial locations, motor responses, and objects: triple dissociation among the hippocampus, caudate nucleus, and extrastriate visual cortex. Exp Brain Res 93(3):462–470

Koger SM, Mair RG (1994) Comparison of the effects of frontal cortical and thalamic lesions on measures of olfactory learning and memory in the rat. Behav Neurosci 108(6):1088–1100

Kopelman MD (2002) Disorders of memory. Brain 125:2152–2190

Lehmann O, Bertrand F, Jeltsch H, Morer M, Lazarus C, Will B, Cassel JC (2002) 5,7-DHT-induced hippocampal 5-HTdepletion attenuates behavioural deficits produced by 192 IgG-saporin lesions of septal cholinergic neurons in the rat. Eur J Neurosci 15:1991–2006

Lopez J, Wolff M, Lecourtier L, Cosquer B, Bontempi B, Dalrymple-Alford J, Cassel JC (2009) The intralaminar thalamic nuclei

contribute to remote spatial memory. J Neurosci 29(10): 3302–3306
Loureiro M, Lecourtier L, Engeln M, Lopez J, Cosquer B, Geiger K, Kelche C, Cassel JC, Pereira de Vasconcelos A (2011) The ventral hippocampus is necessary for expressing a spatial memory. Brain Struct Funct (Epub ahead of print)
Mair RG, Anderson CD, Langlais PJ, McEntee WJ (1988) Behavioral impairments, brain lesions and monoaminergic activity in the rat following recovery from a bout of thiamine deficiency. Behav Brain Res 27(3):223–239
Mair RG, Burk JA, Porter MC (1998) Lesions of the frontal cortex, hippocampus, and intralaminar thalamic nuclei have distinct effects on remembering in rats. Behav Neurosci 112(4):772–792
Mair RG, Burk JA, Porter MC (2003) Impairment of radial maze delayed nonmatching after lesions of anterior thalamus and parahippocampal cortex. Behav Neurosci 117(3):596–605
Mair RG, Koch JK, Newman JB, Howard JR, Burk JA (2002) A double dissociation within striatum between serial reaction time and radial maze delayed nonmatching performance in rats. J Neurosci 22(15):6756–6765
Mair RG, Onos KD, Hembrook JR (2011) Cognitive activation by central thalamic stimulation: the Yerkes–Dodson law revisited. Dose Response 9(3):313–331
McDonald RJ, White NM (1993) A triple dissociation of memory systems: hippocampus, amygdala, and dorsal striatum. Behav Neurosci 107(1):3–22
McDonald RJ, White NM (1994) Parallel information processing in the water maze evidence for independent memory systems involving dorsal striatum and hippocampus. Behav Neural Biol 61(3):260–270
Mena-Segovia J, Cintra L, Prospero-Garcia O, Giordano M (2002) Changes in sleep-waking cycle after striatal excitotoxic lesions. Behav Brain Res 136(2):475–481
Mitchell AS, Dalrymple-Alford JC (2005) Dissociable memory effects after medial thalamus lesions in the rat. Eur J Neurosci 22(4):973–985
Mitchell AS, Dalrymple-Alford JC (2006) Lateral and anterior thalamic lesions impair independent memory systems. Learn Mem 13(3):388–396
Mitchell JA, Hall G (1988) Caudate-putamen lesions in the rat may impair or potentiate maze learning depending upon availability of stimulus cues and relevance of response cues. Q J Exp Psychol 40B(3):243–258
Moran JP, Dalrymple-Alford JC (2003) Perirhinal cortex and anterior thalamic lesions: comparative effects on learning and memory. Behav Neurosci 117(6):1326–1341
Oscar-Berman M, Zola-Morgan SM (1980) Comparative neuropsychology and Korsakoff's syndrome. I. Spatial and visual reversal learning. Neuropsychologia 18(4–5):499–512
Packard MG, McGaugh JL (1992) Double dissociation of fornix and caudate nucleus lesions on acquisition of two water maze tasks: further evidence for multiple memory systems. Behav Neurosci 106(3):439–446
Packard MG, Teather LA (1998) Amygdala modulation of multiple memory systems: hippocampus and caudate-putamen. Neurobiol Learn Mem 69(2):163–203
Parent MB, Baxter MG (2004) Septohippocampal acetylcholine: involved in but not necessary for learning and memory? Learn Mem 11:87–94
Paxinos G, Watson P (1998) The rat brain in stereotaxis coordinates. Academic Press, New York
Savage LM, Castillo R, Langlais PJ (1998) Effects of lesions of thalamic intralaminar and midline nuclei and internal medullary lamina on spatial memory and object discrimination. Behav Neurosci 112(6):1339–1352
Savage LM, Roland J, Klintsova A (2007) Selective septohippocampal—but not forebrain amygdalar—cholinergic dysfunction in diencephalic amnesia. Brain Res 1139:210–219
Sziklas V, Petrides M (1999) The effects of lesions to the anterior thalamic nuclei on object-place associations in rats. Eur J Neurosci 11(2):559–566
Sziklas V, Petrides M (2007) Contribution of the anterior thalamic nuclei to conditional learning in rats. Hippocampus 17:456–461
van der Werf YD, Jolles J, Witter MP, Uylings HB (2003) Contributions of thalamic nuclei to declarative memory functioning. Cortex 39(4–5):1047–1062
van der Werf YD, Witter MP, Groenewegen HJ (2002) The intralaminar and midline nuclei of the thalamus. Anatomical and functional evidence for participation in processes of arousal and awareness. Brain Res Rev 39:107–140
van der Werf YD, Witter MP, Uylings HB, Jolles J (2000) Neuropsychology of infarctions in the thalamus: a review. Neuropsychologia 38(5):613–627
Vann SD, Albasser MM (2009) Hippocampal, retrosplenial, and prefrontal hypoactivity in a model of diencephalic amnesia: evidence towards an interdependent subcortical–cortical memory network. Hippocampus 19:1090–1102
Warburton EC, Baird AL, Morgan A, Muir JL, Aggleton JP (2001) The conjoint importance of the hippocampus and anterior thalamic nuclei for allocentric spatial learning: evidence from a disconnection study in the rat. J Neurosci 21:7323–7330
White NM, McDonald RJ (2002) Multiple parallel memory systems in the brain of the rat. Neurobiol Learn Mem 77:125–184
Wilkinson LS, Mittleman G, Torres E, Humby T, Hall FS, Robbins TW (1993) Enhancement of amphetamine-induced locomotor activity and dopamine release in nucleus accumbens following excitotoxic lesions of the hippocampus. Behav Brain Res 55: 143–150
Winer BJ (1971) Statistical principles in experimental design, 2nd edn. McGraw-Hill, New York
Wolff M, Gibb SJ, Dalrymple-Alford JC (2006) Beyond spatial memory: the anterior thalamus and memory for the temporal order of a sequence of odor cues. J Neurosci 26(11):2907–2913
Wolff M, Gibb SJ, Cassel JC, Dalrymple-Alford JC (2008a) Anterior but not intralaminar thalamic nuclei support allocentric spatial memory. Neurobiol Learn Mem 90(1):71–80
Wolff M, Loukavenko EA, Will BE, Dalrymple-Alford JC (2008b) The extended hippocampal–diencephalic memory system: enriched housing promotes recovery of the flexible use of spatial representations after anterior thalamic lesions. Hippocampus 18:996–1007

nature COMMUNICATIONS

ARTICLE

Received 20 Aug 2012 | Accepted 28 Nov 2012 | Published 8 Jan 2013

DOI: 10.1038/ncomms2341 OPEN

A thermoresponsive and chemically defined hydrogel for long-term culture of human embryonic stem cells

Rong Zhang[1,*,†], Heidi K. Mjoseng[2,*], Marieke A. Hoeve[2], Nina G. Bauer[2], Steve Pells[2], Rut Besseling[3], Srinivas Velugotla[4], Guilhem Tourniaire[1], Ria E.B. Kishen[2], Yanina Tsenkina[2], Chris Armit[2], Cairnan R.E. Duffy[2], Martina Helfen[5], Frank Edenhofer[5], Paul A. de Sousa[2] & Mark Bradley[1]

Cultures of human embryonic stem cell typically rely on protein matrices or feeder cells to support attachment and growth, while mechanical, enzymatic or chemical cell dissociation methods are used for cellular passaging. However, these methods are ill defined, thus introducing variability into the system, and may damage cells. They also exert selective pressures favouring cell aneuploidy and loss of differentiation potential. Here we report the identification of a family of chemically defined thermoresponsive synthetic hydrogels based on 2-(diethylamino)ethyl acrylate, which support long-term human embryonic stem cell growth and pluripotency over a period of 2–6 months. The hydrogels permitted gentle, reagent-free cell passaging by virtue of transient modulation of the ambient temperature from 37 to 15 °C for 30 min. These chemically defined alternatives to currently used, undefined biological substrates represent a flexible and scalable approach for improving the definition, efficacy and safety of human embryonic stem cell culture systems for research, industrial and clinical applications.

[1]EaStChem, School of Chemistry, University of Edinburgh, Joseph Black Building, West Mains Road, Edinburgh EH9 3JJ, UK. [2]Scottish Centre for Regenerative Medicine, University of Edinburgh, Chancellor's Building, 49 Little France Crescent, Edinburgh EH16 4SB, UK. [3]Merck Sharp & Dohme, Molenstraat 110, Oss 5340 BH, The Netherlands. [4]School of Engineering and Electronics, Institute for Integrated Micro and Nano Systems, University of Edinburgh, Edinburgh EH9 3JF, UK. [5]Institute of Reconstructive Neurobiology, Stem Cell Engineering Group, University of Bonn, Life & Brain Center and Hertie Foundation, Sigmund-Freud Straβe 25, Bonn 53105, Germany. * These authors contributed equally to this work. † Present address: School of Materials Science and Engineering, Changzhou University, Changzhou 213164, Jiangsu, China. Correspondence and requests for materials should be addressed to P.A.deS. (email: paul.desousa@ed.ac.uk) or to M.B. (email: mark.bradley@ed.ac.uk).

The use of pluripotent human embryonic stem cells (hESCs) in biomedical research and cellular therapies requires the development of efficacious and cost-effective defined culture systems for cell isolation, growth and differentiation. An important step to achieve these goals is the minimization or elimination of biological reagents which can be a source of pathogens and contribute to variable outcomes during cell processing. To date several feeder-independent and defined media formulations with the capacity to maintain both an undifferentiated hESC phenotype and cellular differentiation potential have been described[1–6]. These contain a broad range of proteins, lipids and small molecules that affect, amongst other things, intracellular signalling pathways controlling differentiation, and rely on extracellular matrix proteins such as laminin, fibronectin and vitronectin or protein-containing extracts[2,5,7,8] as substrates for cell attachment, with growth on such matrices typically being serum or albumin dependent[9–11]. Recently, polymer and peptide-polymer substrates have been reported with a capacity to sustain a hESC phenotype[12–16]. The limitations of these advances include variation in cell line responsiveness[15] and/or requirements for feeder cell conditioning of media or coating of surfaces with serum or serum proteins. Critically, for all substrates reported to date cell dissociation at passaging requires one or more treatments involving mechanical scraping or colony picking, proteolytic enzymatic digestion, or chemically mediated chelation of divalent cations (e.g., calcium and magnesium using EGTA or EDTA)[13–15,17]. Whereas mechanical dissociation is laborious and not readily scalable, enzymatic and chemical treatments can damage cells by removal of important surface proteins or ions (e.g., calcium)[18,19].

A promising alternative to reliance on mechanical, enzymatic or chemical release is binding and growth of cells on stimuli-responsive substrates which include polymers whose physical properties can be reversibly modulated by subtle changes in temperature or light. The utility of thermoresponsive polymers as substrates for cell binding and growth has already been established[20], as has their use in contexts such as tissue engineering[21], gene delivery[22] and reversible molecule absorption[23], with cell dissociation from these substrates achieved by their swelling in response to the physical stimulus.

Previously, we reported the fabrication of chemically defined polymers by inkjet printing[24,25]. In the current study, this method was used to identify combinations of acrylate and acrylamide monomers which generate chemically defined polymers that permit long-term maintenance of hESC and reagent-free dissociation in response to a reduction in ambient temperature.

Results

Polymer library screening. Polymer arrays consisting of 609 different polymers spotted in quadruplicate[25] were synthesized *in situ* by inkjet printing mixtures of 18 monomers in seven different ratios in the presence of the crosslinker *N,N'*-methylene*bis*acrylamide (Supplementary Fig. S1). Monomers were chosen on the basis of their hydrophilicity, known tendency to permit modulation by temperature and pH, and their abilities to bind cells[25,26]. Array screening was performed in the biologically defined medium mTeSR1 (ref. 2). Our approach consisted of three phases of screening hESC for attachment to substrates before commitment to selected polymers for long-term culture (Fig. 1):

First, we selected the top 120 candidates, from two independent polymer screens, which supported cell attachment after 24 h, as determined by 4′,6-diamidino-2-phenylindole (DAPI)-positive nuclear staining (Supplementary Fig. S2). This screen was followed by re-screening of top candidates selected from phase 1 for support of short-term culture of pluripotency-associated transcription factor marker positive hESC for 2, 4 and 7 days (growth data in Supplementary Figs S3 and S4, and expression of Oct3/4 and Nanog in Supplementary Fig. S4). Last, the best 25 polymers were scaled up and tested as coatings on glass coverslips to evaluate their support of hESC attachment, viability and morphology over 7 days of culture, followed by assessment of the efficiency of thermal release by lowering the temperature to 15 °C for 30 min, gentle pipetting and subsequent cell replating (Fig. 1b and Supplementary Fig. S5).

The cumulative outcome of this effort was the identification of three polymers, henceforth called hydrogels (HG), HG19, HG20 and HG21 that were similar to or better than Matrigel for support of short-term attachment and growth of undifferentiated hESC as colonies over 7 days, and from which the majority of undifferentiated hESC colonies, but not spontaneously differentiating cells outside of colonies, could be released by thermomodulation (Fig. 1d). These three HGs formed part of a family that contained the monomers 2-(acryloyloxyethyl) trimethylammonium chloride (AEtMA-Cl) and 2-(diethylamino)ethyl acrylate (DEAEA) in varying ratios. HG21, consisting of AEtMA-Cl and DEAEA in a ratio of 3:1 (Fig. 1c) and providing as much as >90% reagent-free thermal release of cells at passaging (Fig. 1b and Supplementary Movies 1 and 2) was selected based on performance, to assess competence to support long-term maintenance of hESC.

HG21 supports hESC maintenance. To characterize the ability of HG21 to support hESC maintenance, the RH1 hESC line was cultured continuously for more than 20 passages in mTeSR1 on HG21-coated glass coverslips. Undifferentiated hESC colonies were passaged by reducing the temperature to 15 °C for 30 min, followed by gentle pipetting without using any cell dissociation reagents to dislodge cell colonies from the HG substrate (Supplementary Movie 1). Detachment of colonies yielded aggregates similar to those achieved with collagenase-mediated dissociation, which could be fully dissociated to single cells for further culture or analysis by brief (5 min) treatment with trypsin/EDTA at 37 °C if required. Real-time monitoring of shear force applied using a rheometer established that the force required for colony detachment ranged between 75 and 125 Pa, and was dependent on colony size, with larger colonies requiring more force (Table 1 and Supplementary Movie 2).

Cells cultured on Matrigel could not be dislodged even when the shear force was increased to up to 154 Pa. The extent to which HG21-cultured cells remained attached to their matrix upon routine cell passaging also depended on the applied force. Typically, slow gentle pipetting (10–20 times) following thermomodulation resulted in detachment of the population to the extent that the remaining cells did not cover more than 5% of the total surface area (Fig. 1b and data not shown). *In situ* immunocytochemistry (ICC) revealed that, with the exception of cells in small residual colonies, cells which remained attached were predominantly negative for Nanog and Oct3/4 and thus likely to be differentiating derivatives (Fig. 1d).

In practice, RH1 hESC growth on HG21 appeared slower than observed on Matrigel. HG21 cultures routinely took 8–10 days to reach 80% confluence as opposed to 4–5 days for Matrigel, despite being plated at a higher pre-to-post plating ratio of 1:1.5 versus 1:2 wells, respectively. This was confirmed by measurement of cell growth over each of 5 days, which revealed a slower rate of expansion on HG21, and lower total expansion over 5 days from a mean (±s.e.m.) of 17.40-fold (±0.47) to 7.68-fold (±0.04) for Matrigel and HG21, respectively (Fig. 1e; $P<0.0001$). This equates to 4.2 versus 2.8 population doublings over this interval, and population doubling times of ~29 versus 43 h, respectively. There

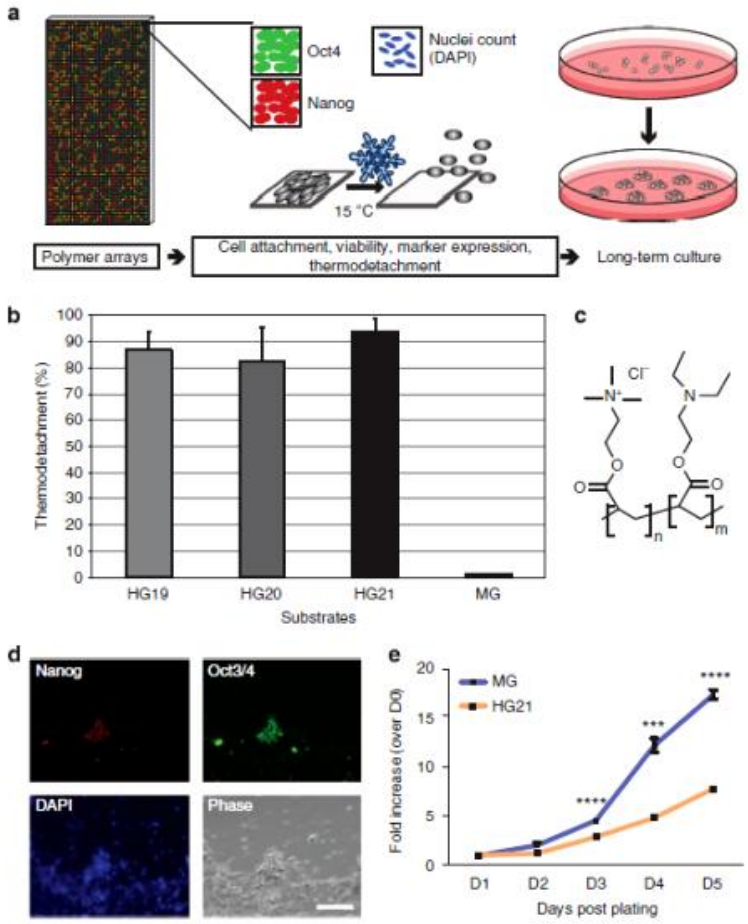

Figure 1 | Screening procedure for selection of polymers that support hESC culture. (**a**) Outline of the screening procedure used to select polymers that support hESC culture and passaging by thermodetachment. Cell attachment (nuclear count following DAPI stain), Oct3/4 and Nanog expression levels (immunocytochemistry) and thermodetachment ability (30 min at 15 °C) were assessed after culture of cells on polymer arrays. Successful polymers were selected for longer-term culture studies. (**b**) Cell detachment following lowering ambient temperature to 15 °C of hESC cultured on the top three polymers or Matrigel as control. Mean ± s.d., $n = 3$. (**c**) Chemical structure of polymers HG19, 20 and 21 with 1:3, 1:1 and 3:1 ratios of AEtMA-Cl/DEAEA, respectively. (**d**) Following thermodetachment of RH1 hESC from HG21 the majority of the remaining cells, visualized by DAPI-stained nuclei (blue) and phase-contrast light microscopy, are negative for Oct3/4 (green) and Nanog (red) (immunocytochemistry). Scale bar, 100 μm. (**e**) Cell growth curves of RH1 hESC cultured on HG21 or MG, plotted as mean fold increase (± s.e.m., $n = 3$ biological replicates) relative to when cells were plated (day 0). ***$P < 0.001$, ****$P < 0.0001$ compared to D1.

Table 1 | Shear stress required for hESC detachment after temperature drop.

Matrix	Shear stress range (Pa)	Cell detachment
HG21	75–125	Nearly all hESC colonies but not differentiated cells detached
MG	>150	Both hESC colonies and differentiated cells remain adherent

hESC, human embryonic stem cell; MG, Matrigel.
Shear stress required to detach cells after incubation of the cells at 15 °C for 30 min was assessed by visualization of cell detachment over time using a camera mounted onto a microscope while applying increasing circular shearing force using a rheometer.

was no apparent increase in non-adherent cells in the medium of HG21-cultured cells compared with Matrigel.

Interaction of HG21 with cell culture medium. To assess whether HG21 could capture or release proteins in mTeSR1 medium, coated coverslips were cultured at 37 °C, followed by washing to remove unbound protein at 37 and 15 °C, and assessment of HG21 incorporated proteins by one-dimensional polyacrylamide gel electrophoresis and mass spectrometry (Supplementary Methods). HG21-captured proteins presented as seven discrete bands, the intensity of which for most (2–7) was

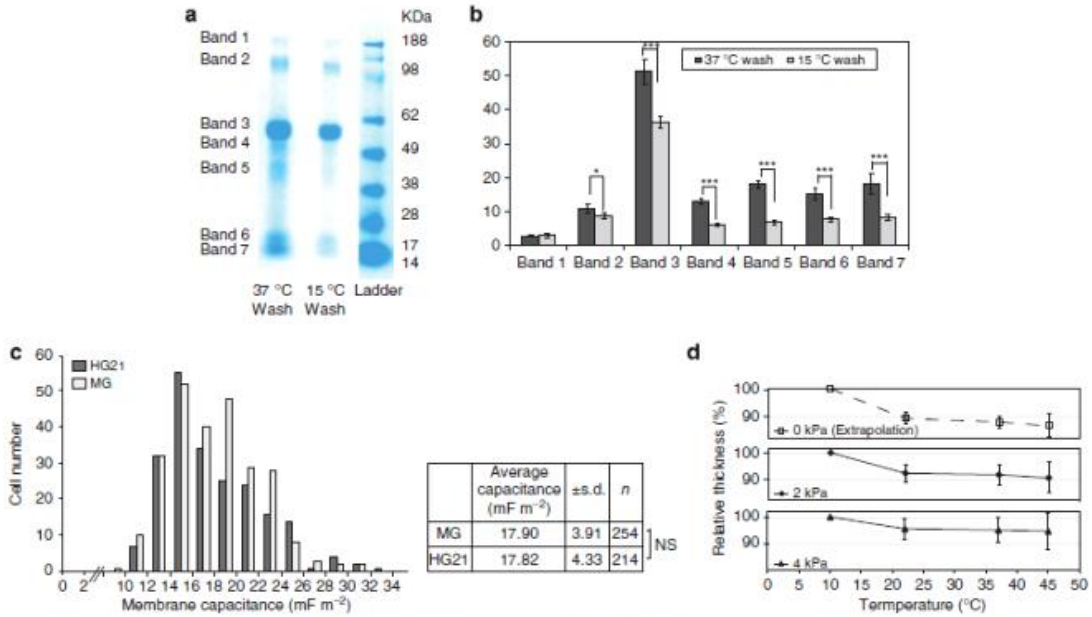

Figure 2 | Membrane capacitance of HG21-cultured hESC and physical properties of HG21. (**a**) Gelcode blue staining of 1-D polyacrylamide gel electrophoresis of proteins incorporated and retained in HG21 after incubation with mTeSR1 at 37 °C, followed by washing with PBS at 37 and 15 °C. Seven bands, ranging in size from ~17–188 kDa, were apparent under both conditions but less abundant in the latter. (**b**) Quantification of mean stained protein band intensity (±s.d; $n = 4$) normalized to background confirmed significant reduction in the retention of most bands (2–7) in HG21 upon temperature reduction (Student's *t*-test, $^{***}P < 0.001$; $^{**}P < 0.01$). (**c**) Long-term culture on HG21 does not significantly alter cell membrane biophysical properties from those observed for cells cultured on Matrigel (MG). Distribution and average cell membrane capacitance values for RH1 populations on HG21 and MG, as measured by dielectrophoresis. No significant difference was observed between cells grown on MG versus HG21 after 20 passages (two-tailed *t*-test, null hypothesis; $P = 0.8338$). (**d**) Change in relative thickness of HG21 as a function of temperature in response to actual (2 and 4 kPa) and extrapolated (0 kPa) compressive forces, confirming swelling of HG21 at lower temperatures. NS, not significant.

significantly reduced after temperature reduction to 15 °C (Fig. 2a,b). Mass spectrometry analyses revealed that all bands represented fragments of bovine serum albumin (BSA; data not shown), a known component of mTeSR1 (ref. 2).

Biophysical properties of hESC cultured on HG21. Next, dielectrophoresis (DEP) was performed to investigate whether culture on HG21 altered the biophysical properties of hESC and their membranes (Supplementary Methods). DEP can identify cellular states associated with cell activation, apoptosis and necrosis[27]. It discriminates distinct cellular identities in heterogeneous populations on the basis of single-cell polarity and membrane capacitance in an electrical field gradient. No difference in the distribution range or average membrane capacitance (two-tailed *t*-test, null hypothesis; $P = 0.8338$) was observed between RH1 cells grown on Matrigel or HG21 (passage 20; Fig. 2c).

Characterization of physical properties of HG21. To determine how bound hESC were thermally detached, mechanical analyses of HG21 were performed (Supplementary Methods). The temperature-dependent alteration of the physical structure of HG21 was examined by rheology in phosphate-buffered saline (PBS) between 10 and 45 °C under constant compressive forces (2 or 4 kPa). Extrapolation to zero compressive force (the situation analogous to cell culture) showed that HG21 increased in relative thickness, when the temperature was reduced from 37 to 15 °C (Fig. 2d). Thus, at 37 °C HG21 allows the attachment and growth of hESC. After 30 min incubation at 15 °C HG21 becomes more hydrated, resulting in the detachment of cell colonies. Similar data were obtained for the two HGs, HG19 and HG20, that are composed of the same monomers as HG21 (but in different ratios), which affects HG thickness following a reduction in temperature (Supplementary Fig. S6). Further analyses of HG21 to assess the expected properties of this HG showed that its storage modulus (G') was much greater than the loss modulus (G'') in the measurement range of strain, a typical property of a HG network (Supplementary Fig. S7)[28], and X-ray photoelectron spectroscopy analysis confirmed the concordance between the actual and theoretical molecular composition of HG21 (Table 2).

Table 2 | Theoretical and experimentally determined composition of HG21.

Element	Coating (%)	Theoretical (%)
Carbon (C 1s)	73.9	67.8
Nitrogen (N 1s)	8.2	10.2
Oxygen (O 1s)	17.8	21.9

Characteristics of hESC cultured on HG21. Similarly to culture on Matrigel, RH1 hESC on HG21 grew as colonies (Fig. 3a),

which were positive for the pluripotency-associated transcription factors Nanog and Oct3/4 (Fig. 3b). Quantitative reverse transcription-PCR (qPCR) confirmed that RNA levels of these transcription factors, in addition to another pluripotent cell transcription factor, Sox2, were similar to respective Matrigel controls (Fig. 3c). Fluorescence activated cell sorting (FACS) of HG21-cultured RH1 cells for pluripotent cell-associated surface markers also confirmed high expression of SSEA-4 and TRA-1-60R, and low expression of SSEA-1 (Fig. 3d). Functional pluripotency to form tissues representative of all three germinal lineages was confirmed by both embryoid body (EB)-mediated differentiation *in vitro* (Fig. 3e) and teratoma formation *in vivo* following injection under the kidney capsule of immunodeficient mice (Fig. 3f). Comparative genome hybridization (CGH) analysis using a Nimblegen 135 k probe whole genome tiling array, with a median probe spacing of 12,524 base pairs (Supplementary Methods), did not reveal any copy number variations in HG21-cultured cells, which were not also apparent following growth on Matrigel. However, microdeletions and duplications ranging from 0.5 to 1.5 Mb were apparent under both culture conditions on chromosomes 8, 9, 13 and 20 (refs 29–31; Fig. 3g, Supplementary Table S1).

HG21 supports multiple hESC lines. To confirm the ability of HG21 to support the continuous culture of other hESC lines, HG21 was evaluated for the support of H9 hESC over 5–10 passages. In practice, cultivation of H9 cells on HG21 was as for RH1, taking longer to achieve confluence than H9 on Matrigel despite seeding at a higher pre-to–post plating ratio (1:1.5 versus 1:2). Assessment of H9 hESC after six passages confirmed comparable expression of pluripotency-associated markers by immunocytochemistry (ICC; Oct3/4 and Nanog) and qPCR (Oct3/4, Nanog, Sox2) (Supplementary Fig. S8). After nine passages injection into immunodeficient mice yielded teratomas with tissues representative of three germinal lineages, supporting preservation of pluripotency (Supplementary Fig. S8). CGH analysis of H9 cells grown on HG21 and Matrigel at this time also revealed no major chromosome aneuploidy. H9 grown on either substrate possessed a micro-duplication of 0.5 Mb on chromosome 20 in common with RH1, and different micro-duplications and deletions on chromosomes 14 and 16 associated with one or the other culture conditions, not observed in RH1 (Supplementary Table S1).

Characterization of hESC attachment to HG21. To understand the basis of hESC attachment to HG21, we evaluated the expression profiles of cell surface proteins known to mediate cell–matrix interactions, for both RH1 and H9 hESC lines on HG 21 and Matrigel by flow cytometry and/or ICC. This included analysis of E-cadherin, epithelial cell adhesion molecule (EpCAM), α-integrins 1–6 and v, β-integrin 1 and 2, and three α/β integrin heterodimers (α5β1, αvβ3 and αvB3). Antibody probes which provided conclusive results for flow cytometry (α1–6, β1, E-cadherin, EpCAM) and ICC (all but α1, E-cadherin and EpCAM) revealed comparable expression of cell adhesion molecules for both cell lines on both matrices, with integrin α4 being the least prevalent of those that were detected by flow cytometry (Fig. 4, Supplementary Figs S9 and S10). To confirm the role for integrins in cell attachment to HG21, RH1 and H9 hESC were incubated with known integrin heterodimer-blocking antibodies (α5β1 or αvβ3) or, as a positive control, a cocktail of all integrin antibodies used for characterization, while in suspension before plating and after plating (Supplementary Methods). Following culture for 4–18 h neither of the two integrin heterodimer-blocking antibodies affected attachment to either HG21 or Matrigel (Supplementary Fig. S11). In contrast, the pan-integrin antibody cocktail interfered with adherence of hESC colonies to both HG21 and Matrigel, resulting in cells in suspension singly and as clusters of loosely and densely packed cells, the latter resembling EB-like structures. (Shown for H9, Supplementary Fig. S11). Treatment with the divalent cation chelating agent EDTA (2.5 mM in mTeSR1) also blocked cell attachment to both substrates (Shown for H9, Supplementary Fig. S11).

Discussion

A number of synthetic substrates supportive of human pluripotent stem cell growth and pluripotency in long-term culture have been reported[11,13–16,32], most of which rely on mechanical dissection at passaging. Though this type of passaging is a favoured means to preserve cell–cell associations important for promoting self-renewal and genetic stability, it is not tractable in large-scale and robotic culture systems. Proteolytic enzymatic digestion using collagenase, and chemically mediated chelation of divalent cations using EDTA represent pragmatic alternatives to dissociate cells as aggregates[13,17]. These methods are more amenable to high-throughput cell culture but still constitute aggressive disruptions of cell–cell and cell–substrate interactions. In addition, they also rely on transient exposure of cells to media and buffers other than the ones in which they are cultured. The thermoresponsive HG (HG21) and related polymers we report here overcome these limitations by providing a gentle method of passaging human pluripotent stem cells. They also enables separation of undifferentiated cell colonies from differentiating cells that remain attached.

Prolonged culture on and adaptation to the HG21 substrate did not detectably affect the character of the cell membrane or its interaction with the substrate, as assessed by dielectrophoretic analysis of membrane capacitance. Most importantly, pluripotency was preserved and the cells did not appear to have adapted by the accumulation of chromosomal aneuploidies. Growth on HG21 was slower than on Matrigel, which might be a reflection of the stimulatory effect of the extracellular matrix components in the latter, including residual growth factors[33]. The absence of these factors in our HGs suggests that either the topography or reactive groups they provide for cell attachment provides sufficient mimicry of a biological substrate to support renewal, at least under the conditions of our study. To our knowledge there is no evidence that slower growth is detrimental to human pluripotent stem properties. In fact, typically it is accelerated growth that is associated with genetic mutation presumed to confer a growth advantage to subpopulations of cells that then come to dominate the culture[34,35].

We and others have reported the suitability of thermoresponsive polymers for mouse embryonic stem cell culture[25,36]. Loh *et al.*[36] observed reduced growth rates when culturing mouse embryonic stem cells on thermoresponsive co-polymers compared with gelatin controls. Although they demonstrated that these gelatin-containing polymers support mouse embryonic stem cell growth and cell release at very low temperature (4 °C), cell cultures lasted only 3–4 days, without cell passaging. To our knowledge, our study is the first to report long-term culture and gentle serial passaging of hESCs using a thermomodulatable synthetic polymer, verified with independent cell lines. Plasma treatment of plastic surfaces[37] followed by simple addition of the appropriate monomers permitted HG polymer coating of conventional plasticware. This surface substrate should therefore be readily applicable in the future to scaled production of hESC in automated systems for industrial and clinical purposes.

It is now accepted that like any other cell in culture, hESC acquire non-random chromosomal aberrations during the course of culture adaptation. In hESC these particularly affect chromosomes 12, 17 and X, similar to aneuploidies observed in germ cell tumours[34,35,38]. These were not observed in our hESC cultured on Matrigel or HGs. Using CGH we did observe deletions and duplications as expected[34,35] ranging in size from 0.5 to 1.5 Mb on chromosomes 8, 9, 13 and 20 in cells cultured on both HG21 and those grown in control conditions. The appearance of the same small changes in both conditions strongly suggests that they were a feature of the cell lines themselves and not a culture adaptation specifically prompted by growth on a thermoresponsive substrate. One of the affected regions was an amplicon on chromosome 20q11.21, which has been associated with adaptation to culture conferring a growth advantage[31]. However, to date there are no reports that such an adaptation would undermine the differentiation potential of cells, and our data presented here confirm that the cells retain their undifferentiated state and pluripotency.

Investigation of the mechanism of hESC attachment to HG21 confirmed similarities in cell adhesion molecule expression to cells grown on Matrigel, and conservation across two

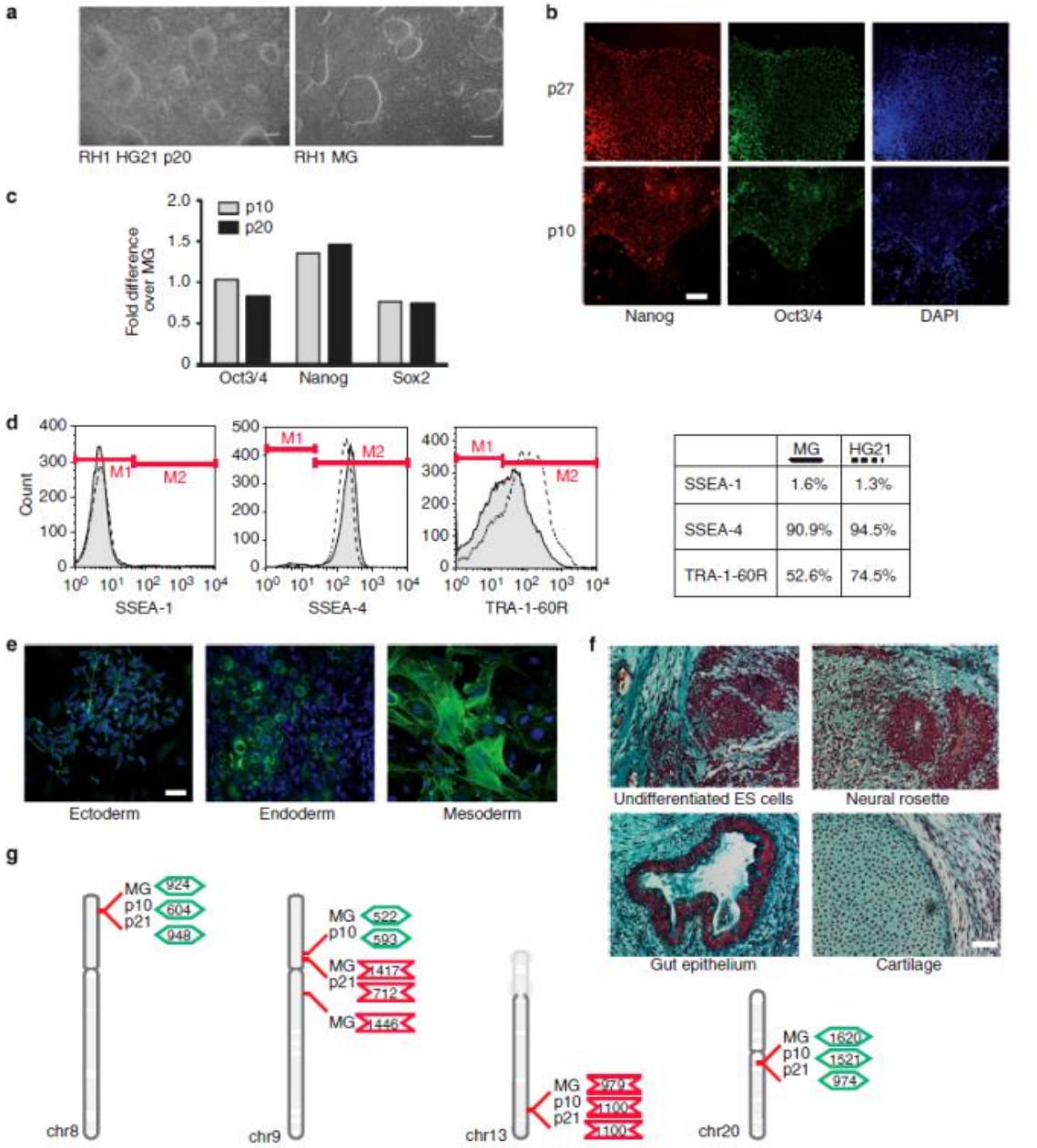

	MG	HG21
SSEA-1	1.6%	1.3%
SSEA-4	90.9%	94.5%
TRA-1-60R	52.6%	74.5%

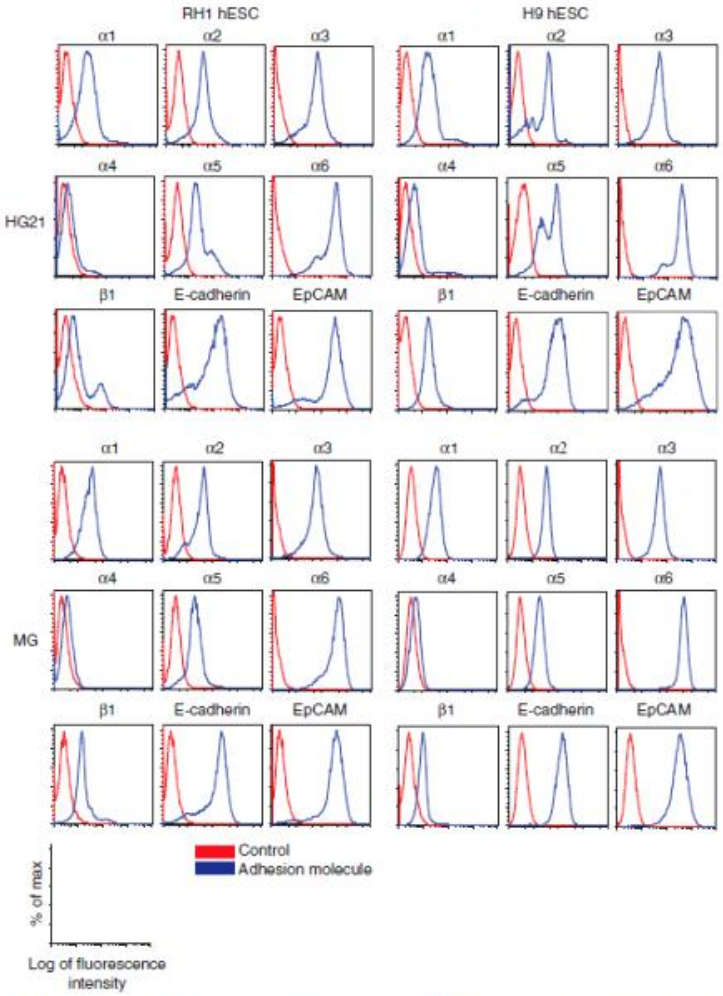

Figure 4 | Analyses of hESC adhesion molecule expression. RH1 (left panel sets) and H9 (right panel set) hESC cultured on HG21 (top panel sets) and Matrigel (MG, bottom panel sets) possess similar expression profiles for integrins α1–6, β1, EpCAM and E-cadherin, as assessed by flow cytometry. Vertical axis, percentage of maximum cell counts on a linear scale. Horizontal axis, fluorescence intensity on a log scale for control background (red) and adhesion molecule specific (blue) signal.

Figure 3 | Characterization of RH1 hESC cultured on thermomodulatable HG21. (**a**) Representative micrographs of hESC colonies cultured on HG21 (left) and Matrigel (MG, right). Scale bar, 100 μm. (**b**) Immunocytochemistry (ICC) for Nanog (red) and Oct3/4 (green) expression in RH1 hESC cultured on HG21 for 10 and 27 passages. Scale bar, 100 μm. (**c**) qPCR analysis of RNA expression of the pluripotency markers Oct3/4, Nanog and Sox2 for RH1 hESC cultured on HG21 for 10 and 20 passages. Expression levels were normalized to glyceraldehyde 3-phosphate dehydrogenase, and data represented as fold-change compared with expression in MG-cultured RH1 hESC. Data are representative examples of minimally two independent qPCR experiments per gene. (**d**) SSEA-1, SSEA-4 and TRA-1-60R cell surface markers are expressed at similar levels on RH1 hESC cultured on HG21 (dashed line) and MG (solid line, grey area), as determined by flow cytometry. M1 and M2 gates discriminate background to signal fluorescence thresholds. Apposing table depicts cell percentages with fluorescence signal intensity above background. (**e**) After 20 passages on HG21, RH1 hESC can differentiate to all three germ layers, as shown by ICC for β-tubulin III (ectoderm; green), α-fetoprotein (endoderm; green) and α-smooth muscle actin (mesoderm; green). Nuclei were stained with DAPI (blue). Scale bar, 20 μm. (**f**) Kidney capsule teratomas, induced by injection of RH1 hESC cultured for 20 passages on HG21 into NOD/SCID mice, contain tissue derived from all three primary germ layers. Clockwise: islands of undifferentiated EC/ES cells, neural rosettes (ectoderm), gut epithelium (endoderm) and cartilage (mesoderm). (Masson's trichrome stain). Scale bar, 100 μm. (**g**) Schematic summary of gene variations detected by CGH analysis of RH1 hESC using a NimblegenTM 135 K probe array following culture on HG21 for 10 and 21 passages (p10, p21) and age-matched MG (MG) (21 passages). Depicted are microdeletions and insertions (> no. <, < no. >, respectively, and their size in kilobase pairs) in relation to their location on chromosomes per genomic DNA sample. No gross chromosomal aneuploidies were detected between HG21 and MG-grown cells. Copy number variations occurring in the former also occurred in the latter on chromosomes 8, 9, 13 and 20.

independent cell lines. Consistent with previous studies[13–15,17], cell adhesion to both substrates was divalent cation and multi-integrin dependent. We observed that BSA and fragments in mTeSR1 incorporate into HG21 at 37 °C and are released at 15 °C. Serum- and serum protein-dependent hESC adhesion to substrates has been previously reported[9–11] and dependence of HG21 on serum albumin and other proteins is a subject of ongoing investigation. In this study, attempts to interfere with cell adhesion by exposure to known blocking antibodies to single integrin heterodimers ($\alpha5\beta1$ or $\alpha v\beta3$) were not successful on either substrate, whereas exposure to a complex cocktail of cell adhesion molecule antibodies was. This is in line with findings by Mei *et al.*[13] who showed that simultaneous blocking of a selection of integrins had a more pronounced effect on abrogating adhesion of hESC to a matrix than the blocking of single integrins, thereby highlighting the redundancy for integrins in mediating adhesion of hESC to substrates. HG swelling induced by thermoreduction was in itself not sufficient to release undifferentiated hESC colonies, which still required gentle shearing forces provided through slow pipetting. Our interpretation therefore is that gel hydration only serves to destabilize interactions between cell adhesion molecules and polymer reactive groups.

In conclusion, our study identifies and validates the utility of a chemically defined and thermomodulatable xeno-free substrate for the support of pluripotent hESC growth in long-term culture. The thermoresponsiveness of this substrate obviates alternative methods for cell passaging that can be damaging to cells and difficult to implement in scaled up and/or automated production. Collectively, these features substantiate the prospective merit of this substrate for pluripotent stem cell manufacture for banking, screening and therapeutic purposes.

Methods

Materials. Unless otherwise stated, cell culture reagents were sourced from Invitrogen. HG microarray fabrication chemicals were purchased from Sigma-Aldrich or ABCR GmbH Co.KG (tridecafluoro-1,1,2,2-tetrahydrooctyl-dimethylchlorosilane). *N*-acryloyl-*N'*-propylpiperazine and 2,2'-(ethylenedioxy) bis(ethylamine) mono-acylamide were synthesized in-house, whereas *N*-isopropylacrylamide was purified by recrystallization as described previously[24,25]. Monomers are listed in Supplementary Table S1.

HG-coated coverslips for upscaling. HG-coated coverslips and slides were prepared as follows: solutions of the monomers, crosslinker and photoinitiator in *N*-methyl-2-pyrrolidone were coated on 3-(trimethoxysilyl)propyl methacrylate-treated coverslips (ϕ13 mm, ϕ19 mm and ϕ32 mm), exposed to 365-nm UV light for 30 min to initiate polymerization, placed overnight in a 50 °C oven, washed with ethanol and acetone, and air dried.[25]

hESC culture. The use of hESC lines in this project was approved by the MRC steering committee overseeing the UK Stem Cell Bank. RCM1 (ref. 39) hESC and RH1 (ref. 40) hESC were derived at the Roslin Institute under a licence from the Human Fertilisation and Embryology Authority to P.A. de Sousa and licenced from Roslin Cells and Geron, respectively. Both lines have been deposited in the UKSCB (www.ukstemcellbank.org.uk). H9 hESC was licensed from WiCell (available from the Wisconsin International Stem Cell Bank (www.wicell.org))[41]. Starting cell populations for all three lines used here were at passage 60–70. All feeder-independent cultures were grown in mTeSR1 medium (STEMCELL Technologies) containing 50 U ml^{-1} penicillin, 50 µg ml^{-1} streptomycin and 2.5 µg ml^{-1} Fungizone (hereafter referred to as mTeSR1 + P/S/Fgz) at 37 °C, 5% CO_2, as reported previously[2]. hESC control cultures were grown on Matrigel (Becton Dickinson) and routinely passaged by mechanical scraping following treatment with collagenase IV (200 digestive units per ml in knockout DMEM). Cells were seeded at a density of ~100,000 cells cm^{-2} and split at a pre-to-post plating ratio of 1:2 wells. Cultures were passaged at 80% confluence every 4–5 days.

hESC culture on polymer arrays. Polymer arrays were screened using RCM1 hESC. Cells were dissociated with trypsin (0.25 g l^{-1})/5 mM EDTA (T/E) at 37 °C to obtain single cells, which were plated (60,000 cells cm^{-2}) on microarray slides in mTeSR1 + P/S/Fgz containing 10 µM ROCK inhibitor (Calbiochem). Cells were incubated for 2, 4 or 7 days in mTeSR1 + P/S/Fgz before fixation in 4% paraformaldehyde in PBS for cell staining.

hESC culture on polymer-coated glass surfaces. Polymer-coated coverslips were placed in tissue culture plate wells. After sterilizing, plates (20 min under UV light) wells were washed with PBS and cells seeded (90,000 cells cm^{-2}). Cells were split at a pre-to-post plating ratio of 1:1.5 wells. Cultures were passaged at 80% confluence every 8–10 days. Thermodetachment was achieved by incubation at 15 ± 3 °C for 30 min. Cell aggregates originating from thermodetached colonies were resuspended in fresh mTeSR1 + P/S/Fgz and replated. Cells were maintained by daily replacement of the medium with fresh mTeSR1 + P/S/Fgz equilibrated to 37 °C.

Assessment of temperature-mediated cell detachment. To quantify temperature-mediated detachment of cells grown on HG21 versus Matrigel, the percentage of cells that detached following temperature reduction was calculated as follows: after placing the culture plates at 15 °C for 30 min, detached cells were harvested, treated with T/E to obtain a single-cell suspension, and counted after Trypan blue staining using a haemocytometer (= Fraction A). The remaining cells were dissociated from the wells by trypsinization and counted (= Fraction B). The percentage of thermodetached cells were calculated as follows: Fraction A/(Fraction A + B) × 100% ($n = 3$).

To measure the (minimal) shear stress required to detach cells from HG21, hESC were cultured for 4 days in Φ35 Petri dishes that were either directly coated with Matrigel or contained an HG21-coated coverslip (glued to the bottom). At day 4, Petri dishes were incubated for 30 min at 15 °C before shear stress analysis, which was performed using a TA AR2000 rheometer with a spinning cone (Φ20 mm, 4°, a truncation gap of 92 mm between cone and the Petri dish surface) to generate a controlled culture medium flow to detach adherent cells. Movies of this detachment were recorded with a homemade imaging module with an × 10 objective in reverse mode, a light-emitting diode light source, and a charge-coupled device camera (0.16 × 0.16 micrometre pixel) (Supplementary Movie 2). Visualization of hESC thermodetachment from HG21 without shear force analysis was performed using a Debut Video Capture system attached to an Infinity 2 Meiji TC 5600 microscope (Supplementary Movie 1).

Immunostaining. Cells on glass coverslips coated with either HG21 or Matrigel were stained using standard immunocytochemistry protocols. hESC were fixed with 4% PFA, incubated overnight with primary antibodies against stem markers (Oct3/4 (Santa Cruz Biotechnology), Nanog (R&D systems), β3-tubulin (Sigma), AFP (Sigma) and α-smooth muscle actin (DAKO)) or against a selection of integrins (Chemicon kit ECM435 and Millipore kit ECM430; all antibodies used at 1/500), and incubated with appropriate Alexafluor-conjugated secondary antibodies (Invitrogen). Nuclei were labelled using DAPI. Imaging was performed with a Leica SPE or Zeiss Observer microscope.

Flow cytometric analysis of population size. To obtain population growth curves, cells grown for 1 – 5 days on HG21-coated coverslips or on Matrigel in 12-well tissue culture plates (in triplicate) were harvested on consecutive days using T/E (5 min at 37 °C). Following quenching (PBS/10% FCS) cells were washed, incubated with 60,000 fluorspheres (Flow-check Fluorspheres, Beckman Coulter) per sample in ice-cold PBS/0.1% BSA and immediately acquired with a FACS-Calibur flow cytometer counting 5,000 fluorspheres per sample. Data were analysed and plotted as fold increase over the cell number at the day of plating (D0), using GraphPad Prism software.

Quantitative reverse transcription-PCR. hESC RNA was prepared from snap-frozen cell pellets using TRIzol Reagent (Invitrogen) according to manufacturer's instructions. cDNA was prepared using a SuperScript 3 reverse transcription kit with oligo-dT as primers. After confirmation of negligible genomic DNA contamination (PCR amplification of human glyceraldehyde 3-phosphate dehydrogenase from cDNA generated in reverse transcription reaction containing no reverse transcriptase) qPCR was performed using SYBR green on a BioRad CFX96 C1000 thermo-cycler. Primer sequences and annealing temperatures are listed in Supplementary Table S2. Three technical replicates were amplified for each sample, with minimally two independent qPCR experiments per gene. Replicates where CT values deviated from others by more than 0.5 were excluded from analysis and experiments repeated in their entirety if two CT values for a sample had to be discarded by this criterion. Results were normalized relative to housekeeping gene glyceraldehyde 3-phosphate dehydrogenase by the ΔΔCT relative method[42].

Flow cytometric analysis of cell surface markers. Following matrix-appropriate cell detachment (thermodetachment for HG21, and collagenase IV treatment followed by mechanical scraping for Matrigel) cells were washed, dissociated by incubation with T/E (5 min at 37 °C), washed (PBS/5% FCS) and resuspended in PBS/0.1% BSA. To assess stemness, cells were incubated with FITC-labelled anti-SSEA-4, phycoerythrin-labelled anti-SSEA-1, and biotinylated anti-TRA-1-60R (all Biolegend) in PBS/0.1% BSA for 30 min on ice. Tra1-60R biotin was detected with

streptavidin-conjugated Allophycocyanine (Biolegend). To assess integrin expression, cells were incubated with a panel of fluorescently labelled anti-integrin antibodies (α1–6, β1 and EpCAM; all BD) (singly stained; 1/50 in PBS/0.1% BSA) for 30 min on ice.

Data were acquired with a FACSCalibur flow cytometer (Becton Dickinson) and analysed using FlowJo software. Per condition data for at least 30,000 live cells were collected. Gating was set relative to unstained controls from the same cell population.

EB-mediated differentiation. EB-mediated differentiation was achieved as previously described[39,43]. In short, cells were grown in suspension for 7 days at 37 °C, 5% CO_2 in EB medium (DMEM, 20% fetal calf serum (Sigma), 2 mM L-Glutamine, 100 nM NEAA, 0.1 mM 2-mercaptoethanol (Sigma)), after which EBs were dissociated in PBS-based enzyme-free cell dissociation solution (Sigma) for 10 min at 37 °C and plated on Matrigel in EB medium plus 10 μM ROCK inhibitor (Calbiochem) overnight. To steer cells towards endoderm, ectoderm and mesoderm, cells were subsequently incubated for 6 days at 37 °C, 5% CO_2 in EB differentiation medium (advanced RPMI-1640, B27 supplement, 50 U ml^{-1} penicillin, 50 μg ml^{-1} streptomycin and 2.5 μg ml^{-1} Fungizone) in the presence of differentiation factors, as described[43], with the exception that ectoderm was obtained by incubating the cells in the presence of 1 μM retinoic acid instead of Noggin.

Teratoma induction. RH1 hESC grown on HG21 were resuspended at 5×10^7 cells ml^{-1} in HEPES-buffered DMEM medium. Twenty microlitres of this cell preparation was placed under kidney capsules of anesthetized NOD/SCID mice (NOD.CB17-Prkdc-scid/J, Jackson Laboratories) ($n = 6$) using a fine glass capillary. Upon detection of teratomas, at least 4 weeks post injection, mice were culled and teratomas dissected, fixed overnight (10% phosphate-buffered formalin) and embedded in paraffin. Sections were stained with Masson's Tricolour stain. Mice were housed in specific pathogen-free conditions and procedures were in accordance with UK home office regulations.

For HG21-grown H9 hESC, teratomas were generated by the injection of cells into testes of narcotized fox chase SCID beige mice (1.2×10^6 cells per animal). After 5 weeks, mice were euthanized, and teratomas dissected, fixed overnight (4% PFA), and prepared for haematoxylin and eosin staining.

References

1. Li, Y., Powell, S., Brunette, E., Lebkowski, J. & Mandalam, R. Expansion of human embryonic stem cells in defined serum-free medium devoid of animal-derived products. *Biotechnol. Bioeng.* **91,** 688–698 (2005).
2. Ludwig, T. E. *et al.* Derivation of human embryonic stem cells in defined conditions. *Nat. Biotechnol.* **24,** 185–187 (2006).
3. Wang, L. *et al.* Self-renewal of human embryonic stem cells requires insulin-like growth factor-1 receptor and ERBB2 receptor signaling. *Blood* **110,** 4111–4119 (2007).
4. Watanabe, K. *et al.* A ROCK inhibitor permits survival of dissociated human embryonic stem cells. *Nat. Biotechnol.* **25,** 681–686 (2007).
5. Xu, C. *et al.* Feeder-free growth of undifferentiated human embryonic stem cells. *Nat. Biotechnol.* **19,** 971–974 (2001).
6. Yao, S. *et al.* Long-term self-renewal and directed differentiation of human embryonic stem cells in chemically defined conditions. *Proc. Natl Acad. Sci. USA* **103,** 6907–6912 (2006).
7. Oh, S. K. *et al.* Long-term microcarrier suspension cultures of human embryonic stem cells. *Stem Cell Res.* **2,** 219–230 (2009).
8. Steiner, D. *et al.* Derivation, propagation and controlled differentiation of human embryonic stem cells in suspension. *Nat. Biotechnol.* **28,** 361–364 (2010).
9. Braam, S. R. *et al.* Recombinant vitronectin is a functionally defined substrate that supports human embryonic stem cell self-renewal via alphavbeta5 integrin. *Stem Cells* **26,** 2257–2265 (2008).
10. Liu, Y. *et al.* A novel chemical-defined medium with bFGF and N2B27 supplements supports undifferentiated growth in human embryonic stem cells. *Biochem. Biophys. Res. Commun.* **346,** 131–139 (2006).
11. Rodin, S. *et al.* Long-term self-renewal of human pluripotent stem cells on human recombinant laminin-511. *Nat. Biotechnol.* **28,** 611–615 (2010).
12. Anderson, D. G., Levenberg, S. & Langer, R. Nanoliter-scale synthesis of arrayed biomaterials and application to human embryonic stem cells. *Nat. Biotechnol.* **22,** 863–866 (2004).
13. Mei, Y. *et al.* Combinatorial development of biomaterials for clonal growth of human pluripotent stem cells. *Nat. Mater.* **9,** 768–778 (2010).
14. Melkoumian, Z. *et al.* Synthetic peptide-acrylate surfaces for long-term self-renewal and cardiomyocyte differentiation of human embryonic stem cells. *Nat. Biotechnol.* **28,** 606–610 (2010).
15. Villa-Diaz, L. G. *et al.* Synthetic polymer coatings for long-term growth of human embryonic stem cells. *Nat. Biotechnol.* **28,** 581–583 (2010).
16. Li, Y. J., Chung, E. H., Rodriguez, R. T., Firpo, M. T. & Healy, K. E. Hydrogels as artificial matrices for human embryonic stem cell self-renewal. *J. Biomed. Mater. Res.* **79A,** 1–5 (2006).
17. Chen, G. *et al.* Chemically defined conditions for human iPSC derivation and culture. *Nat. Methods* **8,** 424–429 (2011).
18. Baran, E. J. Chelation therapies: a chemical and biochemical perspective. *Curr. Med. Chem.* **17,** 3658–3672 (2010).
19. Khalil, W. K. *et al.* The inhibitory effects of garlic and Panax ginseng extract standardized with ginsenoside Rg3 on the genotoxicity, biochemical, and histological changes induced by ethylenediaminetetraacetic acid in male rats. *Arch. Toxicol.* **82,** 183–195 (2008).
20. da Silva, R. M., Mano, J. F. & Reis, R. L. Smart thermoresponsive coatings and surfaces for tissue engineering: switching cell-material boundaries. *Trends Biotechnol.* **25,** 577–583 (2007).
21. Ohashi, K. *et al.* Engineering functional two- and three-dimensional liver systems *in vivo* using hepatic tissue sheets. *Nat. Med.* **13,** 880–885 (2007).
22. Wolff, J. A. & Rozema, D. B. Breaking the bonds: non-viral vectors become chemically dynamic. *Mol. Ther.* **16,** 8–15 (2008).
23. Oya, T. *et al.* Reversible molecular adsorption based on multiple-point interaction by shrinkable gels. *Science* **286,** 1543–1545 (1999).
24. Zhang, R., Liberski, A., Khan, F., Diaz-Mochon, J. J. & Bradley, M. Inkjet fabrication of hydrogel microarrays using *in situ* nanolitre-scale polymerisation. *Chem. Commun. (Camb)* **11,** 1317–1319 (2008).
25. Zhang, R., Liberski, A., Sanchez-Martin, R. & Bradley, M. Microarrays of over 2000 hydrogels—identification of substrates for cellular trapping and thermally triggered release. *Biomaterials* **30,** 6193–6201 (2009).
26. Pernagallo, S., Diaz-Mochon, J. J. & Bradley, M. A cooperative polymer-DNA microarray approach to biomaterial investigation. *Lab. Chip.* **9,** 397–403 (2009).
27. Pethig, R., Menachery, A., Pells, S. & De Sousa, P. Dielectrophoresis: a review of applications for stem cell research. *J. Biomed. Biotechnol.* **2010,** 182581 (2010).
28. Khan, F., Tare, R. S., Oreffo, R. O. & Bradley, M. Versatile biocompatible polymer hydrogels: scaffolds for cell growth. *Angew. Chem. Int. Ed. Engl.* **48,** 978–982 (2009).
29. Amps, K. *et al.* Screening ethnically diverse human embryonic stem cells identifies a chromosome 20 minimal amplicon conferring growth advantage. *Nat. Biotechnol.* **29,** 1132–1144 (2011).
30. Caisander, G. *et al.* Chromosomal integrity maintained in five human embryonic stem cell lines after prolonged *in vitro* culture. *Chromosome Res.* **14,** 131–137 (2006).
31. Narva, E. *et al.* High-resolution DNA analysis of human embryonic stem cell lines reveals culture-induced copy number changes and loss of heterozygosity. *Nat. Biotechnol.* **28,** 371–377 (2010).
32. Higuchi, A., Ling, Q. D., Ko, Y. A., Chang, Y. & Umezawa, A. Biomaterials for the feeder-free culture of human embryonic stem cells and induced pluripotent stem cells. *Chem. Rev.* **111,** 3021–3035 (2011).
33. Kleinman, H. K. & Martin, G. R. Matrigel: basement membrane matrix with biological activity. *Semin. Cancer Biol.* **15,** 378–386 (2005).
34. Baker, D. E. *et al.* Adaptation to culture of human embryonic stem cells and oncogenesis *in vivo*. *Nat. Biotechnol.* **25,** 207–215 (2007).
35. Stephenson, E. *et al.* Safety paradigm: genetic evaluation of therapeutic grade human embryonic stem cells. *J. R. Soc. Interface* **7**(Suppl 6): S677–S688 (2010).
36. Loh, X. J. *et al.* Surface coating with a thermoresponsive copolymer for the culture and non-enzymatic recovery of mouse embryonic stem cells. *Macromol. Biosci.* **9,** 1069–1079 (2009).
37. Kang, I. K., Lee, D. W., Lee, S. K. & Akaike, T. Grafting of lactose-carrying styrene onto polystrene dishes using plasma glow discharge and their interaction with hepatocytes. *J. Mater. Sci. Mater. Med.* **14,** 611–616 (2003).
38. Redon, R. *et al.* Global variation in copy number in the human genome. *Nature* **444,** 444–454 (2006).
39. De Sousa, P. A. *et al.* Clinically failed eggs as a source of normal human embryo stem cells. *Stem Cell Res.* **2,** 188–197 (2009).
40. Fletcher, J. M. *et al.* Variations in humanized and defined culture conditions supporting derivation of new human embryonic stem cell lines. *Cloning Stem Cells* **8,** 319–334 (2006).
41. Thomson, J. A. *et al.* Embryonic stem cell lines derived from human blastocysts. *Science* **282,** 1145–1147 (1998).
42. Livak, K. J. & Schmittgen, T. D. Analysis of relative gene expression data using real-time quantitative PCR and the 2-ΔΔCT method. *Methods* **25,** 402–408 (2001).
43. Klim, J. R., Li, L., Wrighton, P. J., Piekarczyk, M. S. & Kiessling, L. L. A defined glycosaminoglycan-binding substratum for human pluripotent stem cells. *Nat. Methods* **7,** 989–994 (2010).

Acknowledgements

This work was supported by EU FP7 funding for Project 223410 (BEST Stem Cells), co-ordinated by Dr De Sousa. We thank Drs Paz Freile, Kay Samuel and Bruna Corradetti for assistance with flow cytometry experiments; Ms Eirini Koutsouraki for assistance with cell culture; Ms Anke Leinhass (University of Bonn) for assistance with teratoma studies; Prof Ron Pethig (School of Engineering, University of Edinburgh) for

support with the DEP experiment; Ms Mary Shade, Mr Eddy Maher and Mr Roderick Murray (Southeast Scotland cytogenetics laboratory of NHS Lothian university hospitals division) for the CGH analysis of hESCs; Dr Ronald Brown (School of Chemistry, University of Edinburgh) for the XPS analysis; and Dr Michiel Hermes (School of Physics and Astronomy, University of Edinburgh) for his assistance with the analysis of shear force for stem cell detachment.

Author contributions

Polymer screening, cell culture and analyses were performed by H.K.M., R.Z., S.P., M.A.H., N.G.B and R.E.B.K. The polymer library was prepared by R.Z. and G.T. Teratoma studies were carried out by M.H., F.E. and S.P. Integrin analysis was performed by Y.T. The DEP experiment was performed and analysed by S.V. The elastic modulus measurements were performed by R.B. and R.Z. The paper was written by R.Z., H.K.M., M.A.H., N.G.B., S.P., P.A.deS. and M.B. The study was conceived, designed and directed by P.A.deS. and M.B.

Additional information

Supplementary Information accompanies this paper at http://www.nature.com/naturecommunications

Competing financial interests: The authors declare no competing financial interests.

Reprints and permission information is available online at http://npg.nature.com/reprintsandpermissions/

How to cite this article: Zhang, R. *et al.* A thermoresponsive and chemically defined hydrogel for long-term culture of human embryonic stem cells. *Nat. Commun.* 4:1335 doi: 10.1038/ncomms2341 (2013).

Appendices I

S.3.1. Additional behavioural analysis from the radial arm maze study presented in the main thesis body

S.3.1.1. Chronic cerebral hypoperfusion does not affect the visual abilities in mice

As previous pilot studies from our group had demonstrated the occurrence of axonal and myelin damage to the optic tract following hypoperfusion in mice, in the present radial arm maze experiment, the visual abilities of sham and hypoperfused animals trained on the radial arm maze spatial working memory task were tested by means of an optokinetic drum (Thaung et al., 2002) at three different time points (Chapter 2 section 2.3.1.):

1) 3 days prior to surgery (control baseline level),
2) 6 days before the behavioural testing (24 days after surgery),
3) at the end of the behavioural testing (50 days after surgery).

On the pre- surgery screening session (3 days prior to surgery), only 10% (1/10) of the initially included sham and 20% (4/20) of the initially included hypoperfused animals did not show a visual response to the first visual stimulation, but responded to the second visual stimulation. On the first post- surgery testing session (24 days after surgery), only 16.7% (2/15) of the hypoperfused animals did not respond to the first visual stimulation, but showed a visual response on the second trial. All sham animals (10/10) showed a visual response on the first stimulation trial. At the end of the behavioural testing (50 days after surgery), 20% (2/10) of the hypoperfused mice did not respond to the first, but showed a visual response to the second visual stimulation. All sham mice (10/10) showed a visual response to the first stimulation (figure S.3.1.1.).

The results from this visual test subsequently helped to clarify whether the spatial working memory impairment observed in chronically hypoperfused mice was due to actual neuroanatomical changes or alternatively, to a visual deficit following hypoperfusion-induced pathological damage to the optic tract.

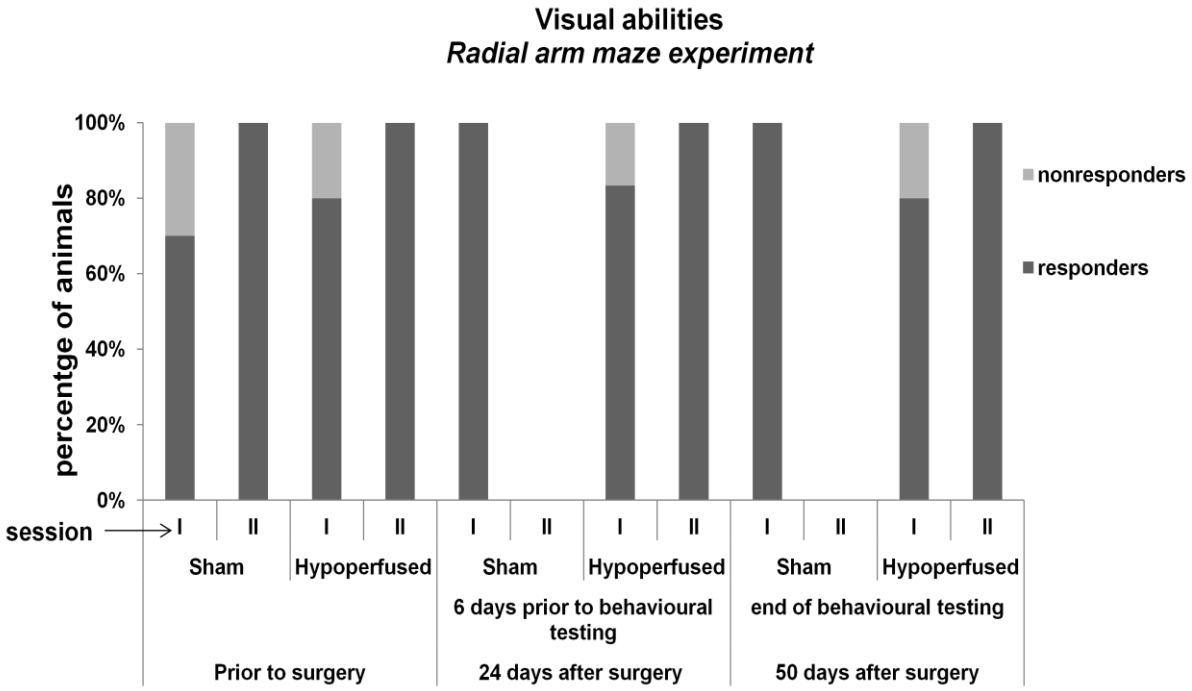

Figure S.3.1.1.: **Visual abilities of sham and hypoperfused mice**

The visual abilities of sham and chronically hypoperfused mice included in the radial arm maze study were tested at three different time points. Although chronic cerebral hypoperfusion induced a significant white matter pathology in the OT of hypoperfused mice, this did not impact on their visual abilities as demonstrated by an intact head movement response to a visual stimulation 24 and 50 days post- surgery

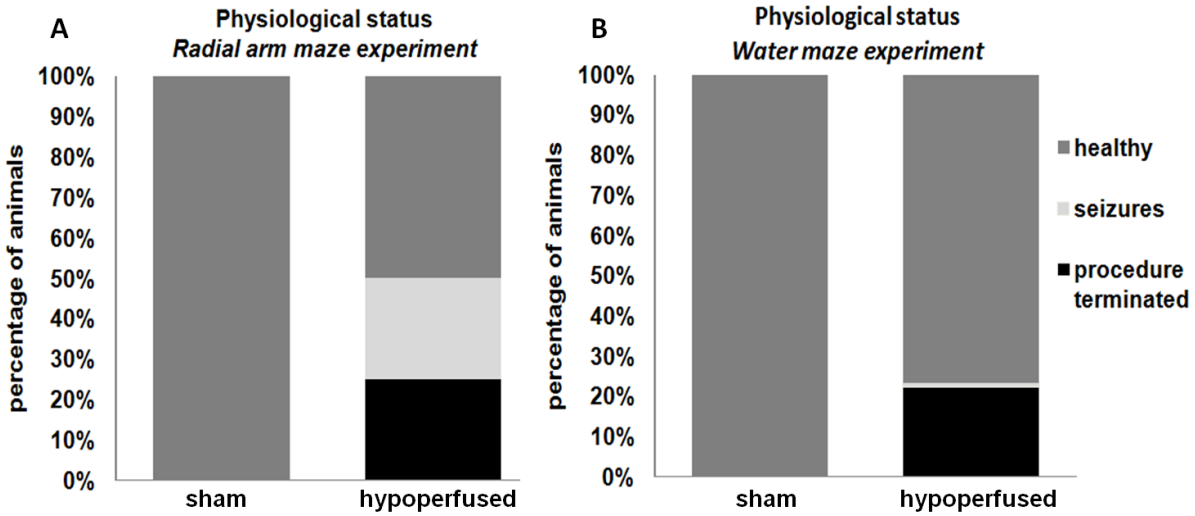

Figure S.3.1.2.: Physiological status of sham and hypoperfused mice

In the radial arm maze study, from the initially included hypoperfused animals 25% were procedure terminated (dead or culled) due to a poor post- surgery recovery, 25% exhibited seizure- like activity, 50% recovered well (healthy) from surgery (**A**).

In the water maze, from the initially included hypoperfused animals 22.8.% were procedure terminated (dead or culled), 0.07% showed seizure- like activity and 77.8% recovered well (healthy) from surgery (**B**).

Sham animals from both studies showed a good post- surgery recovery (**A, B**).

S.3.1.2. Chronic cerebral hypoperfusion leads to significant spatial working memory impairment on a radial arm maze paradigm

S.3.1.2.1. Results: total number of arm entries and trial duration

Two- way repeated measures ANOVA showed that hypoperfused animals (n=10) entered in total significantly more arms ($F_{(1, 18)}$= 26.535, p<0.0001) and completed the task for a significantly longer time (trial duration) ($F_{(1, 18)}$= 11.682, p= 0.003) than sham mice (n= 10) (figure S.3.1. A, B). There was a significant effect of the training day for both the total number of arm entries ($F_{(1,18)}$= 115.724, p<0.0001) and the trial duration ($F_{(1,18)}$= 49. 189, p<0.0001). An absence of a significant training day x group interaction was evidenced for all behavioural measures: the total number of arm entries ($F_{(1,18)}$= 0.184, p=0.673) and the trial duration ($F_{(1,18)}$= 3. 828, p= 0.660). The Tukey`s post- hoc analysis demonstrated that hypoperfused mice entered significantly more arms in total on training day 2 (p=0.001), day 5 (p= 0.0013), day 6 (p=0.010), day 7 (p= 0.003), and day 8 (p=0.031). Significant group differences in the trial duration were observed for training day 2 (p=0.028), day 6 (p=0.023), day 7 (p=0.005), day 8 (p=0.002).

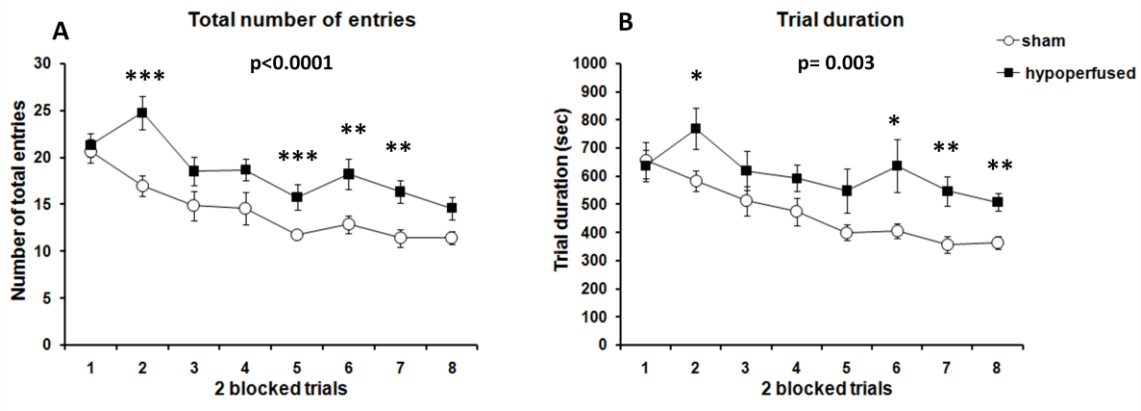

Figure S.3.1.3.: Group performance on a spatial working memory radial arm maze task

(group mean ± SE)

Spatial working memory was significantly impaired in hypoperfused mice. Two- way repeated measures ANOVA demonstrated that chronically hypoperfused mice (n=10) visited significantly more arms in total (**A**) and completed the task for a significantly longer time (**B**) than sham mice (n=10) ($p<0.05$).

Significant group differences as given by the Tukey`s post- hoc analysis: ($p<0.05$)*, ($p<0.01$)**, ($p<0.001$)***

S.3.2. Replica of the radial arm maze study (not presented in the main thesis body)

S.3.2.1 Materials and methods

S.3.2.1.1. Animals and surgery

Three months old C57Bl6/J male mice weighting 25±5gr (Chapter 2, section 2.1.1.; Coltman et al., 2011) were used for the replica of the radial arm maze experiment presented in Chapter 3. The animals were randomly allocated to a sham (n=17) and microcoils (n= 24) surgery performed as described in Chapter 2, section 2.2. All mice were subjected to a food deprivation procedure in order to reduce their body weight to 85-90% from their original one. Only the animals surviving the whole experimental period were included in the final behavioural and pathological analysis.

S.3.2.1.2. Behavioural testing

Spatial working memory was tested one month after surgery using a radial arm maze paradigm (Chapter 2, section 2.3.2.; Shibata et al., 2007; Nishio et al., 2010; Coltman et al., 2011). At the completion of the behavioural procedure (~2 months post- surgery) the animals were perfusion- fixed (Chapter 2, section 2.4.) and their brains were processed for histology and immunohistochemistry (Chapter 2, section 2.5.).

S.3.2.1.3. Pathological assessment

The pathological assessment of grey and white matter integrity for this behavioural study was performed by Dr Karen Horsburgh and therefore the pathological results are not presented in this thesis. The pathological analysis is reported in Coltman et al., 2011.

S.3.2.1.4. Statistical analysis of the behavioral performance

The statistical comparisons were performed on the average of two blocked trials representing the average performance of the animals on two consecutive days of training for each behavioural measure (Shibata et al., 2007; Nishio et al., 2010; Coltman et al., 2011).

For the replica of the radial arm maze experiment only the behavioural performance of hypoperfused animals with white matter pathology (without neuronal ischemic injury at

least at the examined neuroanatomical levels) (n= 7) was statistically compared to the performance of sham animals (n= 17). Group comparisons were performed using a two-way repeated measures ANOVA as described for the first radial arm maze experiment (Chapter 3, section 3.2.4.2.1.). When significant main effects of trial block of group x block interactions ($p<0.05$) were indicated by ANOVA, a Tukey`s post- hoc analysis was applied to determine the exact training day(s) when significant group differences in the behavioural performance between sham and hypoperfused mice occurred.

Significant group differences were reported for p values ($p<0.05$).

S.3.2.2. Results

S.3.2.2.1. Post- surgery recovery and physiological status of the animals

In the replica radial arm maze experiment 0.04% (1/24) of the hypoperfused mice died soon after surgery and 20.0% (5/24) of the hypoperfused mice showed a moderate seizure-like activity during the behavioural testing. The remaining 18 hypoperfused mice (79.0%) and all sham animals (n= 17) recovered well after surgery in the absence of any overt neurological dysfunction and underwent behavioural testing (figure S.3.2.1.)

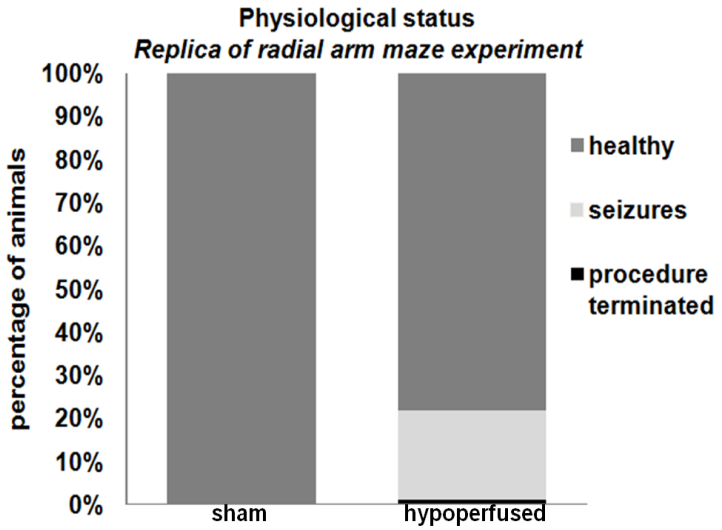

Figure S.3.2.1.: Physiological status of sham and hypoperfused tested on a radial arm maze (replica)

In the replica of the radial arm maze study, from the hypoperfused animals 0.04% were procedure terminated due to a poor post- surgery recovery, 20% exhibited sezure- like activity, 75% recovered well after surgery (healthy). All sham mice showed a good post- surgery recovery.

S.3.2.2.2. Chronic cerebral hypoperfusion leads to spatial working memory impairment in mice

As the major focus of this experimental chapter was on the effects of hypoperfusion-induced white matter pathology on cognitive abilities of mice, the radial arm maze experiment was conducted twice in order to increase the experimental numbers of hypoperfused animals with predominant white matter pathology. For this purpose, for the replica of the radial arm maze experiment only the performance of the hypoperfused animals with white matter pathology (n=7) was statistically compared to sham mice (n=17). The obtained results confirmed the data from the first radial arm maze experiment. Again, hypoperfused mice (n= 7) committed significantly more revisiting errors ($F_{(1, 22)}$= 8.057, p= 0.010), visited significantly fewer new arms in the first 8 arm entries ($F_{(1, 22)}$= 5.619, p= 0.027), and they entered significantly more arms in total ($F_{(1, 22)}$= 6.741, p= 0.016) than sham mice (n= 17) (figure S.3.2.2. A, B, C). There were no significant group differences in the trial duration ($F_{(1, 22)}$= 0.425, p= 0.521) (figure S.3.2.2. D). The post- hoc Tukey`s analysis demonstrated that hypoperfused mice committed significantly more revisiting errors on training day 6 (p=0.008), day 7 (p= 0.014) (figure S.3.2.2. A). They also visited significantly fewer novel arms in the first 8 arm choices on training day 7 (p=0.017) (figure S.3.2.2. B). Hypoperfused mice entered significantly more arms in total on training day 6 (p=0.008), day 7 (p= 0.013) (figure S.3.2.2. C).

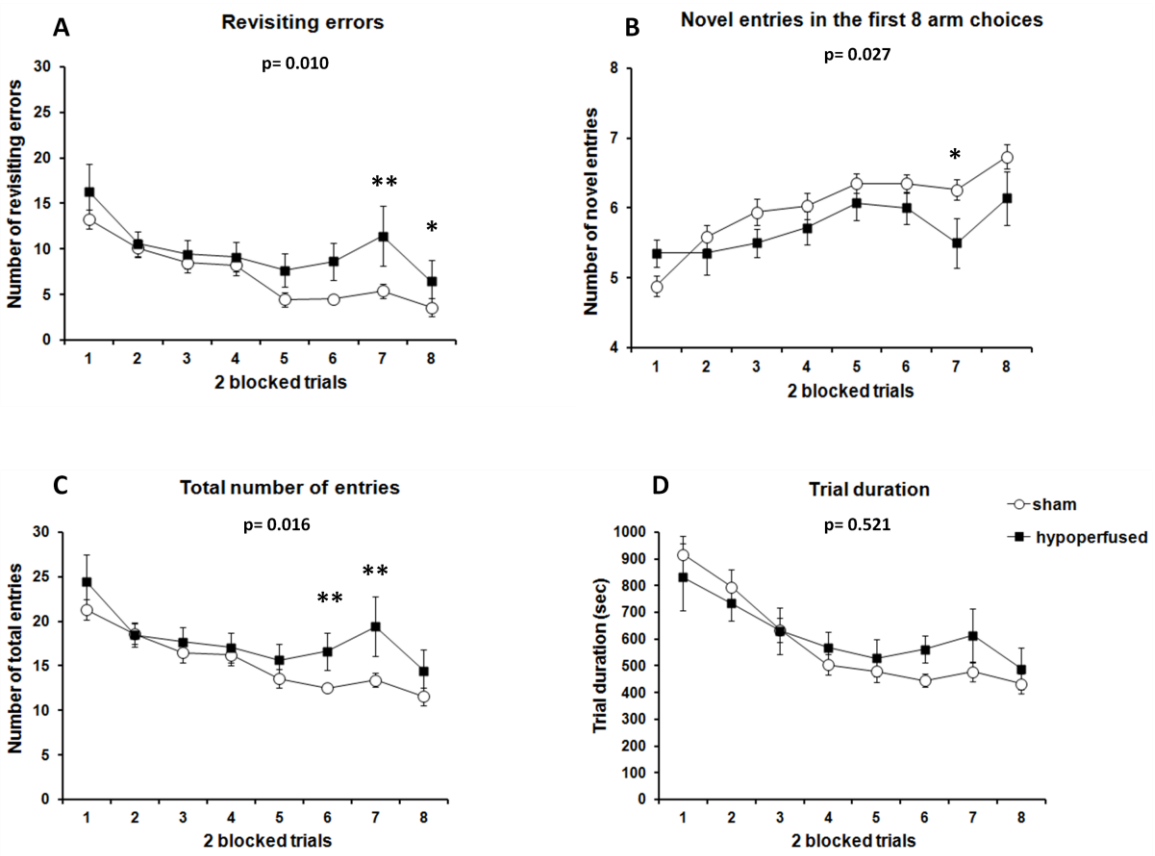

Figure S.3.2.2.: Group performance on a spatial working memory radial arm maze task (replica)

(group mean ± SE)

Hypoperfused mice (n=7) committed significantly more revisiting errors, visited significantly fewer new arms in the first 8 arm choices and entered significantly more arms in total than sham animals (n=17) ($p<0.05$) (**A, B, C**). There was no significant group difference in the trial duration ($p>0.05$) (**D**).

Significant group differences as given by the Tukey`s post- hoc analysis: ns (nonsignficant) ($p>0.05$), ($p<0.05$)*, ($p<0.01$)**, ($p<0.0001$)***

S.3.3. Additional behavioural data from the water maze experiment presented in the main thesis body

S.3.3.1. Chronic cerebral hypoperfusion does not impact on a cue task performance

Since mice are not natural swimmers, their ability to swim and perform a water maze task was tested a day prior to surgery as well as four days before the start of the serial spatial learning and memory task (three weeks after surgery) using a cue task water maze protocol (Chapter 2, section 2.3.3.2.1.). The behavioural performance on this task relies on the ability of mice to remember the spatial association between a hidden escape platform and a landmark cue in the absence of extramaze cues. It also requires intact visual abilities allowing the animals to perceive the landmark indicating the spatial location of the hidden platform.

In the present experiment, the cue task performance prior to surgery allowed to exclude mice exhibiting floating behavior from the subsequent surgical procedure and behavioural testing. The statistical analysis for the pre- surgery data (training day 1) was performed using an unpaired t- test comparing the group mean escape latency to platform. The statistical analysis for the post- surgery data (training day 2- 5) was analyzed using two-way repeated measures ANOVA comparing the group mean escape latency to platform overtime (Chen et al., 2000, Coltman et al., 2011). Significant differences were reported for $p<0.05$.

The analysis showed that prior to the surgical procedure (baseline level), there was no significant difference in the ability of hypoperfused (n=10) and sham (n= 11) mice to perform the cue task (t= 0.689, p= 0.49). Similarly, the statistical analysis of the post-surgery performance on the same water maze task demonstrated an absence of significant differences between hypoperfused and sham animals ($F_{(1,\ 19)}$= 0.695, p= 0.41) (figure S.3.3.).

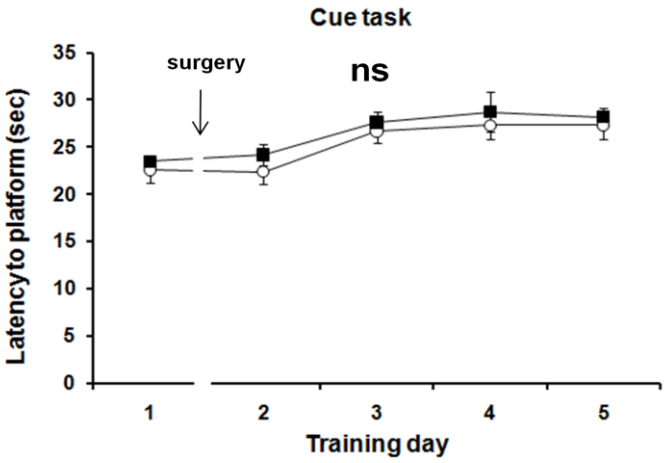

Figure S.3.3.: Cue task performance on a water maze paradigm (group mean ± SE)

Chronically hypoperfused mice (n=10) performed as well as sham animals (n=11) on a cue task water maze paradigm both prior to and 3 weeks after surgery (ns, $p>0.05$).

Behavioural measure	Group statistics	
	PT 10min	PT3h
Percentage of time spent swimming in training quadrant	F(1, 18)= 0.018, p= 0.89	F(1, 18)= 0.151, p= 0.70
Swimming speed	F(1, 18)= 2.021, p= 0.17	F(1, 18)= 3.056, p= 0.09
Percentage of time spent swimming near the walls (thigmotaxis)	F(1, 18)= 0.437, p= 0.52	F(1, 18)= 2.787, p= 0.11
Number of platform crossings	F(1, 18)= 0.065, p= 0.80	F(1, 18)= 1.183, p= 0.29
Latency to platform	F(1, 18)= 0.064, p= 0.80	F(1, 18)= 0.266, p= 0.61

Table S.3.1.: Short and long term memory recall in sham and hypoperfused mice: additional group statistical analysis

There were no significant group differences in the behavioural performance on the short (10min) and long (3h) term PTs on all five tasks as shown by two- way ANOVA for the average percentage of time spent swimming in the training quadrant during the first 60 sec of each PT, the average swimming speed, the average percentage of time spent swimming near the walls of the pool, the average number of platform crossing during the first 60sec of each PT and the average latency to platform ($p>0.05$).

Animal number	Group	Regions of interest						
		Corpus callosum	*External capsule*	*Internal capsule*	*Optic tract*	*Fimbria fornix*	*Hippocampus*	*Cortex*
1	**sham**	0	0	0	0	0	0	0
4	**sham**	0	0	0	0	0	0	0
7	**sham**	0	0	0	0	0	0	0
9	**sham**	0	0	0	0	0	0	0
11	**sham**	0	0	0	0	0	0	0
13	**sham**	0	0	0	0	0	0	0
15	**sham**	0	0	0	0	0	0	0
18	**sham**	0	0	0	0	0	0	0
20	**sham**	0	0	0	0	0	0	0
22	**sham**	0	0	0	0	0	0	0
2	**hypo**	1	1	1	3	3	3	0
3	**hypo**	3	3	3	3	1	3	3
6	**hypo**	0	1	0	3	1	2	2
8	**hypo**	0	0	0	0	0	0	0
10	**hypo**	0	0	0	0	0	3	0
12	**hypo**	1	1	3	3	1	1	2
14	**hypo**	2	1	2	3	0	0	0
16	**hypo**	1	1	3	3	3	1	2
17	**hypo**	1	2	3	2	1	1	2
19	**hypo**	1	1	1	3	1	3	1

Table S.3.2.1.: Individual regional pathological grades of axonal (APP) integrity of sham and hypoperfused mice tested on a radial arm maze paradigm

The animal numbers are the coded experimental numbers used to identify blindly to their treatment the animals during the behavioural and pathological evaluation. In red are indicated the hypoperfused animals without neuronal ischemic injury at the examined brain levels (8, 12, 16). In black are presented all the other animals.

Animal number	Group	Region of interest						
		Corpus callosum	*External capsule*	*Internal capsule*	*Optic tract*	*Fimbria fornix*	*Hippocampus*	*Cortex*
800727	**sham**	0	0	0	0	0	0	0
800729	**sham**	0	0	0	0	0	0	0
800732	**sham**	0	0	0	0	0	0	0
800739	**sham**	0	0	0	0	0	0	0
800743	**sham**	0	0	0	0	0	0	0
800744	**sham**	0	0	0	0	0	0	0
800747	**sham**	0	0	0	0	0	0	0
800752	**sham**	0	0	0	0	0	0	0
800758	**sham**	0	0	0	0	0	0	0
800759	**sham**	0	0	0	0	0	0	0
800760	**sham**	0	0	0	0	0	0	0
800726	**hypo**	0	0	0	1	0	0	0
800728	**hypo**	0	0	0	0	0	0	1
800733	**hypo**	0	0	0	0	0	1	0
800738	**hypo**	0	0	0	0	0	1	1
800746	**hypo**	0	0	0	1	0	0	0
800749	**hypo**	0	0	0	0	0	1	0
800753	**hypo**	0	0	0	2	0	0	0
800754	**hypo**	0	0	0	1	0	0	0
800755	**hypo**	0	0	0	0	0	0	0
800757	**hypo**	0	0	1	0	1	3	0

Table S.3.2.2.: Individual regional pathological grades of axonal (APP) integrity of sham and hypoperfused mice tested on a water maze paradigm

The animal numbers are the coded experimental numbers used to identify blindly to their treatment the animals during the behavioural and pathological evaluation. All hypoperfused animals included in final data analysis of the water arm maze study presented white matter pathology in the absence of grey matter abnormalities (at least at the examined brain levels).

Animal number	Group	Regions of interest				
		Corpus callosum	*External capsule*	*Internal capsule*	*Optic tract*	*Fimbria fornix*
1	**sham**	0	0	0	0	0
4	**sham**	0	0	0	0	0
7	**sham**	0	0	0	0	0
9	**sham**	0	0	0	0	0
11	**sham**	0	0	0	0	0
13	**sham**	0	0	0	0	0
15	**sham**	0	0	0	0	0
18	**sham**	0	0	0	0	0
20	**sham**	0	0	0	0	0
22	**sham**	0	0	0	0	0
2	**hypo**	1	1	1	3	3
3	**hypo**	1	0	1	3	3
6	**hypo**	0	0	2	3	2
8	**hypo**	0	0	0	3	1
10	**hypo**	1	1	2	0	1
12	**hypo**	0	0	2	0	2
14	**hypo**	1	1	2	3	1
16	**hypo**	1	1	3	3	0
17	**hypo**	1	1	2	3	3
19	**hypo**	0	1	1	3	1

Table S.3.2.3.: Individual regional pathological grades of myelin (MAG) integrity of sham and hypoperfused mice tested on a radial arm maze paradigm

The animal numbers are the coded experimental numbers used to identify blindly to their treatment the animals during the behavioural and pathological evaluation. In red are indicated the hypoperfused animals without neuronal ischemic injury at the examined brain levels (8, 12, 16). In black are presented all the other animals.

Animal number	Group	Region of interest				
		Corpus callosum	*External capsule*	*Internal capsule*	*Optic tract*	*Fimbria fornix*
800727	**sham**	0	0	0	0	0
800729	**sham**	0	0	0	0	0
800732	**sham**	0	0	0	0	0
800739	**sham**	0	0	0	0	0
800743	**sham**	0	0	0	0	0
800744	**sham**	0	0	0	0	0
800747	**sham**	0	0	0	0	0
800752	**sham**	0	0	0	0	0
800758	**sham**	0	0	0	0	0
800759	**sham**	0	0	0	0	0
800760	**sham**	0	0	0	0	0
800726	**hypo**	1	1	2	3	0
800728	**hypo**	0	0	1	3	0
800733	**hypo**	0	0	1	1	0
800738	**hypo**	1	1	1	3	1
800746	**hypo**	1	1	1	3	1
800749	**hypo**	1	1	1	3	0
800753	**hypo**	0	0	1	3	0
800754	**hypo**	0	1	2	3	1
800755	**hypo**	1	1	1	3	1
800757	**hypo**	0	0	0	3	0

Table S.3.2.4.: Individual regional pathological grades of myelin (MAG) integrity of sham and hypoperfused mice tested on a water maze paradigm

The animal numbers are the coded experimental numbers used to identify blindly to their treatment the animals during the behavioural and pathological evaluation. All hypoperfused animals included in final data analysis of the water arm maze study presented white matter pathology in the absence of grey matter abnormalities (at least at the examined brain levels).

Animal number	Group	Regions of interest						
		Corpus callosum	*External capsule*	*Internal capsule*	*Optic tract*	*Fimbria fornix*	*Hippocampus*	*Cortex*
1	**sham**	0	0	0	0	0	0	0
4	**sham**	0	0	0	0	0	0	0
7	**sham**	0	0	0	0	0	0	0
9	**sham**	0	0	0	0	0	0	0
11	**sham**	0	0	0	0	0	0	0
13	**sham**	0	0	0	0	0	0	0
15	**sham**	0	0	0	0	0	0	0
18	**sham**	0	0	0	0	0	0	0
20	**sham**	0	0	0	0	0	0	0
22	**sham**	0	0	0	0	0	0	0
2	**hypo**	0	1	2	3	3	3	2
3	**hypo**	3	3	3	3	1	3	3
6	**hypo**	0	1	1	2	1	0	1
8	**hypo**	1	1	0	2	1	0	0
10	**hypo**	0	0	0	0	1	0	0
12	**hypo**	0	0	0	0	0	1	2
14	**hypo**	1	1	2	3	1	0	1
16	**hypo**	0	0	0	0	0	0	0
17	**hypo**	0	0	0	0	0	0	0
19	**hypo**	3	3	3	3	3	3	1

Table S.3.2.5.: Individual regional pathological grades of inflammation (Iba1) of sham and hypoperfused mice tested on a radial arm maze paradigm

The animal numbers are the coded experimental numbers used to identify blindly to their treatment the animals during the behavioural and pathological evaluation. In red are indicated the hypoperfused animals without neuronal ischemic injury at the examined brain levels (8, 12, 16). In black are presented all the other animals.

Animal number	Group	Region of interest						
		Corpus callosum	*External capsule*	*Internal capsule*	*Optic tract*	*Fimbria fornix*	*Hippocampus*	*Cortex*
800727	**sham**	0	0	0	0	0	0	0
800729	**sham**	0	0	0	0	0	0	0
800732	**sham**	0	0	0	0	0	0	0
800739	**sham**	0	0	0	0	0	0	0
800743	**sham**	0	0	0	0	0	0	0
800744	**sham**	0	0	0	0	0	0	0
800747	**sham**	0	0	0	0	0	0	0
800752	**sham**	0	0	0	0	0	0	0
800758	**sham**	0	0	0	0	0	0	0
800759	**sham**	0	0	0	0	0	0	0
800760	**sham**	0	0	0	0	0	0	0
800726	**hypo**	0	1	1	3	0	0	0
800728	**hypo**	0	0	1	3	1	0	0
800733	**hypo**	0	0	0	0	0	0	0
800738	**hypo**	0	0	1	2	0	0	0
800746	**hypo**	0	1	2	2	0	0	0
800749	**hypo**	0	0	2	3	1	0	0
800753	**hypo**	0	1	2	3	1	0	0
800754	**hypo**	0	1	1	2	1	0	0
800755	**hypo**	1	3	3	3	1	0	1
800757	**hypo**	0	1	2	1	0	1	1

Table S.3.2.6.: Individual regional pathological grades of inflammation (Iba1) of sham and hypoperfused mice tested on a water maze paradigm

The animal numbers are the coded experimental numbers used to identify blindly to their treatment the animals during the behavioural and pathological evaluation. All hypoperfused animals included in final data analysis of the water arm maze study presented white matter pathology in the absence of grey matter abnormalities (at least at the examined brain levels).

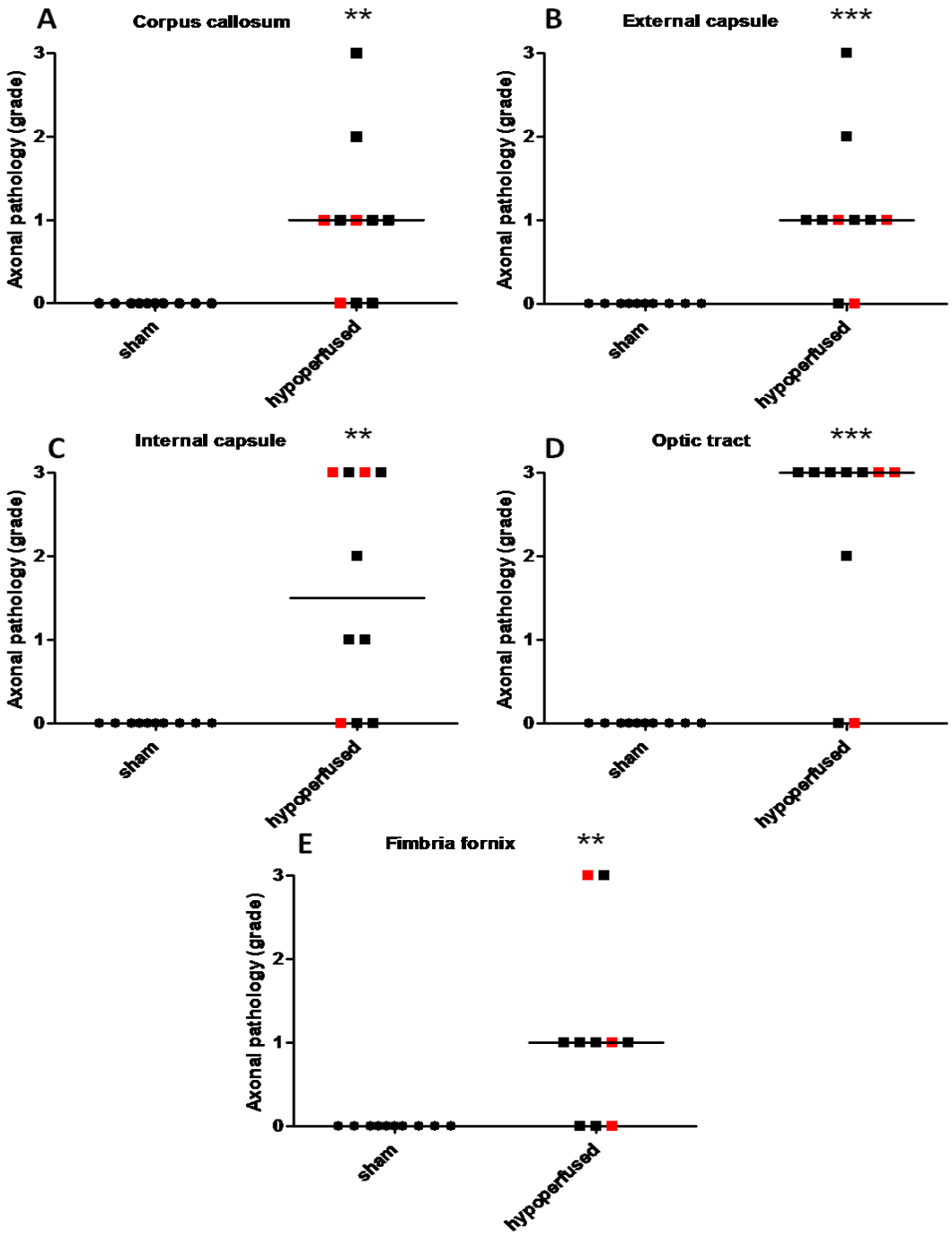

Figure S.3.4.1. A-E: White matter regional group median pathological grades of axonal integrity (the radial arm maze experiment)

Hypoperfused mice (n=10) showed a significantly impaired axonal integrity in all examined white matter ROIs when compared with sham animals (n=10) ($p<0.05$) (**A-E**). In red are indicated hypoperfused mice with without neuronal ischemic injury (at least at the examined brain levels).

Significant group differences as given by Mann- Whitney nonparametric statistics:

($p<0.05$)*, ($p<0.01$)**, ($p<0.0001$)***

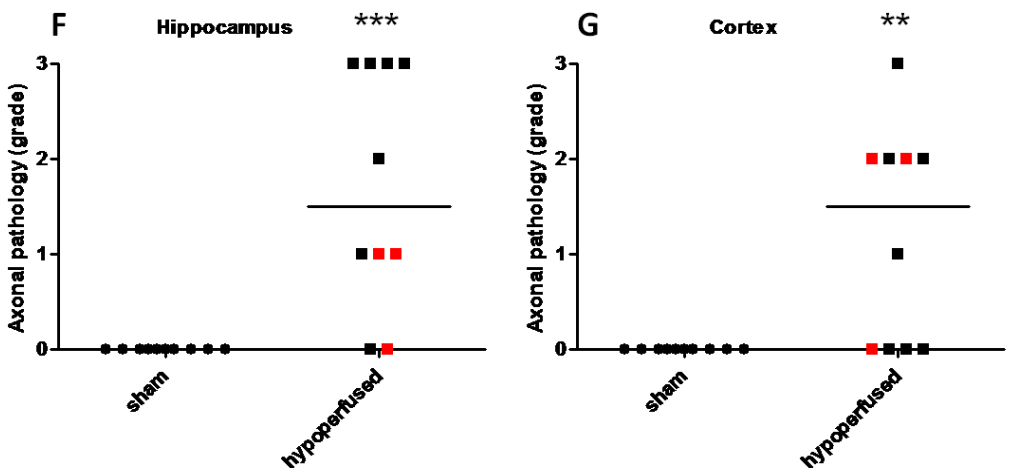

Figure S.3.4.1. F-G: Grey matter regional group median pathological grades of axonal integrity (the radial arm maze experiment)

Hypoperfused mice (n=10) showed a significantly impaired axonal integrity in all grey matter ROIs when compared with sham animals (n=10) ($p<0.05$) (**F, G**). In red are indicated hypoperfused mice with without neuronal ischemic injury (at least at the examined brain levels).

Significant group differences as given by Mann- Whitney nonparametric statistics:

($p<0.01$)**, ($p<0.0001$)***

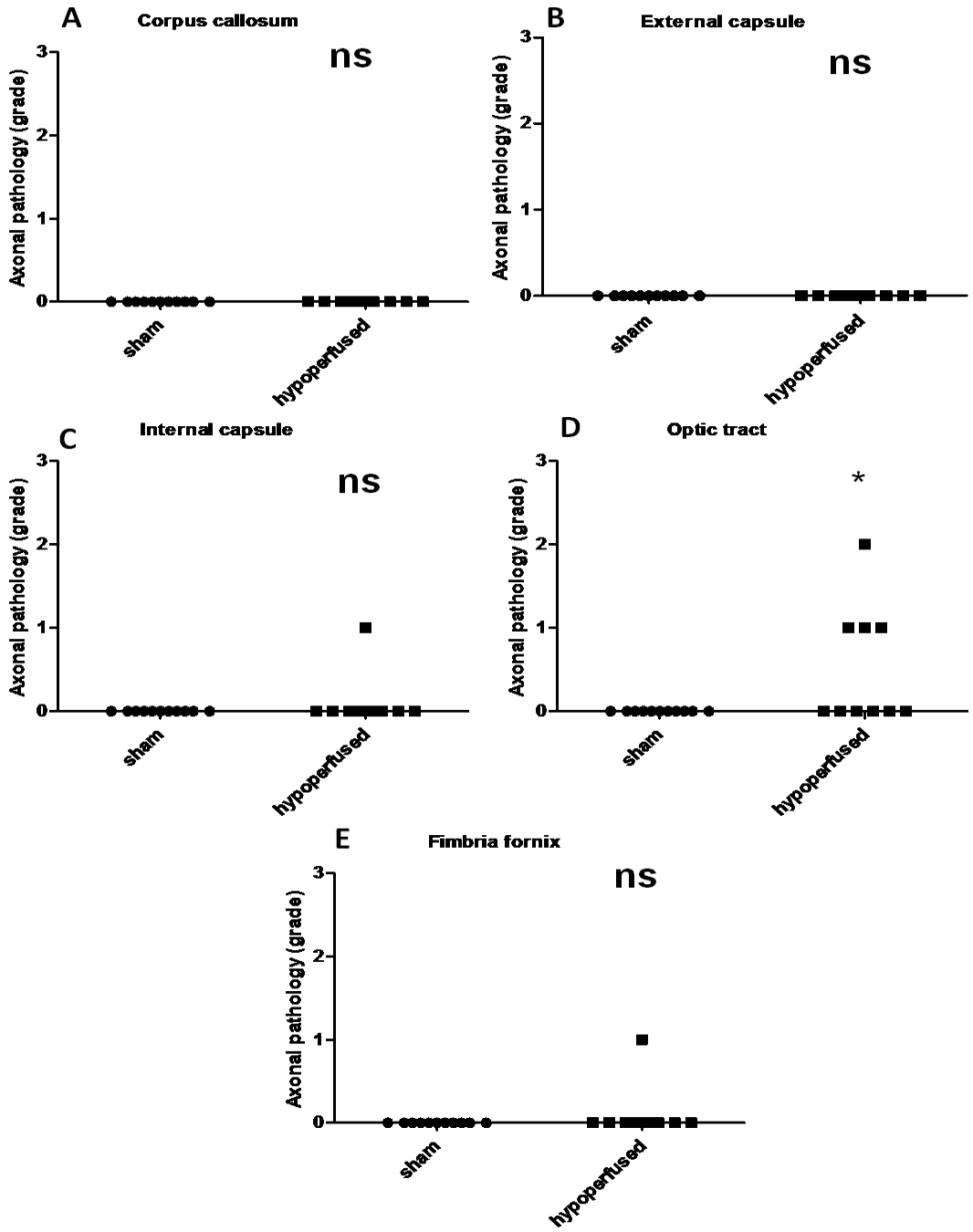

Figure S.3.4.2. A-E: White matter regional group median pathological grades of axonal integrity (the water maze experiment)

Hypoperfused mice (n=10) showed a significantly impaired axonal integrity in the OT (**D**) ($p<0.05$), but not in the rest of the examined ROIs (**A-C, E**) ($p>0.05$) when compared with sham animals (n=11). All hypoperfused mice tested on the water maze paradigm did not exhibit grey matter ischemic injury (at least at the examined brain levels).

Significant group differences as given by Mann- Whitney nonparametric statistics:

($p<0.05$)*, ns (nonsignficant) ($p>0.05$)

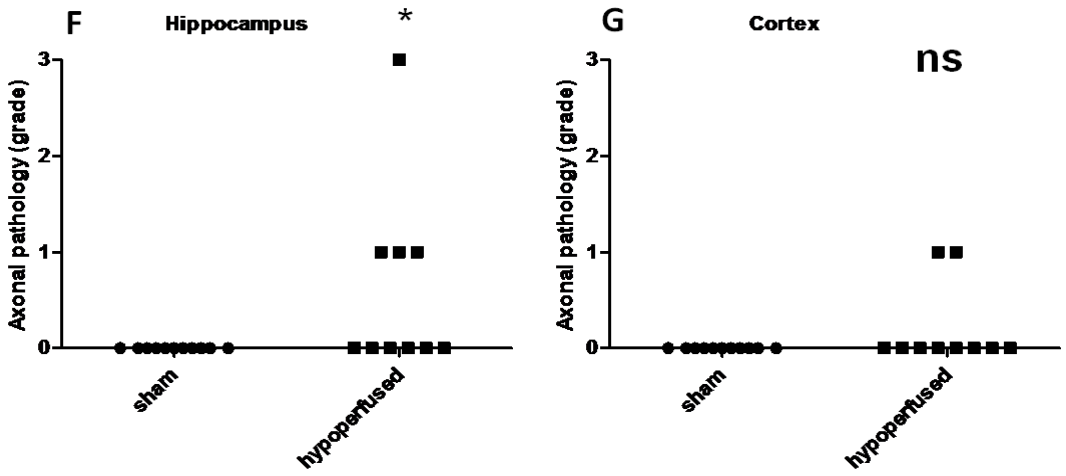

Figure S.3.4.2. F-G: Grey matter regional group median pathological grades of axonal integrity (the water maze experiment)

Hypoperfused mice (n=10) showed a significantly impaired axonal integrity in the hippocampus (**F**), but not in the Cx (**G**) when compared with sham animals (n=11) ($p<0.05$). All hypoperfused mice tested on the water maze paradigm did not exhibit grey matter ischemic injury (at least at the examined brain levels).

Significant group differences as given by Mann- Whitney nonparametric statistics:

($p<0.05$)*, ns (nonsignficant) ($p>0.05$)

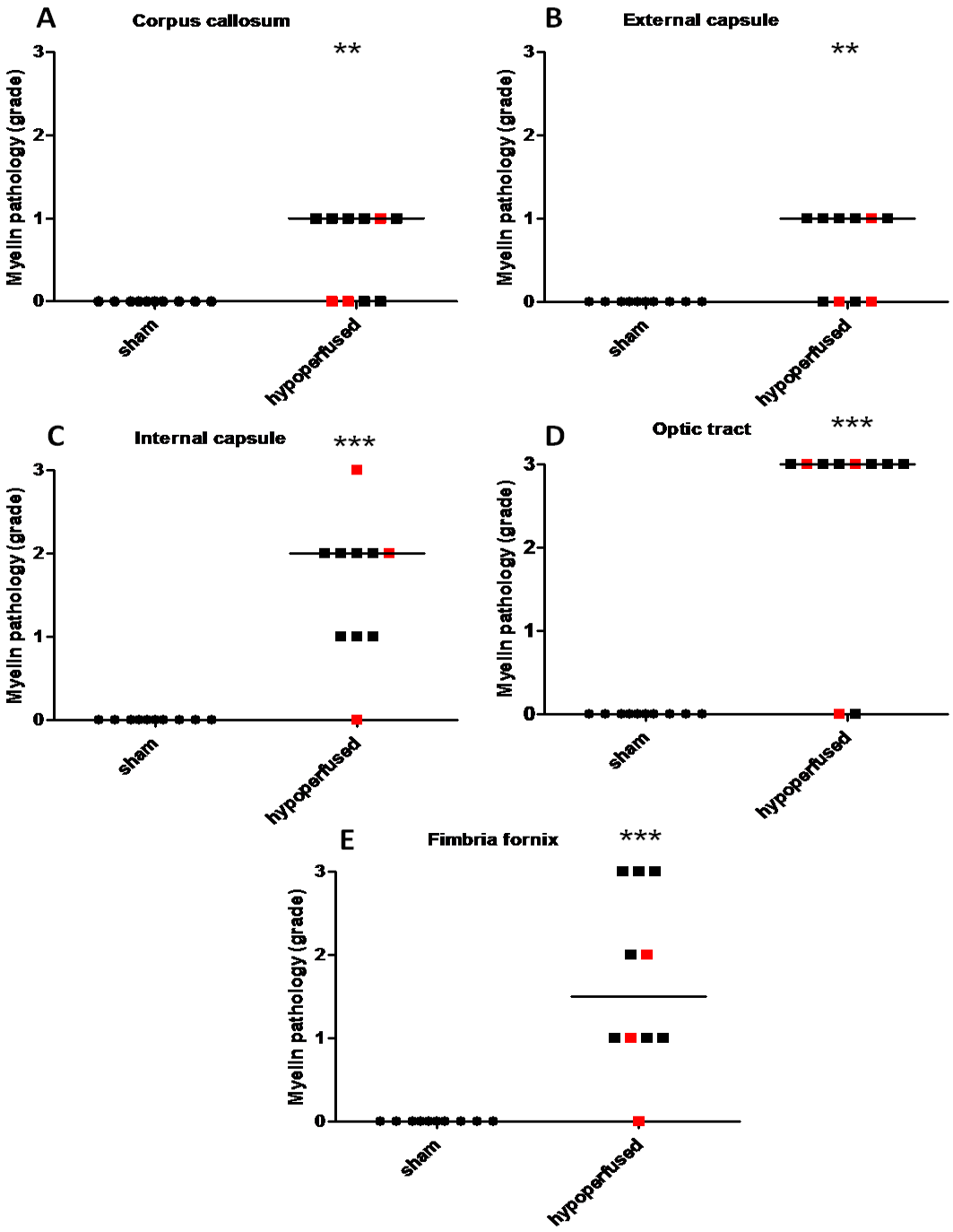

Figure S.3.4.3.: Regional group median pathological grades of myelin integrity (the radial arm maze experiment)

Hypoperfused mice (n=10) exhibited a significant myelin pathology in all examined white matter ROIs when compared with sham animals (n=10) ($p<0.05$) (**A-E**). In red are indicated hypoperfused mice with without neuronal ischemic injury (at least at the examined brain levels).

Significant group differences as given by Mann- Whitney nonparametric statistics:

($p<0.05$)*, ($p<0.01$)**, ($p<0.0001$)***

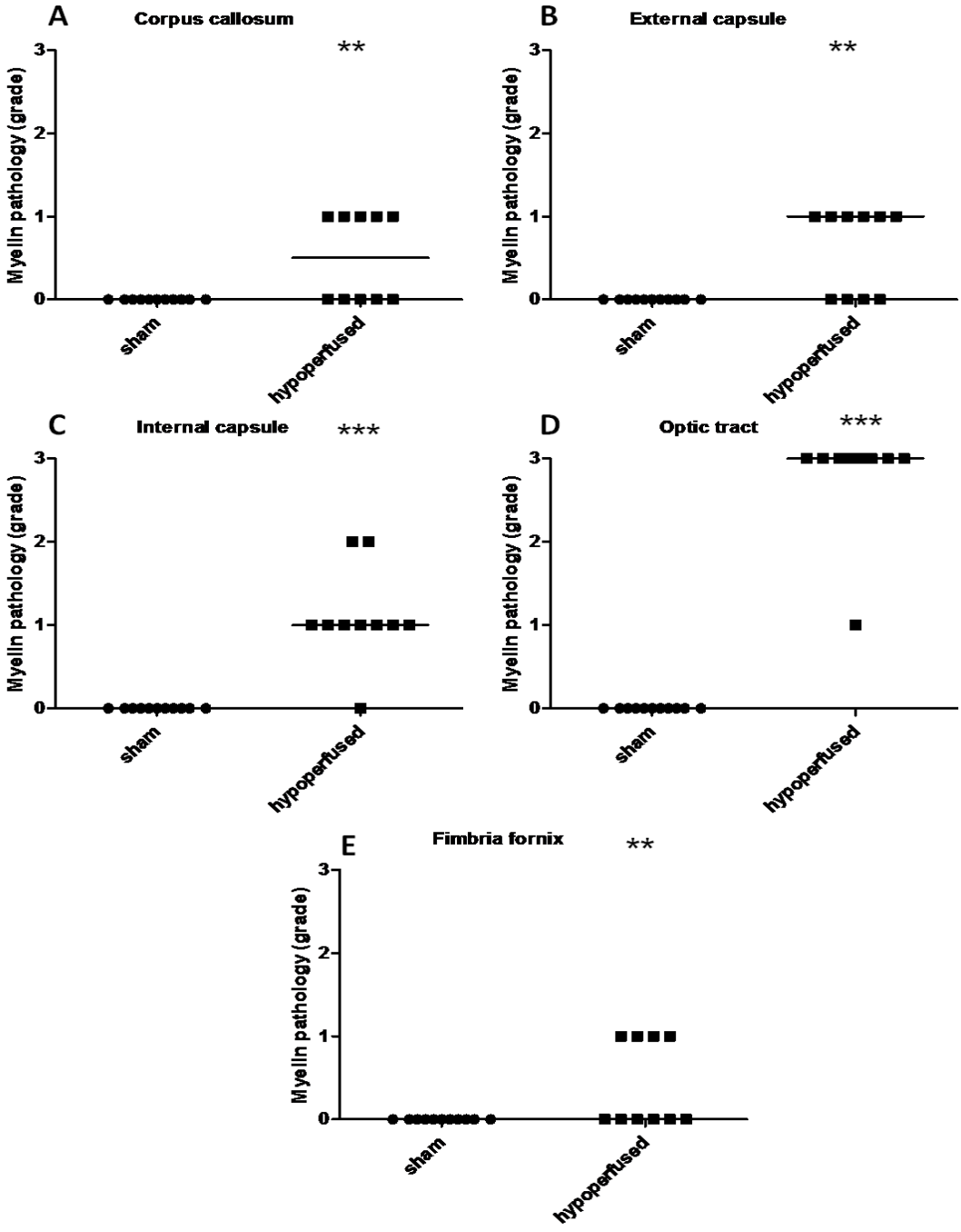

Figure S.3.4.4.A-E: Regional group median pathological grades of myelin integrity (the water maze experiment)

Hypoperfused mice (n=10) showed a significantly impaired myelin integrity in all examine white matter ROIs when compared with sham animals (n=11) ($p<0.05$). All hypoperfused mice tested on the water maze paradigm did not exhibit grey matter ischemic injury (at least at the examined brain levels).

Significant group differences as given by Mann- Whitney nonparametric statistics:

($p<0.01$)**, ($p<0.001$)***

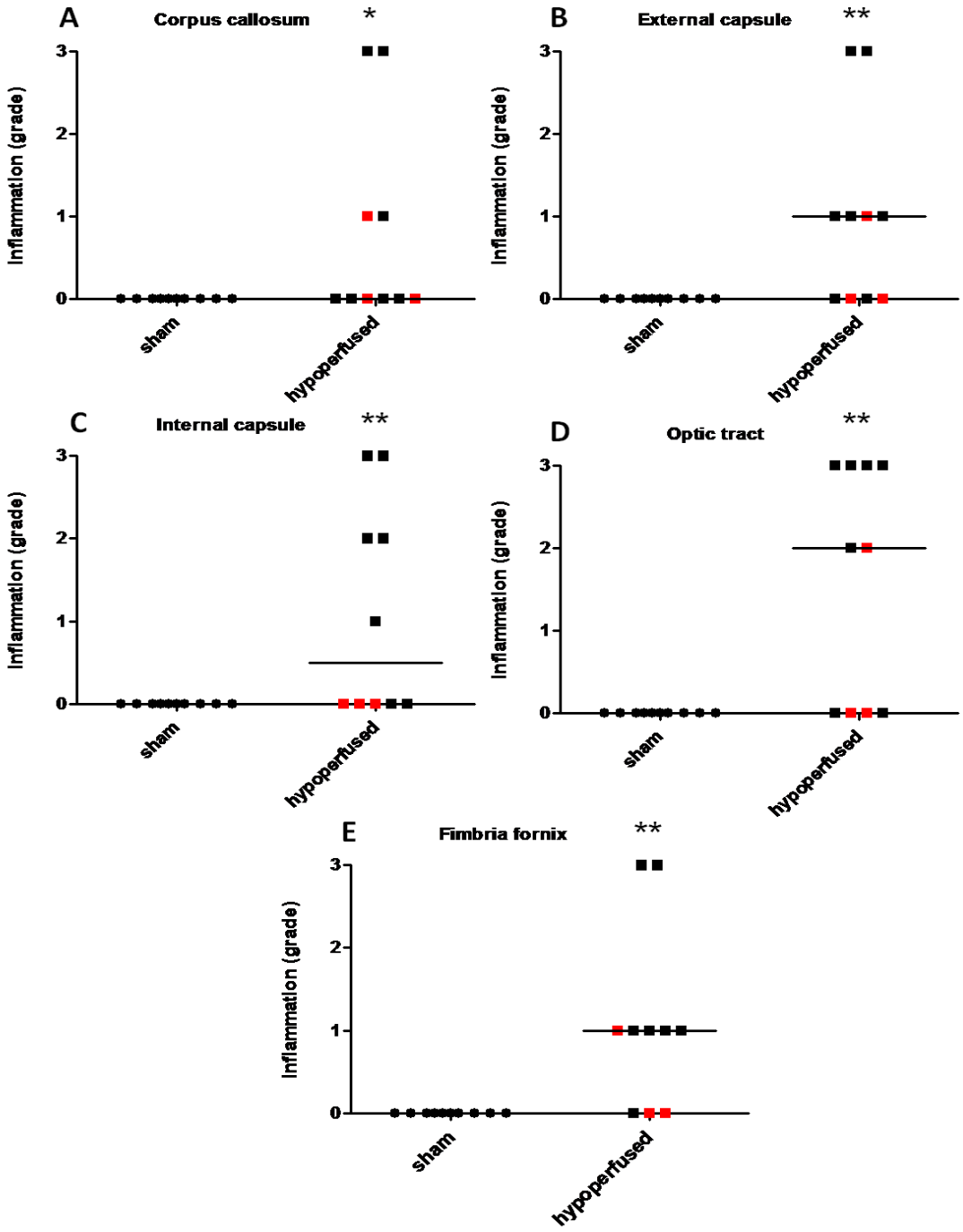

Figure S.3.4.5. A-E: White matter regional group median pathological grades of axonal integrity (the radial arm maze experiment)

Hypoperfused mice (n=10) showed a significantly increased inflammation in all examined white matter ROIs when compared with sham animals (n=10) ($p<0.05$) (**A-E**). In red are indicated hypoperfused mice with without neuronal ischemic injury (at least at the examined brain levels).

Significant group differences as given by Mann- Whitney nonparametric statistics:

($p<0.05$)*, ($p<0.01$)**, ($p<0.0001$)***

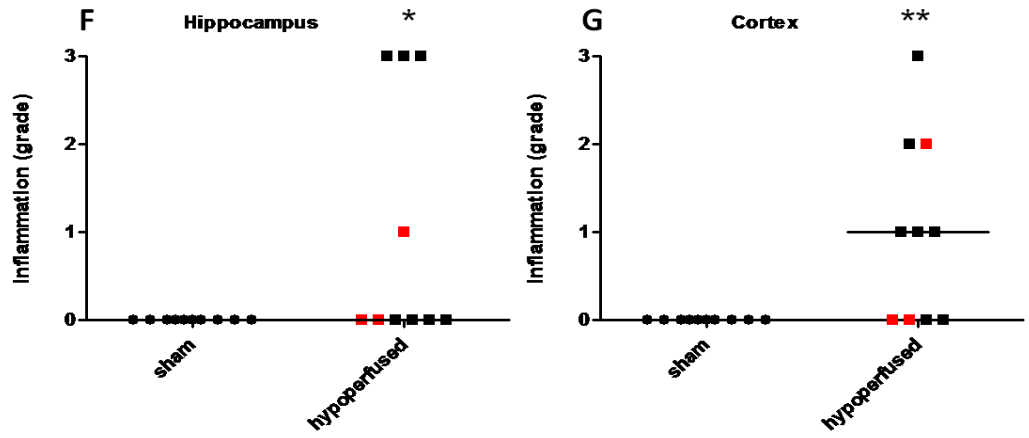

Figure S.3.4.5. F-G: Grey matter regional group median pathological grades of inflammation (the radial arm maze experiment)

Hypoperfused mice (n=10) showed a significantly increased inflammation in grey matter ROIs when compared with sham animals (n=10) ($p<0.05$) (**F-G**). In red are indicated hypoperfused mice with without neuronal ischemic injury (at least at the examined brain levels).

Significant group differences as given by Mann- Whitney nonparametric statistics:

($p<0.05$)*, ($p<0.01$)**

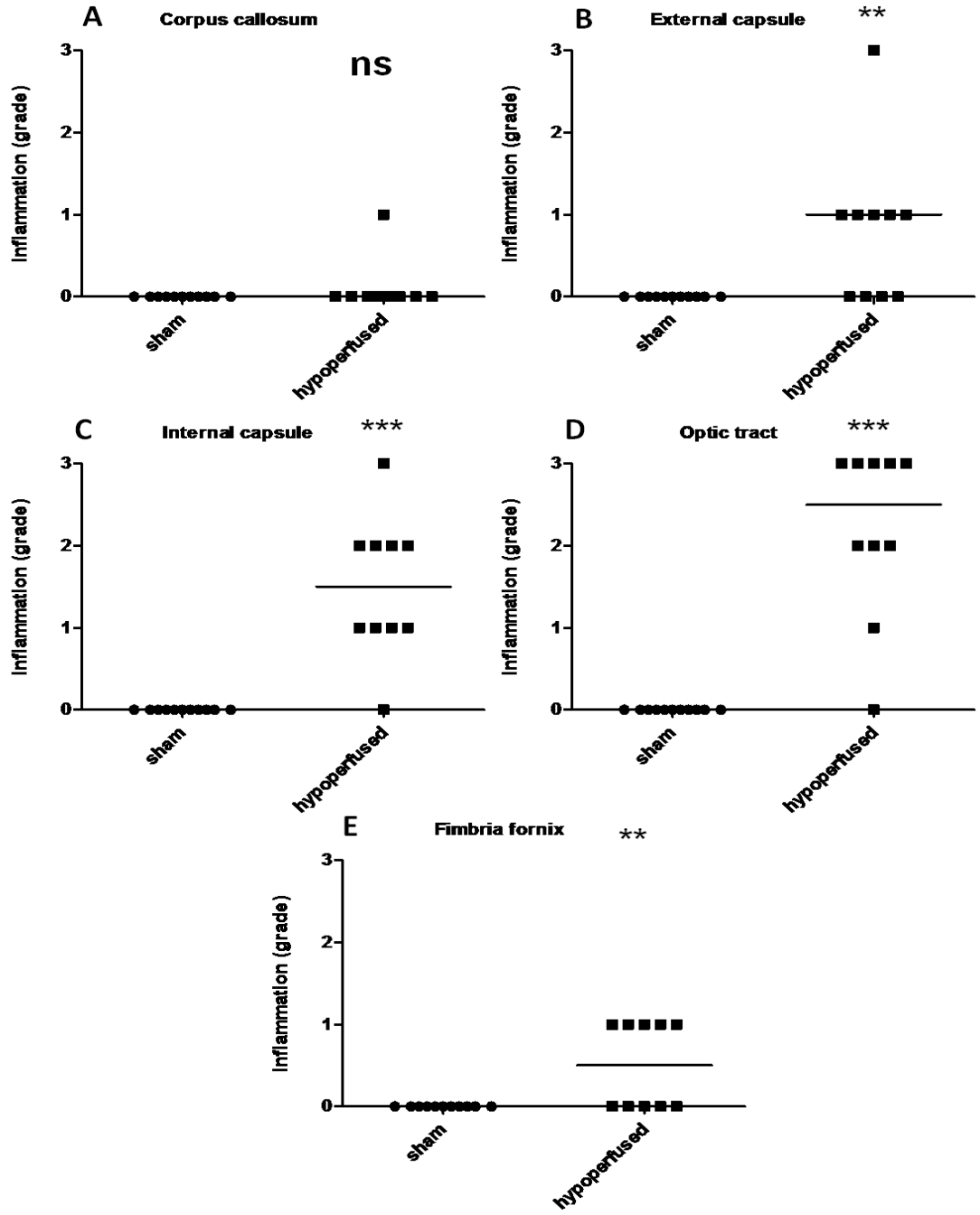

Figure S.3.4.6. A-E: White matter regional group median pathological grades of inflammation (the water maze experiment)

Hypoperfused mice (n=10) showed a significantly increased inflammation in white matter tracts (**B-E**) ($p<0.05$) except in the CC (**A)** ($p>0.05$) when compared with sham animals (n=11). All hypoperfused mice tested on the water maze paradigm did not exhibit grey matter ischemic injury (at least at the examined brain levels).

Significant group differences as given by Mann- Whitney nonparametric statistics:

($p<0.05$)*, ($p<0.01$)**, ($p<0.0001$)***, ns (nonsignificant) ($p>0.05$)

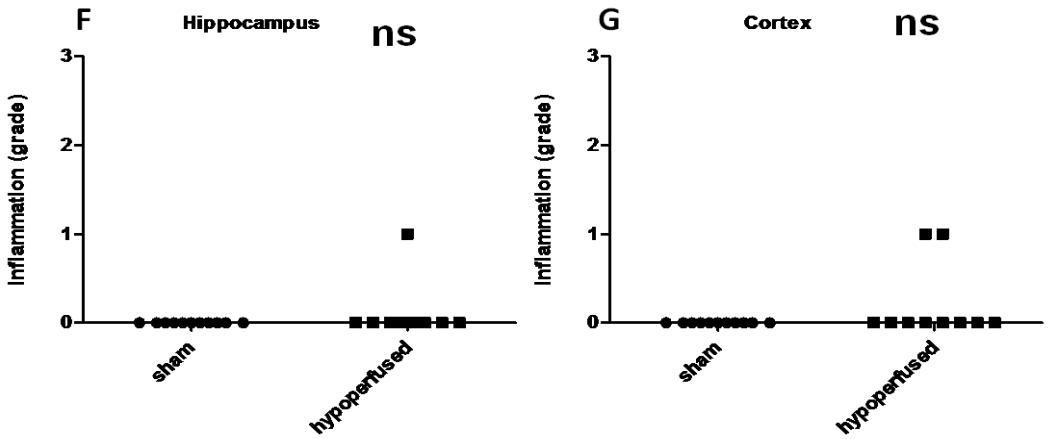

Figure S.3.4.6. F-G: Grey matter regional group median pathological grades of inflammation (the water maze experiment)

Hypoperfused mice (n=10) did not show significantly increased inflammation when compared with sham animals (n=11) in any of the examined grey matter ROIs (**F-G**) ($p>0.05$). All hypoperfused mice tested on the water maze paradigm did not exhibit grey matter ischemic injury (at least at the examined brain levels).

Significant group differences as given by Mann- Whitney nonparametric statistics:

ns (nonsignificant) ($p>0.05$)

Animal number	Group	Total pathological score in white matter		
		APP	*MAG*	*Iba1*
1	**sham**	0	0	0
4	**sham**	0	0	0
7	**sham**	0	0	0
9	**sham**	0	0	0
11	**sham**	0	0	0
13	**sham**	0	0	0
15	**sham**	0	0	0
18	**sham**	0	0	0
20	**sham**	0	0	0
22	**sham**	0	0	0
2	**hypo**	9	9	9
3	**hypo**	13	8	13
6	**hypo**	5	7	5
8	**hypo**	0	4	5
10	**hypo**	0	5	1
12	**hypo**	9	4	0
14	**hypo**	8	8	8
16	**hypo**	11	8	0
17	**hypo**	9	10	0
19	**hypo**	7	6	15

Table S.3.3.1.: Total individual pathological scores across white matter ROIs of sham and hypoperfused mice tested on a radial arm maze paradigm

The total pathological scores of axonal (APP), myelin (MAG) integrity, inflammation (Iba1) were calculated as described in Chapter 2, section 2.7.4., Coltman et al., 2011, Holland et al., 2011.

The animal numbers are the coded experimental numbers used to identify blindly to their treatment the animals during the behavioural and pathological evaluation. In red are indicated the hypoperfused animals without neuronal ischemic injury at the examined brain levels (8, 12, 16). In black are presented all the other animals.

Animal number	Group	Total pathological score in white matter		
		APP	***MAG***	***Iba1***
800727	**sham**	0	0	0
800729	**sham**	0	0	0
800732	**sham**	0	0	0
800739	**sham**	0	0	0
800743	**sham**	0	0	0
800744	**sham**	0	0	0
800747	**sham**	0	0	0
800752	**sham**	0	0	0
800758	**sham**	0	0	0
800759	**sham**	0	0	0
800760	**sham**	0	0	0
800726	**hypo**	1	7	5
800728	**hypo**	0	4	5
800733	**hypo**	0	2	0
800738	**hypo**	0	7	3
800746	**hypo**	1	7	5
800749	**hypo**	0	6	6
800753	**hypo**	2	4	7
800754	**hypo**	1	7	5
800755	**hypo**	0	7	11
800757	**hypo**	2	3	4

Table S.3.3.2.: Total individual pathological scores across white matter ROIs of sham and hypoperfused mice tested on a water maze paradigm

The total pathological scores of axonal (APP), myelin (MAG) integrity, inflammation (Iba1) were calculated as described in Chapter 2, section 2.7.4., Coltman et al., 2011, Holland et al., 2011.

The animal numbers are the coded experimental numbers used to identify blindly to their treatment the animals during the behavioural and pathological evaluation. All hypoperfused animals included in final data analysis of the water arm maze study presented white matter pathology in the absence of grey matter abnormalities (at least at the examined brain levels).

Experiment	Biomarker	Total group median pathological score across examined white matter ROIs *Sham (n=10)*	Total group median pathological score across examined white matter ROIs *Hypoperfused (n=10)*	Group statistics (Mann- Whitney test)
Radial arm maze	*APP*	0	8.5*******	U= 10.000, p= 0.0007
	MAG	0	7.5 ***	U=0.000, p<0.0001
	Iba1	0	5.0***	U= 15.000, p= 0.002
Water maze	*APP*	0	0.5*	U= 27.500, p= 0.01
	MAG	0	6.5***	U=0.000, p<0.0001
	Iba1	0	5.0***	U= 5.500, p<0.0001

Table S.3.3.3.: Total group median pathological scores across white matter ROIs of sham and hypoperfused mice tested on a radial arm maze and water maze paradigm and group statistics

Statistical group comparisons were performed using Mann- Whitney statistics as described in Chapter 3, section 3.2.3.2.

Chronically hypoperfused mice tested on both a radial arm maze and water maze paradigm exhibited significantly more severe total axonal, myelin pathology and increased inflammation in white matter when compared with sham mice.

Significant group differences as given by the Mann- Whitney statistics: ($p<0.05$)*, ($p<0.0001$)***

Appendices II

Animal number	Group	Region of interest				
		Corpus callosum	*External capsule*	*Internal capsule*	*Optic tract*	*Hippocampus*
900835	**WT sham**	0	0	0	0	0
900837	**WT sham**	0	0	0	0	0
900838	**WT sham**	0	0	0	0	0
900843	**WT sham**	0	0	0	0	0
900844	**WT sham**	0	0	0	0	0
900845	**WT sham**	0	0	0	0	0
900846	**WT sham**	0	0	0	0	0
900849	**WT sham**	0	0	0	0	0
900832	**WT hypo**	0	0	0	0	0
900833	**WT hypo**	1	2	2	2	2
900834	**WT hypo**	0	1	0	2	0
900836	**WT hypo**	1	1	1	2	0
900839	**WT hypo**	1	1	2	2	2
900840	**WT hypo**	0	0	0	1	0
900841	**WT hypo**	1	0	1	2	1
900847	**WT hypo**	0	0	0	0	0
900848	**WT hypo**	0	0	0	0	0
900850	**WT hypo**	2	1	2	1	1
900869	**APOEKO sham**	0	0	0	0	0
900870	**APOEKO sham**	0	0	0	0	0
900875	**APOEKO sham**	0	0	0	0	0
900873	**APOEKO sham**	0	0	0	0	0
900874	**APOEKO sham**	0	0	0	0	0
900879	**APOEKO sham**	0	0	0	0	0
900880	**APOEKO sham**	0	0	0	0	0
900878	**APOEKO sham**	0	0	0	0	0
900871	**APOEKO hypo**	1	2	1	1	0
900872	**APOEKO hypo**	0	0	1	0	0
900877	**APOEKO hypo**	0	0	0	2	0
900881	**APOEKO hypo**	0	0	0	0	0
900882	**APOEKO hypo**	2	2	3	2	3
900885	**APOEKO hypo**	2	1	3	2	2
900883	**APOEKO hypo**	1	1	1	1	0
900884	**APOEKO hypo**	1	1	1	1	0

Table S.4.1.1.: Individual regional grades of axonal (APP) integrity in WT and APOKO sham and hypoperfused mice

The animal numbers are the coded experimental numbers used to identify blindly to their treatment the animals during the pathological evaluation. Mouse number 900840 indicated in red is the mouse not included in the experiments presented in Chapter 5.

Animal number	Group	Region of interest			
		Corpus callosum	*External capsule*	*Internal capsule*	*Optic tract*
900835	**WT sham**	0	0	0	0
900837	**WT sham**	0	0	0	0
900838	**WT sham**	0	0	0	0
900843	**WT sham**	0	0	0	0
900844	**WT sham**	0	0	0	0
900845	**WT sham**	0	0	0	0
900846	**WT sham**	0	0	0	0
900849	**WT sham**	0	0	0	0
900832	**WT hypo**	2	2	2	2
900833	**WT hypo**	0	2	3	3
900834	**WT hypo**	0	0	0	1
900836	**WT hypo**	0	1	1	3
900839	**WT hypo**	0	1	2	3
900840	**WT hypo**	0	0	0	3
900841	**WT hypo**	0	0	1	3
900847	**WT hypo**	0	1	1	2
900848	**WT hypo**	0	0	2	2
900850	**WT hypo**	1	2	2	2
900869	**APOEKO sham**	0	0	0	0
900870	**APOEKO sham**	0	0	0	0
900875	**APOEKO sham**	0	0	0	0
900873	**APOEKO sham**	0	0	0	0
900874	**APOEKO sham**	0	0	0	0
900879	**APOEKO sham**	0	0	0	0
900880	**APOEKO sham**	0	0	0	0
900878	**APOEKO sham**	0	0	0	0
900871	**APOEKO hypo**	0	0	1	3
900872	**APOEKO hypo**	1	0	0	0
900877	**APOEKO hypo**	0	0	2	3
900881	**APOEKO hypo**	0	1	3	2
900882	**APOEKO hypo**	2	3	1	3
900885	**APOEKO hypo**	1	1	2	3
900883	**APOEKO hypo**	0	1	1	1
900884	**APOEKO hypo**	0	0	1	0

Table S.4.1.2.: Individual regional grades of myelin (MAG) integrity in WT and APOKO sham and hypoperfused mice

The animal numbers are the coded experimental numbers used to identify blindly to their treatment the animals during the pathological evaluation. Mouse number 900840 indicated in red is the mouse not included in the experiments presented in Chapter 5.

Animal number	Group	Region of interest				
		Corpus callosum	*External capsule*	*Internal capsule*	*Optic tract*	*Hippocampus*
900835	**WT sham**	0	0	0	0	0
900837	**WT sham**	0	0	0	0	0
900838	**WT sham**	0	0	0	0	0
900843	**WT sham**	0	0	0	0	0
900844	**WT sham**	0	0	0	0	0
900845	**WT sham**	0	0	0	0	0
900846	**WT sham**	0	0	0	0	0
900849	**WT sham**	0	0	0	0	0
900832	**WT hypo**	1	1	1	0	0
900833	**WT hypo**	1	1	1	1	1
900834	**WT hypo**	0	0	0	0	0
900836	**WT hypo**	1	2	2	1	3
900839	**WT hypo**	2	2	1	0	1
900840	**WT hypo**	0	1	0	1	1
900841	**WT hypo**	0	0	1	0	3
900847	**WT hypo**	1	1	1	0	1
900848	**WT hypo**	0	1	0	0	1
900850	**WT hypo**	1	0	1	1	0
900869	**APOEKO sham**	0	0	0	0	0
900870	**APOEKO sham**	0	0	0	0	0
900875	**APOEKO sham**	0	0	0	0	0
900873	**APOEKO sham**	0	0	0	0	0
900874	**APOEKO sham**	0	0	0	0	0
900879	**APOEKO sham**	0	0	0	0	0
900880	**APOEKO sham**	0	0	0	0	0
900878	**APOEKO sham**	0	0	0	0	0
900871	**APOEKO hypo**	1	1	1	1	1
900872	**APOEKO hypo**	0	1	0	0	1
900877	**APOEKO hypo**	0	1	1	1	0
900881	**APOEKO hypo**	2	2	2	1	0
900882	**APOEKO hypo**	3	3	1	1	2
900885	**APOEKO hypo**	0	1	1	1	3
900883	**APOEKO hypo**	1	1	1	0	1
900884	**APOEKO hypo**	0	0	1	0	1

Table S.4.1.3.: Individual regional grades of myelin (dMBP) integrity in WT and APOKO sham and hypoperfused mice

The animal numbers are the coded experimental numbers used to identify blindly to their treatment the animals during the pathological evaluation. Mouse number 900840 indicated in red is the mouse not included in the experiments presented in Chapter 5.

Animal number	Group	Region of interest				
		Corpus callosum	*External capsule*	*Internal capsule*	*Optic tract*	*Hippocampus*
900835	**WT sham**	0	0	0	0	0
900837	**WT sham**	0	0	0	0	0
900838	**WT sham**	0	0	0	0	0
900843	**WT sham**	0	0	0	0	0
900844	**WT sham**	0	0	0	0	0
900845	**WT sham**	0	0	0	0	0
900846	**WT sham**	0	0	0	0	0
900849	**WT sham**	0	0	0	0	0
900832	**WT hypo**	0	0	0	0	0
900833	**WT hypo**	2	3	3	3	3
900834	**WT hypo**	0	1	0	2	0
900836	**WT hypo**	1	2	2	3	2
900839	**WT hypo**	0	3	3	3	3
900840	**WT hypo**	2	2	2	3	2
900841	**WT hypo**	0	0	2	3	1
900847	**WT hypo**	0	0	1	0	0
900848	**WT hypo**	0	0	0	3	2
900850	**WT hypo**	2	3	3	2	3
900869	**APOEKO sham**	0	0	0	0	0
900870	**APOEKO sham**	0	0	0	0	0
900875	**APOEKO sham**	0	0	0	0	0
900873	**APOEKO sham**	0	0	0	0	0
900874	**APOEKO sham**	0	0	0	0	0
900879	**APOEKO sham**	0	0	0	0	0
900880	**APOEKO sham**	0	0	0	0	0
900878	**APOEKO sham**	0	0	0	0	0
900871	**APOEKO hypo**	1	0	3	3	3
900872	**APOEKO hypo**	3	2	3	2	2
900877	**APOEKO hypo**	0	0	0	3	0
900881	**APOEKO hypo**	0	0	0	0	0
900882	**APOEKO hypo**	3	3	3	3	3
900885	**APOEKO hypo**	1	3	2	3	3
900883	**APOEKO hypo**	1	1	1	3	1
900884	**APOEKO hypo**	1	1	1	1	0

Table S.4.1.4.: Individual regional grades of inflammation (Iba1) in WT and APOKO sham and hypoperfused mice

The animal numbers are the coded experimental numbers used to identify blindly to their treatment the animals during the pathological evaluation. Mouse number 900840 indicated in red is the mouse not included in the experiments presented in Chapter 5.

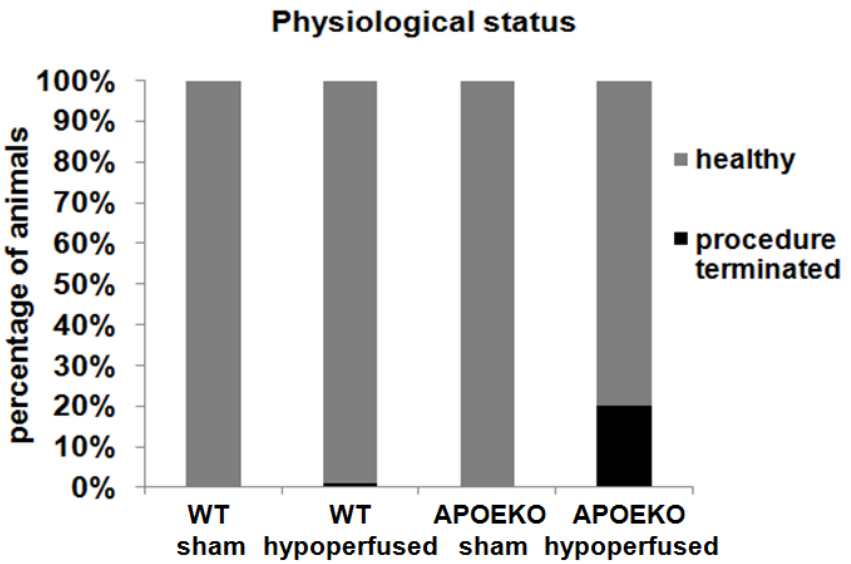

Figure S.4.1.: Physiological status of WT and APOE sham and hypoperfused mice

WT (99.1%) and APOEKO (80%) hypoperfused mice showed a good post- surgery recovery (healthy) at the exception of 0.09% WT and 20% APOEKO hypoperfused mice that were procedure terminated due to a severe sickness. All sham animals from both genotypes recovered well (healthy) after surgery.

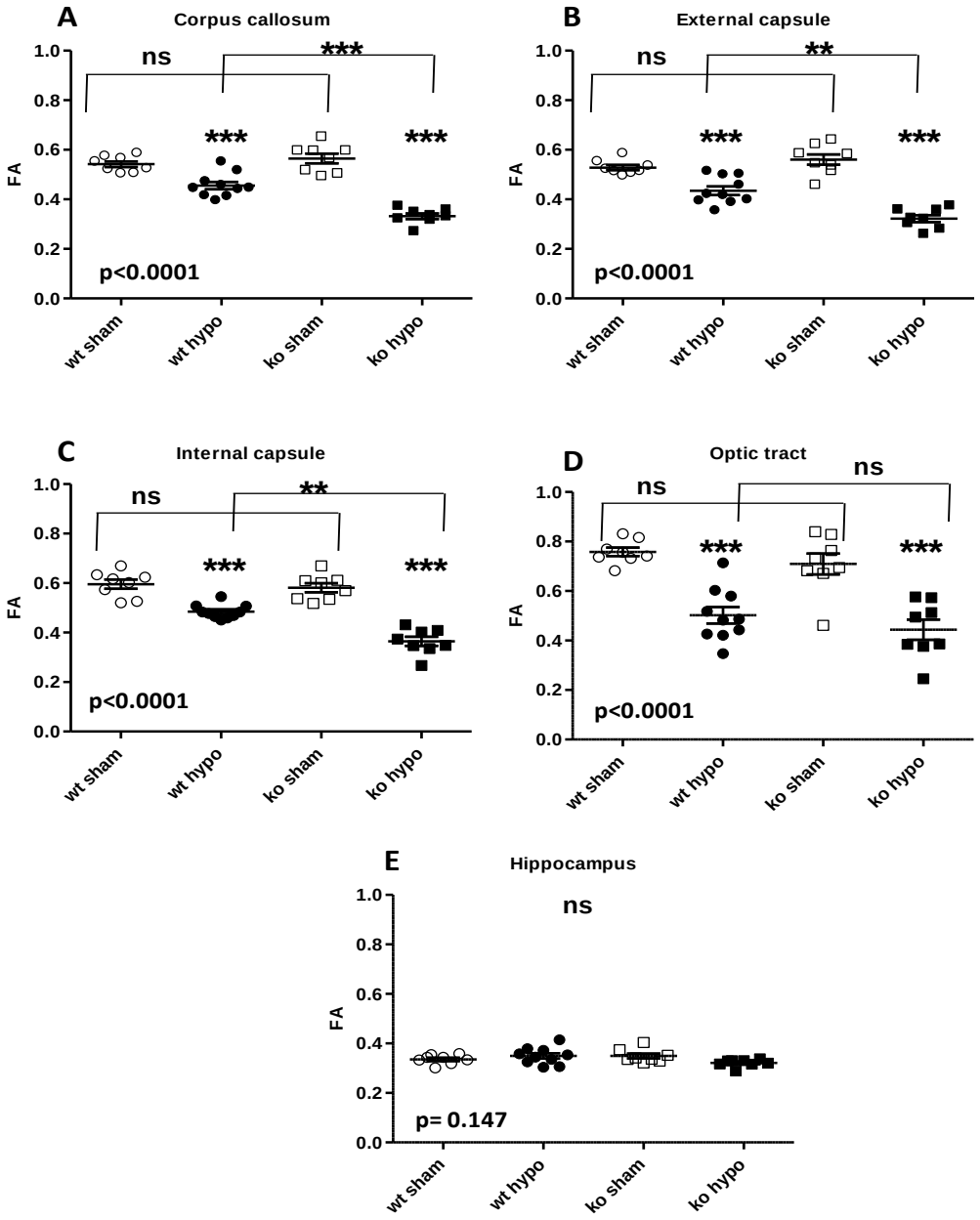

Figure S.4.2.1.: Regional FA parameters

(group mean ± SE)

Significant group differences in FA were evidenced by two- way MANOVA in the CC, EC, IC, and OT ($p<0.0001$), but not in the hippocampus ($p= 0.147$) (**A-E**). These significant changes were significantly more pronounced in APOEKO hypoperfused mice when compared with WT hypoperfused counterparts in the CC, EC and IC ($p<0.01$) (**A, B, C**). There was an absence of significant differences in the regional FA values between WT and APOEKO sham animals in all examined ROIs ($p>0.01$) (**A-E**). Significant group differences as given by the Tukey`s post- hoc analysis: ns ($p>0.05$), ($p<0.01$)**, ($p<0.001$)***

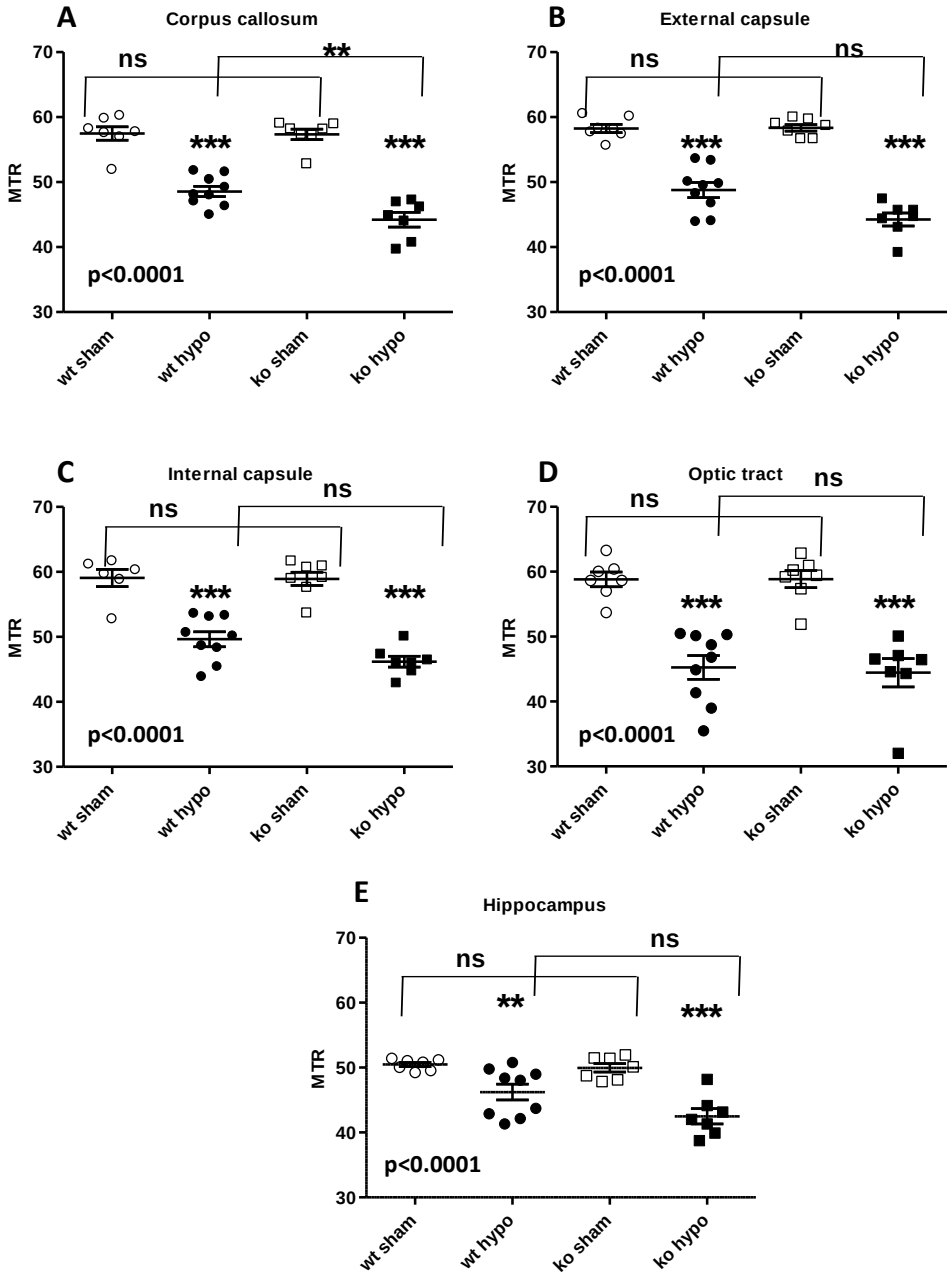

Figure S.4.2.2.: Regional MTR parameters

(group mean ± SE)

Significant group differences in MTR were evidenced by two- way MANOVA in the CC, EC, IC, OT and hippocampus ($p<0.0001$) (**A-E**). These significant changes were significantly more pronounced in APOEKO hypoperfused mice when compared with WT hypoperfused counterparts in the CC ($p<0.01$) (**A, B, E**). There was an absence of significant differences in the regional MTR values between WT and APOEKO sham animals in all examined ROIs ($p>0.01$) (**A-E**). Significant group differences as given by the Tukey`s post- hoc analysis: ns ($p>0.05$), ($p<0.01$)**, ($p<0.001$)***

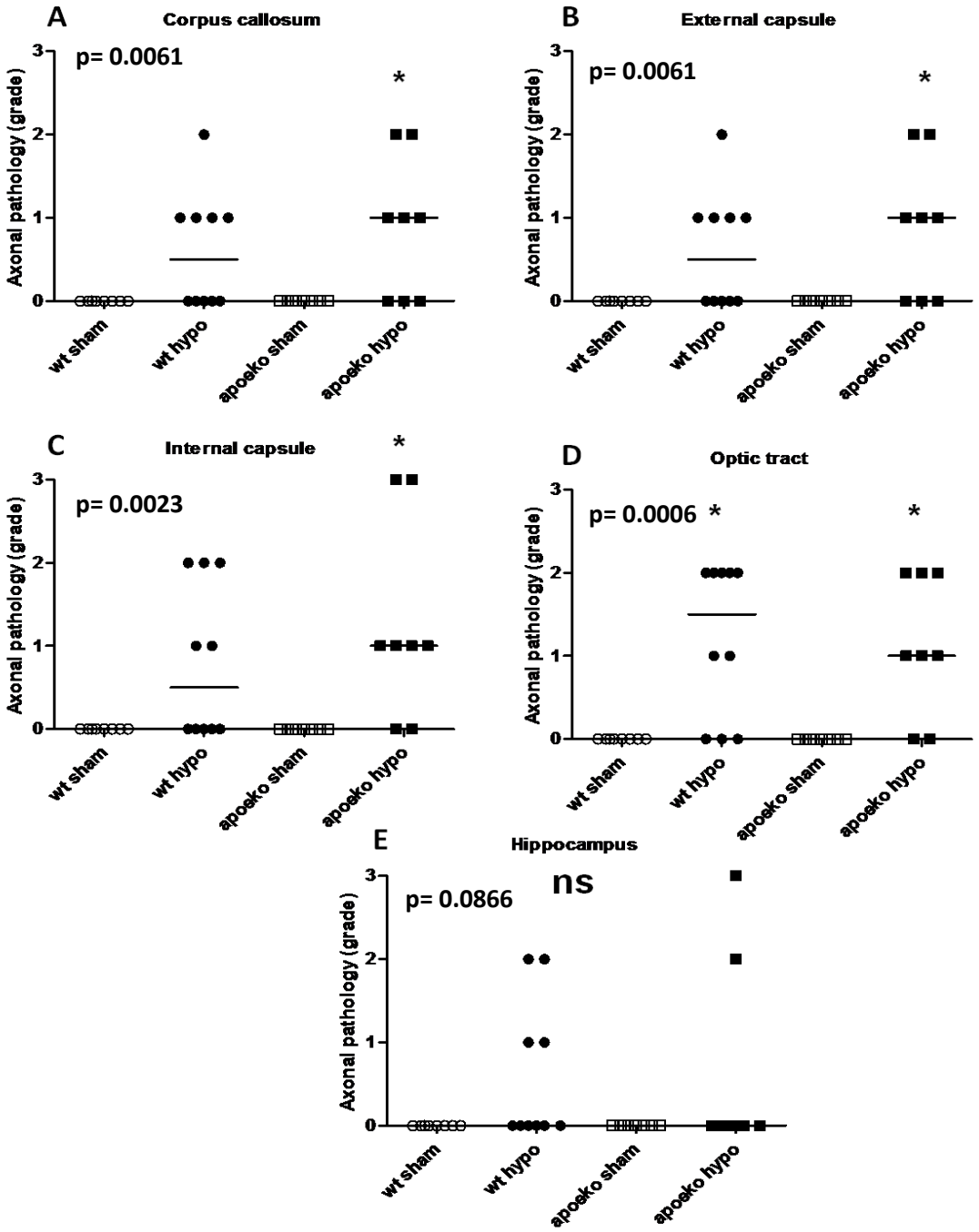

Figure S.4.3.1.: Regional group median pathological grades of axonal integrity

APOEKO hypoperfused mice (n=8) ($p<0.05$), but not WT hypoperfused mice (n=10) ($p>0.05$) developed significantly more severe axonal pathology than WT (n=8) and APOEKO (n=8) sham in the CC, EC, IC (**A, B, C**). In the OT both APOEKO and WT hypoperfused mice exhibited significant axonal injury compared with the two sham group (**D**) ($p<0.05$). In the hippocampus there was no significant group difference in axonal integrity (**E**) ($p>0.05$). There was no significant difference in axonal integrity between WT and APOEKO sham as well as between WT and APOEKO hypoperfused in any of the ROIs ($p>0.05$) (**A-E**). Significant group differences as given by Dunn multiple comparisons`s post- hoc analysis: ($p<0.05$)*, ($p<0.01$)**, ns (nonsignificant) ($p>0.05$)

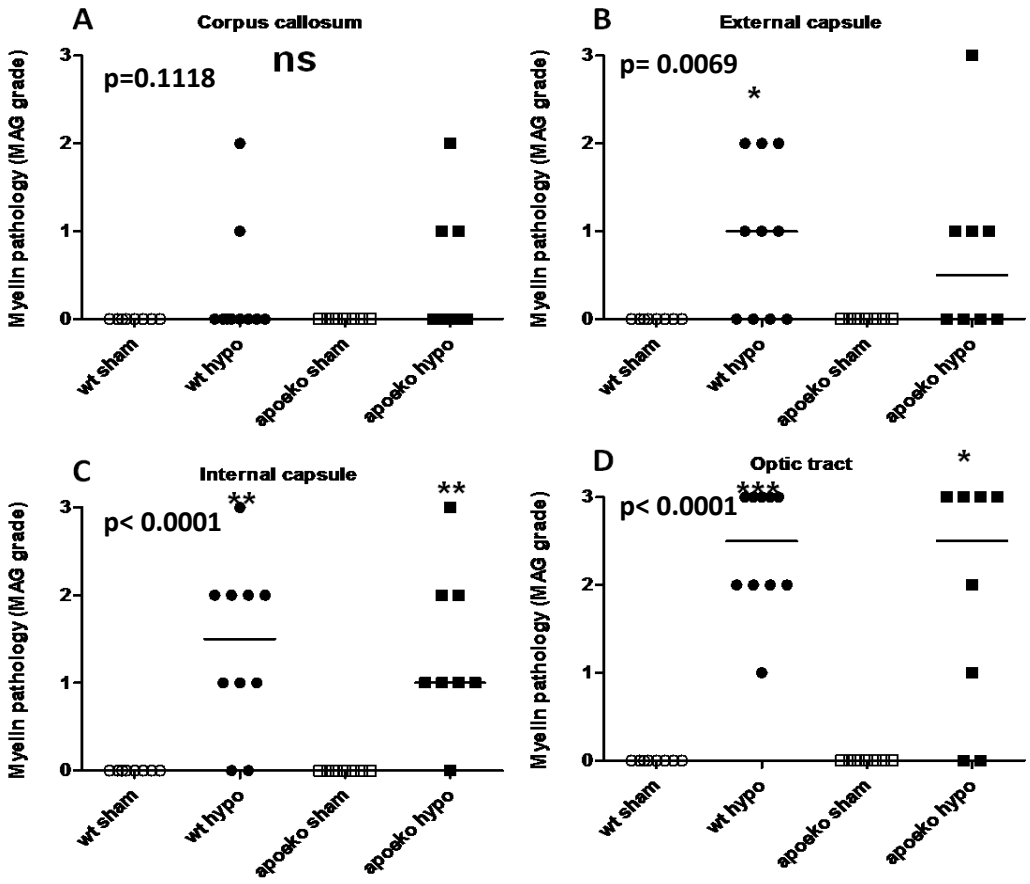

Figure S.4.3.2.: Regional group median pathological grades of myelin integrity (MAG)

Both WT (n= 10) and APOEKO (n=8) hypoperfused mice exhibited significantly impaired myelin integrity when compared with the two sham groups in the IC and OT (**C, D**) ($p<0.05$). In the CC, there was no significant difference in myelin integrity between the four groups (**A**) ($p>0.05$). In the EC, only WT hypoperfused mice ($p<0.05$), but not APOEKO hypoperfused mice ($p>0.05$) showed significantly impaired myelin integrity when compared with sham mice from both genotypes (**B**). There was no difference in myelin integrity between WT and APOEKO sham as well as between WT and APOEKO hypoperfused mice in any of the examined ROIs ($p<0.05$) (**A-D**). Significant group differences as given by Dunn multiple comparisons`s post- hoc analysis: ($p<0.05$)*, ($p<0.01$)**, ($p<0.0001$)***, ns (nonsignficant) ($p>0.05$)

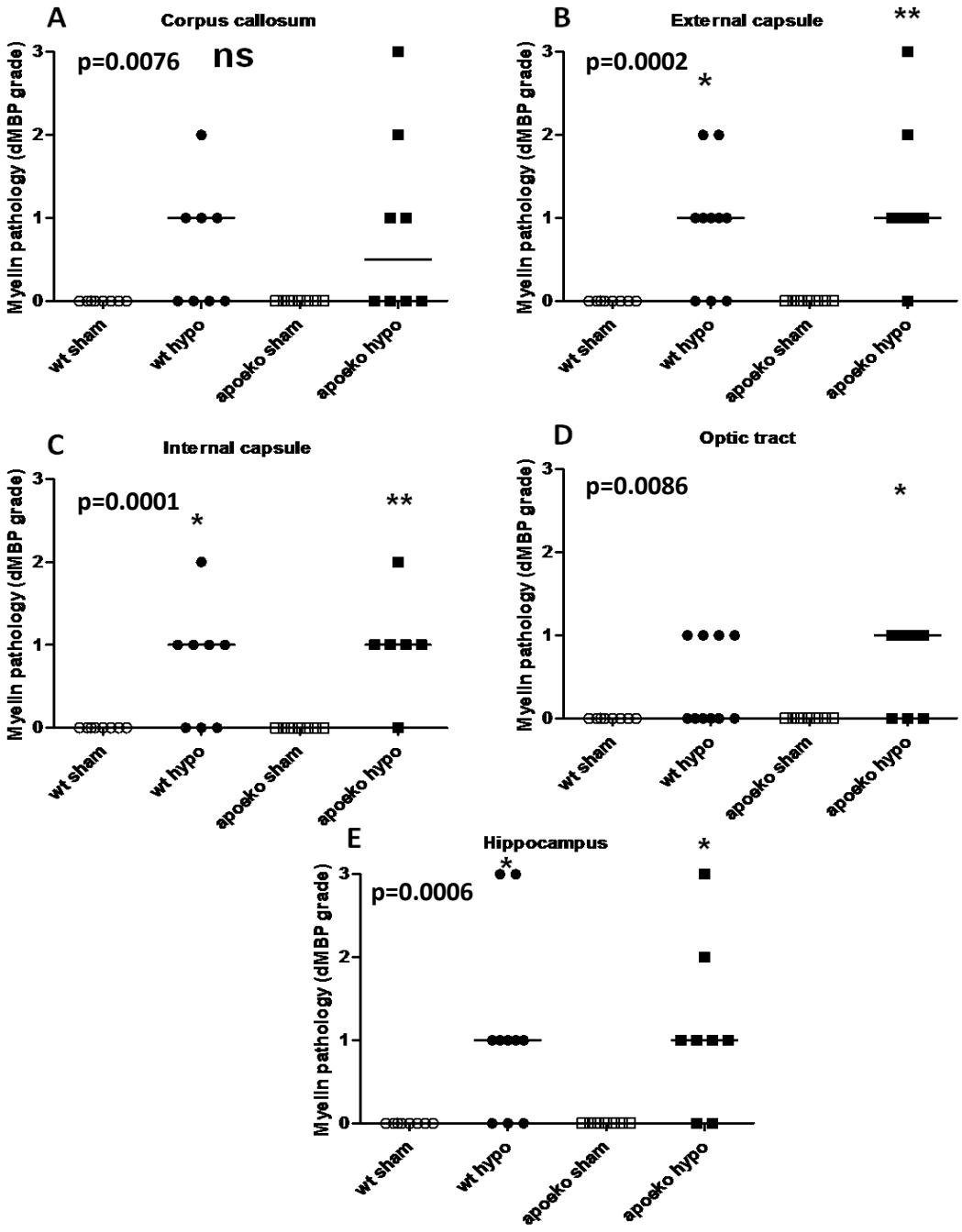

Figure S.4.3.3.: Regional group median pathological grades of degraded myelin (dMBP)

Hypoperfused mice from both genotypes exhibited significantly more degraded myelin in the EC, IC, and hippocampus than the two sham groups (**B, C**) ($p<0.05$). In the OT, only APOEKO hypoperfused group (n=8) ($p<0.05$), but not WT hypoperfused mice (n=10) ($p>0.05$) showed significantly more degraded myelin than the two sham groups. In the CC, there was no significant group difference in dMBP immunoreactivity (**A**) ($p>0.05$). There was no difference in myelin integrity between WT and APOEKO sham as well as between WT and APOEKO hypoperfused mice in any of the examined ROIs (**A**-**E**) ($p>0.05$). Significant group differences as given by Dunn multiple comparisons`s post- hoc analysis: ($p<0.05$)*, ($p<0.01$)**, ($p<0.0001$)***, ns (nonsignficant) ($p>0.05$)

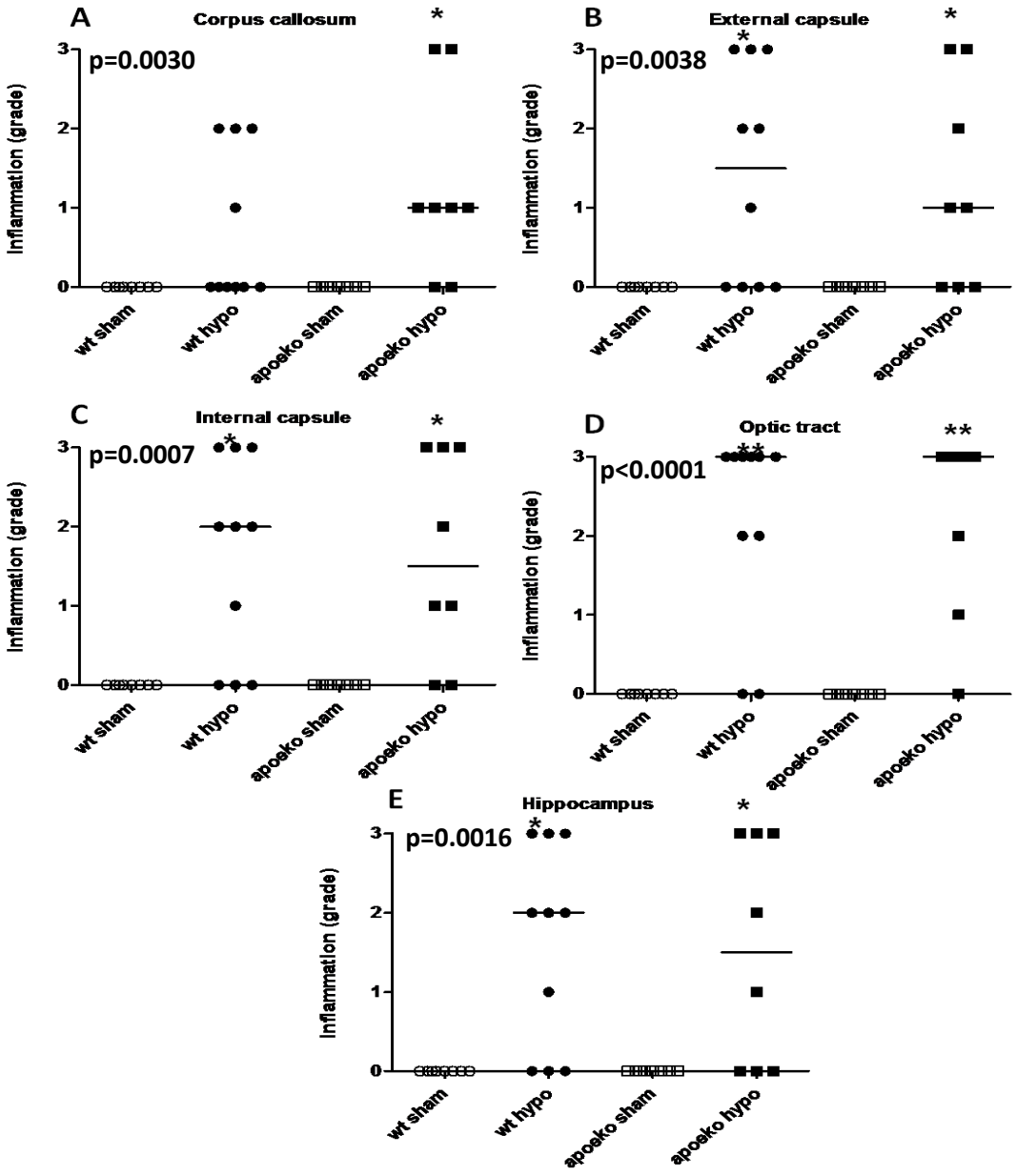

Figure S.4.3.4.: Regional group median pathological grades of inflammation

APOEKO (n=8) and WT (n=10) hypoperfused mice showed significantly increased inflammation in the EC, IC, OT, and hippocampus than the two sham groups (**B-D, E**) ($p<0.05$). In the CC, only APOEKO hypoperfused ($p<0.05$), but not WT hypoperfused ($p>0.05$) mice exhibited significantly increased inflammation than the two sham groups (**A**). There was no difference in inflammatory levels between WT and APOEKO sham as well as between WT and APOEKO hypoperfused mice in any of the examined ROIs ($p>0.05$) (**A-E**). Significant group differences as given by Dunn multiple comparisons`s post- hoc analysis: ($p<0.05$)*, ($p<0.01$)**, ($p<0.0001$)***

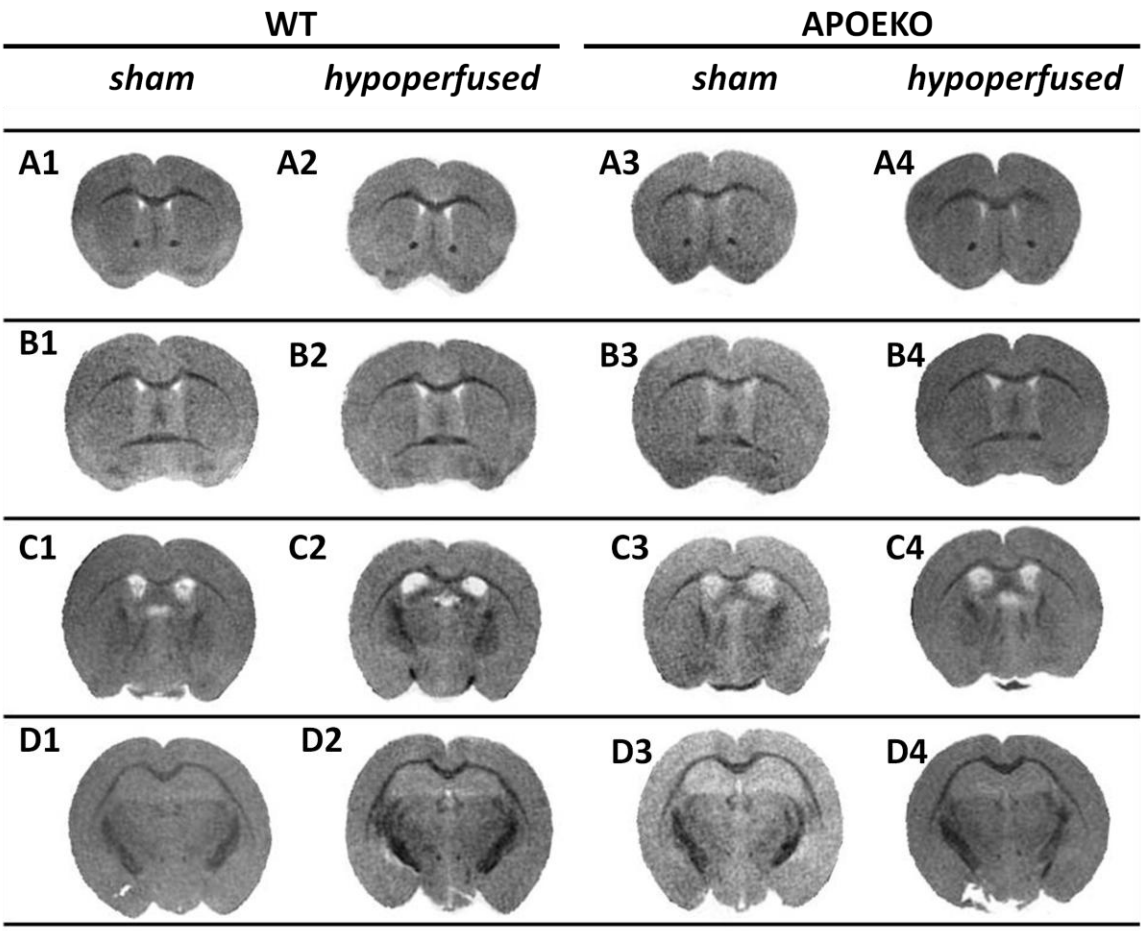

Figure S.4.4.: Grey matter structural integrity on T2- weighted scans of WT and APOEKO sham and hypoperfused mice

Grey matter structural integrity was examined on four consecutive T2- weighted scans corresponding to the following neuroanatomical levels: 0.74mm bregma (**A1- A4**), 0.38mm bregma (**B1- B4**), -0.94mm bregma (**C1- C4**), -2.12mm bregma (**D1- D4**).

An absence of overt grey matter abnormalities were observed in all experimental animals.

S.4.1. Correlation analysis between regional MRI metrics and pathological grades

S.4.1.1. Statistics

Non-parametric Spearman`s test was applied for the correlation analysis of the regional FA and MTR values and the regional median grades of white matter integrity (APP, MAG, dMBP) and inflammation (Iba1). The correlation was considered significant for $p<0.05$.

S.4.1.2. Results

White matter abnormalities related to chronic cerebral hypoperfusion and APOE genotype were revealed by using a combined ex vivo MRI and standard immunohistochemical approach. In order to verify the sensitivity of the developed ex vivo MRI technique to detect changes in white matter integrity in perfusion- fixed brain samples, the regional FA and MTR were correlated with the regional pathological grades of axonal (APP), myelin (MAG) integrity, degraded myelin (dMBP), and inflammation (Iba1).

A significant negative correlation was evidenced between the regional FA and MTR parameters and the corresponding pathological grades of axonal (APP) and myelin (dMBP, MAG) integrity as well as with the grades of inflammatory activity (Iba1) for all white matter ROIs ($p<0.05$). In the control grey matter region- the hippocampus, FA did not correlate significantly with any of the biomarkers ($p> 0.05$). However, MTR showed a significant negative correlation with myelin (dMBP) integrity and inflammatory levels ($p< 0.05$), but not with axonal pathology ($p> 0.05$). A summary of the correlation statistical analysis is provided in table S.4.2. This result suggests that a decrease in both FA and MTR correlates with an increase in the severity of the observed axonal damage, myelin pathology and inflammatory levels evidenced at the histological level in white matter regions.

MRI parameter	Region of interest	Biomarker			
		APP	**MAG**	**dMBP**	**Iba1**
		Axonal integrity	***Myelin integrity***	***Degraded myelin***	***Inflammation***
FA	*Corpus callosum (CC)*	r= -0.4966, p= 0.0028	r= -0.4656, p= 0.0055	r= -0.4666, p=0.0054	r= -0.5491, p= 0.0008
	External capsule (EC)	r= -0.5169, p= 0.0017	r= -0.4635, p= 0.0058	r=-0.6219, p< 0.0001	r= -0.4815, p= 0.0039
	Internal capsule (IC)	r= -0.7016, p< 0.0001	r= -0.7488, p< 0.0001	r= -0.7477, p< 0.0001	r= -0.6817, p< 0.0001
	Optic tract (OT)	r= -0.6290, p< 0.0001	r= -0.7411, p< 0.0001	r= -0.5810, p= 0.0003	r= -0.6040, p= 0.0002
	Hippocampus	r= -0.0790, p= 0.6567		r= -0.1497, p= 0.3981	r= -0.2321, p= 0.1865
MTR	*Corpus callosum (CC)*	r= -0.6314, p= 0.0002	r= -0.4889, p= 0.0061	r= -0.5549, p= 0.0015	r= -0.6130, p= 0.0003
	External capsule (EC)	r= -0.5991, p= 0.0005	r= -0.5320, p= 0.0025	r= -0.6132, p= 0.0003	r= -0.5852, p= 0.0007
	Internal capsule (IC)	r= -0.6699, p< 0.0001	r= -0.6438, p= 0.0001	r= -0.6937, p< 0.0001	r= -0.6459, p= 0.0001
	Optic tract (OT)	r= -0.6478, p= 0.0001	r= -0.7270, p< 0.0001	r= -0.6009, p= 0.0004	r= -0.6642, p< 0.0001
	Hippocampus	r= -0.3068, p= 0.0991		r= -0.4955, p= 0.0054	r= -0.5906, p= 0.0006

Table S.4.2.: Correlation analysis of MRI parameters and pathological grades of axonal (APP), myelin (MAG) integrity, degraded myelin (dMBP), and inflammation (Iba1)

Spearman`s correlation analysis showed a significant negative correlation between MRI (FA and MTR) parameters of white matter integrity and pathological grades of axonal (APP), myelin (dMBP) integrity and inflammation (Iba1) in examined white matter ROIs. In the hippocampus, only MTR, but not FA values correlated significantly with axonal integrity, degraded myelin and inflammation.

The correlation was considered significant for p values ($p<0.05$).

Appendices III

S.5.1. Pathological assessment

S.5.1.1. Materials and methods

The pathological profiles of the hypoperfused and sham animals used for the experimental purposes of the present Chapter 5 are described in Chapter 4. All analysis was performed one month after chronic cerebral hypoperfusion or sham controls. White matter integrity was examined on coronal brain sections at -2.12mm bregma neuroanatomical level (Franklin and Paxinos, 1997) using antibodies that allow detection of alterations in axonal integrity (APP) and the myelin sheath (dMBP and MAG), in the three white matter tracts (CC, EC, IC). White matter pathology was evaluated by means of a semi- quantitative grading scale (Chapter 2, section 2.7.4.) in white and grey matter ROIs of sham and hypoperfused animals (Chapter 2, section 2.8.).

The overall grey matter integrity and the presence of neuronal ischemic injury were examined on 6μm H&E stained coronal brain sections from neuroanatomical levels 0.74 mm; 0.38 mm; -0.94 mm; -2.12 mm bregma (Franklin and Paxinos, 1997) (Chapter 4, section 4.3.2.5.; figure, 4.3.; figure S.4.3.- appendices II). The grey matter ROIs were cortical (the Cx) and subcortical (the striatum, the hippocampus) regions known to be susceptible to blood flow alterations

S.5.1.2. Statistical analysis

As only a subset of the animals from Chapter 4 (hypoperfused n= 9; sham n= 8) were used in the present study, the group median regional pathological grades of axonal (APP) and myelin (MAG and dMBP) integrity were statistically reanalyzed by a nonparametric Mann- Whitney test. This particular statistical test was applied for the data analysis as the pathological grades were nonquantitative values and therefore could not be analyzed by using a standard parametric t- test analysis.

Significant group differences were reported for $p<0.05$.

S.5.1.3. Results

5.3.1.1. Chronic cerebral hypoperfusion affects significantly axonal integrity

Axonal pathology was detected by APP immunoreactivity and identified as intense APP immunoreactivity in swollen and/ or bulbous axons. Axonal injury with a varying degree of severity was evidenced in 6 of the 9 hypoperfused and in none of the 8 sham animals (figure S.5.1. A1- A4). Hypoperfused animals showed significant axonal damage in all white matter ROIs when compared with sham mice: the CC (U= 16.0, p= 0.016), EC (U= 16.0, p= 0.016), IC (U= 16.0, p= 0.016) (table S.5.1.).

The regional pathological grades of axonal integrity for each individual experimental animal are given in table S.4.1.1., appendices II.

5.3.1.2. Chronic cerebral hypoperfusion leads to significant myelin structural abnormalities in EC and IC, but not in CC

Using MAG immunostaining, myelin structural abnormalities with a varying degree of severity were observed in all hypoperfused (9/9) and in none of the sham animals (0/8) (figure S.5.1. B1- B4). A significant group difference in the severity of myelin abnormalities was evident in the EC (U= 12.0, p= 0.007) and IC (U= 4.0, p= 0.001) (table S.5.1.). Interestingly, after chronic cerebral hypoperfusion the myelin structural integrity was relatively preserved in the CC as shown by the absence of significant group difference (U= 28.0, p= 0.169) (table S.5.1.).

The regional pathological grades of myelin integrity as evaluated by MAG immunohistochemistry for each individual experimental animal are given in table S.4.1.2., appendices II.

5.3.1.3. Chronic cerebral hypoperfusion is associated with a significant myelin degradation

Degraded myelin accumulation with a varying degree of severity was detected by dMBP immunoreactivity in 8 hypoperfused (8/9) and none of the sham mice (0/8) (figure S.5.1. C1-C4).. There was a significant group difference in the severity of degraded myelin in all

white matter tracts: the CC (U= 12.0, p= 0.006), EC (U= 12.0, p= 0.006), IC (U= 8.0, p= 0.002) (table S.5.1.).

The regional pathological grades of myelin integrity as evaluated by dMBP immunohistochemistry for each individual experimental animal are given in table S.4.1.3., appendices II

5.3.1.4. Chronic cerebral hypoperfusion does not affect grey matter structural integrity

As described in the previous Chapter 4 there was no overt neuronal perikarya damage in the examined grey matter ROIs (the striatum, the hippocampus, and the cortex) in any of the experimental animals (Chapter 4, section 4.3.2.5.; figure, 4.3.; figure S.4.3.- appendices II).

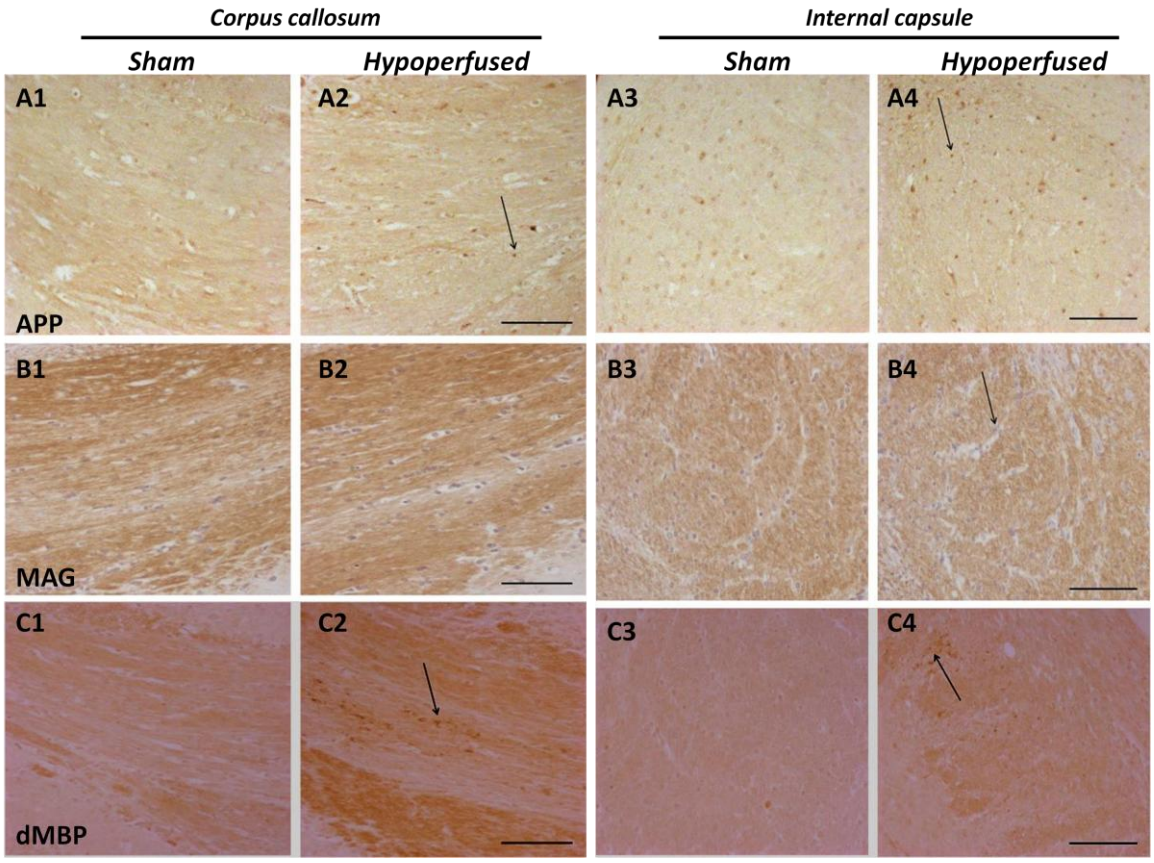

Figure S.5.1.: White matter integrity in sham and hypoperfused mice

Representative images of axonal (**A1- A4**), myelin (**B1- B4**) integrity and degraded myelin (**C1-C4**) in the CC (**A1-A2, B1- B2, C1- C2**) and the IC (**A3-A4, B3-B4, C3-C4**) in sham (**A1-C1, A3-C3**) and hypoperfused (**A2-C2, A4-C4**) mice. Hypoperfused mice exhibited axonal pathology (arrows in **A2, A4**) and degraded myelin (arrows in **C2** and **C4**) in both the CC (**A2, C2**) and the IC (**A4, C4**). Myelin structural integrity evaluated by MAG immunohistochemistry was preserved in the hypoperfused CC (**B2**), but not in the hypoperfused IC where disorganized myelin fibers, vacuoles and myelin debris were observed (arrow in **B4**).

Scale bar represents 20µm (magnification x40).

Biomarker	Region of interest	Sham (n=8) (median)	Hypoperfused (n=9) (median)
APP	*Corpus callosum(CC)*	0	1*
Axonal integrity	*External capsule (EC)*	0	1*
	Internal capsule (IC)	0	1*
MAG	*Corpus callosum(CC)*	0	0
Myelin integrity	*External capsule(EC)*	0	1*
	Internal capsule(IC)	0	2*
dMBP	*Corpus callosum(CC)*	0	1*
Degraded myelin	*External capsule(EC)*	0	1*
	Internal capsule(IC)	0	1*

Table S.5.1.: Regional group median pathological grades

Chronically hypoperfused mice (n=9) exhibited axonal injury (APP), myelin abnormalities (MAG) and increased inflammation (Iba1) in white ROIs compared with sham animals (n=8) a month post- surgery.

Significant group differences as given by Mann- Whitney nonparametric statistics: *($p<0.05$), **($p<0.01$), ***($p<0.001$)

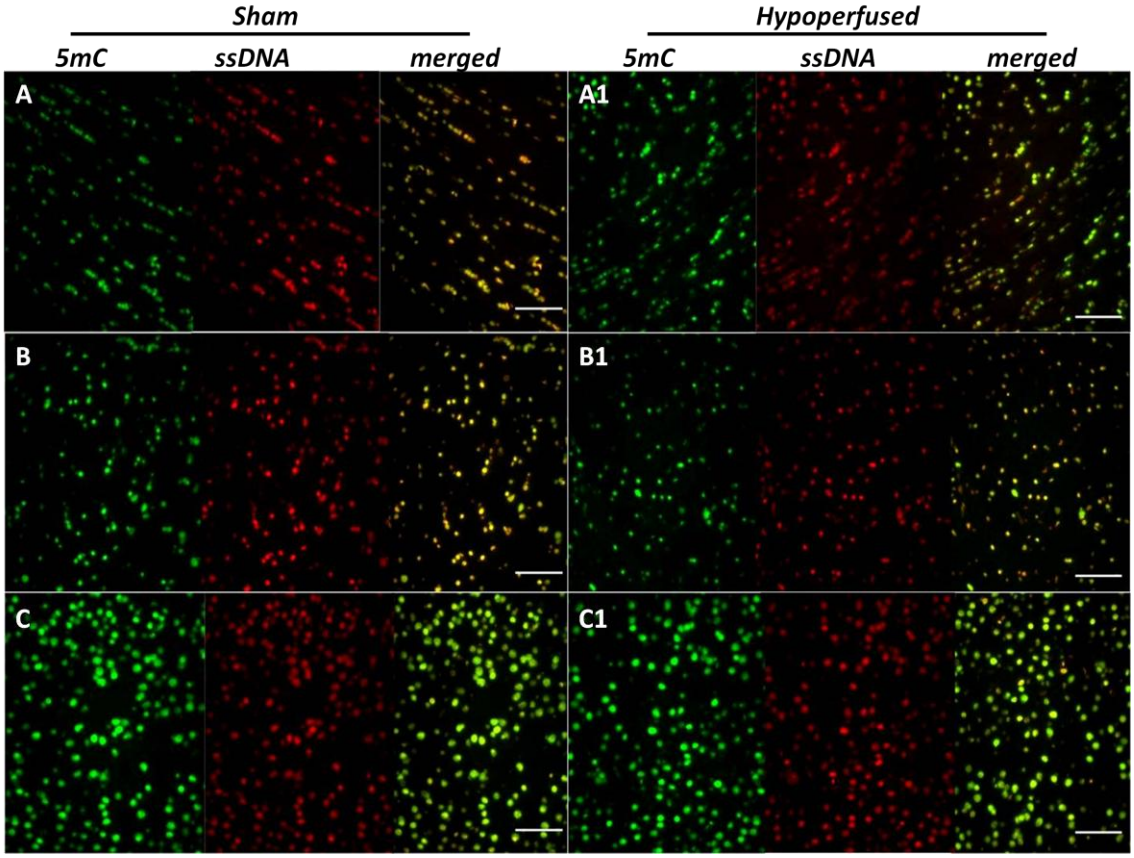

Figure S.5.2.1.: Brain 5mC immunochemical distribution in sham and hypoperfused mice

Representative images of 5mC immunoreactivity with ssDNA counterstaining in CC (**A, A1**), IC (**B, B1**) and Cx (**C, C1**) of sham (**A-C**) and hypoperfused mice (**A1-C1**). Under both normal physiological and chronically hypoperfused conditions methylation was evident in cellular nuclei as demonstrated by co-immunolocalization with ssDNA in white (**A-A1, B-B1**) and grey (**C- C1**) matter regions of the adult mouse brain.

Scale bar represents 20µm (magnification x40).

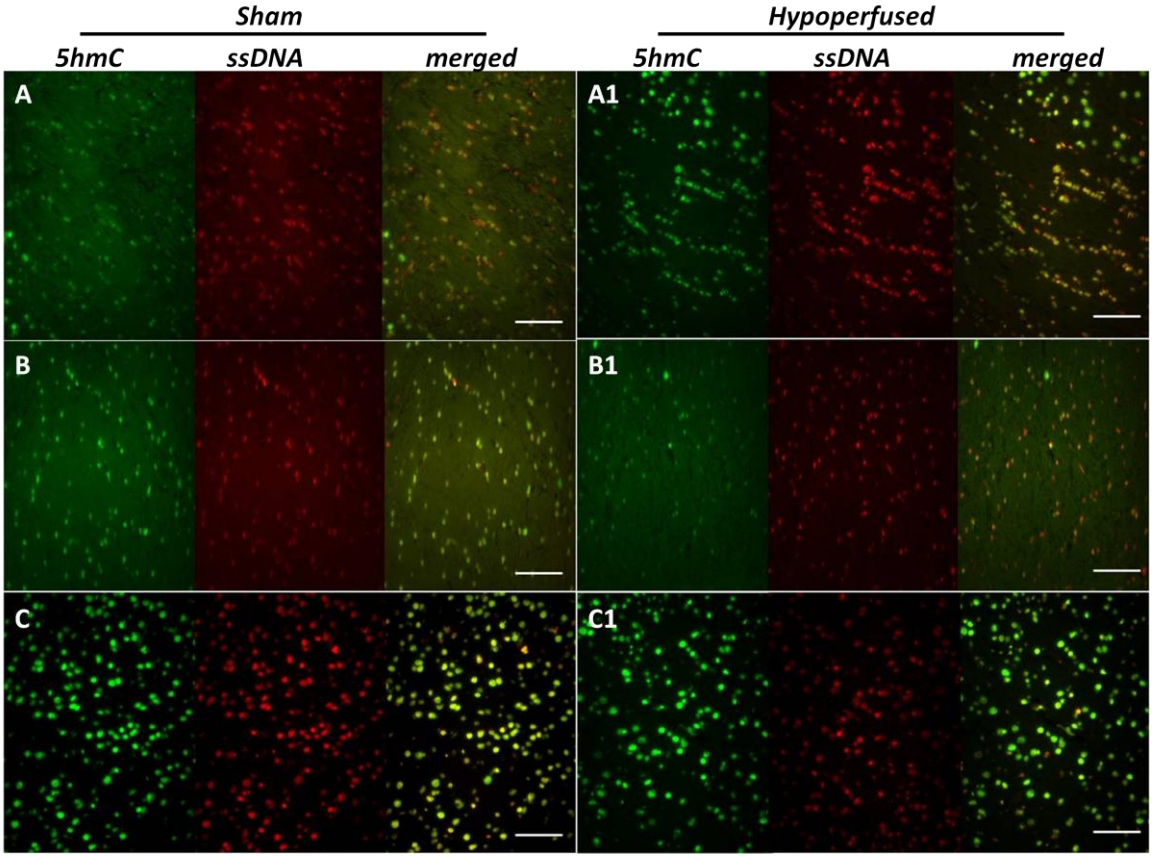

Figure S.5.2.2.: Brain 5hmC immunochemical distribution in sham and hypoperfused mice

Representative images of 5hmC immunoreactivity with ssDNA counterstaining in CC (**A, A1**), IC (**B, B1**) and Cx (**C, C1**) of sham (**A-C**) and hypoperfused (**A1-C1**) mice. Under both normal physiological and chronically hypoperfused conditions, 5hmC was immunodected in cellular nuclei as shown by co- immunocolocalization with ssDNA in white (**A- A1, B- B1**) and grey matter (**C- C1**) areas. Interestingly, under normal physiological conditions not all cells in white matter were 5hmC immunopositive. Chronic cerebral hypoperfusion led to a significant 5hmC upregulation in white matter (the CC- **A1**), but not in grey matter (**C1**) areas.

Scale bar represents 20μm (magnification x40).

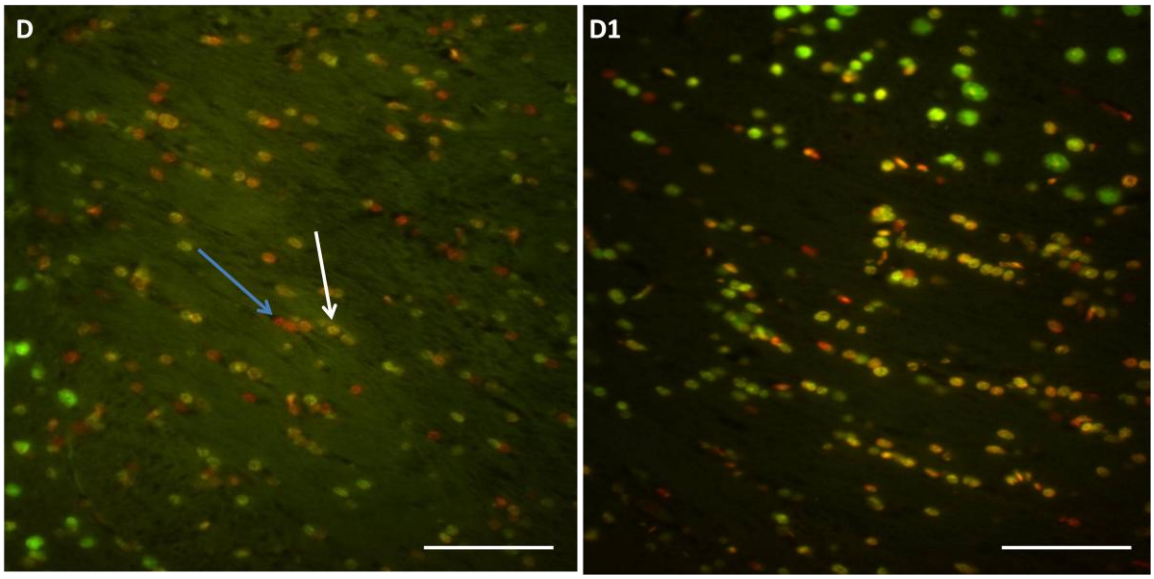

Figure S.5.2.2.: A higher resolution (at the same magnification) of the images shown in figure S.5.2.2. A- A1

Under normal physiological conditions 5hmC was enriched in certain cells present in white matter (white arrows in **D**) and absent in others (blue arrow in **D**). The exact phenotype of 5hmC positive and negative cells in white matter tracts remains unclear. Chronic cerebral hypoperfusion led to a significant increase in the proportion of 5hmC positive cells in the CC (**D1**).

Scale bar represents 20µm (magnification x40).

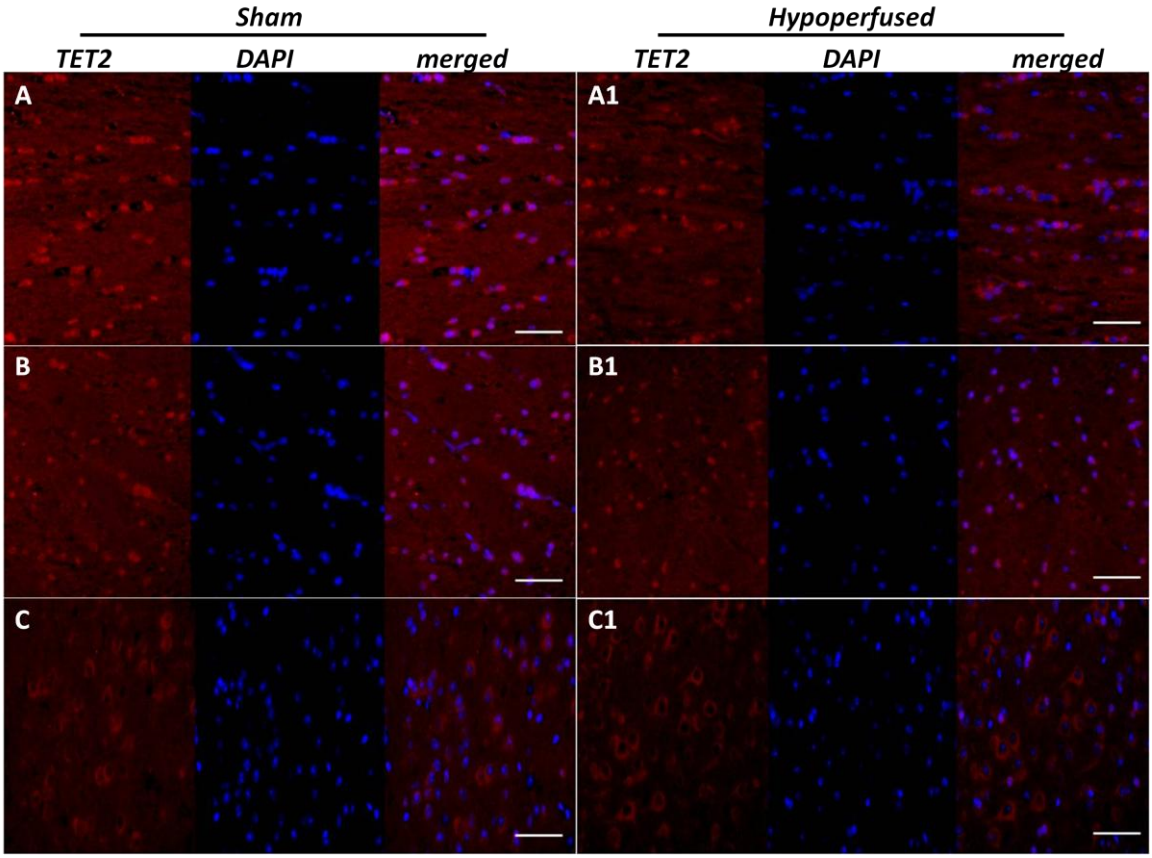

Figure S.5.2.3.: Brain TET2 immunochemical distribution in sham and hypoperfused mice

Representative images of TET2 immunoreactivity with DAPI counterstaining in the CC (**A, A1**), IC (**B, B1**) and Cx (**C, C1**) of sham (**A-C**) and hypoperfused (**A1-C1**) mice. Under normal physiological conditions, TET2 was equally distributed among white (**A, B**) and grey (**C**) matter regions. Chronic cerebral hypoperfusion did not impact on TET2 distribution in white matter (**A1, B1**), but led to a significant TET2 up- regulation in the Cx (**C1**).

Scale bar represents 20µm (magnification x40).

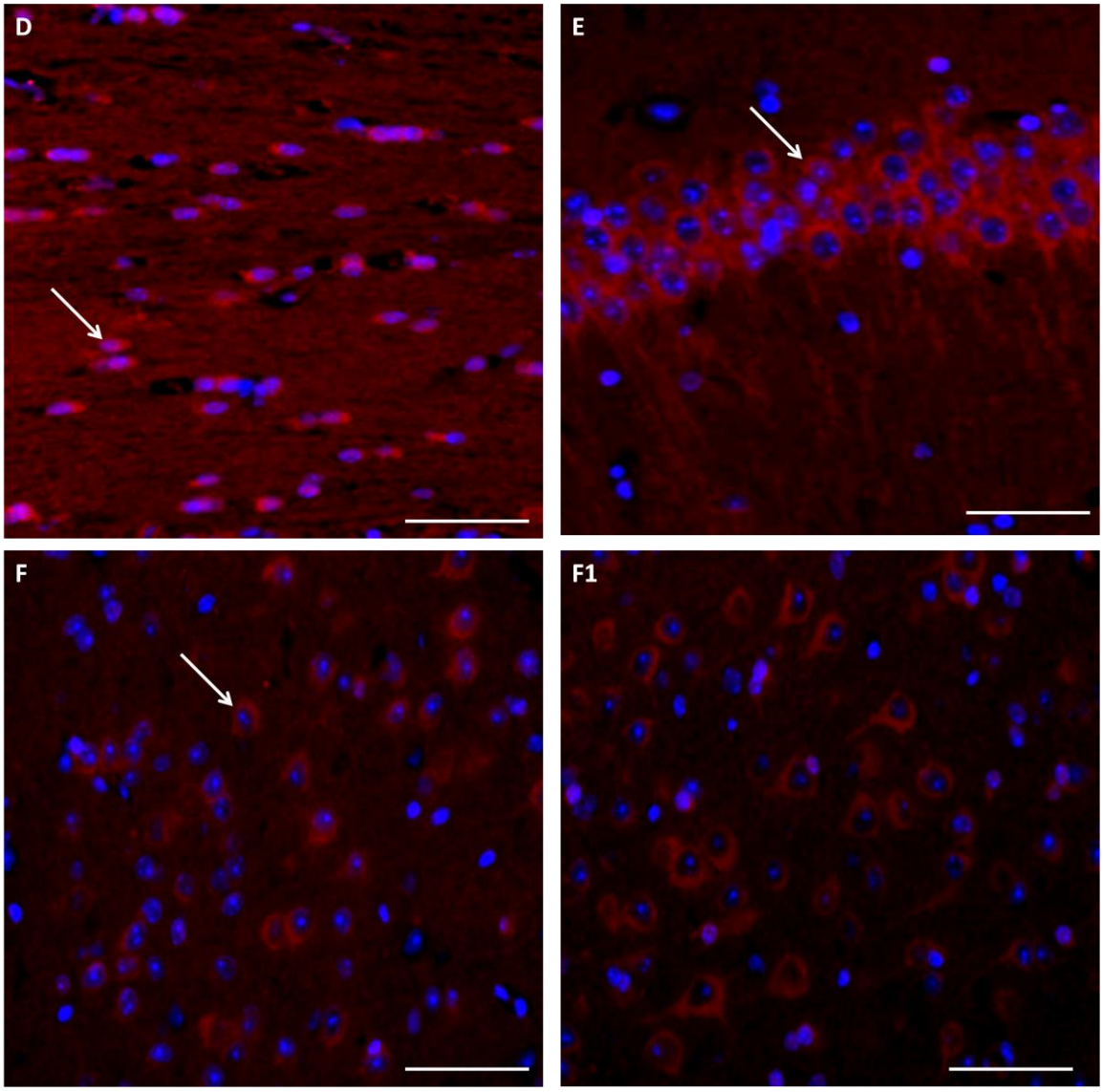

Figure S.5.2.3.: A higher resolution (at the same magnification) of the images shown in figure S.5.2.3. A, C, C1 and an additional image from the CA1 region of the hippocampus (E)

Under both normal physiological and chronically hypoperfused conditions TET2 was found in the cytoplasm of cortical (arrow in **F**) and subcrotical (arrow in **E**) cells (predominantly neurons) as well as in both the cytoplasm and nuclei of cells in white matter (predominantly glia) (arrow in **D**). Chronic cerebral hypoperfusion led a significant increase in cortical TET2 (**D1**).

Scale bar represents 20μm (magnification x40).

Biomarker	Region of interest	Number biomarker positive cells (mean ± SE)		Group statistics	Total number of cells (mean ± SE)		Group statistics
		Sham (n=8)	*Hypoperfused (n=9)*		*Sham (n=8)*	*Hypoperfused(n=9)*	
5mC	*Corpus callosum (CC)*	46 ± 5.7	49 ± 5.5	t= 0.7488, p= 0.4656	59 ± 5.3	59 ± 5.5	t= 0.3671, p= 0.7187
	External capsule (EC)	31 ± 5.5	26 ± 5.1	t= 0.2383, p= 0.8149	40 ± 5.2	34 ± 4.7	t= 0.4162, p= 0.6831
	Internal capsule (IC)	78 ± 7.2	71 ± 7.4	t= 0.1943, p= 0.8485	85 ± 4.3	84 ± 8.2	t= 0.1468, p= 0.8853
	CA1	76 ± 4.0	58 ± 8.4	t= 1.616, p= 0.1269	79 ± 3.1	59 ± 8.0	t= 1.931, p= 0.0726
	Cortex (Cx)	111 ± 8.7	97 ± 9.4	t= 1.077, p= 0.2983	127 ± 7.2	108 ± 8.5	t= 1.410, p= 0.1789
5hmC	*Corpus callosum (CC)*	32 ± 11.1	51 ± 8.6	t= 1.438, p= 0.1710	64 ± 16.7	61 ± 9.2	t= 0.1760, p= 0.8626
	External capsule (EC)	18 ± 4.3	20 ± 4.1	t= 0.3289, p= 0.7467	35 ± 6.1	33 ± 5.1	t= 0.2550, p= 0.8022
	Internal capsule (IC)	70 ± 11.8	70 ± 18.3	t= 0.02759, p= 0.9784	81 ± 10.4	95 ± 15.0	t= 0.8318, p= 0.4186
	CA1	57 ± 12.6	56 ± 8.5	t= 0.1133, p= 0.9113	72 ± 6.6	63 ± 7.9	t= 1.033, p= 0.3315
	Cortex (Cx)	93 ± 10.3	111 ± 8.0	t= 1.525, p= 0.1480	104 ± 11.0	120 ± 9.6	t= 1.213, p= 0.2440
TET2	*Corpus callosum (CC)*	18 ± 4.2	20 ± 4.3	t= 0.2717, p= 0.7895	59 ± 2.5	63 ± 2.5	t= 1.429, p= 0.1735
	External capsule (EC)	9 ± 2.0	8 ± 1.9	t= 0.5438, p= 0.5946	31 ± 2.2	27 ± 1.0	t= 1.698, p= 0.1101
	Internal capsule (IC)	24 ± 2.6	21 ± 3.4	t= 0.6494, p= 0.5259	50 ± 1.9	48 ± 2.5	t= 0.6578, p= 0.5206
	CA1	28 ± 1.6	25 ± 1.7	t= 1.287, p= 0.2175	48 ± 1.7	43 ± 1.5	t= 2.161, p= 0.0572
	Cortex (Cx)	21 ± 3.0	27 ± 2.1	t= 1.708 p= 0.1083	68 ± 2.6	66 ± 2.6	t= 0.3440, p= 0.7356

Table S.5.2.: Regional number of 5mC, 5hmC, TET2 positive cells and total number of cells (group mean ± SE values)

The regional number of 5mC, 5hmC, TET2 positive cells and the corresponding regional total number of ssDNA (for 5mC, 5hmC) or DAPI (for TET2) stained cells did not differ significantly between sham and hypoperfused mice in any of the examined ROIs as indicated by the t- test statistical analysis ($p>0.05$)

Biomarker	Region of interest	Number biomarker positive cells (mean ± SE)		Group statistics	Total number of cells (mean ± SE)		Group statistics
		Sham (n=8)	*Hypoperfused (n=9)*		*Sham (n=8)*	*Hypoperfused (n=9)*	
CC1	*Corpus callosum (CC)*	40 ± 5.6	32 ± 7.7	t= 0.8381, p= 0.4151	58 ± 1.9	61 ± 3.6	t= 0.6400, p= 0.5318
	External capsule (EC)	17 ± 3.7	15 ± 3.1	t= 0.3967, p= 0.6971	31 ± 2.4	31 ± 2.1	t= 0.03228, p= 0.9747
	Internal capsule (IC)	42 ± 3.7	35 ± 4.8	t= 1.147, p= 0.2693	57 ± 3.4	58 ± 3.1	t= 0.2338, p= 0.8183
NG2	*Corpus callosum (CC)*	10 ± 4.1	24 ± 3.2**	t= 2.981, p= 0.0093	60 ± 1.2	59 ± 3.2	t= 0.1817, p= 0.8583
	External capsule (EC)	14 ± 2.6	20 ± 1.3*	t= 2.373, p= 0.0314	34 ± 2.6	37 ± 2.2	t= 0.9881, p= 0.3388
	Internal capsule (IC)	9 ± 2.6	19 ± 3.3*	t= 2.591, p= 0.0205	48 ± 1.6	52 ± 1.7	t= 1.967, p= 0.0680
Iba1	*Corpus callosum (CC)*	4 ± 0.4	7 ± 0.8*	t= 3.546 , p= 0.0029	53 ± 5.5	52 ± 2.4	t= 0.1441, p= 0.8874
	External capsule (EC)	3 ± 0.3	3 ± 0.6	t= 1.051, p= 0.3098	31 ± 1.8	35 ± 1.0	t= 1.979, p= 0.0665
	Internal capsule (IC)	5 ± 0.3	12 ± 2.7*	t= 2.292, p= 0.0368	85 ± 4.5	89 ± 9.1	t= 0.3283, p= 0.7472

Table S.5.3.: Regional number of CC1, NG2, Iba1 positive cells and total number of cells (group mean ± SE values)

The regional number of CC1 positive cells in white matter ROIs and the corresponding regional total number of DAPI (CC1 and NG2), haemotoxylin (Iba1) positive cells for all biomarkers did not differ between sham and hypoperfused mice ($p>0.05$). The number of NG2 (the CC, EC, IC) and the number of Iba1 (the CC and the IC) positive cells increased significantly after chronic cerebral hypoperfusion ($p<0.05$). Significant group differences as indicated by the t- test statistical analysis: ($p<0.05$)*